



UNIVERSITÀ  
DEGLI STUDI  
FIRENZE

DOCTORAL PROGRAMME IN INDUSTRIAL  
ENGINEERING

DOTTORATO DI RICERCA IN INGEGNERIA  
INDUSTRIALE

XXXIV

**Design, Modelling, Simulation and  
Validation of Advanced Mechatronic Control  
Systems for Road Electric Vehicle's Stability  
Performances Improvement**

ING/IND-14

**Doctoral Candidate**

Tommaso Favilli

**Dean of the Doctoral Programme**

Prof. Marco Pierini

**Supervisors**

Prof. Luca Pugi

**External referees**

Prof. Basilio Lenzo

PhD Ing. Lorenzo Berzi

Prof. Edoardo Sabbioni

*Years 2018/2021*

©Università degli Studi di Firenze – School of Engineering  
Via di Santa Marta, 3, 50139 Firenze, Italy

Tutti i diritti riservati. Nessuna parte del testo può essere riprodotta o trasmessa in qualsiasi forma o con qualsiasi mezzo, elettronico o meccanico, incluso le fotocopie, la trasmissione fac simile, la registrazione, il riadattamento o l'uso di qualsiasi sistema di immagazzinamento e recupero di informazioni, senza il permesso scritto dell'editore.

All rights reserved. No part of the publication may be reproduced in any form by print, photoprint, microfilm, electronic or any other means without written permission from the publisher.

*“Invention is the most important product of man’s creative brain. The ultimate purpose is the complete mastery of mind over the material world, the harnessing of human nature to human needs.” - Nikola Tesla (1856-1943)*



# Summary

The intent of my research concern the improvements of electric vehicle's stability performances, while ensuring portability and flexibility properties of the proposed solutions, to be easily adapted and integrated for a large variety of use cases, including non-conventional and innovative traction architectures that should be allowed by current and future technologies, e.g. independent wheel motors.

To reach this goal and accomplish the challenge I work on the development of advanced control algorithms for mechatronic systems, using a systematic model-based methodology. Thus, scalable, modular and real-time capable models are proposed. The controllers are devoted to the optimization of specific tasks, resolving multi-degree of freedom allocation problems.

This document firstly resumes the **background** notions essentials for a complete understanding of the intentions and the improvements. Importance and opportunities for the development of advanced stability control strategies, aiming at the improvement of vehicle performance are introduced. *Vehicle dynamic theory* for longitudinal and lateral body behaviour, as well as tire-road interactions, are given. *Vehicular mechatronic systems* are described, with a special focus on by-Wire technologies for driving handling and active stability purposes, such as brake and steering systems. *Electric vehicle State-of-Art* is outlined for powertrain layouts, performances and braking system. Currently adopted *Electronic Stability Program structures and theories* are introduced, setting a reference baseline for the development of improved control strategies.

Then, the **proposed approach**, based on model-based simulations is described. To account and tackle the *research questions* addressed by the authors and the *open problems* in this field, a *model-based approach* based on V-shape development theory is chosen. For the latter, modelling and simulation methodologies are outlined for intrinsic features, pros and cons. Adopted *reference driving scenarios* are presented. These are related to standardized procedures, fundamental for reliable validation of dynamical behaviour of the vehicle and performance assessment of the proposed ESP controllers. All investigated use cases are supposed to be equipped with an *wheel-independent motors traction layout*, whose features, advantages and disadvantages are presented. A *yaw moment torque vectoring allocator* is developed, which is based on Moore-Penrose pseudo-inverse theory: this constitutes the low-level layer of the proposed ESP controllers. This methodology ensures the application of desired yaw moment to the vehicle's body while minimizing the wheel's torque efforts as compared to the driver's demand.

To achieve the purposes of my work, **methods and tools for preliminary validation activities** are developed. Aims and intents of the *OBELICS project*, which found part of my research are presented. The description of *investigated*

*electric vehicles use cases* follows. *Simulation models* of considered benchmark vehicles are developed to ensure reliable results of the virtual validation process. In particular, a simplified braking plant model is tuned using data arising from a static experimental process. Results show great convergence with real-world tests output performed on a driving track. Enchantment could be reached under several aspects, thanks to the innovative functionalities offered by modern vehicle e-powertrain layouts and control theories, i.e. energy efficiency (with advanced brake blending strategies for coordination of friction and regenerative brakes), functional safety & reliability (concerning the requirements imposed by several standards, using virtual fault tree analysis and fault injection) and stability (for longitudinal and lateral dynamics). These desirable contributions are evaluated during a *preliminary validation simulations* phase.

The main output of my activities is the proposal of **advanced active lateral stability controllers** which can exploit e-motors and by-wire technologies, by proper coordination between steering command and active torque distribution technique, to achieve higher cornering stability performances. The first solution, named *Minimized Tire Adhesion Grip ESP Controller*, intends to stabilize the vehicle while minimizing the engaged grip on each wheel, optimally exploiting the allocation degree of freedom allowed by the over-actuated vehicle systems. The second solution, the *Sliding Mode ESP Controller*, is based on a 2-dimension robust first-order sliding mode methodology that aims at the direct control of the vehicle's yaw rate and side-slip angle to converge to their desired kinematic values. Both controllers exhibit a hierarchical layers structure and share the same low-level torque vectoring Moore-Penrose pseudoinverse allocator. For the latter, validation of the lateral stability controller is performed for relevant use cases and driving scenarios. Results refer to standardized cornering tests, even compared with commercial ESP solutions, in both Software and Hardware-in-the-Loop simulation environments. Simulations outputs clearly state the improvement ensured by these ESP solutions for yaw rate and side-slip angle tracking, leading to enhanced lateral stability. In addition, the torque vectoring allocator ensures at the same time a longitudinal vehicle behaviour in strict accordance with the driver's intentions (speed and accelerations), if compared with conventional differential braking wheel torque allocation methods.

# Preface

Traffic safety is one of the main issues of worldwide automotive mobility and has been attracting considerable attention with an increasing amount of accidents registered in statistics. The growing interest in this field of research concerns both ethical and economical aspects. The costs are estimated at € 160 billion per year. For these reasons in 2001, the *European Commission* set the objective to halve the number of kills on road in the next 10 years (EuroTrans Policy of 2001). A diffused consensus in the literature is that the improvement in road safety requires a holistic approach, considering the three-element of drivers, vehicle technologies and infrastructures.

Typically, human error is the cause most of road accidents (over 90% according to the United States DOT Report of 1992). Due to unpredictable circumstances, such as an obstacle suddenly appearing on the road, or inappropriate driving conditions, e.g. high speeds on a dry surface or low visibility, the vehicle can become unstable by reaching its critical limits. In these situations, adherence of the vehicle's tires is saturated and the driver is no longer able to regain control of the chassis dynamical behaviour [1]. With the introduction of Driving Assistance System (DAS) and active-safety controllers, the pilot is gradually relieved of these tasks having to deal only with high-level decision-making functions. Indeed, newly and innovative vehicle technologies are fundamental for achieving improved road safety, as emphasised in all programs related to this topic.

The Electronic Stability Program (ESP), even known as Electronic Stability Control (ESC) or Vehicle Stability Control (VSC), is widely regarded as one of the most safety-relevant technology, representing the pillar of vehicle stability controllers. Since its first introduction in the market in 1995 by *Mercedes*, the potential of ESP to avoid or mitigate accidents has been analysed and proved in several studies.

The European Accident Causation Survey (EACS) data of [2] highlights that ESP could influence about 67% of fatal accidents involving loss of vehicle control and 42% of the corresponding injury accidents, in Germany. In the US, more than 39% of crash-related fatalities are accounted to vehicle lane departures scenarios [3]. However, data consistency between teams in different countries and lack of national or international representativity in the samples reduce the reliability of these considerations.

Nuessle et al. [4] show that car accidents involving vehicles of Mercedes company are drastically reduced over years, about 30%, if compared to all the Original Equipment Manufacturer (OEM) cars.

A study of 2004 by Baum [5] quantifies the effectiveness of ESP in accident avoidance for Single Vehicle Crash (SVC) in Germany at about 11%, with a 17% reduction of fatalities, supposing single vehicles accidents in skidding conditions.

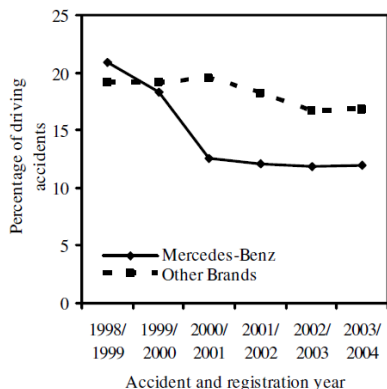


Figure 1: Accident statistic: Mercedes-Benz equipped with ESP vs standard vehicles (Figure from [4])

Nagai et al. [6] investigates traffic road accidents in Japan for the fiscal year 2005. More than 16000 kills were reported. The trend in the long-term scenario of fatalities shows a slight downward trend, related to the effectiveness of safety regulations and strategies (Figure 2). Recent advances in stability controllers and rescue systems determine a decrease in harm and damage to passengers, so the fatalities significantly decline compared to the number of occurred accidents. However, the number of traffic accidents rose, as well as the traffic casualties. Even though the lives of road accident victims can be saved, there are many situations resulting in serious physical damage for the people involved. This fact reveals that we should not be satisfied by only taking a glance at the number of traffic fatalities.

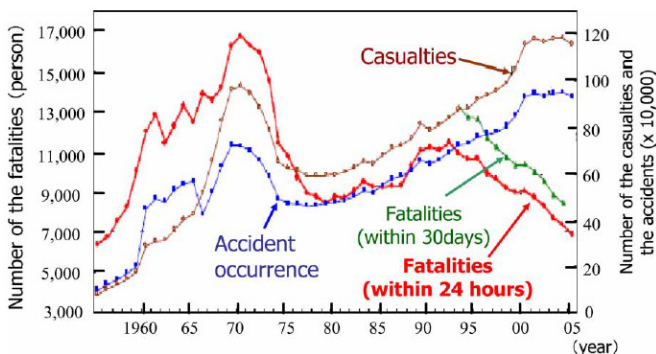


Figure 2: Accident statistics trend in Japan from 1960 to 2005 [6]

In a more recent work of 2019 by Koisaari [7], the calculation of the crashes rate ratio of ESP and no-ESP equipped vehicles show the improvement related to these controllers, which range from 0.17 to 0.81, depending on the accident scenarios.

In summarizing, outputs highlight that in severe driving conditions lateral controllers can contribute to safer driving situations. The effectiveness of ESP is promising enough to stimulate the automotive industry and research groups to develop innovative performing solutions to stabilize the vehicle behaviour in dangerous cornering scenarios [8].



# Contents

<b>Summary</b>	<b>v</b>
<b>Preface</b>	<b>vii</b>
<b>Glossary</b>	<b>xxi</b>
<b>List of Symbols</b>	<b>xxv</b>
<b>1 Introduction</b>	<b>1</b>
<b>2 Background</b>	<b>5</b>
2.1 Vehicle Dynamics . . . . .	5
2.1.1 Tire Forces . . . . .	6
2.1.2 Longitudinal Vehicle Dynamics . . . . .	10
2.1.3 Lateral Vehicle Dynamics . . . . .	14
2.1.4 Vehicle Body Equations . . . . .	16
2.1.5 Understeer Gradient . . . . .	16
2.2 Mechatronic Systems . . . . .	18
2.2.1 Vehicular Mechatronics: By-Wire System . . . . .	19
2.2.2 Brake-By-Wire . . . . .	19
2.2.3 Steer-By-Wire . . . . .	20
2.3 Electric Vehicles . . . . .	22
2.3.1 EV layout . . . . .	24
2.3.2 EV Performances . . . . .	26
2.3.3 Regenerative Brake Systems . . . . .	27
2.3.4 Brake Blending . . . . .	29
2.4 Electronic Stability Program . . . . .	33
2.4.1 Hierarchical Structure . . . . .	35
2.4.2 Control Theory . . . . .	37
2.4.3 ESP Control Solutions . . . . .	40
<b>3 Proposed Approach</b>	<b>43</b>
3.1 Research Question . . . . .	43
3.2 Open Problems . . . . .	44
3.2.1 EVs Heterogeneous Solutions . . . . .	44
3.2.2 Technical Challenges in ESP Developments . . . . .	45
3.2.3 Legislation & Standards . . . . .	48
3.2.4 Standardization . . . . .	50
3.3 Model-Based Methods and Tools . . . . .	50

3.3.1	V-shaped Development Model . . . . .	51
3.3.2	Mechatronic System Simulation . . . . .	52
3.3.3	Vehicle Dynamic Simulation . . . . .	53
3.3.4	Model-based Pros and Cons . . . . .	54
3.3.5	Simulation Toolchains . . . . .	56
3.4	Reference Driving Scenario . . . . .	58
3.4.1	Speed Driving Cycle . . . . .	59
3.4.2	Longitudinal Driving Manoeuvres . . . . .	59
3.4.3	Cornering Driving Manoeuvres . . . . .	60
3.5	Wheel-Independent Motor . . . . .	66
3.5.1	In-Wheel Motors . . . . .	67
3.6	Yaw Moment Torque Vectoring Allocator . . . . .	68
3.6.1	Moore-Penrose Torque Vectoring Approach . . . . .	68
<b>4</b>	<b>Methods, Tools and Preliminary Activities</b>	<b>75</b>
4.1	OBELICS Project . . . . .	75
4.2	Vehicle Use Cases . . . . .	76
4.2.1	FIAT 500e . . . . .	76
4.2.2	SimRod Kyburz . . . . .	77
4.2.3	Valeo Concept 4WD . . . . .	79
4.3	Simulation Model . . . . .	80
4.3.1	MATLAB and VI-Grade Co-simulation Model . . . . .	81
4.3.2	Vehicle Body Model . . . . .	82
4.3.3	Driver Model . . . . .	83
4.3.4	Steering Model . . . . .	85
4.3.5	Brake System Model . . . . .	85
4.3.6	Suspension Model . . . . .	93
4.3.7	e-Powertrain Model . . . . .	93
4.3.8	Stability Control Unit Model . . . . .	94
4.3.9	Brake Blending Controller . . . . .	97
4.4	Preliminary Validation Simulations . . . . .	100
4.4.1	Brake Model Validation . . . . .	101
4.4.2	EV Efficiency Improvements . . . . .	113
4.4.3	EV Safety Improvements . . . . .	126
4.4.4	EV Stability Improvements . . . . .	139
<b>5</b>	<b>Advanced ESP Control Algorithms</b>	<b>151</b>
5.1	Minimized Tire Adhesion Grip ESP Controller . . . . .	152
5.1.1	Introduction . . . . .	153
5.1.2	Torque and Steering Allocation Strategy . . . . .	154
5.1.3	Benchmark Vehicle Model . . . . .	160
5.1.4	Performed Simulations . . . . .	161
5.1.5	Conclusions and Future Developments . . . . .	166
5.2	Sliding Mode ESP Controller [246] . . . . .	169
5.2.1	Control Strategy . . . . .	169
5.2.2	Modelling Approach: High-level layer . . . . .	170
5.2.3	Control Theory: Intermediate-level layer . . . . .	174
5.2.4	Effort Application: Low-level layer . . . . .	175
5.2.5	SiL Test Campaigns: Tuning of the ESP in Co-simulation . . . . .	179
5.2.6	Real-Time Driving Simulator . . . . .	179

5.2.7	HiL Test Campaigns: Performance Evaluations in the Driving Simulator . . . . .	182
5.2.8	SiL Test Campaign: ESP Validation and Optimization in Co-simulation . . . . .	189
5.2.9	Conclusions and Future Developments . . . . .	202
<b>6</b>	<b>Discussion</b>	<b>205</b>
	<b>Bibliography</b>	<b>211</b>
<b>A</b>	<b>Publications</b>	<b>235</b>
A.1	Brake Blending and Optimal Torque Allocation Strategies for Innovative Electric Powertrains [198] . . . . .	235
A.2	Real Time Models of Automotive Mechatronics Systems: Verifications on “Toy Models” [21] . . . . .	240
A.3	Application of Regenerative Braking on Electric Vehicles [198] . . . .	245
A.4	Brake Blending Strategy on Electric Vehicle: Co-simulation Between MATLAB Simulink and Simcenter Amesim [221] . . . . .	253
A.5	Fast modelling and identification of hydraulic brake plants for automotive applications [213] . . . . .	261
A.6	Brake Blending and Torque Vectoring of Road Electric Vehicles: a flexible approach based on Smart Torque Allocation [210] . . . . .	279
A.7	Modeling and Identification of an Electric Vehicle Braking System: Thermal and Tribology Phenomena Assessment [214] . . . . .	292
A.8	Smart Energy Management of Auxiliary Load for Electric Vehicles [223] . . . . .	304
A.9	Regenerative Fuzzy Brake Blending Strategy on Benchmark Electric Vehicle: the FIAT 500e [199] . . . . .	313
A.10	ESC on In-Wheel Motors Driven Electric Vehicle: Handling and Stability Performances Assessment [194] . . . . .	322
A.11	Functional safety and reliability for innovative vehicle braking system and integration with electric traction units [15] . . . . .	334
A.12	48V Electric Vehicle Powertrain Optimal Model-based Design [224] .	354
A.13	Design of a new On-board Energy Storage and Conversion System for a Fast Charging Urban Transport Electric Bus [222] . . . . .	364



# List of Figures

1	Accident statistic: Mercedes-Benz equipped with ESP vs standard vehicles (Figure from [4]) . . . . .	viii
2	Accident statistics trend in Japan from 1960 to 2005 [6] . . . . .	viii
2.1	Three DoF vehicle dynamic model in longitudinal, lateral and yaw motion directions . . . . .	5
2.2	Longitudinal vehicle model . . . . .	6
2.3	Longitudinal tire force as a function of slip ratio (Figure from [3]) . .	7
2.4	Longitudinal driving wheel model for tire forces and deformations definition (Figure from [3]) . . . . .	8
2.5	Experimental result: longitudinal tire force as a function of slip ratio for different vertical load (Figure from [43]) . . . . .	9
2.6	Lateral tire model for slip angle definition (Figure from [3]) . . . . .	9
2.7	Experimental result: lateral tire force as a function of slip angle for different vertical load (Figure from [43]) . . . . .	10
2.8	Normalized friction force as a function of slip ratio for different road status using the Magic Formula (Figure from [3]) . . . . .	11
2.9	Longitudinal vehicle model driving on an inclined road . . . . .	11
2.10	Front and rear axles ideal braking forces plane (Figure from [43]) . .	13
2.11	Front and rear axles admissible braking combination with grip coefficient variation (Figure from [43]) . . . . .	14
2.12	Single-track vehicle model . . . . .	15
2.13	Understeering vehicle behaviour with speed (Figure from [3]) . . . .	17
2.14	Mechatronic engineering fields synergistic integration . . . . .	18
2.15	Automotive brake systems development trend (Figure from [53]) . .	21
2.16	Conceptual schemes of different EV layouts (Figure from [57]) . . . .	26
2.17	Motor torque characteristic: ICE (left) and EM (right) (Figure from [57]) . . . . .	27
2.18	Multi-quadrant torque-speed characteristic of EM . . . . .	28
2.19	Bandwidth response of brake systems (Figure from [84]) . . . . .	30
2.20	Different brake blending strategies: series (left), parallel (center) and hybrid (right) (Figure from [79]) . . . . .	33
2.21	Differential torque allocation and induced yaw moment on a vehicle	35
2.22	Workflow diagram of ESP (Figure from [9]) . . . . .	36
2.23	Simplified block diagram of ESP (Figure from [9]) . . . . .	36
2.24	Over and understeering vehicle behaviors during cornering and ESP control efforts (Figure from [9]) . . . . .	38

3.1	V-shaped development model (Figure from [9]) . . . . .	52
3.2	Simulation time dependability respect to model complexity (Figure from [181]) . . . . .	54
3.3	Simulink and CarRealTime co-simulation blocks . . . . .	57
3.4	Speed profile for the straight line braking manoeuvre as compared to road friction coefficient (Figure from [91]) . . . . .	60
3.5	Input of SwD test (Figure from FMVSS 126) . . . . .	62
3.6	Test track for ISO 3888 DLC (top) and obstacle avoidance (bottom) (Figure from ISO 3888) . . . . .	64
3.7	MATLAB Simulink “Driving Scenario Designer” tool interface . . . . .	65
3.8	Optimal waypoint definition for ISO 3888-1 and ISO 3888-2 tests . . . . .	65
3.9	Reference planar vehicle model for the TV allocation algorithm . . . . .	69
3.10	Yaw moment and torque allocation for 2000Nm yaw moment demand and equal weight on wheels (left) and prioritized rear wheels (right) . . . . .	71
3.11	Yaw moment and torque allocation for 4000Nm yaw moment demand and equal weight on wheels (left) and prioritized rear wheels (right) . . . . .	72
3.12	Yaw moment and torque allocation for 9000Nm yaw moment demand and equal weight on wheels (left) and prioritized rear wheels (right) . . . . .	72
4.1	FIAT 500e vehicle Use Case (UC) . . . . .	76
4.2	Exploded view of FIAT 500e vehicle UC . . . . .	77
4.3	SimRod Kyburz Vehicle UC . . . . .	78
4.4	SimRod Kyburz SCADAS acquisition hardware system . . . . .	78
4.5	Valeo Concept Vehicle UC . . . . .	79
4.6	Valeo 48 V e-machine efficiency map . . . . .	79
4.7	MATLAB and VI-Grade co-simulation model implementation . . . . .	81
4.8	Vehicle chassis and wheels reference systems . . . . .	82
4.9	CarRealTime tire model . . . . .	83
4.10	Preview distance effect of the MacAdam driver model . . . . .	85
4.11	VI-CarRealTime steering model . . . . .	85
4.12	Simplified pseudo-physical model proposed by university of Florence. . . . .	87
4.13	Corresponding table of the brake torque reference respect to the brake command . . . . .	88
4.14	Filtering comparison for the brake pressure acquired in the Simrod Kyburz UC during real-word test . . . . .	90
4.15	Decomposition of the braking plat simulation model in sub-models . . . . .	90
4.16	Equivalent thermal RC network for a single rear brake of the Simrod Kyburz vehicle UC . . . . .	91
4.17	Pad wear coefficient $k$ as a function of the pad temperature . . . . .	92
4.18	Efficiency map of the Valeo EM respect to speed and torque for 25°C temperature implemented in Simulink and CarRealTime . . . . .	94
4.19	Signal flowchart of the stability control units . . . . .	95
4.20	Front/Rear axles braking distribution: (1) optimal; (2) conventional . . . . .	96
4.21	ABS/ASR torque regulation strategy respect to slip $\sigma$ . . . . .	97
4.22	Adopted hybrid brake blending algorithm . . . . .	98
4.23	Equivalent model implementation in Simulink of the BB controller . . . . .	99
4.24	Simplified block diagram of the Brake Blending model . . . . .	100
4.25	Acquisition and sensors system installed on SimRod prototype for the identification of brake plant features . . . . .	102
4.26	Testing center of Aldenhoven (Germany) . . . . .	103

4.27	Evaluation of steady-state values for a three-steps test: brake pressures.	104
4.28	Normalized pressure plant response vs. normalized pedal run. . . . .	104
4.29	Example of fitting performance of the brake model as compared to experimental results on three steps tests used during calibration tests	105
4.30	Comparison of the brake model pressure respect to experimental results during real braking manoeuvre performed on the test circuit of Aldenhoven . . . . .	106
4.31	Comparison of the brake model pressure respect to experimental results during real braking manoeuvre performed on the test circuit of Aldenhoven . . . . .	107
4.32	Comparison of measured and simulated torque profiles during a braking test imposing the same brake pedal displacement . . . . .	107
4.33	Hydraulic brake model response during a $25Hz$ ABS brake modulation	108
4.34	Hydraulic brake model torque during a $50Hz$ ABS brake modulation	108
4.35	Hydraulic brake model torque during a $100Hz$ ABS brake modulation	109
4.36	Response sensitivity of the caliper respect to variation of known input parameters . . . . .	109
4.37	Thermal sensors instrumented on the left-rear brake of the SimRod .	110
4.38	Chassis dynamometer experimental setup . . . . .	111
4.39	Estimated friction coefficient for the different measurement runs as a function of interface temperature $Temp_{if}^{RL}$ . . . . .	112
4.40	Comparison between predicted and simulated temperatures for run 3	112
4.41	Comparison between predicted interface temperature and measured interface temperature for consecutive braking manoeuvre during on-road driving . . . . .	113
4.42	Co-simulation layout implemented in Amesim for the reference UC .	114
4.43	Consumed and regenerated energy during a WLTC class 3 . . . . .	115
4.44	Brake blending with a constant brake demand of 700 Nm. . . . .	116
4.45	Fuzzy brake blending controller . . . . .	116
4.46	Membership functions for: a) brake command; b) EM shaft speed; c) battery SOC; d) battery temperature; e) battery cycle; f) aggregation	119
4.47	Straight line deceleration: regenerative torques at different $SOC_i$ for the full brake test . . . . .	119
4.48	Auxiliary load management control: block diagram . . . . .	121
4.49	Comparison of thermal regulation system's behaviour during a WLTC	122
4.50	Comparison of cabin temperature during a WLTC . . . . .	123
4.51	Auxiliary load management control: flow chart . . . . .	124
4.52	Fully integrated 48V electric vehicle model in Amesim . . . . .	125
4.53	Comparison of SOC (left) and thermal system power (right) during the Barcelona RDE cycle for different environment temperature . . .	125
4.54	Comparison of EV power demand during the barcelona RDE cycle . .	125
4.55	Flowchart of the proposed functional safety assessment methodology	128
4.56	Reference BBW system layout with BB . . . . .	129
4.57	EV block diagram for the FMEA process . . . . .	129
4.58	EV simulation layout of the <i>Simulink model</i> . . . . .	134
4.59	Proposed ABS fault detection and mitigation logic scheme . . . . .	135
4.60	ABS functional decomposition scheme . . . . .	136
4.61	Stopping distance for detected ABS failure without (left) and with FSU (right) during Montecarlo FI simulations . . . . .	137

4.62	Wheel torque (top) and slip (bottom) in normal operative condition (left) and fault condition (right) during Model-based FI simulations .	138
4.63	Vehicle trajectory in a DLC manoeuvre with a speed of $50km/h$ and a friction of 1, supposing different traction architectures . . . . .	140
4.64	Torque vectoring in a DLC manoeuvre with a speed of $50km/h$ and a friction of 1, supposing availability of the ESC . . . . .	141
4.65	Vehicle lateral control strategy block diagram . . . . .	142
4.66	Axle braking force EBD distribution: (1) Ideal; (2) Conventional; (3) Proposed . . . . .	144
4.67	Vehicle braking distance in longitudinal braking maneuver with a speed of $100km/h$ and a friction coefficient of 1, 0.7 and 0.5, supposing availability and unavailability of the ABS control system . . . . .	145
4.68	Vehicle wheels speed in longitudinal braking manoeuvre in accordance to ISO 21994 standard specification with ABS control system . . . .	146
4.69	Vehicle trajectory and lateral acceleration in a j-turn manoeuvre with a speed of $100km/h$ and a friction of 1, supposing availability and unavailability of the ESC . . . . .	146
4.70	Vehicle side-slip angle and yaw rate and lateral acceleration in a j-turn manoeuvre with a speed of $100km/h$ and a friction of 1, supposing availability and unavailability of the ESC . . . . .	147
4.71	Vehicle trajectory in a DLC manoeuvre with a speed of $50km/h$ and a friction of 1, supposing availability and unavailability of the ESC .	147
4.72	Target and effective vehicle side slip angle $\beta$ and yaw rate $r$ during SwD manoeuvre, with a longitudinal speed of $80 km/h$ and a steering wheel angle of $270$ deg, supposing availability and unavailability of the ESC control system . . . . .	148
5.1	Proposed allocator and its interaction with the other systems . . . .	154
5.2	Kamm adhesion ellipse for the $i^{th} - j^{th}wheel$ . . . . .	155
5.3	simplified scheme of proposed algorithm . . . . .	156
5.4	Adopted bicycle model for the Model-based Estimator . . . . .	157
5.5	Benchmark vehicle's architectures of the FIAT 500e . . . . .	161
5.6	Vehicle dynamic response in CSW angle test at $15km/h$ . . . . .	162
5.7	Side-slip angle vs lateral acceleration in different testing scenarios for constant steering wheel angle test at $50km/h$ , supposing availability and unavailability of the ESC . . . . .	162
5.8	Curve radius vs lateral acceleration for constant steering wheel angle test at $50km/h$ , supposing availability and unavailability of the ESC	163
5.9	Steering angle for constant steering wheel angle test at $50km/h$ , supposing availability and unavailability of the ESC . . . . .	163
5.10	Curve radius vs time in different testing scenarios for constant steering wheel angle test at $70km/h$ , supposing availability and unavailability of the ESC . . . . .	164
5.11	Lateral acceleration for lateral transient response test at $60km/h$ , supposing availability and unavailability of the ESC control system .	164
5.12	Lateral displacement for DLC test at $80km/h$ , supposing availability and unavailability of the ESC . . . . .	165
5.13	Steering angle command for DLC test at $80km/h$ , supposing availability and unavailability of the ESC . . . . .	165

5.14	Engaged adherence for for DLC test at $80km/h$ , supposing availability and unavailability of the ESC . . . . .	166
5.15	Normal load estimation on wheels for DLC test at $80 km/h$ . . . . .	166
5.16	Lateral load estimation on wheels for DLC test at $80 km/h$ . . . . .	167
5.17	Normalized lateral acceleration (top), normalized yaw rate (bottom-left) and normalized side-slip angle (bottom-right) for DLC test at $80km/h$ , supposing availability and unavailability of the ESC . . . . .	168
5.18	Block diagram of the SMC controller . . . . .	170
5.19	Block diagram of the low-level SMC controller . . . . .	173
5.20	Block diagram of the intermediate-level SMC controller . . . . .	175
5.21	Definition of control dead-zone . . . . .	176
5.22	Application of corrected steering angle algorithm . . . . .	177
5.23	Application of corrected steering angle algorithm . . . . .	178
5.24	Block diagram of the intermediate-level SMC controller . . . . .	178
5.25	Real-time driving simulator . . . . .	180
5.26	Static simulator setup . . . . .	181
5.27	Control functionality in a Step Steer maneuver . . . . .	184
5.28	Wheel torques in a <i>Step Steer</i> manoeuvre at $150km/h$ and with $90deg$ steering wheel angle in case of Non-controlled (Passive), Commercial-controlled (Active) and SMC-controlled scenarios . . . . .	184
5.29	Vehicle lateral acceleration and longitudinal speed in a <i>Step Steer</i> manoeuvre at $150km/h$ and with $90deg$ steering wheel angle in case of Commercial-controlled (Active) and SMC-controlled scenarios . . . . .	185
5.30	Control functionality in a Sine Steer maneuver . . . . .	186
5.31	Wheel torques in a <i>Sine Steer</i> manoeuvre at $150km/h$ and with $90deg$ steering wheel angle in case of Commercial-controlled (Active) and SMC-controlled scenarios . . . . .	186
5.32	Vehicle lateral acceleration and longitudinal speed in a <i>Sine Steer</i> manoeuvre at $150km/h$ and with $90deg$ steering wheel angle in case of Non-controlled (Passive), Commercial-controlled (Active) and SMC-controlled scenarios . . . . .	187
5.33	Trajectory and longitudinal speed made in a Lane Change maneuver . . . . .	188
5.34	States tracking performances in a <i>Lane Change</i> manoeuvre at $150km/h$ and a lateral displacement of about $3m$ in case of Non-controlled vehicle (Passive), Commercial-controlled vehicle (Active) and SMC controlled . . . . .	188
5.35	Wheel torques in a <i>Lane Change</i> manoeuvre at $150km/h$ and a lateral displacement of about $3m$ in case of Commercial-controlled vehicle (Active) and SMC controlled . . . . .	189
5.36	Gain scheduling of the yaw moment respect to vehicle speed . . . . .	189
5.37	Vehicle understeering characteristic for ramp steer command at $70km/h$ . . . . .	190
5.38	$\beta - \dot{\beta}$ method phase plane plot for ramp steer command at $70km/h$ . . . . .	190
5.39	Results of the constant steering wheel angle test at $120km/h$ , supposing availability and unavailability of the ESC control system . . . . .	191
5.40	Results of the constant steering wheel angle test at $120km/h$ , supposing availability and unavailability of the ESC . . . . .	192
5.41	Results of the constant steering wheel angle test at $120km/h$ , supposing availability and unavailability of the ESC . . . . .	192

5.42	Results of the constant steering wheel angle test at $120km/h$ , supposing availability and unavailability of the ESC . . . . .	193
5.43	Results of the constant steering wheel angle test at $120km/h$ , supposing availability and unavailability of the ESC . . . . .	193
5.44	Results of the SwD test at $80km/h$ , supposing availability and unavailability of the ESC . . . . .	194
5.45	Torque control efforts of the ESP SMC control during the Sine with Dwell test at $80km/h$ , supposing availability and unavailability of the ESC . . . . .	195
5.46	Results of the Double Lane Change (DLC) test at $90km/h$ and $\mu = 1$ , supposing availability and unavailability of the ESC . . . . .	195
5.47	Torque control efforts during the DLC test at $90 km/h$ and $\mu = 1$ , supposing availability and unavailability of the ESC . . . . .	196
5.48	Comparison of the trajectories during the DLC test at $90km/h$ and $\mu = 1$ , supposing availability and unavailability of the ESC . . . . .	196
5.49	Results of the DLC test at $95km/h$ and $\mu = 1$ with Sliding Mode Control (SMC) ESP . . . . .	198
5.50	Results of the obstacle avoidance test at $70km/h$ and $\mu = 1$ , supposing availability and unavailability of the ESC . . . . .	199
5.51	Results of the obstacle avoidance test at $77km/h$ and $\mu = 1$ , supposing availability and unavailability of the ESC . . . . .	199
5.52	Results of the obstacle avoidance test at $80km/h$ and $\mu = 1$ , supposing availability and unavailability of the ESC . . . . .	200
5.53	Torque control efforts during the obstacle avoidance test at $70km/h$ and $\mu = 1$ , supposing availability and unavailability of the ESC . . . . .	200
5.54	Comparison of the trajectories during the obstacle avoidance test at $70km/h$ and $\mu = 1$ , supposing availability and unavailability of the ESC . . . . .	201

# List of Tables

3.1	Exposure classes according ISO 26262 . . . . .	50
3.2	Characteristics of SiL and HiL simulations . . . . .	58
3.3	ISO 4138:2012 test conditions . . . . .	62
3.4	Main UC vehicle parameters . . . . .	71
4.1	Main vehicle parameters: FIAT 500e . . . . .	77
4.2	Main vehicle parameters: SimRod Kyburz . . . . .	78
4.3	Main vehicle parameters: Valeo concept Battery Electric Vehicle (BEV) . . . . .	80
4.4	Cosimulation solver and sample rate settings . . . . .	100
4.5	Simulated dynamical behaviour and corresponding integration features	101
4.6	Vehicle and brake plant datasheet . . . . .	102
4.7	Frequency response calibration of the brake plant . . . . .	105
4.8	Evaluation of additional step tests during the calibration phase . . .	106
4.9	Experimental runs evaluated on the chassis dynamometer . . . . .	110
4.10	Predicted and measured wear on a single rear-left braking pad . . .	113
4.11	Vehicle energy performance during WLTP class 3 cycle . . . . .	115
4.12	Consumed vs recovered energy and pad wear . . . . .	115
4.13	Fuzzy controller implication rules . . . . .	118
4.14	NEDC simulation results at $SOC_i=85\%$ and $DOD=5\%$ . . . . .	120
4.15	Comparison in term of energy consumption . . . . .	122
4.16	Efficiency improvement in RDE cycles . . . . .	123
4.17	Energy consumption in RDE cycles . . . . .	123
4.18	Performance comparison for Gratz and Barcelona RDE cycles . . . .	124
4.19	Influence of the auxiliaries management control on the vehicle model	124
4.20	FMEA of the reference BBW control units . . . . .	130
4.21	FMEA of the reference ABS control unit . . . . .	130
4.22	Automotive Safety Integrity Level (ASIL) target estimation for the EV (autonomous driving level between 0 and 1) . . . . .	131
4.23	ASIL target estimation for the EV (autonomous driving level greater than 2) . . . . .	132
4.24	ASIL target respect to Random Hardware Failure Rate . . . . .	132
4.25	Investigated failure in the Montecarlo simulation campaign . . . . .	137
4.26	Stopping distance of EV in different fault scenario for the BBW subsystems . . . . .	138
4.27	Double lane change test max speed performed by different vehicles powertrain configurations and adherence coefficient . . . . .	140

4.28	Stopping distance of the longitudinal stability tests for different adherence conditions . . . . .	145
4.29	Maximum vehicle speed during Double Lane Change tests for different adherence conditions . . . . .	148
5.1	Input and Output of the proposed Model Estimator . . . . .	157
5.2	ISO7401 test result for $NC$ and $Tv+St$ control . . . . .	163
5.3	Investigated reference manoeuvres . . . . .	182
5.4	Time response data summary of the Sinusoidal Input test . . . . .	194
5.5	ISO3888-1 DLC test RMSE results at different speed and friction values . . . . .	197
5.6	ISO3888-2 obstacle avoidance test RMSE results at different speed .	201

# Glossary

<b>4WD</b>	Four Wheel Drive
<b>AB</b>	Autonomous Braking
<b>ABS</b>	Anti-lock Braking System
<b>AC</b>	Air Conditioning
<b>ACC</b>	Adaptive Cruise Control
<b>Acc Imp</b>	Accuracy Improvement
<b>ADS</b>	Autonomous Driving System
<b>ADAS</b>	Advanced Driver Assistance Systems
<b>AFS</b>	Active Front Steering
<b>AIS</b>	Abbreviated Injury Scale
<b>AMT</b>	Automated Manual Transmission
<b>ANN</b>	Artificial Neural Network
<b>APMC</b>	Auxiliary Power Management Control
<b>ASS</b>	Active Safety System
<b>ASIL</b>	Automotive Safety Integrity Level
<b>ASR</b>	Anti-Spin Regulation
<b>AT</b>	Automatic Transmission
<b>BB</b>	Brake Blending
<b>BBW</b>	Brake By-Wire
<b>BCU</b>	Brake Control Unit
<b>BEV</b>	Battery Electric Vehicle
<b>BoL</b>	Beginning of Life
<b>BW</b>	By-Wire
<b>BMS</b>	Battery Management System
<b>BRD</b>	Block Reliability Diagram
<b>CADC</b>	Common Artemis Driving Cycles
<b>CAN</b>	Controller Area Network
<b>CCL</b>	Charge Current Limit
<b>CNC</b>	Computerized Numerical Control
<b>CoG</b>	Centre Of Gravity
<b>CRF</b>	Centro Richerche FIAT
<b>CRT</b>	CarRealTime
<b>CU</b>	Control Unit
<b>DAE</b>	Differential Algebraic Equations
<b>DAS</b>	Driving Assistance System
<b>DC</b>	Direct Current
<b>DCL</b>	Discharge Current Limit
<b>DDEV</b>	Distributed Drive Electric Vehicle

<b>DIEF</b>	Department of Industrial Engineering of Florence
<b>DO</b>	Disturbance Observer
<b>DOD</b>	Depth Of Discharge
<b>DoF</b>	Degree of Freedom
<b>DLC</b>	Double Lane Change
<b>DYC</b>	Direct Yaw-Moment Control
<b>EACS</b>	European Accident Causation Survey
<b>EBD</b>	Electronic Braking Distribution
<b>ECB</b>	Electronically Controlled Brake
<b>ECMS</b>	Equivalent Consumption Minimization Strategy
<b>ECU</b>	Electronic Control Unit
<b>E/E</b>	Electric/Electronic
<b>Eff Imp</b>	Efficiency Improvement
<b>EHB</b>	Electro-Hydraulic Braking
<b>EKF</b>	Extended Kalman Filter
<b>EM</b>	Electric Motor
<b>EMB</b>	Electro-Mechanical Braking
<b>ENEA</b>	Agenzia Nazionale per le Nuove Tecnologie, l'Energia e lo Sviluppo Economico Sostenibile
<b>EOl</b>	End of Life
<b>EPS</b>	Electronic Power Steering
<b>ESC</b>	Electronic Stability Control
<b>ESP</b>	Electronic Stability Program
<b>ESS</b>	Energy Storage System
<b>EV</b>	Electric Vehicle
<b>EWB</b>	Electronic Wedge Brake
<b>FBB</b>	Fuzzy Brake Blending
<b>FI</b>	Fault Injection
<b>FIS</b>	Fuzzy Inference System
<b>FMEA</b>	Failure Mode and Effect Analysis
<b>vFMEA</b>	Virtual Failure Mode and Effect Analysis
<b>FMECA</b>	Failure Mode, Effect and Criticality Analysis
<b>FPGA</b>	Filed Programmable Gate Array
<b>FSU</b>	Fail Silent Unit
<b>FTA</b>	Fault Tree Analysis
<b>FTP-75</b>	EPA Federal Test Procedure
<b>FWD</b>	Front Wheel Drive
<b>GBW</b>	Gear-By-Wire
<b>H</b>	Hamiltonian
<b>HARA</b>	Hazard Analysis and Risk Assessment
<b>HazOp</b>	Hazard and Operability
<b>HEV</b>	Hybrid Electric Vehicle
<b>HiL</b>	Hardware-in-the-Loop
<b>HV</b>	High Voltage
<b>HVAC</b>	Heating, Ventilation and Air Conditioning
<b>ICE</b>	Internal Combustion Engine
<b>ICEV</b>	Internal Combustion Engine Vehicle
<b>IMU</b>	Inertial Measurement Unit
<b>IWM</b>	In-Wheel Motor
<b>LV</b>	Low-Voltage

<b>LQR</b>	Linear Quadratic Regulator
<b>LQG</b>	Linear Quadratic Gaussian
<b>MBS</b>	Multi-Body System
<b>MBSE</b>	Model-Based System Engineering
<b>MCU</b>	Motor Control Unit
<b>MEMS</b>	Micro-electromechanical Systems
<b>MF</b>	Magic Formula
<b>MIE</b>	Multiple-Impact Events
<b>MiL</b>	Model-in-the-Loop
<b>MIMO</b>	Multiple Input Multiple Output
<b>MISO</b>	Multiple Input Single Output
<b>MPC</b>	Model Predictive Control
<b>MTBF</b>	Mean Time Between Failure
<b>MtF</b>	Mothership Function
<b>NDA</b>	Non-Disclosure Agreement
<b>NEDC</b>	New European Driving Cycle
<b>NL</b>	Non-Linear
<b>NLDO</b>	Non-Linear Disturbance Observer
<b>NVH</b>	Noise, Vibration and Harshness
<b>OBELICS</b>	Optimization of scalaBle rEaltime modeLs and functionaL testing for e-drive ConceptS
<b>ODE</b>	Ordinary Differential Equations
<b>OEM</b>	Original Equipment Manufacturer
<b>PD</b>	Proportional Derivative
<b>PI</b>	Proportional Integral
<b>PID</b>	Proportional Integral Derivative
<b>PIM</b>	Power Inverter Module
<b>PM</b>	Permanent Magnet
<b>RBS</b>	Regenerative Braking System
<b>RDE</b>	Real Driving Emission
<b>RMSE</b>	Root Mean Square Error
<b>RT</b>	Real-Time
<b>RTI</b>	Real-Time Implementation
<b>RTOS</b>	Real-Time Operating System
<b>RWD</b>	Rear Wheel Drive
<b>SBC</b>	Sensotronic Brake Control
<b>SBW</b>	Steer By-Wire
<b>SCU</b>	Steer Control Unit
<b>SIS</b>	Slowly Increasing Steer
<b>SMC</b>	Sliding Mode Control
<b>SOC</b>	State of Charge
<b>SOH</b>	State of Health
<b>SOM</b>	Small Of Minimum
<b>SoA</b>	State of Arts
<b>SiL</b>	Software-in-the-Loop
<b>SISO</b>	Single Input Single Output
<b>SwD</b>	Sine with Dwell
<b>SVC</b>	Single Vehicle Crash
<b>TBW</b>	Throttle-By-Wire
<b>TC</b>	Time Continuous
<b>TCS</b>	Traction Control System

---

<b>TD</b>	Time Discrete
<b>TRFE</b>	Tire-Road Friction Estimation
<b>TV</b>	Torque Vectoring
<b>TTM</b>	Time-To-Market
<b>UC</b>	Use Case
<b>UKF</b>	Unscented Kalman Filter
<b>UNIFI</b>	University of Florence
<b>VDC</b>	Vehicle Dynamic Control
<b>VSC</b>	Vehicle Stability Control
<b>WLTP</b>	World harmonized Light-duty vehicles Test Procedure
<b>WLTC</b>	World harmonized Light-duty vehicles Test Cycle
<b>WIM</b>	Wheel-Individual Motor
<b>XBW</b>	X-By-Wire

# List of Symbols

$x, X$	Vehicle's longitudinal position in $[m]$
$y, Y$	Vehicle's lateral position in $[m]$
$z, Z$	Vehicle's vertical position in $[m]$
$V_x, \dot{x}$	Vehicle's longitudinal speed in $[m/s]$
$V_y, \dot{y}$	Vehicle's lateral speed in $[m/s]$
$V_z, \dot{z}$	Vehicle's vertical speed in $[m/s]$
$a_x, \ddot{x}$	Vehicle's longitudinal acceleration in $[m/s^2]$
$a_y, \ddot{y}$	Vehicle's lateral acceleration in $[m/s^2]$
$a_z, \ddot{z}$	Vehicle's vertical acceleration in $[m/s^2]$
$\Psi$	Vehicle roll angle in $[rad]$
$\gamma$	Vehicle yaw angle in $[rad]$
$\Theta$	Vehicle pitch angle in $[rad]$
$X_w$	Wheel's longitudinal position in $[m]$
$Y_w$	Wheel's lateral position in $[m]$
$Z_w$	Wheel's vertical position in $[m]$
$\Psi_w$	Wheel roll angle in $[rad]$
$\gamma_w$	Wheel yaw angle in $[rad]$
$\Theta_w$	Wheel pitch angle in $[rad]$
$i \in f, r$	Front/Rear index
$j \in l, r$	Left/Right index
$\beta$	Side-slip angle in $[rad]$
$V$	Speed vector in $[m/s]$
$\omega_w$	Wheel rotational speed in $[rad/s]$
$\omega_{EM}$	Electric Motor rotational speed in $[rad/s]$
$r, \dot{\gamma}$	Yaw rate in $[rad/s]$
$R$	Cornering radius in $[m]$
$m$	Mass in $[kg]$
$A_f$	Vehicle frontal area in $[m^2]$
$I$	Rotational inertia in $[kgm^2]$
$a$	Vehicle front wheelbase in $[m]$
$b$	Vehicle rear wheelbase in $[m]$
$t$	Vehicle's track in $[m]$
$p$	Vehicle wheelbase in $[m]$
$h$	Vehicle CoG height in $[m]$
$h_w$	Aerodynamic force application height in $[m]$
$r_w$	Wheel radius in $[m]$
$I_w$	Wheel Intertia in $[kgm^2]$
$\mu$	Friction coefficient

---

$\rho$	Normalized friction force
$\beta$	Side-slip angle in $[rad]$
$\theta$	Road angle in $[rad]$
$\sigma$	Slip ratio in $[rad]$
$\alpha$	Tire slip angle in $[rad]$
$\delta$	Steer angle, wheel orientation in $[rad]$
$\eta$	Efficiency
$\Theta_V$	Orientation of wheel velocity vector in $[rad]$
$t_f$	Vehicle front track in $[m]$
$t_r$	Vehicle rear track in $[m]$
$K_V$	Understeer gradient
$T$	Torque in $[Nm]$
$T_d$	Drive torque in $[Nm]$
$T_b$	Brake torque in $[Nm]$
$T_{EM}$	Electric motor torque in $[Nm]$
$T_{tralim}$	Traction limit torque in $[Nm]$
$T_{reglim}$	Regenerative limit torque in $[Nm]$
$F_x$	Longitudinal force in $[N]$
$F_y$	Lateral force in $[N]$
$F_z$	Vertical force in $[N]$
$F_z^0$	Static load force in $[N]$
$\Delta F_z$	Normal load transfer in $[N]$
$F_w$	Aerodynamic drag force in $[N]$
$C_d$	Aerodynamic drag coefficient $[N * s^2/m]$
$V_w$	Air speed in $[m/s]$
$\rho_{air}$	Air density in $[kg/m^3]$
$F_R$	Rolling resistance force in $[N]$
$F_g$	Gravitational force in $[N]$
$M_{zz}$	Yaw moment in $[Nm]$
$M_{yaw}$	Applied yaw moment in $[Nm]$
$r_w$	Wheel radius in $[m]$
$C_\sigma$	Tire longitudinal stiffness in $[N/rad]$
$C_\alpha$	Tire cornering stiffness in $[N/rad]$
$\theta$	Road slope angle in $[rad]$
$f$	Rolling coefficient
$f_0$	Static rolling coefficient
$f_S$	Speed Rolling coefficient
$K_{rate}$	Transmission rate
$K_{steer}$	Steering rate
$V_{ch}$	Characteristic speed $[m/s]$
$P_{mec}$	Mechanical power in $[W]$
$e$	Error
$K_{ff}$	Driver feed-forward gain
$K_p$	Driver proportional gain
$K_i$	Driver integral gain
$K_{aw}$	Driver anti-windup gain
$K_g$	Driver road slope gain
$L$	Driver preview distance in $[m]$
$\tau$	Driver delay in $s$

---

$A$	Brake's calliper area in $m^2$
$F_{preload}$	Brake's preload force in $N$
$k_{act}$	Brake's calliper stiffness in $N/m$
$y_{gap}$	Brake's calliper run in $m$
$r_{brake}$	Brake's disc mean radius $m$
$f_b$	Brake's friction coefficient
$p$	Brake's pressure in $[Pa]$
$t$	Time in $[s]$
$\omega_n$	Transfer function's eigenfrequency in $[rad/s]$
$\epsilon$	Transfer function's damping factor
$Temp$	Temperature in $[K]$
$\dot{Q}$	Heat rate in $[W]$
$C$	Thermal inertia in $[J/K]$
$PM$	Emitted airborne particles in $[kg]$



# Chapter 1

## Introduction

The number of automobiles is rising all over the world. This pushes the need for more efficient vehicles for energy consumption, safety, comfort and environmental impact. This is extremely difficult since these requirements are often in conflict. To reach these goals, industries and academia are focusing on Electric/Electronic (E/E)-based subsystem, which uses sensors, actuators and feedback control structures. The growing role of these solutions in the automotive field is partially related to the recent advances in electronics and computer technologies. Perhaps, the rising automotive electrification strongly contributes.

In automotive vehicles, the driver is a fundamental element of the control loop and must absolve different functionalities: ensure the comfort and safety of the passengers; maximize performance; optimize consumption and efficiency. With the introduction of a variety DAS (e.g. collision avoidance systems, cruise control, lane departure warning systems, lane-keeping systems, driver condition monitoring systems) and active safety/stability controllers (e.g. braking distributor, anti-slip and anti-spin regulations), the pilot is gradually relieved of these tasks having to deal only with high-level decision-making functions.

The ESP, or ESC, is widely regarded as one of the most safety-relevant technology, representing the pillar of vehicle stability controllers. It applies a unified and synergistic concept to control the vehicle's tendency to slide away [9]. This controller has a significant impact on vehicle stability, enhancing road safety by furnishing the driver with effective support for the aim of maintaining the control of the car in emergencies, allowing him to choose the desired driving path within the limit of adherence conditions. Thus, the evaluation of active safety performances of a vehicle has to be considered in combination with this controller.

Ensuring the lateral stability of road vehicles is a fundamental task, concerning both passenger safety and driving comfort. The recent proliferation of By-Wire (BW) and mechatronic systems in the automotive sector [9–11] along with the rising autonomous drive applications [12], are incentivating researcher and designer in the development of innovative active safety controllers. Indeed, these systems exhibit a higher level of robustness than conventional mechanical ones, due to the reduced number of components and required maintenance, as well as improved reliability and fault-tolerance [13]. Even functional-safety aspect can benefit by the adoption of these components according to ISO26262 regulations [14–17].

In the current literature, many solutions for ESP controllers have been proposed. This task appear extremely challenging. There are plenty reasons: the complexity of the interaction between heterogeneous systems [18]; the large variety of driving conditions at which they may operate, respect to driver input and road status [19]; parameters and variables estimation uncertainties which further penalize a model-based approach [3, 20]; the approximations and assumptions needed to improve predictive control's Real-Time (RT) capability [21].

Electric vehicles exhibit very useful intrinsic characteristics for stability purposes. Despite the easiness of E/E system's integrations, the highly desirable e-drive specifications (e.g. faster bandwidth response, easy and precise torque application, and so on) can be exploited to synthesize advanced control methodology, based on active torque distribution techniques. Recently, academic and industrial interest in the field of Torque Vectoring (TV) techniques is becoming more and more important in the automotive sector, since allows to explore new opportunities for lateral stability control strategies that can be applied [22]. Availability of Wheel-Individual Motor (WIM) traction systems and BW technologies consent the implementation of non-conventional control methodology [23–25], which appear extremely costly or even not feasible without the adoption on E/E devices.

In this PhD thesis, the author intends to propose lateral stability control solutions. Since real-word validation and testing are costly, time-consuming and dangerous (for users, environment and instrumentation), a model-based systematic approach for the controller's virtual assessment is provided. The methodology contributes to a drastic optimization of Time-To-Market (TTM) and industrial costs involved in the development of innovative industrial products by extended use of "In-the-Loop" techniques. When developing such systems, comprehensive frontloading is used to ensure coherence with the V-shaped system design and production workflow. Thus, the models are modular, scalar and parametrized to be applied to relevant industrial and academic vehicle use cases. Efficiency, safety & reliability and stability performances of proposed control strategies are investigated throughout the whole document.

Accurate vehicle sub-systems models are necessary for reliable validation. Even this task is challenging since requires important efforts in terms of cost and time. For these reasons, the vehicle plants are carefully modelled. The modularity features allow for the selection in the virtual environment only the simulated plants which are useful for the intents of the tests.

In particular, a brake plant model is developed and calibrated, using an experimental set-up, as a support for future validation. This functional model is tuned using a limited set of real-world data. A reliable brake model is fundamental for properly simulating each of the vehicle's aspects studied in this work. Also, brake blending algorithms have been implemented to test their performances, concerning energy efficiency improvement and integrability with higher-level controllers (e.g as anti-slip regulation or direct yaw moment control).

A functional safety assessment procedure is developed according to ISO26262 standard specifications. It furnishes a systematic approach to identifying the required integrity level and how to accomplish it. The methodology is based on virtual Failure Mode and Effect Analysis (FMEA) and Fault Injection (FI) simulation techniques to be applied to specified benchmark vehicle layouts.

Finally, non-conventional ESP strategies have been proposed. These controllers have been tested on several vehicles UCs to prove their effectiveness with simulation activities. Both solutions rely on coordinated TV and steering control, exhibit a hierarchical structure and are developed for generalized vehicles. However, these controllers are appropriately parametrized to be easily portable between different vehicle architectures. WIM driven Electric Vehicle (EV) equipped with BW systems prove to be the best car configuration for the task of energy efficiency, functional safety and lateral stability performance improvement purposes [15]. This particular vehicle layout has been the subject of numerous studies in the current literature [26–30]. In this context, independent motor traction layout is assumed for the benchmark vehicles. The available State of Arts (SoA) many papers proposing a coordinated control between steering and differential braking/traction to achieve higher stability performances can be found [31–37].

The application of desired yaw moment is based on Moore-Penrose pseudo-inverse criteria [38] to solve a multi-Degree of Freedom (DoF) problem for over-actuated systems and achieve both vehicle stabilization and a driving path which is in agreement with the driver intentions.

The first ESP control strategy ensures the vehicle’s lateral stability while minimizing the engaged grips on each wheel. A TV allocation methodology is applied to track the desired vehicle yaw rate, while a recursive optimization algorithm is used to adjust in RT the steering command, reducing the Kahm adhesion ellipse utilization. This avoids tire forces saturation, which can lead to undesired and unpredictable Non-Linear (NL) behaviour.

The other solution is based on SMC methodology and has been widely assessed using both Software-in-the-Loop (SiL) and Hardware-in-the-Loop (HiL) methodologies. This controller has been compared to a benchmark ESP solution developed by a well known automotive company, currently implemented on different vehicles in the market. It provides coordinated actions between Steer By-Wire (SBW), Brake By-Wire (BBW) and traction systems to ensure a robust tracking of controlled states: side-slip angle  $\beta$  and yaw rate  $r$ . Optimal control signals, i.e. adjusting yaw moment and correcting steering angle, are calculated through an appropriate Lyapunov candidate. Concerning previously work, based on Sliding Mode strategies [39–42], this algorithm rely on a 2 dimensions model for states and sliding surface, challenging well-known and established lateral stability SMC methods that typically uses separated sliding surfaces for the regulation, decoupling the control dynamics. Moreover, both desired yaw moment and steering command correction are obtained from the same controller, achieving highly compatible control signals.

Although these solutions are best suited for Four Wheel Drive (4WD) with independent traction wheels, the followed developing approach ensures fundamental features, which allows flexibility and portability of the controllers for different vehicle architectures, applications and control structures (e.g. Front Wheel Drive (FWD) or Rear Wheel Drive (RWD) vehicle layout, autonomous driving).

The document is organized as follows: **Chapter 2** presents the background information related to vehicle dynamics, mechatronic systems and electric vehicles with an important focus on e-powertrains, as well as a description of the current ESP controller. In **Chapter 3** the research question is introduced, along with the main purpose of the work and the proposed approach, which allows for tackling the open problems and the technical challenges. The adopted model-based approach, the reference driving scenarios and the WIM traction configuration, used to develop the proposed solutions, are introduced. Vehicle use cases, simulation models and preliminary assessment activities are presented in **Chapter 4**, to ensure an early validation of the proposed approach. The proposed lateral stability controllers are described in **Chapter 5**, with the main simulation results: the *Minimized Tire Adhesion Grip ESP Controller* stabilizes the vehicle while minimizing the engaged grip on each wheel; the *Sliding Mode ESP Controller* is based on a 2-dimension robust first-order sliding mode methodology that aims at the direct control of the vehicle's yaw rate and side-slip angle. Finally, the discussion is reported in **Chapter 6**. In **Appendix**, the author's articles published on conference acts and journals can be founded.

# Chapter 2

## Background

In this chapter background informations, needed for a complete understanding of the rest of the document, are given for a major comprehension of the targeted problem. The next section will introduce the readers to vehicle dynamics, vehicle modelling, mechatronic systems (with a particular focus on By-Wire technologies); electric vehicles and active stability control systems.

### 2.1 Vehicle Dynamics

Vehicle dynamics concern the study of vehicle motion due to the presence of forces acting on it. The vehicle dynamic is influenced by longitudinal and lateral tire forces, aerodynamic drag forces, rolling resistance forces and gravitational forces [3, 43–45].

For the following sub-section, a four-wheel vehicle model with 3-DoF in longitudinal  $x$ , lateral  $y$  and yaw  $\gamma$  is considered (Figure 2.1).  $F_{xij}$  and  $F_{yij}$  are the longitudinal and lateral forces generated in the tire-road contact patch;  $\delta_{ij}$  is the wheel steering angles;  $V_x$  and  $V_y$  are longitudinal and lateral speed;  $\beta$  is the side-slip angle;  $t_i$  is the track;  $a$  and  $b$  are the fronts and rear wheel-base. In all the equations we adopt the same convention in which  $i \in \{f, r\}$  stays for the front or rear axle and  $j \in \{l, r\}$  indicates the left or right wheel, respectively.

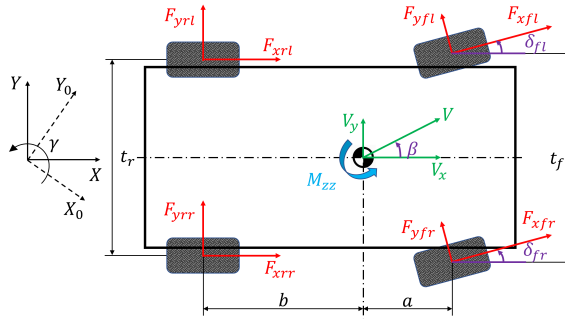


Figure 2.1: Three DoF vehicle dynamic model in longitudinal, lateral and yaw motion directions

### 2.1.1 Tire Forces

Tire-road forces are crucial for the definition of a vehicle's dynamics control strategy since affecting the longitudinal, lateral, yaw and roll motion of the chassis. These forces depend on the normal load on wheel  $F_z$ , slip ratio  $\sigma$ , slip angle  $\alpha_{ij}$  and the friction coefficient  $\mu$ .

#### Friction Coefficient

The friction or adherence coefficient  $\mu$  defines the maximum force a tire can supply in the longitudinal and lateral directions, for a given vertical load [3, 19]. It depends on the characteristic of the road surface and can vary between 0 and 1 in the function of ground status (e.g. dry asphalt, icy road, snow-covered). The normalized friction force  $\rho$ , also known as the coefficient of traction is defined by (2.1), where  $F_x$  is the longitudinal force and  $F_y$  the lateral one.

$$\rho = \frac{\sqrt{F_x^2 + F_y^2}}{F_z} \quad (2.1)$$

#### Normal Load

Normal load on wheel  $F_z$  are influenced by the vehicle weight  $m$ , the longitudinal location of the vehicle's Centre Of Gravity (CoG), longitudinal acceleration, aerodynamic drag forces and road's slope grade. When the vehicle is driving on a straight road,  $F_z$  on the front and rear axle can be calculated imposing the pitch motion has reached a steady-state condition. Taking the moment about the rear tire contact point leads to (2.2). Imposing the same pitch moment equilibrium for the front tire contact point leads to (2.3), with  $h$  the height of the CoG and  $h_w$  the height at which the aerodynamic drag force  $F_w$  act, as for ground (Figure 2.2).

$$F_{zf}(a+b) + F_w h_w + m\ddot{x}h + mgh\sin(\theta) - mgb\cos(\theta) = 0 \quad (2.2)$$

$$F_{zr}(a+b) - F_w h_w - m\ddot{x}h - mgh\sin(\theta) - mga\cos(\theta) = 0 \quad (2.3)$$

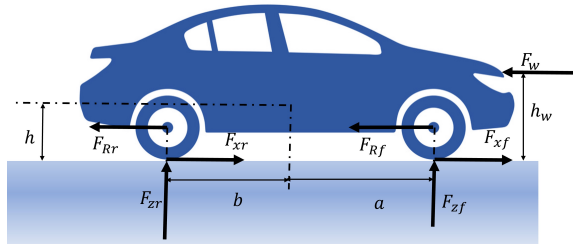


Figure 2.2: Longitudinal vehicle model

Solving (2.2) respect to  $F_{zf}$  and (2.3) respect to  $F_{zr}$  yields to (2.4).

$$\begin{cases} F_{zf} = \frac{-F_w h_w - m\ddot{x}h - mgh\sin(\theta) + mgb\cos(\theta)}{a+b} \\ F_{zr} = \frac{F_w h_w + m\ddot{x}h + mgh\sin(\theta) + mga\cos(\theta)}{a+b} \end{cases} \quad (2.4)$$

## Longitudinal Slip Ratio

Consider the wheel rotation dynamic model represented by (2.5), with  $I_w$  the rotational inertia,  $T_d$  the drive torque,  $T_b$  the brake torque and  $r_w$  the radius of the wheel. Slip ratio of a tire  $\sigma$  is defined according (2.6) as the difference between the actual vehicle longitudinal speed at the wheel axle  $V_x$  and the equivalent rotational speed of the tire  $r_w\omega_w$ , with  $r_w$  in  $m$  and  $\omega_w$  tire radius and rotational speed in  $rad/s$ , respectively.

$$I_w\dot{\omega}_w = T_d - T_b - r_w F_x \quad (2.5)$$

$$\begin{cases} \sigma = \frac{r_w\omega_w - V_x}{V_x} & \text{braking} \\ \sigma = \frac{r_w\omega_w - V_x}{r_w\omega_w} & \text{acceleration} \end{cases} \quad (2.6)$$

Assuming  $\mu = 1$  and  $F_z = \text{const}$ , the longitudinal tire force  $F_x$  vary with the slip ratio  $\sigma$  as in Figure 2.3. If slip ratio is small (less than 0.1) the force is proportional and tire force can be modelled as (2.7), where  $C_{\sigma f}$  and  $C_{\sigma r}$  the tire's longitudinal stiffness. In the NL region a tire model is needed, e.g. Pacejka "Magic Formula" [46].

$$\begin{cases} F_{xf} = 2C_{\sigma f}\sigma_{xf} \\ F_{xr} = 2C_{\sigma r}\sigma_{xr} \end{cases} \quad (2.7)$$

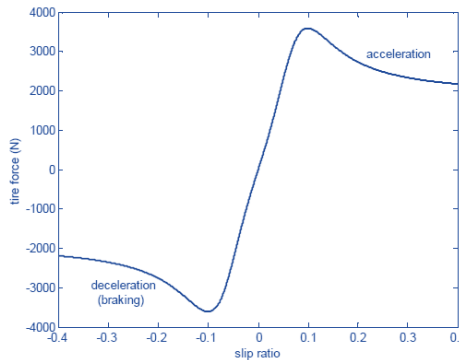


Figure 2.3: Longitudinal tire force as a function of slip ratio (Figure from [3])

A rough explanation of the direct dependence of the tire force on the slip ratio can be given by observing the deformation of the tread elements of the tire, as visible in Figure 2.4. The tread elements can be modelled using the so-called "brush" model, as a series of independent springs that undergo longitudinal deformation and resist with constant longitudinal stiffness. The net velocity at the treads is the slip velocity  $r_w\omega_w - V_x$ . Due to the normal load, the tire contact with the road over a footprint area (contact patch).

First, consider the case in which the wheel is a driving wheel. In this case  $r_w \omega_w > V_x$ , thus the net velocity of the treads is in the opposite direction as compared to the longitudinal velocity of the vehicle. If the slip ratio is small there is a region of the contact patch where the tread elements do not slide to the ground (static region). As the tire rotates, new tread elements enter the contact patch where the speed is 0, since there is no sliding in the static region. In the meanwhile, the top of the tread element moves with the slip velocity. This results in tread elements bending in the direction of the vehicle's motion. The maximum deflection is proportional to the slip velocity and to the time duration for which the tread element remains in the contact patch. The time, however, is inversely proportional to the rotational velocity  $r_w \omega_w$ . This leads to a maximum deflection proportional to the slip ratio, as shown in (2.6). To resume, the net longitudinal force on the tires from the ground is in the forward direction in the case of a driving wheel and is proportional to the slip ratio of the wheel [3].

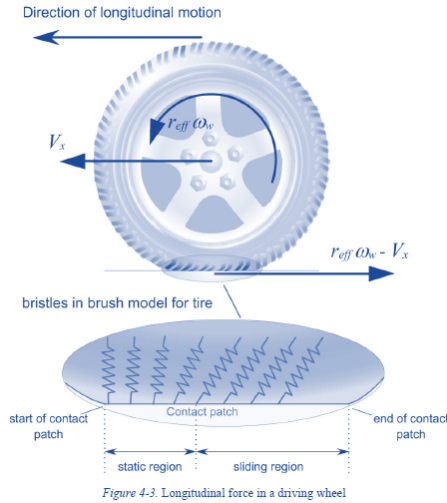


Figure 4.3: Longitudinal force in a driving wheel

Figure 2.4: Longitudinal driving wheel model for tire forces and deformations definition (Figure from [3])

When the wheel is a non-driven one, the longitudinal velocity is greater than the rotational velocity  $V_x > r_w \omega_w$ . Here the tread elements will bend backwards. Hence the tire force on the driven wheel is in the opposite direction of the vehicle's longitudinal speed. Similarly to the previous case, for a small slip, the tire force will be proportional to the slip ratio [3].

Experimental results related to pure braking conditions for different vertical force values exhibit the behaviour of Figure 2.5.

### Lateral Slip Angle

An essential step for a complete overview of lateral vehicle motion dynamics is to model the lateral tire forces  $F_{yf}$  and  $F_{yr}$ . The slip angles at the tires of a front steering vehicle are defined according to (2.8) as the difference between the orientation of the tire  $\delta$  and the one of the velocity vector of the wheel  $\Theta_V$ , as visible in Figure 2.6.

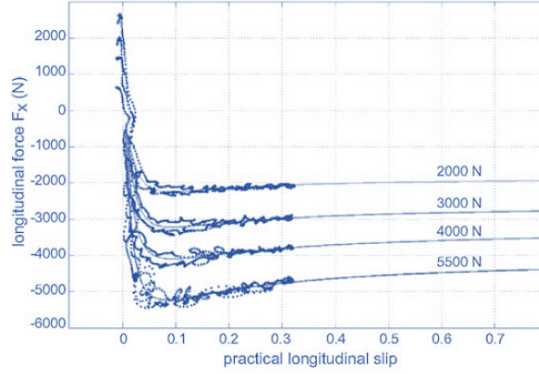


Figure 2.5: Experimental result: longitudinal tire force as a function of slip ratio for different vertical load (Figure from [43])

$$\begin{cases} \alpha_f = \delta - \Theta_{Vf} = \delta - \frac{\dot{y} + a\dot{\gamma}}{\dot{x}} \\ \alpha_r = -\Theta_{Vr} = -\frac{\dot{y} - b\dot{\gamma}}{\dot{x}} \end{cases} \quad (2.8)$$

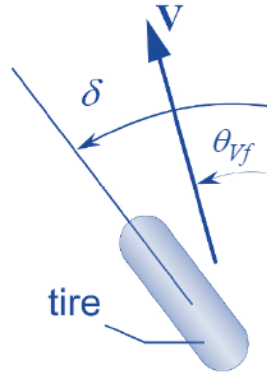


Figure 2.6: Lateral tire model for slip angle definition (Figure from [3])

Lateral forces in the tire-road interface are the one described by (2.9), with  $C_{\alpha_f}$  and  $C_{\alpha_r}$  noted as front and rear tire's cornering stiffness. For small tire slip angles, the lateral tire forces can be approximated as a linear function of tire slip angle. This relation can be explained considering the same tire brush model introduced for the slip ratio. Similarly, in the static region of the contact patch, the tip of each tread in contact with the ground remains stationary. The top of the tread moves as compared to the tip of the tread, resulting in deformations in the tire. Suppose the lateral component of the wheel velocity is  $V_x \sin(\alpha)$ . Thus, lateral deflection of the tread is proportional both to the lateral velocity and to the time spent by the tread in the contact patch. Since the lateral velocity is proportional to speed and slips angle, while the amount of time in the contact patch is inversely proportional to the rotational velocity, the lateral deflection is proportional only to the slip angle.

This lead to a lateral force on the tire depending on the lateral deflection of the treads in the contact patch.

$$\begin{cases} F_{yf} = 2C_{\alpha f}\alpha_f \\ F_{yr} = 2C_{\alpha r}\alpha_r \end{cases} \quad (2.9)$$

Experimental results of Figure 2.7 show the lateral force behaviour for slip angle and different vertical loads. Similarly to the longitudinal forces,  $F_y$  curves are reduced for  $F_z$  less than the nominal one.

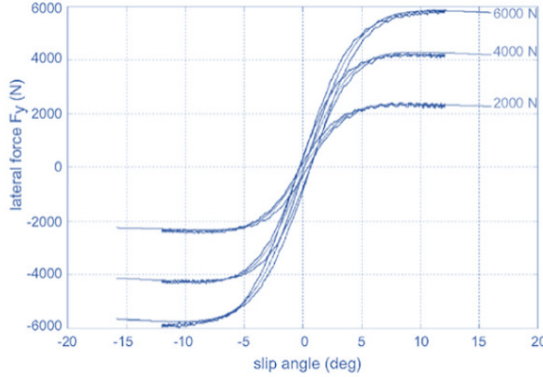


Figure 2.7: Experimental result: lateral tire force as a function of slip angle for different vertical load (Figure from [43])

## Magic Formula

For vehicle dynamics modelling, a mathematical formulation able to consider load and friction variation to build the tire force curves is useful. Generally, these curves have similar shapes: both exhibit an initial proportional growth, reach a maximum and tend to a horizontal asymptote.

The "Magic Formula (MF)" by Pacjecka [46] can account for road status, vertical load and slips, returning different curve for  $\rho$  as a function of  $\sigma$  (e.g. Figure 2.8).

Over years, many formulations of the MF are available; nevertheless are all based on (2.10), where  $B$  is the stiffness,  $C$  the shape factor,  $D$  peak value and  $E$  curvature factor. These values are tabulated as compared to the pneumatic type, arising by experimental validation.  $y(t)$  can be both  $F_x$  or  $F_y$  over time and  $x$  the corresponding slip factor, respectively  $\sigma$  or  $\alpha$ .

$$y(x) = D \cdot \sin\{C \cdot \arctan[B \cdot x - E(B \cdot x - \arctan(B \cdot x))]\} \quad (2.10)$$

### 2.1.2 Longitudinal Vehicle Dynamics

The control of vehicle longitudinal dynamics is done by intervening in the traction and the braking systems. Suppose a vehicle moving on an inclined road for a single-track vehicle model (Figure 2.9), where  $h$  is the CoG vertical displacement to the ground,  $a$  and  $b$  the front and rear wheelbase, respectively. Its longitudinal dynamic is described by (2.11).

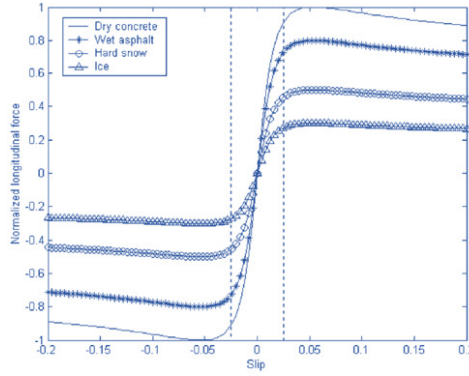


Figure 2.8: Normalized friction force as a function of slip ratio for different road status using the Magic Formula (Figure from [3])

$$m \cdot \ddot{x} = F_{xf} + F_{xr} - F_w - F_{Rf} - F_{Rr} - F_g \quad (2.11)$$

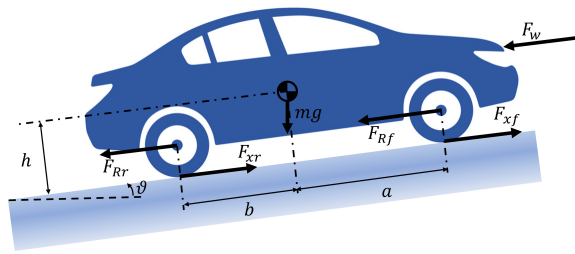


Figure 2.9: Longitudinal vehicle model driving on an inclined road

Rolling resistance  $F_{Ri}$  is calculated by (2.12), with  $F_{zi}$  vertical force,  $f_r$  rolling coefficient and  $\theta$  road angle. Rolling coefficients  $f_0$  and  $f_s$  of (2.13) depend on tire's inflation pressure,  $V_x$  vehicle longitudinal speed in  $km/h$ . For road vehicles, it is sufficient to consider the rolling coefficient as a linear function of speed.

$$F_{Ri} = F_{zi} f_r \cos \alpha \quad (2.12)$$

$$f_r = f_0 + f_s \left( \frac{V_x}{100} \right)^{2.5} \quad (2.13)$$

Aerodynamic drag  $F_w$  or resistance is a function of vehicle speed  $V_x$ , vehicle frontal area  $A_f$ , shape and air density  $\rho_{air}$ , as expressed in (2.14), where  $C_d$  is the aerodynamic drag coefficient (characterized by the shape of the vehicle) and  $V_w$  is the wind speed, with a positive sign when in the opposite direction of vehicle speed.

$$F_w = \frac{1}{2} \rho_{air} A_f C_d (V_x + V_w)^2 \quad (2.14)$$

When a vehicle goes up or down a slope, its weight produces a component that is always directed in the downward direction. The gradient resistance  $F_g$  is (2.15), with  $m$  mass of the vehicle,  $g$  the gravitational acceleration ( $9.81m/s^2$ ) and  $\theta$  the road angle.

$$F_g = mgsin(\theta) \quad (2.15)$$

### Braking Performances

Understanding the braking dynamics of a vehicle is fundamental to reducing the stopping distance and ensuring stable behaviour and vehicle directional capability.

Let's consider the model of Figure 2.9 and suppose it to operate on a flat straight road with uniform grip conditions ( $\theta = 0$  and  $\mu = 1$  on each wheel). Moreover, assume to apply a constant force on the brake pedal. Also, neglect the body pitch oscillation  $\Theta$ . If the resistance forces are low compared to the braking forces, these can be ignored. The equilibrium equations during brake scenarios for longitudinal, vertical and pitch motion are given by (2.16).

$$\begin{cases} m\ddot{x} = F_{xf} + F_{xr} \\ m\ddot{z} = 0 = F_{zf} + F_{zr} - mg \\ \ddot{\Theta} = 0 = (F_{xf} + F_{xr})h - F_{zf}a + F_{zr}b \end{cases} \quad (2.16)$$

The braking forces cannot exceed the tire traction limit ( $F_{xi} \leq \mu F_{zi}$ ), nor the vertical forces be negative ( $F_{zi} \geq 0$ ).

When driving at constant speed ( $\ddot{x} = 0$ ) the static load on each axle  $F_{zi}^0$  are given by (2.17). When accelerating ( $\ddot{x} \neq 0$ ) a longitudinal load transfer occur. Despite their sum must constantly be equal to the vehicle weight ( $F_{zf} + F_{zr} = mg$ ), during braking the transfer load  $\Delta F_z$  of (2.18) move from the rear ( $F_{zr} = F_{zr}^0 - \Delta F_z$ ) to the front ( $F_{zf} = F_{zf}^0 + \Delta F_z$ ).

$$\begin{cases} F_{zf}^0 = \frac{mgb}{a+b} \\ F_{zr}^0 = \frac{mga}{a+b} \end{cases} \quad (2.17)$$

$$\Delta F_z = -\frac{mh}{a+b}\dot{x} \quad (2.18)$$

The best braking performance  $\ddot{x}_{max}$  is obtained if both axles operate at their traction limit (2.19).

$$\begin{cases} F_{xf-P} = \mu F_{zf-P} = \mu (F_{zf}^0 + \Delta F_z) = \mu \frac{mg}{a+b} (b + \mu h) \\ F_{xr-P} = \mu F_{zr-P} = \mu (F_{zr}^0 - \Delta F_z) = \mu \frac{mg}{a+b} (a - \mu h) \end{cases} \quad (2.19)$$

Brake balance, or bias, means how much braking effort should be applied on the front wheels than the rear ones. Thus, it can be promptly calculated by (2.20).

$$b_P = \frac{F_{xf-P}}{F_{xr-P}} = \frac{b + \mu h}{a - \mu h} \quad (2.20)$$

Substituting  $F_{xf} = \mu F_{zf}$  and  $F_{xr} = \mu F_{zr}$  in (2.16) allow to obtain the braking force limited to their constrains (2.21), yielding to the relations between front and rear braking forces. Now is possible to draw the straight lines (2.21) in the  $(F_{xr}, F_{xf})$  plane and identify different regions, visible in Figure 2.10.

$$\begin{cases} F_{xf} = \mu \frac{F_{zf}^0 + \frac{h}{a+b} F_{xr}}{1 - \mu \frac{h}{a+b}} \\ F_{xr} = \mu \frac{F_{zr}^0 - \frac{h}{a+b} F_{xf}}{1 + \mu \frac{h}{a+b}} \end{cases} \quad (2.21)$$

It is interesting to note that points with the same deceleration belong to lines with a  $45deg$  slope, called iso-deceleration lines (dotted in the plot). The area inside the two lines contains all the possible braking combinations. When trespassing the upper line, front-wheel locks occur. Similarly, the rear wheels lock when trespassing the right line. Point  $P$  represent the maximum braking performance. Braking with balance  $b_P$  means moving along the  $OP$  line. Area 1 corresponds to low deceleration where each braking balance can be applied without wheel locking. Area 2 corresponds to the need for a front braking force to fulfil the demanded decelerations. Area 3 is the high deceleration region, which necessarily requires both axles' actuation. The CoG location influences the position of the point  $P$ . When the weight distribution changes the optimal brake balance is affected but not the maximum value  $\mu g$ . In this case the vertex  $P$  moves along the  $45deg$  slope segment on  $\hat{P}$ .

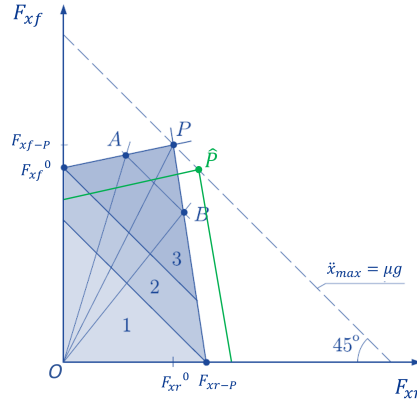


Figure 2.10: Front and rear axes ideal braking forces plane (Figure from [43])

To complete the discussion, the effect of grip variation needs to be addressed, since  $\mu$  is a formulation variable. Indeed, if we extend this study for three different friction coefficients ( $\mu_1 \leq \mu_2 \leq \mu_3$ ) the maximum braking point shift along a parabola curve that collects all the  $P$  vertices, as visible in Figure 2.11. This formulation can be obtained by resolving the equations of (2.19) respect to  $\mu$ , according (2.22).

$$(F_{xf} + F_{xr})^2 + mg \left( F_{xf} \frac{a}{h} - F_{xr} \frac{b}{h} \right) = 0 \quad (2.22)$$

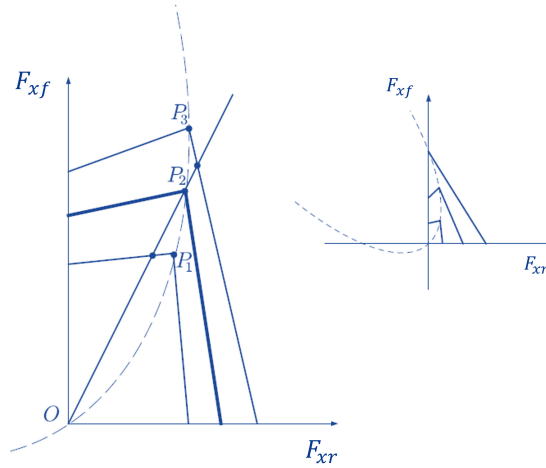


Figure 2.11: Front and rear axles admissible braking combination with grip coefficient variation (Figure from [43])

### 2.1.3 Lateral Vehicle Dynamics

Before describing in detail the vehicle lateral dynamic model is useful to briefly introduce the formulation of the kinematic cornering model, especially for ESP development.

#### Lateral Kinematic Model

A lateral kinematic model of the vehicle provides a mathematical description of the motion without considering the forces. Thus, the equations are purely based on geometric relationships. A single-track model, or bicycle mode, can be used to obtain important information about the lateral behaviour of a vehicle. Here, the lateral properties of an axle are summarized into one effective wheel. The assumption made to build this model are: kinematics and elasto-kinematics of the axle are modelled linearly; lateral force of the tire is linear and the aligning torque is neglected; centre of gravity is assumed to be at road level [9].

Consider the vehicle single-track model of Figure 2.12, where the front and rear axle wheels are represented by one single wheel respectively in points  $A$  and  $B$ . Vehicle CoG is in point  $C$ . The vehicle is assumed to have planar motion, so the model exhibit 3-DoF in longitudinal  $X$ , lateral  $Y$  and yaw  $\gamma$  direction. At low speed is reasonable legit to consider that the velocity vectors in points  $A$  and  $B$  are in the direction of the front and rear axles, making an angle  $\delta_f$  and  $\delta_r$  with the vehicle longitudinal axis. This assumption is equivalent to considering null the tire's slip angles since the lateral forces generated with the road are small. The point  $O$  is the instantaneous rolling centre for the vehicle, defined by the intersection  $AO$  and  $BO$ , perpendicular to the wheel orientation. To drive on a circular path with radius  $R$  (segment  $OC$ ), the total lateral force from both axles is (2.23). The vehicle speed vector  $V$  is perpendicular to  $OC$ . The side-slip angle  $\beta$  is also known as the drifting angle and is defined as the angle between the vehicle's longitudinal axis and the direction of travel at the CoG. It represents the misalignment between vehicle orientation and the direction of the speed vector [47].

$$F_y = \frac{mV^2}{R} \quad (2.23)$$

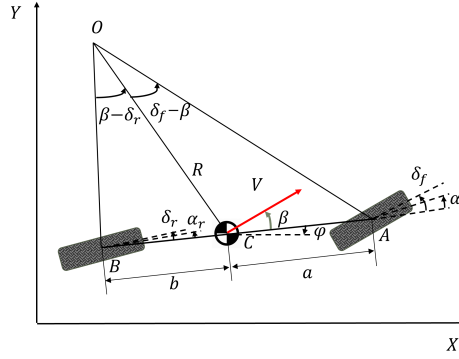


Figure 2.12: Single-track vehicle model

If we assume that the cornering radius changes slowly with low speed, the angular velocity of the vehicle is  $V/R$ . After some simplifications and applying the sine rule to  $OCA$  and  $OCB$  triangles, (2.24) is valid.

$$\dot{\gamma} = \frac{V}{R} = \frac{V \cos(\beta)}{a+b} [\tan(\delta_f) - \tan(\delta_r)] \quad (2.24)$$

Finally, the 3-DoF kinematic vehicle model motion can be described by (2.25), where  $\delta_f$ ,  $\delta_r$  and  $V$  are the inputs.

$$\begin{cases} \dot{X} = V \cos(\gamma + \beta) \\ \dot{Y} = V \sin(\gamma + \beta) \\ \dot{\gamma} = \frac{V}{R} = \frac{V \cos(\beta)}{a+b} [\tan(\delta_f) - \tan(\delta_r)] \end{cases} \quad (2.25)$$

Side-slip angle can be estimated by (2.26).

$$\beta = \tan^{-1} \left( \frac{a \cdot \tan(\delta_r) + b \cdot \tan(\delta_f)}{a+b} \right) \quad (2.26)$$

### Lateral Dynamic Model

At higher vehicle speeds and during cornering manoeuvres, the vector of the wheel velocity is no more oriented in the direction of the tire longitudinal centreline. Thus, a vehicle's lateral model is needed. Lateral and yaw motion dynamics are described by (2.27), where  $m$  is the mass,  $a_y$  lateral acceleration and  $M_{zz}$  the external yaw moment, imposing the equilibrium of lateral forces and momentum about the vehicle's  $z$ -axis respectively.

$$\begin{cases} m \cdot a_y = F_{yfl} + F_{yfr} + F_{yrl} + F_{yrr} \\ I_z \cdot \ddot{\gamma} = I_z \cdot \dot{\gamma} = a(F_{yfl} + F_{yfr}) - b(F_{yrl} + F_{yrr}) + M_{zz} \end{cases} \quad (2.27)$$

### 2.1.4 Vehicle Body Equations

When the vehicle is turning with a front steering angle  $\delta_f$  while accelerating, the motion of a 3-DoF vehicle model is described by (2.28).

$$\begin{cases} ma_x = m(\dot{V}_x - V_y r) = (F_{xfl} + F_{xfr}) \cos \delta_f + F_{xrl} + F_{xrr} - (F_{xfl} + F_{xfr}) \sin \delta_f \\ ma_y = m(\dot{V}_y + V_x r) = (F_{yfl} + F_{yfr}) \cos \delta_f + F_{yrl} + F_{yrr} + (F_{xfl} + F_{xfr}) \sin \delta_f \\ I_z \cdot \ddot{\gamma} = I_z \cdot \dot{r} = a(F_{yfl} + F_{yfr}) \cos \delta_f - b(F_{yrl} + F_{yrr}) + M_{zz} \end{cases} \quad (2.28)$$

### 2.1.5 Understeer Gradient

Several vehicle dynamics performance metrics based on analytical formulations are proposed. These are very important tools for the understanding of the underlying phenomena and how these indices are affected by the tuning variables [48].

The *Roll Gradient* is defined as the vehicle body roll angle derivative to the vehicle's lateral acceleration at its CoG. This parameter quantifies how a vehicle rolls in response to a cornering manoeuvre. Its value should be relatively low.

The *Steering Sensitivity* is defined as the vehicle's lateral acceleration derivative at its CoG to the imposed steering wheel angle. This parameter evaluates the responsiveness of the vehicle to the driver's steering input.

The *Understeer Gradient* is defined as the front tire average steer angle derivative as compared to the vehicle's lateral acceleration at its CoG, according to (2.29). It's usually evaluated through an increasing steering wheel angle test at a constant speed. The understeer gradient is inversely proportional to the steering sensitivity. It can be used to categorize the cornering behaviour of the vehicle.

$$K_V = \frac{\partial \delta_f}{\partial a_y} \quad (2.29)$$

Consider the bicycle model of Figure 2.12, with  $\delta_r = 0$ . Supposing that road radius is much larger than the wheelbase of the vehicle ( $R \gg a + b$ ), (2.30) is valid.

$$\delta_f - \alpha_f + \alpha_r \approx \frac{a + b}{R} \quad (2.30)$$

The steady-state steering angle is (2.31). Hence, force and moment equilibrium are the ones of (2.32).

$$\delta_{ss} = \frac{a + b}{R} + \alpha_f - \alpha_r \quad (2.31)$$

$$\begin{cases} F_{yf} + F_{yr} = m \frac{V_x^2}{R} \\ F_{yf} a - F_{yr} b = 0 \end{cases} \quad (2.32)$$

Front lateral force can be rewritten according (2.33) using the relationship between front and rear tire forces of equation (2.32) (arising by the moment equilibrium) and (2.31), with  $m_i$  the portion of vehicle mass insisting on the axle specified by  $i$ .

$$\begin{cases} F_{yf} = m \frac{b}{a+b} \frac{V_x^2}{R} = m_f \frac{V_x^2}{R} \\ F_{yr} = m \frac{a}{a+b} \frac{V_x^2}{R} = m_r \frac{V_x^2}{R} \end{cases} \quad (2.33)$$

At this point, tire slip angles  $\alpha_i$  can be rearranged as in (2.34), assuming two front and two rear tires.  $K_V$  is the understeer gradient (2.35).

$$\begin{cases} \alpha_f = m \frac{F_{yf}}{2C_{\alpha f}} = \frac{m_f}{2C_{\alpha f}} \frac{V_x^2}{R} \\ \alpha_r = m \frac{F_{yr}}{2C_{\alpha r}} = \frac{m_r}{2C_{\alpha r}} \frac{V_x^2}{R} \end{cases} \quad (2.34)$$

$$K_V = \frac{b \cdot m}{2C_{\alpha f}(a+b)} - \frac{a \cdot m}{2C_{\alpha r}(a+b)} \quad (2.35)$$

Three possible values can exist for the understeer gradient  $K_V$ , in the function of cornering stiffness and mass distribution (Figure 2.13):

1. Neutral steer  $K_V = 0$ : this condition occurs when slip angles are equal for front and rear tires. Here, when driving on a constant radius turn no changes in steering angle are required as speed varies ((2.36));
2. Understeer  $K_V > 0$ : in this case front tires exhibit larger values than the rear ones, so steering angle must be increased proportionally with speed ((2.37));
3. Oversteer  $K_V < 0$ : smaller slip angle at the front need a decrease in the steering wheel when driving in a constant cornering radius as speed increase ((2.38)).

$$\frac{m_f}{C_{\alpha f}} = \frac{m_r}{C_{\alpha r}} \Rightarrow K_V = 0 \Rightarrow \alpha_f = \alpha_r \quad (2.36)$$

$$\frac{m_f}{C_{\alpha f}} > \frac{m_r}{C_{\alpha r}} \Rightarrow K_V > 0 \Rightarrow \alpha_f > \alpha_r \quad (2.37)$$

$$\frac{m_f}{C_{\alpha f}} < \frac{m_r}{C_{\alpha r}} \Rightarrow K_V < 0 \Rightarrow \alpha_f < \alpha_r \quad (2.38)$$

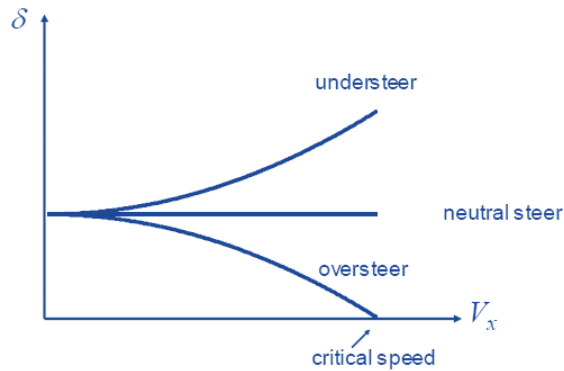


Figure 2.13: Understeering vehicle behaviour with speed (Figure from [3])

The directional controllability of a road vehicle depends on lateral forces in the tire-road contact surface. A locked wheel cannot generate lateral forces to counteract the side-slip trend when cornering, resulting in an understeering behaviour. Indeed, lateral adhesion suddenly drops with a high slip ratio. In this case, the front wheels lose their steerability. Nevertheless, due to the inertial forces, a self-correcting moment about the yaw centre of the rear axle will be developed to push the vehicle back on a straight path. Indeed, when the rear wheels lock the vehicle's rear end might start to slide sideways, compromising the directional stability.

Understeer is generally the preferred condition since is inherently safer. Hand-wheel steering angle has to be increased from the driver to follow the desired radius path in a turn with increasing speed since the front of the car steer out in the turn more than the rear end. In oversteering vehicle, instead, rear-end steer out of the turn more than the front and the driver must reduce the steering angle. This condition is better suited for professional and experienced drivers since may be counter-intuitive for a standard user.

## 2.2 Mechatronic Systems

The historical divisions between the various branches of engineering and computer science become less clearly defined. This stimulates a closer interconnection between these technological disciplines, providing a roadmap for nontraditional solutions. The consequent improvement in single-domain subjects (mechanics, electronics, information processing and control) are merged into a multi-domain discipline, called *Mechatronics*.

The term was first introduced in 1969 by a Yaskawa Electric engineer, composed of “mecha” from the mechanism and the “tronics” from electronics and soon became popular. The growing availability of reliable and low cost embedded microcomputers, along with information technologies and software advances, are pushing the development of mechatronic systems [49].

Despite the details of the formulations [50, 51], all definitions agree in recognizing the collaboration between mechanic, electronic and software disciplines to build a synergistic system as the pillar of mechatronics [49] (Figure 2.14).

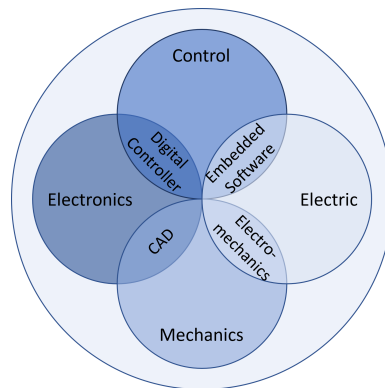


Figure 2.14: Mechatronic engineering fields synergistic integration

Mechatronic systems are developed following a holistic approach [10], aiming at an optimal compromise between the following properties: basic mechanical structure, interfaciability with sensors and actuators, automated digital information processing and implementation of control strategies through Electronic Control Unit (ECU). This latter specification represents the core feature of mechatronics and its synergy with the other elements can result in new and innovative solutions. Also, a new level of safety diagnosis and fault tolerance needs to be considered [52].

To summarize, the development of mechatronic systems must aim at achieving a synergistic optimization of mechanical engineering, electronic hardware and software programs to perform more and new functions at lower cost, less weight and installation space, while improving quality and reliability. The success of these products in solving the tackled problems resides upon the interactions of heterogeneous disciplines that were previously kept separate [9]. The general technological trend is that the mechanical part is continually decreasing, meanwhile electrical and software contributions are growing rapidly [52].

### 2.2.1 Vehicular Mechatronics: By-Wire System

Mechatronics is central to most of the innovations in automotive products, recognized as the main driving factor for the development of new vehicle features. Academic and industrial attention to embedded software technologies is growing rapidly and software-based solutions are continuously replacing mechanical components, due to technological and economical reasons. Indeed, the recent evolution in hardware components allows reducing its cost while improving both performance and reliability aspects. Moreover, E/E technologies are further increasing the opportunities, allowing to explore innovative control solutions which can be very costly or even not feasible using mechanical/hydraulic conventional systems.

Literature refers to the Anti-lock Braking System (ABS) by Robert Bosch GmbH as the first mechatronic device in vehicles, introduced in 1978. Another example is the Anti-Spin Regulation (ASR) or Traction Control System (TCS). Moreover, DAS are strictly integrated with mechatronics systems, e.g. the so-called Adaptive Cruise Control (ACC).

Now, the concept of “X-By-Wire (XBW)” can be introduced, where this term is intended for the replacement of mechanical/hydraulic systems embedded in automotive applications with fully E/E solutions [11]. It is important to note that, for critical-safety tasks, the mechanical components cannot be completely removed and replaced by XBW technologies: those are essential to work in conjunction with E/E devices and fundamental as redundant fall-back system in case of failure. Perhaps, the main problem of XBW concerns their reliability aspects, when related to safety functions. Mechatronics is playing an increasingly vital role in automotive applications. Malfunctions of SBW, BBW or Throttle-By-Wire (TBW) will compromise the whole vehicle’s manoeuvrability and controllability, resulting in unpredictable vehicle dynamics and, subsequently, jeopardising the safeness of the occupants.

### 2.2.2 Brake-By-Wire

Traditional braking systems haven’t changed much in the last century; in this sense, the brake by wire system represents an important innovation in the field of braking systems used in the automotive sector. This technology allows control of these systems electronically and can be designed to work with conventional or with

specially designed actuators. The development trend of the automotive braking control solution is visible in Figure 2.15 where the axis of the plot reflects the safety and comfort of the product. As can be seen, electronic “Brake-By-Wire” mechatronic systems intend to replace traditional hydro-mechanical connections between the driver pedal and the brake callipers, consisting of boosters, master cylinders, wheel cylinders and vacuum pumps. Thus, Electro-Hydraulic (EHB) or Electro-Mechanical (EMB) solutions have recently engaged the interest of manufacturers [53].

The mechanical decoupling of the brake pedal and actuators make the braking effort modulation process more flexible and enable a simpler implementation for the cooperative regenerative/friction braking allocation in EVs [54]. More simplistic and faster assembly, robust electric interface and easily upgradable firmware contribute to their dissemination [55].

Thus, BBW offer many benefits, respect to conventional hydraulic brakes:

- **Efficiency and Stability:** greater braking efficiency and more precise stability control thanks to the ability to independently, quickly and precisely distribute the braking torques on all wheels;
- **Safety:** the time delay between driver command on pedal and brake actuation is strongly reduced;
- **Cost and Manutenibility:** remove many mechanical components to reduce production, assembly and maintenance costs. It contribute also to weight and dimension reduction, with a positive impact on efficiency and design freedom. Even reliability is improved due to the reduced number of components;
- **Diagnostic:** the widespread presence of sensors and the continuous signals processing by the ECUs guarantees RT control of the braking system functionalities;
- **Integration:** ensuring simpler interfaciability with higher-level controllers, e.g. ABS or ESP, without requiring complex mechanical/hydraulic components;
- **Environmental Impact:** allows to significantly reduce the release of fine particles into the environment by removing all parts subject to wear. This is essential in a perspective of reducing particles such as PM10 and PM2.5, especially in urban areas.

The main disadvantage of BBW is the higher safety requirements needed to meet the traditional brake plant reliability. The absence of mechanic-hydraulic links between pedal and callipers is detrimental from this point of view. So, failure rate of BBW must be decreased [13]. This leads to the need for fault tolerance and fail-safe system architecture. The underlying approach is to provide redundancy in power supply, sensors, hardware, Control Unit (CU) and signals.

The major component of typical BBW is brake actuators, pedal simulator, communication lines, ECU, backup system and power supply. A Wheel Speed Sensor (WSS) is also equipped on each tire. The backup brake system will intervene when the BBW system fails, supplying the required brake effort.

### 2.2.3 Steer-By-Wire

Purely mechanical steering systems can be divided into two categories: rack and pinion steering and ball and nut steering. The loss of steering control due to

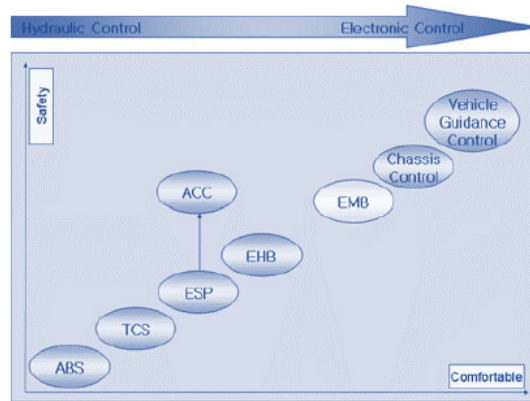


Figure 2.15: Automotive brake systems development trend (Figure from [53])

failures in the steering system is not considered, since these are developed to ensure appropriate safety margins. Indeed, given standards impose on manufacturers to design steering systems with high-reliability characteristics. ECE R-79 regulates the designing and development aspects of steering systems.

The modern solution is usually hydraulic power steering systems, consisting of a mechanical part working in conjunction with a hydraulic system. With this architecture the driver is assisted, reducing the total effort that must be applied to the steering wheel to perform the desired cornering manoeuvre. In case of a failure, the handling of the vehicle is not compromised, resulting only in an increase of steering effort from the pilot.

The research is currently investigating newly steering system, where the column is omitted to further reduce mechanical parts by removing the direct connection between the steering wheel and steered tires. Nevertheless, failure in such plants may lead to dangerous situations, since the controllability of the vehicle is completely compromised. For this reason, important reliability considerations must be considered for the design of such systems.

Despite that, many advantages can be achieved thanks to this BW configurations. A remarkable improvement in driving comfort and more desirable steering behaviour in oversteer/understeer conditions can be reached, due to the variable steering ratio. This feature allows the steering ratio between the hand wheel and the wheels to adapt according to the driving conditions. Another benefit can be obtained acting on the CU software during  $\mu$ -split braking situations: in case of asymmetric adherence different torque can be delivered to right and left wheels. Finally, completely removing the steering column, which is one of the heaviest components of the vehicle. This can significantly decrease the weight of the vehicle, thus reducing fuel consumption, providing more design freedom in the engine compartment and improving Noise, Vibration and Harshness (NVH) performances. Concerning efficiency, an electrically powered steering system is the best solution [10]. The electric-powered solution can save about 90% of fuel consumption if compared to a hydraulic steering plant.

## 2.3 Electric Vehicles

Internal Combustion Engine (ICE) automobiles are one of the greatest achievements of modern technology by satisfying the need for mobility. Though road vehicles made fundamental contributions to the definition of modern society, the rising number of automotive products in the world is still causing several issues for the environment and life. Indeed, transportation is a major energy-demanding sector, whose main source is still a fossil fuel [56]. In the last decades, oil consumption in this field has grown at a higher rate than any other application. Air pollution, global warming and rapid depletion of petroleum resources are now major threats to human beings of paramount concern. Recent regulations regarding stringent emission and fuel consumption emphasized interest in the development of safer, cleaner and more efficient transportation. Electric, hybrid and fuel cell drivetrain technologies have been addressed as the most promising solutions for replacing conventional Internal Combustion Engine Vehicles (ICEVs), attracting rising attention from vehicle constructors, governments, and academics. Primarily because of the absence of fuel emissions, higher efficiency and smooth operation [57].

Central focus in on the development of EVs, which use Electric Motor (EM) for traction and batteries as Energy Storage System (ESS). These cars can help to meet the challenges of energy crisis and pollution imposed by government agencies and organizations [58]. Specifically, European Commission intends to eliminate conventionally fuelled cars in cities by 2050 [59].

Current and future development of electric mobility is deeply affected by the opportunities offered by recent and incoming technological advancements concerning actuation, power management and embedded/distributed computing. All these achievements are often indicated as topics of mechatronics and industry 4.0. These innovations applied to vehicles design and management should produce the following trends:

- **Reduction of Environmental Impact**

- *Direct*: reduction in CO<sub>2</sub> emissions, that must fit the normative limits produced by EU Commissions and international treaties [60, 61]. Also reduction of particulate matter emissions related to ICE and to brake wear [62];
- *Indirect*: higher efficiency and electric propulsion technologies make possible usage of renewable resources and their optimal allocation respect to distribution/grid constraints and consumption profile [63];

- **New functionalities**

- *Energy management*: optimize this aspect can yield to improvement in vehicles autonomy and efficiency [54, 64];
- *Safety and Stability*: both can benefit in terms of longitudinal and lateral dynamics. Portability constraints should be respected for an easier integration with incoming and future high-level functionalities with the opportunity to expand the regulation algorithms with the insertion of nested feedback loops [64];
- *By-Wire system*: full electrification of the vehicle should lead to a drastic redesign of the whole system, allowing innovative solutions and configurations such as unconventional wheels layout or powertrain schemes.

In this sense, an extensive use of BW technologies should contribute to higher level of safety and performances of the system [13, 14, 16, 54];

- **Higher performances:** electric actuation systems allow superior performances both for traction and control purposes respect to conventional ICE and auxiliary devices currently installed, in terms of controllability, response time, reduced maintenance [63], optimization of system layout and complexity, depending on adopted technologies;
- **Coherence with V-shaped development process:** according to the V-model design and production workflow (described in the next chapter 3.3.1), modelling design and testing procedures should contribute to a drastic optimization of TTM and manufacturing costs involved in the development of innovative industrial products by extended use of “in-the-Loop” methodologies.

Recent development in the power electric field made available several technologies (semiconductors, calculation capacities of embedded CU, energy storage systems) at an acceptable cost, which are critical for the mass-market penetration of electrified mobility solutions, triggering the comeback of e-vehicles [59]. Modern EV appear in the early 1990s when GM release EV1 and PSA cars. Although important improvements were reached, the problem of the reduced driving range ever obstacle their market penetration. Indeed, energy storage represents the weakest element of electric powertrains. Since this, the tendency is to introduce systems with on-demand power instead of those with continuous idle power needs, e.g. replacement of engine-driven hydraulic Electronic Power Steering (EPS) with electrohydraulic or pure electric solutions [65].

Improvement in energy efficiency for road vehicles can be achieved in three ways [66]: operating each component with its optimal efficiency; reducing dissipation terms of rolling; recovering kinetic and potential energy during brake.

It is stated that electrified vehicles are more economic in terms of energy efficiency, which has been proven by several authors by calculating the well-to-wheel overall energy consumption [58]. ICE shows a rather low-efficiency percentage, in the order of middle twenties for gasoline vehicles and middle forties for diesel solutions. These low fuel efficiencies make the automotive industry one of the largest sources of greenhouse gas emissions [56]. To reach a more sustainable transportation system, the development of higher-efficiency automobiles is a key enabling factor. On the other hand, power electronics and electrical machine efficiencies can range from the high nineties to the high eighties. Also, battery efficiencies can be in the eighties. Considering all the electrical components taken together, the overall system efficiency can be placed at about 70% for EV. So, from the user’s point of view, automotive electrification can represent a valuable candidate for conventional vehicles in terms of fuel economy. Besides the favourable environmental-friendly impact, even driving pleasure, comfort and performances are pushing for the introduction of EV [67], thanks to shorter response time and their torque-speed characteristics which match better with traction requirements [56].

From the viewpoint of vehicle dynamic, EVs are the most exciting target for advanced motion control methodologies. This additional distinct aspect is often not well recognized. A great advantage is the quick and precise torque generation offered by EM. Without considering this merit, e-vehicle properties may not be fully exploited. If we considering also the benefit in control performance and success in the purpose of the new concept mobility product, a brighter future will be expected for EV [68]. The mass commercialization of these automobiles will allow emancipating from fossil fuels, enabling a more green mobility system. However, the premature technology of e-vehicle is still demanding more reliable, compact, lower weight, and higher-efficiency solutions. Moreover, the additional cost of electrified vehicles may take several years to be recovered [69]. Costumers may not necessarily be pushed by environmental consideration but rather by economics. Indeed, from a user's viewpoint, the prize can become the deciding factor, concerning fuel and life cycle costs, as well as maintenance and disposal. Another important element is the driving range, which, for fully electric vehicles, is still very limited. Thus, to achieve widespread use of EVs and engage the market interest, the industry requires the realization of cost-competitive and long drive range cars to make them more attractive. Adequate incentive programs may emphasized their desirability [56, 69].

### 2.3.1 EV layout

Research effort on novel electrified powertrains development and energy management algorithms has dominated automotive engineering for the first two decades of the twenty-first century, which are relentlessly reviewed throughout the literature. However, additional challenges are emerged, demanding innovative alternatives to the well-established ICE technologies, concerning powertrain layouts, chassis, and vehicle dynamic controls.

In their recent implementation, EVs were born by conversion of existing ICE cars, replacing the engine and tank with EM and battery pack, respectively. ICE powertrain consist of a series of NL systems, such as combustion motor, clutch, transmissions, gearbox, differential and axle, which drive the wheels. Drawbacks such as weight, poor performance and lower flexibility cause these solutions to disappear soon. Indeed, the best approach for the design and development of these vehicles is to completely rearrange the vehicle traction layout, by proposing a new structure that best exploits the unique characteristic of e-powertrains. This makes out the best of e-propulsion, fitting the requirements of new trends in mobility, both from industry and users' perspectives.

One of the biggest technological challenges in mobility electrification lies in the development of powerful, efficient and economic battery systems. The energy density of automotive batteries is significantly low if compared to fossil fuels tanks:  $100 - 150Wh/kg$  for Li-Ion battery vs  $12000Wh/kg$  for gasoline fuel. To achieve comparable driving ranges in BEV, very large battery packs have to be equipped, which affects negatively the net weight and costs of e-vehicles.

In modern EVs, more than 100 different EM can be found, since extensive work in terms of research in this area from various sources is being done. This results in a segmented market with, Permanent Magnet (PM), Direct Current (DC), induction, synchronous, synchronous brushed, reluctance and flux machines, depending on desired topologies and design requirements of EVs [59]. From the literature review, a clear challenge that emerges is to reach the high-efficiency target, to be maintained from 10 to 100% speed range [70].

The electric drive train consists of three major subsystems [57]: electric propulsion (power converter, electric motor and transmission to deliver torques to the wheels), energy storage system (battery and its ECU) and auxiliary systems.

Keep in mind that power can also go in the direction of the battery in case of regenerative braking. Indeed, the kinetic energy of the vehicle can be converted to electrical form and restored in the storage system. All these operation are executed in cooperation with the Battery Management System (BMS), which in RT estimate the State of Charge (SOC) and State of Health (SOH) to avoid under-discharging or over-charging conditions.

For what concern EV architectures plenty solutions are available, respect to the powertrain design [57, 71]. With e-propulsion, the possibility of powertrain frames substantially grows. The substitution of ICE with an EM is only one of the few options. We can find Hybrid Electric Vehicle (HEV) where combustion and electric machines coexist in the same shaft or different axles. Further concepts can be seen with separate EM on axles or for each wheel, even targeting super sports cars (e.g. Mercedes-AMG SLS E-CELL) [65].

Interesting aspects are quantity and layout of EM and energy storage, as well as their characteristics (Figure 2.16):

- (a) The most common configuration has a single EM as the central motor, which simply replaces the engine of a conventional internal combustion vehicle. The transmission of power is done with the aid of a clutch and a gearbox in series to a differential mechanism;
- (b) The fixed gearing is replaced by a multi-speed gear-box to remove the clutch. E-motor show a constant power characteristic in a wide speed range;
- (c) Fixed gearing and differential are integrated into a single assembly;
- (d) Electric machines can optionally also be installed near the wheels. When using this topology two EM is series to a fixed gear, driving one side wheel individually, are installed and differential is not required anymore;
- (e) Also known as WIM configuration. The planetary gear is adopted to reduce motor speed and increase the torque;
- (f) The previous topology can be further simplified by placing the e-motors directly inside the wheel's hub, from which the name Hub motors or In-Wheel Motor (IWM). This allows to fully remove any mechanical gearing between EM and driven wheels, reducing friction losses, space and weight.

The key component connecting e-vehicle performance with vehicle dynamic behaviour control is certainly the EM, which shows many attributes that can be exploited when developing stability controllers. The following advantages open the way for the implementation of novel motion control techniques [68, 72, 73]:

- Quick and accurate torque generation: torque response is 10-100 times faster than ICE and hydraulic brake, in the order of milliseconds. This essential feature enables the implementation of precise feedback speed and torque control in wider operational ranges for stability purposes, without requiring intervention in the driver command interface. Due to the availability of acceleration and deceleration torques thanks to the multi-quadrant operational modes, ABS and TCS functionalities can be integrated [74];

- Distributed motor location: EM can be attached to each wheel, allowing the implementation of enhanced VSC strategies, such as Direct Yaw-Moment Control (DYC);
- Reliable and easy motor torque measurement: a smaller uncertainty in traction or braking torque generation is possible due to the motor current control. This also enable simple "driving force observer", to estimate in RT the force produced in the tire-road interface[75].

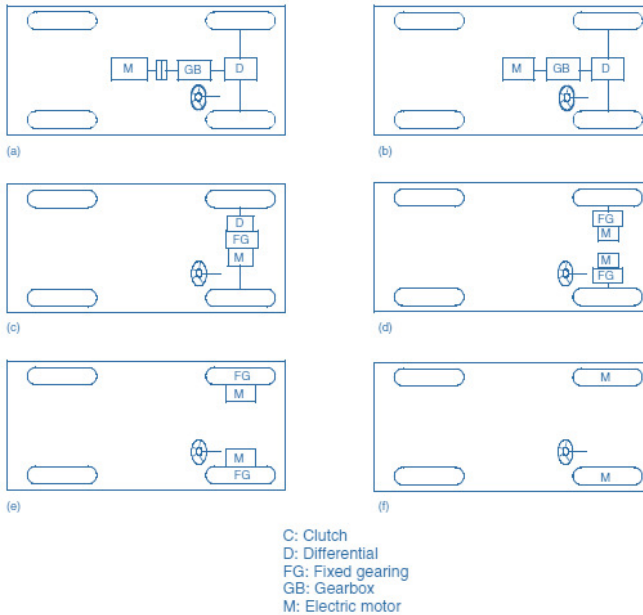


Figure 2.16: Conceptual schemes of different EV layouts (Figure from [57])

### 2.3.2 EV Performances

Design requirements of automotive EM concern several aspects, i.e. control performance, reliability, and affordability. E-powertrains should have high power density (power to weight ratio), high torque at low speed and operate in a wide speed range and on rough roads with high efficiency, under severe temperature conditions over a long period. However, these new technologies pose tremendous challenges for vehicle dynamics, affecting driving safety [64].

In automotive applications, the ideal power plant characteristic is constant power over the full speed range. Efficiency of electric motors depends on the working point, as for ICE [59]. Since motor mechanical power  $P_{mec}$  is (2.39) where  $\eta$  is the efficiency,  $T_{EM}$  the torque and  $\omega_{EM}$  the speed of the EM, expressed respectively in  $[N \cdot s]$  and  $[rad/s]$ , the torque effort must decrease following a hyperbolic function, once the base speed is reached.

$$P_{mec} = \eta \cdot T_{EM} \cdot \omega_{EM} \quad (2.39)$$

At low speeds, maximum torque is available and maintained constant. Optimal sizing of the motor is obtained by constraining the starting torque to not exceed maximum longitudinal force  $F_{x-max}$  that can be generated in the tire-road interfaces of the driven wheels without slipping, supposing full adhesion conditions. This can depend on vehicle mass and pneumatic characteristics. So, assuming a friction coefficient  $\mu$  of 1, the maximum deliverable motor torque  $T_{EM-max}$  should be equal to the vehicle weight (mass  $m$  per gravitational acceleration  $g$ ) multiplied by the wheel radius  $r_w$  and a gear ratio of the transmission  $K_{rate}$ , as described by (2.40).

$$T_{EM-max} = F_{x-max} \cdot r_w \cdot K_{rate} = \mu \cdot m \cdot g \cdot K_{rate} \quad (2.40)$$

The internal combustion engine shows torque-speed characteristics far from the ideal one. Figure 2.17 on the left report ICE torque and power map over speed, when the motor is combined with a multi-gear transmission. In contrast, EM exhibit a speed-torque characteristic which closely match the ideal one (Figure 2.17 on the right). Thus, a single-gear or double-gear transmission is usually employed.

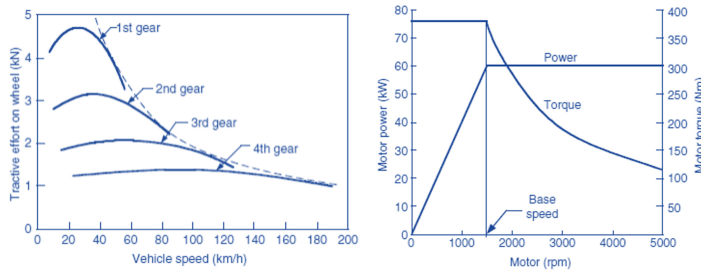


Figure 2.17: Motor torque characteristic: ICE (left) and EM (right) (Figure from [57])

The performance of a vehicle is usually described by maximum cruising speed, gradeability, and acceleration [57]. *Maximum speed* is the constant cruising speed that the vehicle can reach with full throttle on a flat road. Is defined by the equilibrium point between traction force and resistances. *Gradeability* is the road angle that the vehicle can overcome at a certain speed, typically the one referred to 100km/h.

*Acceleration performance* is described by the time and distance covered from 0 speed to 100km/h.

### 2.3.3 Regenerative Brake Systems

Future automotive makers have to propose new technologies able to satisfy both reduced emissions and environmental impact, as well as increasing performance demands [53]. As compared to these tasks, an inherent valuable feature of EVs, which has become more and more important, is their ability to work on multi-quadrant operational modes. As visible in Figure 2.18 and according to the sign of torque and speed, the mechanical power (2.39) is positive in the first and third quadrants where the e-machine works as a motor (traction), while is negative in the second and fourth quadrants when operating as a generator (braking).

This offers the possibility of performing regenerative braking, probably one of the most significant applications of vehicular mechatronics: is a multi-objective

optimization problem, whose design must meet the compromise between the aims of improving energy efficiency, system complexity, brake performance, brake comfort, cost, safety and reliability [66, 76]. Regenerative Braking System (RBS) allows for the recovery of a large part of vehicle kinetic and potential energy of the vehicle mass during the braking phase, instead of dissipating it as heat through friction brakes [77].

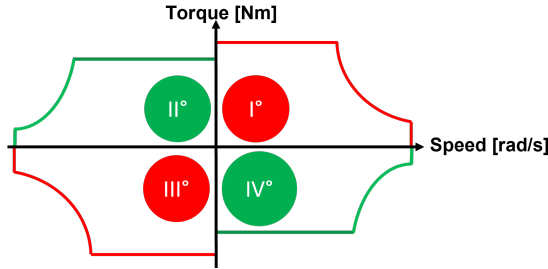


Figure 2.18: Multi-quadrant torque-speed characteristic of EM

### Regenerative Braking Energy

The quantity of energy that can be recovered by RBS during braking it's an important indicator of regeneration technology's viability, as well as for evaluating the potential of this system concerning greenhouse gas emissions, local pollutants, energy insecurity and driving fuel costs. It may depend on several factors, i.e. motor characteristics, drive train layout, energy storage capacity, battery SOC (which rarely is the limiting factor), battery SOH (if it is approaching its end-life condition) and driving styles of the driver (including the car usage pattern) [78]. The bigger constraints to deal with it certainly the power characteristic over the speed of the EM and the maximum allowable charging current of the battery. In the regenerative braking energy management process, a vital role is also played by the driving style, influencing recovery efficiency and safety [76].

The braking power demand can be divided into *dissipative*, transformed into unrecoverable heat (rolling resistance  $P_r(t)$  and air drag  $P_w(t)$ ), and *conservative*, as kinetic  $P_{acc}(t)$  and potential  $P_g(t)$  power. The regenerated brake energy  $E_{reg}$  is the integral of braking power  $P_{brake}(t)$  supplied by the EM according to (2.41), with  $\eta_{reg}$  the conversion efficiency from wheel to battery, comprising drive unit, motor, transmission and battery efficiencies [79].

$$E_{reg} = \int P_{brake}(t)\eta_{reg}dt = \int (P_{acc}(t) + P_g(t) - P_r(t) - P_w(t))\eta_{reg}dt \quad (2.41)$$

Regenerated power depends on generator size, storage capacity and power electronics. Despite what one can think, choosing the biggest possible e-powertrain is not necessarily the optimal solution. Indeed, the majority of braking events are moderate, generally lower than  $20kW$  and within  $0.3g$  in most used drive cycles [66, 80]. This means limited power e-machine should be able to recover almost the available braking energy, making a larger motor unnecessary for deceleration aspects and avoiding the over-sizing of the electric powertrain.

Different studies have measured the effective impact of regenerative braking in terms of energy consumption, for different UC and driving cycles, with a percentage up to 46% [81, 82].

Nevertheless, it should be noted that RBS can introduce some disadvantages. Additional weight, charge/discharge efficiencies of the storage system and the limited fraction of the entire drive mission in which regeneration is so effective should be considered when calculating the overall advantages of the regenerative plant [10].

### Regenerative Braking and Vehicle Dynamics

Despite that, even active safety systems can benefit from RBS, since it enables faster braking effort applications and the adoption of more sophisticated controlling techniques. Concerning vehicle stability purposes, when using a RBS it is important to exploit the e-powertrain for the development of control strategies, not only during the braking and traction phase but also in cornering manoeuvres [83]:

- Higher torque bandwidth response in contrast to hydraulic friction brakes, which improve open-loop and closed-loop control performances;
- Highly precise torque and speed control if compared to ICE or disc brakes, due to the electric current-based control structure which can be handled with fewer uncertainties;
- More accurate knowledge of the motor torque can be used for the application of advanced stability control algorithms, enhancing the estimation of the road friction coefficient and tire slips as well.

Undoubtedly, the braking system is one of the main safety-related plants of all automotive vehicles. A successfully designed braking system must meet distinct demands: ensure the shortest stopping distance in emergency braking situations, maintain the travelling direction stable and controllable, being able to supply in every working scenario sufficient braking torque on the wheels. However, the required braking forces to fulfil these conditions typically exceed the one e-machines can produce. So in EVs, RBS and the mechanical friction brake system must coexist and cooperate. Therefore, the optimized design of the coordinated control of both mechanical and the electric brake is an important topic [10, 66]. Disabling the RBS in dangerous stability situations may appear a good solution, especially when braking performances are safety-related, e.g. cornering on low friction roads. However, this solution overlooks one important feature of the electric actuator: the fast torque response, which can be exploited for advanced control algorithms. As pointed out in Figure 2.19, the EM should be regarded as a braking device, which can extend the bandwidth response of the brakes [84].

#### 2.3.4 Brake Blending

The benefits arising from the usage of a RBS in electrified vehicles are obvious, strongly improving the efficiency, especially in city driving with frequent stop/go operations. However, regenerative braking could not be available or is limited only to a modest percentage. The limiting factors are [60, 73, 79, 84]:

- i. Battery rate of charge: limiting the overall maximum current that the BMS makes available. The SOC of the energy storage system have a strong influence, since, to avoid battery over-charging, regenerated power is reduced or even disabled when approaching its full charge state. Also, it depends on battery ageing (SOH) and actual temperature, which rather imply a reduction of the battery capacity;
- ii. E-powertrain characteristics: the torque availability in e-machine is speed dependent. For instance, beyond the EM's base, speed power must be held constant, so torque is severely reduced in the field weakening region, to be less or equal to the ideal torque characteristic. Moreover, at low speed proper electric braking is not guaranteed: at full stop the torque needed to compensate for the external forces is hard to be estimated, causing the vehicle to move forwards or backwards. So, under a certain velocity, RBS is deactivated and brake efforts are applied by the friction system;
- iii. Overall efficiency: to convert vehicle kinematic energy into usable electric form, it is necessary to transform the braking mechanical power into electric current in the EM and store back it into the battery. This involves e-machine, power electronics, inverters and battery charging efficiency, introducing additional power constrains and, thus, reducing the final recoverable energy;
- iv. Braking system regulations: to ensure braking safety, the maximum braking torque on each axle should be constrained for front/rear distribution criteria. ECE R-13 standard provides the rules, based on vehicle properties and braking severity. In case the vehicle electronics malfunction the vehicle should still be able to come to a standstill.

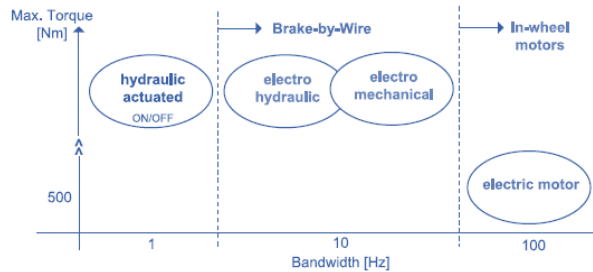


Figure 2.19: Bandwidth response of brake systems (Figure from [84])

### Concern on Design Hybrid Brake System

Keeping in mind these limitations and knowing that for all automotive vehicles minimum braking performances must be ensured for achieving driving safety, an acceptable braking behaviour and avoiding e-oversized motors, RBS must be integrated with conventional hydraulic backup brakes. Indeed, when the braking torque provided by the EM cannot meet the driver's demand, the friction brake system should deliver the extra torque. When designing a hybrid brake system for electrified vehicles there are three major concerns [85, 86]:

1. Application of required braking effort: a proper torque must be allocated to the front and rear axle to quickly reduce the vehicle speed and maintain a reduced braking distance while ensuring a stable and controllable directional behaviour . So a proper front/rear brake force distribution must be achieved;
2. Energy recover maximization: favour the RBS in braking effort allocation is fundamental to improve vehicle efficiency, especially when driving in stop-and-go patterns in urban areas;
3. Enable integration and coordination with an active stability system: to preserve safety, driving comfort and torque transient response.

In all EVs there is a redundant brake system, where mechanic and electric braking should be mutually complementary [87]. The key problem of this over-actuated system is to find an optimal trade-off between braking performance and maximized energy recovery while maintaining acceptable costs. If a cooperative behaviour of the brake actuators is not achieved, even driving comfort and braking feeling can be greatly affected [88]. All the constraints deal with the Brake Blending (BB) allocation problem for over-actuated brake system [54].

Thus, to attain the first point and consider the safety-related purpose of a vehicle brake system, a mechanical or BW friction brake backup is needed to deliver the desired braking torque. The BB controller must be able to automatically compensate for any unexpected electric braking unavailability, adjusting output torque values to meet the driver's deceleration demand when the driving conditions suddenly change [89].

To satisfy the second point and recover as much braking energy as possible, a feasible solution is the adoption of optimal power management techniques. For this, the storage system should admit high recharge current values while EV is braking.

The third point deal with the optimal coordination within the braking systems, aiming to improve driving comfort and ensure no dynamic effect from the passenger's viewpoint during the application of the brake efforts. Conventional hydraulic brakes can provide the driver with a subjectively acceptable brake feel. Using BBW system is inevitable when realizing a blended brake control, in which part of the braking efforts are delivered by RBS. This is because desired friction torque depends on EM and ESS states. An additional aspect concern the pedal feel. The feedback pedal force should be controlled independently by employing a pedal simulator since the human perception of vehicle deceleration when braking must remain the same. It is widely accepted that driver must be unaware of the braking actuators, letting the braking performance and perception its only concerns [60, 73].

### **Brake Effort Allocation**

The process of braking effort allocation is done in three steps. Firstly, the total amount of the required braking force is calculated according to driver demand. At this point, the individual braking torque is established for each tire, accounting for the information arising by the higher-level controller, e.g. ESP, which may require differential efforts between left and right wheels, to induce a correcting yaw moment. Then, the maximum available regenerative braking torque is defined, according to e-powertrain and ESS states. Finally, the regenerative and dissipative brake effort are calculated according the driver demand and the adopted blending strategy [53, 84, 87].

To keep the BB strategy consistent with the previous specifications, friction braking forces must be regulated in RT in the function of the regenerative torque availability. This specification is particularly relevant for control strategies that require a fast wheel's torque modulation. This multi-objective optimization task defines a complex challenge. The control framework should be able to tackle several optimization goals when deciding how to split the brake demand on available actuators, taking into account the system's dynamics and actuator's constraints. This requires a flawless coordination strategy for satisfactory control performance. A common element in the majority of most advanced proposed BB approaches is the definition of a nested control loop: the inner one deal with the torque allocations problem, assigning torque references to the actuators to assure desired braking performance (torque tracking) and, e.g., prioritizing regenerative brake to improve energy recover; while the outer loop target the driving comfort task, including the different actuator dynamic and constrain compensations along with a cascade control architecture for wheel slip control [90].

### Hybrid Brake Systems Categories

Despite the typologies of RBS, ECE 13H have the compulsory requirement of granting any ABS to override priority to control braking [89]. The application of regenerative braking is allowed when (1) the intrinsic variations of the regenerative braking torque are automatically compensated using foundation brakes and (2) braking rates always remain related to the driver's braking demand. These legal requirements heavily influence the regenerative braking control strategy design, currently under investigation by original equipment manufacturers (OEMs) and research groups worldwide. These specifications have driven the development of the regenerative braking systems, as well as the test and verification procedures [91].

In literature, a wide diffused classification of the BB, divide the solutions into three branches, i.e. *Series*, *Parallel* and *Hybrid*, summarized in Figure 2.20 [10, 79, 92–94]. These blended braking algorithms may occur individually or switch between each other frequently during operation. So, it becomes relevant to properly coordinate these brake actuators to ensure maximum braking performance and improve energy efficiency.

*Series* BB algorithms, also known as "series braking with optimal energy recover", impose that the vehicle is decelerated using the RBS when requested brake torque can be completely provided by the e-motor. The main idea is to prioritize the use of regenerative braking while adjusting friction braking to satisfy the total braking requirement. Keep in mind that regenerative braking is effective only for the driven axle. As visible in Figure 2.20 on the left, the issue is there isn't an ideal front-rear brake distribution and the car is stopped only by its electric driven axle. This solution is the most efficient since allows for fully exploiting regenerative braking. On the other hand, when braking the car at the driven axle no front-rear repartition is realized, which may lead to unstable vehicle behaviour.

Indeed, for *Parallel* BB solutions, regenerative and friction braking are applied together (central plot of Figure 2.20). In contrast to series BB, the mechanical brake is always present at both driven and non-driven axle, ensuring front-rear effort allocation. Even in this case, RBS is used until its maximum deliverable torque, but its effort is always merged with the one arising by the backup system, typically using a fixed blending ratio between them. Energy recovery is reduced, but higher stability performance is ensured while braking. Indeed, regeneration is

not possible on a locked axle, so optimal front-rear allocation is desirable even for efficiency improvement.

The last BB algorithm is the *Hybrid* one, or "series braking with optimal braking feel", reported in Figure 2.20 on the right. Even in this case, there is always front-rear brake repartition, since the non-driven axle is actuated by dissipative brakes. Here, at the driven axle regenerative braking is applied until maximum capacity is reached. When the required braking force become larger and RBS is no longer able to fulfil the requested torque the friction brake is activated to compensate for EM unavailability. This strategy ensures the best compromise between vehicle regeneration efficiency and braking stability, preserving also a good pedal feeling.

A comparison of series, parallel and hybrid BB strategies has shown a capability of recapturing 36%, 15%, and 30%, respectively, of the overall output electric energy.

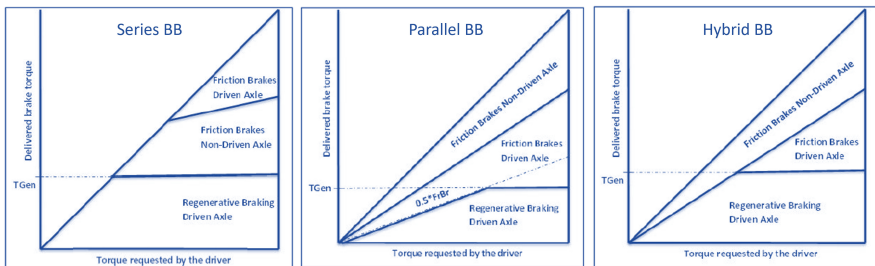


Figure 2.20: Different brake blending strategies: series (left), parallel (center) and hybrid (right) (Figure from [79])

## 2.4 Electronic Stability Program

As mentioned in the *Preface*, a large portion of road accidents results from a loss of control of the car due to human error and its limited perception of vehicle dynamical response. External circumstances and improper driving styles, e.g. obstacles suddenly appearing on the road, poor adherence conditions or driving at inappropriately high speeds can lead the vehicle to reach its critical limits and become uncontrollable. When the adhesion limit is exceeded, the car behaviour became extremely NL. The system appears unstable and the average driver may panic. As a result, the vehicle may suddenly spin, putting in risky situations the users. To regain control of the car, the driver may apply steering corrections, which in some cases worsens the situation.

To assist the pilot in the control of vehicle dynamics in longitudinal, lateral and yaw motion direction, active stability control systems implemented through ECUs are introduced. These controllers adapt the actuator's efforts (e.g. brakes, drivetrain, steer) according to their constraints and current vehicle behaviour. The goal is to maximize the range of driving operation, stabilizing it in a bounded linear region. When using a feed-forward solution, the adhesion limit can be exceeded. To keep the vehicle in safe and stable conditions the control commands have to be actively adjusted in RT. In the current SoA feedback control strategies are the most popular in the vehicle dynamic control field. Thus, stability CUs are designed to take over the leadership for a short time and correct the vehicle motion [95].

Active lateral control systems have the aim to prevent automotive vehicles from spinning and drifting out. The main functionality of yaw stability controllers is to restore the vehicle yaw rate as much as possible to the motion behaviour desired by the driver [3]. ESP controller, also known as ESC or Vehicle Dynamic Control (VDC), applies a unified and synergistic concept to control the vehicle's tendency to slide away instead of obeying the attempted steering commands. At the same time, it must ensure stability to prevent breakaway risks, keeping the vehicle remains within its physical limits. Improved dynamical behaviour is enabled by providing the following assets [9]:

- *Increased directional stability under all operating conditions*, keeping the vehicle on track during emergency stops, standard braking, coasting, acceleration and so on;
- *Increased handling and manoeuvrability at the limits of traction*, e.g. during abrupt steering manoeuvres or driver's panic responses, reducing skidding and breakaway scenarios;
- *Interactive integration with other safety systems*, maintaining the vehicle within its physical limits.

The adopted control approach of current commercial ESP relies on brakes and engine as a tool for "steering" the vehicle. A closed-loop system is designed to improve vehicle handling, manoeuvrability and braking response through coordinated action between braking and traction systems. When stability-control functionality operates, the priorities which govern these actuators shift. Acceleration and deceleration basic commands assume secondary importance when ESP intervenes to stabilize the vehicle in a certain trajectory. Specific braking interventions are directed to individual wheels, such as the inner rear wheel to counter understeer or the outer front wheel during oversteer. These allocation techniques are also known as "selective braking" or "differential braking". Similarly, intervention can also be on the engine, to accelerate or decelerate the driven wheels. To generalize, these methodologies can be classified as "differential allocation", where an equivalent yaw moment is induced on the vehicle body to counteract undesired behaviour (Figure 2.21).

This controller show capabilities extending far beyond those of ABS and TCS combined, by integrated coordination between them. ESP relies on active TV methodologies at wheels, where vehicle response is used to close the control loop. In specific, the algorithm can use brake, propulsion and steer systems to produce the desired set of lateral forces on the wheels, leading the actual response to converge with the ideal one under the given circumstances. This solution provides highly precise performance, selectively adjusting the dynamic longitudinal and lateral forces on each wheel [9].

To summarize, within the invariable limits imposed by the laws of physics, ESP keeps the vehicle on the road and reduces the risk of accidents and overturning. The majority of ESP currently in production rely on differential braking technique, which utilizes ABS and TCS to apply different torque efforts between the right and left wheels, developing a yaw moment which preserves vehicle stability when it would otherwise be compromised. The performance requirements of the ESP are primarily related to the support of average drivers. This controller should help to maintain the directional control of the car in any driving situation, including

abrupt steering or acceleration. To achieve this a specific control action (e.g. yaw moment) must be quickly generated.

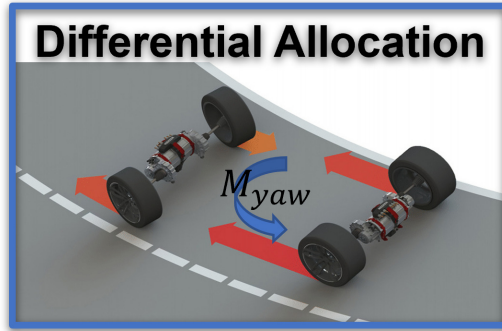


Figure 2.21: Differential torque allocation and induced yaw moment on a vehicle

### 2.4.1 Hierarchical Structure

Current ESP closed-loop stability controllers intend to prevent the longitudinal, lateral and yaw speed from exceeding the ultimate control limits. This is done using a hierarchical frame. Firstly, the driver command is translated into the expected dynamic vehicular response, using car and road characteristics. The action of this active safety system is based on the gap between the vehicle's ideal behaviour and the actual one. Actuators are regulated to minimize this difference (control deviation), indirectly or directly influencing the forces acting at the tires. The workflow is represented in Figure 2.22.

According to the majority of the current SoA, a ESP controller has a three layers hierarchical structure [22, 96].

1) *Reference Generation*: the VDC is the uppermost layer and deals with the reference path generation. It combines information from sensors and estimators (concerning driver input and vehicle dynamical states) to establish an ideal desired drive path. This reference is intended to be followed by the lower controller's levels to ensure stable and comfortable vehicle behaviour. Typically, the reference path relies on both the ideal yaw rate and side-slip angle.

2) *Control Effort Definition*: in the intermediate level the control efforts are calculated as a function of the information arising from the upper-level sub-controller. Depending on the actual dynamical state and driver demands, optimal control signals are defined for the available actuators to achieve the intended goals. In particular, the defined signals can be the desired vehicle yaw moment, as well as the ideal steering wheel command.

3) *Actuator Allocation*: the optimal control efforts are converted into actuator's references (e.g. driven wheels or equipped BW systems). As an example, the desired yaw moment can be mapped into equivalent torque demand for each wheel. In the case of steering control, the corrected steering command is applied to the steered wheel as a contribution to the driver's demand.

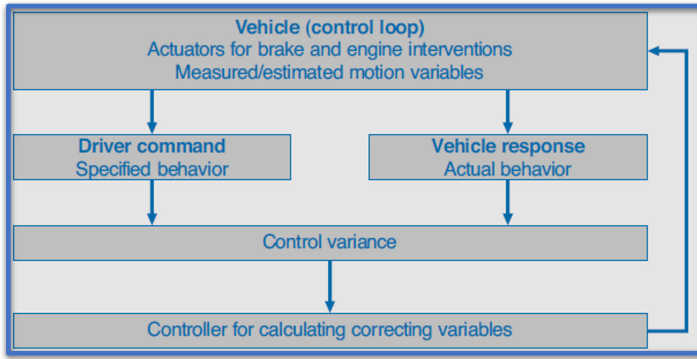


Figure 2.22: Workflow diagram of ESP (Figure from [9])

Figure 2.23 show a simplified schematic diagram of ESP and its main components:

- Sensors: which measure the dynamical states, representing the input parameters of the controller;
- ESP control unit: constituting the core of the controller. It features the high-level task and the integration with the other safety-relevant CUs;
- Actuators: like brake, engine and in some cases, steering system, used for the application of the control efforts.

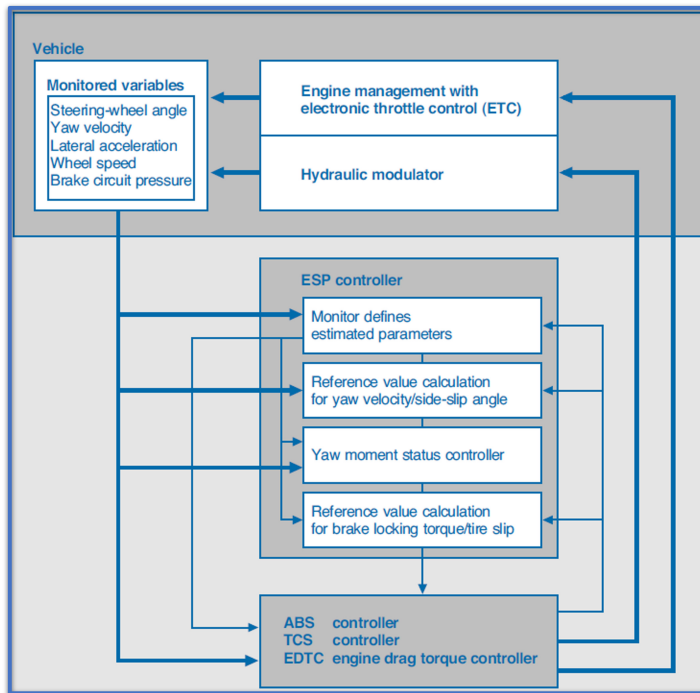


Figure 2.23: Simplified block diagram of ESP (Figure from [9])

Thus, the responsibility of the ESP sub-layers concerns the determination of the desired and current vehicle status, the definition of the optimal control efforts and the regulation of the actuators to achieve maximum convergence between the vehicle's response and expected ideal response. The desired vehicle behaviour is obtained from the driver demand, by merging the information arising from Motor Control Unit (MCU), Brake Control Unit (BCU) and Steer Control Unit (SCU). The current behaviour is calculated from the vehicle states, either sensed or estimated. Monitored variables, which are directly measured (i.e. yaw speed, steering-wheel angle, lateral acceleration and longitudinal speed) can be used to determine lateral forces on the wheel, tire slip angles, vehicle side-slip angle and vehicle lateral speed. The trajectory correction is obtained by the generation of a yaw momentum around the vehicle's vertical axis and/or correcting steering command. These efforts are allocated to motors, brakes and steering systems. When braking or accelerating the wheels the tire slip rates are modified to indirectly influence the longitudinal and lateral forces. To avoid excessive slippage burden on subordinated ABS and TCS controllers. Indeed, keeping wheel slip within a limited range could maximise the available traction force and retain a lateral force capability to maintain vehicle directional stability.

### 2.4.2 Control Theory

In the SoA, ESP system intends to address the specific needs for ride and handling qualities of a vehicle, and how it responds to environmental disturbances and driver control inputs. It is important to distinguish these definitions. Good ride handling requires appropriate feedback through steering and pedal systems, thus is related to driver perception. Ride quality concern the vibration feel and deal with passenger comfort.

Innovative lateral stability controllers directly govern the two status parameters of yaw speed  $r$  and side-slip angle  $\beta$ , which are the most significant variables of the vehicle lateral motion behaviour. The entity of the applied yaw moment may depend on the deviation between these values and the reference one. The ideal response of the vehicle can be based on a single-track model, while the dynamic patterns can be determined from steady-state skid-pad testing.

It is important to limit the target variables with the available friction to keep the vehicle on the predefined physically feasible track. In particular, passenger cars can achieve up to  $10m/s^2$  lateral acceleration. However, the linear region is restricted to  $0.5 - 5m/s^2$ , where the vehicle motion can be described by the single-track model. In the critical range above  $5m/s^2$ , the car response is highly NL.

When a vehicle is oversteering (tendency to rotate too quickly) and the reference yaw speed is exceeded, the ESP should brake the outer-curve wheels and accelerate the inner-curve wheel to generate a yaw moment which impresses a counterclockwise rotation on the body, thus suppressing the vehicle's tendency to break away. Viceversa, in understeering situations (tendency to rotate too slowly around its vertical axis), braked and accelerated wheels are inverted as compared to the previous case to impress a clockwise rotation, thus suppressing the vehicle's tendency to push over the front axle. Both cases are represented in Figure 2.24.

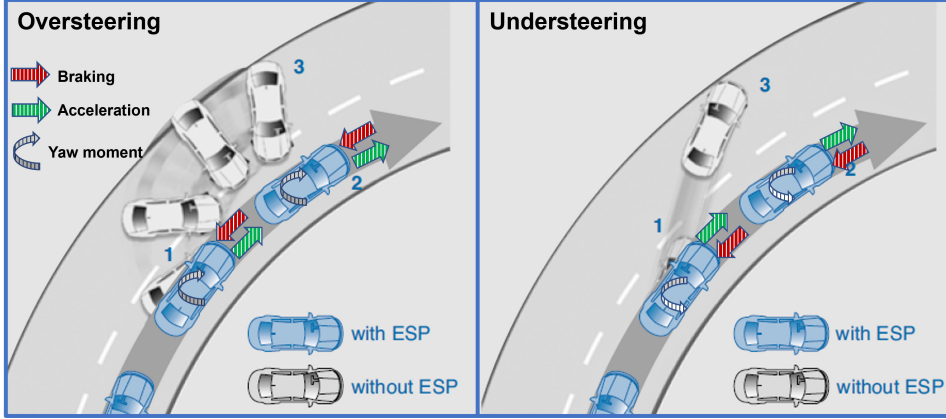


Figure 2.24: Over and understeering vehicle behaviors during cornering and ESP control efforts (Figure from [9])

According to current vehicle acceleration, a longitudinal load transfer occur between the front and rear wheels. Thus, when deciding how to allocate the yaw moment on wheels, maintaining a proper axle torque distribution assume relevant importance. When braking, the front wheel's vertical forces increase and so should do the demanded forces on related tire-road interfaces. On the other side, during acceleration phases, rear wheels should be prioritized. In general, the ideal torque distribution introduced in Chapter 2.1.2 and visible in Figure 2.11 should be respected to avoid wheel slippage or spin. This ensures an increased stability margin since a greater yaw moment can be delivered.

A general explanation of how conventional ESP works is given here. If the states of the car (yaw rate  $r$  and/or side-slip angle  $\beta$ ) differs from its nominal values ( $r_{id}$  and  $\beta_{id}$ ), the dynamics controller firstly checks if this difference is within some tolerable dead zone  $\Delta r_{DZ}$  and  $\Delta \beta_{DZ}$ . If the control errors (2.42) and (2.43) exceed the dead zones, a yaw moment has to be generated to let the controlled states converge to the reference ideal states. Human behaviour is accounted for in the algorithm, reducing the response time of yaw velocity control action until the nominal slip angle of the car is reached. This is done to counteract the driver's tendency to increase the steering angle[95].

$$e_r = \begin{cases} 0, & \text{if } r_{id} - r \leq \Delta r_{DZ} \\ r_{id} - r, & \text{if } r_{id} - r > \Delta r_{DZ} \end{cases} \quad (2.42)$$

$$e_\beta = \begin{cases} 0, & \text{if } \beta_{id} - \beta \leq \Delta \beta_{DZ} \\ \beta_{id} - \beta, & \text{if } \beta_{id} - \beta > \Delta \beta_{DZ} \end{cases} \quad (2.43)$$

The specifications of the control algorithms, however, are completely unknown from our side, since the companies do not intend to spread this information. Nevertheless, we can assume, from empirical and reverse engineering consideration, a Proportional Derivative (PD) control approach according to (2.44).

$$M_{yaw} = k_r e_r + \Delta_r \dot{e}_r + k_\beta e_\beta + \Delta_\beta \dot{e}_\beta \quad (2.44)$$

## Direct Yaw-Moment Control

Most diffused ESP are based on DYC. As pointed out, an induced yaw moment, generated on a vehicle by an uneven left-to-right torque distribution, leads to a change in the yaw velocity of the car. This can be applied by controlling the slip at each wheel and actuating brakes and motor.

When the aim of the ESP control system is to track the desired yaw rate, its feasibility appears easily implementable, since the rotational speed around the vehicle z-axis is simply observable with common automotive sensors (e.g. IMU) [3].

To fully exploit the DYC capabilities, accurate tire-road friction estimation is useful to update the reference yaw rate. This is especially true for continuously active ESP, which demands a smooth reference yaw rate profile. Supposing a friction coefficient greater than the actual one may lead to an oversteering behaviour since the controller over-estimated the available adhesion and apply not-negligible control efforts. On the other hand, when under-estimating the available friction the control actions can be insufficient for the stability purpose. As mentioned before however, the adherence conditions are hard to be estimated.

The actuation of this strategy can be done using conventional dissipative brakes, electronic differential or WIM. The first solution causes a vehicle speed reduction, thus compromising driveability and comfort. For this reason, is recommended in emergencies only. TV capable differentials introduce significant complexity and cost. Finally, independent motor solutions are far the most desirable due to the faster bandwidth response and precise individual torque control [97].

## Yaw Rate and Side-Slip Angle Control

As an alternative to continuously updated reference yaw rate based on friction status, the ESP can be coupled with a side-slip angle controller [98]. Highly performing lateral control systems intend to track both desired yaw rate and side-slip angle, whose superior stability improvement has been widely studied and proven. As claimed by Tchamna et al. [99], yaw rate is mainly related to driving feeling, while side-slip deals more with stability and handling [100].

Shibahata et al. [101] explain through the  $\beta$ -method that to preserve a good vehicle handling even in severe cornering situations and prevent it to spin, ESP has to limit the side-slip to ensure acceptable yaw moment gain. If  $\beta$  reach the critical values driver may experience vehicle control loss and may start to panic. ESP must intervene before it happened. However, at the characteristic slip angle values, a large yaw moment can still be generated by [102].

When considering solely vehicle kinematic behaviour, the side-slip angle depends upon lateral acceleration, vehicle mass distribution and rear axle slip angles. If a dynamic modelling approach is used, its value is influenced by the tyre's properties and road conditions too (e.g. cornering stiffness, friction coefficient). Indeed, when a poor tire-road condition occurs (e.g. wet or icy roads) side-slip angles exhibit a larger variation gradient. Side-slip angle and its rate serve also as driver feedback, providing important information in the eventual upcoming instability, affecting the user's perception and confidence with the vehicle [47].

Due to the NL characteristics of the pneumatic, a prompt control action from the ESP is fundamental to prevent the side-slip angle to become too large, especially in low friction conditions. So, the intervention must be quick enough to avoid the wheel's behaviour to digress into the saturation range. Otherwise, can be too late to

restore vehicle controllability. This control solution is more complex to be realized due to the difficulty in the vehicle's actual  $\beta$  measurement. Unfortunately, no sensor for the direct measurement of side-slip angle and adhesion in the tire-road interface is available, so these missing variables require a robust estimator.

Furthermore, the concurrent yaw rate and side-slip angle control represent an important challenge, since this contemporaneous regulation deals with contrasting requirements: control objectives cannot be simultaneously achieved and are likely to be contradictory. That implies a proper tuning of the controller to achieve the desired vehicle behaviour. Thus, an optimal compromise between these requirements is needed [22].

Most common lateral dynamic approaches consist of a yaw rate tracking controller coupled with a side-slip angle limiter. Despite this, a considerable part of the literature deal with cooperative regulation of both [100]. The latter are Multiple Input Single Output (MISO) controller, with the desired yaw moment as the sole output. Alternatively, two separated Single Input Single Output (SISO) controllers can be used to track individually yaw rate and side-slip angle, where the ultimate control effort is chosen between the two with a predefined criterion, e.g. weighting factor or prioritization. A viable solution is a SISO controller, in which the reference yaw rate is corrected as a function of the actual side-slip angle. In this ambit, many works are available in the literature. Lenzo et al. [22, 98, 103] present a summary of the activities in this field and develop a switched linear system validated using phase-plane analysis, virtual simulations and real-world experimental data. The controller proves to be effective in the continuous control of yaw rate and side-slip angle.

### 2.4.3 ESP Control Solutions

The vehicle dynamic of conventional automobiles has been well understood and various active lateral control systems have been developed to enhance dynamic performance and driving safety. These systems are highly effective from a safety perspective and represent a standard for every vehicle in the market.

Vehicle motions in the roll-plane, pitch-plane and yaw-plane of EVs need further investigation. Indeed, these aspects are strictly correlated, affecting vehicle dynamics and controls in a very complex manner. Although their mutual interaction, stability and performance characteristics can be partially decoupled [73]. The integration of such control systems can bring further advances in in-vehicle dynamic characteristics and stability, typically developed in stand-alone conditions.

Vehicle handling performance and directional stability are characterized by the yaw dynamic behaviour and control strategies. Here, the most important aspect concern the combined steady and transient-state handling characteristics. Indeed, an optimal trade-off between vehicle steering responsiveness (depending on yaw rate and lateral acceleration) and directional stability (influenced by side-slip and roll angles) must be achieved.

The steady-state vehicle cornering dynamic is determined by the set of vehicle design and chassis tuning parameters (e.g. geometrical parameters, front/rear load distribution ratio, tyre stiffness properties). When using an e-powertrain these properties can vary, thus modifying the steady-state vehicle lateral dynamics. Transient-state, in a similar way, strongly depends on vehicle mass, yaw moment of inertia and damping. A desired transient cornering behaviour must ensure the greatest lateral response to be perceived on the front axle (yaw motion pivoting

about the rear axle), followed by a roll motion. Responses should be smooth and with reduced overshoot. Even in this case, an electrified powertrain can alter the transient-state response negatively, due to the lesser DoF in the vehicle's packing and due to heavy batteries.

Modern and future handling control solutions should also increase driver enjoyment and fun-to-drive. Brake-based systems are highly intrusive since can cause sudden and abrupt deceleration. To solve this problem, alternative actuation and control systems are therefore being considered to provide vehicle stability without the intrusiveness effect of current control approaches.

## Literature Review

The simplest implementation for a ESP control algorithm is based on Proportional Integral Derivative (PID) control methodologies [104–111], using as a feedback the errors between reference and actual state variables. PID controllers require a model linearization about an equilibrium point [100]. However, when vehicle behaviour becomes non-linear this approach performs poorly.

Even fuzzy logic has been extensively investigated, which is a knowledge-based control approach [112–114]. An additional drawback of these strategies is related to the higher level of abstraction for vehicle dynamical modelling, as well as the tuning process.

In recent literature, other control methodologies have been proposed and investigated to address the above gaps. More advanced solutions rely on complex control theory, which adopts a model-based approach. It is important to note that model-based controls suffer from model uncertainties, system parameter variations and disturbances [97]. These aspects must be considered for a robust design. Gain scheduling could be a useful tool for online controller tuning.

Model Predictive Control (MPC) are widely adopted [30, 32, 115–121] due to the recognized advantages: allows the predict the future vehicle behaviour and to define an appropriate control action in RT; enable the management of several actuators while accounting for the corresponding constraints at each time steps [100]; the high flexible formulation consent to consider model non-linearities or time-varying features of the system [122]. Additional methodologies includes  $H_\infty$  [123–126], linear parameter varying controllers [127] and Linear Quadratic Regulator (LQR) solutions [97, 105, 114, 128–134]. The latter resolve the Jacobi-Riccati equation for the optimisation the controller gain. Robust control, such the ones of [135–137] are available in the SoA. Many ESP strategy based on SMC have been proposed [39–42, 99, 111, 138–141]. A comparisons between this model-based control approach is presented in [29].

In the recent SoA a comprehensive overview of the energy aspect of electrically driven cars is given. However, very little effort related to their dynamic is investigated, due to the perception that their behaviour is essentially similar to one of the conventional ICE vehicles. Thus, are treated to have the same fundamental characteristics [65] and the impact of vehicle electrification on dynamics and control systems has received minimal attention.

## Torque Vectoring

Torque allocation control has received substantial attention in the research field due to its highly desirable features from a stability perspective. Its first application concern the individual brake intervention to generate a yaw moment and perform DYC. This enhances the safety and driveability of the vehicle. Thus, variable torque allocation could also be performed with electronically controlled differential and twin-clutch torque biasing differentials, where the torque can be delivered to inner and outer wheels in different ratios [3, 98, 142]. Similarly, front/rear axle torque distribution can be actively controlled using the centre differential. However, this solution exhibits high manufacturing cost, weight and energy losses during its functionality. Moreover, with such a traction structure is impossible to allocate more torque on the faster wheel of the driven axle [22]. As an example, active differential or independently distributed traction layouts allows the application of active torque distribution techniques. These systems are traditionally known as traction-enhancing devices and have the potential for significant improvements in vehicle stability as compared to the conventional brake-based system while increasing driving comfort and enjoyability [143].

The ability to distribute desired amounts of torque at different wheels is known as Torque Vectoring. This feature can be exploited to improve active safety system performance, providing continuous and smooth control action to correct the vehicle handling and yaw response, by reshaping the vehicle's understeer characteristic [41, 106]. The adoption of this technology is a solution to many drawbacks and may enhance the traction and handling of the vehicle. Yaw stability control can be achieved during acceleration without requiring differential brake activation. Perhaps, an important topic is the integration of TV instability control. WIM offer many advantages for TV control, furnishing the opportunity for simple and efficient individual force control at the four wheels of a vehicle, which effectively overcomes these drawbacks. This makes appear the vehicle an over-actuated system, so the additional allocation DoF have to be carefully optimized for the specific objective (e.g. balanced tyre force based on tyre's friction circle, energy efficiency maximization) [73]. This aspect, along with the inherent non-linearities of the vehicle lateral response, introduces an important challenge for the ESP strategy design [122].

Different TV control algorithms can be employed depending on specific performance requirements [22], enabling the design of the cornering response with the additional benefit of increasing yaw and side-slip damping during transients [98]. In literature, the most common approach for the management of the multi-DoF solutions of TV control relies on optimization methodologies. In this way, modern ESP can allocate the wheel's torque to effectively improve handling characteristics, relying on a model-based approach. The main drawback of these solutions is the RT estimation of the vehicle's motion to update the reference model parameters, especially in abrupt cornering manoeuvres. Vignati et al. [144] further investigate these aspects, by developing a strategy that coupled the optimal LQR steady-state control theory, which uses an Extended Kalman Filter (EKF) for friction and side-slip angle estimation, with an index logic for the parameters update and the transient-state control [134]. The yaw index is directly related to the vehicle under-steering behaviour. The study has been conducted by comparing the results for different powertrain layouts. As pointed out, the 4WD layout with independent motors outperform the other traction architectures from a stability viewpoint.

# Chapter 3

## Proposed Approach

During the 3 years of my PhD journey, I mainly focus on the development of automotive lateral stability controllers. This choice has been driven by the interdisciplinary aspect of this task, which perfectly sticks with my acquired competencies and expertise. I'm a "hybrid" mechanical/automation engineer and this topic allows me to merge these skills, which required both knowledges of vehicle dynamic behaviour and robust control design. However, enhancing this aspect can appear extremely challenging, considering the complex interaction between involved systems and the large variety of driving conditions in which vehicles may operate. The growing availability of mechatronics and by-wire systems have recently engaged the interest of designers and researchers in the development of these controllers. Also, the rapid transition towards electric vehicles with non-conventional powertrain layouts is further increasing the opportunities, allowing to explore innovative control solutions which can be very costly or even not feasible using mechanical systems.

### 3.1 Research Question

The purpose of my research is aimed at answer a fundamental question:

**How can the EV's stability performances be improved?**

During the first year I concentrate my effort on a deep SoA investigation and literature review, acquiring competencies and knowledge on various topics of the electric automotive field: *Vehicle dynamics* [3, 43–45] and his interaction with the other safety-related on-board subsystems and stability controllers [9]; *Electric powertrain*, starting from the analysis of the traction architecture, high and low-level control strategies and power management [59, 72]; and *BW technologies*, which consent a better integration within mechatronics systems, such longitudinal and lateral stability controller [10, 11, 13].

What strongly emerge is that, among different possibilities, one feasible solution to answer the addressed research question is the *optimization of the electric powertrain management strategy* in combination with a *proper coordination within By-Wire systems technologies*, specifically BBW and SBW. Multiple aspects can benefit from this approach:

- From an energetic point of view, is found an increase in the vehicle's efficiency and autonomy due to the possibility to implement advanced energy management policies [65, 73, 78, 79];

- From a stability perspective instead, increased longitudinal and lateral stability can be reached, thanks to a faster bandwidth response and adoption of specific controlling techniques [65, 84, 91];
- For what concern the safety performances, the availability of an over-actuated system can bring reliability advantages, due to redundancy of the plant. Also, the possibility to implement an advanced control strategy can improve the functional safety aspect [91, 145, 146].

## 3.2 Open Problems

Before going into the core of my activity, it is important to highlight the major open problem that needs to be addressed to reach the intended goals of developing innovative control systems for lateral stability EV's improvements.

### 3.2.1 EVs Heterogeneous Solutions

The first very big challenge I need to address concerns the vehicle layout. Indeed, EVs are an established industrial reality and an academic growing topic. However, a wide range of different solutions has been taken into consideration for powertrain topologies, ESS and control strategies. This constitutes a major open problem. In particular, what is not well defined is which layout is the most feasible and suitable, considering the man-hour and economical cost, the industrial process trend and the required performances. These new vehicle concepts and technologies lead to a highly competitive and dynamic market. However, at this point, it is uncertain which solution prevail in the future. Manufacturers are proposing many different solutions each year, so it becomes important to develop controllers which are portable between multiple architectures.

In the past century, several kinds of traction architecture have been developed concerning driven wheels. However, a conclusive solution for the best package has not been found [147]. This fact is even aggravated by vehicle electrification, one of the main trends in current vehicle development, enabling the development of a multitude of hybrid and full electric configurations. More than 350 EVs were presented between 2002 and 2012. About 130 of these vehicles are produced in series and available in the market. Another 220 e-vehicle solutions are proposed as concepts or prototypes by OEM. The trend which emerges clearly shows the growing importance of EVs.

Considering the different e-machine which are available, a classification can be proposed respect to [56, 71]: technology, traction configuration, performance, manufacturability and cost. EM can be installed in several configurations: one single central motor, axle-split-motor and inside the wheel-hub (IWM). This last layout usually supposes 2 or 4 motors, allowing for superior driving dynamics in terms of TV and all-wheel drive.

The introduction of supplemental energy storage and energy converter devices consented to the OEM to improve efficiency performances while meeting the ambitious CO<sub>2</sub> reduction targets. This leads to a variety of different propulsion concepts being investigated. In EVs, the ESS can be realized with different technologies, e.g. batteries, super-condenser, fuel cell, and so on. Recently, the use of Lithium-Ion batteries set a clear trend. However, in the long term, it is not yet sure which battery will be the most competitive [71].

### 3.2.2 Technical Challenges in ESP Developments

Many challenges can be encountered when developing ESP solution, which can be categorized as driver intent recognition, control development philosophy and vehicle side-slip estimation [148, 149].

#### Driver Intent Recognition

An active stability control system affects the vehicle's attitude and motion, a function normally reserved for the driver. For this reason, it needs to accurately interpret the desired driving path of the pilot to provide added directional control, without compromising the driving intention. The driver expresses the directional intent through the steering wheel and the pedals. The challenge is to improve customer value by using reliable sensors and developing algorithms that quickly and accurately determine the driving intention and apply control effort following the desired motion behaviour. The basic approach to determining the driver's directional intent is to establish the desired yaw rate based upon a simplified vehicle bicycle model. This information will then be used by the controller to understand when it needs to intervene to control the vehicle. Comfort and confidence are ensured if the ESP action appear responsive to the driver's commands, dynamically consistent with the base vehicle, smooth and reasonably constrained by the physical limits of the vehicle and road surface. It is important to note that the reference kinematic model has to be tuned with the following parameters: mass, CoG location of the front and rear axles, the moment of inertia in the yaw axis, front and rear cornering stiffness and the maximum yaw moment [150].

#### Control Development Philosophy

The literature about the lateral stability control for Distributed Drive Electric Vehicle (DDEV) is huge. To cite only few, consider the following [23, 24, 26, 27, 64, 84, 86, 105, 114, 123, 148, 149, 151–170]. These papers address the specific need for the definition of a robust and reliable TV control for over-actuated WIM driven vehicles. At the same time, is important to ensure a good trade-off between control action and informing the driver that the cornering capability has been reached.

To maintain the same vehicle's handling characteristic in all operative situations the control efforts should be progressive and non-intrusive in entity to increase sensitivity and prevent provoking a panic reaction. Also, the deviation should not be zero, but small to advert the driver of the adverse driving conditions. Without this feedback, the driver could be deprived of critical information necessary for adapting to the driving behaviour. To summarize, transparency, progressive and non-intrusive stability control concepts can contribute to a safer driving experience, optimizing the driver-environment-vehicle interactions. In the meanwhile, the action by ESP must appear reliable, effective and smooth in the rejection of disturbances introduced by the surrounding environment. This constitutes a challenge in stability control, which consider both increased stability and driver's perception.

This heterogeneity in the adopted control approaches suggests that a predominant methodology has not been identified yet. For this reason, it is fundamental to develop controllers distributed in more layers with modularity and integration features.

## Tire Slip Estimation

Tire-Road Friction Estimation (TRFE) is an important research area as the interest in information technology in vehicles increases. Its objective is to predict the value of the traction force each wheel can provide. Friction coefficient  $\mu$ , introduced in section 2.1.1, depends on the type of road surface condition, such as icy, snow-covered, gravel, and dry asphalt.

For achieving the best performance in active stability controls, an accurate RT TRFE is needed. Indeed, for DYC controllers, the knowledge of the actual tire-road friction is fundamental to determine the desired yaw rate of the vehicle, ensuring its safety under all driving conditions: this will improve the performance of ESC on slippery surfaces, prevent the slip angle from becoming too large, reduce high lateral acceleration and avoid vehicle's skidding. Another benefit of TRFE is to inform the driver (machines or people) of dangerous conditions so they can change their driving style to prevent emergencies [171]. For adaptive cruise control and collision-avoidance systems, estimating  $\mu$  enables the braking distances to be adjusted in real-time, thus improving the safety and effectiveness of these active controllers.

Research in tire-road friction modelling and estimation for individual vehicles is abundant [19, 171–178]. The “magic formula” gives a good approximation of experimental results and is widely used in automotive research and industries. However, this model is analytically complex and its parameters are difficult to be identified. Therefore, the Pacejka formulation is mainly used for simulation than for control purposes.

TRFE approach can be classified into two branches. **Direct friction sensor methods** uses special sensors that directly attempt to measure friction coefficient. Acoustic sensors and optical sensors solutions have been investigated in the literature. Also, a method based on strain sensors vulcanized into the tire treads for measuring the tire deformation, and thus the tire-road forces, is proposed in [179]. However, direct friction sensor methods suffer from reliability and robustness problems, along with a not-negligible cost. Due to these issues, **vehicle-dynamics-based estimation methods** are far the preferred solutions. Here vehicle motion information is used to indirectly estimate the friction coefficient. The main advantage of this solution is that utilizes only sensors that are commonly available in every road vehicle equipped with an ABS. The goal is to compute certain parameters from standard sensors in the car, which depend directly or indirectly on the friction. Again, these solution can be divided into two categories [179]:

- Average Friction Coefficient Estimation: the friction coefficient is assumed to be the same for all the wheels. Some examples are slip-slope methods, Kalman filtering and lateral-dynamics-based solutions;
- Individual Wheel Friction Coefficient Estimation: the friction coefficient is independently estimated for each wheel. This enables both traction and stability control systems to provide optimum drive torque and/or brake inputs to the individual wheels to maximize traction, reduce skid and enhance stability.

However, the dynamics-based estimation method exhibit the following issues: it requires the design of an adaptive parameter estimator able to track fast parameter variations; needs the determination of the physical relationship between these parameters and the maximal friction forces [180].

## Side-slip Angle Estimation

The primary objective of an ESP is to provide vehicle stability and handling predictability, achieved by reducing the deviation of the intended lateral response as compared to the actual one. The lateral response of the vehicle can be described not only by yaw rate but by a combination of it with side-slip angle, side-slip gradient and path radius of curvature.

When trying to control a vehicle's cornering behaviour, both yaw and side-slip dynamics should be accounted for in a robust design. Indeed, yaw rate can be easily measured through sensors, e.g. Inertial Measurement Unit (IMU). However, the definition of a target yaw rate requires a reliable tire-road friction estimation, which is difficult to obtain.

The side-slip angle cannot be directly sensed and must be estimated using state variables. This estimation has been a major challenge since the first ESP implementation in the early '90s [47]. Among the many possibilities available in the SoA, the estimation methods can be grouped into observer-based (which uses a vehicle reference model) or network-based (which adopts an input-output black-box relationship). However, complex models are needed and sensed variables may be the object of drifts and uncertainties, while Artificial Neural Network (ANN) need continuous RT updating [47]. To date, there is no commercial ESP system based on side-slip angle measurement. Thus, if considering the side-slip angle  $\beta$  according (3.1), another challenge concern the integration of ESP with robust estimator of vehicle lateral speed in the presence of road surface friction coefficient estimation, vehicle model uncertainty, sensor noise and bias [150, 181].

$$\beta = \tan^{-1} \left( \frac{V_x}{V_y} \right) \quad (3.1)$$

Estimation of  $V_y$  involves the knowledge of tire lateral forces, tire slip angles, normal forces and adherence coefficient in the tire-road interface [150, 181]. For example, the observer can be based on yaw velocity and lateral speed vehicle dynamic equations [181]. The side-slip angle can be estimated using the differential equation (3.2), valid when neglecting pitch and roll angle and moving on a flat road.

$$\dot{\beta} = \frac{1}{1 + \beta^2} \cdot \left( \frac{\dot{V}_y}{V} - r - \beta \frac{\dot{V}_x}{V} - \beta^2 r \right) \quad (3.2)$$

If the slip-angle is small and the vehicle velocity is constant, (3.2) can be simply integrated. However, depending on driving conditions, the accuracy of vehicle side-slip angle is different. Since a reliable value of  $\beta$  can't always be obtained, a cascade control with a yaw speed inner-loop control can be introduced to constitute a good basis for the outer loop slip angle control. This strategy is a model following control. Using a vehicle single-track model a first value of the nominal yaw velocity  $r$  is obtained (3.3), where  $L$  is the wheelbase,  $K_{steer}$  is the steering ratio and  $V_{ch}$  the characteristic speed. This relation is valid only in the linear region of the tyre characteristic [181].

$$\dot{\gamma} = r = \frac{V_x \cdot \delta}{L \cdot K_{steer} \cdot \left[ 1 + \left( \frac{V_x}{V_{ch}} \right)^2 \right]} \quad (3.3)$$

However, when  $\beta$  rise, the yaw moment gain decreases. This means that at large slip angles the vehicle's lateral motion, and thus the yaw moment, is hardly influenced by steering command. In these conditions, the manoeuvrability of the car is compromised, since the stability requirements demanded by yaw rate and side-slip angle tracking are difficult to be achieved contemporaneously. Thus, limiting  $\beta$  while achieving increased vehicle stability performance is difficult. For instance, the steerability physical limit is reached for  $\pm 12deg$  on dry asphalt roads, while is about  $\pm 2deg$  on ice. So, when the friction coefficient with the road is low the controller may not be able to entirely achieve the nominal value that would be reached on a high-friction surface and the DYC would only partially succeed.

### Yaw Rate and Side-Slip Angle Saturation

It is important to define a saturation limit for the yaw rate and side-slip control in dependence on the maximum friction coefficient  $\mu_0$  between the tyres and road. Nominal yaw speed needs to be limited through (3.4) and (3.5). Accordingly, saturation for side-slip control can be derived using the  $\beta$  method [181]. Alternatively, side-slip angle can be limited according to (3.6) and (3.7).

$$|\dot{\gamma}| = |r| \leq \left| \frac{\mu_0 \cdot g}{V_x} \right| = |r_{bound}| \quad (3.4)$$

$$\begin{cases} r_{tar} = r & \text{if } |r| \leq r_{bound} \\ r = r_{bound} \cdot \text{sign}(r_{des}) & \text{if } |r| > r_{bound} \end{cases} \quad (3.5)$$

$$|\dot{\beta}| \leq |\tan^{-1}(0.02\mu g)| = |\beta_{bound}| \quad (3.6)$$

$$\begin{cases} \beta_{tar} = \beta & \text{if } |\beta| \leq \beta_{bound} \\ \beta_{tar} = \beta_{bound} \cdot \text{sign}(\beta) & \text{if } |\beta| > \beta_{bound} \end{cases} \quad (3.7)$$

Since these simplification assumptions can lead to a poor estimation, an observer based on a 4-wheel vehicle model can be used. The characteristic handling behaviour of the car may change during its lifetime (e.g. due to tire wear), so these modifications have to be carefully considered.

### 3.2.3 Legislation & Standards

Apart from technical issues, which should be accounted for when developing a new ESP system, also legislation and standards must be considered. To assist designers in ensuring the highest safety standards and lead the development of safe automotive systems, specific regulations should be investigated.

*ECE R-13* & *R-79* regulates respectively brake and steering automotive systems. Both of them must be respected when high-level interactions of these systems exist with ESP controllers. In particular, UN/ECE R-13H requires all M1 category vehicles to be equipped with directional stability controllers, including ESP. Performance requirements for this system concern the result of Sine with Dwell (SwD) open-loop manoeuvre. The functionalities shall be demonstrated by the comparison of the vehicle with stability control enabled and disabled for given test boundary conditions. Additional tests may be done, e.g. reduced radius test, steady-state circular test, asymmetrical one-period sine steer and double lane change manoeuvres

[181]. Moreover, since all the investigated stability algorithms are implemented through ECU, standards related to these devices must be ensured. To cope with the growing complexity of E/E systems, vehicle manufacturers have to comply with different regulations.

## ISO 26262

The automotive industry is entering a new era of EV and HEV. The increased presence of E/E devices, devoted to improving efficiency, driver comfort and performance, has reached a humongous limit. This rapid growth has to be carried out to guarantee the achievement of required target levels of quality and functional safety features as an integral part of each automotive system's development phase.

The management of safety-critical decisions by the E/E system in the automotive sector inevitably increases the complexity of the vehicle architectures, where electronic devices can provide several functionalities, especially for active dynamic control purposes. The *ISO 26262* series of standards [182] is the adaptation of IEC 61508 [183] to address the sector-specific needs of E/E systems within road vehicles. It concern the functional safety, defined as the absence of unreasonable risk due to hazards caused by malfunctioning behaviour of systems.

The development and integration of this component must follow a specific process and respect several criteria to prove their safety since whenever mechatronic and software systems are used, the intrinsic systematic and random failure risk always exists. ISO 26262 intend to provide guidance and tools to develop such vehicular systems, avoiding dangerous failure and proving their reliability for the addressed tasks. Furthermore, it provides a risk-based approach to determine the ASIL classes, useful for specifying an item's safety requirements for achieving an acceptable residual risk during a predefined operational situation. ASIL of a specific fault modality can be determined through 3 parameters and its values ranging from QM (minimum) to D (maximum). ISO 26262 guide developers in the definition of *Severity*, *Exposure* and *Controllability*.

*Severity* is related to the level of risk for the users resulting from the fault occurrence. This value is established using the Abbreviated Injury Scale (AIS), developed by the Association for the Advancement of Automotive Medicine. Respect to these values, the standard provides a direct correspondence with a new scale ranging from *S0* (min) to *S3* (max).

*Exposure* is strictly dependent on the probability to be in a specific driving scenario in which the fault could occur. All the operative situations should be considered, e.g. road condition and typology, weather conditions or performed manoeuvres. In this work, both the table proposed by IEC 61508 and ISO 26262 are considered. Exposure value range from *E0* (incredible) to *E4* (high probability).

*Controllability* replicate the concepts of fault detection and reaction, indicating which amount of common driver can manage and handle the considered fault event to avert or minimize the extent of risk. Even in this case, the standard proposes a corresponding table, with values ranging from *C0* (controllable in general) to *C3* (less than 90% of drivers can handle the harm situation). These parameters could be mitigated by appropriate reports to inform the driver and diagnostic procedures.

When investigating a specific device, related task and working conditions, the equivalent ASIL is determined according to Table 3.1.

Severity	Exposure	Controllability		
		<i>C1</i>	<i>C2</i>	<i>C3</i>
<i>S1</i>	<i>E1</i>	QM	QM	QM
	<i>E2</i>	QM	QM	QM
	<i>E3</i>	QM	QM	A
	<i>E4</i>	QM	A	B
<i>S2</i>	<i>E1</i>	QM	QM	QM
	<i>E2</i>	QM	QM	A
	<i>E3</i>	QM	A	B
	<i>E4</i>	A	B	C
<i>S3</i>	<i>E1</i>	QM	QM	A
	<i>E2</i>	QM	A	B
	<i>E3</i>	A	B	C
	<i>E4</i>	B	C	D

Table 3.1: Exposure classes according ISO 26262

### 3.2.4 Standardization

The previous described open problems (availability of heterogeneous vehicle solutions, technical challenges and normative specifications) need to be addressed. As a consequence, there is a clear need for simple, computationally efficient, easily tunable, and effective solutions for the control design, aimed at drivetrain optimization.

To overcome it is fundamental to develop mechatronic control algorithms accounting for these requirements and dealing with issues related to code modularity, customization for different vehicle layouts and easy integration with higher-level functionalities (assisted or autonomous driving and coordinated/inter-vehicle functionalities, like platooning). Standardization is essential in the optics of implementing and integrating controllers in a multi-layer structure. This ensures modularity and interfaceability characteristics. All the proposed systems must respect important features to be validated through simulation activities: scalability, abstraction, parameterization, modularity, flexibility and RT capability.

For doing this **model-based methods and tools** are used. The coherence of the models with these features is fundamental for ensuring portability between different vehicle architectures and autonomous driving implementation purposes.

## 3.3 Model-Based Methods and Tools

This work intends to provide development tools that use physical/mathematical Time Continuous (TC) models coupled with Time Discrete (TD) control algorithms for an exhaustive virtual assessment of the developed solutions. The models must show high portability and allows their reuse ("plug-and-play" feature). Also, the computational load have been appropriate for the target hardware, so it should be kept low as possible. Indeed, the proposed control algorithm should address specifications regarding computational limits of on-board ECU installed on vehicles, in order to better exploit distributed or heterogeneous computational resources that should cooperate through industrial field bus or wireless connections.

Simulation models can be used to investigate key design aspects, especially in the early development phases, where no prototype is available. These include all the models which are explicitly aimed at investigating physic phenomenological aspects of a system or process. This is even more important when developing vehicular control and mechatronic systems, where the cost and risks related to prototype testing are extremely severe.

Automotive vehicles are becoming more and more complex due to the increasing number of mechatronic systems. Thus, simulation efforts for combining all the sub-sub systems in a single platform are rising as well. The desired solutions require that these sub-models are available in a central library with specific documentation, describing the physical behaviour, equations and interfaces.

At this point, another question may be asked: *Why I should follow a model-based approach? In which way it could be useful?* There are many reasons, which must be sought for the development of mechatronic control systems.

### 3.3.1 V-shaped Development Model

Industrial products typically follow a development V-shaped model process. This is composed of a top-down *Verification Phase* (concerning the virtual assessment), a horizontal *Manufacturing Phase* (where the device is physically deployed) and a bottom-up *Validation Phase* (using a real prototype of the investigated products). These main phases are subdivided into sub-tasks, assisting the designer and supplier through the whole development process.

The **Verification Phase** is the first one in the V-shaped deployment model and consists of a virtual assessment of the components. This stage relies mainly on Model-in-the-Loop (MiL) simulations, with the objectives of overall optimization and achieving a detailed system understanding. Is composed of the following sub-tasks:

- Requirement Analysis: consist in obtaining enough detail to know when a design has solved the problem satisfactorily. Desired performances and functionalities must be expressed to support the engineering decision. This step forms the basis for a model system description;
- System-level design: the product is framed in the whole system architecture, considering all the involved physical domains and sub-systems it interacts with. Multiple concepts that might satisfy the requirements are identified here;
- Component-level design: targeting the single product or element.

In every design level requirement specifications are accounted. Similarly, performance specifications, describing how a requirement can be met, are given to the following levels to validate the correctness of each design stage.

The **Manufacturing Phase** is where the device is physically produced as a prototype, using the information and guidelines arising from the previous phase.

Once the product is available, the bottom-up **Validation Phase** starts. This stage retraces the same level of the verification phase but in the opposite direction using real components.

The process is inherently recursive, with each high-level design decision producing a simpler design problem at a lower level of abstraction, whose schematic flow-chart

is visible in Figure 3.1. This allows to significantly shorten the development time due to the usage of simulations, rapid prototyping and simultaneous engineering tools. This enables a continuous exchange between verification and validation phases to improve the design aspect and propose suitable/tailored products through an organized process.

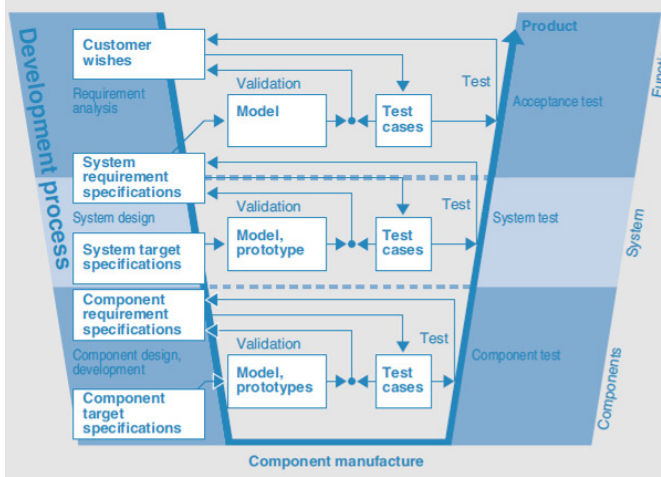


Figure 3.1: V-shaped development model (Figure from [9])

Mechatronic systems are evaluated at component and system levels to verify the appropriateness of the developed solution for the requirement specification. This ensures an easy and reliable exchange in both horizontal and vertical directions. According to Bosch, this methodology yields multiple benefits. Design quality can be increased from the early stages of development, while efficiency increase too. Also, the variants of the product can be evaluated easily before the physical realization, ensuring higher flexibility due to the model-based system design description [10].

### 3.3.2 Mechatronic System Simulation

Conventional design methods for the vehicular mechatronic system are sequential and the different engineering domains are managed and optimized individually, before being integrated. Nevertheless, the design of such devices requires a holistic approach. To deal with the mechatronic system design challenge, Bosch started the initiative "Systems Engineering Mechatronic", to reach higher design efficiency (time and cost) and quality [184].

There are two ways engineers and companies develop mechatronic systems. The first approach is the so-called *Functional Modelling*, based on conventional design methodologies for mechanical disciplines. As the name suggests, it is focused on user-defined functions the modelled system has to perform, by capturing and processing the information about its goal and the roles of its components to fulfil the purpose. The second one is the *Model-Based Design*, situated in the context of Model-Based System Engineering (MBSE) [10, 52]. Several attempts to standardize this approach have been done. This solution allows to model and simulates any part of the system within one environment using a graphical model to describe the project requirements and identify issues in the early phase, to reduce the products

TTM. MBSE is formalized and supports different modelling languages. In contrast with functional modelling, it allows the reuse of the proposed model as a basis to create, specify and explore system variants. The development criteria are a higher level of abstraction, modularity and support tools.

The conceptual and logical differences in the virtual assessment of software, electrical and mechanical systems reside in the development methodologies and traditions coming from the respective disciplines. These factors make the design and modelling of mechatronic systems difficult when using a holistic approach, due to their domain-spanning feature. Other key points should be considered when simulating mechatronic solutions: suitable abstraction level of the physical modelling and software design for efficient handling; integration with control part; choice of the right virtual simulation tools.

To mitigate the enormous complexity, time and costs involved in the development of vehicular mechatronics systems, legislation has allowed the use of simulation tools and methods to complement physical testing. For example, an important aspect of UN/ECE R-13H is that both real word tests and computer simulations test results may be submitted for validation, under certain conditions. So, within specified limitations, this normative explicitly allows the use of simulations to establish the effectiveness of the proposed stability control algorithm. Even ISO 26262 standard authorize the adoption of virtual assessment. It provides methods and techniques which should be integrated into the development process to ensure the required functional safety level of E/E devices in road vehicles. In particular, it states the necessity to assist traditional reliability assessment solutions, e.g. FMEA, Failure Mode, Effect and Criticality Analysis (FMECA), Fault Tree Analysis (FTA) or Block Reliability Diagram (BRD) with FI simulation strategy.

### 3.3.3 Vehicle Dynamic Simulation

When dealing with automotive stability controllers, vehicle dynamics play an important role in their development. If a simulation approach is adopted, it is important to properly model the dynamic behaviour of the car for an effective ESP design. Indeed, in case of vehicle prototype unavailability, the use of simulations is a possibility to cope with this objective. Consistence with the V-model can be achieved by considering in the decreasing line (Verification phase) the ESP development and in the increasing line (Validation phase) the performance assessment [181].

Multi-Body System (MBS) is based on the physical modelling of a vehicle by rigid bodies connected by joints, springs and dampers. External torques and forces act on them to reproduce the effect of external ambient and dynamic. These relations are typically expressed in the form of motion equations (Newton and Euler).

The complexity and accuracy of the vehicle models depend on investigation requirements, e.g. component design, topology analysis, energy and pollution assessment, energy management, optimal control [58]. The components and behaviour involved by the designed component must be represented realistically. The dynamical behaviour of the car and its interactions with sub-systems (e.g. suspension, tires, engine, brakes) can be represented by look-up tables, analytic equations or complex multi-body systems (for non-linear dynamic manoeuvres) [48].

Despite the chosen solutions, the model should always guarantee a close relationship between simulated and real results. As visible in Figure 3.2, when the level of detail in the model increase so does the simulation time, until the simulation

environment's RT capability is exceeded. Thus, to reduce development effort, a compromise between model accuracy and intended goals must be met.

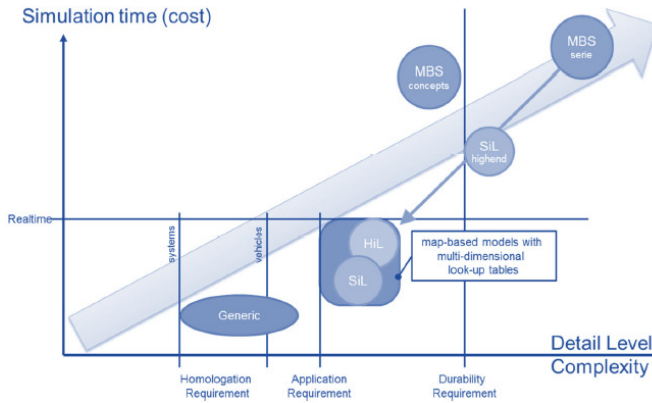


Figure 3.2: Simulation time dependability respect to model complexity (Figure from [181])

When reliability investigation is the aim, simplified vehicle models are generally sufficient. In contrast, when evaluating the CU performances for stability purposes, more vehicle model's DoF must be considered. For the objective of SiL and HiL system validation, more detailed models are required. Generally, SiL simulations are more flexible. When using variable step-size the RT capability can no longer be ensured but the results are more accurate since the discontinuous effect can be resolved.

Simulation-based homologation needs high-quality dynamic models. To be consistent with the vehicle behaviour all the sub-components must be simulated. Chassis clearance analysis, kinematics and compliance of the suspensions, as well tire-road interaction should be investigated for the general purpose of accurate simulations. To perform vehicle ride and handling investigations, chassis, suspensions, tyres and wheels road, powertrain, brakes and steering system models are needed. Even controller functionalities are included in the simulation environment to reproduce the strategy for the actuators regulations [181].

### 3.3.4 Model-based Pros and Cons

Modelling and simulation are fundamental tools for the successful development of systems, such as devices and machines. Recent improvements in computational power and memory have enabled faster simulations and high-fidelity models in a wide range of technical domains. Many simulation software are available. Moreover, availability of co-simulation environment, holistic cross-domain simulations are possible by coupling different RT platforms [185].

The model-based design has become a state-of-art method for developing new systems and products, especially in the automotive, aerospace and defence sectors. The key feature resides in the opportunity to run simulations at any development process steps. Modelling a system serve many purpose in the design process [20, 49] and introduce the following *pros*:

- **Consistent between documentation and implementation:** concepts, assumptions and requirements are inherited features of each model. Also, documentation can help provide analogies with a similar system and prior experience, useful for solving the problem. A perfect example are the Bond graphs;
- **Continuous verification and validation:** allowing tests at every project stage of development. Problems can be tackled in the earliest possible phases, reducing the costs for late and potentially risky product changes;
- **Graphical description of the system:** which ensures high-level understandability and reduces documentation costs. Insight of the system's behaviour can be acquired when the complexity rises (e.g. presence of feedback loops);
- **Hierarchical framework:** allowing the concurrent work on different sub-systems by division in tasks of the design process;
- **Results Accuracy:** enable highly reliable simulations output, compared to real-world data;
- **Reduced coding effort:** automatic code generation ensure simple implementation;
- **Robustness respect to errors and debugging;**
- **Code re-use:** the models can be included in a library, allowing higher flexibility and portability for different UCs, variants and in successive phases of product life-cycle;
- **Identification of ignorance:** leading to a possible estimation of parameter ranges and designing an experiment to determine the model uncertainties.

Portability has important consequences both for the lifetime and design development cycle. In this specific case, the computational techniques used for ESP control only have a lifetime of 3-5 years. To ensure high competitive controllers, the algorithm needs to take advantage of the ever-increasing computational capability. Thus, to be cost-efficient, the control solution must be easily portable from original to new target processors. RT constraints, however, further complicate portability. A good methodology is to introduce a higher layer of abstraction for the real-time environments to bypass incompatibility issues [186].

Nevertheless, the model-based approach have the following *cons*:

- **Difference between prototype and series code;**
- **Adapting the toolchain to the target hardware:** requiring detailed information into the code generation process and producing significant cost and delay;

- **Implementation of special functions:** in some cases may be necessary to manually implement C-code since provided libraries are limited;
- **Model implementation:** which require a significant amount of practice and expertise [48];
- **Computational running time:** can be penalized by the multiple accounted variables and dynamics, which can be a problem for numerical optimisation procedures that demand a very high number of iterations to get to an optimum design [48];
- **Formalism representation:** due to the high abstraction level of the adopted formalism.

### 3.3.5 Simulation Toolchains

Implementation of new advanced functionalities of on-board vehicle systems involves an increase in the system's complexity and needed computational resources. Advanced design, testing and validation methods should be powerful tools that help developers fully exploit the potentiality of new technologies, for the development of innovative industrial products. Attention should be focused on the rapid prototyping of EV's components, particularly for control algorithms.

Simulation is very important during product development. For vehicular mechatronic, however, is extremely difficult to properly simulate the whole system due to the multi-domain feature. There are many toolchains to be used when modelling complex multi-domain systems. The adoption of RT simulation environment is fundamental, especially when hardware and software parts are developed simultaneously. In this way, the TTM reduced [49]. Indeed, RT software differ from conventional ones since results must be delivered instantaneously, in addition to being numerically and logically correct. Thus, input and output signals show the same time-dependent values as the real dynamically operating components. Another reason for using RT simulation platforms resides in the capability to monitor each of the simulated components and signals.

Thus, the simulation platforms must embody the concept of duration and time-step, allowing the usage of mixed continuous and discrete-time sub-models. As an example, by simulating malfunctions with the correct timing the safety-critical aspect can be optimized accordingly [13].

Although a simplified model can generally fulfil the homologation requirements, the reliability of the model must be verified. Therefore, it is recommended to use a well-documented toolchain that ensures traceability between the simulated and real vehicle's results [181].

### Co-simulations

Despite the chosen methodology and toolchain, is important that mechatronic system development solutions allow for specific physical domain design, as well as model integration and simulation. Tools based on MATLAB Simulink ensure: an interdisciplinary development process along all the design stages, enable synchronization of discipline-specific design (fundamental to reproduce the interactions between the disciplines), and support the dynamic reuse of the model at every phase (update and changes during the redesign cycles) and, finally, link domain-specific

design to a meta-model for integration purposes. This results in a functional global system with domain-specific partial models (mechanic, electric and software), while preserving the internal design concept of the domain-specific discipline [52].

Multi-domain simulation environments, however, are usually limited to domain-specific tools. An alternative solution is to interconnect existing tools, exploiting the best of each software (Figure 3.3). The general idea is to use a specialized software tool to model certain components in detail, coupled with a general modelling/simulation environment. Indeed, MATLAB Simulink consent co-simulation process with other software (e.g. Simcenter Amesim, VI-Grade). Since these features are highly recommendable when developing mechatronic systems, this software is largely in these activities.

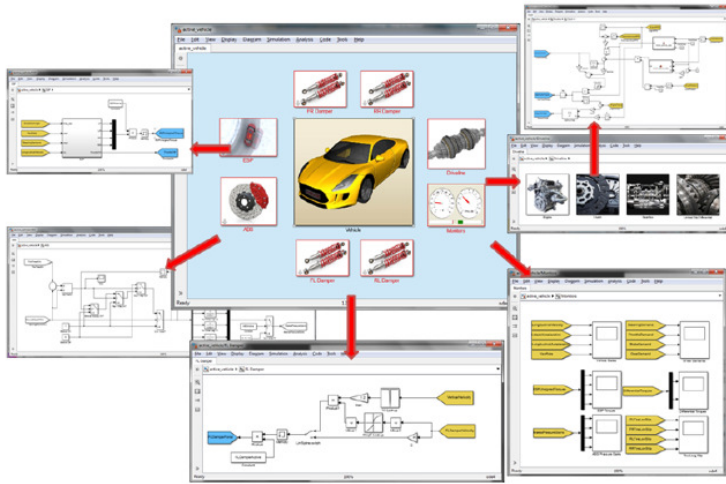


Figure 3.3: Simulink and CarRealTime co-simulation blocks

In this work, a modelling framework that includes mechanical, electrical and electronic/control systems is proposed to achieve an accurate systematic process for mechatronic modelling. Moreover, the co-simulation features of Simulink have been exploited in conjunction with accurate vehicle dynamic modelling software. In particular, the driver and ECUs (including ESP) has been modelled in Simulink, while the vehicle's dynamical behaviour is managed by the other platforms.

### Software-in-the-Loop Simulation

In SiL simulations the system is simulated in a virtual environment independently by the nature of the component. This allows to easily and quickly verify both software and hardware models for real control strategies and components. In automotive SiL simulations, vehicle body and sub-systems are modelled according to chosen approach. However, the complexity of each sub-model can be defined according to the simulation's objective. For example, if only the regenerative brake energy performances are of interest, a 1-DoF longitudinal vehicle, engine and e-powertrain models are sufficient for the scope. In contrast, when a ESP controller need to be validate, 6-DoF chassis, suspensions, steering, tire-road interface and CU software must be considered too [181].

## Hardware-in-the-Loop Simulation

The distinctive characteristic of HiL simulations is to couple real components with a virtual environment, where the remaining part of the system is simulated. The reason is that hardware and control algorithms form a single integrated sub-system and the actuators are often difficult to be modelled properly and simulated in RT.

Main advantages and disadvantages of SiL and HiL approaches are summarized in Table 3.2 [49, 181]. In both cases experiments are repeatable and a reduction of development effort is achieved. Also, both ensures the design and testing of systems without operating a real process in the laboratory, avoiding related risks.

Table 3.2: Characteristics of SiL and HiL simulations

Software-in-the-Loop	Hardware-in-the-Loop
<i>Advantages</i>	
No complex hardware needed	Certainty of results
Fast execution	Testability of Extensive functions
Low cost of test bench	Performance, functional and safety test
<i>Disadvantages</i>	
Complexity the models	Instrumentation effort
Parameterisation effort	Higher costs of test benches
Quality and uncertainty of results	
Absence of safety software	

## 3.4 Reference Driving Scenario

Results of the research activities should be evaluated according to well-defined criteria or “metrics”, that should be agreed upon widely by academic and industrial companies to ensure reliable comparative outputs. In the context of vehicle model-based simulations, assessment of achievable performances is done using reference driving scenarios, accurately reproducing in the virtual environment.

The investigated improvement concerns mainly three aspects. The first is related to *energy efficiency and polluting emissions* of the e-vehicle UC. Here the optimization algorithms are evaluated as compared to several solutions, which can differ from the powertrain architecture viewpoint or the control strategies. The driving range, efficiency and emission are established from standardized and Real Driving Emission (RDE) speed mission profiles for the developed BB allocation policies and the alternative traction layouts. Then, the *functional reliability* of some relevant vehicle sub-systems is investigated. According to ISO26262, many braking manoeuvres are observed during fault-injection simulations to evaluate the impact of different failures on vehicle dynamics (e.g. on brake distance). The third aspect is the *dynamical stability* performance, both for longitudinal and lateral behaviour. In this case, regulations specify the boundary conditions of the tests to properly assess the achievement allowed by the proposed control allocation strategy.

### 3.4.1 Speed Driving Cycle

The driving cycles are well-known speed mission profiles. These represent a standardized procedure to evaluate and compare vehicle driving performances in a reproducible way. In particular, are speed-time sequences specifically developed for a certain type of vehicle to reproduce real-world driving patterns, measure exhaust emissions and monitor fuel consumption. The idea is to impose on the car a reference speed across the time to assess driving ranges and polluting emissions [187]. These cycles are produced by organizations and OEM automotive engineers to furnish reliable metrics for the comparability of the results between different vehicle solutions in simulations, laboratory (e.g. power-adsorbing chassis dynamometer) and road tracks tests. These can be directly referred to specific cities or general driving missions. The adoption of a simulation approach ensures the repeatability of the tests, increasing the level of accuracy of the comparison.

The most common is surely the New European Driving Cycle (NEDC), lastly updated in 1997. Nevertheless, today is obsolete since poorly reproduce real world driving patterns. The World harmonized Light-duty vehicles Test Procedure (WLTP) proposed by UNECE on the contrary, is currently the most diffused since is a globally harmonized standard, able to mimic rear driving behaviour [188]. Also, several cycles have been developed for the United States, European and Japanese countries.

RDE cycles have been proposed to accurately reproduce real-world conditions for CO<sub>2</sub> and NO<sub>x</sub> emissions. The recent diffusion of EVs is demanding for its investigation, even using tailored drive cycles [146]. The reason is the limited driving range and the relevance of auxiliary power demand [187]. Also, the availability of regenerative braking can greatly influence the results. In this work several drive cycles are used to estimate the performances of the BB and RBS control algorithms, supposing different vehicle UCs and traction layouts.

It is preferred to test different cycles in order to verify the robustness of obtained results for specific features of simulated mission profiles. The choice of adopting different driving scenarios allows, also, to prevent that specific system calibration, optimally tuned for certain driving cycles, is not robust for different driving conditions.

### 3.4.2 Longitudinal Driving Manoeuvres

In this context, analysis of the vehicle's brake performance is realized through a straight-line braking manoeuvre on a specific  $\mu$  surface. This is one of the most frequently occurring braking scenarios. In this work, is used for the investigation of the BB strategy features [91]:

- Brake performance, in terms of deceleration and stopping distance;
- Regenerative capabilities for flat dry road or low adhesion conditions;
- RBS interaction and influence on brake modulations from ABS controller;

ISO 21994:2007 is related to the determination of the stopping distance in straight line deceleration with ABS in open-loop test methodology. The maximum speed is generally  $27.78m/s$ , and in full adherence roads, the stopping distance should be lower than  $40m$  with a deceleration of about  $1g$ , according to ECE-R13 specifications.

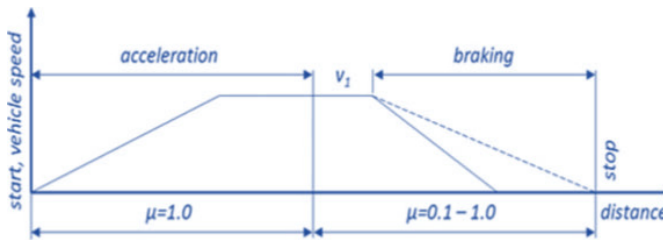


Figure 3.4: Speed profile for the straight line braking manoeuvre as compared to road friction coefficient (Figure from [91])

### 3.4.3 Cornering Driving Manoeuvres

Vehicle characterization is defined as the process by which a vehicle's dynamic behaviour is classified by quantitatively measuring its response to certain inputs command under standard test conditions. The main objective of the testing process is to assess the handling behaviour of the vehicle, which exhibits transient and steady-state responses. This information is useful to compare the performances of different UC and to validate related models.

Any given vehicle, together with the driver and the environment, forms a unique closed-loop system. Therefore, evaluating the dynamic behaviour is challenging, since there is a significant interaction between these elements and the active safety systems. For this reason, some reference manoeuvres are tested in the simulation environment. It is possible to group the tests into two branches [189]:

- Open-Loop Tests: utilized to objectively determine steady-state and transient-state vehicle response. The driver model is excluded from the loop to establish inner handling vehicle capacities. These tests are naturally repeatable, especially if performed with an automated driver;
- Closed-Loop Tests: able to subjectively assess the performances of the lateral stability controller. These kinds of tests are strongly affected by driver interventions. Thus, achievements are a combination of vehicle holding abilities and pilot manoeuvrability skills. These are more difficult to perform with an acceptable level of repeatability and accuracy.

For ESP homologation, legal authorities propose several tests and criteria. All the following ISO standards provide repeatable and discriminatory results that enable the characterisation of a vehicle's dynamic properties. Each test focus on specific vehicle behaviour, replicating as closely as possible real driving scenarios. These tests allow the characterisation of the investigated UC and enable meaningful comparisons between vehicles that perform the same test. However, results have limited significance for the overall dynamic vehicle response and must be considered only in the context of the addressed variables.

Investigation of ride and handling properties is done with specified load cases. For performance evaluation, manoeuvres defined for a physical vehicle are also suitable for simulations. The aim is to reach a certain performance within the expected tolerance band. A major concern is to test repeatability in real-world conditions. In contrast, simulations ensure higher reliability from this point of view.

To better understand the effect of the control techniques and to comparatively evaluate the results, tests are repeated supposing different driving scenarios, in

which the vehicle is alternatively controlled and non-controlled with the proposed ESP. So, once the passive model is validated, the controller software can be included. This allows also fine-tuning of the gains.

It is recommended to conduct vehicle testing in strict compliance with ISO standards when the purpose is to compare the results between different vehicles undergoing the same test since repeatability must be ensured. However, when the intention is to validate virtual models or assess the performance achievements for advanced control strategies, the tests can be executed considering different boundary conditions. In this work, some simulated experiments are performed supposing more severe operative conditions from the stability viewpoint as compared to the mandatory specifications of the regulations. This enables to investigate the proposed safety controller at the limit of their effectiveness [190].

### Open-Loop Test

Open-loop tests are executed imposing to the vehicle-specific input with previously specified timing and amplitude, excluding any kind of human intervention during the test. This lets developers investigate inner vehicle capabilities or skills as compared to the task, not relying on feedback controls. An objective analysis is ensured when using open-loop manoeuvres, comparing different vehicles experiencing the same command inputs.

**Sine with Dwell** UN/ECE-R 13H define the SwD test as performance requirements for ESP controllers. The manoeuvre is described in **FMVSS 126** standard, established by the United States National Highway Traffic Safety Administration (NHTSA). This over-steering test has the steering input of Figure 3.5 with a frequency of  $0.7Hz$  and an amplitude defined by a previous Slowly Increasing Steer (SIS) test. Vehicle speed is fixed at  $80km/h$ . Firstly, the vehicle is driven at the test speed and the steering angle is increased with a  $13.5deg/s$  rate until a lateral acceleration of  $0.5g$  is reached. The steering wheel associated with  $0.3g$  lateral acceleration is  $A$ . The steering pattern of Figure 3.5 is applied to the vehicle with  $\delta = Gain \cdot A$ . Initially,  $Gain$  is equal to 1.5 and sequentially increased by 0.5 in the following tests, until a value of  $\delta \in [270; 300]deg$  is achieved.

Functional and performance requirements of the ESP are given. The lateral stability criteria are defined as the ratio of vehicle yaw rate at a specified time to the first local peak yaw rate generated by the  $0.7Hz$  SwD steering input. In particular,  $1s$  after the completion of the steering input the yaw rate of the vehicle has to be less than or equal to 35% of the first local peak. Also,  $1.75se$  after completion of the steering input, the yaw rate of the vehicle has to be less than or equal to 20% of the first local peak.

In addition to this, a responsiveness criterion is introduced in this evasive test, to evaluate the ability of the vehicle to adequately respond to a driver's steering inputs during ESP intervention. Is defined as the lateral displacement of the vehicle CoG for the initial position during the manoeuvre. At  $1.07s$  after the start must be at least  $1.83m$ .

Together, the lateral stability and responsiveness criteria ensure that the ESP system achieves acceptable stability performance.

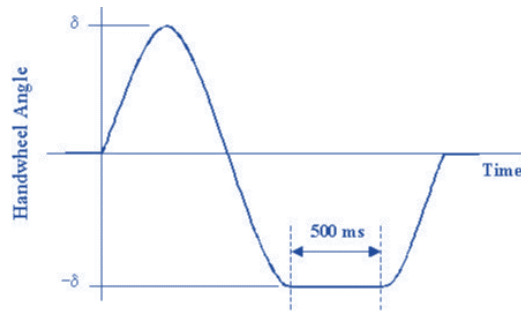


Figure 3.5: Input of SwD test (Figure from FMVSS 126)

**Steady-State Circular Driving Test** ISO 4138:2012 allow us to investigate the steady-state circular driving behaviour of passenger cars. It gives three different methods, described in Table 3.3 (constant-radius test method; constant steering-wheel angle test method; the constant-speed test method). However, the nature of a stable steady-state does not depend on the adopted methodology. So, the equilibrium set for speed, steering-wheel angle and turning radius can be achieved by holding one constant, varying another one and measuring the third.

Table 3.3: ISO 4138:2012 test conditions

Test Method	Constant	Varied	Measured
<i>Const radius</i>	Radius	Speed	Steering-wheel angle
<i>Const steering-wheel angle</i>	Steering-wheel angle	Speed	Radius
<i>Const speed with discrete turn radii</i>	Speed	Radius	Steering-wheel angle
<i>Const speed with discrete steer angles</i>	Speed	Steering-wheel angle	Radius

**Lateral Transient Response Test** Concerning vehicle lateral transient response behaviour, the reference normative is the **ISO 7401:2003**. It uses the time domain (step and sinusoidal steering wheel angle input) and frequency domain (random, pulse, continuous sinusoidal and sinusoidal sweep steering wheel angle input) to characterize vehicle transient response. Also, for the *step input test* (or J-turn manoeuvre) the normative require the calculation of different parameters:

- Steady State: Yaw velocity response gain  $(\frac{r}{\delta})_{SS}$ ;
- Lateral acceleration: Response time  $T_{a_y}$ , Peak response time  $T_{a_y-max}$ , Overshoot  $U_{a_y}$ ;
- Yaw rate: Response time  $T_r$ , Peak response time  $T_{r-max}$ , Overshoot  $U_r$

In contrast, *sinusoidal input test* specifies that one full period sinusoidal steering-wheel angle must be applied to the vehicle while driving at a constant speed. The frequency of the sinusoidal can be  $0.5Hz$  or  $1Hz$ . The amplitude of input steering signal is determined performing a SIS until a lateral acceleration level of  $2m/s^2$ ,  $4m/s^2$  or  $6m/s^2$  is obtained. It is also strongly suggested to plot the side-slip angle yaw rate for lateral acceleration. For the full understanding of the vehicle behaviour, the following data should be acquired:

- Time lags between steering-wheel angle and lateral acceleration: first peak  $T(\delta_H - a_y)_1$ , second peak  $T(\delta_H - a_y)_2$ ;
- Time lags between steering-wheel angle and yaw rate: first peak  $T(\delta_H - r)_1$ , second peak  $T(\delta_H - r)_2$ ;
- Lateral acceleration absolute gain  $|\frac{a_y}{\delta_H}|$
- Yaw rate absolute gain  $|\frac{r}{\delta_H}|$

**Ramp Steer Test** ISO 19364 is a standard that regulates the vehicle dynamics simulation and validation of steady-state circular driving behaviour. It specifies a method for the virtual simulation of the ISO 4138 and SIS tests. The purpose of the test is to demonstrate that model-based tools can accurately simulate vehicle behaviour.

### Closed-Loop Tests

The subjective determination of the vehicle stability properties is done using a closed-loop test, in which the driver can actively contribute to the final purpose. Road conditions and vehicle feature plays a fundamental role, so it's difficult to distinguish the different contribution to stabilization performed by pilot and control algorithm, since are a combination of vehicle dynamics and the road-holding ability of the car. Indeed, Gillespie [44] define the vehicle and its driver as a closed-loop system in which the pilot uses sensory feedback to correct the deviations from the desired motion.

In contrast to UN/ECE-R 13H, UN/ECE-R 13/11 establish that vehicle stability controller functionalities must be demonstrated by closed-loop tests. Typically, a comparison is done between the simulation results related to a vehicle with stability functions enabled and disabled, at given boundary conditions. However, here test procedures and evaluation criteria are not clearly defined. Despite this, the chosen metrics for yaw and rollover prevention controls should be agreed booth from the manufacturers and the technical committees for type approval.

**Severe Lane-Change Test** Several criteria are discussed in the literature, but surely the most relevant closed-loop test concern the obstacle avoidance task, agreed upon by car manufacturers, legal authorities and test institutes. **ISO 3888** is the most representative, also known as a severe lane-change manoeuvre or Moose test. The standard is composed of two-part: DLC (ISO 3888-1:2018) and obstacle avoidance (ISO 3888-2:2011). The test tracks and boundary conditions are specified to ensure repeatability of the tests and comparability of the results (Figure 3.6).

These types of tests are very common and well established in the automotive world for the validation of lateral stability control systems, but also the verification

of the goodness of a car design. Regarding this test, a historical mention is necessary: the test was conceived in Sweden in the 70s, to evaluate how effectively the cars were able to avoid collisions with wild animals. This test has become more and more important in the automotive sector, also thanks to the famous accident that occurred to the Mercedes-Benz A-Class in 1997, which could not perform the test without tipping over. The designers of this car thus were forced to install the very first ESP system to solve the problem. From this point on, the test has become a reference and its specifications are subject to regulations that are still constantly revised today.

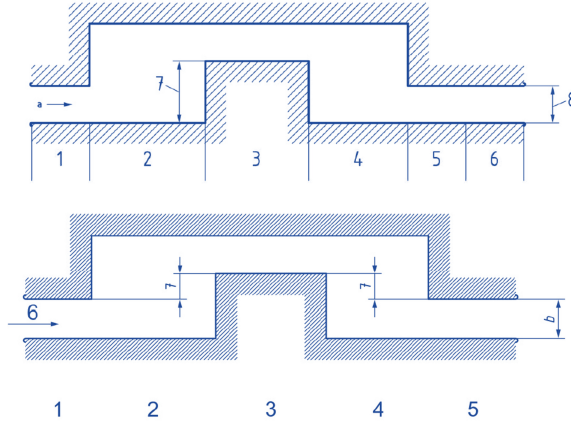


Figure 3.6: Test track for ISO 3888 DLC (top) and obstacle avoidance (bottom) (Figure from ISO 3888)

These tests are repeated at increasing driving speed until the vehicle exit from the designated track, typically delimited by cones. The maximum speed at which the manoeuvre can be performed correctly represents the vehicle stability limits.

This test allows us to analyse the effect of tire load variation in the two consecutive turns and the interaction with human driver intervention. Such investigation is especially valid for systems utilising WIM architecture with torque vectoring control. In this case, the ability to rapidly increase/decrease the regenerative braking torque for the wheels individually will determine the vehicle's lateral dynamics. For these reasons, this test is highly recommended for preliminary tuning and validation of ESP controllers and related integration with regenerative brake system [91].

### ISO3888 - Optimal Waypoints Definitions

The reference path for a closed-loop test, such DLC, is very important for the lateral stability performances. To ensure smooth behaviour when approaching and tracking the desired trajectory an appropriate definition of optimal waypoints and corresponding matching curves is fundamental.

For both ISO3888-1 and ISO3888-2 tests, the MATLAB tools “driving scenario designer” (Figure 3.7) is used to establish the ideal pattern to be replicated [191]. After the specification of the waypoints, the matching curves are approximated using splines. In Figure 3.8 it is possible to observe the reference trajectories generated with the previously described method, based on bibliographic studies and

observations of physical tests conducted by expert drivers. ISO3888-1 manoeuvre track is long enough to let the ideal path be straight in the central area, allowing the vehicle to recover stability. On the other hand, in test ISO3888-2, it can be seen that the trajectory is a continuous curve due to the shorter path, which does not allow to stabilize the trajectory during the crossing of the central area; this makes the test certainly more demanding for the lateral dynamics of the vehicle and consequently requires an adequate control to be supplied to the predictive driver.

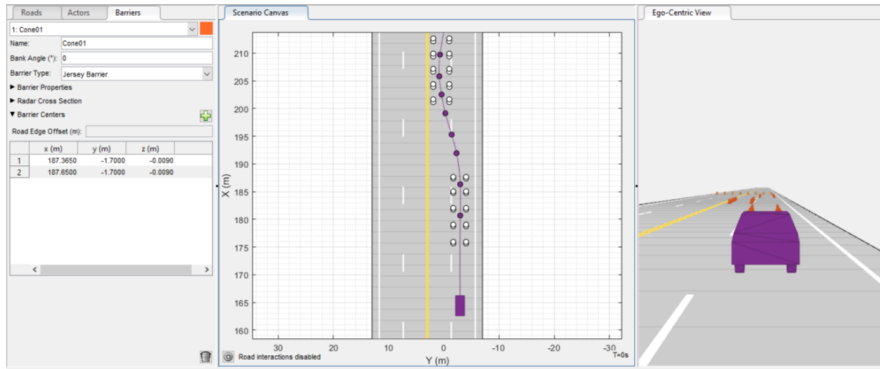


Figure 3.7: MATLAB Simulink “Driving Scenario Designer” tool interface

Finally, to take into account the frontal dimensions of the vehicle which would otherwise hit the boundary cones, a special simulation tool was used during the construction of the route, which, once the geometric characteristics of the car have been set, faithfully reproduces the displacements along the generated trajectory, simulating an ideal test conducted in perfect kinematic conditions and without wheel slippage.

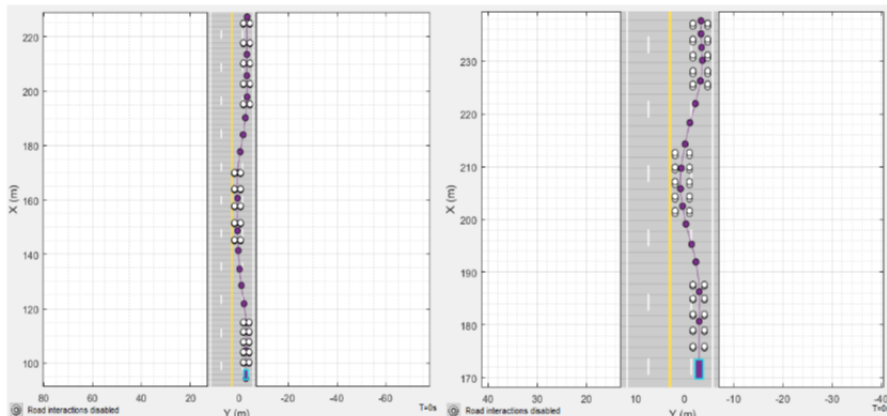


Figure 3.8: Optimal waypoint definition for ISO 3888-1 and ISO 3888-2 tests

The optimal DLC reference trajectory is only introduced for the activities presented in Chapter 5. ISO 3888 tests of Chapter 4 are performed imposing to the driver a simplified target path, realized using a series of broken lines.

### 3.5 Wheel-Independent Motor

The technological features of modern electric motors combined with a distributed traction layout (e.g. hub motors, IWM, or onboard motors) offer to designers a wide range of functionalities that are very innovative as compared to constraints affecting ICE conventional solutions. These technologies enable the redesign of the powertrain architecture, allowing the full exploitation of EM features, such:

- High-power density: ensuring reduced motor weight and size, or higher performances;
- Easy and precise torque and speed control;
- Fast bandwidth response: providing efforts even 10 times faster for both the combustion engine and hydraulic brake;
- Independent torque allocation: which allows the possibility to apply advanced torque vectoring techniques;
- Four-quadrant operational mode: which consents to the application of positive and negative torques, e.g. regenerative braking;
- Direct wheel torque transmission: no driveshaft is needed, avoiding the undesired low natural frequency effects of its stiffness, allowing a good motor response.

Full regenerative capacity can't be reached with only one driven axle. When using 4WD with independent e-motors on each wheel higher efficiency is ensured. With such configuration, also an optimal front/rear torque allocation, depending on longitudinal load, can be applied to further increase energy recuperation.

With EM the measure of delivered torque is simple and reliable (using the current), allowing a more accurate tire state estimation. In this way, it is possible to generate a yaw moment to control the vehicle both in linear and non-linear regions, where cornering forces saturate. Exploiting this feature consent improvement of the vehicle lateral stability performance [129].

Despite this technology being highly promising, has not yet established itself on the market and only a few prototypes have been built and developed to accommodate this innovation. In literature, we can find many papers dealing with this kind of traction system [192, 193], but any WIM configurations have reached the series production. Among the reasons, there is certainly the inability to completely exploit its features. Their development is still in an embryonic phase while developing such solutions require a large dataset related to testing campaigns. Nowadays, we have been used to think a vehicle with the main engine and a distribution system that powers 2 or 4 wheels. This new architecture, however, completely changes the concept that has always been affirmed and which is continuing to be represented also on current EVs.

In this work, for each investigated vehicle UC, an alternative traction layout with WIM solution is considered to furnish the reader with results related to this architecture compared with the conventional frame. In the following sub-sections advantages and disadvantages are discussed in detail.

### 3.5.1 In-Wheel Motors

IWM are credited as one of the most important key technology in the next future to be used on EVs, resulting in a distributed powertrain layout [144]. These solutions enable the development of innovative control techniques, thanks to their highly desirable properties.

Even if the adoption of this traction solution appears a very attractive idea, mass production and market spread have not been achieved. Indeed, these motors cannot be installed inside every wheel for space reasons. Nowadays, many prototype and concept cars solution has been proposed has test vehicles, e.g. GM's Hy-wire platform or Mitsubishi's IWMEV [59].

In a study by Murata [147], feasibility and implementability of IWM solutions have been widely investigated. The difficulty to install a IWM depending on the suspension type is studied and quantified from the standpoint of the space inside the wheel as a score point. The factors that can contribute to the installability of IWM unit are motor size reduction, motor offset thanks to counter gear and installation of reducers inside the hub. Indeed, these kinds of e-motors do not require any heavy power-transmission mechanisms between wheel-clutch, such as transmission, driveshafts, and differentials. Thus, this provides significant weight and space reduction, as well as minor energy loss and manufacturing cost savings.

The fact that IWM for passengers vehicles are yet at a prototype level can be explained by their inner technological difficulties. As already pointed out, any type of e-motor cannot be the sole source of braking, so dissipative disk brakes must be installed on the vehicle. Since the space in the wheel is almost completely occupied by the electric actuators the conventional brake system needs a re-design, even if it is preferred this assembly remain unmodified.

The sprung and unsprung mass ratio of a vehicle plays a crucial role in the ride comfort and handling of automobiles. The weight of IWM inevitably increases the unsprung mass, affecting the vehicle's road-holding ability. When this condition occurs, the frequency response function of the sprung masses shifts in the  $[4 - 8]Hz$  band which falls in the highest human body sensitivity level for vertical vibration [83]. Despite the presence of motor, transmission gears and other parts, IWM's not suspended mass is only 23% higher. When comparing the overall vehicle mass of the traction system, overall weight is reduced due to the elimination of many torque transmission elements. Thus, the differential is removed and the available room in the chassis is enlarged, allowing a better mass distribution of the sub-components [144]. For example, the battery can be installed in that space. This aspect, in combination with the elimination of the ICE located in the vehicle front, contributes to substantially lowering the CoG, increasing the rear axle load.

Another important aspect concern the change of driving force action point. The reaction force is located at the suspension so the motor's torque effort acts directly on the tyre-road contact point. In contrast, for a conventional engine, the driving force is applied at the wheel centre.

A reason that further limits the application IWM traction frames is the increase in costs: four electric motors significantly increase the number of components and this affects the production cost. If we also take into account the current problem of raw materials supplying, fundamental for the production of these components, the issues that are difficult to overcome in the short term are clearly outlined.

A problem often underestimated is the reliability of this architecture. Increasing the components lead to more elements being sensitive to wear and possible breakages.

In addition, the fact that IWMs are housed in the wheels means that are subject to dirt and impacts, further increasing their criticality.

To summarize, three elements are necessary to improve vehicle dynamic performance: a grater mass distribution on the rear axle, an all-wheel-drive layout and different-sized tyres at the front and rear. IWM can guarantee all these aspects, allowing higher DoF in the traction layout design.

### 3.6 Yaw Moment Torque Vectoring Allocator

The proposed ESP controllers differ in the way the control efforts are calculated. However, a common element between each solution concern the external yaw moment allocation algorithm. In conventional ICE vehicle these control efforts are applied by differential braking between left and right wheels. In a more sophisticated EV layout the availability of multi-quadrant electric motors allows taking advantage also of traction torque [194]. In this case, the desired  $M_{zz}$  is applied to the vehicle using an advanced TV technique. Indeed, WIM allow not only to decelerate but also to accelerate the EV's wheels, resulting in a higher value of applicable momentum around the vehicle's z-axis.

This approach contemplates a constrained control problem because of the multi-DoF solutions that are available. Supposing an all-wheel traction layout, in DDEV an actuation redundancy is obtained. This lead to 4-DoF for the definition of the effort allocation algorithm, resulting in  $\infty^4$  available solutions for the WIM torque commands. When using a DYC approach, desired yaw moment and total demanded torque are imposed respectively by the ESP and the driver. Thus, introducing these constraints the possible combinations are reduced to  $\infty^2$  [195]. The remaining 2-DoF can be used to achieve different intents. For example, in [22, 96, 195, 196] energy-efficient allocation criteria are proposed.

However, to the knowledge of the author, there is no work in the literature concerning the adoption of a TV to stabilize the vehicle while ensuring a vehicle's longitudinal behaviour is as close as possible to the one intended by the driver. Thus, for the range of feasible torque distributions, a novel optimal allocation strategy based on Moore-Penrose pseudo-inverse [38] is proposed. In this case, an optimal trade-off between vehicle stability and driver intention is satisfied, by minimizing the norm 2 of the torque delivered on the wheels by the TV allocator and the pilot request on the accelerator/braking pedals.

#### 3.6.1 Moore-Penrose Torque Vectoring Approach

Consider the planar vehicle model of Figure3.9, where  $t_f$  and  $t_r$  are front and rear tracks and  $r_w$  is the wheel radius. Assume that  $T_{ij}$  is the wheel torque demanded by the driver, where  $i$  and  $j$  inherit the same convention for the forces described in chapter 2. This value is established from the brake or throttle pedal's travels by the driver and by the Electronic Braking Distribution (EBD) controller. Assume  $T_{ij}^*$  is the ESP torque command, which is not prior assigned but results from the high-level layers of the control algorithm.  $\Delta T = T - T^*$  is the column vector of the difference between these values.

In order to correct vehicle trajectory, ESP has to allocate a known correction torque  $M_{zz}$  which, for example, can be a function of the error between desired  $r_{ref}$  and estimated  $r_{feed}$  yaw rotational speed, as in (3.8).

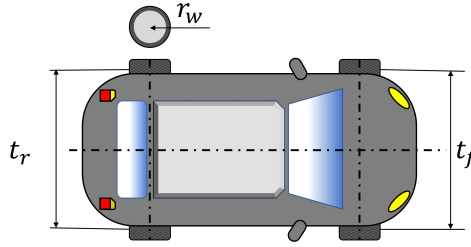


Figure 3.9: Reference planar vehicle model for the TV allocation algorithm

$$M_{zz} = f(r_{ref}, r_{feed}) \quad (3.8)$$

Stability controllers perform vehicle torque vectoring by modulating the braking efforts applied on left and right wheels, to produce the desired correction torque  $M_{zz}$  as in (3.9). A second objective is to regulate the yaw moment by keeping as low as possible the total longitudinal correction efforts, in accordance with (3.10).

$$M_{zz} = \sum \frac{T_{ij} - T_{ij}^*}{r_w} \cdot \frac{t_i}{2} \quad (3.9)$$

$$\sum T_{ij} - T_{ij}^* \approx 0 \quad (3.10)$$

The allocation problem is given by (3.11), which is composed of two-row: the first one ensures a desired stable lateral behaviour of the vehicle by the application of  $M_{zz}$ , as in (3.9); the second one account the necessity of producing wheel torques in agreement with the driver purpose. Thus, the intent is to accomplish two different tasks: (1) ensure a desired stable lateral behaviour of the vehicle and (2) produce a minimum correction moment, which must be also in accordance with the driver's intent. As can be seen, the first row corresponds to task (1), while the second row reflects task (2). In some cases, however, these objectives can demand opposed corrective actions.

$$\underbrace{\begin{bmatrix} -\frac{t_f}{2R_w} & \frac{t_f}{2R_w} & -\frac{t_r}{2R_w} & \frac{t_r}{2R_w} \\ 1 & 1 & 1 & 1 \end{bmatrix}}_L \overbrace{\begin{bmatrix} T_{fl} - T_{fl}^* \\ T_{fr} - T_{fr}^* \\ T_{rl} - T_{rl}^* \\ T_{rr} - T_{rr}^* \end{bmatrix}}^{\Delta T} = L\Delta T = \begin{bmatrix} M_{zz} \\ 0 \end{bmatrix} \quad (3.11)$$

The redundant controls should realize the optimal control  $[M_{zz}; 0]^T$  using minimum control power (3.12). If the control is unable to satisfy the equality condition, it is desirable to minimize the error (3.13), where  $\Delta T$  is subject of constrains  $\Delta T_{min} \leq \Delta T \leq \Delta T_{max}$ .

$$\min P_1 = \frac{1}{2} \Delta T^T \Delta T \quad (3.12)$$

$$\min P_2 = \frac{1}{2} (L\Delta T - [M_{zz}; 0]^T)^T (L\Delta T - [M_{zz}; 0]^T) \quad (3.13)$$

Desired yaw moment determines whether or not the condition (3.11) can be satisfied within the control limits for a given system with fixed  $L$ ,  $T_{min}$  and  $T_{max}$ . If the equality can be satisfied is chosen the solution which minimizes  $P_1$ , otherwise norm solution  $P_2$  is minimized. Equations (3.12) and (3.13) are general formulations of control allocation problems and the Moore-Penrose method is a powerful tool for solving them. It is noteworthy that accordance with driver intention and improved vehicle stability in severe driving conditions are two conflicting indexes that require to be traded off [197]. Solution (3.14) respect these conditions, with  $L^+$  the pseudo-inverse of  $L$ , according to (3.15). The controller guarantee that  $M_{zz}$  is achieved since representing the priority task. As a secondary objective,  $\Delta T$  is minimized.

$$\Delta T = L^+ \cdot \begin{bmatrix} M_{zz} \\ 0 \end{bmatrix} \quad (3.14)$$

$$L^+ = (L^T L)^{-1} L^T \quad (3.15)$$

In general, the pseudo-inverse torque allocator finds a least-square solution as compared to the torque demand arising by the upper-level controller, which can be the EBD.

A valuable feature of this approach resides in the possibility to apply different allocation weight  $\kappa_{ij}$  on each wheel in accordance to (3.16), thanks to the simplified parameterized interface. Weights distribution must respect (3.17).

$$\begin{bmatrix} -\frac{1}{\kappa_{fl}} \frac{t_f}{2R_W} & \frac{1}{\kappa_{fr}} \frac{t_f}{2R_W} & -\frac{1}{\kappa_{rl}} \frac{t_r}{2R_W} & \frac{1}{\kappa_{rr}} \frac{t_r}{2R_W} \\ \frac{1}{\kappa_{fl}} & \frac{1}{\kappa_{fr}} & \frac{1}{\kappa_{rl}} & -\frac{1}{\kappa_{rr}} \end{bmatrix} = L \quad (3.16)$$

$$\kappa_{fl} + \kappa_{fr} + \kappa_{rl} + \kappa_{rr} = 4 \quad (3.17)$$

If the corresponding weights are fixed to 1 the solution is to evenly distribute the torque variations between the four wheels. Otherwise, wheels can be prioritized to achieve additional purposes. As an example, if the front axle is electric its effort can be maximized to ensure higher regeneration during braking manoeuvres, by choosing  $\kappa_{fl} = \kappa_{fr} = 2$  and  $\kappa_{rl} = \kappa_{rr} = 0$ . Other optimization criteria can be realized by changing in RT the corresponding weights. When the UC exhibit different tracks for the axle, their contribution to the yaw moment is different. Thus, normalization factors  $\frac{t_f}{t_r}$  and  $\frac{t_r}{t_f}$  must be considered for rear wheels and front wheels, respectively.

To give an example, suppose a WIM drive an electric vehicle. The main parameters of the vehicle UC are summarized in Table 3.4. Consider also that the high-level ESP controller demands a  $2000Nm$  yaw moment  $M_{zz}$  while the vehicle is accelerating with  $200Nm$  torque on the front wheels and  $150Nm$  on the rear wheels. When the weights are set to 1 for each wheel the demanded torques are the ones of Figure 3.10 on the left. As can be seen, the wheel's actuators can provide the requested yaw moment. Since the vehicle is accelerating, the torque allocator prioritizes driven torque to deliver an equivalent positive force in the tire-road interface. This leads to a longitudinal behaviour in accordance with the driver's demand, respecting front/rear effort distribution as required by the EBD. On the other side, when prioritizing rear wheels by choosing  $\kappa_{fl} = \kappa_{fr} = 0.7$  and  $\kappa_{rl} = \kappa_{rr} = 1.3$ , the same yaw moment is delivered but with different allocation criteria.

Table 3.4: Main UC vehicle parameters

<i>Name</i>	<i>Symbol</i>	<i>Value [unit]</i>
<i>Vehicle Parameters</i>		
Vehicle Mass	$m$	1094 [kg]
Front Wheelbase	$a$	0.915 [m]
Rear Wheelbase	$b$	1.055 [m]
Front track	$t_f$	1.295 [m]
Rear track	$t_r$	1.295 [m]
Wheel radius	$r_w$	0.3094 [m]
<i>e-Powertrain Parameters</i>		
Electric Motor Nominal Power	$P_{EM}$	15 [kW]
Max Motor Torque	$T_{EM-max}$	55 [Nm]
Max Motor Speed	$\omega_{EM-max}$	20000 [rpm]
Gear Ratio	$T_{rate}$	8 [/]
<i>Wheel Torque Parameters</i>		
Max Front Wheel Traction Torque	$T_{tra-f}$	520 [Nm]
Max Rear Wheel Traction Torque	$T_{tra-r}$	520 [Nm]
Max Front Wheel Braking Torque	$T_{brk-f}$	1500 [Nm]
Max Rear Wheel Braking Torque	$T_{brk-r}$	1500 [Nm]

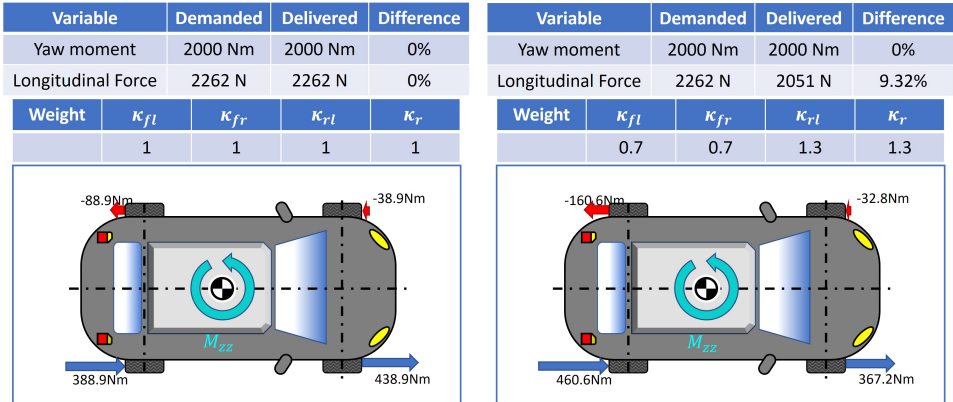


Figure 3.10: Yaw moment and torque allocation for 2000Nm yaw moment demand and equal weight on wheels (left) and prioritized rear wheels (right)

When considering a 4000Nm yaw moment instead, both left wheels' torques are saturated to their limits for equal sharing conditions (Figure 3.11). However, the corresponding longitudinal force is penalized as compared to the yaw moment objective. Thus, using a prioritized rear allocation strategy, the same longitudinal acceleration is achieved while fulfilling the ESP yaw moment demand.

Finally, for yaw moment up to 9000Nm each wheel is saturated, thus the solution is unique for every combination of weights (Figure 3.12). This is due to an if statement in the algorithm which maximizes the applied yaw moment, despite the weight allocation.

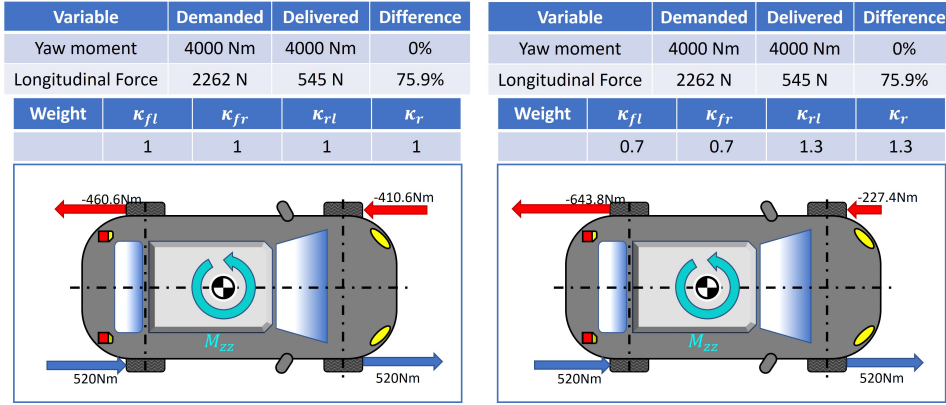


Figure 3.11: Yaw moment and torque allocation for 4000Nm yaw moment demand and equal weight on wheels (left) and prioritized rear wheels (right)

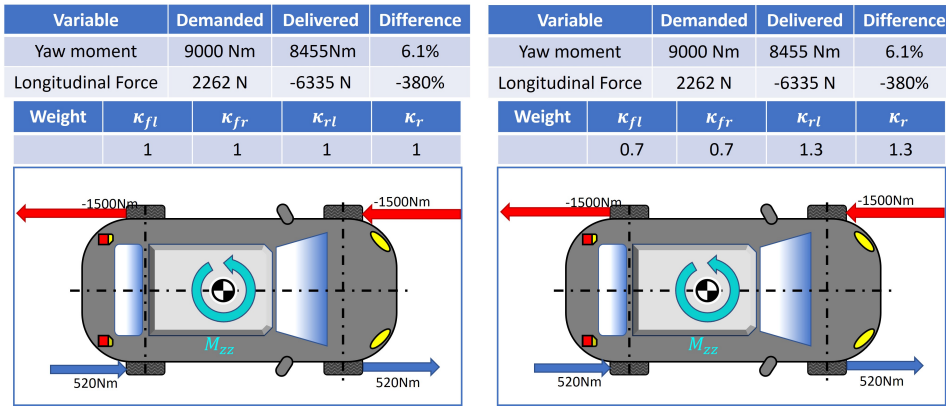


Figure 3.12: Yaw moment and torque allocation for 9000Nm yaw moment demand and equal weight on wheels (left) and prioritized rear wheels (right)

One can notice that, when  $\mu$ -split conditions occur, different friction coefficients are supposed on the wheels. Thus, the ideal yaw moment can not be completely met since the wheels contribute differently to the total  $M_{zz}$ . Future development can be a higher-level weight allocator which distributes  $\kappa_{ij}$  depending on adherence conditions and performed the manoeuvre.

Also, the constraints of the wheel actuators (e-motor and brake) are managed at this level: (3.14) is solved in 4 sequential  $k$ -steps. In each of them the elements of  $T^*$  vector are cross-checked with upper  $T_{ij-tralim}$  and lower  $T_{ij-reglim}$  torque limits for the specified tire, according to (3.18).

$$\begin{aligned}
 if(T_{ij} \leq 0) &\Rightarrow \begin{cases} T_{ij-elm} = \min(T_{ij}, T_{ij-reglim}) \\ T_{ij-brk} = \min(T_{ij} - T_{ij-reg}, 0) \end{cases} && \text{"braking"} \\
 else &\Rightarrow \begin{cases} T_{ij-elm} = \min(T_{ij}, T_{ij-tralim}) \end{cases} && \text{"traction"}
 \end{aligned} \tag{3.18}$$

When wheels constrain are exceeded, a feedback loop fixes the values to the admitted limits and the solution is recalculated in the next  $(k + 1)$ -step, excluding from the system the row related to the  $k - th$  wheel, whose effect is considered according to (3.19). This increases the robustness for motor and/or brake failures. When a diagnostic system updates the allocator with the current actuator's torque capability, the algorithm can account for these scenarios by re-allocating the efforts on the other wheels, accordingly. Thus, if the demanded torque of a wheel is set to its maximum capability, the calculation of (3.14) is repeated solving a system in which the value of the corresponding element is fixed to the saturated value. The calculation is then repeated until a valid solution is found, or when every torque actuator is saturated.

$$M_{zz}(k + 1) = M_{zz}(k) - L(k, 1) \cdot \Delta T(k) \quad (3.19)$$

The resulting method is quite efficient since in the worst case four iterations are needed. From a computational point of view, the most demanding task is represented by the inversion of the  $L$  matrix. However, as the number of computational steps increases from one to four, also the size of the problem decreases, further reducing the corresponding computational load.

Summarizing, this control algorithm serves many purposes:

- Ensure the achievement of desired yaw moment, which is always a priority;
- Minimize the difference between a high-level torque demand (from the driver and/or EBD) and ESP driving intentions;
- Allow the usage of different allocation weights in RT for each wheel to optimize specific requirements;
- Account for the actuator's constraints, automatically reallocating the effort accordingly to reach the yaw moment within the physical limitations imposed by brakes, motors and available friction.

This low-level controller is parametrized to be easily applied to different traction architectures and control theories. This ensures portability and flexibility of the whole proposed strategy, allowing the application of advanced TV techniques, regardless of vehicle layout and control methodologies. In doing so, we are also facing a secondary control allocation problem for over-actuated systems [25]: the BB task. This controller can be coupled with a BB algorithm, which split the braking demand between the actuators in the function of torque availability, prioritizing regenerative braking to improve vehicle energy consumption [198, 199].



# Chapter 4

## Methods, Tools and Preliminary Activities

Before presenting the developed coordinated steering and torque vectoring ESP controllers, it is important to properly build and validate the simulation environment which will be used for the performance assessment of the control strategies. So, following the model-based simulation approach described in Chapter 3, the models of the vehicles and related sub-systems as been developed in the virtual environment.

### 4.1 OBELICS Project

My first two-year activities have been executed in the ambit of the Optimization of scalaBle rEaltime modeLs and functIonal testing for e-drive ConceptS (OBELICS) European project (<https://obelics.eu/>), where a consortium of 19 renowned industrial and academic partners propose new methods, tools and standards for the efficient development of next-generation EVs, demonstrated via relevant UCs.

A great part of current mobility technologies is switching from conventional transportation to electric solutions. This constitutes a major challenge for the automotive industry. A combination of EVs affordability, industrial capacity, real operation performances and durability is crucial for future mass-market deployment. However, the current SoA cannot reach these targets nowadays due to limited technical maturity and constrained investment in the recent past. To achieve a short period EVs mass-production, and implement new components and architectures for higher operation efficiency, great research and development efforts at the industrial level are required. The fast-changing automotive landscape and market opportunities are demanding a faster and more efficient vehicle design to enable mass production and affordability. To achieve this, OBELICS intend to provide innovative, systematic, reliable and RT-capable modelling approaches which ensure models' scalability and compatibility for different components and systems. These model-based methods and tools must be coherent with SiL and HiL validation techniques in each development phase. As pointed out in the section 3.3.1, the V-model is the current standard for system developments, where integration and testing are traditionally performed on the right side, where no systematic test procedure can be done until the system is physically realized. Within OBELICS the testing efforts are transferred to the left side, reducing the development time and effort.

Nevertheless, detailed and accurate models are needed, which may increase computational costs. So it becomes equally important to reduce the model's complexity when RT capability is needed. A scalable model is helpful to adapt for higher accuracy or high computational speed of the simulations, depending on the requirements and objectives of the virtual test.

The overall intent of the project is the development of a systematic and comprehensive framework for the design, development and testing of advanced e-powertrains and EV's line-ups, to reduce development efforts by 40% while improving the efficiency of the e-drivetrain by 20% and increase safety by a factor of 10 using advanced heterogeneous model-based testing methods and tools; as well as scalable and easy to parametrize models.

## 4.2 Vehicle Use Cases

To verify these properties and assess performances for different vehicle solutions, three vehicles use cases are investigated in collaboration with the OBELICS project partners. These benchmark vehicles have high relevance since address both commercial and prototype/concept cars. The idea is to test and validate the control algorithms on vehicles that exhibit industrial and research impact.

### 4.2.1 FIAT 500e

The investigated vehicle is the *FIAT 500e* (Figure 4.1), a fully FWD EV, in which a single permanent magnet EM is used to actuate the front wheels through a differential mechanism. The main UC parameters are summarized in Table 4.1, which are freely available on-line.



Figure 4.1: FIAT 500e vehicle UC

The FIAT 500e powertrain is 100% electric and composed of three main components: an advanced high-voltage lithium-ion battery pack, a high-power electric-drive motor and a power inverter module to help manage power flow. The battery pack is a  $24kWh$  lithium-ion battery and it is strategically located to improve front-to-rear balance (4.2). For the gasoline version, in the FIAT 500e, the coil spring ride is increased to deal with the higher curb weight, mainly related to the heavy battery package. The electric motor, located in the front of the vehicle, is a three-phase synchronous drive motor with an interior permanent magnet, provided by BOSCH, which guarantee the vehicle traction using single-speed gearbox transmission.

More specifications for the vehicle UC can't be given, since the cooperation with Centro Ricerche FIAT (CRF) is still covered by NDA.

Table 4.1: Main vehicle parameters: FIAT 500e

<i>Name</i>	<i>Symbol</i>	<i>Value [unit]</i>
<i>Vehicle Parameters</i>		
Vehicle Mass	$m$	1355 [kg]
Vehicle Length	$L_{tot}$	3.616 [m]
Vehicle Width	$W_{tot}$	1.628 [m]
Front Wheelbase	$a$	0.989 [m]
Rear Wheelbase	$b$	1.311 [m]
Front track	$t_f$	1.407 [m]
Rear track	$t_r$	1.397 [m]
Tyre Type	/	185/65 R15
Max Vehicle Speed	$V_{max}$	141 [km/h]
<i>e-Powertrain Parameters</i>		
Electric Motor Nominal Power	$P_{EM}$	83 [kW]
Electric Polar pair	$n_p$	6 [/]
Motor Rotor Inertia	$I_{EM}$	0.178 [kgm <sup>2</sup> ]
Max Motor Torque	$T_{EM-max}$	200 [Nm]
Average Motor Efficiency at $T_{EM-max}$	$\eta_{EM}$	95.7 [%]
Max Motor Speed	$\omega_{EM-max}$	12800 [rpm]
Gear Ratio	$T_{rate}$	9.59 [/]
Battery Nominal Voltage	$V_{batt}$	364 [V]
Battery Max Voltage	$V_{batt-max}$	400 [V]
Battery Capacity	$C_{batt}$	64 [Ah]



Figure 4.2: Exploded view of FIAT 500e vehicle UC

### 4.2.2 SimRod Kyburz

The SimRod Kyburz, represented in Figure 4.3, is an electric sports car developed by a Swiss automotive company (E-Rod). The rear-wheel electric drive in conjunction with the low centre of gravity is intended to attract buyers who want to have fun during driving. In the picture, can be seen the wheel force transducers. The investigate UC has been modified by Siemens Leuven Research laboratory with more than 150 sensors and a Simcenter SCADAS acquisition system (Figure 4.4). Main UC's specifications are summarized in Table 4.2.



Figure 4.3: SimRod Kyburz Vehicle UC

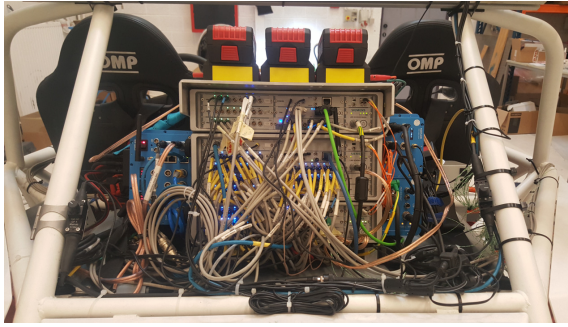


Figure 4.4: SimRod Kyburz SCADAS acquisition hardware system

Table 4.2: Main vehicle parameters: SimRod Kyburz

<i>Name</i>	<i>Symbol</i>	<i>Value [unit]</i>
<i>Vehicle Parameters</i>		
Vehicle Mass	$m$	720 [kg]
Front Wheelbase	$a$	1.249 [m]
Rear Wheelbase	$b$	1.101 [m]
Vertical Dist. Ground to CoG	$h$	0.317 [m]
Front track	$t_f$	1.420 [m]
Rear track	$t_r$	1.425 [m]
Tyre diameter	$d_w$	0.576 [m]
<i>e-Powertrain Parameters</i>		
Electric Motor Nominal Power	$P_{EM}$	15 [kW]
Electric Motor Peak Power	$P_{EM-max}$	25 [kW]
Max Motor Torque	$T_{EM-max}$	140 [Nm]
Max Motor Speed	$\omega_{EM-max}$	8000 [rpm]
Gear Ratio	$T_{rate}$	7.13 [/]
Battery Voltage	$V_{batt}$	96 [V]
Battery Capacity	$C_{batt}$	200 [Ah]

The current version of the SimRod prototype is not equipped with any stability mechatronics system aiming to improve vehicle stability; vehicle brake plant consist of a TT layout with two master cylinders to control front and rear brakes separately. This allows for good control of the front-rear brake balance. Both front and rear brakes use discs, but only the front ones have cooling vanes. Master cylinders amplify the command provided through a conventional brake pedal.

### 4.2.3 Valeo Concept 4WD

A 4WD BEV with a single 48V battery pack concept car has been supposed (Figure 4.5). The hypothetical e-powertrain layout consists of 4 IWM connected to each wheel and intends to target the A/B car segment. Supposed EM are 48V e-machines developed by VALEO Industries. Their performances and characteristics (maximum and minimum torque, losses for shaft speed) are mapped as in Figure 4.6, while vehicle specifications are summarized in Table 4.3.



Figure 4.5: Valeo Concept Vehicle UC

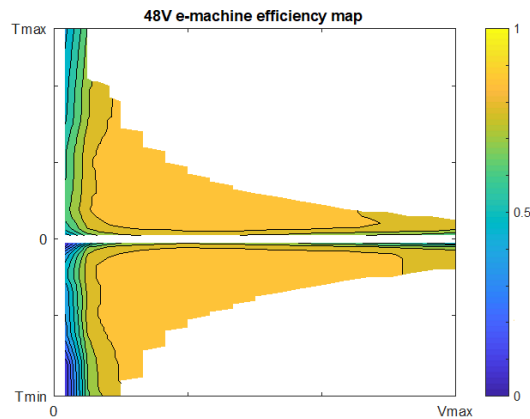


Figure 4.6: Valeo 48 V e-machine efficiency map

Table 4.3: Main vehicle parameters: Valeo concept BEV

<i>Name</i>	<i>Symbol</i>	<i>Value [unit]</i>
<i>Vehicle Parameters</i>		
Vehicle Mass	$m$	1094 [kg]
Front Wheelbase	$a$	0.915 [m]
Rear Wheelbase	$b$	1.055 [m]
Front track	$t_f$	1.295 [m]
Rear track	$t_r$	1.295 [m]
<i>e-Powertrain Parameters</i>		
Electric Motor Nominal Power	$P_{EM}$	15 [kW]
Max Motor Torque	$T_{EM-max}$	55 [Nm]
Max Motor Speed	$\omega_{EM-max}$	20000 [rpm]
Gear Ratio	$T_{rate}$	8 [/]
Battery Voltage	$V_{batt}$	48 [V]
Battery Capacity	$C_{batt}$	42.5 [kWh]

### 4.3 Simulation Model

Over the years, the test methodologies to quantify the effectiveness of stability control systems have multiplied quickly, thanks also to the advent of increasingly precise simulation software for the study of vehicle dynamics. If in the past the tests were carried out on purpose-built prototypes, today the approach is based on virtual vehicle modelling. This solution contributes to significantly reducing both costs and time associated with production. Issues that in the past were separate now go to merge, increasing the overall complexity as well as the needed computational load. The aim is to bring the project to a superior functional abstraction level for mechatronic and multi-domain physical models to ensure code porting. That leads to a completely scalable and layer-structured solution. Using low order and discrete fixed time step simulation solvers allow the interface with superior functions and heterogeneous vehicles, keeping the computational cost at acceptable levels.

Another fundamental aspect is to simulate the effect of coupling TC and TD systems. Delays and issues related to deterministic data transfer between physical models and ECU should be considered to address their drawbacks and specific need. For example, for TD systems a  $100Hz$  sampling frequency is chosen, while for the TC ones it is selected a frequency two orders of magnitude higher  $10.000Hz$ .

For what concerns the simulation complexity, it is important to develop tailored sub-models depending on the investigated aspects. Indeed, to avoid unnecessary computational costs the virtual environment should include only the sub-systems directly correlated with the simulation purpose. If the intent is an efficiency evaluation over a standardized drive cycle, powertrain and longitudinal vehicle models are needed for an accurate estimation of the consumption, while ESP and lateral vehicle dynamics are not required and can be removed to speed up the simulations. On the other hand, if the intent is to establish the lateral stability controller performance, safety controllers and vehicle cornering dynamics are fundamental, while the battery model can be removed. This highlights the importance of a modular vehicle model which allows to specifically select the simulated sub-systems.

The ultimate and most dynamical accurate solution is a full non-linear integrated performance, handling and ride model that involves all the DoF of the vehicle body in space, together with sprung and unsprung mass motion and wheel dynamics [83].

Since EVs are very complex multi-physical systems, a graphical block diagram representation formalism is the most suitable to ensure a high level of understandability, organizing the sub-models and underlying the main properties, as well as highlight the interchanged signals. A mathematical formalism is also needed, e.g. state-space formalism. This enables a functional description of the models and related relationships, highlighting system properties [58].

### 4.3.1 MATLAB and VI-Grade Co-simulation Model

To ensure high fidelity simulation output, most of the virtual validation has been performed using a co-simulation environment between MATLAB Simulink and VI-Grade CarRealTime. In this way, the boundary conditions in which the vehicle can operate during real driving scenarios are accurately reproduced [194].

The main purpose of these activities intend to assess the possible improvement arising from the proposed ESP in terms of the vehicle's dynamical behaviour. Thus, the vehicle model has been developed using a co-simulation approach between the above-mentioned platforms, according to the following specifications:

- *MATLAB Simulink*: in which reside the control logic (driver, EBD and ESP controllers, e-powertrain and brakes control units)
- *VI grade Simulator*: which replicates the vehicle behaviour with a 16-DoF model (chassis, steering system, suspension system, ABS and TCS controllers, wheels and tire-road interaction, brake, powertrain and transmission models).

In particular, the models are coupled using the MATLAB platform as master and VI-Grade as a slave. To ensure no losses in the data exchange process during RT simulation tests, proper sample rates and solvers are imposed. The exchanged signals are visible in Figure 4.7. From the Simulink environment the steer, brake and motor commands are delivered to the CarRealTime interface block. Additional boolean signals are used to enable or disable specific controllers (e.g. ABS). The CarRTealTime environment manages this information to compute the vehicle's physical behaviour. These values are delivered back to the Simulink model to close the feedback control loops and enable a fast RT data visualization.

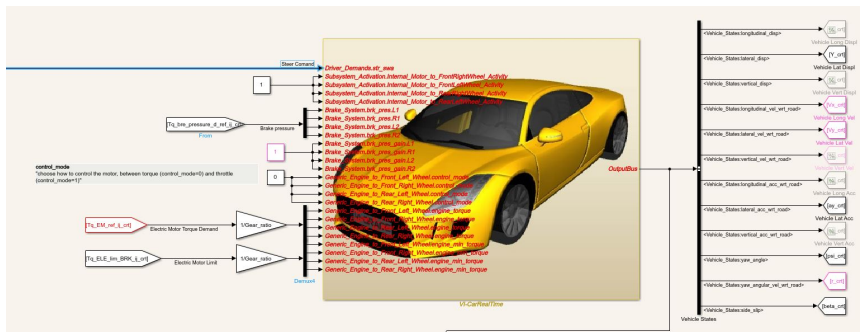


Figure 4.7: MATLAB and VI-Grade co-simulation model implementation

### 4.3.2 Vehicle Body Model

The Vehicle model intends to accurately predict overall vehicle behaviour for cornering, braking, and acceleration performance for four-wheeled cars.

The vehicle body is modelled through well-known and widely accepted dynamic equations [44], able to reproduce the chassis motion in all directions. This model includes both body and wheels, whose reference systems are visible in Figure 4.8. To properly simulate tire-road interactions, a contact adhesion model must be considered [83].

If only the longitudinal vehicle dynamic is of interest, a **5-DoF** vehicle body model is sufficient. It considers longitudinal chassis motion  $X$  and the four wheels' rotation around their  $Y_w$  axis,  $\Theta_w$ .

Instead, when the vehicle cornering dynamic is needed, a **9-DoF** can be used to account for lateral  $Y$  and yaw motion  $\gamma$  of the chassis, allowing also both front axle wheels to steer, rotating around their relative vertical axis  $Z_w$  of an angle  $\delta$  for the tire's yaw motion  $\gamma_w$ .

However, a **16-DoF** model must be used if more accurate vehicle behaviour is required. It include all the chassis motion (longitudinal  $X$ , lateral  $Y$ , vertical  $Z$  and related roll  $\Psi$ , pitch  $\Theta$  and yaw  $\gamma$ ), for a total of 6-DoF, along with 2-DoF for each wheel (pitch  $\Theta_w$  and vertical motion  $Z_w$ ) for a total of 8-DoF, and steering of the front wheel (yaw  $\gamma_w$ ), adding additional 2-DoF. Lateral and longitudinal displacement of the wheels  $X_w$  and  $Y_w$  are not considered since these movements are constrained to the vehicle axle and no relative motion is permitted. This is without a doubt the most complete vehicle body model and is used in conjunction with a suspension model to consider wheel vertical motions.

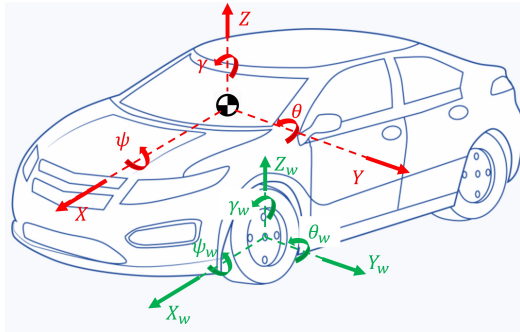


Figure 4.8: Vehicle chassis and wheels reference systems

### Tire-Road Contact Model

In vehicle dynamics simulations, tire modelling assumes great relevance. Its behaviour must be reproduced accurately to ensure reliable results. In the MATLAB Simulink environment, the interaction between the vehicle's tires and the road is modelled according to the Pacejka "Magic Formula" (MF) equations [46], assuming a combined slip wheel model. This modelling approach relies on empirical data and furnishes a reliable estimation of the tire-road interface response in terms of exchanged forces, longitudinal slip  $\sigma$  (2.7) and side slip  $\alpha$  (2.8) if we assume a combined slip wheel model.

When using Amesim or CarRealTime, the MF-tyre model is the one developed by Delft, which is an extension of the Pacejka formulation. It allows to detect and calculate tire slip and relevant forces between the road and a pneumatic, along with the aligning torque. With this solution, a wide range of steady-state, transient-state and high-frequency analyses can be performed (Figure 4.9). However, all the above-mentioned software allows for directly specifying the pneumatic type on their modelling interfaces to automatically inherit the tyre's characteristic parameter from an internal database, ensuring high fidelity simulations.

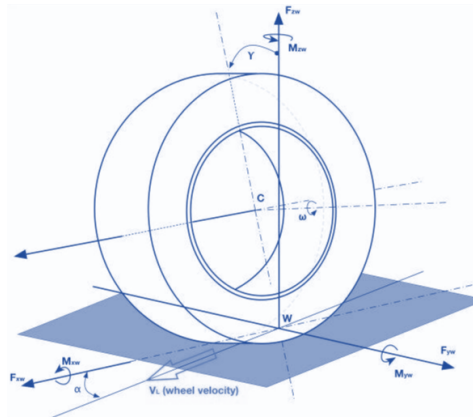


Figure 4.9: CarRealTime tire model

### 4.3.3 Driver Model

In real-world conditions, the closed-loop tests are executed by expert drivers. In SiL virtual simulations the behaviour of the pilot should be accurately reproduced to ensure the reliability of the manoeuvres, as well as the output comparability. When simulating the vehicle longitudinal dynamics, such as standard or RDE mission profiles, a simple PID controller to track the desired speed (acting on both throttle and brake pedals) is sufficient. Nevertheless, if cornering manoeuvres have to be performed, a model acting even on a wheel steering is needed.

A predictive model solution is surely the best one, able to account for road status, and accurately fit the driver's response for low-friction scenarios. However, these features are challenging to be reproduced in a virtual environment, since depending on a multitude of factors [200]. Another problem is the desired path definitions, due to its high dependency on driving conditions (e.g. speed, road friction  $\mu$ ).

In this context, the predictive driver model of MATLAB has been optimally tuned to fit these capabilities. Based on the literature, a comparison has been made with other virtual models, to have direct feedback on their effectiveness. This model rely of MacAdam works [201, 202], which are nowadays the SoA. For the tracking of the longitudinal vehicle's dynamic, a cruise control logic is implemented using a Proportional Integral (PI) with anti-windup and feed-forward gain, according to (4.1), with  $q$  the adimensional output. When  $q \in (-1; 0]$  the vehicle is braking, while when  $q \in [0; 1)$  is accelerating.  $K_{ff}$ ,  $K_p$ ,  $K_i$ ,  $K_{aw}$  and  $K_g$  are the feed-forward, proportional, integrative, anti-windup and wheel road slope gains, respectively.  $V_{ref}$

is the vehicle reference speed,  $e_{ref} = V_{ref} - V_x$ ,  $e_{out} = y_{ref} - y$  the control errors.

$$q = \frac{K_{ff}}{V_x} V_{x-ref} + \frac{K_p e_{ref}}{V_x} + \int \left( \frac{K_i e_{ref}}{V_x} + K_{aw} e_{out} dt \right) + K_g \Theta \quad (4.1)$$

The lateral dynamic is implemented through a single-point preview (look-ahead) control. The model allows defining a path-following manoeuvre acting on the wheel steering command. The main features are: the vehicle's dynamical behaviour is simplified using the single-track kinematics; the functional cost error (4.2) at the specified point forward in time  $t^*$  is minimized, with  $y(t)$  and  $y_{ref}(t)$  the vehicle lateral displacement and related reference; driver input delay are accounted; a feedback loop respect to actual yaw rate is considered.

$$J = \frac{1}{T^*} \left[ \int_{t_0}^{t_0+t^*} [f(t) - f_{ref}(t)]^2 dt \right] \quad (4.2)$$

The model require the definition the following parameters to calculate the preview time  $T^*$  (4.3) and account for human input delay (4.4):

- Preview distance  $L$ : define the distance in which the driver intends to collide with the desired trajectory. The smaller it is, the more the driver will tend to spin faster. On the contrary, the action will be smoother;
- Driver delay time  $\tau$ : representing the time between desire and actual steering action, since humans are the object of perceptual and neuromuscular mechanisms which inevitably introduce a delay;
- Longitudinal Speed  $V_x$ : a restrained value allows to use smaller preview distance. In these activities, the preview distance value has been scheduled for the speed to ensure accurate modelling.

$$t^* = \frac{L}{V_x} \quad (4.3)$$

$$H(s) = e^{-s\tau} \quad (4.4)$$

In Figure 4.10, the effect of the preview distance on driver steer actuation and related trajectory can be seen. The performed tests require the simulation of highly skilled and professional drivers. For this reason,  $\tau$  is chosen equal to 0.1s.

Has mentioned before, the performance of the active stability algorithms is a combination of vehicle, controller and driver. So, it is important to ensure, for each test, the repeatability of the driving style. This is essential in the optic of comparing the results of manoeuvres performed with and without the ESP controller. This factor enables a more reliable comparison for a real-world test. Every human driver, although his experience, will always be affected by small variations between one test and another. Virtual validation, in this sense, can provide important information and ensure high comparability levels by eliminating the human factor from the final assessment.

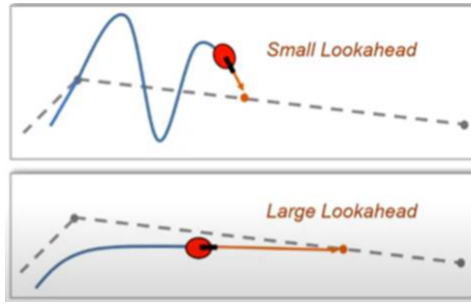


Figure 4.10: Preview distance effect of the MacAdam driver model

### 4.3.4 Steering Model

From the driver model, an adimensional signal from -1 to 1 is given to the steering model, representing respectively maximum left and right wheel turning. The steering model receives this information and provides the wheel's steering angles for the steered wheels, depending on the selected mechanism.

The Simulink model allows selecting the steering system typologies, e.g. Ackermann, to define the whole system kinematic. CarRealTime instead, models the steering system with a 3D spline curve, depending on driver command, rack travel and jounce of the suspension (Figure 4.11). It provides the rack displacement including all the dynamics of the command line (friction, inertia and so on). It is important to note that the cooperation between the kinematic of the suspensions, which have it's one geometry, and the steered wheel are compatible.

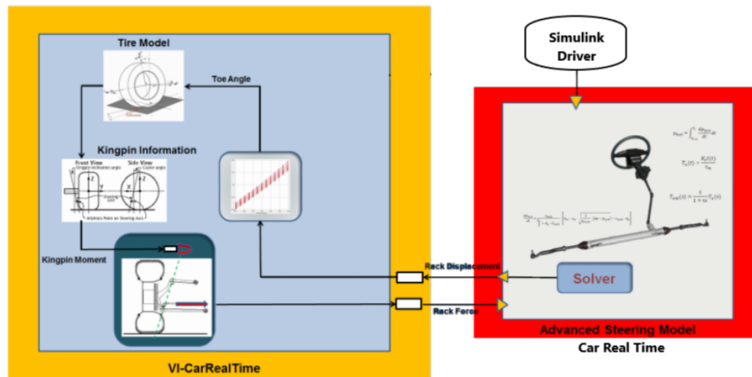


Figure 4.11: VI-CarRealTime steering model

### 4.3.5 Brake System Model

To ensure reliable simulation results, an accurate model for the hydraulic brake is needed. There is a wide literature concerning simulation of conventional automotive brake plants [61, 203–206], which is usually performed using customized commercial tools. However, development of electric powertrains [207] and pervading diffusion of autonomous or assisted driving systems [12, 208] are encouraging the application of brake-by-wire technologies [209].

Indeed, there is an increasing interest in studies concerning innovative brake plant configurations [21, 198, 210] to improve both performances and implemented functionalities. Literature works [211, 212] emphasize different aspects of a common topic: the need for increased integration between a conventional brake system, e-drivetrain and various sub-systems of the vehicle CUs.

In literature, there is a gap in what concerns simplified models that can be used to fit plant functionalities, abstracting from the specific physical features of components and subsystems. In addition, very accurate models involve the availability of a large amount of data and the calibration of many parameters, which are often not available. For these reasons, a general-purpose procedure that should be used to reproduce the behaviour of different braking plants is proposed in this work.

In this sense, the original research contribution is the definition of a systematic methodology to build an accurate, flexible, modular and RT-capable brake system model, based on a limited set of experimental results. The approach should be used for different tasks and activities: preliminary design, simulations and numerical optimizations; Real-Time Implementation (RTI) for HiL, SiL and MiL systems, re-use of proposed models as part of model-based filters, controllers and estimators.

A hybrid functional model is proposed. Simplified physical elements are introduced to perform an easy calibration. More complex functionalities are implemented with interpolated piece-wise linear transfer functions, able to reproduce a wide variability of phenomena, acting on a reduced set of parameters. Piece-wise linear transfer functions are a powerful tool that is commonly used to approximate systems with a strong non-linear behaviour, minimizing the number of integrated states and maintaining a high level of continuity on calculated states and corresponding derivatives. **Kyburz SimRod** has been used as the benchmark test vehicle.

The main differences between this research respect to the current literature are:

- Functional decomposition of the plant: proposed model is not a simplified physical representation of the plant, but its functionalities.
- Piece-wise transfer functions: poles of linear transfer functions are scheduled as compared to state values and their derivatives. Thus, it is possible to reproduce complex NL phenomena affecting both amplitude and frequency response of the plant. The resulting model maintains a reduced number of integrated states and assures a numerically smooth behaviour.

The hydraulic brake plant model has to reproduce the behaviour of the dissipative brake system, which converts the brake demand in real clamping to produce the desired brake torques on the wheels. The model has been calibrated and validated using a limited set of real-world vehicle data for the UC, in collaboration with Siemens Leuven research centre. The method appears efficient and reliable for modelling purposes. It is RT capable, parametrized and can reproduce typical hydraulic brake system non-linearities (e.g. hysteretic behaviour) [213].

For conventional models available in the literature, here the attention is focused on numerical stability for fixed-step RTI: this is an issue often under-evaluated since the integration of hydraulic systems is performed on commercial codes with variable step solvers, that are almost unsuitable for RTI in which fixed-step implementation is mandatory [198, 210].

The main features of the model are described in Figure 4.12. Brake demand is pre-processed using piece-wise second-order transfer functions. Static gain is scheduled for the plant response in terms of amplitude, while poles of the transfer function are scheduled respect to the system states, to reproduce the dynamic response of the brake plant. Output is an equivalent pressure reference, corresponding to the desired torque that must be transmitted to braking units. This reference pressure is modulated considering an independent actuation unit for each wheel. To model the hydraulic plant of callipers, a multi-physics approach [13] is followed. Fluid compressibility is modelled as a single RC circuit that simulates equivalent capacity and losses of the plant, according to the Bond's graphs.

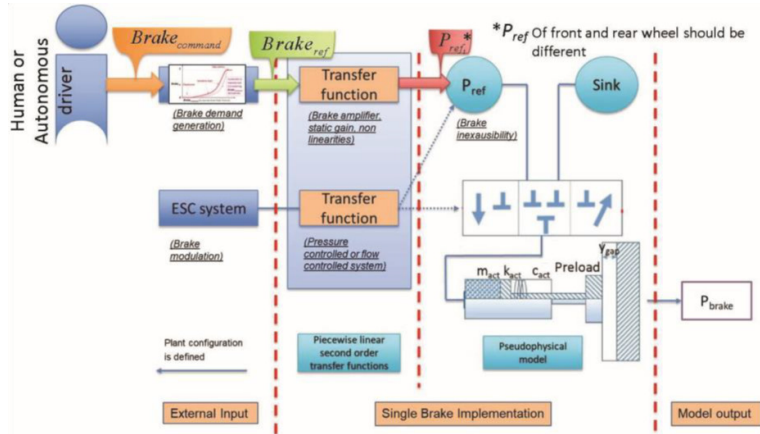


Figure 4.12: Simplified pseudo-physical model proposed by university of Florence.

### Functional Decomposition Modelling Approach

The Brake unit adopted here is a hydraulic servo-amplification and actuation system. The latter is also analysed in terms of the functions that are performed by its different subsystems and then translated into an equivalent functional model. Adopted model maintains only some limited features of the simulated plant, i.e. [210, 213, 214]:

- *Brake Demand Generation*: desired brake demand is generated by a human driver or by automatic/autonomous systems that assist or substitute his action. It's simulated as a converted and servo-amplified command signal which represents a clamping force reference and, consequently, a torque one;
- *Plant Configuration*: driver brake demand and system configuration are affected by mechatronics subsystems. According to the current plant state, applied commands are modified to reproduce the response of corresponding fluid components. In a real plant, this modulation is performed by valves, which are also needed to produce a specific variation of the plant topology. All these functionalities are simulated in a simplified way by assuring the possibility of direct access from external commands, arising from onboard systems. Applied friction brake commands are filtered by transfer functions, that could be customized to reproduce the response of corresponding fluid components;

- *Brake Modulation*: clamping pressures applied to brakes are typically regulated by electro-hydraulic valves that can connect the actuator with a pressure source or discharge it. A single effect actuator controlled by a 3/3 valve is the best way to approximate the plant response;
- *Brake Inexhaustibility*: the action of the brake plant and its interactions with onboard systems should produce an increased demand for hydraulic power. Safety of brake plant involves the availability of supply pressure in every working condition. This feature is important for mechatronics systems, like ABS and ESP, whose fluid consumption are difficult to be evaluated when complex regulation patterns are involved. Real plants have additional capacities and feeding/pumping units to assure pressurization in almost every condition.

### Brake Demand Generation

$Brake_{ref}$  represents the required braking performance generated by an input signal  $Brake_{command}$ . The output torque is tabulated as a function of the command and its rate to reproduce non-linearities of the system, such as dead zones, variable gains and saturation effects, as visible in Figure 4.13.

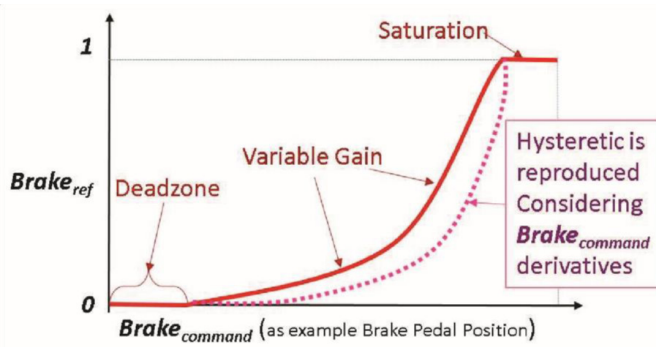


Figure 4.13: Corresponding table of the brake torque reference respect to the brake command

Once desired longitudinal forces are known, corresponding values of steady-state pressure can be calculated according to (4.5). The following symbology is adopted:  $A$  is the equivalent area of the calliper (including friction surfaces and actuators);  $F_{preload}$ ,  $k_{act}$  and  $y_{gap}$  are respectively the pre-load, stiffness and run of the calliper;  $r_{brake}$  and  $r_w$  are the mean disc radius and the mean rolling radius of the wheel;  $f$  is the friction factor between brake pads and discs;  $p_{max}$  is the steady-state value of brake pressure to obtain the desired brake force  $F_x$ , in steady-state conditions.

$$F_x = (p_{max}A - F_{preload} - k_{act}y_{gap}) \frac{r_{brake}f}{r_w} \quad (4.5)$$

Real brake modulation valves have a finite response bandwidth, which is reproduced by inserting a second-order filter. Assuming to model the system as an equivalent pressure-controlled loop, transfer function described in (4.6) is used to represent evolution of  $p_{ref}$  respect to the desired steady-state value  $p_{max}$ .

$$P_{ref}(s) = Brake_{ref}(s)P_{max} \overbrace{\frac{\omega_n^2}{s^2 + 2\epsilon\omega_n s + \omega_n^2}}^{G(s) \text{ transfer function}} \quad (4.6)$$

In (4.6)  $\omega_n$  is the equivalent eigenfrequency/pole of the pressure loop,  $\epsilon$  is the damping factor. Second-order transfer functions are often used to approximate the dynamical behaviour of both flow-controlled and pressure-controlled valves. Transfer functions are a rough approximation of plant response, so is adopted a piece-wise linear transfer function in which parameters are scheduled as functions of system states. In this way, it's possible to change the coefficients with a continuous smooth behaviour: even a step variation of transfer function coefficients produces an output signal which is at least C1 (continuity of function and its first derivative), properly shaping a smooth and continuous behaviour of simulated pressure reference.

### Plant Configuration

In modern vehicles, the brake plant is interconnected with several onboard control and safety systems. These systems may overrule or modulate the demanded braking efforts. This functionality is assured by fast response valves which intercept the fluid flow that is provided for brake clamping. Since ABS operates with high switching frequencies, modelling must take count of the dynamic response of these valves. Behaviour can be modelled using a 2nd order transfer function  $G_v(s)$  adopting an approach that is substantially like the one adopted in (4.7) to model the dynamic response of the brake amplifier.  $G_v(s)$  is the ratio between  $x_{vi}$  and coil current command  $i_{vi}$ .

$$G_v(s) = \frac{x_{vi}}{i_{vi}} = \frac{\omega_{nv}^2}{s^2 + 2\epsilon_v\omega_{nv}s + \omega_n^2} \quad (4.7)$$

### Data Post Processing

The measured data needs to be processed, to eliminate the instrumentation noise. This is important, especially for real-world tests in which the power electronics could generate not negligible electrical noise. For the standstill calibration tests, we used two types of filters:

- Moving mean filter, with a window of 70 points before and after each measured point;
- Butterworth filter, or low-pass filter, with a cut frequency of 100Hz.

As shown in Figure 4.14, the two filters are similar. For this reason, the latter is selected, which is also easy to implement and control in MATLAB.

The second phase is the removal of offset and dead-band of the measurements. Each run starts and ends with a 3s measurement reference, with no action applied to the brake system. If the reference is still different from zero, the function automatically calculates the mean offset, subtracting that quantity from all the measurement data.

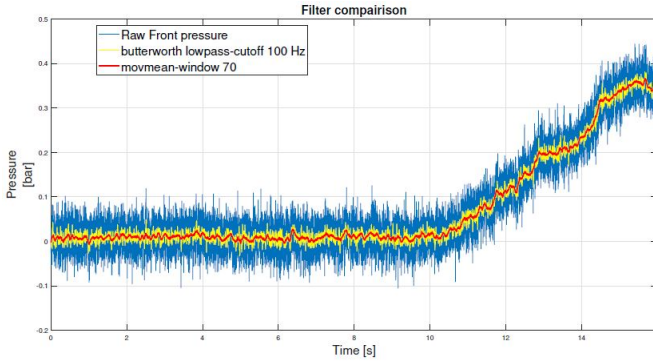


Figure 4.14: Filtering comparison for the brake pressure acquired in the Simrod Kyburz UC during real-word test

### Thermal and Wear Model

The brake plant model is divided into sub-models, each representing a specific component of the system and related physical phenomena (Figure 4.15). The braking torques on each wheel affect the dynamic behaviour of the vehicle, which is here summarised by the vehicle longitudinal speed  $V_x$  and acceleration  $a_x$ . The model can compute the temperature of different components of the brake system, including the disc-pad interface temperature  $Temp_{if}^i$ . The latter is fed back to the torque sub-model since the friction coefficient between the pad and the disc is a function of this temperature.

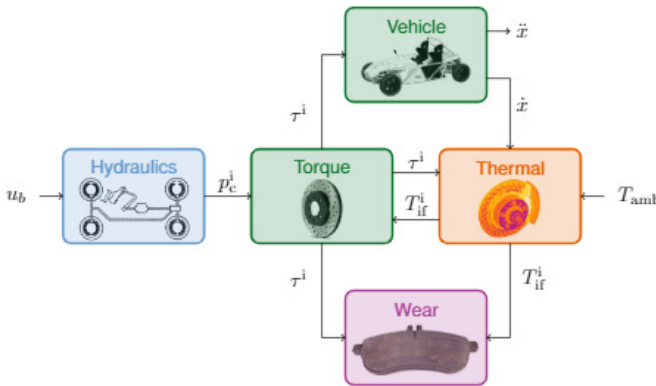


Figure 4.15: Decomposition of the braking plant simulation model in sub-models

The thermal behaviour of the braking system is modelled using an equivalent electrical circuit [215]. This circuit is composed of multiple basic elements:

- The temperature source imposes a constant temperature gradient  $\Delta Temp = Temp_s$  across its terminals. It can be used for instance to define the ambient temperature  $Temp_{amb}$  for the thermal reference.

- The heat transfer rate source imposes a constant heat rate  $\dot{Q} = \dot{Q}_s$  through its circuit branch. A common application is the modelling of the generated heat at the interface between the braking pad and the disc.
- The thermal resistance models the heat transfer between two bodies at different temperatures  $\Delta Temp = R_{th}\dot{Q}$ . This element can be used to model both conduction and convection phenomena.
- The thermal mass represents the thermal inertia of a body. It imposes the temperature of the body as a function of the rate of heat  $\dot{Q} = C_{th} \frac{d\Delta Temp}{dt} = C_{th} \frac{dTemp}{dt}$ .

The model focuses on the thermal behaviour of the calliper assembly and the non-vented braking disc of the rear brakes (Figure 4.16). The interface region between the disc and one of the pads, indicated in red, is represented by a heat source  $\dot{Q}^i$  and an equivalent thermal mass  $C_{if}$ . The latter represents the local mass around the pad-disc interface which heats up during braking manoeuvres and whose temperature is  $Temp_{if}^i$ . The resulting heat is then further propagated either towards the disc or the pad. The disc thermal capacity and resistance are given by  $C_{disc}$  and  $R_{disc}$ , respectively. The hub temperature  $Temp_{hub}^i$  is defined by the thermal resistance  $R_{hub}$  and capacitance  $C_{hub}$ . On the other side, the generated heat is propagated to the pad, the piston, the calliper and the braking fluid. When the pressure  $p_c^i$  is greater than zero, the pad-to-air convection resistance  $R_{pad,conv}$  is very high, as the pad surface is in contact with the disc and no longer with air.

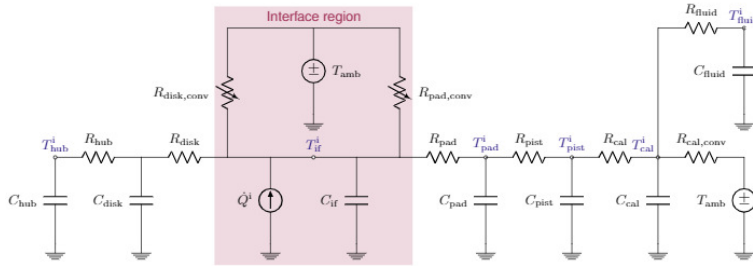


Figure 4.16: Equivalent thermal RC network for a single rear brake of the Simrod Kyburz vehicle UC

It is assumed that all the energy dissipated by the friction between the pad and the disc is converted into heat. Thus, the heat is divided equally amongst both brake pads symmetrically along the half-plane of the disc. The injected heat into the thermal model of the braking system is given by (4.8). The major difference with the front brakes model, besides the geometry, is that the front discs are vented on the SimRod. This improves the convection cooling of the system. Therefore, is assumed a speed-varying thermal resistance.

$$\dot{Q}^i = \frac{|T_{ij}\omega_{ij}|}{2} \quad (4.8)$$

The wear of friction materials is modelled according to the Archard's law, which can be expressed in polar coordinates as in (4.9) [216, 217], where  $h_p$  is the worn height of a pad,  $k_p$  is the associated specific wear coefficient,  $p_p$  is the contact pressure between the disc and the pad and  $r_p$  is the radius at which the wear occurs.

$$\frac{dh_p}{d\theta} = k_p p_p r_p \quad (4.9)$$

Finally, this equation is applied to a single pad inside one of the brake callipers of the car, after multiplying both sides for rotational speed  $\omega_p$ . It is furthermore assumed that the wear occurs at a constant average radius  $r_p = r_p^i$ . Therefore, integrating from the start of the experiment time  $t_0$  until the end  $t_f$ , (4.10) is valid.

$$h^i = \int_{t_0}^{t_f} k_p p_p^i r_p^i \omega_p^i dt \quad (4.10)$$

In (4.10),  $h^i$  is the worn height of a single pad,  $p^i = p_c^i A_{pist}^i / A_{pad}^i$  the contact pressure between the disc and the pad,  $r^i$  the mean braking radius and  $\omega_i$  the angular speed of the disc.

The wear coefficient  $k$  is a function of the interface temperature  $T_{if}^i$ , which is predicted by the previously described thermal model. The curve, represented in Figure 4.17, is a bi-linear approximation of the fading phenomenon and represents a wear increase at high temperatures due to the degradation of the mechanical properties of the material.

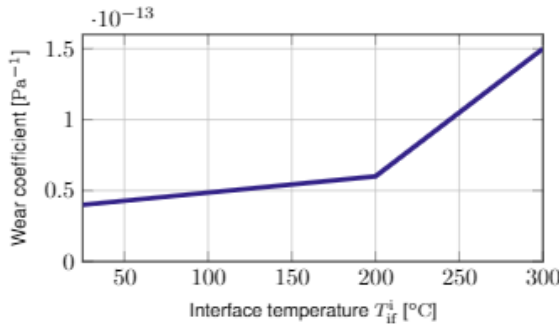


Figure 4.17: Pad wear coefficient  $k$  as a function of the pad temperature

The worn mass  $m_f^i = \rho_{pad} h^i A_{pad}^i$  per pad is obtained assuming that the pads wear uniformly across their surface. The resulting mass of emitted airborne particles in the environment  $m_{PM}^i$  corresponds on average to 35% of the total worn mass  $m_f^i$  [218]. Those particles can then be divided into two main groups, according to their size:  $PM_{10}^i$  and  $PM_{2.5}^i$  as in (4.11).

$$\begin{aligned} PM_{10}^i &= 0.8m_{PM}^i \\ PM_{2.5}^i &= 0.63m_{PM}^i \end{aligned} \quad (4.11)$$

One should note that the fraction of particles  $PM_{10}^i$  also includes  $PM_{2.5}^i$ . To obtain the total worn mass for the entire car, the wear on the four callipers should be summed, considering two pads per calliper as in (4.12).

$$\begin{aligned} PM_{10}^{tot} &= 2 \sum_i PM_{10}^i \\ PM_{2.5}^{tot} &= 2 \sum_i PM_{2.5}^i \end{aligned} \quad (4.12)$$

### 4.3.6 Suspension Model

The suspension model is integrated when using at least 2-DoF wheel models to account for vertical relative displacement between axles and tires suspensions attachment points. This is essential when analysing vehicle dynamics during transient-state cornering manoeuvres, since relevant lateral and longitudinal load transfer occurs, which produces not negligible roll and pitch chassis movement. In real-world driving conditions, the tire-road interaction is transmitted to the vehicle body through the suspension system, so its dynamical behaviour is essential for the analysis of ESP controller performance for handling and comfort.

However, the suspension system structure is one of the most complex systems in the modelling of an automotive vehicle; in fact, presents a great variety of possible configurations and the geometric properties that are assigned to the individual components can also significantly influence the performance.

Both Simulink and CarRealTime provide an intuitive interface for the suspension model parameterization. Typical parameters are spring stiffness, spring pre-load, shock damping coefficient, tire/axle connection point positions, tire/axle compliance interface and so on. The main outputs are the forces delivered to the body and wheels, the suspension jounces and travels. A dependence of toe, caster and camber angle with these variables can be assumed in the model.

VI-Grade tool is also able to perform a preliminary kinematic and elastokinematic analysis on the suspension for jounce and steering. By selecting the specific suspension type, the software allows tailoring the system characteristics by specifying the geometry parameters.

### 4.3.7 e-Powertrain Model

The electric powertrain consist of several component, i.e. ESS, inverter, EM and corresponding CUs. Depending on the purpose of the simulations, their modelling can be more or less detailed. When evaluating EV drive range and energy efficiency, accurate modelling of the electric system loss, RBS availability and battery response are demanded. If the intent is to analyse traction and braking performances the modelling effort should be focused on reliable power-plant characteristics in terms of power, torque and speed. Finally, for lateral stability control assessment, the torque delivered to the wheels must be accurately calculated in RT.

#### Electric Motor Model

A 4-quadrant EM model has been developed. For generalization purposes for the different vehicle UCs, it's parametrized respect to characteristic e-machine parameters. Specifying nominal power, nominal shaft speed, maximum shaft speed and maximum torque it is possible to obtain the ideal EM characteristics. The available output torque is mapped for the motor shaft speed using a 1-dimension look-up table. Also, the MCU is simulated, which receives from the upper-level TCS or BB controllers the demanded electric torque and set the machine output torque equal to or less than the reference one, depending on the actual EM state.

For the Valeo UC, more parameters are available. In particular, the efficiency map of Figure 4.6 was given for different EM temperatures and battery voltage. Thus, 3-dimensions lookup tables have been developed both for the output torque and efficiency for different temperatures.

In VI-CarRealTime a similar implementation is given. The model enables to specify the traction system layout (e.g. ICE, central EM, IWM) and the corresponding torque vs speed maps (for traction, coasting and braking) through look-up tables (Figure 4.18).

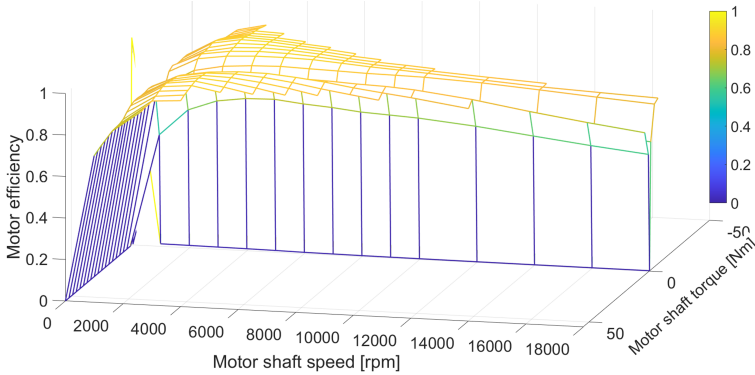


Figure 4.18: Efficiency map of the Valeo EM respect to speed and torque for 25°C temperature implemented in Simulink and CarRealTime

### Energy Storage System Model

The ESS is composed by battery, BMS and driver for the e-motor. In current literature, there are plenty of battery modelling approaches. For the purpose of this research, it is interesting to monitor the overall electrical parameters of the battery pack, avoiding the high computational cost related to accurate cell modelling and balancing strategy. For this reason, an equivalent Thevenin circuit battery model with two Resistive-Capacitive (RC) circuits, based on forgetting factor theory, is used to meet an optimal trade-off between energy storage behaviour representability and reduced code complexity.

Battery management system is responsible to calculate in RT the storage system SOC, Charge Current Limit (CCL) and Discharge Current Limit (DCL) in function of past and present current demand. The ageing effect, accounted for by the SOH presents a slower dynamic, so its calculation is performed with a higher-order sampling rate. These parameters are used to establish the torque availability, both for traction and electric braking to preserve ESS integrity and avoid fast ageing effects of the battery cells. In particular, regenerative braking should be prioritized by the BB controller when the SOC is low; on the other end, RBS should be derated or even disabled when approaching the full charging condition. From this consideration, it is evident that the BMS must operate in strict conjunction with the brake effort allocator and the MCU to avoid over-charging or under-discharging situations.

### 4.3.8 Stability Control Unit Model

Different ECUs devoted to vehicle stability are included in the model, which is implemented in accordance with the scheme visible in Figure 4.19. For the longitudinal dynamic, EBD, ABS and TCS are implemented. Except when explicitly

specified, the implemented solutions faithfully reproduce the algorithm proposed by Bosch.

This is done in the optics to ensure reliable results for a real vehicle. Perhaps, when testing newly ESP controllers it is recommended to prove its interoperability with the already existing active-safety systems. This allows us to verify that the coupling of such systems produces no counteracting effects. At this level is considered also the BB controller.

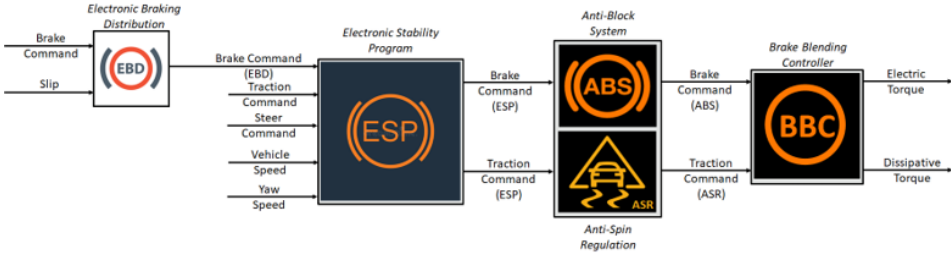


Figure 4.19: Signal flowchart of the stability control units

## EBD Controller Model

A desirable braking behaviour with neutral steering and equal tire wear is achieved when adhesion is the same for each wheel. During acceleration variations, a dynamic axle load shift occurs due to vehicle pitch movement. In braking scenarios, the front axle load rise while the rear decrease, so brake effort must be applied accordingly to avoid the wheel's locking. When friction change from sticking to sliding, the tire available cornering forces suddenly drop, leading to limited steerability in case of the front wheels slippage and instability for the rear wheels slippage [92].

The steady-state vertical load ratio between the front and the rear wheel is defined according to the car CoG location, as described by (2.17). On the contrary, when the vehicle is accelerating, the axle load distribution varies according to the formulation mentioned in section 2.1.2. Thus, the set of optimal braking points changes in the function of the brake intensity and available friction, forming a parabola curve defined by (2.19). The curve (1) of Figure 4.20 define the load distribution coefficients between the axes which maximize the available deceleration while avoiding wheels sliding. Optimal front/rear braking distribution burden on EBD: the basilar design relay on the assumption that the rear wheel should never lock up before the front ones. Since a vehicle understeering behaviour is generally preferred, a common and well-diffused strategy is to apply a fixed brake balance coefficient that prioritizes front braking, leaving to the ABS the task to avoid rear wheel locks. The strategy is described by the curve (2) of Figure 4.20, where the anti-slip controller intervention are visible [194]. For EVs equipped with BBW systems instead, the front-rear brake allocation can be regulated in RT during the braking phases. The mechanical decoupling of the brakes with the pedal allow to apply an ideal distribution, achieving higher regeneration efficiency while preserving driveability [74].

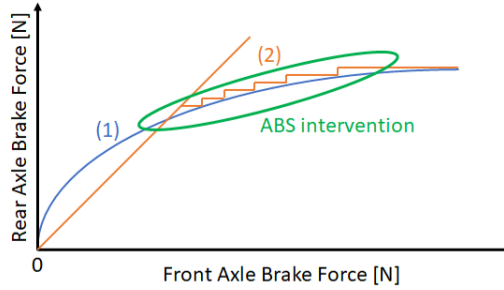


Figure 4.20: Front/Rear axles braking distribution: (1) optimal; (2) conventional

### ABS/ASR Controllers Model

To ensure stability during braking and traction conditions and improve the handling of the vehicle, both in longitudinal and cornering manoeuvres, ABS and ASR units are recommended. ABS avoid the wheels locking, reducing the corresponding stopping distance and the under/oversteering behaviour of the vehicle in a cornering scenario. To reach this goal, the braking torque is reduced until the wheel slip falls within the desired band. ASR, also known as TCS, avoid the wheels spinning, increasing the vehicle acceleration capability on the low friction surface, according to the available grip. Its action is handled by reducing the drive torque at the wheels. Both controllers ensure stable behaviour in accordance with the driver steer input. This wheel slip ratio  $\sigma$  should remain below  $[0.05; 0.15]$  absolute value (depending on the type of pneumatic), where the available friction is maximum.

The formulation used in this work relies on a functional modelling approach. The hybrid ABS/ASR controllers require specific tuning. Here, 4 different region can be identified, where  $x$  is the admitted dead-band (Figure 4.21):

1. ABS total regulation: the slip is lower than the threshold  $\sigma_{ABS}(1+x)$ , so the brake torque is totally removed;
2. ABS partial regulation: the slip is in the regulation bandwidth  $[\sigma_{ABS}(1+x); \sigma_{ABS}(1-x)]$  and the brake effort are linearly reduced with  $\sigma$ ;
3. No regulation: no regulation is applied in the band  $[\sigma_{ABS}(1-x); \sigma_{ASR}]$ ;
4. ASR total regulation: the slip is greater than the limit  $\sigma_{ASR}$  and the braking torque is increased with a quadratic function respect to  $\sigma$ . Alternatively, the traction torque is reduced with the same law.

Issues related to TRFE, introduced in section 3.2.2, are not accounted for in the following simulation activities, which is assumed the availability of reliable estimation of the friction coefficient  $\mu$ . Thus, the friction coefficient is assumed to be known.

### ESP Controller Model

Among these controllers figure also the ESP, whose foundations are widely introduced before. However, the specifications of the innovative solutions developed during these activities will be specifically addressed in the next section. In all the presented activities, the ESP controllers are coupled with the developed low-level TV allocator described in section 3.6.1.

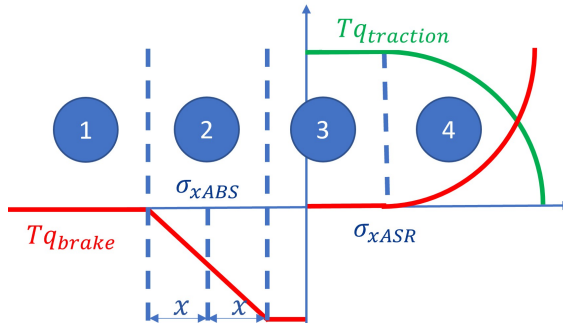


Figure 4.21: ABS/ASR torque regulation strategy respect to slip  $\sigma$

### 4.3.9 Brake Blending Controller

Braking control is the most safety-relevant vehicle functionality. With the growing diffusion of electric traction systems in the automotive sector is growing the opportunity of exploiting their four-quadrant capabilities to perform an extensive use of regenerative braking, mainly to optimize energy consumption. However, to benefit from these features, good cooperation between the friction brakes plant and RBS further complicates the controller design [219].

Optimal BB criteria, aiming at the cooperative control of both plants to assure desired braking performances, while avoiding any undesired dynamical effect that should arise from the contemporaneous application of braking forces produced by different actuators, is essential. Optimization of brake blending is challenging since exerted braking efforts also influence lateral stability. Modulation of braking forces is used by on-board control subsystems, such as ESP, to stabilize the trajectory of the vehicle. Poorly conditioned BB logic may reduce stability and comfort while increasing the corresponding stop distance.

Brake Blending Controller have to decide how to split the torque demand ( $T_{ref-ij}$ ) between the conventional brake ( $T_{ref-br-i}$ ) and the regenerative one ( $T_{ref-reg-i}$ ), according to (4.13).

$$T_{ref-ij} = T_{ref-br-ij} + T_{ref-reg-ij} \quad (4.13)$$

The allocation scheme adopted here is well described by Figure 4.22, known as the hybrid brake blending algorithm. The action of the BB regulation has to be “transparent” for the user: the system has to compensate for different performances and availability levels of electric and conventional actuators, maintaining a stable vehicle behaviour [53, 198, 220]. This also ensures simple and reliable integration with on-board CUs. In this way, it is sufficient to furnish the BB controller with the single wheel torque references to allocate the desired driving efforts, without requiring an additional interface with an active-stability controller, located before or after this controller. Thus, first, the brake distributor calculates the optimal braking performance for the front and rear axles. Then, ESP perform an optimal TV allocation. Anti-slip regulators avoid the slip or spin of the wheel.

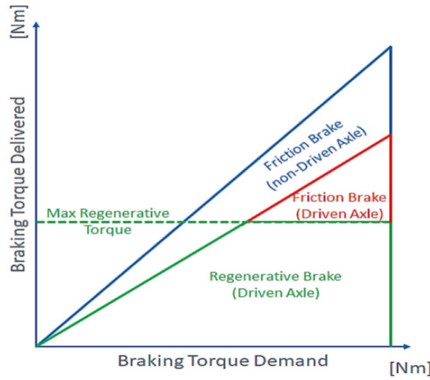


Figure 4.22: Adopted hybrid brake blending algorithm

The presence of two brake sources makes appear the vehicle like an over-actuated system. Motivated by this redundancy, the torque efforts must be constrained by some steady and variable physical limit conditions. The controller is composed by:

- **Brake Blending Controller:** producing the actuators effort references; EM torques should be limited according to powertrain and battery status.
  - *Electric Motor:* it must be controlled in order to perform the ideal traction/braking characteristic [147];
  - *Battery:* to avoid over-charge and under-discharge situations, overheating, fast ageing or other undesired occurrences, electric traction power must be limited at low SOC, while regenerative braking must be limited at high SOC.
- **Friction Brake Units:** constrained by maximum hydraulic deliverable braking torque.

Proposed brake blending logic, for a single motorized wheel, is represented in Figure 4.23, whose principal features are:

- a) *Power and Current Limits:* according to the state of the motor and of the ESS, the BB controller evaluates the drivetrain performance limitations, in terms of maximum and minimum deliverable torque, as a function of power and current that are tolerable by the electric powertrain, automatically selecting the most cautionary/restrictive condition;
- b) *Torque Demand Creation:* a reference torque demand  $T_{ref-ij}$  is evaluated according to the brake and traction commands of the vehicle driver. These torque references can also be modified/established by upper-level CUs;
- c) *Electrical Torque Saturation:* to maximize the usage of regenerative brakes for conventional brakes, the torque reference is supposed to be entirely exerted by electric motors. Generated torque reference is saturated for the known limitations of the electric plant previously calculated by (a), producing a corresponding regenerative torque reference  $T_{ref-reg-ij}$ ;

- d) *Mechanical/Dissipative Braking Torque*: to satisfy the torque demand, the difference between desired braking torque  $T_{ref-ij}$  and the one available for regenerative braking  $T_{ref-reg-i}$  is used to calculate the desired torque  $T_{ref-br-ij}$  exerted by the conventional brake;
- e) *Dynamic Compensation*: since electric and mechanical brake plants have quite different dynamical behaviour, an additional calibration filter should be imposed on the electric braking torque reference to compensate RBS faster behaviour and avoid undesirable effects in the torque references generation. Specifically, the faster RBS response must be controlled to be similar to the response of the dissipative brake, to maintain good braking performance and feel [88]. The hydraulic brake response can be modelled through a second-order transfer function (4.14), with  $\omega_{br}$  natural frequency,  $\epsilon_{br}$  the damping coefficient and  $\tau_{br}$  the time delay. Thus, the RBS response is filtered by this function to obtain a behaviour as similar as possible to one of the dissipative brakes.

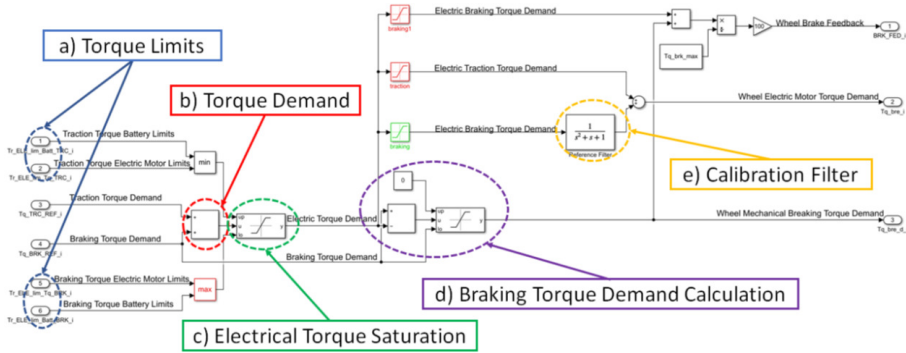


Figure 4.23: Equivalent model implementation in Simulink of the BB controller

$$\frac{P_{ij-br}}{P_{ij-ref-br}} = \frac{\omega_{br}^2}{s^2 + 2\omega_{br}\epsilon_{br}s + \omega_{br}^2} e^{-\tau_{br}s} \quad (4.14)$$

Substantially, the BB controller of Figure 4.24 receives the traction and the braking command produced by the driver. Relying on these signals, the brake allocator decides how to split the requested brake demand between the hydraulic brake and the regenerative one, in the respect of the electric powertrain torque constraints, while attempting to completely exploit the electric braking in the motorized wheels. Regenerative torque reference must be saturated to the maximum available value, reproducing the limitations of the simulated components. The BB regulation should be able to compensate for the unavailability of the actuation systems in several working situations, working adaptively and ensuring at the same time a certain minimum level of performance, able to guarantee the desired vehicle behaviour and safety level.

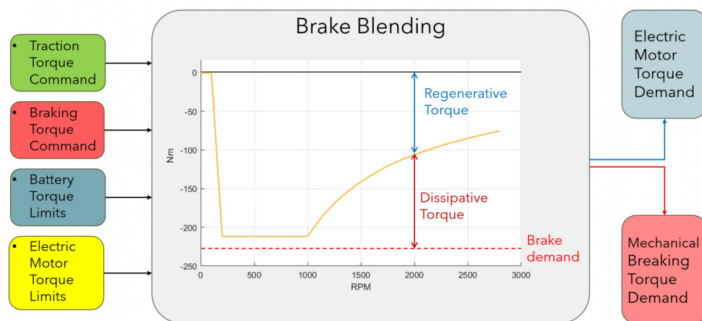


Figure 4.24: Simplified block diagram of the Brake Blending model

## 4.4 Preliminary Validation Simulations

In the following sub-sections, preliminary simulation activities are presented. These are grouped for the intent and the addressed goals. The different works are described individually in the appendix, which concerns energy efficiency, safety/reliability, and longitudinal/lateral stability.

When investigating a vehicle's feature in a simulation environment, system modelling is fundamental. The higher complexity is due to the multiple interconnected physical subsystems and the scales of the different dynamics [58]. For what concerns the virtual validation potentiality, it seems that the use of a cooperative simulation environment can lead to the possibility of to use of different solvers and sample times for the integration of the implemented subsystems while ensuring a fast data exchange between the used software. The actual implementations allow the coupling of different sub-models, whose integration is performed with the help of different solvers and sampling steps, reported in Table 4.4. The proposed co-simulation layout replicates the behaviour of a realistic EV, both for what concerns the brake system as its energy performance. The integration appears robust and reliable [221], automatically executing data extrapolation of the input signals to ensure the continuity of the exchange data between the software. This feature is fundamental to compensate for the delay effect arising from the use of different solver's sample rates and communication intervals.

Table 4.4: Cosimulation solver and sample rate settings

Cosimulation settings		
<i>System</i>	<i>Sample</i>	<i>Solver</i>
Vehicle Model	0.0001 [s]	Standard
Hydraulic Model	0.001 [s]	ODE14x (Extrap.)
Stability Controller	0.01 [s]	ODE1 (Euler)
Communication	0.01 [s]	ODE1

The flexibility properties of the models are met. Modularity and portability are proven since it was possible to use the same models for different vehicle UC and simulation software. Even RT capability is ensured, since both SiL and HiL testing are enabled [21, 198]. Indeed, a good organization of tasks is fundamental to optimising computational efficiency. Thus, it adopted a physical-based distinction

between “Continuous” and “Discrete” subsystems. Continuous models represent physical systems whose mutual interaction has to be modelled minimizing the delays introduced by the execution on a real-time target, which is necessary discrete. Computational delays are tolerable only if they are relatively negligible for the typical time scale of the phenomena to be reproduced, as shown in Table 4.5.

Each subsystem of the vehicle is implemented as an independent model instance, allowing a separate execution of each sub-model with different sampling frequencies and solver features. In this way it’s possible to perform a fixed-step concurrent execution of each plant in separated tasks, allowing a fast RT execution. Also, execution in separated threads allows verifying potentially negative drawbacks, in terms of stability, due to delay that necessarily affect the communication between time continuous and discrete systems.

Table 4.5: Simulated dynamical behaviour and corresponding integration features

System description	Physical domain	Continuous/ Discrete (Num.Stiffness)	Mean integration freq. (ODE1 solver)
Multibody Vehicle Model	Mechanical	Continuous <sup>a</sup> (Stiff)	$10^3-10^4$ [Hz]
Tire/Road Contact Models	Mechanical	Continuous <sup>a</sup> (Stiff)	$10^3-10^4$ [Hz]
Hydraulic Plant/Brake Models	Mainly Fluid	Continuous <sup>a</sup> (Stiff)	$10^3-10^4$ [Hz]
On board Digital Control Systems	Math/Digital	Discrete (Not stiff)	$10^1-10^3$ [Hz]
Electric Motor and Drives	Electric	Continuous (Stiff)	$10^3-10^4$ [Hz]
Low Lev. Control of Power	Math/Digital	Discrete (Not stiff)	$10^4$ [Hz]
Battery Models	Electro-Chem.	Continuous <sup>a</sup> (Stiff)	$10^3-10^6$ [Hz] <sup>b</sup>
Efficiency, Thermal and Wear Models	Thermal/Other	Continuous <sup>a</sup> (Stiff)	$10^1-10^2$ [Hz] <sup>b</sup>

#### 4.4.1 Brake Model Validation

For the aim of this work the **SimRod Kyburz** vehicle UC has been used. Regenerative braking was disabled so only the conventional hydraulic brake plant is used to decelerate the vehicle. The vehicle was equipped with the measurement system described in Figure 4.25, comprising IMU, Wheel Force Transducer (WFT) and others. All data are collected using a Siemens Simcenter SCADAS. For the particular purpose of this work, the hydraulic plant was equipped with additional sensors. All brake-related measured quantities are acquired with a sampling frequency of  $1024Hz$  (Table 4.6). This general approach applies to several different kinds of brake plants, including brake-by-wire ones, in which these kinds of signals are often generated by different components and subsystems:

- Vehicle dynamics and localization: vehicle kinematics and position are identified using a fully integrated OXTSTM RT3003 Inertial Measurement Unit (IMU) (6 D.O.F inertial measurements, GPS and magnetometer);
- Wheel-road interaction: forces exchanged between road and tyres are measured through a 6-axis Wheel Force Transducer (WFT) of the RoaDyn™ series, from Kistler; these sensors are installed on wheels;
- Electric drive system: battery and electric drive are continuously monitored, respectively by BMS and by Motor Control unit MCU;
- Additional sensors: the vehicle is customized to be easily adapted to different testing activities (a maximum of about 150 signals not fully listed here can be acquired). Also, the braking plant is monitored by measuring pressures on callipers and brake pedal position.

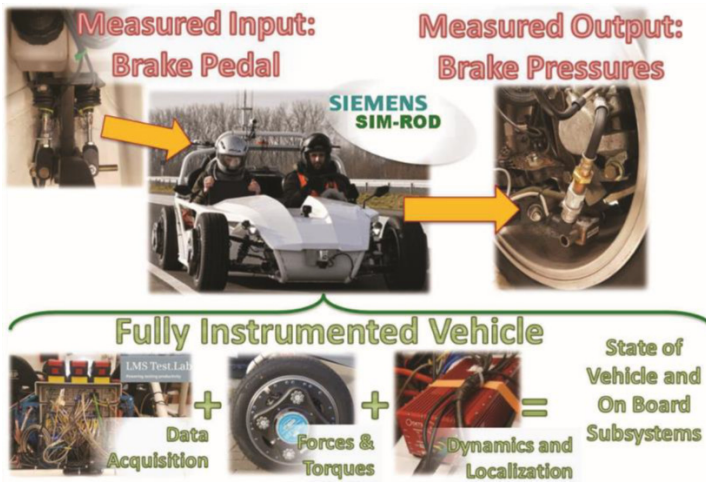


Figure 4.25: Acquisition and sensors system installed on SimRod prototype for the identification of brake plant features

Table 4.6: Vehicle and brake plant datasheet

Phys. Quantity	Symbol	Sensor	Measured
Force(f)	$F_f$	Strain gauge	Strain [ $\mu\epsilon$ ]
Force(r)	$F_r$	Strain gauge	Strain [ $\mu\epsilon$ ]
Displ(f)	$x_f$	Potentiometer	Displ [mm]
Displ(r)	$x_r$	Potentiometer	Displ [mm]
Pressure(f)	$p_{brake-f}$	Pres. sens.	Pressure [bar]
Pressure(r)	$p_{brake-r}$	Pres. sens.	Pressure [bar]

### Aim and Organization of Testing Campaign

The performed campaign aims to verify how the proposed model can fit the response of a real plant with a reduced set of known data and experimental results. The test campaign has been organized as follows:

- Standstill Tests: known inputs are applied to brake pedals, to identify hydraulic plant behaviour, in terms of clamping pressure inside callipers. The proposed model implements a decoupled scheduling of both amplitude and frequency response of the brake plant;
- Dynamic Test on Circuit: some additional tests with the vehicle running on a circuit are performed. The purpose of this activity is to verify how various braking patterns performed on a circuit by a driver should be fitted by a model calibrated with a limited number of step tests in standstill conditions. Tests were executed on the circuit of Aldenhoven (Germany) visible in Figure 4.26.

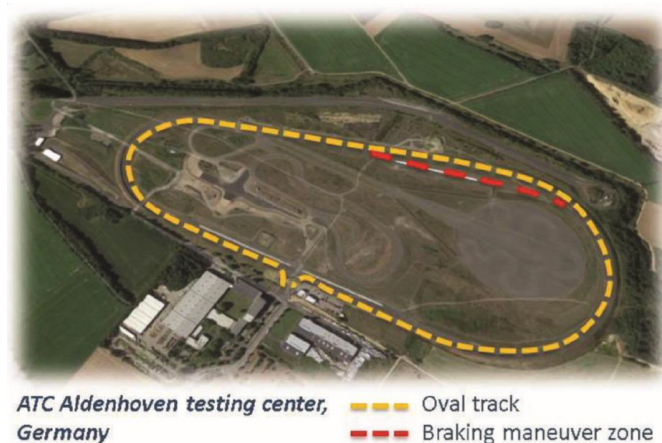


Figure 4.26: Testing center of Aldenhoven (Germany)

### Amplitude Response Identification

To identify the amplitude response of the plant, some simple tests are executed: first, the brake pedal is lowered slowly to identify the dead band or some compliance that has to be recovered in terms of pedal displacements. Then test with multiple braking applications are executed: brake pedal position is imposed and corresponding pressures on callipers are measured. In each test, the pedal position is increased from the lower end run to the upper one, with three consecutive steps. The amplitude of each intermediate step is randomly perturbed and their duration is high enough to assure the achievement of steady-state conditions before the application of the following step (the duration of  $t_{wait}$  is much bigger than the system time constant). After the maximum run is reached, the pedal returns to the lowest position through three falling steps that are generated with the same random procedure. This cycle is repeated at least ten times to have data corresponding to a population of at least 60 random steps (30 rising and 30 falling steps). To calibrate the scheduled relation between pedal displacement and corresponding steady-state pressure of the brake plant, it is recommended to observe the system output after transient becomes negligible.

Figure 4.27 is visible an example of this procedure: when derivatives of observed signals are sufficiently low, a running mean of the observed pressure is performed. In this way, it is possible to evaluate two interpolated curves for the rising and falling values of the reference, that approximately describe the amplitude response of the system, including its hysteresis. In particular, according to the sign of  $Brake_{ref-i}$ , an upper rising gain profile and a falling one can be defined. Results of Figure 4.28 are scaled for maximum input displacements and maximum brake pressures of front and rear callipers, respectively.

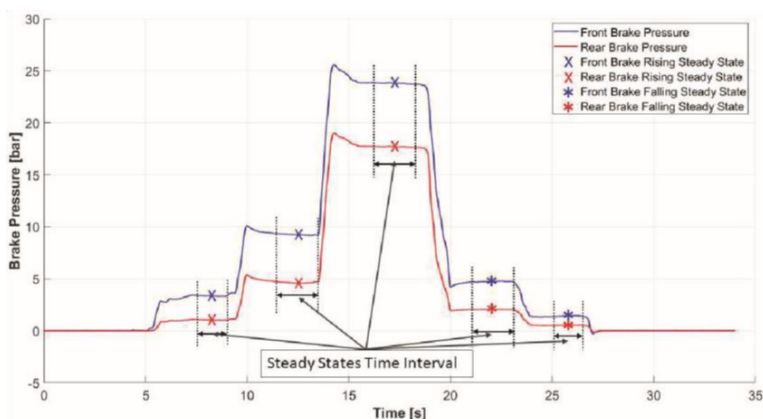


Figure 4.27: Evaluation of steady-state values for a three-steps test: brake pressures.

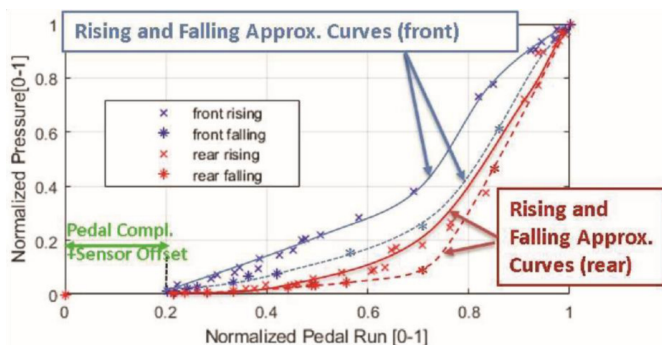


Figure 4.28: Normalized pressure plant response vs. normalized pedal run.

## Frequency Response Identification

Parameters that have to be tuned, to fit plant response, are  $\omega_n$  and  $\epsilon$  of the second-order transfer function. These parameters should be scheduled for measured inputs and their corresponding derivatives: coefficients are tabulated as compared to the sign of the derivatives of  $Brake_{ref-i}$  and  $p_{ref-i}$ , as described in Table 4.7. Since experimental data were naturally noisy, pressure and brake command derivatives must be calculated with relatively aggressive filtering (Butterworth 3rd order with a cutting frequency of about  $100rad/s$ ).

Table 4.7: Frequency response calibration of the brake plant

	$Brake_{ref-i} \geq 0$	$Brake_{ref-i} < 0$
$\dot{p}_{ref-i} \geq 0$	$\begin{cases} \omega_n = 13.5[rad/s] \\ \epsilon = 0.15 \end{cases}$	$\begin{cases} \omega_n = 10[rad/s] \\ \epsilon = 4000 \end{cases}$
$\dot{p}_{ref-i} < 0$	$\begin{cases} \omega_n = 67.5[rad/s] \\ \epsilon = 2.25 \end{cases}$	$\begin{cases} \omega_n = 40[rad/s] \\ \epsilon = 2 \end{cases}$

### Calibration Tests

By applying both over-explained amplitude and frequency scheduling, it was possible to fit in the quite satisfying way experimental behaviour of calibration tests. A comparison between brake pressure on vehicle callipers recorded during real-world tests and simulation results from the *5-DoF Simulink model* are visible in Figure 4.29. Even with the simple manual calibration, the model can reproduce some typical non-linearity of the performed test.

As visible in Table 4.8 tests are performed considering a single sequence of brake and release manoeuvres or a sequence of three incremental braking steps followed by three release steps as described in Figure 4.29. Results are evaluated according to the following performance criteria: maximum errors between simulated and experimental results in terms of absolute and relative values and delay of the maximum gradient on release manoeuvres. Higher errors are related to the difficult detection of hysteretic phenomena during the transition between braking and release manoeuvres. Indeed this evaluation must be performed by observing local derivatives which have to be filtered to avoid noisy performances.

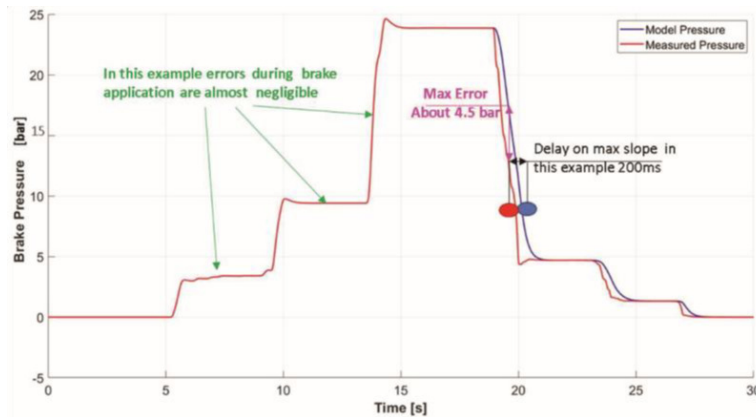


Figure 4.29: Example of fitting performance of the brake model as compared to experimental results on three steps tests used during calibration tests

Table 4.8: Evaluation of additional step tests during the calibration phase

Test N.	Type	Max Pressure Front//Rear	Max Abs	Max Rel.	Max Slope
			ErrorFront//Rear	ErrorFront//Rear	Delay*Front//Rear
1	Single Step	47.7[bar]//35[bar]	3.1[bar]//4.2[bar]	6.5%/12%	63[ms]//142[ms]
2	Single Step	51.2[bar]//36.9[bar]	4.2[bar]//3.1[bar]	8.2%/8.4%	51[ms]//123[ms]
3	Single Step	61.1[bar]//46.7[bar]	2.2[bar]//3.6[bar]	3.6%/7.7%	89[ms]//87[ms]
4	Single Step	61.1[bar]//46.7[bar]	3.5[bar]//5.1[bar]	5.7%/11.1%	41[ms]//52[ms]
5	Single Step	61.4[bar]//46[bar]	3.9[bar]//3.4[bar]	6.7%/7.4%	63[ms]//63[ms]
6	Single Step	62.5[bar]//48[bar]	3.5[bar]//5.3[bar]	5.6%/11%	52[ms]//42[ms]
7	Single Step	60.8[bar]//48.8[bar]	3.1[bar]//4.1[bar]	5.1%/8.4%	78[ms]//86[ms]
8	Single Step	64.4[bar]//47[bar]	2.9[bar]//3.7[bar]	4.5%/7.9%	143[ms]//78[ms]
9	Single Step	59.2[bar]//40.9[bar]	4.5[bar]//2.9[bar]	7.6%/7.1%	32[ms]//96[ms]
10	Single Step	68.5[bar]//49[bar]	3.7[bar]//2.5[bar]	5.4%/5.1%	69[ms]//113[ms]
11	Single Step	61.2[bar]//47.3[bar]	4.1[bar]//3.5[bar]	6.7%/7.4%	87[ms]//105[ms]
12	3-Step	26.8[bar]//16[bar]	1.5[bar]//1.5[bar]	5.6%/9.4%	35[ms]//132[ms]
13	3-Step	14.3[bar]//9[bar]	2.8[bar]//1.8[bar]	19.6%/20%	42[ms]//69[ms]
14	3-Step	14.4[bar]//8[bar]	1.5[bar]//2.2[bar]	10.4%/27.6%	41[ms]//78[ms]
15	3-Step	13.4[bar]//8[bar]	1.7[bar]//2.3[bar]	12.7%/28.8%	63[ms]//84[ms]

## Validation Process

For the validation process, the SimRod vehicle was transported to the test circuit of Aldenhoven, where it was possible to perform various manoeuvres at different speeds. By imposing the same recorded input to the calibrated model of the brake plant, it was possible to compare the simulation results for corresponding brake pressures measured during the experimental activities. In Figure 4.30 and Figure 4.31, some of these comparisons are shown: obtained results are very good in terms of fitting capability. Higher errors are mainly due to the modelling of hysteretic effects.

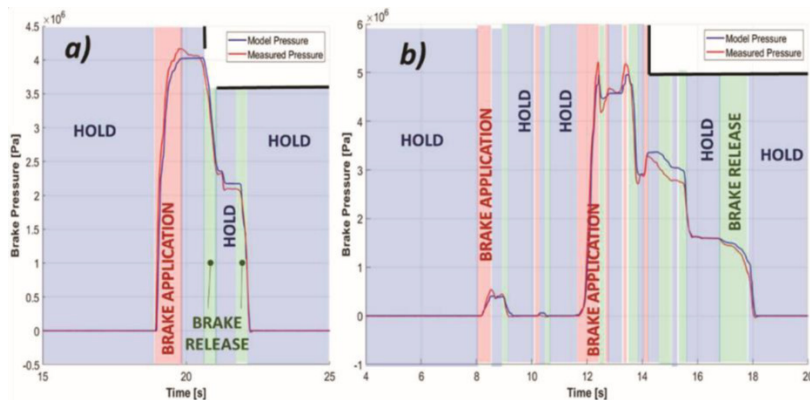


Figure 4.30: Comparison of the brake model pressure respect to experimental results during real braking manoeuvre performed on the test circuit of Aldenhoven

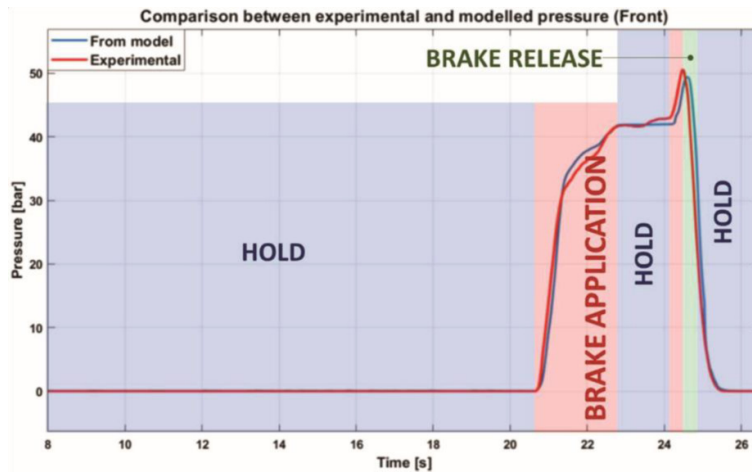


Figure 4.31: Comparison of the brake model pressure respect to experimental results during real braking manoeuvre performed on the test circuit of Aldenhoven

Knowing the friction factor of the pad, simulated brake pad torques are compared with corresponding experimental torque measurements (wheels of Simrod are also equipped with force and torque sensors) as shown in Figure 4.32.

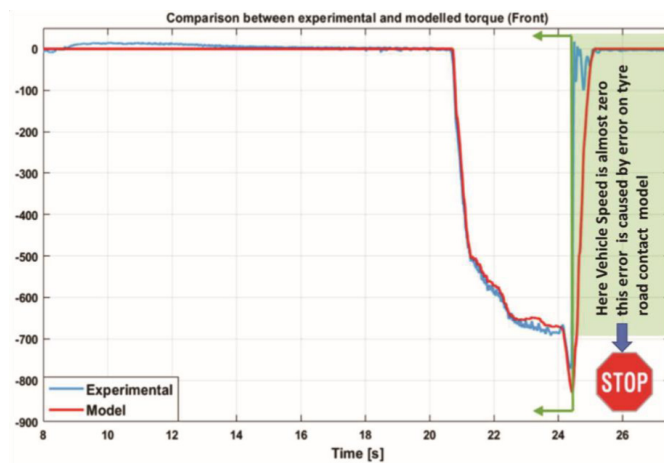


Figure 4.32: Comparison of measured and simulated torque profiles during a braking test imposing the same brake pedal displacement

Brake modulation tests are performed to assess the brake model's response to high-frequency torque demand patterns. Suppose a vehicle braking on a flat straight road with reduced friction conditions. Figure 4.33 shows the application of full braking followed by a modulation pattern due to ABS intervention with a duty cycle of 50%, resulting in a braking effort modulated at about  $25\text{Hz}$ . Results refer to brake pressure, actuator run and clamping force normalized as compared to their maximum values. The proposed model can reproduce some typical fast transient features of the plant. Indeed, the limited bandwidth of brake systems assures a relatively smooth behaviour of applied clamping and braking forces.

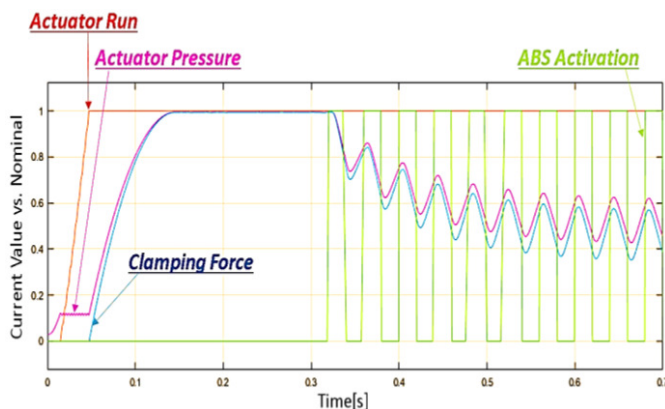


Figure 4.33: Hydraulic brake model response during a  $25Hz$  ABS brake modulation

Consider also that the ABS demand for a brake modulation pattern of  $50Hz$ , with  $225Nm$  torque on front wheels and  $150Nm$  on the rear ones. The corresponding model behaviour is the one of Figure 4.34. In contrast, Figure 4.35 shows a similar test with a  $100Hz$  frequency brake request from ABS, where it can be seen that the brake plant is approaching its frequency bandwidth.

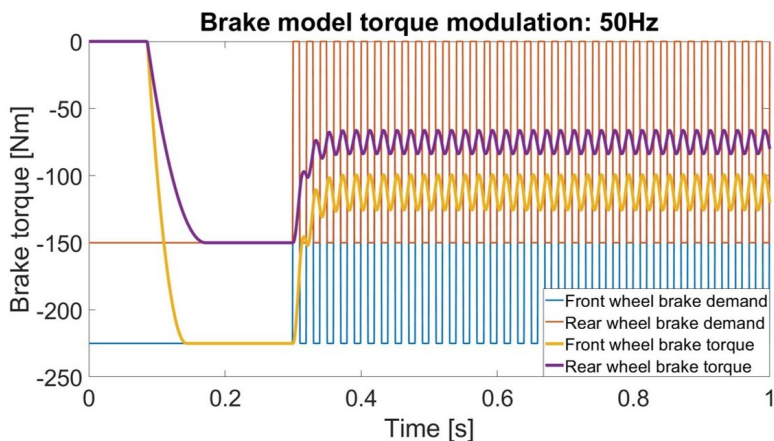


Figure 4.34: Hydraulic brake model torque during a  $50Hz$  ABS brake modulation

The response of the brake model is calibrated as compared to real experimental data. The system response can be easily changed by managing some parameters. As visible in Figure 4.36, the simulated response of the system can be customized, working on a limited number of parameters:

- *Calliper run*: represents the run of calliper hydraulic actuation, which simulates the requirement of a minimum volume of fluid to produce the desired clamping force. It's very useful to replicate a fixed delay in the plant, without introducing complicated or hard-to-tune dynamics. Increasing the calliper run introduce also a moderate degradation of system bandwidth. This feature is useful to reproduce the fact that the final volume of the simulated plant is slightly increased;

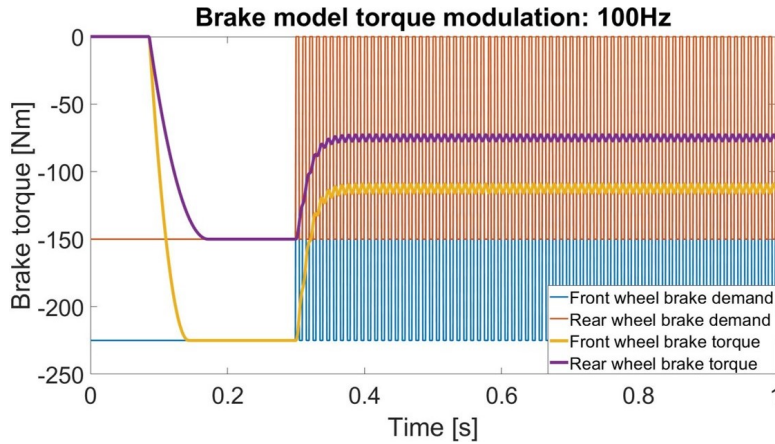


Figure 4.35: Hydraulic brake model torque during a 100Hz ABS brake modulation

- *Bulk modulus and compressibility effects*: by reducing fluid bulk modulus a higher volume of oil has to be transferred to the calliper to obtain the same response. As consequence, by doubling the consistency of the compressibility effects the response of the system is slower. An equivalent reduction of bulk modulus should be used also to take count of elastic compliance of pipes or additional plant dead volumes;
- *Hydraulic losses*: an increase of friction losses in pipes and valves introduces a slower response of the plant, also increasing fixed delays;
- *Additional parameters*: by modifying the preloads, equivalent inertia of the calliper and frequency response of valves, is possible to further reshape the response of the valves. This simplifies the customization of the plant respect to the experimental data.

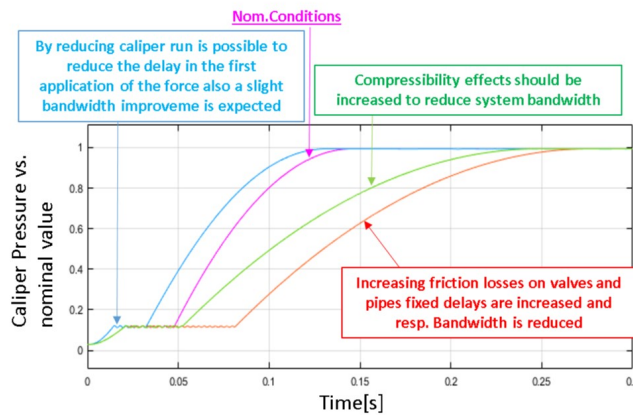


Figure 4.36: Response sensitivity of the caliper respect to variation of known input parameters

## Thermal and Wear Model Validation

The braking system of the **SimRod Kyburz** has been instrumented with several thermal sensors for the identification of the simulation model parameters (Figure 4.37). These are placed on the rear-left brake, following the different measurement points indicated in the equivalent thermal RC network of Figure 4.16. Regular thermocouples are used due to their lower cost and wide availability. Both a rubbing thermocouple and an infra-red sensor are equipped to measure the disc interface temperature. Additionally, a thermocouple is used to measure the internal temperature in the pad.

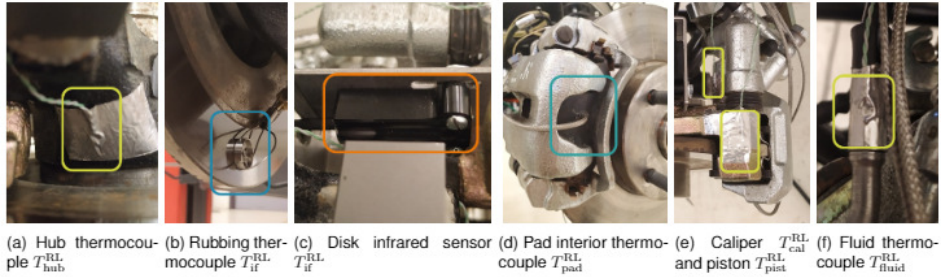


Figure 4.37: Thermal sensors instrumented on the left-rear brake of the SimRod

Other physical quantities are measured on the car during the tests. The pressure is measured next to the rear-left and the front-right callipers. The rotational speed of the wheels is acquired using optical sensors and zebra tapes. GPS data are acquired during outdoor measurements. Finally, all of the data are collected using a multi-physical Simcenter SCADAS and Testlab data acquisition system. The sampling frequency is fixed at  $100Hz$  for all the sensors. The identification measurements take place in the controlled environment of a chassis dynamometer (Figure 4.38). The braking pedal position is fixed. The rear wheels of the car are spinning at a constant speed imposed by the test bench. Different measurement runs are recorded considering several speeds and pedal displacements (Table 4.9).

Run	$p_{c,0}^{RL}$ [bar]	$V_x$ [km/h]
1	8	10
2	7	5
3	2	30
4	4	50

Table 4.9: Experimental runs evaluated on the chassis dynamometer

Then, real-world validation tests are performed on parking using the same instrumentation, where wheel lock-up is avoided during those experimental runs.

Finally, new braking pads are installed on the car before the first test on the chassis dynamometer. Their weight is measured before and after the runs listed in Table 4.9 and the real-world tests for the evaluation of the wear model.

One of the most important parameters in the simulation model is the friction coefficient  $\mu$  between the pad and the disc, as it directly links the braking pressure and the resulting torques. On the dynamometer, the dissipated power  $P_{br}$  is

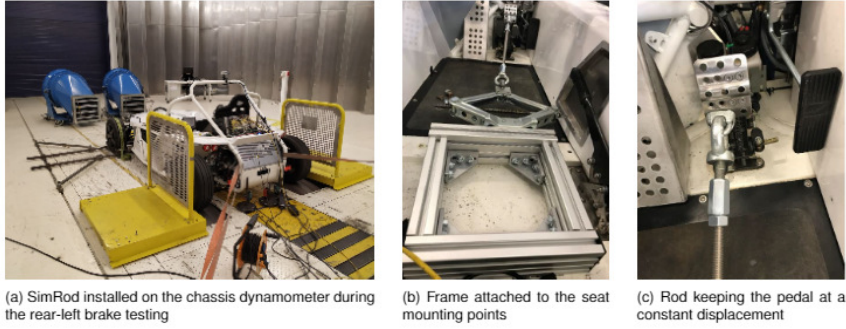


Figure 4.38: Chassis dynamometer experimental setup

obtained from the product between the rotational speed  $\omega_i$  and the torque  $T_{ij}$  of the rear wheels. In (4.15) it is assumed that the left and rear sides of the car behave equally.

$$P_{br} = T_{rl}\omega_{rl} + T_{rr}\omega_{rr} = 2T_{rl}\omega_{rl} \quad (4.15)$$

Hence, the friction coefficient  $\mu$  can be computed for all experimental runs as a function of  $Temp_{if}^i$  according to (4.16).

$$\mu(Temp_{if}^i) = \frac{P_{br}}{2\omega^i p^i A^i r^i} \quad (4.16)$$

Subsequently, these data are filtered to obtain smoother curves using a zero-phase filter to avoid adding a phase shift in the system. Finally, those curves are arithmetically averaged for each interface temperature  $Temp_{if}^i$  to obtain a unique friction curve  $\mu(T_{if}^i)$  which can be used inside the simulation model.

The final tuning of the different thermal parameters is done using a top-bottom approach. The experimentally measured torque is imposed on the model. Therefore, the dissipated heat at the disc-pad interface is computed based on the acquired data for all measurement runs. It's then imposed as an input to the simulation model and the resulting predicted and measured temperatures are compared. The parameters are tuned to find a good correspondence between experimental and simulated temperatures. The friction coefficient  $\mu$  is evaluated for the different runs using (4.16). The results were plotted as a function of the interface temperature  $Temp_{if}^{RL}$  in Figure 4.39.

After identifying the different thermal resistances and capacities of the system, the simulation model is executed on the different recorded runs for its validation. For this purpose, measured pressure and speed are imposed directly on the model and the thermal responses of the different braking system components are compared. Firstly, a good match is observed between the measured and the predicted temperatures of the interface region and the piston (Figure 4.40). During the first 1500s of the run, the temperature increases up to 200 °C. Subsequently, the brake pedal locking mechanism is retracted before restarting the test bed at its initial speed.

The short period during which the wheels are not rotating corresponds to the slow decrease in interface temperature. Once the dynamometer is restarted, the decrease in temperature accelerates again thanks to the increased convection.

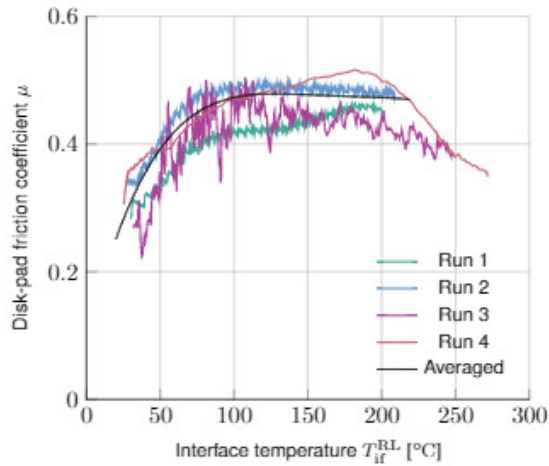


Figure 4.39: Estimated friction coefficient for the different measurement runs as a function of interface temperature  $Temp_{if}^{RL}$

Similarly, a comparison between the pad and calliper temperatures is provided (Figure 4.40/b).

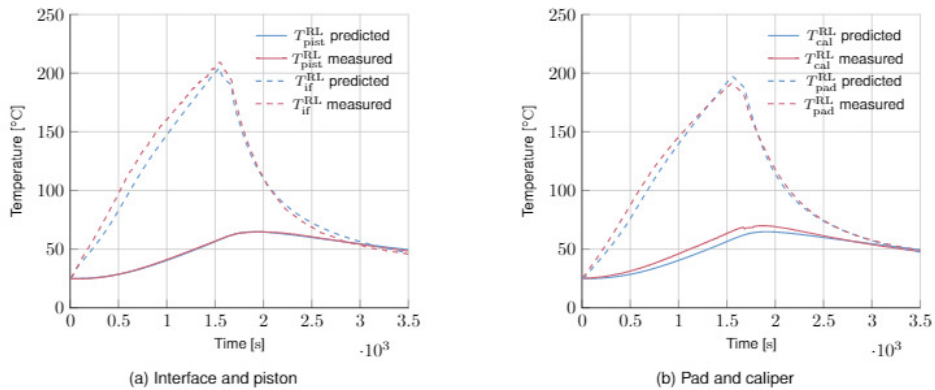


Figure 4.40: Comparison between predicted and simulated temperatures for run 3

Finally, the solely *thermal and wear simulation model* is used to predict the thermal behaviour of the braking system in a real-world driving scenario (Figure 4.41). During the first part of the experiment ( $t \approx 100$  s), the driver quickly alternate between accelerating and braking manoeuvres to increase the interface temperature. Afterwards, the car is stopped to let the system cool. The measured pressure and GPS speed are used as inputs to the simulation model. A good match is observed between the predicted and the measured results.

A first validation for the wear model is performed by comparing the mass of the newly installed braking pad before and after all the tests. The predicted wear mass is also computed by the model (Table 4.10). Although a good match is observed between measured and predicted wear, further tests are required to more accurately validate this part of the simulation model.

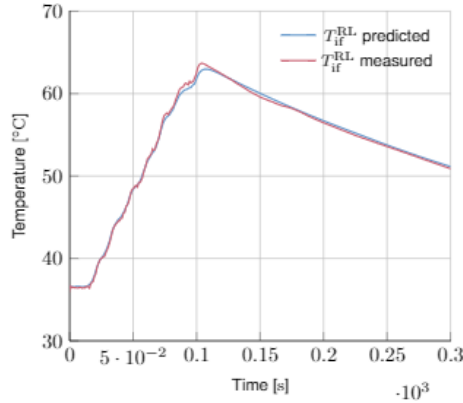


Figure 4.41: Comparison between predicted interface temperature and measured interface temperature for consecutive braking manoeuvre during on-road driving

Parameter	$m_{pm}^{RL}$ [g]	$h^{RL}$ [mm]
Measured	1.7	6.5e-2
Predicted	1.5	5.9e-2
Error	11.7%	8.8%

Table 4.10: Predicted and measured wear on a single rear-left braking pad

## Conclusions

A scalable model of the braking system is presented with a focus on the thermal, friction and wear behaviour. An experimental setup and identification methodology are also proposed and evaluated. The resulting parametrized models show a promising correlation with the experimental results [213, 214]. Preliminary validation results obtained on a test circuit are quite encouraging. These indicate that brake pressures are reproduced quite precisely, and recorded errors produce negligible errors in terms of simulated vehicle dynamics. The models showed a promising correlation with the experimental results. Finally, simulations on the emissions associated with brake pad wear highlight that it is important to consider also the emissions associated with braking, along with the combustion ones [198, 214].

Proposed models offer interesting features for preliminary sizing and optimization of brake blending policies. The tool is also designed and optimized for real-time implementation and HiL testing.

### 4.4.2 EV Efficiency Improvements

Many activities have been conducted for the EV's use cases to investigate the energetic aspects. An appropriate brake blending strategy must be used to maximize regenerated energy. In this implementation is assumed that every wheel is equipped with its BB controllers to ensure higher energy harvesting capacity. In addition to BB algorithm [21, 198, 199, 210, 221, 222], advanced energy management strategy (e.g. RBS coordination and power flow control) are proposed [223, 224].

Since the final goal is to bring the energy flow control to an upper level, understanding the functionalities of the sub-components is essential. Thus, a functional model appears more appropriate than a structural one. Results prove the efficiency improvements allowed by the BB allocation algorithm and the optimal energy management policies proposed in these activities, which have been applied on **FIAT 500e** and **VALEO concept car** vehicle models.

### Brake Blending Control

The developed hybrid BB controller consent advantages in terms of efficiency. In a co-simulation activity between *Simulink* and *Amesim* [221], the *5-DoF* model of the **FIAT 500e** (Figure 4.42) was used to establish the regenerated energy during a World harmonized Light-duty vehicles Test Cycle (WLTC). Two different drive configuration was compared: the conventional FWD central motor layout with the differential transmission; 4WD traction configuration with independent wheel motors and, thus, independent brake effort allocation control for each wheel.

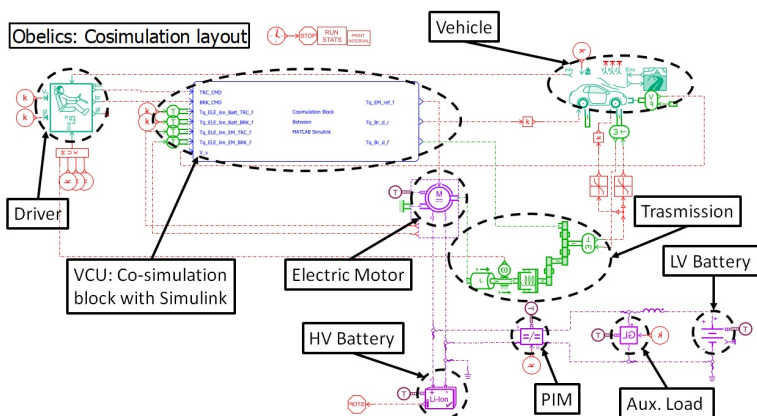


Figure 4.42: Co-simulation layout implemented in Amesim for the reference UC

The availability of the regenerative brake system consents to the recovery of part of the total consumed energy, depending on the adopted powertrain configuration, increasing the overall efficiency and autonomy. As visible in Figure 4.43 and Table 4.11, about 15-18% of the consumed energy can be recovered using the developed BB strategy. Simulations have been repeated for different test cycles (NEDC, WLTP, FTP-75) to verify the robustness of obtained results [198]. Results are visible in Table 4.12: as expected, a four inwheel powertrain is desirable in terms of regenerated energy and stability.

Another interesting result is represented by the comparative evaluation of brake pad wear, which is far lower for the four in-wheel powertrains. The high RBS efficiency can be easily explained considering the limited deceleration associated with simulated test cycles: for the four in-wheel powertrain deceleration is almost completely assured by electric braking.

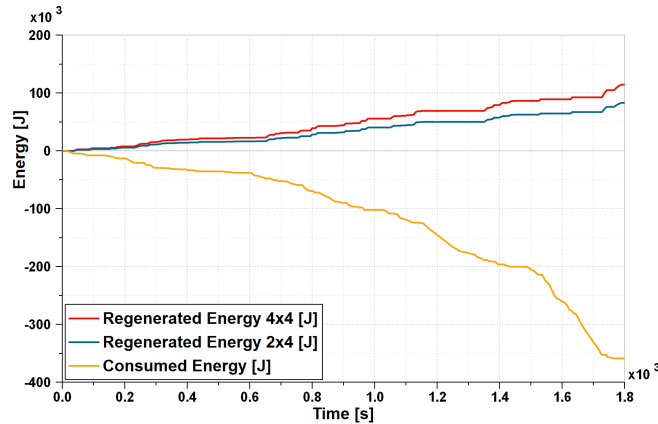


Figure 4.43: Consumed and regenerated energy during a WLTC class 3

Table 4.11: Vehicle energy performance during WLTP class 3 cycle

Vehicle Energy Performances				
Cases	Consumed Energy [kJ]	Regenerated Energy [kJ]	Regenerated Energy [%]	$SOC_f$ [%]
No Reg Brake	1582.1 kJ	0 kJ	0%	41.2%
2x4 Reg Brake	1353.6 kJ	225.5 kJ	14.25%	43.9%
4x4 Reg Brake	1306.3 kJ	275.8 kJ	17.4%	44.5%

Table 4.12: Consumed vs recovered energy and pad wear

Drive Cycle Simulation Test			
Drive Cycle	Traction Layout	Reg vs. Cons energy	Pad Wear Reduction
<b>NEDC</b>	2x4 (A)	0.258	About 60%
	4x4 (B)	0.427	About 99%
<b>WLTP</b>	2x4 (A)	0.287	About 68%
	4x4 (B)	0.454	About 99%
<b>FTP-75</b>	2x4 (A)	0.393	About 66%
	4x4 (B)	0.601	About 99%

The controller proved to be flexible since it was possible to use the same model for both powertrain configurations proposed for the benchmark vehicle model. Also, the BB strategy appears to be extremely efficient and reliable, since addresses the maximum of the requested braking effort to the electric motor, in the respect of the corresponding constraints, leaving the disc brake the burden to compensate for a possible gap between the required torque and the one delivered by the EM. In Figure 4.44 an example is shown: the algorithm allocates the maximum available braking torque to the RBS. The remaining one is applied through a conventional brake system.

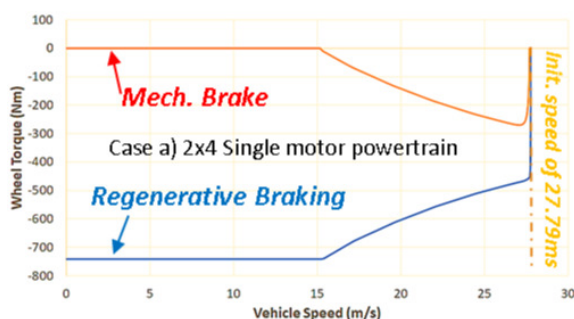


Figure 4.44: Brake blending with a constant brake demand of 700 Nm.

### Fuzzy Brake Blending Controller

For the same *5-DoF model* of **FIAT 500e** benchmark vehicle, a simulation campaign was performed in *Simulink* to evaluate the performances of a novel **Fuzzy Brake Blending** solution [199]. The intent is to evaluate the improvement permitted by the Fuzzy Brake Blending (FBB) controller in terms of regenerated energy and battery ageing.

Fuzzy logic can be considered as a simplified neural network whose primary benefit is to approximate systems behaviour when analytic functions or numerical models don't exist, are poorly structured [225] or object of a high level of measurement uncertainty [226]. This solution is a widely adopted tool for the control of a complex system which involves several devices and components belonging to quite different physical fields: this is the case of the BB [227]. This methodology enables the prediction of the state's evolution to avoid undesired situations while assuring the full exploitation of the EM torques availability. Indeed, conventional controllers are often restricted to linear ranges of variables.

Proposed Fuzzy Inference System (FIS) logic controller, whose block diagram is represented in Figure 4.45, aims the control the blending strategy. By doing so, it is possible to account for the following variables.

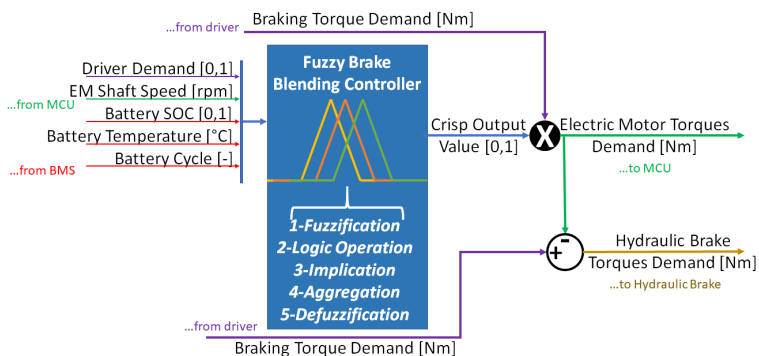


Figure 4.45: Fuzzy brake blending controller

1) **Driver Demand:** establish the requested torques on each wheel. For medium SOC value a regenerative brake is still desired, but it achieves its maximum value of 1 only if the entity of the requested brake exceeds a threshold, corresponding to a minimum level of regeneration. Indeed, if the brake command is smaller than this established value, the reduced amounts of recovered energy could not justify the increased complexity in energy management. The *Driver demand* is then fuzzified through three different Mothership Function (MtF)s, respectively *full*, *derate* and *no* for low, medium and high SOC values.

2) **EM shaft speed:** essential for the evaluation of the available torque by the electric powertrain and the avoidance of shaft overrunning. The full exploitation of the EM characteristics is achieved by making sure that the delivered torque closely matches the ideal traction/braking curve. To realize this assumption in the FIS, we build a 2 MtFs variable dependency: the *start* function, used to avoid vehicle going in a reverse direction, and the *stop* function, which turns off the regenerative braking above the maximum admitted shaft speed. The Iso-Torque and Iso-Power curves arise from the MCU.

3) **Battery SOC:** fundamental for averting dangerous conditions of the storage system. The power constrains are implemented by 3 MtFs named *low*, *medium* and *high*, reflecting the corresponding SOC states defined by (4.17), where  $C_{nom}$  is the battery capacity. This variable is essential to avoid fast performances degradation due to high level of requested Depth Of Discharge (DOD), as pointed out in [228], where  $DOD = 1 - SOC$ .

$$SOC = 100 \left( 1 - \frac{1}{C_{nominal}} \int_0^t i(t) dt \right) \quad (4.17)$$

4) **Battery Temperature** it is recommended to reduce the power flowing in the battery when low or high temperatures condition occurs. Similarly, in the previous case, temperature effects increase the ageing rate of the battery [228, 229]. So it is advisable to limit the battery C-rate when operating at a temperature that differs from the nominal. We adopt a Gaussian MtF in the function of the battery temperature to reduce the current for low and high temperatures.

5) **Battery ageing** used to implement energy limitations of storage according to capacity fade effects. As the battery ages its capacity decreases, so it is recommended to limit the amount of power recovered during regenerative braking scenarios. Otherwise, we could accelerate the decay performance law.

To quantify the ageing effects we consider the severity factor  $\Phi$ , an indicator of the battery degradation respect to the nominal number of admitted cycle  $N_{EoL}$ . In particular, the severity factor, at a given *DOD* and temperature  $T_{batt}$ , is defined by (4.18), with  $i(t)$  the current actually flowing in the battery.

$$\Phi = \frac{Ah - throughput_{nominal}}{\int_0^{t_{EoL}} |i(t)| dt} \quad (4.18)$$

A value of  $\Phi$  higher than 1 corresponds to more severe operating conditions for the baseline. In [228] the severity factor is mapped respect to *DOD* and  $T_{batt}$ , highlighting that at higher temperature and depth of discharge the severity factor is increased, as the ageing rate. In this work, we assume three different values for  $\Phi$ . In these scenarios is recommended to reduce the flowing current when the effective battery Ampere-hour throughput is approaching his End of Life (EoL) value. To implement these functionalities we use a single MtF for the performed equivalent

cycles. The severity factor  $\Phi$  is used as adjusting coefficient for the calculation of the effective battery  $Ah$ -throughput $_{eff}$ , according to (4.19).

$$Ah - throughput_{eff} = \int_0^t \Phi(t) |i_{batt}(t)| dt \quad (4.19)$$

At this point the  $Ah$ -throughput $_{eff}$  is used to establish the equivalent number of performed cycles  $N_{eff}$ , subdividing it by the nominal  $Ah$  consumed during a cycle in nominal condition, which is double the nominal capacity of the battery, supposing a cycle composed by a full charge and discharge process.

**6) Output** the fuzzy logic requires the definition of proper output MtFs to fulfil the implication phases. Those are *max* and *min*.

Once established the inputs fuzzy values using the corresponding MtFs during the fuzzification process, the fuzzified input variables, whose degrees of membership are comprised between 0 and 1, have to be processed according to specified rules. Adopted implication rules, summarized in Table 4.13, have the objective to join model-based constraints with poorly structured reliability aspects of the electric powertrain. In the meanwhile, it enables to maximize of the regenerated energy. The resolving of those statements is done according to AND operator logic (min).

Table 4.13: Fuzzy controller implication rules

Implication Rules: Statements						
$n^\circ$	$Brake_{CMD}$	$EM_{rpm}$	$SOC_{batt}$	$T_{batt}$	$Cycle_{batt}$	output
1	full	start	low	cycle	T	max
2	derate	start	medium	cycle	T	max
3	no	start	high	cycle	T	min
4	stop	/	/	/	/	min

For each rule, a single degree of membership is obtained using an OR operator between fuzzified input and corresponding output MtFs, during the implication phase. The following aggregation stages conjugated the previously described rules, while the final defuzzification phase returns a single crisp final value using a Small Of Minimum (SOM) logic. The FIS controller uses a *mamdani-type* inference method and the output signals are continuous (instead of discrete for the *sugeno-type*). This final value corresponds to the desired EM brake ratio that can be exerted by the electric powertrain, respecting the actuator constrain. This solution concretized the attempt to reproduce a model-based concept in a fuzzy controller. The above mentioned input and output MtFs are visible in Figure 4.46.

For evaluating the performances of the proposed FBB controller, the models of the investigated EV (the *FIAT 500e*) has been implemented in *Simulink*.

Performed tests can be grouped into two branches:

**Full Braking** : consist of the execution of straight-line deceleration at fixed boundary condition, varying the corresponding initial charge. In this way it is possible to show the influence of  $Brake_{CMD}$  and  $EM_{speed}$  Membership Functions on the blending strategy. During these full braking manoeuvres the blending controller prioritizes the RBS when available. Initial vehicle speed  $V_x = 27.78m/s$  and battery temperature  $Temp_{batt} = 20C$  are supposed constant, while consecutive simulation

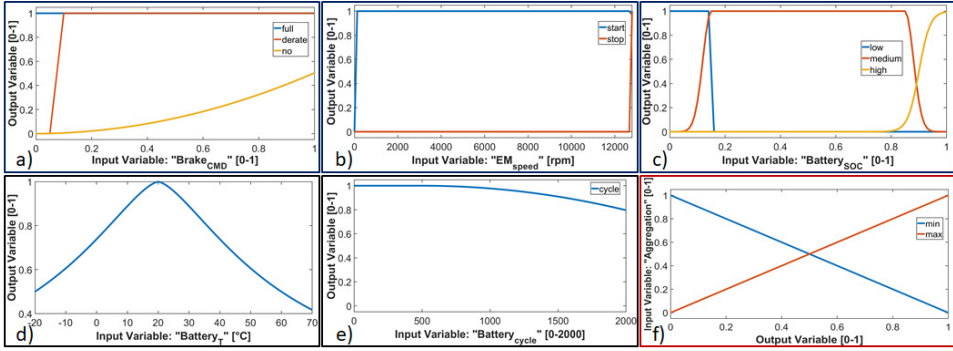


Figure 4.46: Membership functions for: a) brake command; b) EM shaft speed; c) battery SOC; d) battery temperature; e) battery cycle; f) aggregation

have been performed at different battery initial charges  $SOC_i$ . Outcomes of the tests, for the FWD vehicle UC, are the torque references summarized in Figure 4.47.

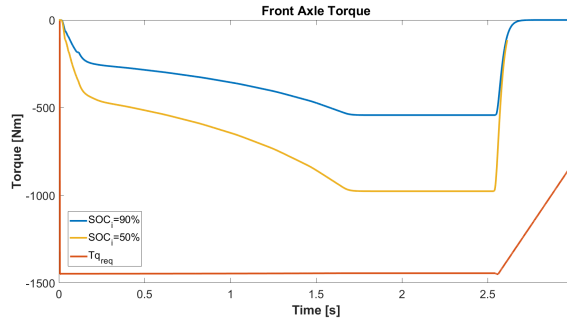


Figure 4.47: Straight line deceleration: regenerative torques at different  $SOC_i$  for the full brake test

**Driving Cycles** : making the vehicle perform specific driving cycles at different initial battery temperature  $Temp_{batti}$ , to account for the effect of the FBB controller on storage reliability aspects. Though more significant driving cycles are available and frequently used, e.g. WLTP, which better replicates real driving conditions by involving a wide spectrum of acceleration and speed ranges, we still opted for the NEDC. This is since experimental data have been made available by CRF concerning this cycle, useful for the model and controller design. Tests are repeated, for both the electric powertrain configurations, supposing the unavailability and availability of the FBB controller to metrical asses its performances. Interesting output are regenerated energy respect to the consumed one, final  $SOC_f$  and effective  $Ah$ -throughput impact on one equivalent performed cycle (4.20). These results are visible in Table 4.13, assuming the data arise from simulation performed with conventional BB as a reference baseline for the improvement evaluations.

$$Ah - throughput_{\text{impact}} = \frac{Ah - throughput_{\text{eff}}}{2C_{\text{nom}}} \quad (4.20)$$

Results of Figure 4.47 show how the proposed controller correctly assigns the EM's torque references, according to the battery SOC and motor shaft speed: when a high level of charge occurs the FBB strategies reduces the RBS effort to avoid over-charging. Regarding the driving cycle simulations, we expect a faster performance degradation when the BB strategy does not account for thermal and ageing phenomena. Data of Table 4.14 are in agreement with these assumptions since more severe operative conditions accelerate the performance decay. Indeed, according (4.18)-(4.18) and [228], the impact in the battery ageing of cycles performed at temperatures different from the nominal, is greater.

Table 4.14: NEDC simulation results at  $SOC_i=85\%$  and  $DOD=5\%$

<b>Initial Condition: <math>T_{batt0}=20^{\circ}C</math>; <math>\Phi = 1</math></b>				
<i>Layout</i>	<i>Fuzzy BB</i>	$SOC_{battf}[\%]$	$E_{reg}/E_{cons}[\%]$	$Cycle_{impact}[\%]$
FWD	ON	80.1	16.24	3.24
	OFF	80.2	16.28	3.45
4WD	ON	80.5	21.72	3.40
	OFF	80.5	21.76	3.61
<b>Initial Condition: <math>T_{batt0}=45^{\circ}C</math>; <math>\Phi = 1.5</math></b>				
<i>Layout</i>	<i>Fuzzy BB</i>	$SOC_{battf}[\%]$	$E_{reg}/E_{cons}[\%]$	$Cycle_{eff}$
FWD	ON	79.9	10.87	4.93
	OFF	80.2	16.28	5.17
4WD	ON	80.0	14.47	5.09
	OFF	80.5	21.76	5.41
<b>Initial Condition: <math>T_{batt0}=60^{\circ}C</math>; <math>\Phi = 2</math></b>				
<i>Layout</i>	<i>Fuzzy BB</i>	$SOC_{battf}[\%]$	$E_{reg}/E_{cons}[\%]$	$Cycle_{eff}$
FWD	ON	79.7	8.14	6.42
	OFF	80.1	16.23	6.90
4WD	ON	79.9	10.85	6.57
	OFF	80.5	21.71	7.22

An important consideration about the proposed controller could be done observing that the amount of energy regenerated is minor for higher battery temperatures. A first look at this output could suggest some error in the simulations activities since we expect a less significant decrease of the energy recovered ratio by the RBS when the tests are performed at severe temperature conditions. However, these results are justified considering the limited vehicle accelerations involved by the NEDC.

The most significant results of the simulations are the energy performances and reliability improvements obtained. Supposing different powertrain layouts allows for comparatively evaluating the outcomes, as well as the assessment of scalability and portability properties of the developed control strategy.

## Energy Management Control of Auxiliary Load

In this work, a decentralized power management strategy that can be easily implemented in almost every vehicle is proposed. The system aims to force an increased statistical correlation between the applied auxiliary loads and vehicle dynamics: in this way it's possible to save energy when the traction system is requiring more power, shifting as much as possible the application of auxiliary loads during the regenerative braking phase, thus when a reverse flow of power can be exploited.

**FIAT 500e** The scheme is visible in Figure 4.48, applied to the **FIAT 500e 5-DoF model in Simulink-Amesim co-simulation** environment [223]. After a battery charging phase and many more situations of interest – At the system initialization, the Power Management System collect some data from the other ECUs installed on board and associated with the different vehicle subsystems to estimate the CCL and the DCL of the powertrain. According to these values, the controller decided how the auxiliary loads should be managed to preserve the battery against overloads. It is defined as a binary state called "ECOMODE" which is sent and shared with the various electronic control units. According to the state of ECO MODE, each connected subsystem will define its energy management policy privileging performance or energy saving. In this way, the proposed system indicates to connected devices the opportunity of enabling a more aggressive or conservative power policy, but how this choice is implemented in each sub-system's controllers. To implement the proposed control strategy the speed of the compressor of the chiller/heat pump of the HVAC is regulated to maintain the temperature of the processed air to a known reference temperature.

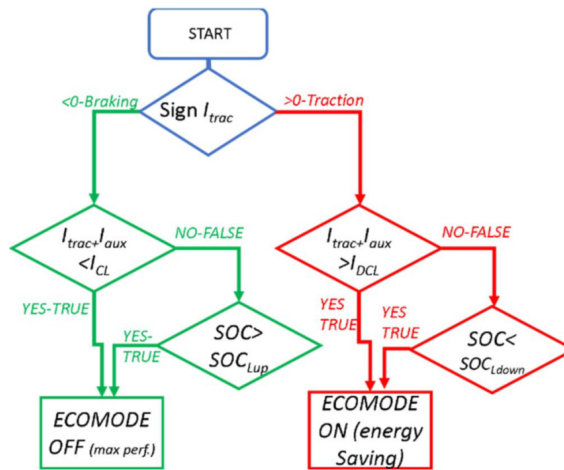


Figure 4.48: Auxiliary load management control: block diagram

Air mass flow is regulated through a speed-controlled blower; its speed reference is generated by a temperature loop aiming to regulate the internal temperature of the cabin. So, a higher temperature error in the cabin corresponds to greater performance in terms of exchanged heat flows. The following modifications have been introduced: both regulators are supposed to be proportional and not controlled by a discrete state logic; also it's introduced a variable dead-band on the evaluation of both temperature errors.

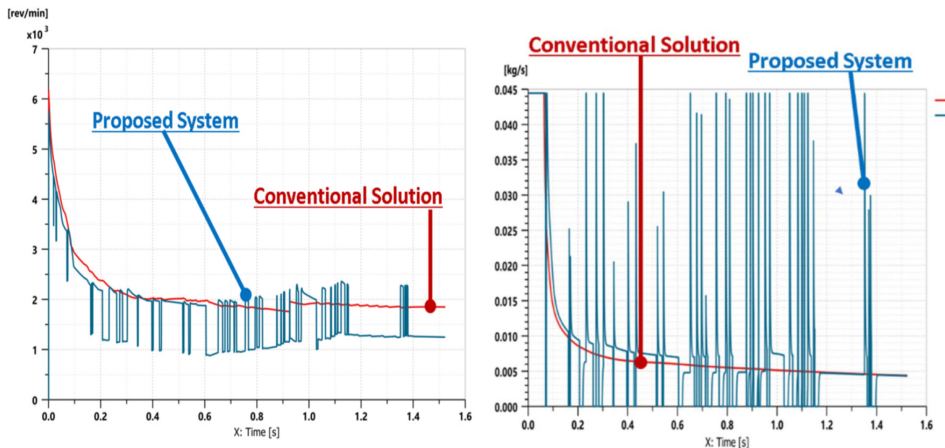
This dead band is a function of the ECOMODE state: if the ECOMODE state is “ON” (system needs to save energy) dead band is increased. Otherwise is near null and the performances of both loops are higher. Thus, in ECOMODE, intervention concern both the control loop gain modifications and variable tolerance dead-zones.

As visible from the result of Table 4.15, the proposed system assures an increase of the residual vehicle autonomy during a WLTC mission profile, thanks to energy saved by HVAC: most of the energy-saving is assured by more efficient use of HVAC compressor while the consumption of the blower is almost the same.

Table 4.15: Comparison in term of energy consumption

	<i>ECOMODE</i>	<i>Conventional</i>	<i>Difference %</i>
Blower Energy	25.8 [Wh]	25.6 [Wh]	-0.8%
Compressor Energy	134 [Wh]	193 [Wh]	-30%
Distance	7234 [m]	6682 [m]	+9%

In Figure 4.49 power profiles of compressor and blower are shown: it is quite clear how blower and compressor switching are well-synchronized for traction and braking manoeuvres. Looking to cabin temperature profiles visible in Figure 4.50, it is visible that these relevant improvements are obtained with limited consequences on controlled temperature, since the increased dead band produced negligible temperature fluctuations.



(a) Comparison of compressor rotational speed)

(b) Comparison of blower flow

Figure 4.49: Comparison of thermal regulation system's behaviour during a WLTC

RDE cycles concerning urban, extra-urban and highway scenarios are simulated supposing different external conditions with a cabin target temperature of 23C. Assuming the energy consumption as the reference metric, energy efficiency improvement related to the Auxiliary Power Management Control (APMC) is visible in Table 4.16. The major benefits found in the urban and extra-urban cycles, as compared to the highway ones, are justified by the increased traction demand required which reduces the overall improvement in percentage.

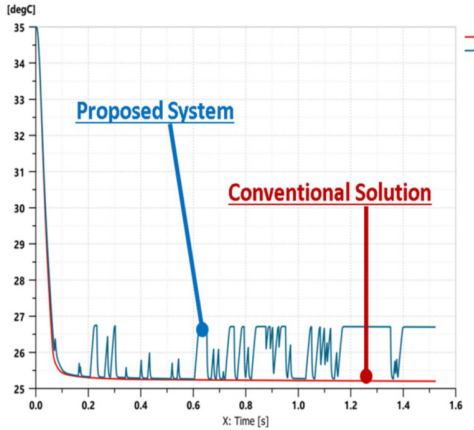


Figure 4.50: Comparison of cabin temperature during a WLTC

Table 4.16: Efficiency improvement in RDE cycles

Efficiency improvement [%]			
Externat Temp	Urban (430s)	Extraurban (1045s)	Highway (3330s)
35°C	5.16	1.12	0.26
10°C	8.67	4.04	1.74
35°C	6.86	2.92	1.84

As visible in Table 4.17, when is supposed an initial battery, the overall energy consumption is increased to assure a fast cooling of the storage system. Current fluctuations are less than 1C for a difference between external and internal temperature of 10C so the recorded increase of efficiency (30%) is largely justified by more efficient use of available energy.

Table 4.17: Energy consumption in RDE cycles

	<i>ECO bat overheating</i>	<i>ECO bat nominal</i>
Blower Energy	32 [Wh] (+6.2)	25.8 [Wh]
Compressor Energy	186 [Wh] (+62)	124 [Wh]

**Valeo concept car** A similar controller has been applied to the **concept Valeo** vehicle UC using RDE drive cycles [224], exploiting the same *6-DoF co-simulation model of Simulink-Amesim*. A simplified flow chart of the APMC is visible in Figure 4.51. The process is recursively iterated ad each time steps of the APMC. Does the controller allow the verification of two *if* statements: (1) is the value of current SOC is below a specified desired value? (2) The total requested current is above admitted DCL? Results of the rules are evaluated through an OR logical operator. If verified, ECO-mode will trigger, otherwise, no action on auxiliary systems is

performed.

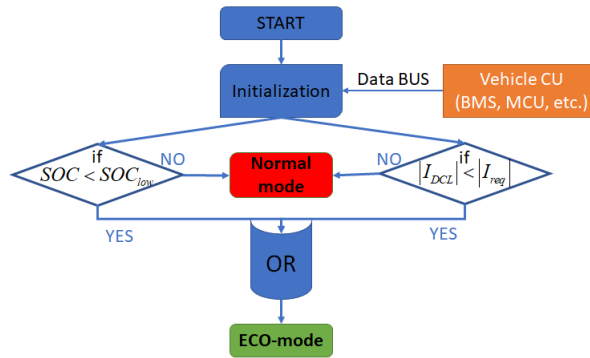


Figure 4.51: Auxiliary load management control: flow chart

Campaign tests have been performed in the model of Figure 4.52. RDE cycles reply the driving condition of *Barcelona* and *Gratz* cities. The model *Energy Improvement* is calculated considering the 4WD Amesim vehicle at 20°C as a baseline. The energy consumption increases due to the activation of the thermal regulation systems (air conditioning, heat pump). Results are visible in Table 4.18. Thus, final SOC is increased by 4% when the environment temperature is 35°C and 9% when the environment temperature is 0°C, as shown in Figure 4.53. The results of Table 4.19 show that energy improvement is achieved thanks to APMC. Indeed, as illustrated in Figure 4.54 the ECO mode reduces the Heating, Ventilation and Air Conditioning (HVAC) system power consumption, increasing battery autonomy.

Table 4.18: Performance comparison for Gratz and Barcelona RDE cycles

RDE cycle simulation results		
<i>RDE Cycle</i>	<i>Temperature</i>	<i>Energy Improvement [%]</i>
Gratz	35°C	13.9
	0°C	29.6
Barcelona	35°C	14.2
	0°C	28.6

Table 4.19: Influence of the auxiliaries management control on the vehicle model

Initial conditions: SOC 90% and 35°C			
<i>Layout</i>	<i>RDE Cycle</i>	<i>APMC</i>	<i>Eff. Imp. [%]</i>
ECMS	Gratz	OFF	4.46
		ON	7.4
ECMS	Barcelona	OFF	5.44
		ON	8.79

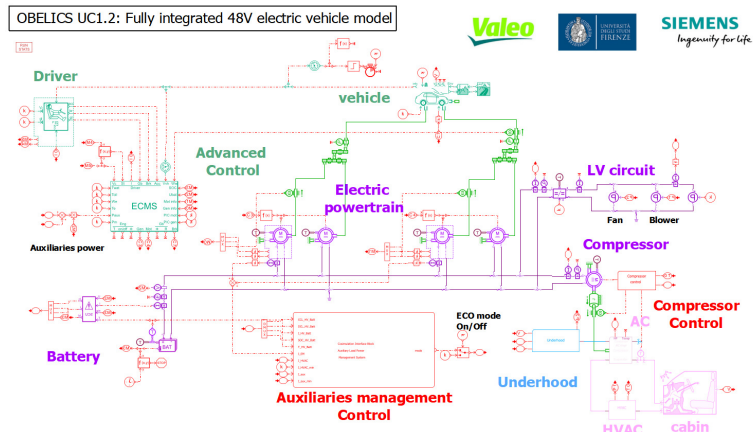


Figure 4.52: Fully integrated 48V electric vehicle model in Amesim

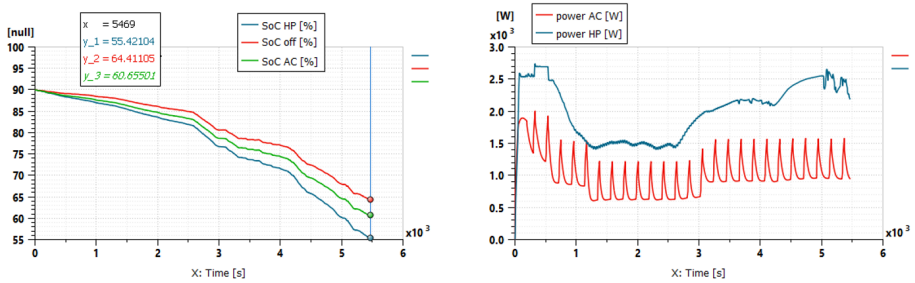


Figure 4.53: Comparison of SOC (left) and thermal system power (right) during the Barcelona RDE cycle for different environment temperature

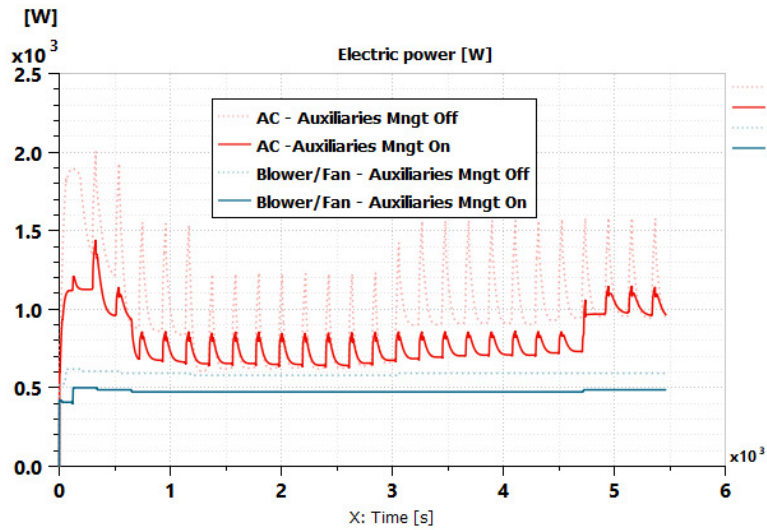


Figure 4.54: Comparison of EV power demand during the Barcelona RDE cycle

## Conclusions

The *fuzzy brake blending solution* ensures the maximum flexibility of the controller since has been developed as an algorithm that owns important scalability and portability properties. In addition, improvements in the driver dynamic feedback are achieved: conventional blending policies could generate abrupt accelerations when passing from one usage of braking actuators to another. A smoother dynamic instead, reduce the passenger's perception. The proposed fuzzy BB policies could increase battery reliability and lifespan, selecting more conservative power constraints when limit conditions occur. However, adopting FBB reduce the overall energy which could be recovered for the RBS in those scenarios.

Investigated *optimal power management strategy* could bring from 4% up to 9% of improvement of energy consumption in the performed RDE cycles. A non-secondary advantage of this implementation is computational time efficiency, even considering the increasing complexity of the phenomena involved by vehicle sub-systems models. Indeed, virtual tests are running 11.5 times faster than in real-time. So, models can be easily integrated into HiL target to validate the control algorithms.

### 4.4.3 EV Safety Improvements

EV safety both concerning functional, users safety and environmental impact must be considered when proposing an advanced traction layout in combination with innovative control strategies. A lot of research is done in the qualitative reliability and failure mode field, considering the whole safety life cycle. Safety-related control and design of BW system are based on reliability and fault-tolerant analysis, to minimize hardware and software failure, maximize the fault-tolerance and reduce maintenance costs. Moreover, when studying multi-motor vehicle configurations, safety implications of failure either of an individual wheel or axle motor inevitably pose some difficult challenges in practice [73]. WIM driven vehicle require an accurate torque distribution for all the wheels to run stably. When unbalanced force distribution occurs due to a failure in the actuators or the allocation control, EV may experience a spin or loss of steering ability, leading to dangerous conditions. The safety and riding comfort of vehicles are strongly influenced by the braking performance. Thus, a fail-safe structure is needed [87].

Reliability and Safety are crucial factors for the correct operation of a product, especially for E/E devices adopted in the automotive sector, whose development process must follow rigorous procedures. Indeed, essential drive functionalities are implemented through CU, so a safety-critical active system should be developed in accordance with the severe functional reliability concept. Standard *ISO 26262* [182] provide useful guidelines, assisting designers through all main phases of the V-shape procedure to develop a product that respects required safety performances. More in detail, relevant examples of BW commands on the latest generation's vehicles are throttle, braking and steer. All of them are fundamental for vehicle safety and controllability. The literature describes the main design criteria for such applications, including appropriate system topology, and the testing procedures needed to quantify their functional reliability, fault tolerance and applicability on-road vehicles [230, 231]. In this context, *ISO 26262* provides a solid framework for system development which is applicable to XBW analysis, possibly integrated with modelling activities [17, 232–236].

To avoid these situations, a systematic procedure for the design, development and validation of automotive systems could be a feasible solution to avoid a dangerous and harmful scenario. For the actual SoA, the current activities propose the definition of a systematic methodology based on Virtual Failure Mode and Effect Analysis (vFMEA) approach and ISO 26262 standard specifications. This task can be challenging considering the growing complexity of vehicle architectures, due to the ever-increasing relevance of ECUs and BW systems. Standard strongly suggests supporting the validation protocol with FI techniques. In particular, a multi-level FI approach is adopted, which consists of the simulation of failure modes, useful to establish their effects on the vehicle behaviour. The proposed approach allows the evaluation of the product's tolerance and recovery from a fault condition. This study aims to identify the major weakness of the brake plant and establish a proper solution to fit the previously determined safety requirement. The methodology will reduce the man-hour and cost of the reliability analysis by recursively simulating the effect of the failure in the vehicle's stopping distance, resulting in a quite reliable output.

### Functional Safety Assessment Methodology

To reach the intended goals a risk-based approach is proposed [15] to determine the ASIL class of the targeted system, ranging from QM through D. The aim is to achieve the safety requirements and acceptable residual risk, based on ISO26262. Indeed, this methodology can support the manufacturers in the design of tailored securing solutions, providing the requirements for validation and confirmation measures [13].

The purpose of this activity concerns different aspects: ensure braking performances of the EV and the BBW system reliability and ensure the availability of safety-related functionalities in which brake is involved, despite the operation of the various subsystems dealing with brake effort management and application. A flowchart of the proposed methodology is visible in Figure 4.55, which consists of different phases:

1. **SoA investigation:** an in-depth literature review is conducted to identify the failure rate and distribution of the brake component [16].
2. **FMEA:** Failure Modes and Effects Analysis is executed on the target BBW components. This step aims to identify the failure mode, causes and consequences of involved components. FMEA constitutes an essential methodology in the development process of a product, allowing reliable forecast. By doing so, designers can focus on the most critical plant parts, assisting them in the application of securing mechanisms to be implemented to fulfil minimum safety requirements.
3. **ISO 26262 guidelines application:** guidelines of the standards have been applied to the reference brake system, to evaluate target and actual ASIL for the investigated plant functionalities.
4. **Simulation-based FI:** consists in the execution of simulation tests in which the behaviour of the EV is observed when one or more faults are injected [185, 237]. In particular, FI is used to evaluate if the response of the system fulfils the specification when faults occur. The standards encourage the application of multi-level FI to define and tune specific solutions to increase system functional safety.

5. **Securing Solutions:** finally, plant modification and securing strategy are proposed and implemented in the *Simulink* environment, to better understand their impact of them on brake system reliability and performance.

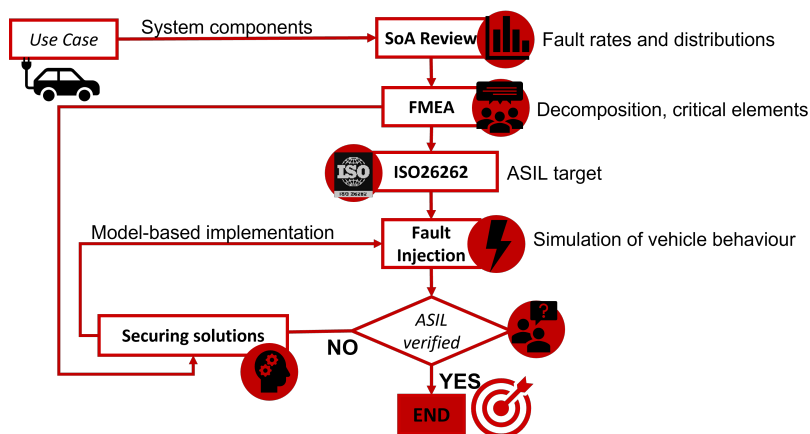


Figure 4.55: Flowchart of the proposed functional safety assessment methodology

Once the benchmark vehicle is chosen, the physical and functional scheme of the corresponding BBW system is identified. Failure rates and probability distributions of the brake plant components are identified during the SoA review. Then, follows the analysis of the causes, modes and effects of the investigated faults. This phase is fundamental to selecting the most critical malfunctionalities and proposing securing solutions. At this point, guidelines of ISO 26262 standard are applied to establish the target of the ASIL and the FI simulation activities to be performed to assess the plant reliability aspect. If the target ASIL is reached, the process ends and can be stated that the system fulfils standard specifications; otherwise, appropriate securing mechanisms are implemented in the vehicle models and the simulations are repeated to confirm their effectiveness.

### Benchmark Electric Vehicle

Investigated EV is the fully electric **Valeo Concept Car**, equipped with 4 independent IWMs. For the UC is possible to identify the following elements: brake pedal interface, ECUs and vehicle equipment.

This consideration allows a conceptual abstraction for the considered vehicle layout, to propose a flexible methodology that can effectively be applied to different powertrain architectures and UCs, allowing man-hour and cost reduction, thanks to the possibility to automatically adapt the proposed approach to several EV's e-powertrain and brake system configurations. In this context, it should be considered the integration of a multiple braking actuation, in which the mechanical brake system is coupled with the electric one. This makes the BEV an over-actuated system from the braking functionalities aspects, offering opportunities to achieve increased ASIL, due to the redundancy of the brake plant.

The integration in the system of a BB strategy is accounted for using the EV architecture represented in Figure 4.56, in which each wheel is equipped with its controller. This layout assures a higher level of redundancy since the BB ECU

failure affects only one wheel. On the other hand, specific securing procedures have to be implemented to avoid undesired vehicle dynamics behaviour. Our investigation focuses on this architecture, which is used only with the aim of the higher possible generality to 4WD vehicles.

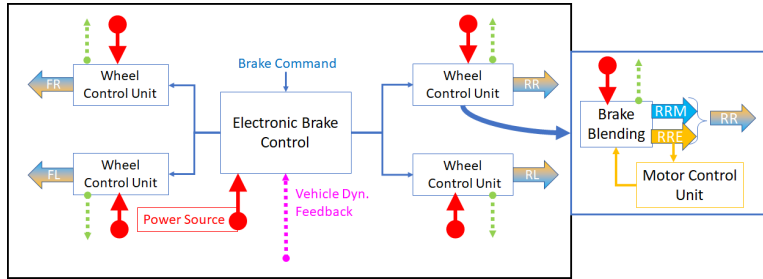


Figure 4.56: Reference BBW system layout with BB

### Failure Mode and Effect Analysis

FMEA is a versatile and flexible bottom-up failure identification systematic process, applied to the EV layout of Figure 4.56. It is essential to identify the major weakness of the BBW plant, letting the designer focus mainly on the most critical elements and define an appropriate securing strategy. The output of this phase is the EV’s block diagram of Figure 4.57. It is assumed the presence of an additional CU, the *Supervisor Controller*, which superintends the securing strategy functionalities.

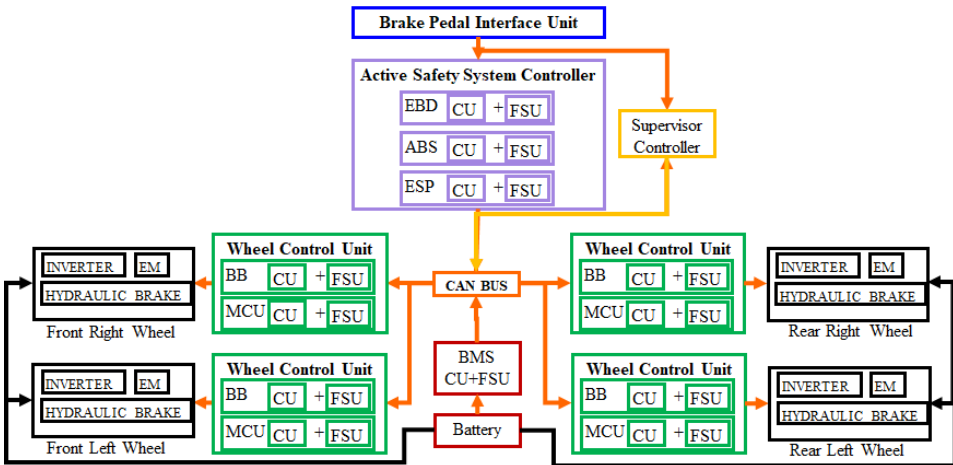


Figure 4.57: EV block diagram for the FMEA process

FMEA of the whole EV’s BBW model components are summarized in Table 4.20, where a column is dedicated to the proposal of safety solutions that can be implemented. Also, specific fault mode and effect analysis have been applied to ABS functionalities. FMEA considers all the existing interactions between the single plant’s elements in Table 4.21. For this analysis are considered only the main functionalities related to E/E systems. In particular, the proposed solutions concern:

- Fault prevention: failure forecasting is done by evaluating systems behaviour, for injection.
  - Qualitative evaluation: identification and classification of fault mode and/or combinations.
  - Quantitative/probabilistic evaluation: reliability measurements, such as Mean Time Between Failure (MTBF) or failure rate.
- Fault tolerance: integrating technique of management, detection, correction of fault and redundancy, to define fault-tolerant system architecture.
- Fault removal: aiming at reducing fault occurrences during the development stage. This consists of a verification process that leads to the system's weak diagnosis.

Table 4.20: FMEA of the reference BBW control units

Component	Failure	Effects	Causes	Securing
Pedal unit	Pedal fail	No pedal stroke No signal to EBD	Power supply fail Sensor fail	Redundancy
EBD	ECU fail	No f/r allocation No signal to ESP	Power supply fail Sensor fail	Redundancy Bypass EBD
ESP	ECU fail	No lateral stability No signal to ABS	Power supply fail Sensor fail	Redundancy Bypass ESP
ABS	ECU fail	Wheels locking No signal to BB	Power supply fail Sensor fail	Redundancy Bypass ABS
BB	ECU fail	No regeneration	Power supply fail Sensor fail	Redundancy Bypass BB
BMS	ECU fail	Overcharging Underdischarging	Power supply fail Sensor fail	Redundancy Hydr. braking
MCU	ECU fail	No electric torque	Power supply fail Sensor fail	Redundancy Hydr. braking
HCU	ECU fail	No hydraulic torque	Power supply fail Sensor fail	Redundancy

Table 4.21: FMEA of the reference ABS control unit

Component	Failure mode	Effects	Causes	RPN	Securing
Sensors	No signal	ABS off	Operative fault	18	Redundancy
	Wrong signal		Operative fault	96	Warning light
Wires	No signal	ABS off	Short circuit	18	Redundancy
	Wrong signal		Disconnection		Warning light
ECU	No signal	ABS off	Operative fault	108	Redundancy
	Wrong diagnostic		Software fault		Warning light
	Wrong signal		Software fault		

RPN: Risk Priority Number

## ISO 26262

The management of safety-critical decisions by the E/E system in the automotive sector inevitably increases the complexity of the vehicle architectures. Indeed, the risk of systematic and random hardware failure is greater. To assist designers in ensuring the highest safety requirements, specific regulations should be considered. This adaptation applies to all activities during the life-cycle of safety-related systems, comprised of electrical, electronic and software components. It provides methods and techniques which should be integrated into the development process to ensure the required functional safety level. ISO 26262 furnish guidelines to determine the ASIL for specific systems and functionalities, estimated using three indicators [10]: Severity, Exposure and Controllability. Target ASIL of the system of Figure 4.57 are defined in accordance with the specifications provided by ISO 26262. These values are visible in Table 4.22 and Table 4.23, regarding respectively vehicle with human driver or Advanced Driver Assistance Systems (ADAS).

In the autonomous driving scenarios, values of Severity could be increased, since it is legit to assume distracted passengers and therefore more dangerous consequences. Only for some failure modes is assumed a major Controllability, related to more sophisticated diagnostic procedures. Generally speaking, ADAS requires higher ASIL since the level of demanded automation is greater. For each scenario that results in target  $ASIL > QM$ , one or more *safety goal* are formulated, which represent the safety requirements that should be achieved to avert the risk. If similar safety goals are formulated for several events related to the same sub-component, these must be combined into a single security goal with the highest ASIL among those which are considered. In this activity, the evaluation of the appropriateness of the BBW system with the ISO 26262 specifications is performed by observing the *Random Hardware Failure Rate*, whose requirements are those of Table 4.24.

Table 4.22: ASIL target estimation for the EV (autonomous driving level between 0 and 1)

Component	Severity	Exposure	Controllability	ASIL
Pedal CU	S3	E4	C3	D (max)
EBD CU	S2	E4	C2	B
ESP CU	S3	E3	C3	C
ABS CU	S3	E3	C3	C
BB CU	S2	E4	C2	B
BMS CU	S2	E4	C2	B
MCU	S2	E4	C2	B
Hydraulic CU	S3	E4	C3	D (max)

Table 4.23: ASIL target estimation for the EV (autonomous driving level greater than 2)

Component	Severity	Exposure	Controllability	ASIL
Pedal CU	S3	E3	C2	B
EBD CU	S3	E4	C2	C
ESP CU	S3	E3	C2	B
ABS CU	S3	E3	C3	C
BB CU	S2	E4	C2	B
BMS CU	S2	E4	C2	B
MCU	S2	E4	C2	B
Hydraulic CU	S3	E4	C3	D (max)

Table 4.24: ASIL target respect to Random Hardware Failure Rate

ASIL	Failure Rate $\lambda$ [1/h]
B	$< 10^{-7}$
C	$< 10^{-7}$
D	$< 10^{-8}$

### Simulation Based Fault Injection

The Fault Injection (FI) phase consists of the execution of controlled experiments where the behaviour is observed upon the introduction of one or more failures [238–240]. The injection of faults allows determining if the response of the system, in the presence of a defined set of faults, corresponds to the specifications. In particular, is useful to establish a proper securing strategy, aiming at fault prevention and removal. Fault prevention solutions are typically based on statistical tests, which simulate the distribution and rate of specific failure. Fault removal, instead, is based on functional modelling of the system. The introduction of FI in ISO 26262 [241] has renewed the interest in this methodology for the automotive sector. The standard motivated the adoption of new solutions for the safety assessment of a product, redefining specific reliability concepts which should be applied during development phases, and supporting conventional failure analysis methods.

Developed simulation test campaigns consist of two different steps. In the first phase, a recursive **Montecarlo simulation campaign** of a simplified vehicle model (high level of physical abstraction) is performed at a high computational speed, considering the real value of the component’s fault occurrences and probability distributions. The impact of several brake system failure modes on the vehicle stopping distance is evaluated. High integrity and safety levels of the brake system are involved to embed the current mechatronic system within a higher-level system. In this stage, components of the plant which are more inclined to fail and/or had a major impact on vehicle braking performances can be established.

Then, once establish from the latter phase a specific number of dangerous scenarios for functional safety, **Model-based simulation campaign** of specific failure events are repeated using a more precise accurate vehicle model, from a physical and functional point of view. This allows evaluating the appropriateness of the proposed approach and securing solutions, comparing results obtained at this stage and in the previous one to propose fault removal solutions. Also, it consents

to better identify the causes and effects of failure, improving the knowledge of the mechanism of their occurrence and related impact on functional safety.

In both cases, the simulation environment involves 2 sub-models: *Target system*, which is the vehicle model; *FI controller*, consisting of a *Fault Injector*, which contains the vectors of the possible fault and schedules their onset; the *Fault Monitor*, which detects malfunctions and communicates with the *Supervisor controller*.

It is important to note that a delay is considered between the fault occurrences and its detection. This delay replicates the physiological lag of the communication channels (e.g. flooding of the CAN bus system) and time step interval (of 50 ms). An additional 300ms time-out is supposed, to avoid false-positive fault detection by the *Supervisor controller*. The latter monitors the failure occurrences turns on the warning light in the driver dashboard and triggers specific securing algorithms to start the failure mitigation procedures.

The reason behind the choice of this process is mainly referred to the necessity of reducing the simulation computational effort and time. vFMEA activities require the execution of billion recursive simulations to observe failure events, which are in the magnitude of  $10^{-7} - 10^{-8}$  occurrences per hour. So, it is necessary to identify the system weakness in a shorter time and lower energy/cost consumption, in the optics of implementing fault mitigation solutions in the early phases of design, evaluating their effectiveness on safety requirements.

The developed model has the following characteristics:

- *Numerical efficient*: able to perform a large number of simulations, considering several combinations of faults and performance degradation in different operational conditions and scenarios. RT implementation is required;
- *Simple and standardized*: models flexibility is ensured by proper scalability and portability properties, to be easily portable for different vehicle UCs, as well as for different simulation environments and boundary conditions;
- *Robust and reliable*: respect to the physical abstraction, which in some cases can lead to complex dynamic behaviour that introduces further integration problems, especially when a fault occurs.

**Montecarlo Simulation:** In this phase, each component of the investigated BBW system is abstracted by its primary functionality and considered as a simplified element [242], identified only by its own Mean Time Between Failure (MTBF) and fault distribution. Probability of fault occurrences is estimated from SoA, literature, data-sheet and technical considerations [16, 243]. This abstraction concept, based on system BRD, is useful to implement an efficient and effective Montecarlo recursive study, aimed to establish the stopping distance of the vehicle when one or more components of the brake system experience fault situations. This probabilistic-based implementation, from the computational effort perspective, is designed to perform  $10^3 - 10^{12}$  consecutive iteration, using a simple functional approach devoted to parallel computing. This simulation campaign is based on the vehicle longitudinal dynamic equation, according to the formula of the stopping distance calculation during a braking manoeuvre (4.21), where  $s$  is the stopping distance expressed in meter,  $V_0$  the initial vehicle speed,  $a_x$  the longitudinal acceleration and  $d$  the time delay.

$$s = \frac{V_0^2}{2a_x} + V_0 d \quad (4.21)$$

The output of this test campaign constitutes a preliminary supporting tool for the following model-based FI: the information arising from the Montecarlo simulations allows understanding the system weakness and to identify the specific plant components which mainly experience fails. At this point, it is possible to deeply study the select scenario, by their implementation in a more sophisticated simulation environment. Considered fault event are:

- Boolean Fault: the component can appear as completely healthy (ON) or dead (OFF). When a fault occurs its functionalities are considered lost;
- Derating Fault: the component can be partially available, and its functionalities reduced in the magnitude order of a percentage.

**Model-based Simulations:** A more complete vehicle equipment test is performed in the Simulink environment, using the *9-DoF vehicle model* to assess the effect of the BBW E/E devices failure on the car vehicle behaviour. For this work, however, models have been modified to account for fault effect by the introduction of FI controller.

The detailed FI model (Figure 4.58) is designed for  $10^0 - 10^3$  iterative simulations and it is useful to evaluate the consequence of a fault or to validate expected results on a worst-case scenario, established in the previous step. This full vehicle equipment functional model consists in: Driver, Vehicle Chassis, Torque Regulation Controller (EBD, ABS, ASR, ESP, BB controller), Torque Actuation (EM and hydraulic brake system) and Monitor (to observe model behaviour when one or more faults occur). The usage of these more accurate models is devoted mainly to confirming the coherence with the dynamic vehicle behaviour established during the Montecarlo methodology. Moreover, model-based simulations are useful also to endorse the achievement of target ASIL and evaluate the improvement permitted by plant modifications.

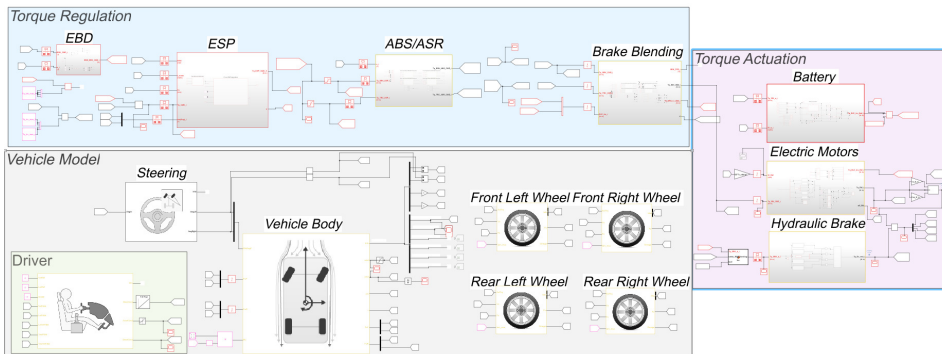


Figure 4.58: EV simulation layout of the *Simulink model*

## Securing Solutions

The proposal of securing solutions to be implemented in the vehicle model concerns the necessity to fulfil the minimum safety performances established from ISO 26262 perspective. Indeed, to reach target ASIL of Table 4.22, plant modifications and advanced control algorithm are required to fit the functional safety level in accordance with the standard specifications. In relation to Figure 4.57, for the vehicle CU is assumed the presence of a redundant electronic controller, called Fail Silent Unit (FSU). Also, an addition ECU, named *Supervisor Controller* is considered, whose task concerns the application of the securing strategy. Fault detection for ABS/ASR system is done following the logical scheme of Figure 4.59. Other securing strategies, summarized in Table 4.21, are realized in analogy with this one.

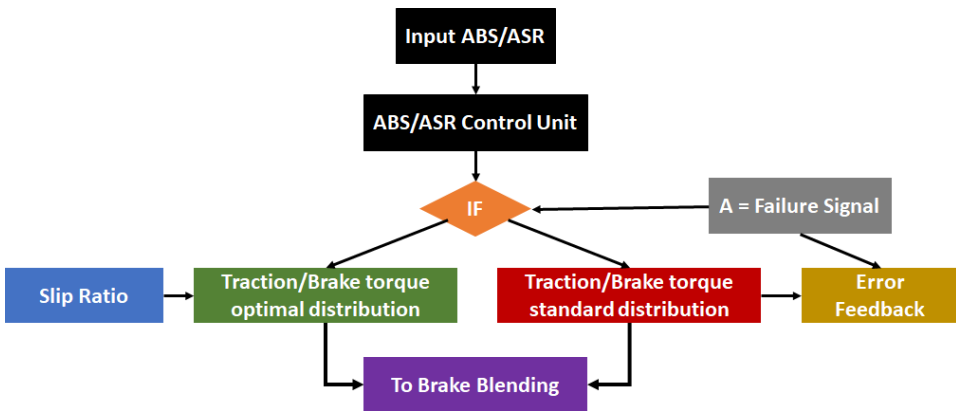


Figure 4.59: Proposed ABS fault detection and mitigation logic scheme

## Results and Discussions

In this section are summarized the result concerning the FI simulation campaign, obtained from the application of the proposed methodology to the benchmark EV, supposing different faults. Also, it assumes a specific fault of the CU related to anti-lock braking functionalities, whose simplified scheme is represented in Figure 4.60, in which are evident the interconnection within other BBW components. It is important to know that the proposed *Supervisor Controller* can perform diagnostic functions, turning off ABS system when errors are detected. This implemented securing strategy allows the application of braking torque to wheels, which, however, are not modulated to keep the slip in the admitted bandwidth.

For this simulation campaign, the boundary condition of the simulated tests is the one provided by ISO 21994:2007, related to the determination of the stopping distance in Straight line deceleration with ABS in open-loop test methodology, which should remain under 40m from an initial speed of 100km/h.

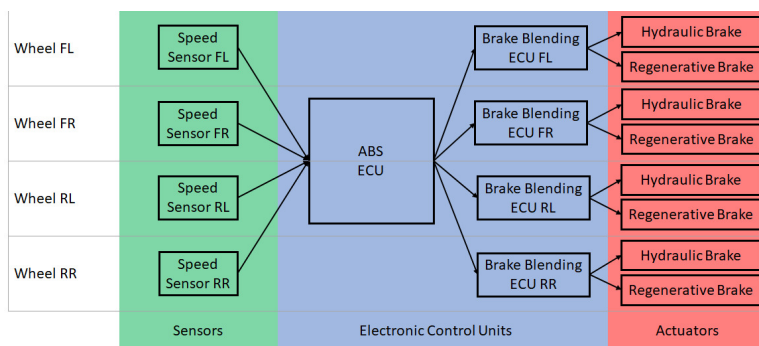


Figure 4.60: ABS functional decomposition scheme

### Montecarlo Simulation Campaign Results

In this kind of test, different failures are supposed, whose specifications, for the BBW system layout of Figure 4.57, are summarized in Table 4.25, along with some parametric variable, needed to simulate different braking conditions (e.g. vehicle mass variation). For the E/E control units a redundant solution with FSU is suggested. This consideration is due to the high ASIL required. The results of the tests are in agreement with these assumptions since the detection of the failure will result in an acceptable stopping distance. Consider the simulation results of Figure 4.61, which refers to the fault of ABS CU for a population of 100 millions of straight-line deceleration events. These outcomes correspond to about 72 billion operative hours of the brake system. This fact is due to the failure rates of Table 4.25, which are expressed in terms of occurrences per hour, while the reference manoeuvre only lasts about 5s. Thus, between these rates there is a factor of 720 ( $\lambda[1/h] = \lambda[1/3600s] = \lambda[1/5s] \cdot \frac{1}{720}$ ).

Figure 4.61 shows the FSU which markedly improves the braking by replacing the primary electronic regulator after the time-out. In the case of a single CU instead, the intervention of the *Supervisor Controller* is needed.

### Model-based FI Campaign Results

The braking manoeuvre is repeated for the full vehicle model, supposing the fault occurrences of all the subsystems dealing with braking performances and BBW functionalities. In the model-based simulation are investigated the effect on vehicle behaviour of the securing strategy.

Output of Figure 4.62 shows wheel torques and slips in normal operative condition (left) and ABS control unit fault (right). In the second case, the *Supervisor Controller* applies the securing solution of Figure 4.59. So, even in the extremely rare case of simultaneous failure of CU and FSU, is still possible to apply braking torques to the wheels. However, these are not properly modulated, so wheel locking occurs, resulting in an increased stopping distance (Table 4.26). Making the vehicle replicate, for each investigated fault, the same manoeuvre allows to comparatively evaluate the effect on stopping distance. Note that the first two rows of the table refer to the full working vehicle stopping condition; the first one presents a stopping distance of 46.6m, which corresponds to an average-condition surface; while the second one presents a stopping distance of 39.3m, which corresponds to a good-condition

Table 4.25: Investigated failure in the Montecarlo simulation campaign

Sub-system	Failure	Rate [1/h]	Distr.	Parameters
Brake Pedal Inter.	ECU (D)	$5.88 \cdot 10^{-7}$	Uniform	$a_{nom}; d_{nom}$
	ECU (ND)	$3.46 \cdot 10^{-13}$	Uniform	$a_{min}; d_{max}$
	CAN bus	$5.69 \cdot 10^{-9}$	Uniform	$a_{min}; d_{max}$
Safety CU	ECU (D)	$5.88 \cdot 10^{-7}$	Uniform	$a_{nom}; d_{nom}$
	ECU (ND)	$3.46 \cdot 10^{-13}$	Uniform	$a_{ABS}; d_{max}$
	CAN bus	$5.69 \cdot 10^{-9}$	Uniform	$a_{min}; d_{max}$
Wheel Brake CU	ECU (ND)	$1 \cdot 10^{-7}$	Uniform	$3/4a_{nom}; d_{nom}$
	CAN bus	$5.69 \cdot 10^{-9}$	Uniform	$a_{min}; d_{max}$
Power Supply	Unavailable	$3.77 \cdot 10^{-7}$	Uniform	$a_{min}; d_{max}$
Load	Variation	/	Normal	$[0.8; 1.2]a_{nom}$
Pad-Disc Friction	Variation	/	Normal	$[0.8; 1.2]a_{nom}$
Slope	Variation	/	Normal	$[0.95; 1.05]a_{nom}$

$a_{nom} = 9.81m/s^2; d_{nom} = 0.005s; a_{min} = 0.1m/s^2; d_{max} = 0.035s; a_{ABS} = 8m/s^2$   
D: detected; ND: not detected

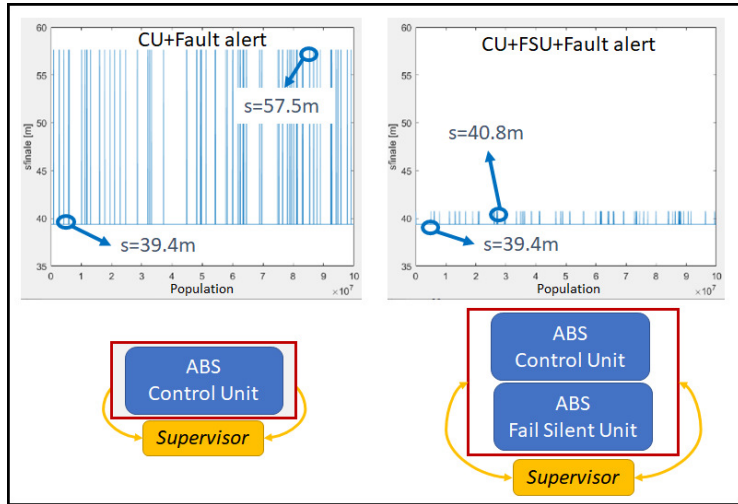


Figure 4.61: Stopping distance for detected ABS failure without (left) and with FSU (right) during Montecarlo FI simulations

surface. All other rows are calculated assuming the same conditions expressed on the first row.

**Conclusions**

Results of these tests, as already pointed out, concern several aspects: Definition of the actual ASIL, for the investigated brake plant functionalities; Proposal of securing intervention, to let the system fulfil the ISO 26262 standard requirements as compared to brake functionalities; Assessment of the procedure coherence and robustness with results arising from functional safety identification methodology.

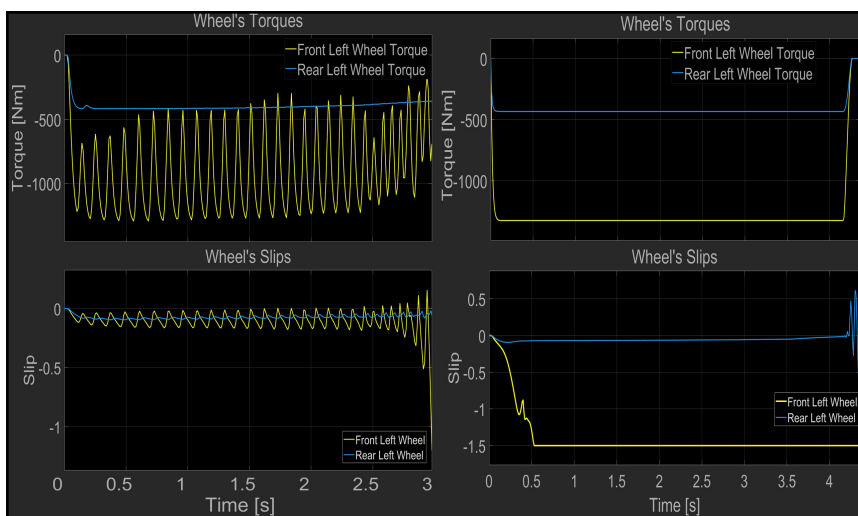


Figure 4.62: Wheel torque (top) and slip (bottom) in normal operative condition (left) and fault condition (right) during Model-based FI simulations

Table 4.26: Stopping distance of EV in different fault scenario for the BBW subsystems

Case	Stopping Distance [m]	Max Deceleration [ $m/s^2$ ]
Normal	46.6	9.81
Normal (Best Case)	39.3	10.65
EBD Fault	50.6	9.31
ABS Fault	57.1	9.69
BB Fault	47.3	9.88
BMS Fault	47.7	9.84
EM Fault	49.6	9.36
Hydraulic CU Fault	72.6	8.01

The proposed vFMEA procedure has been applied to several components dealing with EV braking performances. Modified block able to support FI has been proposed and implemented on an existing *MATLAB Simulink* model, representing an electric vehicle equipped with four IWM and a conventional hydraulic braking system, integrated with BB policies. The model is useful to verify the consequences of the events considered more critical and to verify the implications in terms of stopping distance, considering implemented securing strategy. Simulation involves two environments: Montecarlo and Model-based solution.

In particular, for ABS functionalities, the simplified Montecarlo model provides quite reliable output (Figure 4.61), in accordance with the stopping distance of Table 4.26 identified during model-based simulation campaign. The developed models include the possibility to vary parameters that are sensitive to the target performance achievements, such as failure recognition delay and mitigation strategy. The model is defined on a “high level” representation, so real system topology is not reproduced.

In *conclusion* it can be stated that:

- A tool for the reliability assessment of a target Brake-By-Wire system has been developed, through systematic Virtual FMEA methodology;
- Proposed solution, following ISO 26262 standard, adopts FI technique to be applied on vehicle models with different levels of detail. This lets the users scale the methodology according to the desired results;
- Applied to the reference vehicle UC ABS system, allows verifying the effectiveness of the proposed securing solution, making the system fulfil standard specifications for the random hardware failure metric, which is about  $10^{-12}[1/h]$ .

#### 4.4.4 EV Stability Improvements

Results of **EV stability improvement** are show for longitudinal and lateral achievements [21, 194, 210, 244–246]. For the following activities, alternative WIM vehicle configurations have been supposed for each UCs. From these preliminary validations activity, the Moore-Penrose pseudoinverse approach for the TV allocation, described in section 3.6.1, prove to be efficient and reliable in improving handling performances while respecting effort constrain of the over-actuated system. Results of the cornering tests show the improvement allowed by the coordinated integration of this controller with the IWM and the brake actuators. This solution is further integrated with the advanced ESP strategy, described in Chapter 5.

##### First Implementation in Simulink

Firstly, the torque allocation algorithm is tested on the virtual model of the **FIAT 500e**: a planar 3-DoF body model is adopted; rotation of each wheel is considered, as well as front-wheel steering, for a total of *9-DoF vehicle model*. Also, high-level control sub-systems, are introduced: the human driver model, EBS, ABS/ASR, and ESP. For the prescribed benchmark vehicle, two different powertrain configurations are considered:

- a *Single traction Motor*: a conventional powertrain layout in which a single electrical motor is used to distribute power to frontal wheels.
- b *Four In-wheel Motors*: the same power of the previous case is divided between four identical motors, each one directly connected to a wheel.

Over-described models have been developed in Matlab Simulink™, where each subsystem is implemented as an independent model instance, allowing a separate execution of threads with different solvers and sampling frequencies.

Using the FIAT 500e vehicle model allows for simulating the multiple interactions between the braking plant and installed onboard subsystems, dedicated to the preservation of the vehicle stability [210]. Some simulations of a DLC test have been performed. Tests were performed with different powertrain layouts and different adherence conditions. Results in terms of maximum speed for which vehicle stability is verified during the DLC manoeuvre are visible in Table 4.27: the model highlight the benefit obtained by the application of the ESP control.

Table 4.27: Double lane change test max speed performed by different vehicles powertrain configurations and adherence coefficient

Double Lane Change Simulation Test			
<i>Adherence</i>	<i>Vehicle Layout</i>	<i>ESP</i>	<i>Maximum Speed</i>
0.5	2x4	No	30 [km/h]
		Yes	35 [km/h]
	4x4	No	35 [km/h]
		Yes	45 [km/h]
0.75	2x4	No	70 [km/h]
		Yes	75 [km/h]
	4x4	No	70 [km/h]
		Yes	80 [km/h]
1	2x4	No	85 [km/h]
		Yes	90 [km/h]
	4x4	No	85 [km/h]
		Yes	90 [km/h]

Results in terms of compared vehicle trajectories are shown in Figure 4.63: simulations are performed considering a travelling speed of 80 km/h and the availability of full adhesion conditions ( $\mu = 1$ ). Best performances are obtained by the vehicle equipped with four in-wheel motors and the ESP system able to perform a full torque vectoring of the applied traction efforts. In Figure 4.64, torque vectoring control actions on the four in-wheel motors are shown.

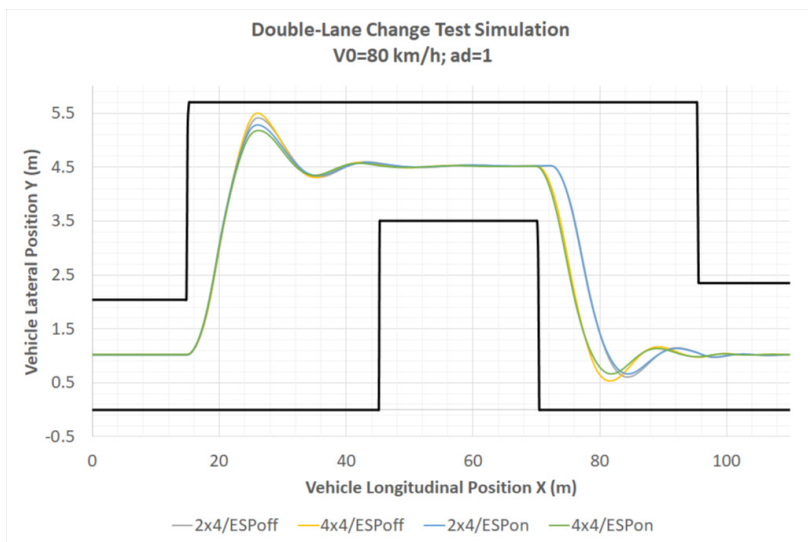


Figure 4.63: Vehicle trajectory in a DLC manoeuvre with a speed of 50km/h and a friction of 1, supposing different traction architectures

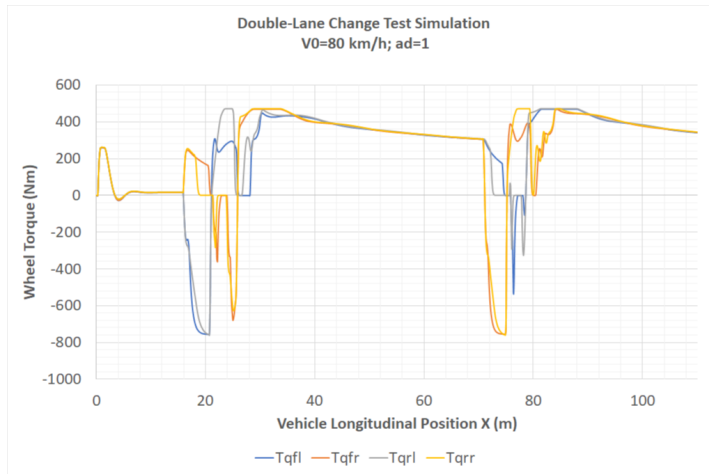


Figure 4.64: Torque vectoring in a DLC manoeuvre with a speed of  $50\text{km/h}$  and a friction of 1, supposing availability of the ESC

### Implementation in Co-Simulation

Another activity is done to evaluate the allocation algorithm in co-simulation environments. A newly LQR-based ESC strategy using an Unscented Kalman Filter (UKF) vehicle state estimator [13] and More-Penrose pseudoinverse based torque vectoring technique [247] is proposed, which aim at minimizing the difference between the driving performances requested by the driver and the controllers, ensuring enhanced stable behaviour by fully exploiting IWM traction and braking characteristic. The vehicle model, inspired by a real existing sports car, is a RWD vehicle configuration. However, we suppose a 4WD architecture with IWMs. Detail of the benchmark UC cannot be presented here for non-disclosure reasons.

The interfacing between the *16-DoF vehicle model* of VI-Grade and the Stability Controllers in Simulink is done according to the block diagram scheme of Figure 4.65.

Using a reference vehicle model, the ESC controller firstly calculates the expected yaw rate and side-slip angles. Then, these values are compared with the ones that the vehicle is effectively experiencing, typically estimated through IMU sensors platform and ANN-UKF algorithm, as reported in [248]. If there is a not negligible error, evaluated with a proper dead-zone, the ESC apply the Moore-Penrose torque vectoring technique to ensure the vehicle follows as close as possible to the desired states (yaw rate and side-slip angle), delivering an equivalent yaw moment according to the driver's steering ideal command  $\delta_c$ . However, for the reference UC, lateral stability enhancement is achieved thanks to IWM specifications. Indeed, each actuator can both accelerate and decelerate, increasing the  $M_{yaw}$  that could be applied to the vehicle body. The lateral control algorithm, shown in Figure 4.65, is composed of three sub-systems.

1) *Reference Dynamic Model*: according to driver commands the vehicle body reference system varies with time. However, to underline inner vehicle characteristics (manoeuvrability) and control the under-steering/over-steering behaviour of the chassis, estimating the steady-state values of the yaw rate (4.22) and sideslip angle (4.23) it's essential. These equations are based on the dynamical modelling of the

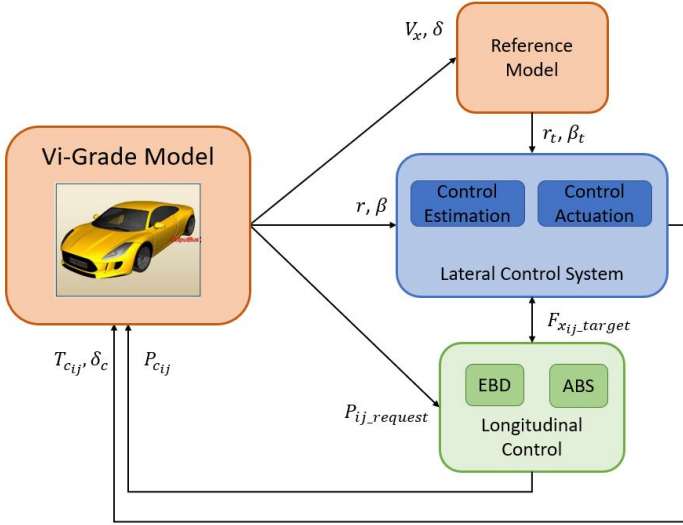


Figure 4.65: Vehicle lateral control strategy block diagram

vehicle and are expressed as a function of the *under-steering gradient*  $K_V$ .

$$r_t = \frac{u}{(a+b) + u^2 K_V} \delta \quad (4.22)$$

$$\beta_t = \frac{b - \frac{m a u^2}{(a+b) C_{yf}}}{(a+b) + u^2 K_V} \delta \quad (4.23)$$

Since every lateral stability test is performed supposing nominal friction condition, related to a dry asphalt road, variation of target states with  $\mu$  is neglected.

To ensure a stable behaviour of the vehicle during cornering manoeuvres, the ESC should control the available actuators to make the yaw rate  $r$  and the sideslip angle  $\beta$  strictly follow their optimal values, established from the *Reference Dynamic Model*. Nevertheless, expressions (4.22) and (4.23) don't account for degraded adhesion conditions of the wheels, thus their values must be saturated to an upper threshold, depending on the available friction coefficient in the tire-road contact surface. Saturation is done according (3.4) and (3.6) as a constrain limitations. In doing so, the reference model is implemented to provide the yaw rate and the side-slip angle references, once knowing the steering angle and the longitudinal speed.

2) *Control Estimation System*: the implemented ESC strategy is based on LQR, an optimal control that can find, during the driving scenario, the desired yaw torque and the ideal steering wheel angle which ensure stable behaviour of the chassis, as well as improved dynamic performances. Conventional LQR estimator works for a single linear dynamic model and is tuned specifically to reset the input variable [248]. The proposed solution, as reported in [249], integrates a gain-scheduling control methodology, able to accurately follow the target value imposed by the *Reference Dynamic Model*, by adaptively tuning itself in RT. The states of the

system are estimated by a single-track vehicle model (4.26), where  $A$  (4.24) and  $B$  (4.25) are the coefficients matrices.

$$A = - \begin{bmatrix} \frac{C_{yf}+C_{yr}}{m*vel_x} & \frac{1+C_{yf}*a-C_{yr}*b}{m*vel_x^2} & 0 & 0 \\ \frac{C_{yf}*a-C_{yr}*b}{J} & \frac{C_{yf}*a^2+C_{yr}*b^2}{J*vel_x} & 0 & 0 \\ 0 & 0 & \frac{1}{\tau_\beta} & 0 \\ 0 & 0 & 0 & \frac{1}{\tau_r} \end{bmatrix} \quad (4.24)$$

$$B = \begin{bmatrix} \frac{C_{yf}}{m*vel_x} & 0 \\ \frac{C_{yf}*a}{J} & \frac{1}{J} \\ 0 & 0 \\ 0 & 0 \end{bmatrix} \quad (4.25)$$

$$\begin{Bmatrix} \dot{r} \\ \dot{\beta} \\ \dot{r}_t \\ \dot{\beta}_t \end{Bmatrix} = A * \begin{Bmatrix} r \\ \beta \\ r_t \\ \beta_t \end{Bmatrix} + B * \begin{Bmatrix} \delta_c \\ M_y \end{Bmatrix} \quad (4.26)$$

In (4.26) the dynamic states evolution is expressed by vehicle geometric parameters, i.e., the front and rear wheelbase  $a$  and  $b$ , the vehicle mass  $m$  and yaw moment of inertia  $J$ , the front and rear cornering stiffness,  $C_{yf}$  and  $C_{yr}$  respectively, and the longitudinal vehicle speed, which is scheduled at intervals of  $10m/s$ .

Defining the output of the controller as the difference between reference and actual states, it's possible to establish the optimal controller gains. This allows to correctly determine the control signals: a steering wheel angle  $\delta_c$ , which is the ideal driver's steer command; and an equivalent yaw moment  $M_{yaw}$ , delivered to the vehicle body by the EM and by the hydraulic brake plant (4.27). The formulation of the LQR controller automatically defines the optimal control efforts to reach the expected vehicle behaviour. Thus, there is no need to divide the control objective as compared to the available actuators since the desired yaw moment and steering angle are calculated contemporaneously, based on the same modelling approach. However, optimal steering correction control is not implemented for this activity. For the RTI all the control logic is discretized with a sample time of  $0,001s$ .

$$\begin{Bmatrix} \delta_c \\ M_{yaw} \end{Bmatrix} = \begin{bmatrix} K_{\delta r} & K_{\delta \beta} & K_{\delta r_t} & K_{\delta \beta_t} \\ K_{M r} & K_{M \beta} & K_{M r_t} & K_{M \beta_t} \end{bmatrix} * \begin{Bmatrix} r \\ \beta \\ r_t \\ \beta_t \end{Bmatrix} \quad (4.27)$$

3) *Control Command Actuation*: the optimal allocation strategy proposed here is based on the Moore-Penrose pseudoinverse method introduced in section 3.6.1.

The EBD is a control unit widely adopted in the automotive field, used to privilege braking performances of the vehicle's axes, in the function of front/rear longitudinal load transfer. According to [43], the set of optimal points, as the adhesion coefficient in the tire-road interface changes, is a parabola, visible in Figure 4.66(a). This curve is calculated by solving (4.28).

$$F_{zf} = \frac{F_{xf}}{\mu} = F_{zf}^0 + \frac{h}{l}(F_{xf} + F_{xr}) \quad (4.28)$$

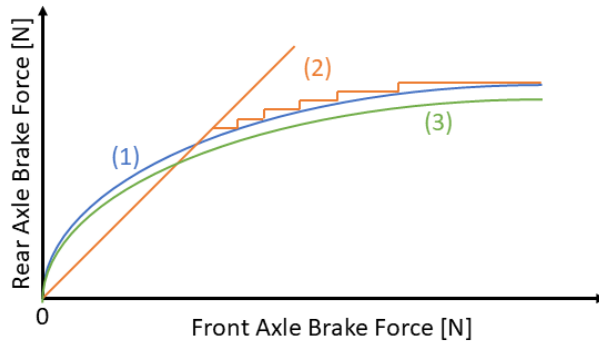


Figure 4.66: Axle braking force EBD distribution: (1) Ideal; (2) Conventional; (3) Proposed

The curve defines the load distribution coefficients between the axes which, for the specified friction coefficient, maximize the available deceleration while avoiding wheels sliding. Using a more conservative strategy could reduce the onset of wheel slippage, but underestimate the available deceleration performances. However, the new architecture of the by-wire system used allows for reducing the delay for the one in modern EV, thanks to the positioning of the hydraulic component close to the wheel. The use of four independent actuators ensures to obtain the optimal brake distribution and increases system safety with redundancy. To compensate for the uncertainty of the adhesion coefficient we adopt a parabola that slightly deviates from the ideal curve (Figure 4.66(3)). In this way, the front/rear braking allocation strategy appears more robust in avoiding rear-wheel slippage.

### Longitudinal Stability Test

To ensure the stability during braking actuation and improve the handling of the vehicle, both in longitudinal and cornering manoeuvres, an ABS is recommended (Fig.4.65). It is implemented a PID controller that allows following the target longitudinal wheel slip [250], given by the ESC and by the driver's request, at each wheel. In this way it is possible to avoid the wheels locking when braking, reducing the corresponding stopping distance and the under/over-steer behaviour of the vehicle in the cornering scenario, ensuring a stable behaviour in accordance with the driver steer input. The target wheel slip is calculated from the desired longitudinal force, arising from the EBD or the ESC system. Knowing the longitudinal front and rear stiffness of the tires and assuming a linear behaviour of the latter, target longitudinal slip is calculated through (4.29).

$$\sigma_t = \frac{F_x}{C_x} \quad (4.29)$$

This value is saturated from zero, so that the control only works when braking, to near 0.05, ensuring that the wheel maintains itself in the linear dynamic range. The PID output is the single wheel brake pressure which, if applied on every wheel, reduces the error between the target and actual value of the slip.

The virtual tests consist of the execution of straight-line deceleration for several friction coefficient values. Indeed, for degraded tire-road adhesion conditions, EBD and ABS controllers are essential to ensure the minimum braking performances required by the standards ISO 21994, reducing the corresponding vehicle braking distance.

Results are shown in Figure 4.67 and summarized in Table 4.28 for the vehicle UC, supposing the availability and unavailability of the ABS controller, showing also the corresponding improvement in terms of distance percentage. In addition, in Figure 4.68 the wheels' and vehicle speed are shown, to underline the avoidance of wheel locking and the driver comfort improvement with the ABS implemented, compared with the conventional bang-bang wheels acceleration controller. Result of Figure 4.67 and Table 4.28 suggest that the ABS controller is fundamental to ensure a safe behaviour during straight line deceleration. Instead, Figure 4.68 indicates that the proposed ABS strategy smooths the braking effort for on-off control of the wheel acceleration. It's interesting to note also that, for normal adherence conditions, the adopted policy successfully fulfils the limitations imposed by the mandatory standards by actively controlling the wheel's longitudinal slip.

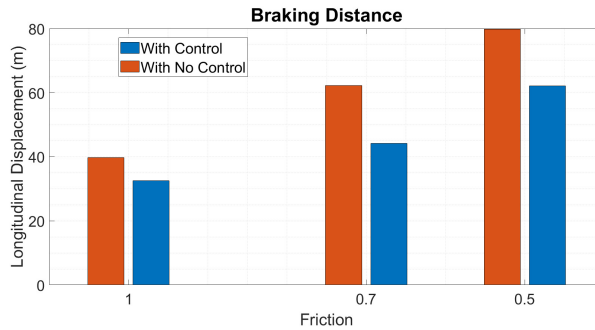


Figure 4.67: Vehicle braking distance in longitudinal braking maneuver with a speed of  $100\text{km/h}$  and a friction coefficient of 1, 0.7 and 0.5, supposing availability and unavailability of the ABS control system

Table 4.28: Stopping distance of the longitudinal stability tests for different adherence conditions

Initial Speed: $V_{x-i}=27.78 \text{ [m/s]}$			
Adherence $\mu$ [0-1]	ABS	Stopping Dist. [m]	Improvement [%]
1	ON	32.56	18.13%
	OFF	39.77	
0.7	ON	44.14	29.02%
	OFF	62.19	
0.5	ON	62.12	22.17%
	OFF	79.82	

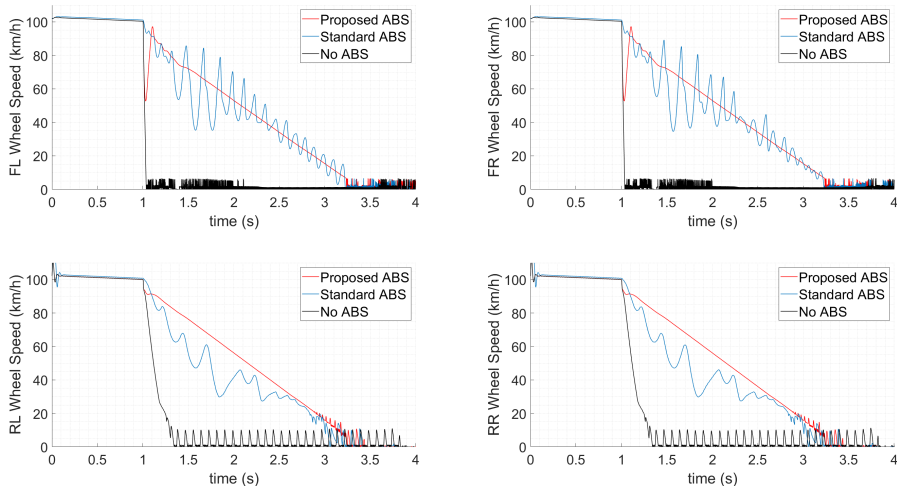


Figure 4.68: Vehicle wheels speed in longitudinal braking manoeuvre in accordance to ISO 21994 standard specification with ABS control system

### Lateral Stability Test

These simulations campaign are executed in order to asses the effect of the proposed ESC algorithm on lateral stability performances. Three different tests are executed: *constant steering wheel angle*, *DLC* and *SwD* tests.

When performing the j-turn manoeuvre at  $100\text{km/h}$ , it can be seen from Figure 4.69 that the oversteering behaviour of the benchmark EV is corrected by the ESP interventions in the trajectory plot, as well as the higher lateral acceleration respect to the steering angle. Thus, the controller ensures higher tracking performance of both side-slip angle and yaw rate (Figure 4.70).

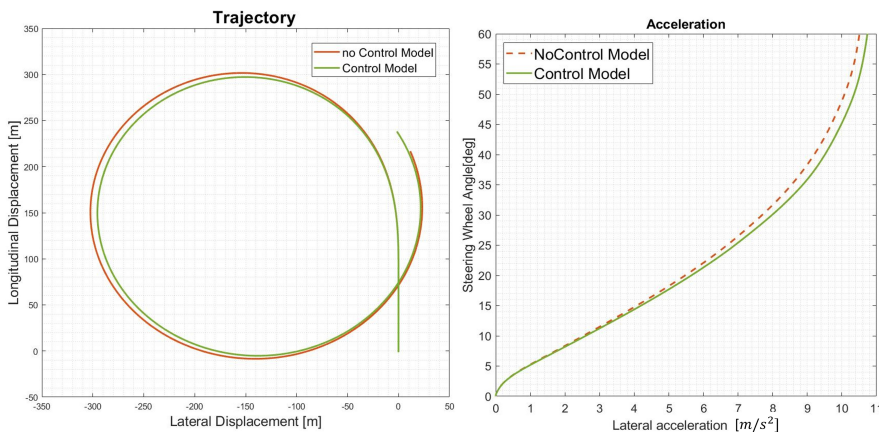


Figure 4.69: Vehicle trajectory and lateral acceleration in a j-turn manoeuvre with a speed of  $100\text{km/h}$  and a friction of 1, supposing availability and unavailability of the ESC

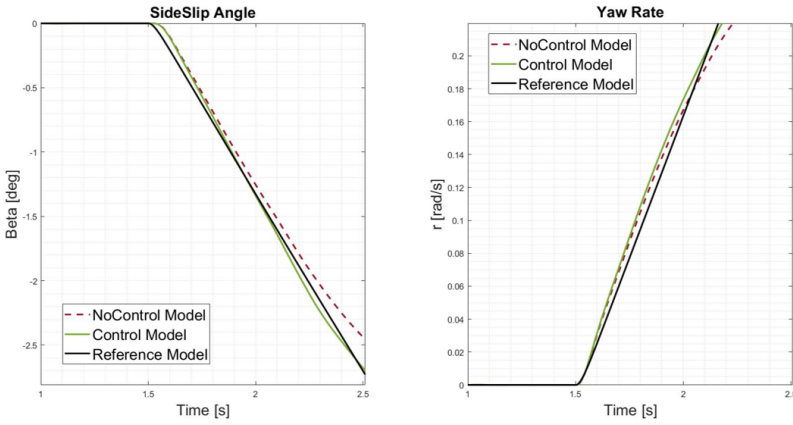


Figure 4.70: Vehicle side-slip angle and yaw rate and lateral acceleration in a j-turn manoeuvre with a speed of  $100km/h$  and a friction of 1, supposing availability and unavailability of the ESC

For the DLC, tests are repeated increasing the reference speed, until the vehicle can correctly perform the trajectory, supposing availability and unavailability of the proposed controlling method. The improvement is evaluated by observing the maximum speed at which the vehicle executes the imposed steering manoeuvres without leaving the admitted zone and hitting the corners. Figure 4.71 shows how the vehicle equipped with the proposed control can manoeuvre  $60km/h$ . Instead, a vehicle with only standard ESC, i.e. excluding the Moore-Penrose pseudoinverse from the control algorithm, is unable to fulfil test requirements at the same speed. In addition, the comparison of the speed during DLC manoeuvre for the investigated UCs shows a lesser vehicle speed reduction in the second phase of the trajectory and a faster return to target speed, due to a better distribution of the vehicle torque values.

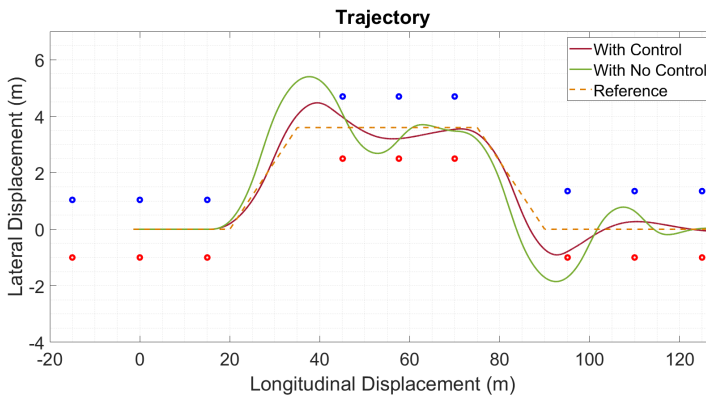


Figure 4.71: Vehicle trajectory in a DLC manoeuvre with a speed of  $50km/h$  and a friction of 1, supposing availability and unavailability of the ESC

Looking at the outputs of Table 4.29, the proposed ESC strategy can ensure a stable lateral behaviour of the vehicle, by increasing the speed at which the reference trajectory could be executed and by reducing the Root Square Mean Error (RSME) respect to the ideal curve of the manoeuvre (centred respect to the admitted zone).

Table 4.29: Maximum vehicle speed during Double Lane Change tests for different adherence conditions

Double-Lane Change			
<i>Adherence</i> $\mu$ [0-1]	<i>ESP</i>	<i>Max. Speed</i> [km/h]	<i>RSME</i>
1	ON	50	0.52
	OFF	40	0.78
0.7	ON	40	0.40
	OFF	30	0.53
0.5	ON	30	0.11
	OFF	30	0.28

The performance evaluation of the ESC during the SwD manoeuvre is done by evaluating two key parameters: the sideslip angle  $\beta$  and the yaw rate  $r$ . Figure 4.72 shows the target and actual values of the yaw rate and the sideslip angle. Plots display both, supposing availability and unavailability of the controller.

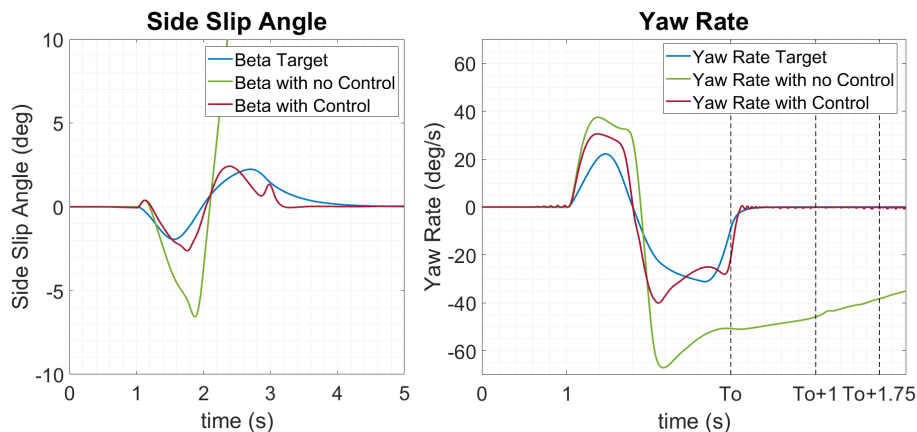


Figure 4.72: Target and effective vehicle side slip angle  $\beta$  and yaw rate  $r$  during SwD manoeuvre, with a longitudinal speed of 80 km/h and a steering wheel angle of 270 deg, supposing availability and unavailability of the ESC control system

## Conclusions

In conclusion, the assumption to alternatively suppose availability and unavailability of the stability controller are done to comparatively assess the simulation outputs of the performed tests. In particular, the results of the tests in which the controller systems are disabled are assumed as a reference baseline for the metrical evaluation of the obtained improvements.

Results suggest that the ABS controller is fundamental to ensuring a safe behaviour during straight-line deceleration. Instead, indicates that the proposed ABS strategy, based on PID control logic of the longitudinal slip, makes effective and smooth the braking effort as compared to an on-off control based on the wheel rotational acceleration. Indeed, for different adherence conditions, the Anti-slip strategy appears effective, since reduces the corresponding longitudinal distance between the starting of the brake manoeuvres and the complete stopping of the vehicle. For normal adherence conditions, the adopted policy successfully fulfils the limitations imposed by the mandatory standards.

The j-turn test highlight how the controller can correct the oversteering vehicle behaviour. Concerning the Double-Lane Change, it can be stated that the proposed ESC strategy can ensure a stable lateral behaviour of the vehicle, by increasing the speed at which the reference trajectory could be executed. Results of the Sine with Dwell tests clearly show that the ESC controller increase the stability performances, reducing the error between target and real value of  $\beta$  and  $r$  and enabling the correct execution of the imposed manoeuvre.

Thus, we can conclude by saying that, in this work, the proposed controller is correctly integrated to accomplish enhanced stability behaviours of the IWM driven vehicle, both in longitudinal and lateral directions.



## Chapter 5

# Advanced ESP Control Algorithms

By-Wire and E/E systems have offered designers previously precluded possibilities, allowing the development of advanced and complex control solutions. Increased computational power of stable and reliable platforms [251] with extended and flexible HiL capabilities [252] support the development of advanced control functionalities. Further improvements in terms of ECU's computational resources are incentivized by newly hardware resources and task scheduling techniques, developed to implement DAS on modern vehicles [253].

All these considerations contribute to a rapidly changing scenario, in which environmental issues have pushed toward the electrification of vehicles, opening up to totally new configurations. WIM traction structure is certainly one of the most innovative and promising technology from the point of view of stability control. Distributed and electrified vehicle powertrains make possible the development of newly traction configurations that allows efficient four-quadrant controls of longitudinal forces applied on each wheel [194, 254–257]. BBW technology [258] and corresponding improvements of brake units assure more precise control of applied braking forces, allowing fast and reliable application of correction efforts on each wheel. SBW instead, can be easily interfaced with high-level CU to control vehicle lateral behaviour and assist the driver during dangerous and risky manoeuvres. A wide diffused application is the lane-keeping function, in which the steering system is automatically actuated to keep the vehicle between the road lines.

From a SoA review, many work related to coordinate active steering and TV action for active stability system design can be found: Ando [31] define a DYC with active front/rear steering and wheel force distribution for lateral force control and a method of yaw moment compensation to attenuate tracking error in this controller, also using a wheel workload equalization technique; Di Cairano et al. [32] propose a coordinate Active Front Steering (AFS) and differential brake using a MPC, controlling vehicle in the tire-slip angle domains; in [259] Burgio presents the application of state feedback linearization technique to integrate brakes and steering actuators in vehicle lateral dynamics control; a novel vehicle controller is proposed by Dincmen [33], combining two control loops: the inner loop regulates the individual tire force generation and prevents saturation, the outer loop is a LQR optimal controller to assure the overall lateral stability; a control architecture

that simultaneously utilizes AFS and differential braking for vehicle lateral stability while minimizing longitudinal perturbations based on MPC is used in [260] by Choi; Doumiati [261] coordinate these actuators through a suitable gain scheduled Linear Parameter Varying (LPV) controller for yaw control purpose; Falcone et al. [118] propose a path following MPC-based (MPC) scheme utilising steering and braking to track a desired path for obstacle avoidance manoeuvre; Guvenç [34] revise different control techniques for braking and AFS coordination; a four wheel independent steering EV is controlled with a NL SMC by Hang in [262]; Lee combine active steering and differential braking to achieve yaw stability and rollover avoidance [263]; Li [264] define a DYC with 4 wheel driven omni-directional vehicle using optimal steering and driving actuator distribution; an integrated control of active front steer angle and direct yaw moment control is developed by Nagai [265] to improve vehicle handling and stability of a vehicle; Ren et al. [119] adopt a MPC-based yaw stability control for in-wheel-motored EV via active front steering and motor torque distribution to stabilize a vehicle along the desired states; in [36] authors use a dynamic control approach for automotive vehicle yaw stabilization, coordinating AFS and adaptive brake allocation for DYC; a coordinated differential assist steering and VSC for 4WD independent vehicle is proposed by Wang in [266]. Other papers can be found [123, 267–269].

The current chapter is dedicated to the description of two different lateral stability control strategies which rely on TV technique and steering command. Despite the majority of work in literature, which addresses only one layer at the time of the hierarchical framework described in section 2.4.1, in these activities the three-level are encompassed. This approach ensures a smoother integration between the blocks by including their mutual interactions during the design phases.

First solution concern the mutual correction of vehicle cornering behaviour and minimization of engaged grips in the tire-road interfaces. The second control methodology is based on a first-order SMC to ensure both vehicle's yaw rate  $r$  and side-slip angle  $\beta$  asymptotically reach their target values, estimated using a 2 dimension model-based approach. Actuator constraints are accounted and specific control dead zones are defined. Performances are evaluated on standardized cornering manoeuvre tests, supposing 4WD-layout actuated by IWMs.

## 5.1 Minimized Tire Adhesion Grip ESP Controller

In this section, an optimal torque and steering allocation strategy for the control of a road vehicle's lateral behaviour is designed, developed and investigated [245]. The aim is to find the best compromise between road vehicle lateral stability and minimum available adhesion on tires, by performing *Steering* and *Active Torque Distribution* corrections. The TV allocation strategy is designed for integration on RT systems, requiring modest computational and a limited set of input data, which is affordable with sensors that are currently installed on vehicles. The solution involves a constrained double minimum least-square optimization control, which minimizes at the same time correction torques on wheels and corresponding engaged road adhesion. Performances are assessed on a standardized cornering manoeuvre test in a simulation environment. Finally, the main features of the allocation strategy are evaluated for a benchmark vehicle model, which also simulates complex interactions arising with other onboard subsystems.

### 5.1.1 Introduction

Improvements in different technologies in the automotive field are continuously increasing the interest of both scientific and industrial communities for TV and AFS techniques aiming to improve directional stability of road vehicles, especially when degraded wheel-road adhesion conditions occur. Increased computational power of stable and reliable platforms [251] with extended and flexible HiL capabilities [252] support the development of advanced control functionalities. Further improvements in terms of computational resources of wide diffused ECU are incentivized by the increasing level of hardware resources and task scheduling techniques developed to implement DAS on modern vehicles [253]. BBW technology [258] and corresponding improvements of brake units assure more precise control of applied braking forces, allowing fast and reliable control of correction efforts applied on each wheel. Distributed and electrified vehicle powertrains make possible the development of newly traction configurations, such as WIM layouts, which allow efficient four-quadrant controls of longitudinal forces applied on each wheel [194, 254–256]. In this case, applicable corrections are constrained by specific features of the chosen solutions [257]. Adoption of SBW systems [270] offers the possibility of a further enhance vehicle dynamical behaviour [271].

The object of this work is the design of optimal allocation criteria to properly stabilize vehicle trajectory with a mixed array of corrections in terms of torques applied to wheels and steering angle, optimized for available adhesion in the tire-road interface. This topic is still the subject of study and debate in the technical-scientific literature and is destined to become increasingly important for the development of autonomous or assisted driving systems that tend to support, or even eliminate, the driver's intervention. By their nature, these systems require very effective vehicle stability controls that allow managing complex scenarios once entrusted to the user's experience and competence.

The proposed allocator is designed to take as inputs the required traction/brake demand and the desired yaw moment to correct the vehicle's driving path. Allocation problem show multi-DoF solutions, so the final control efforts must be chosen between several possible conditions as a trade-off between lateral stability and reduced adhesion committed by the vehicle's wheels, which must take count of different non-linearities. These over-actuated systems are limited and perturbed by the complex variety of driving conditions. For this reason, an allocator is necessary to manage optimally the control DoF.

In this sense, the analysis of the data from the simulations has provided many interesting insights. The choice of using the Moore-Penrose pseudoinverse TV allocator was certainly found to be very valid. Indeed, the controller can guarantee greater stability, while reducing at the same time the committed adherence.

The innovative contribution of this work is represented by the idea that this problem can be solved following the typical approach adopted in robotics for over-actuated systems [272], by resolving a constrained minimization problem related to the actuator's efforts. This concept has been proposed recently both for energy optimization [273] and lateral stability purposes [31], but the extension of this concept to merge the task of vehicle stabilization and available adherence minimization is innovative, not previously mentioned in the literature. Steering and TV control produce a redundant set of forces on wheels that must be compared to a homogeneous criterion/metric.

### 5.1.2 Torque and Steering Allocation Strategy

In the scheme of Figure 5.1 is visible the block diagram of the proposed *Allocator*, which summarize its main interactions with other on-board systems and ECUs.

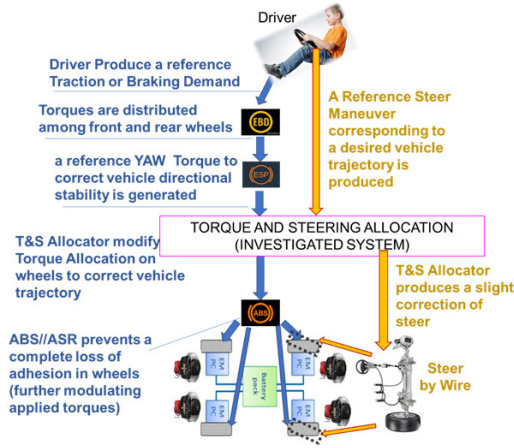


Figure 5.1: Proposed allocator and its interaction with the other systems

### Control Objectives

The controller should perform two different tasks: *Vehicle lateral stabilization*, by the application of a correcting yaw moment; *Minimization of the engaged grips*, introducing steering corrections that improve vehicle controllability. Considering the inherently contrasting nature of these control objectives is important to finely tune the controllers in order to achieve both the aims.

**Vehicle Lateral Stabilization:** this control is realized using a simplified approach, in which the desired yaw moment is calculated through a gain scheduling method based on desired and actual yaw rate, steering angle and longitudinal speed. Desired yaw velocity  $r_{tar}$  is defined by (5.1). The yaw moment  $M_{yaw}$  to be applied by the TV technique is (5.2), where  $k_{yaw}$  is the proportional gain, calculated to minimize the RMSE between actual and desired lateral displacement during the manoeuvres.

$$r_{tar} = \frac{\cos[\tan^{-1}(\frac{b \cdot \tan(\delta)}{a+b})V_x]}{a+b} \tan(\delta) \quad (5.1)$$

$$M_{yaw} = k_{yaw}(r_{tar} - r) \cdot \delta \cdot V_x \quad (5.2)$$

**Minimization of the engaged grips:** one of the biggest issues in the field of vehicle dynamical control deals with the estimation of available adherence with the road. This methodology instead, wants to challenge conventional and widely adopted techniques. This model-based solution is abstracted by the concept of friction estimation, proposing an approach which the manoeuvrability margin of the vehicle, especially in poor adherence cornering situations. The adherence evaluation metric is the engaged grip on each wheel  $\mu_{ij}$  (5.3), calculated in terms of equivalent dimension of Kamm adhesion circle/ellipse [274], as shown in Figure 5.2.

$$\left(\frac{F_{yij}}{f_S F_{zij}}\right)^2 + \left(\frac{F_{xij}}{F_{zij}}\right)^2 = \mu_{yij}^2 + \mu_{xij}^2 = \mu_{ij}^2 \quad (5.3)$$

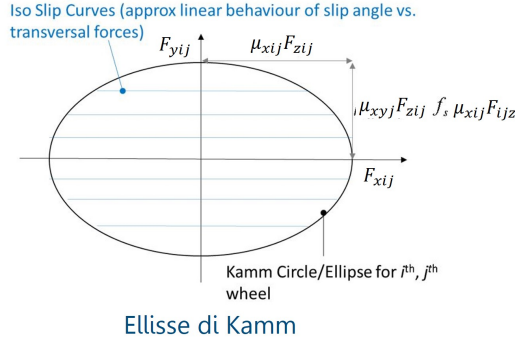


Figure 5.2: Kamm adhesion ellipse for the  $i^{\text{th}} - j^{\text{th}}$  wheel

Optimal solution corresponds to a minimum value of  $\|\mu_{eng}\|_2$  defined according to (5.4), where  $f_S$  is the scaling factor between  $\mu_{yij}$  and  $\mu_{xij}$  on the same contact patch ( $\mu_{yij} = f_S \mu_{xij}$ ),  $F_{xij}$  and  $F_{yij}$  are the wheel contact forces and  $F_{zij}$  are the normal forces.

$$\|\mu_{eng}\|_2 = \sqrt{\mu_{rl}^2 + \mu_{fl}^2 + \mu_{rr}^2 + \mu_{fr}^2} \quad (5.4)$$

For the definition of normal loads on wheels authors propose an estimator relying on a quasi-static vehicle model, that can be executed with relatively modest numerical resources. According to scheme of Figure 5.3, inputs of investigated algorithm are:

- Desired longitudinal effort  $T_x$ , applied to the vehicle according to driver pedal inputs;
- Correction yaw moment  $M_{zz}$ , applied according to decisions performed by ESP controller to correct vehicle driving path.

The output of the Coordinated Steer and TV Allocator are:

- Corrections forces to wheel  $dT_x$ , which represents the implementation of active torque distribution technique;
- Steering correction angle  $d\delta$ , introducing a correction of the steering angle.

### Model-based Estimator

There is a wide literature concerning model-based estimators of vehicle behaviour [105, 275, 276]. Cited examples are mainly related to the estimation of vehicle dynamics and kinematics which is indispensable to providing state feedback for proper control of vehicle dynamics. This estimation is often performed using Kalman recursive/servo-filters in their different implementations.

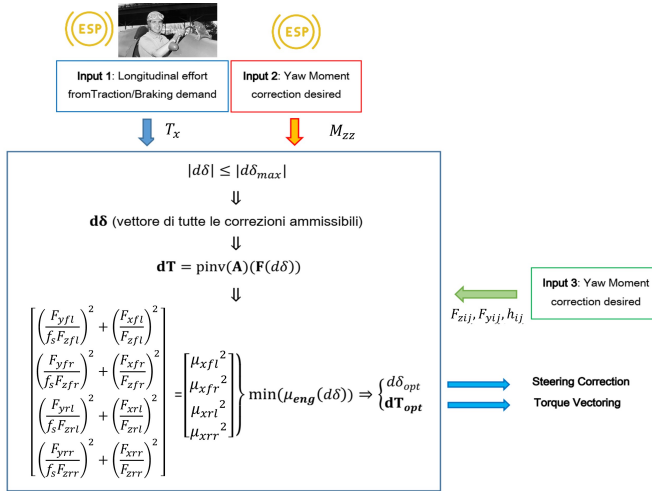


Figure 5.3: simplified scheme of proposed algorithm

It is also interesting to notice that vehicle state estimators adopted by [105] are integrated into a TV regulator that slightly resembles the one developed in this activity, differing essentially for three main features: (1) TV solution of Xiong et al. does not consider the possibility of correcting the steering angle; (2) Overall optimization criteria perform a weighted least square optimization of both actuation and performed correction concern the available adhesion, while the proposed allocator aims to execute a two-step least-square optimization of actuation and adhesion; (3) This strategy avoid the use of on-line estimators, privileging a simple but robust approach, whose parameters are simpler to be calibrated.

Here, an explicit model is considered: proposed controllers and estimators rely on ideal measurements from common automotive sensors. A developed vehicle estimator can assure a relatively fast and simple execution, which is also a fundamental feature for the future integration in a recursive filter: as visible in Table 5.1, the estimator assumes as known some inertial parameters of the vehicle, or at least approximately identified. The output of the proposed model is rough estimations of normal  $F_{zij}$  and lateral  $F_{yij}^*$  contact forces currently applied to the vehicle. The model calculates linearised coefficients  $h_{yij}$  to correlate the performed steering corrections to the corresponding variations of lateral forces. Cautionary limitation of  $d\delta_{max}$  is calculated to avoid excessive and abrupt steering corrections for which it can correspond to undesired non-linear behaviour.

The bicycle model of Figure 5.4 is used to calculate the distribution of lateral contact forces between the front and rear tyres. Impose the planar equilibrium of the vehicle respect to lateral direction and rotational around  $z$  axis is done according (5.5). Relation (5.6) is obtained. Distribution of applied lateral forces  $T_{yij}$  are assumed proportional to applied normal loads  $F_{zij}$ , according (5.7).

$$\begin{cases} F_y = \frac{m\dot{x}^2}{R} = F_{yf} \cos(\delta) + F_{yr} \approx F_{yf} + F_{yr} \\ F_{yfa} = F_{yrb} \end{cases} \quad (5.5)$$

Table 5.1: Input and Output of the proposed Model Estimator

Model Estimator Input/Output		
<i>Name</i>	<i>Symbol</i>	<i>Description</i>
<i>Input</i>		
Yaw Rate	$\dot{\gamma}$	Measured (from sensors)
Long. Speed	$\dot{x}$	Measured (from sensors)
Steering Angle	$\delta$	Measured (from sensors)
Mass	$m$	Known or estimated (filter)
CoG position	$a, b, h$	Known or estimated (filter)
Braking/Traction Forces	$F_x$	Known
Maximum Steer Correction	$d\delta_{max}$	Imposed
<i>Output</i>		
Normal Forces	$N$	Estimated
Lateral Forces	$T_y$	Estimated
Linearized Coeff.	$h_y$	Calculated

$$\left. \begin{aligned} F_{yf} &= \frac{m\dot{x}^2}{R} \frac{b}{a+b} \\ F_{yr} &= \frac{m\dot{x}^2}{R} \frac{a}{a+b} \end{aligned} \right\} \begin{aligned} F_{yf} &= \frac{m\dot{x}^2}{R} \frac{b}{a+b} = \frac{b}{a} \\ F_{yr} &= \frac{m\dot{x}^2}{R} \frac{a}{a+b} = \frac{a}{a+b} \end{aligned} \quad (5.6)$$

$$\left\{ \begin{aligned} F_{yffj} &= T_{yf} \frac{F_{zffj}}{F_{zff}} = \frac{m\dot{x}^2}{R} \frac{b}{a+b} \frac{F_{zffj}}{F_{zff}} \\ F_{yrfj} &= F_{yr} \frac{F_{zrfj}}{F_{zr}} = \frac{m\dot{x}^2}{R} \frac{a}{a+b} \frac{F_{zrfj}}{F_{zr}} \end{aligned} \right. \quad (5.7)$$

Vertical forces cannot be directly calculated with static considerations, since neglecting tyre and suspension deformations result in considering the structure over-constrained/hyperstatic; this problem is solved by performing the calculation of the inertial load transfer in two separate steps [221]: transfer between front and rear wheels is considered by imposing equilibrium against pitch rotations ( $y$  axis), while the lateral one is obtained by solving the equilibrium respect to roll movement ( $x$  axis).

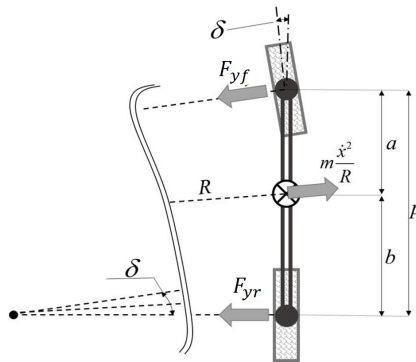


Figure 5.4: Adopted bicycle model for the Model-based Estimator

Finally, distribution of normal loads is calculated according (5.8), with  $h$  height of the vehicle CoG and  $t/2$  the half-track of front and rear axles.

$$F_{zij} = F_{zi} \frac{b}{2(a+b)} - m\ddot{x} \frac{h}{2(a+b)} - m \frac{\dot{x}^2}{R} \frac{h}{4t} \quad (5.8)$$

For what concerns the third output of Figure 5.3, linearized coefficients are calculated by differentiating (5.7) as compared to the steering angle around the current configuration. This calculation is approximated and valid only in the case of ideal steering: in this way calculated  $h_{yij}$  overestimates the increase of  $F_{yij}$ , assuring a further safety factor for excessive steering with degraded adhesion conditions. The same simplified approach is also used to calculate the value of  $\Delta\delta_{max}$  that should be investigated by the least square optimization. The aim of this calculation is only to provide a boundary limit for the iterative optimization of the allocator, avoiding excessive computational efforts and further protecting the system from unfeasible or dangerous solutions. According to the bicycle model of Figure 5.4, it is possible to calculate the maximum values of lateral forces that can be exerted on the front and rear wheels according (5.9), assuming a nominal value of adhesion  $\mu_0$ .

$$F_{yi(max)} = \mu_0 F_{zi} \quad (5.9)$$

By differentiating (5.10), (5.11) is obtained, where  $p$  is the vehicle wheel-base.

$$F_{yfl} = \frac{m\dot{x}^2}{R} \frac{b}{p} \frac{F_{zfl}}{F_{zf}} = \frac{m\dot{x}^2}{R} \frac{b}{p} \frac{F_z \frac{b}{2p} - m\ddot{c} \frac{h}{2p} - m \frac{\dot{x}^2 h}{R2c}}{F_z \frac{b}{p} - m\ddot{x} \frac{h}{p}} \quad (5.10)$$

$$dF_{yfl} = - \frac{m\dot{x}^2}{R} \frac{b}{p} \frac{F_z \frac{b}{2p} - m\ddot{c} \frac{h}{2p} - m \frac{\dot{x}^2 h}{R2c}}{F_z \frac{b}{p} - m\ddot{x} \frac{h}{p}} dR \quad (5.11)$$

Then, combining (5.11) with the assumption (5.12), the linearised coefficient  $h_{fl}$  can be estimated with (5.13). Similarly, the coefficients for the other wheels can be calculated.

$$\delta \approx \frac{p}{R} \rightarrow d\delta \approx - \frac{p}{R^2} dR \rightarrow dR = -d\delta \frac{R^2}{p} \quad (5.12)$$

$$\Delta T_{yfl} = m\dot{x}^2 R \frac{\overbrace{b \frac{F_z \frac{b}{2p} - m\ddot{c} \frac{h}{2p} - m \frac{\dot{x}^2 h}{R2c}}{F_z \frac{b}{p} - m\ddot{x} \frac{h}{p}}}}{p^2} d\delta \quad (5.13)$$

Then maximum steering correction is chosen imposing reasonable limits as (5.14). Linearised coefficients  $h_{yi}$  are defined according (5.15).

$$d\delta_{max} = \min \left( \max \left( \frac{F_{yi(max)} - F_{yi}^*}{h_{yi}}, 0 \right) \right) \quad (5.14)$$

$$h_{yi} = \frac{dF_{yi}^*}{d\delta} = \frac{h_{yil} + h_{yir}}{2} \quad (5.15)$$

### Optimal Allocation Criteria

Starting from the scheme of Figure 5.3, the corrections of longitudinal and lateral contact forces  $dT_{kij}$  introduced by the TV allocator have to satisfy (5.17): efforts must produce no modifications in terms of vehicle's longitudinal accelerations, assuring at the same time a desired yaw correction moment  $M_{zz}$  calculated by the ESP system, to improve the directional stability. Wheel effort can be controlled independently by modulating traction and braking forces supposing an IWM 4WD vehicle layout; variations of lateral forces  $\Delta T_{yij}$  are produced by introducing a steering correction. So, (5.17) can be rewritten by considering the linearised coefficients  $h_{yij}$  defined by (5.15). Thus, (5.18) is valid, with  $k$  the normalized factor (5.16) which allows to express lateral tire force variations  $\Delta F_{yij}$  in function of steer command corrections  $\Delta\delta$ . Finally, System of (5.18) can be rearranged as (5.19).

$$k = -b(h_{yrl} + h_{yrr}) + a(h_{yfl} + h_{yfr}) \quad (5.16)$$

$$\begin{bmatrix} 0 \\ M_{zz} \end{bmatrix} = \begin{bmatrix} 1 & 1 & 1 & 1 & 0 & 0 & 0 & 0 \\ -t/2 & -t/2 & t/2 & t/2 & -b & a & -b & a \end{bmatrix} \begin{bmatrix} \Delta T_{xrl} \\ \Delta T_{xfl} \\ \Delta T_{xrr} \\ \Delta T_{xfr} \\ \Delta T_{yrl} \\ \Delta T_{xfl} \\ \Delta T_{yrr} \\ \Delta T_{yfr} \end{bmatrix} \quad (5.17)$$

$$\begin{bmatrix} 0 \\ M_{zz} \end{bmatrix} = \begin{bmatrix} 1 & 1 & 1 & 1 & 0 \\ -t/2 & -t/2 & t/2 & t/2 & k \end{bmatrix} \begin{bmatrix} \Delta T_{xrl} \\ \Delta T_{xfl} \\ \Delta T_{xrr} \\ \Delta T_{xfr} \\ \Delta\delta \end{bmatrix} \quad (5.18)$$

$$\underbrace{\begin{bmatrix} 0 \\ M_{zz} - k\Delta\delta \end{bmatrix}}_F = \underbrace{\begin{bmatrix} 1 & 1 & 1 & 1 \\ -t/2 & -t/2 & t/2 & t/2 \end{bmatrix}}_A \overbrace{\begin{bmatrix} \Delta T_{xrl} \\ \Delta T_{xfl} \\ \Delta T_{xrr} \\ \Delta T_{xfr} \end{bmatrix}}^{\Delta T} \quad (5.19)$$

Once assigned the value of the steering correction  $\Delta\delta$ , (5.19) can be solved by applying the Moore-Penrose pseudoinverse of the matrix  $A$  as described in (5.20).

$$dT = pinv(A)F \quad (5.20)$$

It can be easily demonstrated that the TV correction calculated according (5.20) is the minimum in term of norm 2 [194, 252, 277]; so chosen solution is optimal in terms of least square torques applied on wheels. Corrections are applied through real actuators whose behaviour should be saturated to reproduce typical limitations in terms of response amplitude and operational quadrant. This is a common problem that has been investigated in previous studies [278]. In this work, it is simply solved by iterating (5.20) until all constraints are respected. Also, the optimal control signal is filtered using a low-pass filter with a 40Hz pass-band, according to (5.21).

$$F(s) = \frac{1}{0.02s + 1} \quad (5.21)$$

As previously introduced this calculation is repeated for multiple values of steering correction  $\Delta\delta$ . A function of possible solutions is obtained. Interval of investigated steering corrections defines a vector whose elements are constrained to be lower than a maximum allowable value  $\Delta\delta_{max}$ .

For each value of  $\Delta\delta$  is possible to calculate the corresponding vector of tangential contact forces  $T(\Delta\delta)$  (5.22), where: Longitudinal contact forces  $T_{xij}(\Delta\delta)$  are calculated as the sum of corrections  $\Delta T_{xij}$  and corresponding reference traction/braking demand  $T_{xij(ref)}$ , generated by driver command and eventually corrected by others ECU; Lateral contact forces  $T_{yij}(\Delta\delta)$  are calculated as the sum of corrections  $\Delta T_{yij} = h_{yij}\Delta\delta$  and  $T_{yij}^*$ , that are evaluated by a model-based estimator according to current kinematic behaviour of the vehicle.

$$\overbrace{\begin{bmatrix} T_{xrl}(\Delta\delta) \\ T_{xfl}(\Delta\delta) \\ T_{xrr}(\Delta\delta) \\ T_{xfr}(\Delta\delta) \\ T_{yrl}(\Delta\delta) \\ T_{yfl}(\Delta\delta) \\ T_{yrr}(\Delta\delta) \\ T_{yfr}(\Delta\delta) \end{bmatrix}}^{T(\Delta\delta)} = \begin{bmatrix} \Delta T_{xrl} \\ \Delta T_{xfl} \\ \Delta T_{xrr} \\ \Delta T_{xfr} \\ \Delta T_{yrl} \\ \Delta T_{yfl} \\ \Delta T_{yrr} \\ \Delta T_{yfr} \end{bmatrix} + \begin{bmatrix} T_{xrl(ref)} \\ T_{xfl(ref)} \\ T_{xrr(ref)} \\ T_{xfr(ref)} \\ T_{yrl}^* \\ T_{yfl}^* \\ T_{yrr}^* \\ T_{yfr}^* \end{bmatrix} \quad (5.22)$$

Once  $T(\Delta\delta)$  is calculated for each value of steering correction is possible to calculate  $\mu_{eng}(\Delta\delta)$  according (5.3). Associated correction of longitudinal forces on wheels is known. This ‘‘optimal’’ solution has the following properties:

- For a known set of the desired length, effort  $T_x$  and yaw torque  $M_{zz}$ , the chosen optimal solution minimizes the required  $\mu_{eng}$  for performed manoeuvre. Since corrections of vehicle dynamics are often performed with limited wheel-road adhesion this is a highly desirable feature;
- Proposed criteria allow for optimisation corrections regarding both steering angle and applied longitudinal efforts with a unified adhesion-based criterion;
- Corrections of longitudinal efforts applied to wheels are minimized with least-square criteria for known limits of actuators and driver intentions.

### 5.1.3 Benchmark Vehicle Model

Evaluation of achievable performances is executed on the **FIAT 500e** benchmark vehicle implemented in the *9-DoF Simulink model*. For this validation we suppose a 4WD traction layout with independent IWM and front steering wheels (Figure 5.5). However, the proposed allocation algorithm is parametrized to be further generalized for different vehicle architectures.

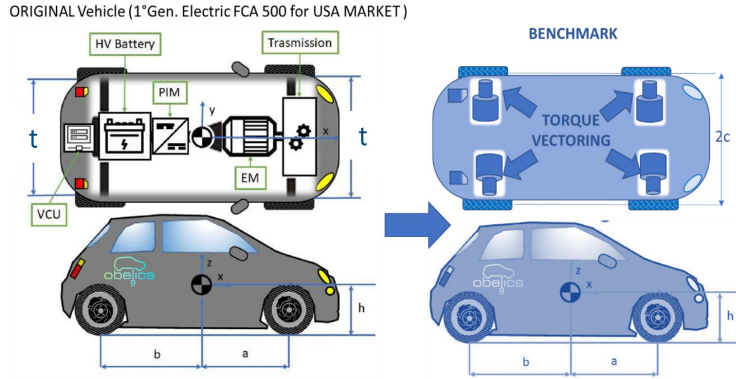


Figure 5.5: Benchmark vehicle's architectures of the FIAT 500e

The 9-DoF model consist of several sub-systems: **Driver**; **Chassis**, 3 DoF model which reproduce longitudinal, lateral and yaw motion dynamical behaviour of the vehicle body and four wheel models, which add 1 DoF each; **Electronic Control Units**, devoted to perform different functionalities, defining control objectives and braking effort allocation (Brake Blending Controller); **Proposed Allocator**, which apply the described control strategy; **Actuators**.

#### 5.1.4 Performed Simulations

Assessment of the *Allocator* performances are related to standardized vehicle cornering tests, executed in simulation environment and properly initialized according required boundary conditions. For a comparative evaluation, each test is performed assuming four different scenario: *No Control (NC)*; *Torque Vectoring (Tv)*; *Steering (St)* and *Torque Vectoring + Steering (Tv+St)*.

It is important to distinguish the nature of the proposed reference manoeuvres: **Open-Loop tests**, which provide the condition to objectively evaluate vehicle inner manoeuvrability and handling abilities, by excluding the driver from the control rig; **Closed-Loop tests**, utilized to assess active stability performance both concerning vehicle and driver capabilities.

##### Open-loop Test: ISO4138 - Constant Steering Wheel Angle

The vehicle is driven holding constant the steering wheel angle. Output refers to curve radius and lateral acceleration. The fixed steering angle is the one related to a 30m curve radius at the lowest speed possible, according to  $\delta(30m) = (a + b)/R = 0.076 \approx 4.35deg$ . Results are visible in Figure 5.6. The test is repeated for increasing vehicle speed until the handling and controllability of the car are completely lost. Result for 50km/h which compare non-controlled and controlled vehicle are visible in Figure 5.7 and Figure 5.8. Steering angle commands are visible in Figure 5.9. When the control is enabled lower side-slip angles are reached, as the wheel a curve radius closer to desired ones. When observing the curve radius for 70km/h vehicle speed of Figure 5.10, it can be noted that the coordinate TV and steering control ensure reach the desired curve in less time. However, a greater overshoot in radius over time can be seen.

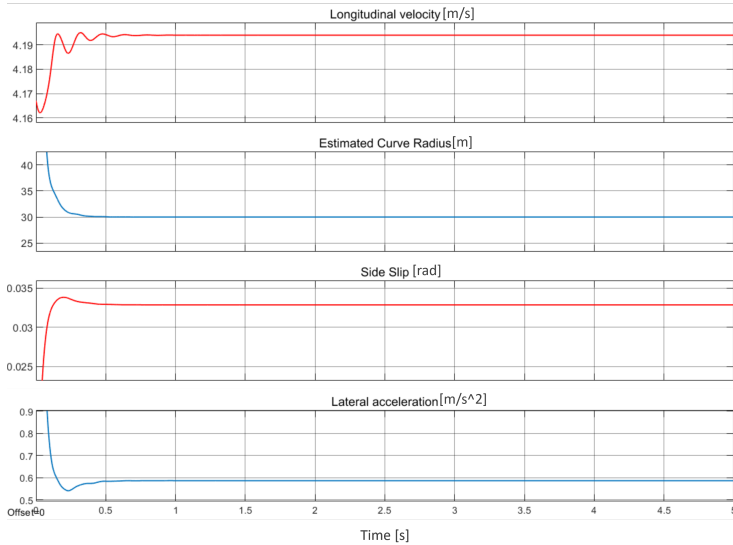


Figure 5.6: Vehicle dynamic response in CSW angle test at  $15\text{km/h}$

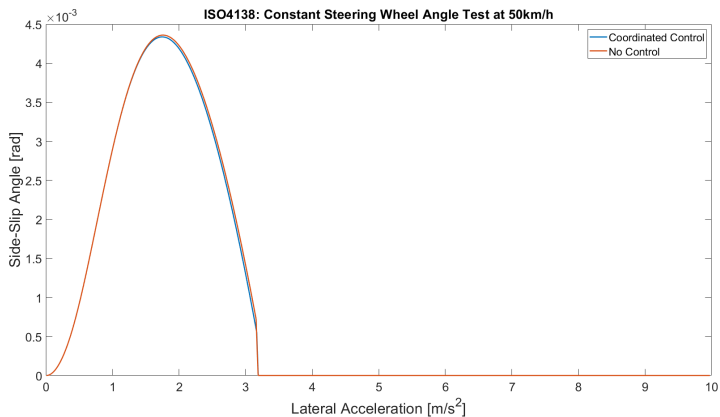


Figure 5.7: Side-slip angle vs lateral acceleration in different testing scenarios for constant steering wheel angle test at  $50\text{km/h}$ , supposing availability and unavailability of the ESC

### Open-loop Test: ISO7401 - Lateral Transient Response

A **Step Input Test** is performed to quantify peak response time and overshoot of steering wheel angle, lateral acceleration and yaw rate. Also, the steady-state yaw velocity response gain  $(\dot{\gamma}/\delta_H)_{SS}$  is calculated. The vehicle is driven at the required test speed ( $60\text{km/h}$ ) to identify the steady-state wheel angle which produces a lateral acceleration of  $4\text{m/s}^2$ . The throttle pedal is held to a constant value, letting the vehicle maintain the manoeuvre's entrance speed. The result of Table 5.2 shows that lower value of lateral acceleration and yaw rate response times are allowed by the controller. Overshoot of lateral acceleration is slightly improved, as can be seen from Figure 5.11. However, the yaw rate is penalized.

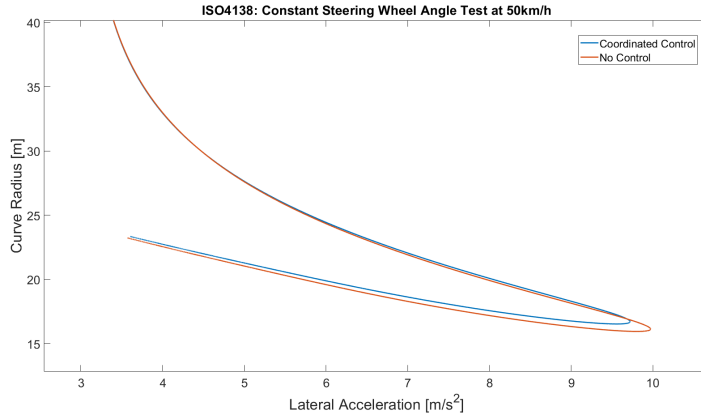


Figure 5.8: Curve radius vs lateral acceleration for constant steering wheel angle test at  $50\text{km}/h$ , supposing availability and unavailability of the ESC

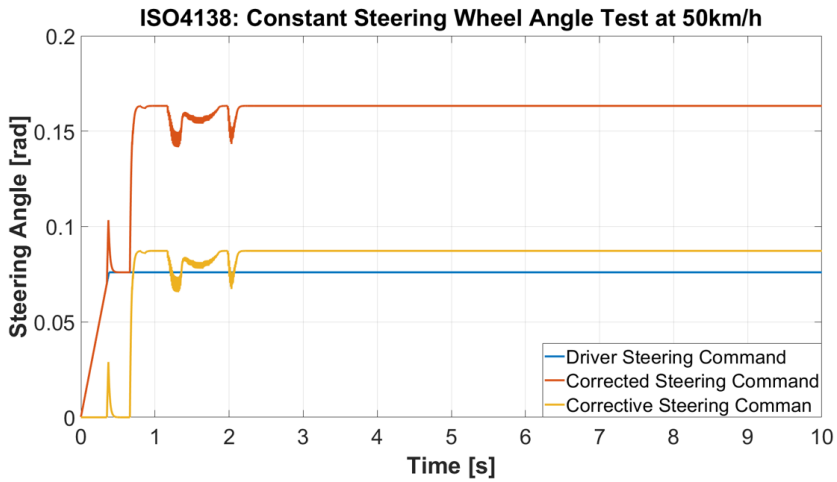


Figure 5.9: Steering angle for constant steering wheel angle test at  $50\text{km}/h$ , supposing availability and unavailability of the ESC

Table 5.2: ISO7401 test result for  $NC$  and  $Tv+St$  control

<i>Parameter [Unit]</i>	<i>Symbol</i>	<i>NC</i>	<i>St+Tv</i>	<i>Impr. [%]</i>
Yaw Rate Response Gain [ $s^{-1}$ ]	$(\frac{\dot{\gamma}}{\delta})_{SS}$	7.194	7.134	0.82
Lat. Acc. Resp. Time [s]	$T_{aY}$	0.673	0.663	1.48
Yaw Rate Resp. Time [s]	$T_r$	0.455	0.445	2.19
Lat. Acc. Peak Resp. Time [s]	$T_{aY,max}$	1.62	1.59	1.85
Yaw Rate Peak Resp. Time [s]	$T_{r,max}$	1.42	1.39	2.11
Lat. Acc. Overshoot [ $m/s^2$ ]	$U_{aY}$	0.098	0.097	1.02
Yaw Rate Overshoot [ $rad/s$ ]	$U_r$	0.066	0.067	-1.51

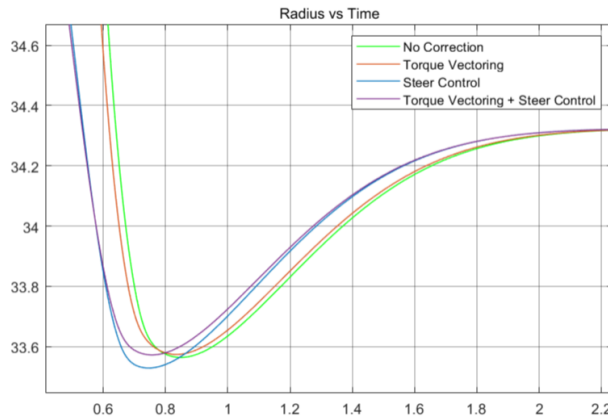


Figure 5.10: Curve radius vs time in different testing scenarios for constant steering wheel angle test at  $70\text{km/h}$ , supposing availability and unavailability of the ESC

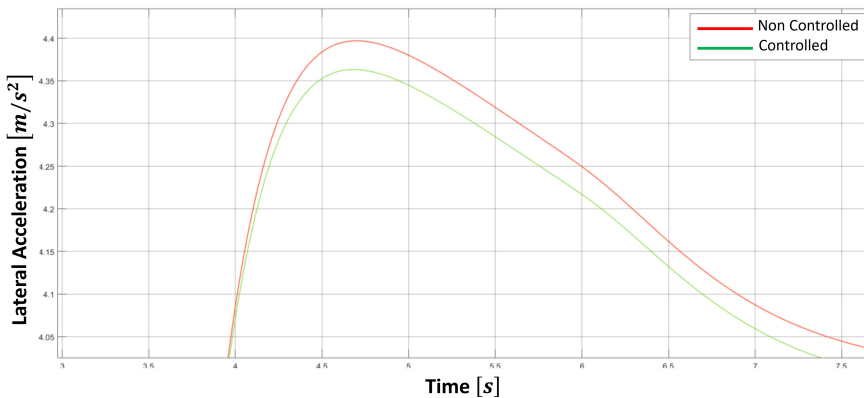


Figure 5.11: Lateral acceleration for lateral transient response test at  $60\text{km/h}$ , supposing availability and unavailability of the ESC control system

### Closed-loop Test: ISO3888 - Double Lane Change

The standard related to the **DLC manoeuvre** specifies the track dimension for the test, which must be respected to consider it successfully executed. In particular, the vehicle should perform 2 consecutive lane changes with a lateral displacement of  $3.5\text{m}$ , without touching the admitted boundaries. Result of Figure 5.12, Figure 5.13 and Figure 5.14 refer to  $80\text{km/h}$  vehicle speed. Here is evident that the proposed coordinated control between *Steering* and *Torque Vectoring* is highly desirable, both in terms of stability (DLC is performed with a higher safety margin) and engaged adherence minimization (in full control mode, adherence  $\mu$  is lower and at least equal to the one related to solely TV solution).



Figure 5.12: Lateral displacement for DLC test at 80km/h, supposing availability and unavailability of the ESC

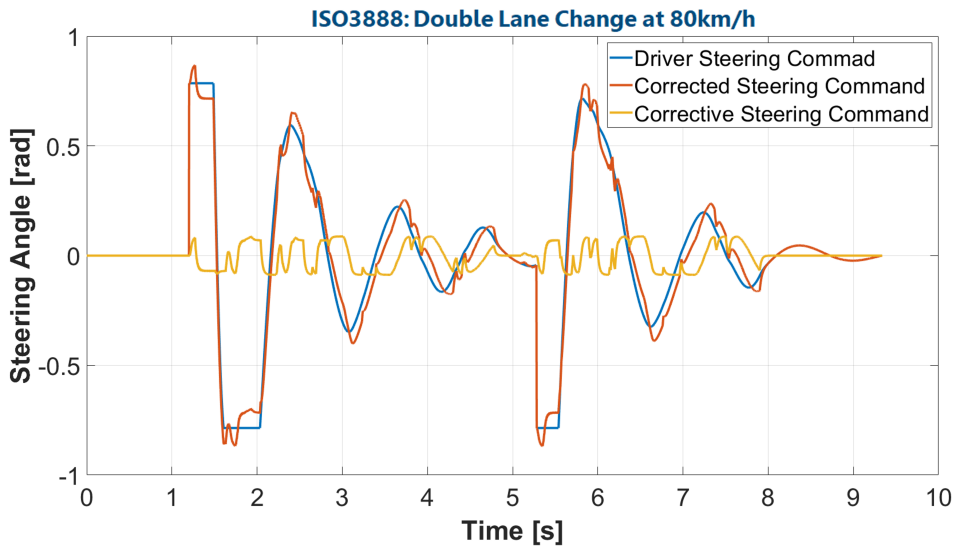


Figure 5.13: Steering angle command for DLC test at 80km/h, supposing availability and unavailability of the ESC

This test was also useful to evaluate the tracking performances of the vertical and lateral load estimators, comparing results for the calculation performed by the model natively implemented in Simulink. Figure 5.15 and Figure 5.16 show good performances, since the normal forces are calculated with acceptable level of confidence.

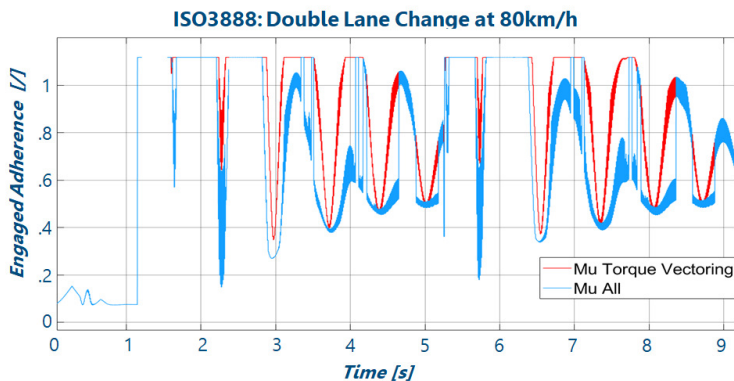


Figure 5.14: Engaged adherence for for DLC test at  $80\text{km/h}$ , supposing availability and unavailability of the ESC

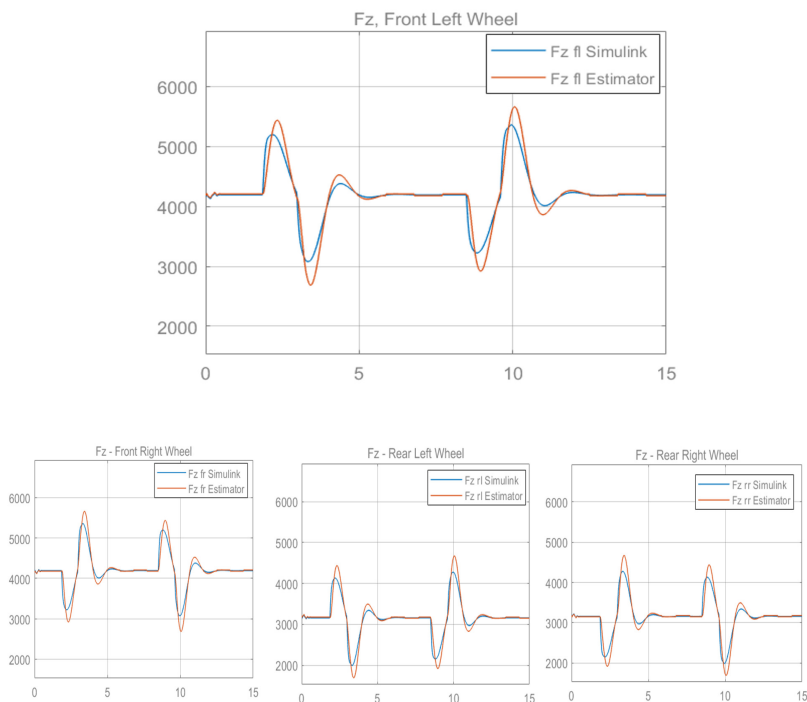


Figure 5.15: Normal load estimation on wheels for DLC test at  $80\text{ km/h}$

### 5.1.5 Conclusions and Future Developments

The result of the performed simulations shows that the coordinated steering and TV optimal control approach appear efficient and reliable respecting the tasks of vehicle lateral stabilization and engaged adherence minimization. The proposed ESP model is scalable, RT capable and parametrized, so its architecture is portable for different vehicle UC and can be easily interfaced with higher-level trajectory planning system (e.g. ADAS).

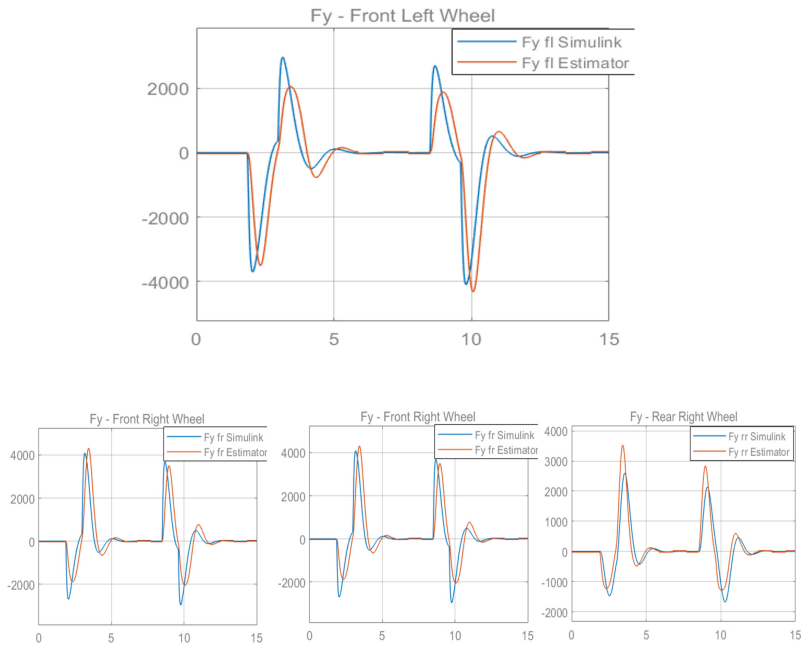


Figure 5.16: Lateral load estimation on wheels for DLC test at 80 km/h

The output of the test, however, highlights also lacks strategy. Loads on wheels are evaluated with a simplified estimator based on the quasi-static vehicle model. Indeed, estimators show poor performances when operating at boundary conditions for simplification assumptions. Also, noise or disturbances are not modelled in this case, so further improvement can concern this topic. This aspect, along with the simplified vehicle's modelling approach (based on a single-track model) makes the improvement achievement appear marginal if compared to an uncontrolled vehicle. A more robust estimation algorithm, considering filtering solutions (e.g. Unscented Kalman filters), a more reliable vehicle behaviour modelling could represent possible future developments.

Another aspect which contributes to a limited stability improvement is the contrasting nature of the addressed tasks: in some driving conditions reducing the committed grip on the wheels may lead to a corrective action which conflicts with the lateral stability task. An example is certainly the constant radius turn, in which the driver can actively adjust the trajectory acting on the steering wheel. Thus, when such driving condition occurs, these can be recognized by the estimators to act on controller gain scheduling and/or dead-zone definition.

Finally, since the controller does not directly address the vehicle's dynamical states as a control objective, during the DLC test performances related to lateral acceleration, yaw rate and side-slip angle are penalized. These results are summarized in Figure 5.17, which shows their normalized values as compared to the peak of the non-controlled driving scenario. Indeed, the ideal yaw moment is determined by a simple proportional control for the yaw rate error, steering angle and vehicle speed. Side-slip angle is not addressed as a control objective, nor lateral acceleration. Thus, coupling the tire adhesion minimization algorithm with a more robust ESP strategy could lead to better stability improvement.

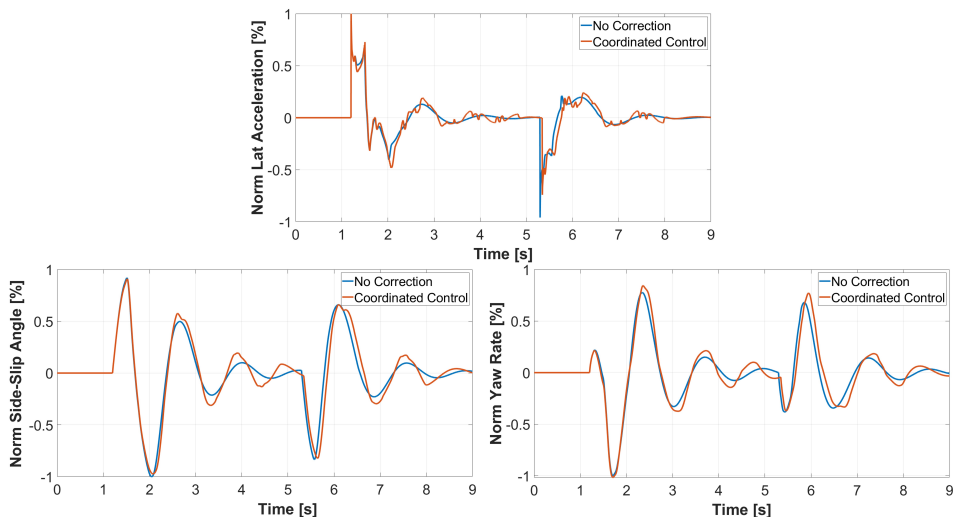


Figure 5.17: Normalized lateral acceleration (top), normalized yaw rate (bottom-left) and normalized side-slip angle (bottom-right) for DLC test at  $80\text{km/h}$ , supposing availability and unavailability of the ESC

## 5.2 Sliding Mode ESP Controller [246]

In the vehicle dynamics control topic, several sliding modes-based control algorithms are available in the literature. The main advantage of this technique concern the robustness of system uncertainties accounted for during the development phases.

Uematsu et al. [279] have compared the robustness of sliding controllers supposing alternative sliding surfaces. Bobier [280] designed a sliding controller to minimize the weighted combination of yaw rate error and side-slip angle. Alipour [28] develop a sliding mode controller coupled with a neural network observer and a fuzzy logic controller. Chung [281] use a 3-DoF vehicle motion model. Ding [141] adopt sliding mode in conjunction of non-linear disturbance observer techniques. Goggia et al. [40] present an integral sliding mode formulation, similarly to Hu [282]. Tota [41], extend the integral sliding mode control theory to a 4WD electric vehicle with independent driven wheels. Second-order sliding surface methodologies are summarized by Bartolini in [39]. Canale [42] propose this solution integrated with a feedforward contribution to enhance transient response.

As compared to previous work based on Sliding Mode strategies [39–42], this algorithm relies on a 2 dimensions model for states and sliding surface, challenging well-know and established lateral stability SMC methods, typically using separated sliding surfaces which decouple the yaw rate and side-slip angle control dynamics. The feed-forward term of the sliding control approach is completed with a feed-back PI control term based on the state's errors. Moreover, desired yaw moment and steering command correction are obtained from the same robust controller, achieving a highly compatible control signal.

### 5.2.1 Control Strategy

This lateral stability solution is based on the Sliding Mode methodology. The objective is the direct control of vehicle side-slip angle  $\beta$  and yaw rate  $r$  by the application of AFS and TV efforts. The SMC-based ESP algorithm simplified block diagram is visible in Figure 5.18. The Multiple Input Multiple Output (MIMO) control unit is developed on three different layers, depending on the task the sub-controller must accomplish:

- **High-level layer:** which define the control objective according to driver intention and vehicle states, e.g. longitudinal speed, side-slip angle, yaw rate;
- **Intermediate-level layer:** consisting in a first order sliding mode controller;
- **Low-level layer:** devoted to the generation of the control references for the actuators, i.e. SBW, BBW and TCS.

In-depth information about each controller layer can be found in the following sub-chapters. However, it is worth nothing to say that the proposed solution respects fundamental features to exhibit portability and flexibility properties, being able to be implemented for different vehicle architectures. For this specific ESP controller, the needed sensors are a steering wheel angle sensor, speed sensors on each wheel, IMU (for vehicle longitudinal speed yaw rate measurement) and a side-slip angle estimator (typically requiring vehicle lateral speed).

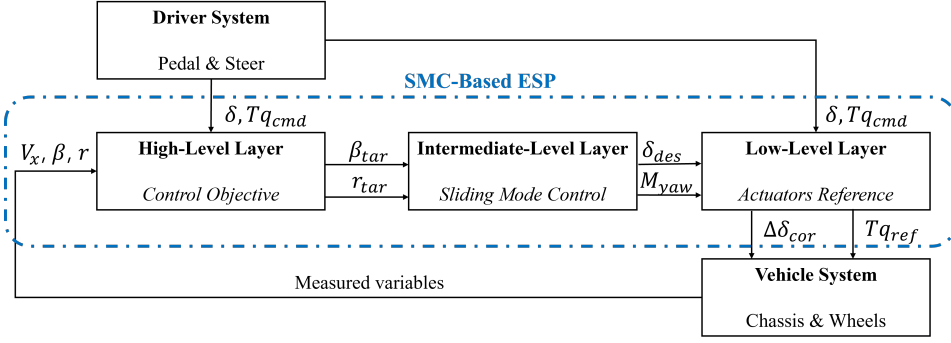


Figure 5.18: Block diagram of the SMC controller

## 5.2.2 Modelling Approach: High-level layer

The High-Level control layer relies on ideal and simplified vehicle equations to define the control objectives [3]. It combines information from sensors and estimators about vehicle actual states and driver input, thereby generating the state's references. Since the SMC aim at the direct control of the vehicle's side-slip angle and yaw rate, it is important to define the state space of the above-mentioned variable. A four wheel vehicle model with 3-DoF in longitudinal  $x$ , lateral  $y$  and yaw  $\gamma$  is considered (Figure 2.1).

### Assumptions

The modelling approach is based on the following assumptions:

- (a) The steering angle is small:  $\delta < 10deg$ ;
- (b) Left and right wheel steer angles are equal:  $\delta_{fl} = \delta_{fr} = \delta$ ;
- (c) The vehicle longitudinal speed is constant:  $V_x = cost$ ;
- (d) Tire slip angle are small:  $\alpha \ll 1$ ;
- (e) Tires cornering stiffness are known and constant:  $C_{yf} = cost$ ;  $C_{yr} = cost$ .

These conditions are fundamental to account for parametric RT estimation uncertainties, both concerning dynamics and kinematics variables. Neglecting the effect of road bank angle and applying the Newton's second law for the  $y$ -axis vehicle's motion gives (5.23), where  $a_y$  is the inertial acceleration of the vehicle at the CoG. It can be seen that 2 terms contribute to  $a_y$ :  $\ddot{y}$  is the acceleration due to the lateral motion,  $V_x \dot{\gamma}$  is the centripetal acceleration. System (5.24) represent assumptions (a) and (c). Combining (5.23) with (5.24) lead to (5.25).

$$a_y = \left( \frac{d^2 y}{dt^2} \right) = \ddot{y} + V_x \dot{\gamma} \quad (5.23)$$

$$\begin{cases} \beta = \frac{V_y}{V_x} = \frac{\dot{y}}{V_x} \\ \ddot{y} = V_x \cdot \dot{\beta} \end{cases} \Rightarrow \beta = \frac{V_y}{V_x} = \frac{\dot{y}}{V_x} \quad (5.24)$$

$$a_y = \ddot{y} + V_x \cdot \dot{\gamma} = \ddot{y} + V_x \cdot r = V_x \cdot \left( \frac{d\beta}{dt} + \dot{\gamma} \right) \quad (5.25)$$

Small tire slip angle ( $d$ ) and constant cornering stiffness ( $e$ ) instead, are abstracted through (5.26) and (5.27), assuming a linear behaviour of wheel's lateral forces for side-slip angles  $\alpha_i$ , where  $\theta_{v_i}$  is the angle between the velocity vector form with the vehicle longitudinal axis. For further improvements, assumption ( $b$ ) can be removed by considering different steering angles for right and left front tires. This leads to an increased dimension of the state space model.

$$\begin{cases} F_{yfl} = F_{yfr} = C_{\alpha_f} \cdot \alpha_f \\ F_{yrl} = F_{yrr} = C_{\alpha_r} \cdot \alpha_r \end{cases} \quad (5.26)$$

$$\begin{cases} \alpha_f = \delta - \theta_{vf} = \delta - \beta - \frac{a \cdot r}{V_x} \\ \alpha_r = -\theta_{vr} = -\beta + \frac{b \cdot r}{V_x} \end{cases} \quad (5.27)$$

## Vehicle Dynamics

As already pointed out, the SMC aim at the direct control of the vehicle's side-slip angle and yaw rate. So, it is important to define the state space of the above-mentioned variable. External yaw moment  $M_{zz}$  expression can be described by (5.28), applied through differential torque allocation between left and right wheels.

$$M_{zz} = -\frac{t_f}{2}(F_{xfl} - F_{xfr}) \cos \delta_f - \frac{t_r}{2}(F_{xrl} - F_{xrr}) + a(F_{xfl} + F_{xfr}) \sin \delta_f \quad (5.28)$$

Combining (5.25), (5.26) and (5.27) in the system (2.27) lead to (5.29).

$$\begin{cases} mV_x \left( \frac{d\beta}{dt} + r \right) = 2C_{\alpha_f} \left( \delta - \beta - \frac{ar}{V_x} \right) + 2C_{\alpha_r} \left( -\beta + \frac{br}{V_x} \right) \\ I_z \dot{r} = 2aC_{\alpha_f} \left( \delta - \beta - \frac{ar}{V_x} \right) - 2bC_{\alpha_r} \left( -\beta + \frac{br}{V_x} \right) + M_{zz} \end{cases} \quad (5.29)$$

System (5.29) can be expressed making explicit  $\beta$  and  $r$ , yielding to (5.30).

$$\begin{cases} \frac{d\beta}{dt} = -r + 2 \frac{C_{\alpha_f}}{m \cdot V_x} \left( \delta - \beta - \frac{ar}{V_x} \right) + 2 \frac{C_{\alpha_r}}{m \cdot V_x} \left( -\beta + \frac{br}{V_x} \right) \\ \frac{dr}{dt} = 2a \frac{C_{\alpha_f}}{I_z} \left( \delta - \beta - \frac{ar}{V_x} \right) - 2b \frac{C_{\alpha_r}}{I_z} \left( -\beta + \frac{br}{V_x} \right) + \frac{M_{zz}}{I_z} \end{cases} \quad (5.30)$$

Rearranging (5.30) allow us to obtain the state space model (5.31) of the controlled variable  $x = [\beta; r]^T$ , with  $u = [\delta; M_{zz}]^T$  the control inputs,  $A$  the state matrix and  $B$  the control matrix. This modelling approach could also be applied to a front and rear wheels steering vehicle, by including  $\delta_r$  in (5.27) and by increasing the dimension of matrix  $B$  to 3x2 in (5.31), with control input  $u = [\delta_f; \delta_r; M_{zz}]^T$ .

$$\dot{x} = \begin{bmatrix} \dot{\beta} \\ \dot{r} \end{bmatrix} = \begin{bmatrix} -2 \frac{C_{\alpha_f} + C_{\alpha_r}}{m V_x} & -1 - 2 \frac{a C_{\alpha_f} - b C_{\alpha_r}}{m V_x^2} \\ 2 \frac{b C_{\alpha_r} - a C_{\alpha_f}}{I_z} & -2 \frac{a^2 C_{\alpha_f} + b^2 C_{\alpha_r}}{I_z V_x} \end{bmatrix} x + \begin{bmatrix} 2 \frac{C_{\alpha_f}}{m V_x} & 0 \\ 2 \frac{a C_{\alpha_f}}{I_z} & \frac{1}{I_z} \end{bmatrix} u = Ax + Bu \quad (5.31)$$

## Target Vehicle States

Desired side-slip angle (5.33) and yaw rate (5.34) appear linearly dependent by  $\delta$  if it is assumed that the front steering vehicle is in steady-state conditions. Indeed, in this situation, (5.32) is the steering angle for negotiating a curve radius  $R$ , with  $K_V$  the vehicle under-steer gradient. It is important to highlight that target states rely on ideal dynamic vehicle behaviour supposing steady-state conditions, while the *High-Level layer* is based on a dynamic modelling approach as compared to yaw rate and side-slip angle. Even in this case, variation of target states with the friction coefficient  $\mu$  is neglected.

$$\delta_{ss} = \frac{a+b}{R} + \left( \frac{m_f}{2C_{\alpha f}} - \frac{m_r}{2C_{\alpha r}} \right) \frac{V_x^2}{R} = \frac{a+b}{R} + K_V a_y \quad (5.32)$$

$$\beta_{des} = \frac{b - \frac{amV^2}{2C_{\alpha r}(a+b)}}{a+b + \frac{mV^2(bC_{\alpha r} - aC_{\alpha f})}{2C_{\alpha f}C_{\alpha r}(a+b)}} \delta = K_{\beta} \cdot \delta \quad (5.33)$$

$$\dot{\gamma}_{des} = \frac{\dot{x}}{R} = \frac{\dot{x}}{a+b + \frac{m\dot{x}^2(bC_{\alpha r} - aC_{\alpha f})}{2C_{\alpha r}C_{\alpha f}(a+b)}} \delta = K_r \cdot \delta \quad (5.34)$$

Consider the vector  $x_{des} = [\beta_{des}; r_{des}]^T$  and the assumption (5.35), with  $k$  the  $k$ -th sampling step at a rate of  $T_s$ . The model of (5.36) is valid and correspond to the state space model of the desired side-slip and yaw rate, obtained by differentiation of the kinematic equations (5.33)-(5.34).

$$\dot{x}_{des} = \frac{d}{dt} x_{des} = \frac{x_{des}(k) - x_{des}(k-1)}{T_s} \quad (5.35)$$

$$\dot{x}_{des} = \frac{1}{T_s} \begin{bmatrix} \beta_{des}(k) - \beta_{des}(k-1) \\ r_{des}(k) - r_{des}(k-1) \end{bmatrix} = \begin{bmatrix} \frac{K_{\beta}}{T_s} & 0 \\ \frac{K_r}{T_s} & 0 \end{bmatrix} u - \frac{1}{T_s} \begin{bmatrix} \beta_{des}(k-1) \\ r_{des}(k-1) \end{bmatrix} = B_{des} u + g \quad (5.36)$$

However, desired side-slip angle and yaw rate (5.33)-(5.34) cannot always be obtained, e.g. in poor tire-road friction condition. For these reason, target states must be bounded considering safety factors. If the lateral acceleration at the vehicle CoG is defined by (5.37),  $a_y$  can be expressed in function of  $\beta$  and  $r$  from (5.39), since (5.38) is valid. Lateral acceleration is upper by bounded by the friction coefficient  $\mu$  according (5.40). Assuming that  $\beta$  and its derivative are small, the second and the third term of (5.39) are negligible, while the first one dominates.

$$a_y = \dot{x}r + \ddot{y} \quad (5.37)$$

$$\dot{y} = \dot{x} \tan(\beta) \quad (5.38)$$

$$a_y = \dot{x}r + \ddot{x} \tan(\dot{\beta}) + \frac{\dot{x}\dot{\beta}}{\sqrt{1 + \tan(\beta)^2}} \quad (5.39)$$

$$a_y \leq \mu g \quad (5.40)$$

Considering a safety factor of 0.85, the target yaw rate can be bounded by (5.41), as described in (5.42). In this way, we suppose that the second and third terms of (5.39) contribute only 15% to the total lateral acceleration.

$$|r_{bound}| \leq 0.85 \frac{\mu g}{\dot{x}} \quad (5.41)$$

$$\begin{cases} r_{tar} = r_{des} & \text{if } |r_{des}| \leq r_{bound} \\ r_{tar} = r_{bound} \cdot \text{sign}(r_{des}) & \text{if } |r_{des}| > r_{bound} \end{cases} \quad (5.42)$$

Limiting the target side-slip angle is also very important since at higher value tires lose their linear behaviour, approaching the limit of adhesion.  $\beta$  is upper bounded by the empirical relation (5.43), as visible in (5.44). This relation correspond to an upper bound of  $\beta \leq 10deg$  when  $\mu = 0.9$  (dry road) and  $\beta \leq 4deg$  when  $\mu = 0.35$  (snowy road).

$$|\beta_{bound}| \leq r_{tar} \left( \frac{b}{V_x} - \frac{m \cdot a \cdot V_x}{2C_{yr} \cdot (a + b)} \right) \quad (5.43)$$

$$\begin{cases} \beta_{tar} = \beta_{des} & \text{if } |\beta_{des}| \leq \beta_{bound} \\ \beta_{tar} = \beta_{bound} \cdot \text{sign}(\beta_{des}) & \text{if } |\beta_{des}| > \beta_{bound} \end{cases} \quad (5.44)$$

To ensure  $x$  to asymptotically converge to  $x_{tar}$ , the modelling approach described in this section is fundamental. Indeed, optimal control effort calculated by the **Intermediate-level layer** using SMC requires the knowledge of actual and target-controlled states. A second-order transfer function (5.45) is used both for the target side-slip angle and yaw rate to include the real dynamic behaviour of the vehicle, which exhibit smoother conduct for the one calculated in (5.33)-(5.34).

$$\frac{x_{tar}^*}{x_{tar}} = \frac{w_n^2}{s^2 + 2w_n s + w_n^2} \quad (5.45)$$

The control objectives are calculated at each time step, fixed in this case at  $0.001s$ , to update the current desired path behaviour. This allows the calculation of optimal control efforts. The specifications of this low-level controller are summarized in Figure 5.19.

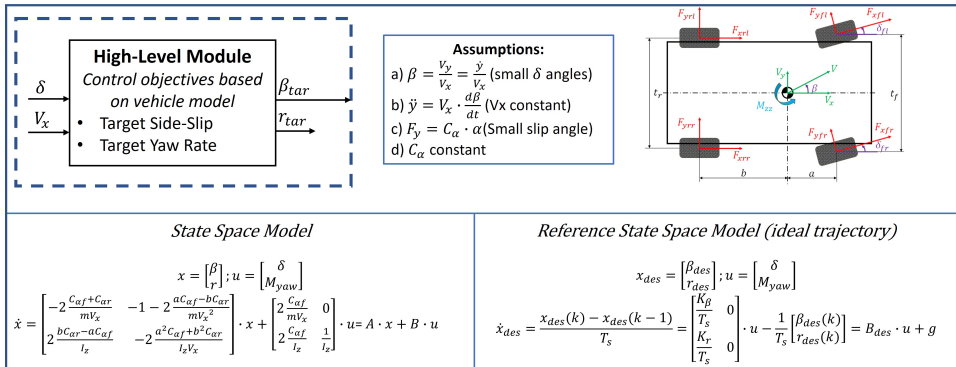


Figure 5.19: Block diagram of the low-level SMC controller

### 5.2.3 Control Theory: Intermediate-level layer

The Intermediate-level receive the control objectives from the upper controller, along with the driver inputs and vehicle states, to define desired wheel steer demand and equivalent yaw moment to be applied to the vehicle.

**Control action:** To lead the states  $\beta$  and  $r$  converge to the target values a first-order *Sliding Mode Controller* is proposed. It's action is typically composed by a feed-forward impedance control terms (based on model considerations) and a feed-back compensation terms (similar to a PID control effort). The *Feed-forward term* is defined by imposing to 0 the desired states error (5.46) and it's derivative (5.47), starting from formulation (5.31) and (5.36).

$$\tilde{x}_{des} = x - x_{des} = \begin{bmatrix} \beta - \beta_{des} \\ r - r_{des} \end{bmatrix} = 0 \quad (5.46)$$

$$\dot{\tilde{x}}_{des} = \dot{x} - \dot{x}_{des} = Ax + Bu - (B_{des}u + g) = Ax + (B - B_{des})u - g = 0 \quad (5.47)$$

The feed forward term  $u_{fwd}$  is obtained by resolving (5.47) respect to  $u$ , as visible in (5.48). This ensure that the derivative states error  $\tilde{x}_{des}$  tend asymptotically to 0. It worth nothing to note that matrix  $(B - B_{des})$  of (5.45) is non-invertible, so a pseudo-inverse operator is used.

$$\begin{aligned} u_{fwd} &= (B - B_{des})^+ \cdot (g - Ax) \\ &= \begin{bmatrix} -2\frac{C_{\alpha f} + C_{\alpha r}}{mV_x} - \frac{K_\beta}{T_s} & -1 - 2\frac{aC_{\alpha f} - bC_{\alpha r}}{mV_x^2} \\ 2\frac{bC_{\alpha r} - aC_{\alpha f}}{I_z} - \frac{K_r}{T_s} & -2\frac{a^2C_{\alpha f} + b^2C_{\alpha r}}{I_{zz}V_x} \end{bmatrix}^+ \left( -\frac{1}{T_s} \begin{bmatrix} \beta_{des}(k-1) \\ r_{des}(k-1) \end{bmatrix} - Ax \right) \end{aligned} \quad (5.48)$$

The *Feed-back term*  $u_{bck}$  depend on target error  $\tilde{x}_{tar} = x - x_{tar}$  to produce the proportional, integral and sign compensation components, according to (5.49).

$$u_{bck} = (B - B_{des})^+ \cdot (-k_P \tilde{x}_{tar} - k_I \int \tilde{x}_{tar} dt - k_s \text{sing}(S)) \quad (5.49)$$

The optimal control input  $\hat{u}$  is (5.50), as the sum of (5.48) and (5.49).

$$\hat{u} = \begin{bmatrix} \delta_{cor} \\ M_{yaw} \end{bmatrix} = (B - B_{tar})^+ \left( \underbrace{g - Ax}_{\text{Feed-forward}} \overbrace{-k_P \tilde{x}_{tar} - k_I \int \tilde{x}_{tar} dt - k_s \text{sing}(S)}^{\text{Feed-back}} \right) \quad (5.50)$$

**Ljapunov candidate function:** The Ljapunov stability of the SMC-based ESP is guaranteed by the function candidate of (5.51) [28], whose convergence is ensured by condition (5.52). Substituting  $u$  into (5.52) lead to (5.53).

$$\begin{cases} S = \tilde{x}_{des} + \xi \int \tilde{x} dt \\ V(t) = \frac{1}{2} S^2 + \int \epsilon |S| dt \end{cases} \quad (5.51)$$

$$\dot{V}(t) = S\dot{S} + \epsilon |S| = S[Ax - g + (B - B_{des})u + \xi \tilde{x}_{des}] + \epsilon |S| \leq 0 \quad (5.52)$$

$$(\xi - k_P)\tilde{x}_{tar}S - k_I \int \tilde{x}_{tar} dt S - k_S|S| + \epsilon|S| \leq 0 \quad (5.53)$$

**Proof:** Selecting  $k_P$ ,  $k_I$  and  $k_s$  according (5.54) the Ljapunov stability is proved. However, to obtain the best stability control performances from the SMC the multiple gains have to be tuned properly. This process is carried out during the preliminary test phases. The tasks performed by the intermediate-level controller are visible in the block diagram of Figure 5.20.

$$\begin{cases} k_P = \xi \\ k_I > 0 \\ k_s \geq \epsilon - k_I \int \tilde{x} dt \cdot \text{sign}(S) \end{cases} \quad (5.54)$$

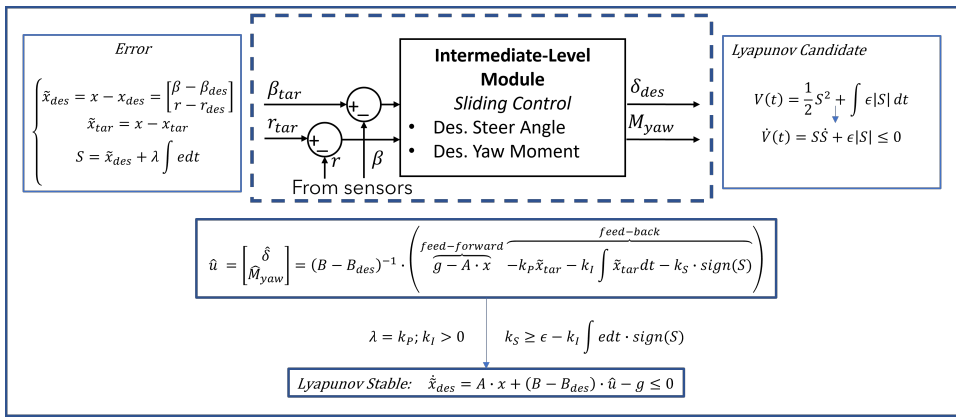


Figure 5.20: Block diagram of the intermediate-level SMC controller

The current formulation of the sliding mode controller ensures an optimal trade-off between side-slip angle and yaw rate tracking tasks. These objectives, as previously mentioned, are often conflictual, especially in risky driving situations. However, the adoption of the 2-dimensions sliding surface couple both the dynamics and defines control efforts in agreement with the contrasting aim of direct yaw rate and side-slip contemporaneous regulations.

#### 5.2.4 Effort Application: Low-level layer

Even if optimal control signals (5.50) secure the controlled states converge to desired states, an allocation problem still needs to be solved. Indeed, the controller should stabilize the vehicle as well as produce control effort that should be in accordance with the driver's intention, keeping unaltered the driving path.

The effectiveness of the sliding mode approach in suppressing bounded disturbances is due to the discontinuous terms based on the error sign. However, chattering in the control action is induced. This may lead to either mechanical/electrical stress and wear, as well as undesired vibrations during normal operation. To avoid the typical chatter [29], specific saturation and dead-zone are defined (Figure 5.21). The adopted criteria are state errors and vehicle longitudinal speed. By a proper definition of these dead zones, only the non-linear region of the vehicle’s lateral behaviour is affected. In contrast, when the vehicle operates in a linear range and its response is proportional to the steering command, ESP does not intervene.

Note that using these functions to deal with SMC output discontinuities could be detrimental since the controller formulation loses its robustness properties [40]. Asymptotic convergence to zero of the tracking error can no longer be proved, except for its boundedness.

Specific smoothing transfer functions are adopted in the definition of the control dead zones. Thus, this solution provides a useful tool to avoid the fast transient yaw moment command demanded by the upper controller during abrupt cornering manoeuvres, letting to use relatively high control gains while averting undesired spikes during the torque allocation phase.

At this level, are managed also by the actuator constraints, which is often a critical point for the application of sliding mode techniques to real cases. This allows to simultaneously achieve smooth transient performance and hold the inequality constraints of the actuators.

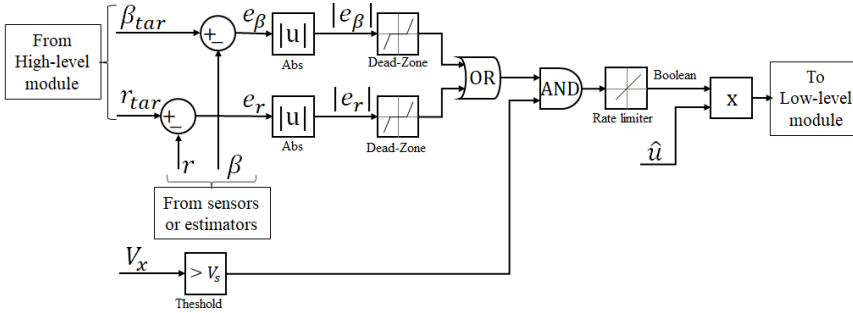


Figure 5.21: Definition of control dead-zone

### Steer Command

Optimal steer angle is applied as a correction for the desired trajectory: it shouldn't directly overwrite the driver command. For doing so,  $\delta_{cor}$  is limited to the 10% of the steering angle command, to avoid abrupt deviation which could lead to unpredictable vehicle dynamics. Indeed, during fast transient phases a greater wheel steering angle correction can bring the tires outside the linear behaviour boundaries, saturating the available friction in the contact patch (high slip angles  $\alpha$  and slip ratios  $\lambda$ ). Also, the rate of the steering correction  $\dot{\delta}_{cor}$  is limited to  $1500deg/s$  to not exceed the maximum driver capability of steering angle speed application [283]. The block diagram of the steer correction application algorithm is visible in Figure 5.22.

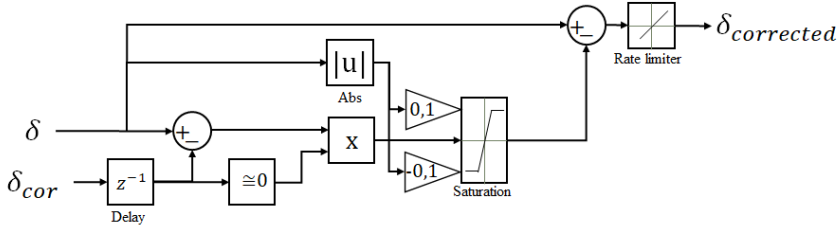


Figure 5.22: Application of corrected steering angle algorithm

### Yaw Moment

In a more sophisticated EV layout the availability of multi-quadrant electric motors or active differential consent to take advantage also of traction torque for the task of mapping the desired yaw moment into equivalent torque demand for each wheel. In this case, the desired  $M_{zz}$  is applied to the vehicle using an advanced TV technique. However, this approach contemplates a constrained control problem, because of the multi-DoF solutions that are available. Indeed, independent wheel torque control implicates 4-DoF. This lead to  $\infty^4$  possible solutions [22]. For this reason, the optimal allocation strategy based on the Moore-Penrose pseudo-inverse is adopted [245], where TV efforts are limited to the maximum deliverable torques of each wheel. Even in this case, a good trade-off between vehicle stability and driver intention must be satisfied.

The optimal yaw moment  $M_{yaw}$  calculated by (5.50) is the  $M_{zz}$  defined in (5.28). However, some modifications are assumed. Firstly, the last term of (5.28) is neglected. This assumption is coherent with the proposed testing procedure and the conditions (a) and (d) defined earlier. As can be seen later, the maximum wheel steering angle during the reference manoeuvre is about  $6deg$ , which limits the contribution of the steer component to a maximum of 10% on the yaw moment. Thus, is neglected. For further activities, this term will be accounted. Also, the allocation problem is formulated to account for the different steering angles of the left and right front tires,  $\delta_{fl}$  and  $\delta_{fr}$ , respectively. The correcting yaw moment imposed on the torque allocator is the one described in (5.55).

$$M_{yaw} = -\frac{t_f}{2}[F_{xfl}\cos(\delta_{fl}) - F_{xfr}\cos(\delta_{fr})] - \frac{t_r}{2}(F_{xrl} - F_{xrr}) \quad (5.55)$$

The allocation problem is given by (5.56), where:  $\Delta T = T - T^*$  is the vector of the difference between wheel torque demanded by the driver  $T_k$  and the ESP torque command  $T_k^*$  (with  $k \in \{1, 2, 3, 4\}$  for front left, front right, rear left and rear right wheel),  $r_{wf}$  and  $r_{wr}$  are front and rear wheel radius, respectively. The two rows composing (5.56) reduce the overall control solution to  $\infty^2$ . One DoF is removed by imposing the application of  $M_{yaw}$ , ensuring a desired lateral behaviour of the vehicle (first row); the second row corresponds to the need for demanding wheel torques in agreement with the driver's purpose, which removes another DoF.

$$L \cdot \Delta T = \begin{bmatrix} -\frac{t_f}{2r_{wf}} & \frac{t_f}{2r_{wf}} & -\frac{t_r}{2r_{wr}} & \frac{t_r}{2r_{wr}} \\ 1 & 1 & 1 & 1 \end{bmatrix} \begin{bmatrix} \Delta T_{fl} \\ \Delta T_{fr} \\ \Delta T_{rl} \\ \Delta T_{rr} \end{bmatrix} = \begin{bmatrix} M_{yaw} \\ 0 \end{bmatrix} \quad (5.56)$$

The *Moore-Penrose pseudoinverse* methodology [38], introduced in section 3.6.1,

is adopted to select the optimal solution among all those are available. The allocation process must also respect actuator constraints.

$$\Delta T = L^+ \cdot \begin{bmatrix} M_{yaw} \\ 0 \end{bmatrix} \tag{5.57}$$

Indeed, (5.57) is solved in 4 sequential  $k$ -steps to compare with the upper and lower torque limit of the reference wheel. A common torque allocation case is the one of Figure 5.23, where a desired counter-clockwise yaw moment is applied to the vehicle body by braking the left wheels and accelerating the right ones. Forces  $F_{xij}$  are calculated from the desired wheel's torques  $T^*$  divided by tire radius.

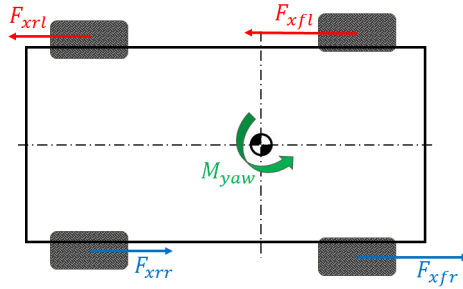


Figure 5.23: Application of corrected steering angle algorithm

This low-level controller is parametrized to be easily applied on different traction architectures. This ensures portability and flexibility of the whole proposed strategy, allowing the application of advanced TV techniques, regardless of vehicle layout. It is important to point out that the longitudinal stability task, i.e. front/rear axle longitudinal effort distribution, anti-slip and anti-spin regulations, rely on dedicated controllers. These are already implemented in the vehicle model. Figure 5.24 show a block diagram of the high-level control layer.

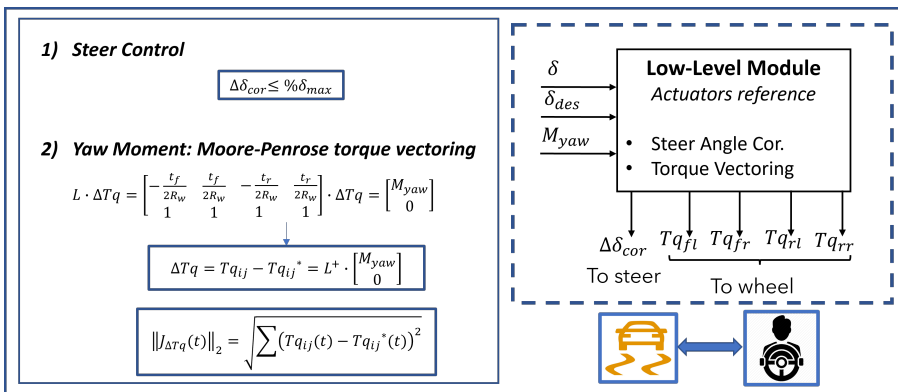


Figure 5.24: Block diagram of the intermediate-level SMC controller

### 5.2.5 SiL Test Campaigns: Tuning of the ESP in Co-simulation

Before the testing phase in the HiL system for the benchmark vehicle with reference commercial ESP, the controllers are firstly implemented in the co-simulation environment between MATLAB and VI-Grade. The *16-DoF vehicle model* used for this SiL tuning campaign and the following HiL implementation refers to a **commercial sports cars**, whose main parameters and specifications can not be given here for non-disclosure reasons. The task which burden on Simulink are the ones related to discrete/logic control operations, i.e. the ESP control algorithm, trajectory path definition and predictive driver model, ESS model, BB controller, optimal EBD strategy. CarRealTime environment, instead, simulate the physical domain aspect, i.e. road-tire interaction, IWM powertrain, suspensions, chassis, aerodynamic and rolling resistances, ABS, TCS and steering system.

Thus, a preliminary test campaign aimed at the tuning of the multiple gains is conducted for the SMC controller. In addition, a recursive optimization algorithm is used to identify the tire cornering stiffness  $C_{yf}$  and  $C_{yr}$  of the vehicle model. These are assumed constant and known for the control objectives calculations, but appear non-linear for the tire modelling approach adopted in VI-Grade [46]. For this stage, a *Step Steer* test is performed. However, there is still the risk the gains are tuned optimally only for these specific test boundary conditions, showing poor performances when the vehicle operates in quite different scenarios for the one considered during the optimization phase. To avoid the tuning process being affected by these problems, multiple functional costs are evaluated. Investigated vehicle states are lateral displacement, lateral acceleration, yaw rate and side-slip angle. This is done to better understand the effect of the controlling techniques on the outcomes of the reference drive test. Different Root Mean Square Error (RMSE) are evaluated according (5.58). In particular, cost function are considered respect to lateral displacement  $J_y(t)$ , lateral acceleration  $J_{a_y}(t)$  and controlled states side-slip  $J_\beta(t)$  and yaw rate  $J_r(t)$ , both supposing full and degraded adherence condition, to assess performances even under poor tire-road friction conditions.

$$J_F(t) = \frac{1}{t} \sqrt{\int_0^t (f(t) - f_{des}(t))^2 dt} \quad (5.58)$$

### 5.2.6 Real-Time Driving Simulator

To test the stability performances allowed by the proposed ESP strategies, the controllers are evaluated in the RT driving simulators of Figure 5.25. HiL test rig allows to understand which impact these solutions introduce, both on vehicle behaviour and driver perception, supposing real driving conditions. Indeed, Human-in-the-Loop validation plays an essential role in the design process of a ESP controller, due to the continuous interaction between driver, vehicle and environment which constitute the closed-loop control elements [281].

The experimental activity has been carried out on the static simulator supplied by *Meccanica 42 srl*, equipped with a steering wheel, brake pedal and throttle pedal as human-interface devices. It is composed of three main parts (Figure 5.26):

- **Real-Time simulator:** consisting of a concurrent-RT machine that manages the simulation environment and the vehicle model. For non-disclosure reasons, the detailed specifications of the benchmark UC cannot be described, which is a real existing car. However, its implemented with stability CU, i.e. EBD, ABS, TCS and commercial ESP solutions. Also, it is assumed that the vehicle's RWD powertrain is actuated by an active differential transmission;
- **EPSiL steering bench:** reproducing the real behaviour of the steering system, including the Electric Power Steering system (EPS) and a steering wheel;
- **Braking unit:** a by-wire system that includes all the components of a real disc brake plant with independent control of each wheel callipers. Also, a virtual sensing regulation loop is considered.

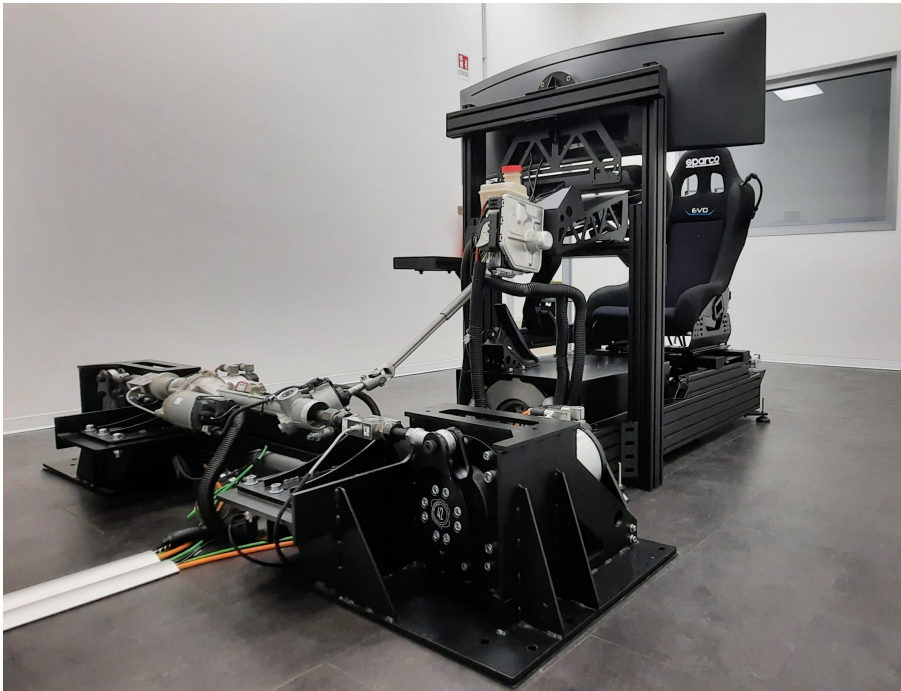


Figure 5.25: Meccanica 42 s.r.l. real-time driving simulator.

### EPSiL steering bench

The EPSiL steering bench integrates a complete steering system, implemented in a HiL driving simulator. Two torque motors and transmissions act directly on the tie-rods of the real steering system by the means of a rocker, accurately reproducing the kinematic movement of the suspensions. With this architecture the rig can reproduce all the forces acting beyond the  $XY$  plane, improving the reliability of the vehicle model by accurately reproducing the actual efforts insisting on the car chassis. The tie-rods, equipped with load cells, rack, EPS, steering column, and steering wheel are integrated into the system.

The described steering layout replicates exactly the commercial solution equipped on the simulated vehicle. The steering bench is included in the simulation loop, enhancing the driving experience and providing the necessary tool for steering virtual development. Indeed, through CAN connection, it is possible to observe the feedback signals and tune the parameters of the EPS parameters to calibrate the system, while the driver can assess the effect of each modification on multiple testing conditions. The unit proved itself capable of accurately reproducing real vehicle tie-rod forces, resulting in an efficient and reliable steering feeling.

## Braking Unit

A commercially available brake-by-wire system, known as **MKC1** produced by Continental GmbH, has been implemented on the simulation rig. The installation layout is described in Figure 5.26. The stock brake plant is mounted on the simulator. It includes the brake tubes (with the correct diameter and length), which are connected to the electro-mechanical units of 4 independent stock brake callipers, acting on the original brake discs. The brake pedal is directly integrated into the unit, and it constitutes the main braking unit driver-machine interface device.

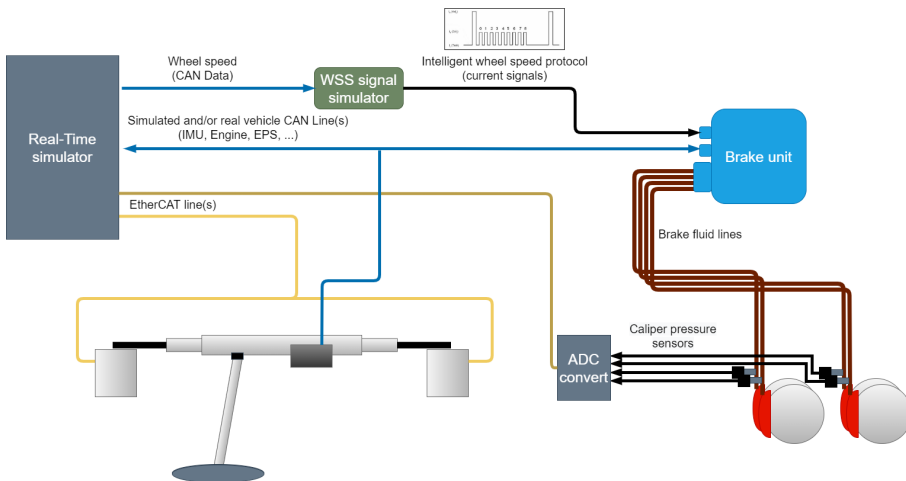


Figure 5.26: Static simulator setup

The brake unit communicates through the communication lines using a Controller Area Network (CAN) protocol, receiving all the signals that are usually exchanged on real vehicles, simulated by the model on the RT computer. In addition, this unit needs intelligent wheel speed signals via a direct communication line. For this reason, virtual wheel speed sensors have been implemented, which convert the wheel speeds (received via CAN from the RT machine) to the typical signal type provided by intelligent wheel speed sensors [284].

Finally, 4 pressure sensors have been installed on the callipers and their signals are sent back to the vehicle model via an EtherCAT measurement line to close the loop, which controls the vehicle deceleration after a brake demand from the driver.

The unit functionalities have been extensively tested to compare response and behaviour on the static simulator for a real vehicle. Results prove its effectiveness on a previously validated vehicle model.

### 5.2.7 HiL Test Campaigns: Performance Evaluations in the Driving Simulator

In this phase, a driver replicates some reference cornering test, using the above-described RT driving simulator through the HiL interface system and exploiting the same control rig of the previous scenario (ESP in *MATLAB Simulink* and 16-DoF vehicle model in the *VI-Grade*). To assure reliable comparative metrics, reference closed-loop manoeuvres are repeated supposing three scenarios, in which the vehicle model is alternatively implemented with the controlling techniques:

**Controlled Scenario:** in this case, the vehicle is driven without the assistance of any kind of lateral stability controller. Thus, it was possible to establish inner vehicle manoeuvrability and test the driver's capabilities. Many free driving tests are conducted to identify the limit of controllability.

**Commercial-Controlled Scenario:** tests are conducted with the *Continental GmbH* proprietary ESP controller. The strategy, from our side, is completely unknown. However, we can make some assumptions, supposing the control technique is advanced and represent the SoA of the industrial ESP solutions, which are implemented on different vehicles in the market.

**SMC-Controlled Scenario:** here the *Sliding Mode Lateral Stability Controller* is investigated. It acts both on wheel torque distribution and active steering.

The reference manoeuvres are repeated many times, selecting as results the ones which appear more comparable. Indeed, to ensure reliable comparative metrics it's fundamental to reproduce the close-loop test as similar as possible. Selected cornering tests are summarized in Table 5.3.

Table 5.3: Investigated reference manoeuvres

Name	Standard	Purpose
<i>Ramp Steer</i>	FMVSS No.126 & ISO 19364:2016	Calibration
<i>Step Steer</i>	ISO 7401:2003	Calibration & Validation
<i>Sine Steer</i>	ISO 7401:2003	Validation
<i>Lane-Change</i>	ISO 3888-1:2018	Validation

However, boundary conditions specified by the related standards are modified to guarantee more severe conditions, in terms of stability performances. This is useful to highlight the results [190]. Indeed, due to the excellent handling capabilities of the vehicle model, using the reference operative scenario produce no unstable behaviour, making it difficult to assess the improvements related to the investigated controllers. The main contributions of ESP systems concern the stabilization of vehicle trajectory and desired driving path when NL behaviour onset.

To ensure an easy understanding of the results, output plots are presented for the SMC-based lateral controller, compared with Non-controlled and Commercial-controlled scenarios.

### Open-loop Test: FMVSS126 Ramp Steer

The *SIS* test is used here to observe the linear behaviour between steering angle and the lateral response of the vehicle in the different controlling situations. The vehicle is driven at  $120\text{km/h}$  with a steering angle linearly increased from  $0\text{deg}$  to  $270\text{deg}$ . Even in this case the test is conducted for right and left cornering directions. Following standard FMVSS 126, this manoeuvre is adopted to characterize the lateral dynamics of the vehicle in the different controlling scenarios. The ratio of applied steering angle is as slow as to assure steady-state behaviour, avoiding abrupt deviation in the manoeuvre until stability margin is reached, e.g. manifest of wheel side slipping, non-linear and undesired behave. The SIS test is useful to establish the upper and lower limit of controlling intervention, regarding actuators systems.

### Open-loop Test: ISO7401 Step Steer

Inspired by the ISO 7401:2003 standard, a *Step Input* test is performed in both directions: left and right turning. For the reference manoeuvres, this one is carried out in closed-loop conditions with the initial longitudinal speed of  $150\text{km/h}$  and wheel steering angle of  $90\text{deg}$ . It is worth nothing to say that this lateral test exhibits a ramp steering command. Indeed, a human driver can't apply an instantaneous angle to the steering wheel [283]. However, the steering rate is high enough to produce a rapid cornering manoeuvre, letting us investigate the vehicle's fast transient behaviour.

Results of Figure 5.27 clearly show that the controller succeeds in tracking yaw rate and side-slip angle if compared to a Non-controlled and Commercial-controlled scenario. Controlled state errors are reduced for the SMC solution, thanks to the application of optimal control efforts of Figure 5.28. It is inserted to highlight that both proposed controllers apply different torque vectoring efforts for the benchmark ESC. In the first stage (at about  $1.5\text{s}$ ) both the stability systems perform quite similar, although the SMC solution shows higher control actions. In the steady-state phase of the manoeuvre, indeed, the sliding controller actuates the wheels on the opposite side for a Commercial-controlled scenario. This is since the developed solutions aim at the control of side-slip angle, in addition to yaw rate, which typically is the sole control objective of wide diffused ESC in the market. Figure 5.29 shows the vehicle's lateral acceleration and longitudinal speed for the simulated scenarios. For SMC-controlled vehicles, speed is maintained high as in the non-controlled vehicle, due to the Moore-Penrose TV solution.

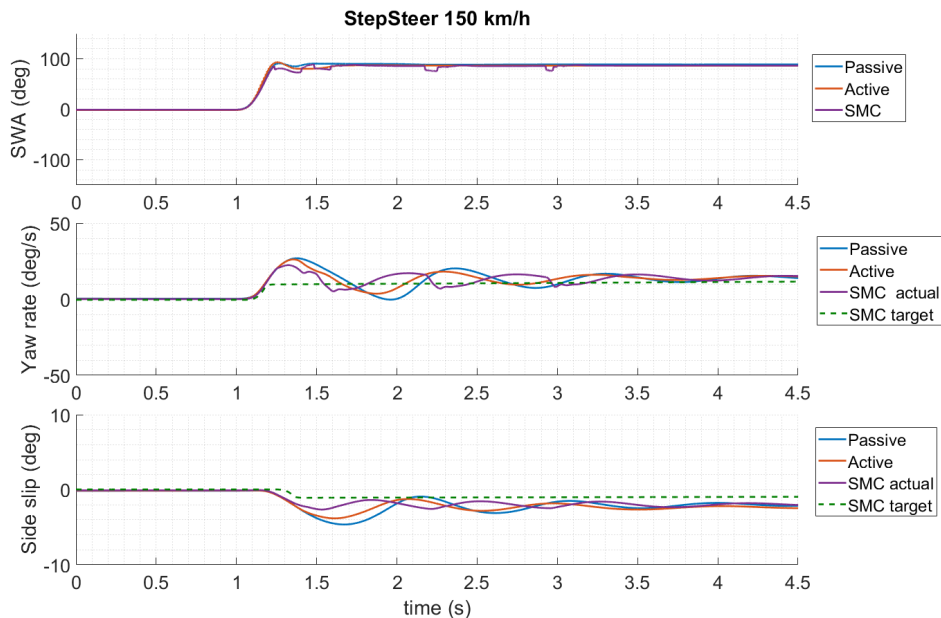


Figure 5.27: States tracking performances in a *Step Steer* manoeuvre at 150km/h and with 90deg steering wheel angle in case of Non-controlled (Passive), Commercial-controlled (Active) and SMC-controlled scenarios

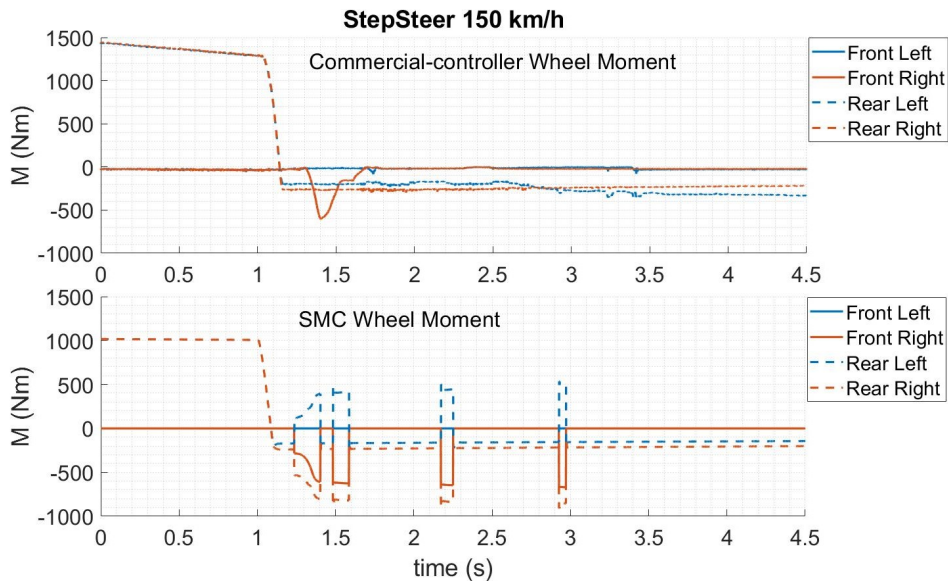


Figure 5.28: Wheel torques in a *Step Steer* manoeuvre at 150km/h and with 90deg steering wheel angle in case of Non-controlled (Passive), Commercial-controlled (Active) and SMC-controlled scenarios



Figure 5.29: Vehicle lateral acceleration and longitudinal speed in a *Step Steer* manoeuvre at  $150\text{km/h}$  and with  $90\text{deg}$  steering wheel angle in case of Commercial-controlled (Active) and SMC-controlled scenarios

### Open-loop Test: ISO7401 Sine Steer

A sine path wave of  $90\text{deg}$  on the steering wheel is realized by the driver while travelling at  $150\text{km/h}$ , to evaluate the responsiveness of the controlling techniques during this test. These manoeuvres allow us to investigate the correctness of implemented dead-zone on the state's errors since both yaw rate and side-slip consecutively cross 0 values. In the top plot of Figure 5.30, the steering angle imposed by the driver is visible for the different scenarios. For the SMC-Controlled solutions, the impact of the steering correction control technique is shown.

Even in this case, the proposed controller performs quite well for the task of tracking the controlled states. In Non-controlled solutions vehicle is unstable, while for the SMC scenario both vehicle yaw rate and side-slip angle are controlled by active torque distributions effort of Figure 5.31, exhibiting improved stability performances even for the Commercial-controlled scenario. As for *Step Steer* test, SMC control actions show higher control effort values respect to reference ESP controller. This leads to improved tracking performances of the controlled states, especially for the side-slip angle, achieving a higher safety margin. Acceleration in the lateral direction  $a_y$  and driving speed  $V_x$  of the vehicle during this test are visible in Figure 5.32. Even in this case, longitudinal speed is maintained higher.

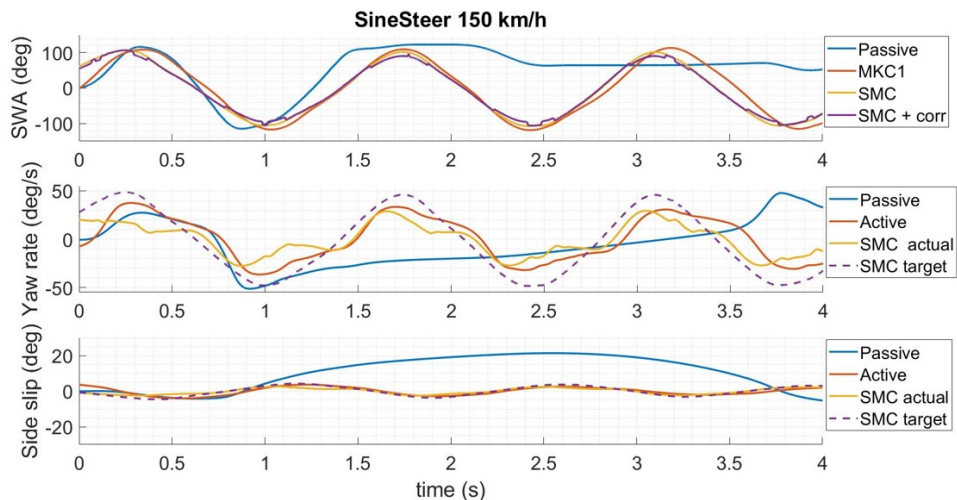


Figure 5.30: States tracking performances in a *Sine Steer* manoeuvre at  $150\text{km/h}$  and with  $90\text{deg}$  steering wheel angle in case of Non-controlled (Passive), Commercial-controlled (Active) and SMC-controlled scenarios

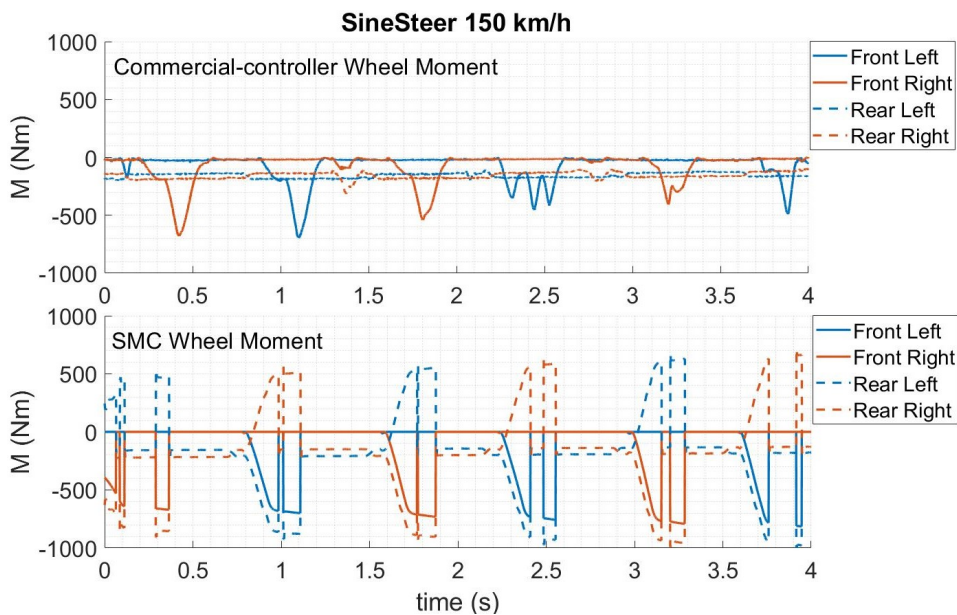


Figure 5.31: Wheel torques in a *Sine Steer* manoeuvre at  $150\text{km/h}$  and with  $90\text{deg}$  steering wheel angle in case of Commercial-controlled (Active) and SMC-controlled scenarios

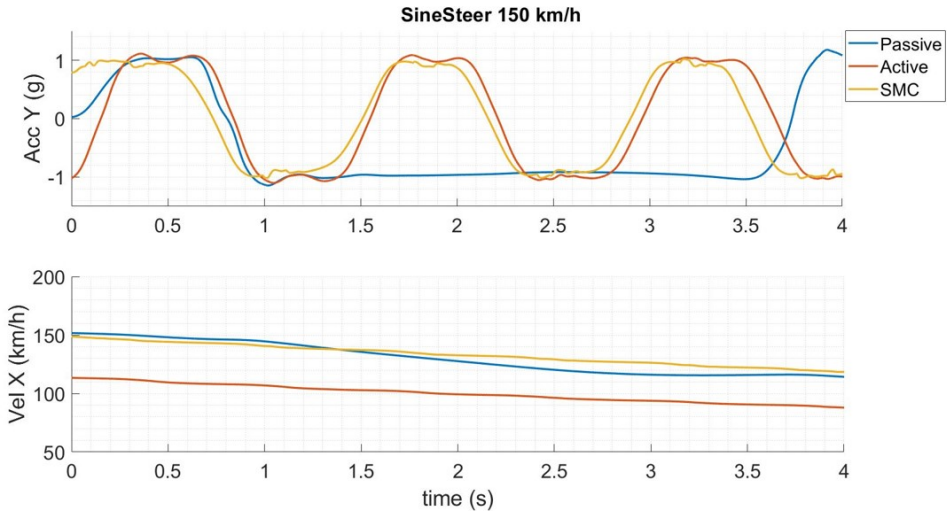


Figure 5.32: Vehicle lateral acceleration and longitudinal speed in a *Sine Steer* manoeuvre at  $150\text{km/h}$  and with  $90\text{deg}$  steering wheel angle in case of Non-controlled (Passive), Commercial-controlled (Active) and SMC-controlled scenarios

### Closed-loop Test: Single-Lane Change

A single Lane-Change manoeuvre test is conducted to subjectively determine vehicle stability aspects. For previous tests, this is the only one that is specified as closed-loop by the reference standard (ISO 3888). The vehicle is driven at  $150\text{km/h}$  and a steering path is imposed by the pilot to obtain a lateral displacement of about  $3\text{m}$ . Subsequently, another steer command is applied to re-orient the car in the longitudinal direction. Figure 5.33 shows the driving path performed by the vehicle during the manoeuvre and the vehicle's longitudinal speed. Yaw rates and side-slip angles are visible in Figure 5.34. The plot of the torques control efforts is the one in Figure 5.35.

It is interesting to note that the uncontrolled vehicle's trajectory exhibits a slight overshoot in the lateral displacement for the centre-line, with the reduced speed for other scenarios. SMC, indeed, tracks desired trajectory with a smoother behaviour. This is since sliding control adopts a PI criterion with fixed dead zones, reducing the control effort when approaching target states. For what concerns the speed, the sliding mode solution allows to perform the reference manoeuvre in accordance with the driver's intention, maintaining the entrance longitudinal speed by the exploitation of the traction forces of the powertrain.

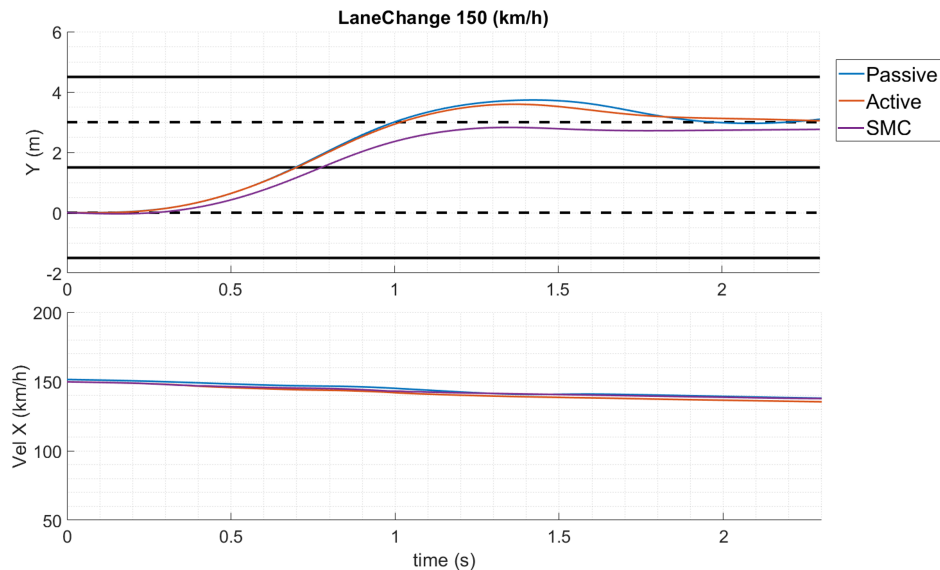


Figure 5.33: Trajectories and longitudinal speeds in a *Lane Change* manoeuvre at 150km/h and a lateral displacement of about 3m in case of Non-controlled vehicle (Passive), Commercial-controlled vehicle (Active) and SMC controlled

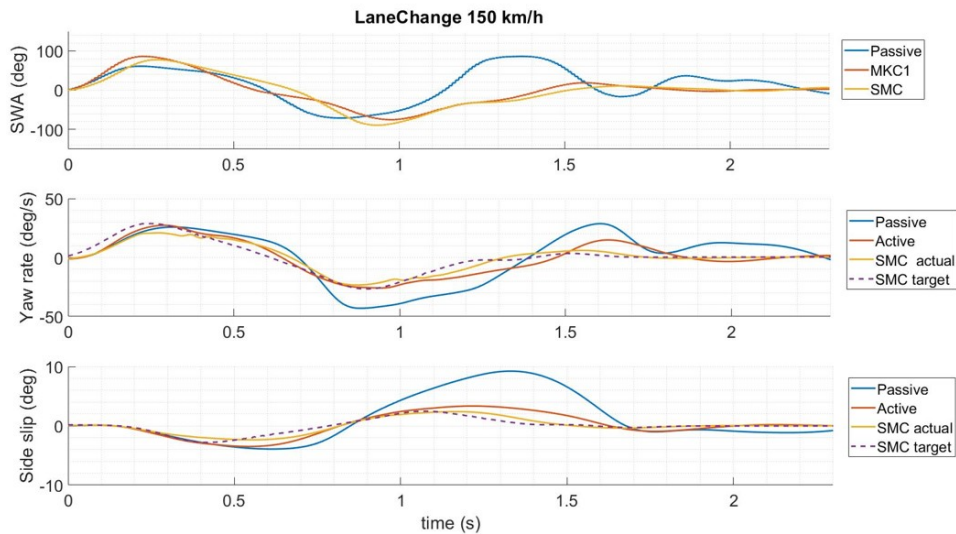


Figure 5.34: States tracking performances in a *Lane Change* manoeuvre at 150km/h and a lateral displacement of about 3m in case of Non-controlled vehicle (Passive), Commercial-controlled vehicle (Active) and SMC controlled

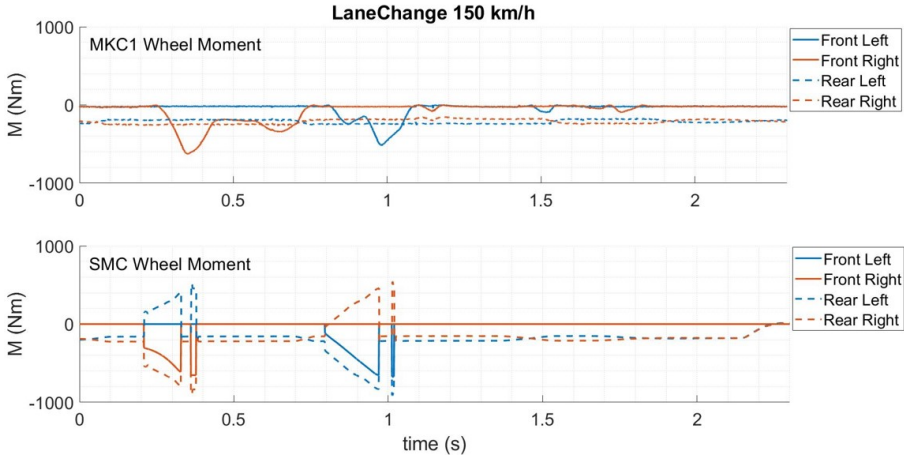


Figure 5.35: Wheel torques in a Lane Change manoeuvre at 150km/h and a lateral displacement of about 3m in case of Commercial-controlled vehicle (Active) and SMC controlled

### 5.2.8 SiL Test Campaign: ESP Validation and Optimization in Co-simulation

This final validation has been implemented on the co-simulation environment of Simulink and VI-CarRealTime on the **FIAT 500e 16-DoF vehicle model**. To further improve the tracking performances of the SMC-based ESP, for yaw rate and side-slip angle, the gain of the TV action has been scheduled for the vehicle’s longitudinal speed. In the first implementation, this gain has been applied to the optimal yaw moment  $k_{yaw}M_{yaw}$  calculated by (5.50) as a fixed value. Instead, here has been tabled with the velocity using a recursive optimization algorithm, which varies its value to minimize a functional cost. The cost function is a weighted linear combination of the normalized RMSE of yaw rate  $r$ , side-slip angle  $\beta$ , lateral acceleration  $a_y$  and lateral displacement  $y$ , according to (5.59), where  $p_r, p_\beta, p_{a_y}$  and  $p_y$  are the corresponding weight. The points found with this process have been approximated using a polynomial curve (Figure 5.36).

$$k_{yaw} = k \{ J_{global} = p_r J_r + p_\beta J_\beta + p_{a_y} J_{a_y} + p_y J_y \}_{min} \tag{5.59}$$

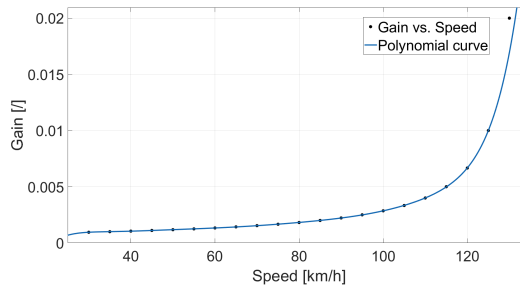


Figure 5.36: Gain scheduling of the yaw moment respect to vehicle speed

### Open-loop Test: FMVSS126 Ramp Steer

Before proceeding with the test validation, it is interesting to observe the plot of Figure 5.37. A ramp command is imposed on the steering wheel to observe the understeer characteristic of the vehicle at  $70\text{km/h}$ , comparing non-controlled and coordinated controlled scenarios. An additional test is performed when both dead-zones on yaw rate and side-slip angle are disabled (Figure 5.21), resulting in the controller starting its intervention from the beginning of the manoeuvre, and not when NL lateral dynamic behaviour occur (at about  $6\text{m/s}^2$  lateral acceleration). As can be seen, the SMC-based ESP controller extends the linear region of the vehicle steering response, allowing also a greater lateral acceleration (from  $7.94\text{m/s}^2$  to  $8.20\text{m/s}^2$ ). In addition, the steering responsiveness is further improved when no dead zones are used and continuous active ESP is used. Indeed, a lower understeer gradient  $K_V$ , which represents the slope of the curve in the linear region, results in a more reactive vehicle, since is closer to a neutral behaviour [22].

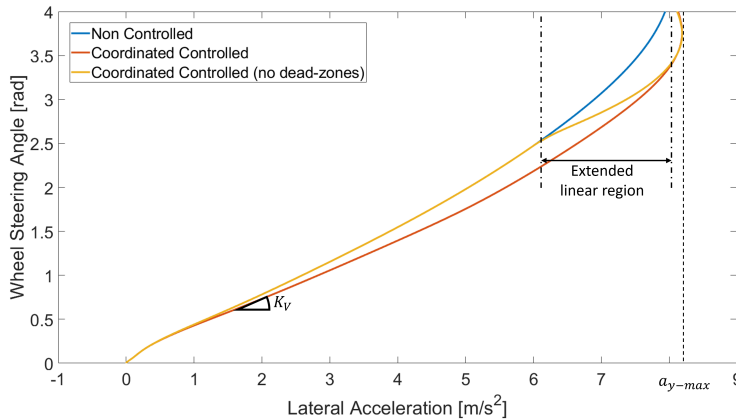


Figure 5.37: Vehicle understeering characteristic for ramp steer command at  $70\text{km/h}$

In this context, the phase plane  $\beta - \dot{\beta}$  according to the  $\beta$  method is plotted. As can be seen in Figure 5.38, when adopting a continuous active control technique higher stability margins are achieved.

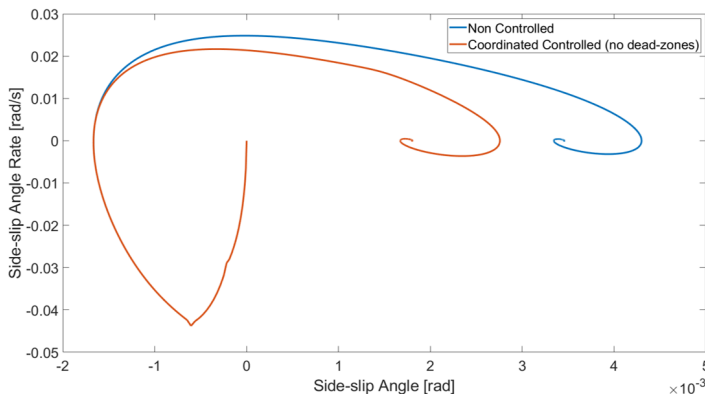


Figure 5.38:  $\beta - \dot{\beta}$  method phase plane plot for ramp steer command at  $70\text{km/h}$

### Open-Loop Test: ISO4148 Constant Steering Wheel Angle

Figure 5.39 shows the results related to the test performed at  $120km/h$ , with and without active ESP control, respectively. The stationary conditions are reached after about  $5s$  from the start of the test.

The steering angle is increased in the test with ESP, due to the effect of the corrective steering action carried out by the proposed logic. The value that most confirms the effectiveness of the SMC lateral stability control is the minimum radius of curvature in steady-state conditions, thanks to the combined intervention of torque vectoring and steering angle correction. When observing  $\beta$  vs  $a_y$ , steady condition are reached when ESP is activated. In addition, both side-slip angle and yaw rate peaks are reduced, as compared to non-controlled vehicles.

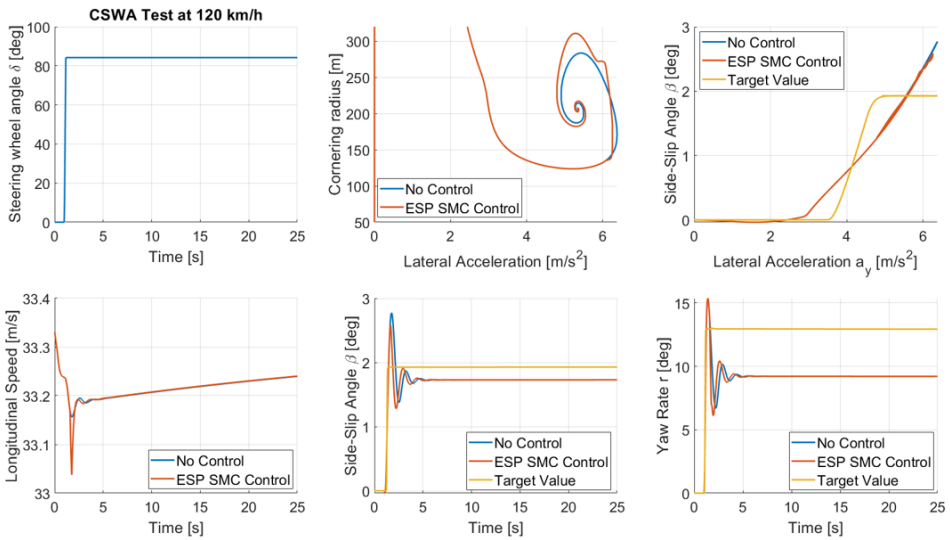


Figure 5.39: Results of the constant steering wheel angle test at  $120km/h$ , supposing availability and unavailability of the ESC control system

### Open-loop Test: ISO7401 Sine Steer

A sinusoidal input test at  $100km/h$  is performed. To reach a lateral acceleration of  $6m/s^2$  for  $0.5Hz$  and  $1Hz$  sinusoidal steering command frequencies, a steering amplitude of  $1.85rad$  and  $2.7rad$  is applied respectively. Figure 5.40 resume the result of the  $0.5Hz$  test in the time domain, while tracked states respect to lateral acceleration are visible in Figure 5.41. Similarly, Figure 5.42 and Figure 5.43 show the same results for the  $1Hz$  sinusoidal steering angle input frequency. Results highlight the superior tracking performance of the SMC ESP control strategy for the controlled states. Finally, Table 5.4 summarizes the time delay between the peaks of lateral acceleration and yaw rate for the steering angle. Corresponding lateral acceleration and yaw rate gains referred to the amplitude steering command are computed. These are reduced, thanks to the implemented lateral stability controller. Output data highlight how the vehicle steering responsiveness is improved for both the input signal peaks.

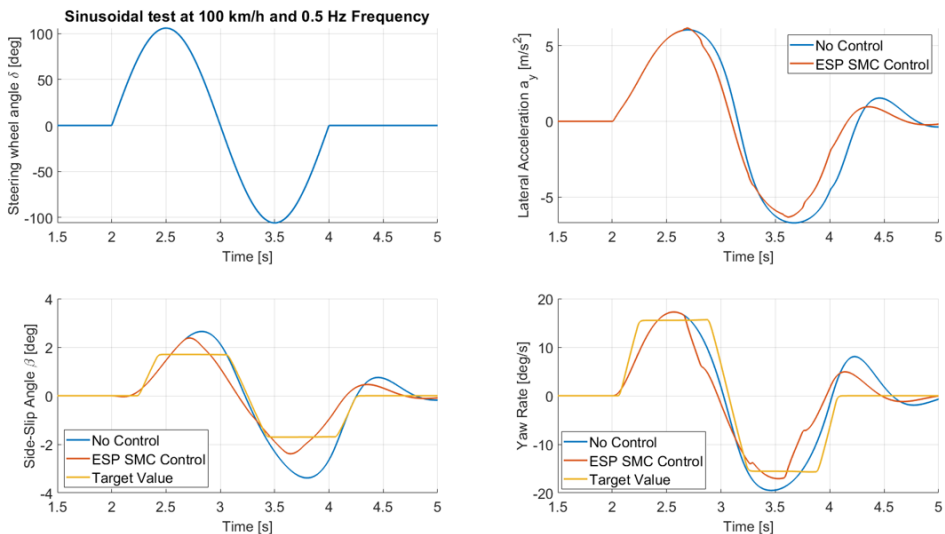


Figure 5.40: Results of the constant steering wheel angle test at  $120km/h$ , supposing availability and unavailability of the ESC

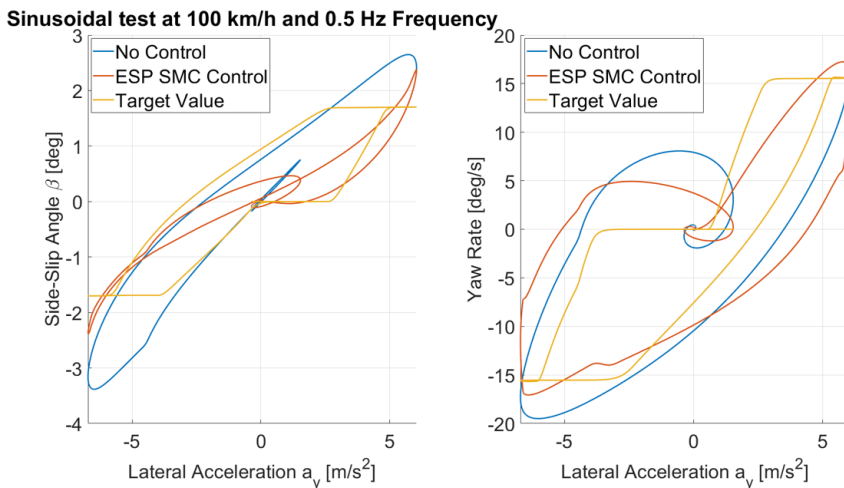


Figure 5.41: Results of the constant steering wheel angle test at  $120km/h$ , supposing availability and unavailability of the ESC

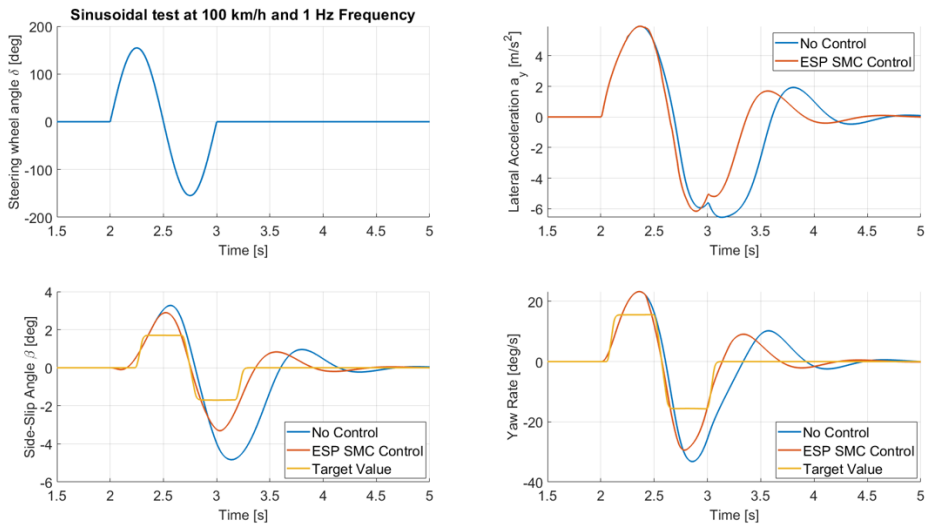


Figure 5.42: Results of the constant steering wheel angle test at  $120km/h$ , supposing availability and unavailability of the ESC

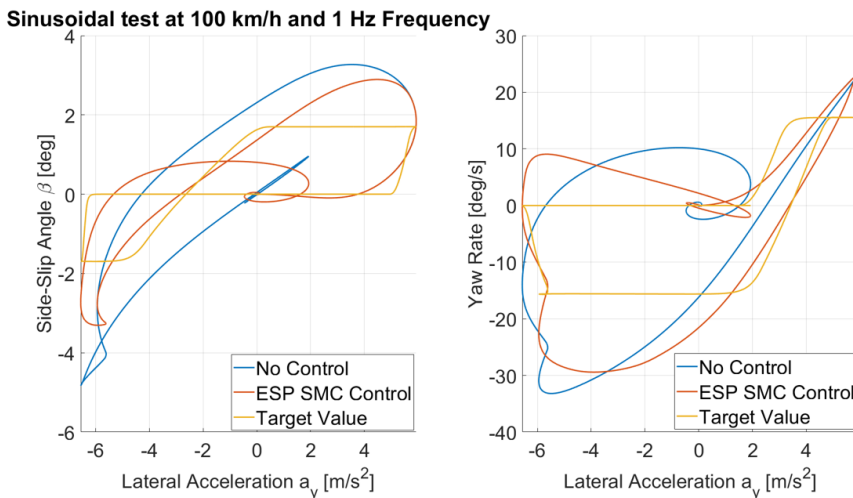


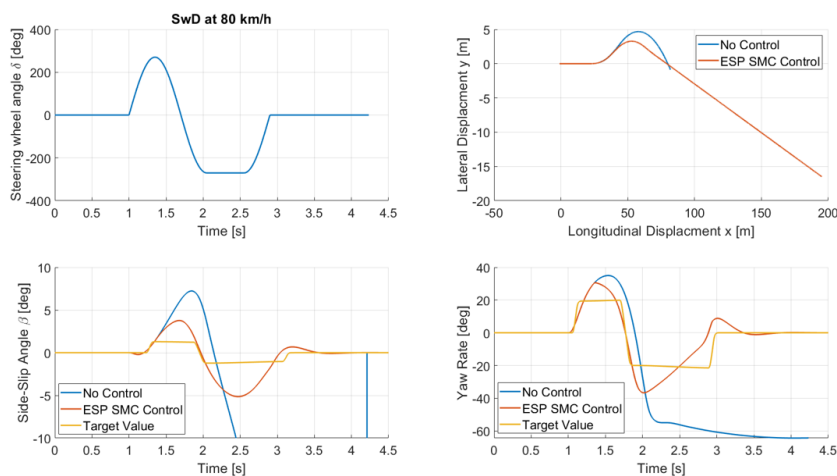
Figure 5.43: Results of the constant steering wheel angle test at  $120km/h$ , supposing availability and unavailability of the ESC

### Open-loop Test: FMVSS126 Sine with Dwell Test

The SwD test is particularly interesting to show the effectiveness of the stabilizing action of the control. In fact, without its support, the test is not passed and the vehicle undergoes a total loss of control at the second steering peak (Figure 5.44). In the presence of stabilizing corrections, it was possible to pass the test at a  $300deg$  steering angle: the yaw rate values are kept within the limits imposed by the ideal model by the ESP control which, acting on TV, ensure optimal control. Torque control efforts are visible in Figure 5.45.

Table 5.4: Time response data summary of the Sinusoidal Input test

<i>Parameter</i>	<i>ESP</i>	<i>0.5 Hz</i>	<i>1 Hz</i>
<b>Time lag between steering-wheel angle and lateral acceleration [s]</b>			
First peak $T_{(\delta_H - a_y)_1}$	ON	-0.19	-0.12
	OFF	-0.22	-0.12
Second peak $T_{(\delta_H - a_y)_2}$	ON	-0.12	-0.14
	OFF	-0.17	-0.40
<b>Time lags between steering-wheel angle and yaw rate [s]</b>			
First peak $T_{(\delta_H - r)_1}$	ON	-0.05	-0.10
	OFF	-0.05	-0.10
Second peak $T_{(\delta_H - r)_2}$	ON	-0.02	-0.03
	OFF	0.05	-0.10
<b>Lateral acceleration gain</b>			
Absolute peak $ \frac{a_y}{\delta_H} $	ON	3.41	2.28
	OFF	3.62	2.42
<b>Yaw rate gain</b>			
Absolute peak $ \frac{r}{\delta_H} $	ON	0.16	0.19
	OFF	0.18	0.21

Figure 5.44: Results of the SwD test at  $80\text{km/h}$ , supposing availability and unavailability of the ESC

### Closed-loop Test: ISO3888-1 - Double-Lane Change

As suggested by the standard, the DLC test has been conducted at increasing speed, to establish the top velocity at which the vehicle can correctly perform the track, without leaving the admitted path. Figure 5.46 refers to a  $90\text{km/h}$  test with nominal friction condition with the road when the 4WD e-car is driven by the predictive driver model. This speed is the one at which the vehicle began to experience lateral instability behaviour. The same test conditions are replicated with ESP activated.

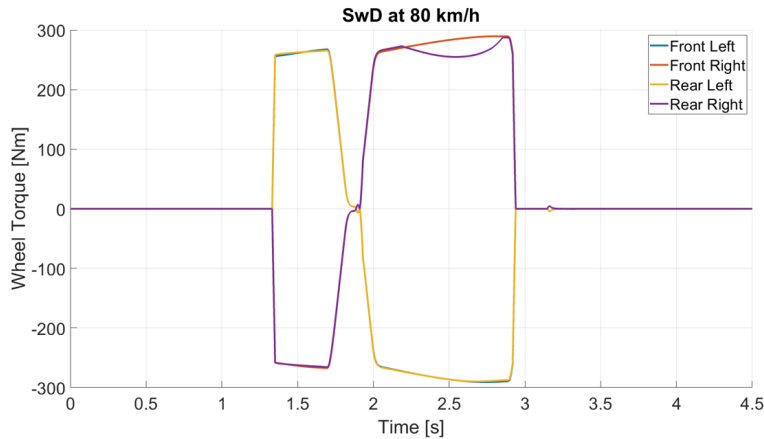


Figure 5.45: Torque control efforts of the ESP SMC control during the Sine with Dwell test at  $80\text{km/h}$ , supposing availability and unavailability of the ESC

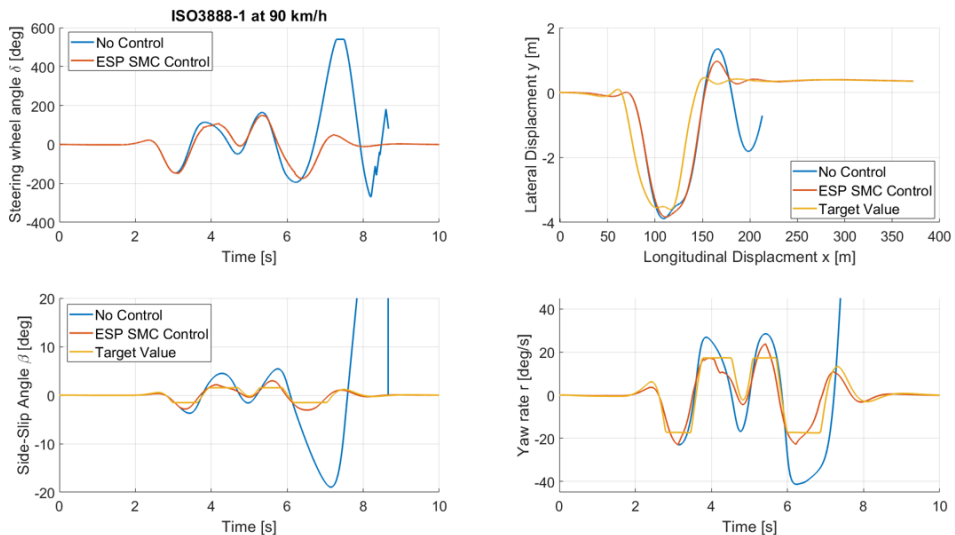


Figure 5.46: Results of the DLC test at  $90\text{km/h}$  and  $\mu = 1$ , supposing availability and unavailability of the ESC

The effectiveness of the proposed ESP can be seen by comparing these outputs. The lateral stability control intervenes to stabilize the vehicle by applying the TV efforts, as visible in the plot of Figure 5.47. Here, the direct yaw rate and side-slip angle control are efficient and can ensure higher tracking of the desired states, allowing the test is passed. Otherwise, when the control algorithm is disabled, the vehicle is unable to perform the DLC manoeuvre, leaving the admitted zone and hitting the cones while spinning away. The performed trajectories are reported in Figure 5.48, for both the scenarios in which the controller is disabled and enabled.

The controller ensures the correct execution of this test even at  $95\text{km/h}$  (top speed), whose results are the one in Figure 5.49.

The following Table 5.5 show the comparative results for different vehicle speed and friction values, in terms of RMSE respect to yaw rate  $r$ , side-slip angle  $\beta$  and lateral displacement  $y$  with the corresponding references, according to (5.58). The more these values are close to 0, the more the test is satisfied. It can be seen that until  $85\text{km/h}$  ESP intervene only for low friction conditions. For this speed, the controller is fundamental to reduce the RMSEs and pass the tests.

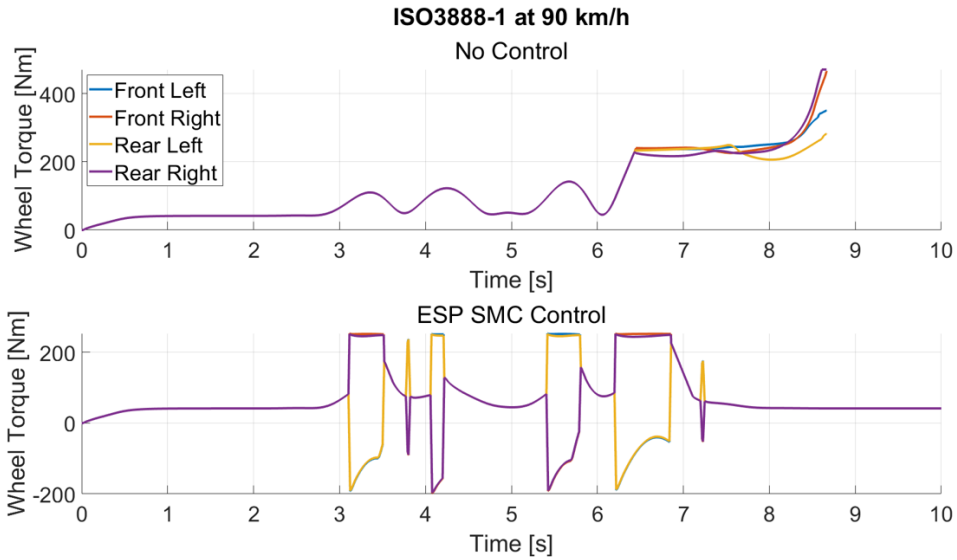


Figure 5.47: Torque control efforts during the DLC test at  $90\text{ km/h}$  and  $\mu = 1$ , supposing availability and unavailability of the ESC

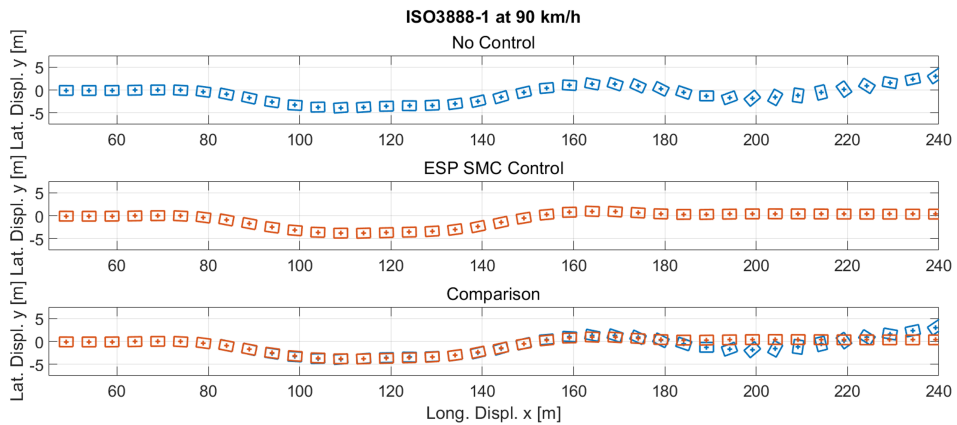


Figure 5.48: Comparison of the trajectories during the DLC test at  $90\text{ km/h}$  and  $\mu = 1$ , supposing availability and unavailability of the ESC

Table 5.5: ISO3888-1 DLC test RMSE results at different speed and friction values

<i>Adherence</i>	<i>ESP</i>	$J_r$	$J_\beta$	$J_y$	<i>Test</i>
<b>Initial speed: 75 km/h</b>					
$\mu = 0.5$	OFF	0.3283	0.0774	2.2795	pass
	ON	0.3464	0.0130	2.25393	pass
$\mu = 0.8$	OFF	0.3831	0.0110	2.3167	pass
	ON	0.3935	0.0103	2.3176	pass
$\mu = 1$	OFF	0.3536	0.0093	2.2831	pass
	ON	0.3536	0.0093	2.2831	pass
<b>Initial speed: 80 km/h</b>					
$\mu = 0.5$	OFF	/	/	/	fail
	ON	0.3563	0.0185	2.6789	pass
$\mu = 0.8$	OFF	0.1771	0.0283	2.2778	pass
	ON	0.2477	0.0137	2.2894	pass
$\mu = 1$	OFF	0.1963	0.0162	2.2264	pass
	ON	0.2353	0.0132	2.2383	pass
<b>Initial speed: 85 km/h</b>					
$\mu = 0.5$	OFF	/	/	/	fail
	ON	0.4211	0.0309	3.4422	pass
$\mu = 0.8$	OFF	/	/	/	fail
	ON	0.2230	0.0198	2.2721	pass
$\mu = 1$	OFF	0.1543	0.0409	2.1952	pass
	ON	0.2188	0.0182	2.2060	pass
<b>Initial speed: 90 km/h</b>					
$\mu = 0.5$	OFF	/	/	/	fail
	ON	0.4560	0.0421	4.3228	fail
$\mu = 0.8$	OFF	/	/	/	fail
	ON	0.2238	0.0290	2.2644	pass
$\mu = 1$	OFF	/	/	/	fail
	ON	0.2182	0.0289	2.1790	pass
<b>Initial speed: 95 km/h</b>					
$\mu = 0.5$	OFF	/	/	/	fail
	ON	0.4576	0.0463	5.0201	fail
$\mu = 0.8$	OFF	/	/	/	fail
	ON	0.2659	0.0548	2.3069	pass
$\mu = 1$	OFF	/	/	/	fail
	ON	0.2590	0.0621	2.1961	fail
<b>Initial speed: 100 km/h</b>					
$\mu = 0.5$	OFF	/	/	/	fail
	ON	0.4758	0.0530	5.8224	fail
$\mu = 0.8$	OFF	/	/	/	fail
	ON	0.3099	0.0734	2.3491	fail
$\mu = 1$	OFF	/	/	/	fail
	ON	0.2845	0.0694	2.3012	fail

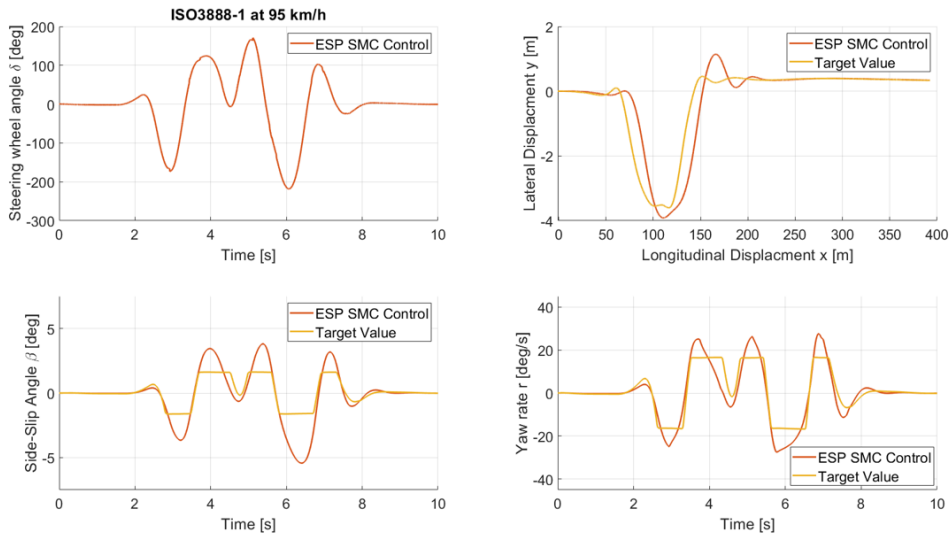


Figure 5.49: Results of the DLC test at  $95\text{km/h}$  and  $\mu = 1$  with SMC ESP

### Closed-loop Test: ISO3888-2 - Obstacle Avoidance

The ISO3888-2 test immediately appears more demanding, both concerning the stability and the modelling of low adherence conditions. Even at lower speeds, the car without an ESP system was unable to complete the test, not only hitting the cones but also losing general controllability. Figure 5.50 shows that at a speed of  $70\text{km/h}$  the car became completely unstable after the first corner and finds itself in an uncontrolled skid condition. Instead, when the ESP control is ON, the stability conditions significantly improve. Figure 5.50, Figure 5.51 and Figure 5.52 show the results for  $70\text{km/h}$ ,  $77\text{km/h}$  and  $80\text{km/h}$  vehicle speed, respectively. In Figure 5.53 the torque interventions are visible: the inner wheels are braked while the outer ones are accelerated. Yaw rate and side-slip angles are actively controlled to be as close as possible to the references. However, the manoeuvre is very severe, especially in the second turn. Thus, for high speed, the test is failed (Table 5.6). The driving path performed by the benchmark EV during the tests is the one of Figure 5.54.

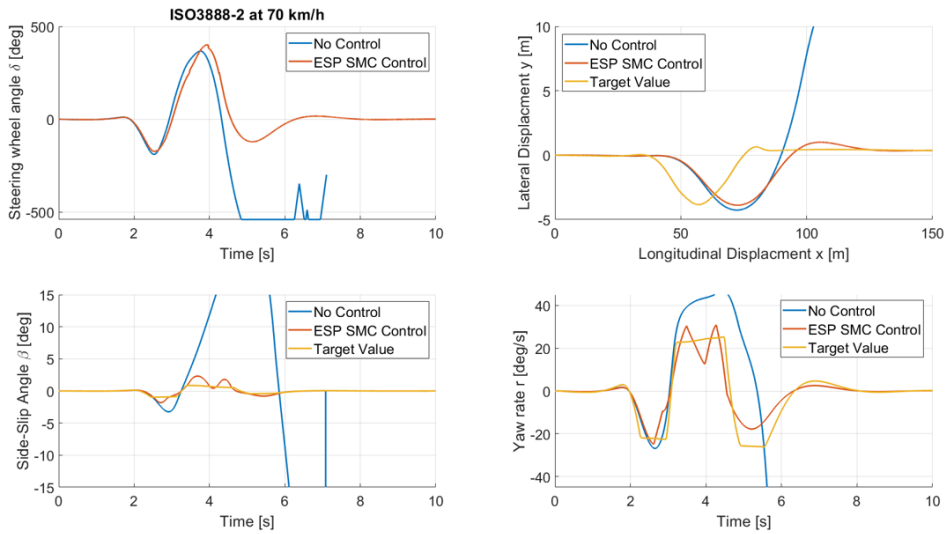


Figure 5.50: Results of the obstacle avoidance test at  $70\text{km}/h$  and  $\mu = 1$ , supposing availability and unavailability of the ESC

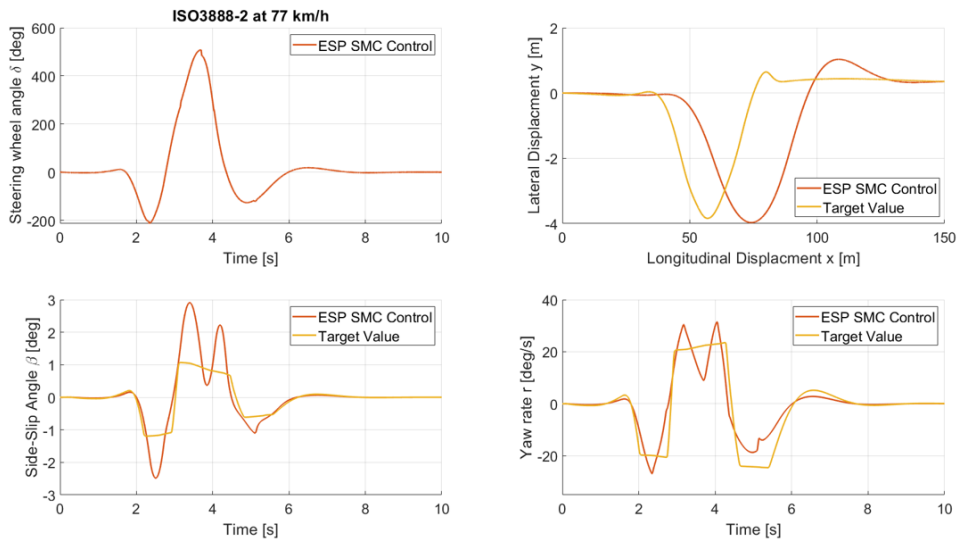


Figure 5.51: Results of the obstacle avoidance test at  $77\text{km}/h$  and  $\mu = 1$ , supposing availability and unavailability of the ESC

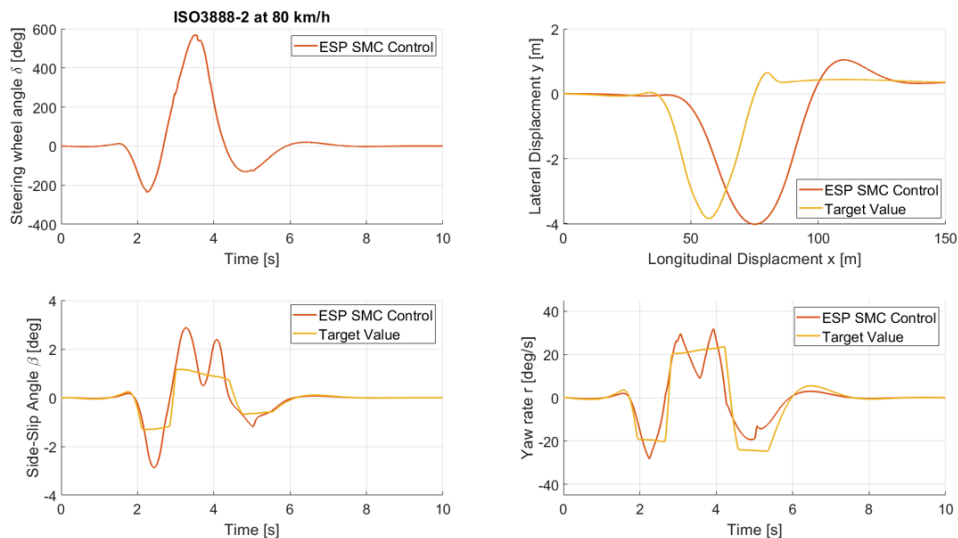


Figure 5.52: Results of the obstacle avoidance test at  $80\text{km/h}$  and  $\mu = 1$ , supposing availability and unavailability of the ESC

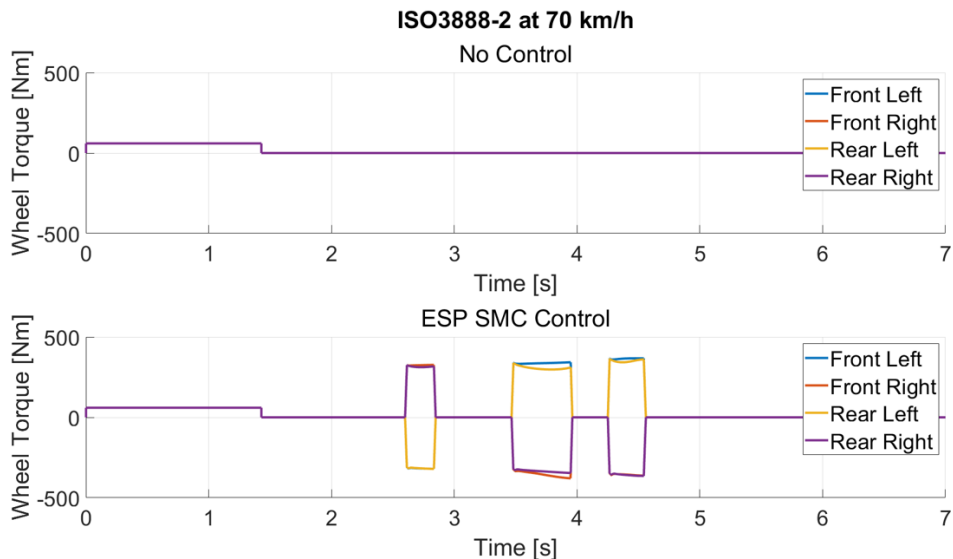


Figure 5.53: Torque control efforts during the obstacle avoidance test at  $70\text{km/h}$  and  $\mu = 1$ , supposing availability and unavailability of the ESC

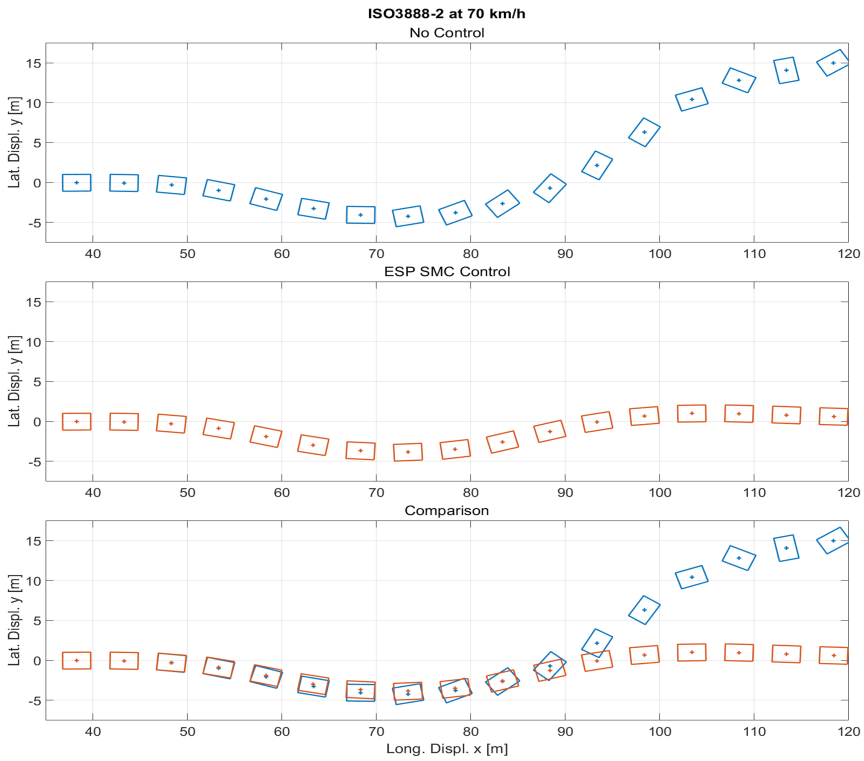


Figure 5.54: Comparison of the trajectories during the obstacle avoidance test at  $70\text{km/h}$  and  $\mu = 1$ , supposing availability and unavailability of the ESC

Table 5.6: ISO3888-2 obstacle avoidance test RMSE results at different speed

<i>ESP</i>	$J_r$	$J_\beta$	$J_y$	<i>Test</i>
<b>Initial speed: 70 km/h</b>				
OFF	1.8194	1.1224	14.5372	fail
ON	0.2729	0.0195	4.1566	pass
<b>Initial speed: 73 km/h</b>				
OFF	/	/	/	fail
ON	0.3409	0.0292	4.2813	pass
<b>Initial speed: 75 km/h</b>				
OFF	/	/	/	fail
ON	0.2767	0.0249	4.3168	pass
<b>Initial speed: 77 km/h</b>				
OFF	/	/	/	fail
ON	0.2815	0.0265	4.3865	pass
<b>Initial speed: 80 km/h</b>				
OFF	/	/	/	fail
ON	0.2886	0.0274	4.5203	pass

### 5.2.9 Conclusions and Future Developments

The proposed SMC-based control algorithm aim at the direct regulation of the vehicle's yaw rate and side-slip angle to achieve stability improvements for the conventional solution, based on solely yaw rate tracking. It has been developed respecting important features to ensure flexibility and portability of the strategy for quite different powertrain architectures. Its simple implementation relies on a limited set of parameters. The best performance of this controller can be obtained by considering independent electric hub-motors for 4WD vehicles, which guarantee a higher applicable yaw momentum thanks to the easiness of 4-quadrant torque control, enabling the exploiting of traction forces. In addition, the 2-dimension sliding surface formulation enables the option to apply even steer angle corrections.

In these activities, the evaluation of the SMC-based lateral stability controller is performed. The simulation campaign consists of different validation activities.

A SiL co-simulation approach between Simulink and CarRealTime is used for the SMC's gain tuning, on a benchmark sports vehicle. For this stage and the online one, the vehicle UC data can't be given since this activity is covered by an NDA. The model DoF are 16. *Ramp Steer* was fundamental for the definition of the effort constraints, adopted as saturation limits for brake pressures and wheel torques. Instead, *Step Steer* tests with low lateral acceleration were useful for the tuning of parameters related to control objective definitions (e.g. tires cornering stiffness).

The online test phase assessment of the ESP is done in a co-simulation environment exploiting a RT driving simulator hardware system, which allows a driver to perform different reference manoeuvres, piloting the vehicle through steer and pedals interface devices. Results are compared with a benchmark reference ESP solution already used in different car models actually in the market. The vehicle UC is a sports car. The manoeuvres are inspired by standardized cornering tests, to assess achievement in terms of lateral stability using a Human-in-the-Loop approach. This means that a control rig composed of the vehicle, environment and driver is required. Evaluating the stability performances in this kind of test is very challenging since there is a significant interaction between these elements. So, the results are combinations of inner car handling dynamics and driver road-holding capabilities. To highlight the outputs, more severe operative situations have been simulated for the boundary conditions specified by the ISO regulations. This is because performance achievements related to standardized vehicle speed and steer command are quite negligible since the vehicle operates in steady-state mode. Instead, bringing the vehicle near unstable conditions allows us to make more evident the effects of the controllers, which aim at leading the vehicle back to a linear behaviour. Executed cornering manoeuvres could show some gaps between each other, in terms of steering amplitude and rate as well as speed tracking. This is due to the inability of any human driver to assure the perfect repeatability of the tests. However, to mitigate this aspect multiple tests are conducted, comparing the most similar ones. The *on-line test phase* refer to standard cornering manoeuvre in HiL configuration. Results highlight as the proposed control algorithm enable improved performances for Non-controlled and Commercial-controlled vehicle scenarios. Indeed, actual yaw rates and side-slip angles exhibit lower errors for target values using the SMC stability program solution. In particular, in the *Step Steer* manoeuvre is evident how the tracking efforts exhibit different control actions between developed ESP solutions and the Commercial ones, achieving better stability and dynamic perform-

ance of the car. This is also shown in the *Sine Steer* test. Furthermore, the need for stability control is essential: the driver with a Non-Controlled vehicle is unable to manoeuvre without losing control of the car; instead, the configuration with an ESP ensures to maintain stability and manoeuvrability. The performance of the optimal control solution can be seen also in the *Lane Change* test. To improve the tracking performances of both yaw rate and side-slip angle, this manoeuvre shows the achievements allowed by the exploitation of traction torques. SMC assist the driver, enhancing vehicle handling aspects for Commercial-controller. However, the sliding approach allows a smoother response of the car to the driver's intentions, letting to maintain the target longitudinal vehicle entrance speed and producing desired yaw moment by the usage of traction command and steering, in addition to conventional differential braking technique.

Finally, a conclusive test campaign is performed in SiL co-simulation conditions, exploiting again the FIAT 500e benchmark use case. The vehicle and sub-systems models have been implemented in CarRealTime (CRT), while the control algorithm resides in the MATLAB environment. The gain-scheduling of the TV technique further improves the tracking performance for both yaw rate and side-slip angle. In open-loop testing, results show the improvement allowed by the SMC controller as compared to lateral stability. In the first case, by approaching the desired cornering radius in steady-state conditions; in the second case by allowing the vehicle to pass the test. The general performance improvement for the closed-loop test can be attributed also to the enhanced predictive driver model tuning and the specification of the optimal waypoints. For the DLC manoeuvre, outputs show that the test can be performed correctly up to  $95\text{km/h}$ . These outputs highlight how the controller contributes to the stabilization of the vehicle. Similar results are obtained for the obstacle avoidance manoeuvre. This test is passed for speed up to  $77\text{km/h}$ .

## Future Developments

The optimal control solutions investigated in this activity could be an object of further improvements to increase the adaptability of the control action to the environmental condition and driver needs. The reference values are based on an ideal kinematic model, so do not account for dynamic aspects acting on the vehicle in the tire-road contact interfaces. This uncertainty, along with the assumptions, clearly affects the tracking performances, especially for lateral acceleration.

The definition of a gain scheduling technique for tire-road contact patch conditions (e.g. cornering stiffness), in addition to the implemented RT speed gains regulation, could lead to higher tracking performances, both for linear and non-linear dynamical behaviour. Also, a robustness analysis for estimation uncertainties is necessary to ensure stability in different driving conditions. Thus, the modularity of the algorithm allows the coupling with an MPC controller to implement the update of the reference model, e.g. respect to cornering stiffness. Indeed, accounting for the road status in the reference states calculation can bring great advantages. As an example, coupling an RT friction estimator with a gain scheduling protocol can improve the target values assignment of the high-level ESP's layer, which can assume faster side-slip angle variations in poor adherence driving conditions.

Another major problem concern the chattering of the controlled states around steady-state desired values. A reduction of this effect is obtained by the proper definition of dead-zone and SMC gains, but the phenomenon is still present. To solve this, the adoption of a second-order sliding mode controller could be useful. Defining

the sliding surface for  $\dot{\beta}$  and  $\dot{\gamma} = \dot{r}$  will bring side-slip rate and yaw acceleration errors to converge asymptotically to 0, ensuring lower chatter effects by removing the direct dependencies between controlled and desired states. Indeed, the *sign*( $\cdot$ ) component of (5.50) will be removed, which is the major source of spikes and step variation of the controlling efforts. In this case, a continuous active ESP algorithm can be adopted.

A contribution to further enhance the performance could be the definition of an anti-windup for the integral term of sliding mode controller [41].

Finally, the output of the system  $y = [r; a_y]^T$  (5.60) could be used for the definition of a Disturbance Observer (DO) to reject uncertainties related to tire-road contact model assumptions. Indeed, cornering stiffness is assumed constant. However, their values are strictly dependent on pavement conditions and normal forces acting on the pneumatic, thus affecting the accuracy performances of the state space model estimations. The lateral acceleration error, whose real value can be easily obtained through IMU, can be introduced in the observer to compensate for those perturbations. This solution could enable improvement under the response time perspective since the control gain can be tuned to higher values while avoiding overshooting problems.

$$y = \begin{bmatrix} r \\ a_y \end{bmatrix} = Cx + Du \quad (5.60)$$

# Chapter 6

## Discussion

This document presents the background, methodologies, tools and materials adopted by the author for the developments of innovative control strategies for EVs performance improvement. Despite the efficiency and functional safety enhancement, mainly attributable to the highly desirable features offered by the electric traction system, a special attention has been dedicated to the proposal of lateral stability controllers, which relies on active torque distribution and steering control actions.

**Background** Respect to the actual SoA, tools and systematic methodologies which allow the full exploitation of e-powertrain characteristics to increase EVs performances are provided. Proposed solutions, concerning mechatronics and By-Wire technologies, are modelled along with the vehicle equipments and implemented in simulation environments. At first, *Vehicle Dynamics* modelling approach is presented. The importance of vehicular *Mechatronics Systems* is underlined. Current *Electric Vehicles* solutions are investigated, both concerning powertrain configurations and performances. The basilar implementation for *Electronic Stability Program* is defined. Literature agrees in develop ESP controller with a hierarchical structure distributed on three layers, dealing with control objectives definitions, optimal control definition and efforts allocation.

**Proposed Approach** The *Research Question* is addressed respect to the open problems of heterogeneous EVs solution which are available and technical challenges for an efficient and reliable development of ESP controllers. Even legislations and standards needs are accounted. Considering the complex interaction arising by the coupling of systems belonging to heterogeneous engineering fields, all the simulation activities are executed on models which fulfil stringent specifications to be easily adapted to different EV. This highlights the clear need for simple, computationally efficient, easily tunable, and effective models, to simplify the development of control allocation controllers. The gap is tackled by the following solutions:

*Standardization* is identified as a viable way to overcome these open problems, by proposing models and control algorithms which are modular, customizable, portable and integrable between the several vehicle architecture and control layers. In particular, the adopted modelling methodology must ensure scalability, abstraction, parametrization, modularity, flexibility and Real-Time capability properties. These aspects allow to overcome the open problem of the many vehicle solutions which are available.

A *Model-Based Method and Tools* in accordance with the V-shaped development approach is proposed to fulfil the design requirements of the control strategies. This needs the adoption of a robust virtual simulation environment for SiL and HiL testing. Achievable performance are evaluated respect to *Reference Driving Scenario*, as standardized cornering test manoeuvres, to produce highly repeatable and comparable results.

The investigated vehicle's layout is the electric *Wheel Independent Motor* traction architecture. When multiple motors and braking system are available, an actuation redundancy is obtained. The increased DoF for the torque allocation purpose allows the definition of novel controller aimed at improving specific vehicle aspects, since driver's intention can be realized through an infinite number of feasible wheel effort distribution combinations. The SoA analysis concerning this powertrain structure highlight the innovative potentiality respect to handling and lateral stability improvement. Main disadvantages are also described. Trough the whole range of allocation solution, a novel solution for improved handling performance and higher correspondence with the desired longitudinal behaviour is proposed here. Thus, a newly *Yaw Moment Torque Vectoring Allocator*, based on Moore-Penrose pseudoinverse theory is proposed. The most innovative contribution of this novel low-level allocation framework concern the fact that driving or braking torques are delivered to the wheels to produce a desired yaw moment, while ensuring a longitudinal vehicle behaviour in strict accordance with the driver intention. Thus, optimal compromise between stabilization control actions and driving performance is meet. This low-level controller is parametrized in order to be easily applied on different traction architectures. This ensure portability and flexibility of the whole proposed strategy, allowing to exploit the allocator for all the vehicle configurations, as well as high level controller policies.

**Methods, Tools and Preliminary Activities** At this point preliminary validation activities are executed. The vehicle sub-systems models refer to several UCs, which exhibit high relevance for both industrial interest and research/academic impact. Specifically, the FIAT 500e, the SimRod Kyburz and the Valeo BEV concept car. Part of these studies are done in collaboration within important industrial and academic partners of the *OBELICS Project* consortium, which share with us benchmark *Vehicles Use Cases* data, as well as expertise and knowledge both for modelling and controlling. The described *Simulation Models* for vehicle chassis, tire-road interface, e-powertrain and controllers are developed in accordance with the standardization specifications and the V-shaped development process given above, ensuring high correspondence with real-word test results. These models are suitable and tailorable for a wide range of traction architectures and UCs, aiming at reducing man-hour and cost for the testing and performance assessment of the developed control algorithm. Comparative evaluation is done for several car solutions to verify effectiveness and efficiency of the controller, using reliable metrics for high reproducible tests. The flexibility, modularity and portability are proven, since it was possible to use the same models for different vehicle UC, traction configurations, control algorithm and simulation software. RT capability is ensured for both SiL and HiL by an efficient system organization respect to TC and TD sub-models. However, in these works the attention is mainly focused on DDEV, due to their relevant and desirable features.

The developed *hydraulic brake model* has been validated using real world test data [213, 214]. Preliminary validation results obtained on a test circuit are quite encouraging [213, 214]. Results clearly indicate that brake pressures are reproduced quite precisely, and recorded errors produce negligible errors in terms of simulated vehicle dynamics. A thermal, friction and wear brake models are developed. An experimental set-up and identification methodology were also proposed and evaluated. The resulting parametrized models showed a promising correlation with the experimental results. Finally, simulations on the emissions associated with brake pad wear underlying the importance of its environmental impact. Proposed models offer interesting features for preliminary sizing and optimization of brake blending policies for electric vehicles. The tool is also designed and optimized for RTI and HiL testing. The virtual environments for the evaluation of efficiency, safety and stability performance improvements is introduced.

*Energy efficiency improvement* are due to the developed BB control and the optimal power management strategy. BB strategy proved to be flexible since it was possible to use the same model for different powertrain configurations and benchmark e-vehicles. In addition, regenerated energy up to 18% of the consumed one can be achieved. Concerning the fuzzy brake blending solution, results highlight that increased battery reliability and lifespan is achieved by selecting more conservative power constrains when limit conditions occurs. However, adopt FBB reduce the overall energy which could be recovered for the RBS in those scenarios. This strategy, attempt to find an optimal comprise between energy regeneration and energy storage system preservation. In addition, the driver dynamic feedback is enhanced, since a smoother dynamic, which reduce the passengers perception, is ensured. Optimal power management system, assessed on both standard and real driving emission drive speed mission profile, can lead to a 9% drive-range improvement and 4% up to 8% of energy consumption reduction.

*Functional safety enhancement* are investigated proposing a risk-based approach, to determine the ASIL class of the targeted system to achieve the safety requirements and acceptable residual risk imposed by ISO 26262. Specifically, a systematic model-based methodology based on vFMEA and FI analysis is proposed in the optic of ensuring braking performances of the EV, the BBW system reliability and availability of safety-related functionalities in which brake is involved. Also, support to the manufactures in the design of tailored securing solutions is given, providing the requirements for validation and confirmation measures as well as time and cost effort reduction.

Then, *lateral stability performances* are evaluated for the innovative *Moore-Penrose TV allocation* technique. The assumption to alternatively suppose availability and unavailability of the stability controller is done in order to comparatively asses the simulation outputs of the performed tests. This allocation strategy can ensure a stable lateral behaviour of the vehicle, by increasing the speed at which the reference trajectory could be executed, reducing the RSME respect to the ideal trajectory of the manoeuvre and achieving a longitudinal behaviour in agreement with the driver intentions, if compared with non-controlled vehicle solution. The controller is correctly integrated with other CUs in order to accomplish enhanced stability behaviours of the WIM driven vehicle, both in longitudinal and lateral directions. The IWM layout is the best configuration for lateral stability purposes.

**Advanced ESP Control Algorithms** Between the different aspects, I decided to mainly focus on automotive *Advanced ESP Control Algorithms*, not only dealing with roll-over prevention but more generally on lateral stabilization. The growing diffusion of mechatronic and By-Wire systems on modern vehicles recently engaged the interest of designers for active safety devices development purposes. Thus, the availability of highly performing E/E platforms, from a computational point-of-view, allows the implementation of advanced control strategies, which can be extremely expensive or even not feasible using conventional mechanical systems. In addition, the rapid transition towards vehicle electrification is further increasing the opportunities to develop innovative control solutions. Indeed, WIM traction configurations exhibit the most desirable features respect to dynamical behaviour control of automotive vehicles, allowing the application of complex TV allocation techniques. The majority of approaches in literature focus only on one of the controller layers. Here, all three levels are encompassed to ensure a smooth integration between each block since their development is not completely independent from the other. In particular, two different lateral stability control strategies which relies on TV and AFS techniques are developed and investigated.

*Minimized Tire Adhesion Grip ESP Controller:* The first proposed ESP controller is based on an *optimal allocation criteria* to properly stabilize lateral vehicle behaviour, with mixed array of corrections in terms of torques applied to wheels and steering angle. The control effort are optimized as compared to available adhesion in the tire-road interface. The innovative contribution of this work is represented by the idea that resolving a two-step least-square optimization of actuation and allocated adhesion, a set of wheels torque commands and corrective steering angle is produced to both stabilize the vehicle in cornering manoeuvre while minimizing the engaged grip. This model-based solution is abstracted by the concept of friction estimation, proposing an approach which increase the manoeuvrability margin of the vehicle, especially in poor adherence cornering situations. Here, an explicit model is considered: proposed controllers and estimators rely on ideal measurements from IMU and common automotive sensors. Developed vehicle estimator is able to assure a relatively fast and simple execution, which is also a fundamental feature for the future integration in a recursive filter. This strategy avoid the use of on-line estimators, privileging a simple but robust approach, whose parameters should be relatively more simple to be calibrated. The model calculates linearized coefficients  $h_{ijy}$  to correlate performed steering corrections to corresponding variations of lateral forces. Cautionary limitation of  $d\delta_{max}$  is calculated to avoid excessive and abrupt steering corrections for which it can be correspond undesired non-linear behaviour. This “optimal” solution has the following properties:

- For a known set of desired longitudinal effort  $T_x$  and yaw torque  $M_{zz}$ , chosen optimal solution minimizes required  $\mu_{eng}$  as compared to performed manoeuvre. Since corrections of vehicle dynamics are often performed with limited wheel-road adhesion this is a highly desirable feature;
- Proposed criteria allow to optimize at the same time corrections regarding both steering angle and applied longitudinal efforts with a unified adhesion-based criterion;
- Corrections of longitudinal efforts applied to wheels are minimized with a least square criteria respect to known limits of actuators and driver intentions.

Result of the performed simulations show that the coordinated steering and TV optimal control approach, proposed in this work, appear efficient and reliable respect the tasks of vehicle lateral stabilization and engaged adherence minimization. Output of the test, however, highlight also lacks of the strategy. Normal loads on wheels are evaluated with a simplified an estimator based on quasi-static vehicle model.

*Sliding Mode ESP Controller:* The second solution is based on *first order sliding mode control*, which aim at the direct control of vehicle side-slip angle  $\beta$  and yaw rate  $r$  by the application of corrective steering and TV efforts. Respect to previously work, this algorithm rely on a 2 dimensions model for states and sliding surface, challenging well-know and established lateral stability SMC methods, typically using separated sliding surfaces which decouple the control dynamics. To lead the states converge to the target values, the control action is composed by a feedforward model-based terms and a feedback PI compensation terms. Optimal control inputs, defined by a specific Ljapunov candidate, ensure the state errors asymptotically converge to 0, where the error is used for proportional, integral and sign components. Even in this case, the controlling approach require only a limited numbers of sensed signals, currently available in almost any vehicle.

Optimal steer angle is applied as a correction respect to the desired trajectory, constrained to the 10% of the steering angle command, in order to avoid abrupt deviation which could lead to unpredictable vehicle dynamics. Thus, its contribution is quite limited. Desired yaw moment is mapped into equivalent torque demand for each wheel with the Moore-Penrose pseudoinverse approach. At this level, are managed also the actuator inequality constrains to achieve also a smooth transient performance. Preliminary results in Simulink clearly highlight the benefit allowed by the proposed coordinated TV and steering control, from the lateral stability perspective. Also, the integration with the other on-board ECUs and sub-system is ensured. However, the 3-DoF body vehicle model of MATLAB environment poorly reproduce the lateral behaviour when severe operative conditions occurs.

The proposed ESP strategies is evaluated also in a RT driving simulators, compared with a benchmark reference ESP solution already used in different car models actually in the market. HiL test rig allows to understand which impact these solutions introduce, both on vehicle behaviour and driver perception, supposing real driving conditions. Indeed, Human-in-the-Loop validation plays as essential role in the design process of a ESP controller, due to the continuous interaction between driver, vehicle and environment which constitute the closed loop control elements. To highlight the outputs, more severe operative situations have been simulated as compared to the boundary conditions specified by the ISO regulations. Sliding mode control leads to improved tracking performances of the controlled states, achieving higher safety margin even respect a ESP commercial solution. For what concern the speed, the sliding mode solution allows to perform the reference manoeuvre in accordance with the driver intention, maintaining the entrance longitudinal speed by the exploitation of the traction forces of the powertrain.

The final validation has been implemented on the co-simulation environment of MATLAB Simulink and VI-CarRealTime on the Fiat 500e vehicle 16-DoF model. To further improve the tracking performances of the SMC-based ESP, respect to yaw rate and side-slip angle, the gain of the TV action as been scheduled respect to the vehicle's longitudinal speed. As can be seen, the sliding mode controller extend the linear region of the vehicle steering response, allowing also a greater lateral acceleration. In addition, the steering responsiveness can be further improved when no dead-zones are used and continuous active ESP is used. In this context, the phase plane  $\beta - \dot{\beta}$  plot show that higher stability margin is achieved. Output data highlight how the vehicle steering responsiveness is improved for both the input signal peaks. Yaw rate and side-slip angles are actively controlled to be as close as possible to the references. The general performance improvement for the closed-loop test can be attributed also to the enhanced predictive driver model, gain scheduling tuning and the specification of the trajectory optimal way-points. Best performance of this controller can be obtained by considering independent electric hub-motors for 4WD vehicles, which guarantee an higher applicable yaw momentum thanks to the easiness of 4-quadrant wheel torque independent control, enabling the exploiting of traction forces.

However, these results point out also limitations and gaps of the sliding mode approach. The optimal controls investigated in these activities could be object of further improvements to increase the adaptability of the control action to the environmental condition and driver needs.

# Bibliography

- [1] D. Yang, B. Jacobson and M. Lidberg, ‘Benefit prediction of passenger car post impact stability control based on accident statistics and vehicle dynamics simulations’, p. 13, 2009.
- [2] R. Sferco, ‘Potential effectiveness of electronic stability programs (ESP) - what european field studies tell us’, p. 10, 2001.
- [3] R. Rajamani, *Vehicle Dynamics and Control* (Mechanical Engineering Series). Boston, MA: Springer US, 2012. DOI: 10.1007/978-1-4614-1433-9.
- [4] M. Nuessle, R. Rutz, M. Leucht, M. Nonnenmacher and H. Volk, ‘OBJECTIVE TEST METHODS TO ASSESS ACTIVE SAFETY BENEFITS OF ESP®’, p. 8, 2004.
- [5] H. Baum, S. Grawenhoff and T. GEIßLER, ‘Cost-benefit analysis of the electronic stability program (ESP)’, p. 35, 2008.
- [6] M. Nagai, ‘The perspectives of research for enhancing active safety based on advanced control technology’, *Vehicle System Dynamics*, vol. 45, no. 5, pp. 413–431, May 2007. DOI: 10.1080/00423110701275162.
- [7] T. Koisaari, T. Kari, T. Vahlberg, N. Sihvola and T. Tervo, ‘Crash risk of ESC-fitted passenger cars’, *Traffic Injury Prevention*, vol. 20, no. 3, pp. 325–331, 18th Mar. 2019. DOI: 10.1080/15389588.2019.1579907.
- [8] A. Lie, C. Tingvall, M. Krafft and A. Kullgren, ‘The effectiveness of ESP (electronic stability program) in reducing real life accidents’, *Traffic Injury Prevention*, vol. 5, no. 1, pp. 37–41, Mar. 2004. DOI: 10.1080/15389580490269164.
- [9] K. Reif, Ed., *Automotive Mechatronics: Automotive Networking, Driving Stability Systems, Electronics*, Wiesbaden: Springer Fachmedien Wiesbaden, 2015. DOI: 10.1007/978-3-658-03975-2.
- [10] D. Frede, M. Khodabakhshian and D. Malmquist, ‘A state-of-the-art survey on vehicular mechatronics focusing on by-wire systems.’, p. 67, 2010.
- [11] N. Navet, F. Simonot-Lion, Y. Qiong Song and C. Wilwert, ‘Design of automotive x-by-wire systems’, in *The Industrial Communication Technology Handbook*. CRC Press, 23rd Feb. 2005, vol. 20050668, pp. 29–1–29–19, Series Title: Industrial Information Technology. DOI: 10.1201/9781420037821.ch29.
- [12] D. Gonzalez, J. Perez, V. Milanés and F. Nashashibi, ‘A review of motion planning techniques for automated vehicles’, *IEEE Transactions on Intelligent Transportation Systems*, vol. 17, no. 4, pp. 1135–1145, Apr. 2016. DOI: 10.1109/TITS.2015.2498841.

- [13] L. Yu, X. Liu, Z. Xie and Y. Chen, ‘Review of brake-by-wire system used in modern passenger car’, in *Volume 3: 18th International Conference on Advanced Vehicle Technologies; 13th International Conference on Design Education; 9th Frontiers in Biomedical Devices*, Charlotte, North Carolina, USA: American Society of Mechanical Engineers, 21st Aug. 2016, V003T01A020. DOI: 10.1115/DETC2016-59279.
- [14] S. Huang, C. Zhou, L. Yang, Y. Qin, X. Huang and B. Hu, ‘Transient fault tolerant control for vehicle brake-by-wire systems’, *Reliability Engineering & System Safety*, vol. 149, pp. 148–163, May 2016. DOI: 10.1016/j.ress.2016.01.001.
- [15] T. Favilli, M. Delogu, L. Pugi and L. Berzi, ‘Functional safety and reliability for innovative vehicle braking system and integration with electric traction units’, *IOP Conference Series: Materials Science and Engineering*, vol. 1038, no. 1, p. 012020, 1st Feb. 2021. DOI: 10.1088/1757-899X/1038/1/012020.
- [16] P. Sinha, ‘Architectural design and reliability analysis of a fail-operational brake-by-wire system from ISO 26262 perspectives’, *Reliability Engineering & System Safety*, vol. 96, no. 10, pp. 1349–1359, Oct. 2011. DOI: 10.1016/j.ress.2011.03.013.
- [17] Hyungju Kwon, R. Itabashi-Campbell and K. McLaughlin, ‘ISO26262 application to electric steering development with a focus on hazard analysis’, in *2013 IEEE International Systems Conference (SysCon)*, Orlando, FL: IEEE, Apr. 2013, pp. 655–661. DOI: 10.1109/SysCon.2013.6549952.
- [18] H. Tseng, D. Madau, B. Ashrafi, T. Brown and D. Recker, ‘Technical challenges in the development of vehicle stability control system’, in *Proceedings of the 1999 IEEE International Conference on Control Applications (Cat. No.99CH36328)*, vol. 2, Kohala Coast, HI, USA: IEEE, 1999, pp. 1660–1666. DOI: 10.1109/CCA.1999.801221.
- [19] R. Rajamani, G. Phanomchoeng, D. Piyabongkarn and J. Y. Lew, ‘Algorithms for real-time estimation of individual wheel tire-road friction coefficients’, *IEEE/ASME Transactions on Mechatronics*, vol. 17, no. 6, pp. 1183–1195, Dec. 2012. DOI: 10.1109/TMECH.2011.2159240.
- [20] A. Bergmann, ‘Benefits and drawbacks of model-based design’, *KMUTNB International Journal of Applied Science and Technology*, vol. 7, no. 3, pp. 15–19, 30th Sep. 2014. DOI: 10.14416/j.ijast.2014.04.004.
- [21] L. Berzi, T. Favilli, E. Locorotondo, M. Pierini and L. Pugi, ‘Real time models of automotive mechatronics systems: Verifications on “toy models”’, in *Advances in Italian Mechanism Science*, G. Carbone and A. Gasparetto, Eds., vol. 68, Series Title: Mechanisms and Machine Science, Cham: Springer International Publishing, 2019, pp. 141–148. DOI: 10.1007/978-3-030-03320-0\_15.
- [22] A. Mangia, B. Lenzo and E. Sabbioni, ‘An integrated torque-vectoring control framework for electric vehicles featuring multiple handling and energy-efficiency modes selectable by the driver’, *Meccanica*, vol. 56, no. 5, pp. 991–1010, May 2021. DOI: 10.1007/s11012-021-01317-3.

- [23] S.-Y. Ko, J.-W. Ko, S.-M. Lee, J.-S. Cheon and H. Kim, 'A study on in-wheel motor control to improve vehicle stability using human-in-the-loop simulation', *Journal of Power Electronics*, vol. 13, no. 4, pp. 536–545, 20th Jul. 2013. DOI: 10.6113/JPE.2013.13.4.536.
- [24] B. Jin, C. Sun and X. Zhang, 'RESEARCH ON LATERAL STABILITY OF FOUR HUBMOTOR- IN-WHEELS DRIVE ELECTRIC VEHICLE', *International Journal on Smart Sensing and Intelligent Systems*, vol. 8, no. 3, pp. 1855–1875, 2015. DOI: 10.21307/ijssis-2017-833.
- [25] C. Feng, N.-g. Ding, Y.-l. He, G.-y. Xu and F. Gao, 'Control allocation algorithm for over-actuated electric vehicles', *Journal of Central South University*, vol. 21, no. 10, pp. 3705–3712, Oct. 2014. DOI: 10.1007/s11771-014-2354-0.
- [26] Y. Chen, S. Chen, Y. Zhao, Z. Gao and C. Li, 'Optimized handling stability control strategy for a four in-wheel motor independent-drive electric vehicle', *IEEE Access*, vol. 7, pp. 17 017–17 032, 2019. DOI: 10.1109/ACCESS.2019.2893894.
- [27] J.-S. Hu, Y. Wang, H. Fujimoto and Y. Hori, 'Robust yaw stability control for in-wheel motor electric vehicles', *IEEE/ASME Transactions on Mechatronics*, vol. 22, no. 3, pp. 1360–1370, Jun. 2017. DOI: 10.1109/TMECH.2017.2677998.
- [28] H. Alipour, M. Sabahi and M. B. Bannae Sharifian, 'Lateral stabilization of a four wheel independent drive electric vehicle on slippery roads', *Mechatronics*, vol. 30, pp. 275–285, Sep. 2015. DOI: 10.1016/j.mechatronics.2014.08.006.
- [29] L. De Novellis, A. Sorniotti, P. Gruber and A. Pennycott, 'Comparison of feedback control techniques for torque-vectoring control of fully electric vehicles', *IEEE Transactions on Vehicular Technology*, vol. 63, no. 8, pp. 3612–3623, Oct. 2014. DOI: 10.1109/TVT.2014.2305475.
- [30] L. De Novellis, A. Sorniotti, P. Gruber, L. Shead, V. Ivanov and K. Hoeppeing, 'Torque vectoring for electric vehicles with individually controlled motors: State-of-the-art and future developments', *World Electric Vehicle Journal*, vol. 5, no. 2, pp. 617–628, 29th Jun. 2012. DOI: 10.3390/wevj5020617.
- [31] N. Ando and H. Fujimoto, 'Yaw-rate control for electric vehicle with active front/rear steering and driving/braking force distribution of rear wheels', in *2010 11th IEEE International Workshop on Advanced Motion Control (AMC)*, Nagaoka, Japan: IEEE, Mar. 2010, pp. 726–731. DOI: 10.1109/AMC.2010.5464040.
- [32] S. Di Cairano, H. E. Tseng, D. Bernardini and A. Bemporad, 'Vehicle yaw stability control by coordinated active front steering and differential braking in the tire sideslip angles domain', *IEEE Transactions on Control Systems Technology*, vol. 21, no. 4, pp. 1236–1248, Jul. 2013. DOI: 10.1109/TCST.2012.2198886.
- [33] E. Dinçmen and T. Acarman, 'Active coordination of the individually actuated wheel braking and steering to enhance vehicle lateral stability and handling', *IFAC Proceedings Volumes*, vol. 41, no. 2, pp. 10 738–10 743, 2008. DOI: 10.3182/20080706-5-KR-1001.01820.

- [34] B. Guvenc, T. Acarman and L. Guvenc, 'Coordination of steering and individual wheel braking actuated vehicle yaw stability control', in *IEEE IV2003 Intelligent Vehicles Symposium. Proceedings (Cat. No.03TH8683)*, Columbus, OH, USA: IEEE, 2003, pp. 288–293. DOI: 10.1109/IVS.2003.1212924.
- [35] Junmin Wang and R. Longoria, 'Coordinated vehicle dynamics control with control distribution', in *2006 American Control Conference*, Minneapolis, MN, USA: IEEE, 2006, 6 pp. DOI: 10.1109/ACC.2006.1657573.
- [36] J. Tjonnas and T. A. Johansen, 'Stabilization of automotive vehicles using active steering and adaptive brake control allocation', *IEEE Transactions on Control Systems Technology*, vol. 18, no. 3, pp. 545–558, May 2010. DOI: 10.1109/TCST.2009.2023981.
- [37] S.-H. Yu and J. J. Moskwa, 'A global approach to vehicle control: Coordination of four wheel steering and wheel torques', *Journal of Dynamic Systems, Measurement, and Control*, vol. 116, no. 4, pp. 659–667, 1st Dec. 1994. DOI: 10.1115/1.2899265.
- [38] J. Jin, 'Modified pseudoinverse redistribution methods for redundant controls allocation', *Journal of Guidance, Control, and Dynamics*, vol. 28, no. 5, pp. 1076–1079, Sep. 2005. DOI: 10.2514/1.14992.
- [39] G. Bartolini, A. Pisano, E. Punta and E. Usai, 'A survey of applications of second-order sliding mode control to mechanical systems', *International Journal of Control*, vol. 76, no. 9, pp. 875–892, Jan. 2003. DOI: 10.1080/0020717031000099010.
- [40] T. Goggia *et al.*, 'Integral sliding mode for the torque-vectoring control of fully electric vehicles: Theoretical design and experimental assessment', *IEEE Transactions on Vehicular Technology*, vol. 64, no. 5, pp. 1701–1715, May 2015. DOI: 10.1109/TVT.2014.2339401.
- [41] A. Tota *et al.*, 'On the experimental analysis of integral sliding modes for yaw rate and sideslip control of an electric vehicle with multiple motors', *International Journal of Automotive Technology*, vol. 19, no. 5, pp. 811–823, Oct. 2018. DOI: 10.1007/s12239-018-0078-0.
- [42] M. Canale, L. Fagiano, A. Ferrara and C. Vecchio, 'Vehicle yaw control via second-order sliding-mode technique', *IEEE Transactions on Industrial Electronics*, vol. 55, no. 11, pp. 3908–3916, Nov. 2008. DOI: 10.1109/TIE.2008.2003200.
- [43] M. Guiggiani, *The Science of Vehicle Dynamics*. Dordrecht: Springer Netherlands, 2014. DOI: 10.1007/978-94-017-8533-4.
- [44] T. Gillespie, *Fundamentals of vehicle dynamics, 2nd edition*, 2nd. Warrendale: SAE Internationals, 2021.
- [45] G. Genta and L. Morello, *The automotive chassis* (Mechanical engineering series). Dordrecht: Springer, 2009, 1 p., OCLC: ocn316513661.
- [46] H. B. Pacejka and I. Besselink, *Tire and vehicle dynamics*. Reino Unido; Estados Unidos; Estados Unidos: Butterworth - Heinemann Distributed in conjunction with SAE International : 2012, OCLC: 1112868686.

- [47] D. Chindamo, B. Lenzo and M. Gadola, 'On the vehicle sideslip angle estimation: A literature review of methods, models, and innovations', *Applied Sciences*, vol. 8, no. 3, p. 355, 1st Mar. 2018. DOI: 10.3390/app8030355.
- [48] D. Vilela and R. S. Barbosa, 'Analytical models correlation for vehicle dynamic handling properties', *Journal of the Brazilian Society of Mechanical Sciences and Engineering*, vol. 33, no. 4, pp. 437–444, Dec. 2011. DOI: 10.1590/S1678-58782011000400007.
- [49] R. H. Bishop, Ed., *Mechatronics: an introduction*, Boca Raton: Taylor & Francis, 2006, 1 p.
- [50] F. Harashima, M. Tomizuka and T. Fukuda, 'Mechatronics - "what is it, why, and how?" an editorial', *IEEE/ASME Transactions on Mechatronics*, vol. 1, no. 1, pp. 1–4, Mar. 1996. DOI: 10.1109/TMECH.1996.7827930.
- [51] R. Isermann, *Mechatronische Systeme: Grundlagen ; mit 103 Tabellen*, 2., vollst. neu bearb. Aufl. Berlin Heidelberg: Springer, 2008, 623 pp.
- [52] A. B. Fotso and A. Rettberg, 'State of the art for mechatronic design concepts', in *Proceedings of 2012 IEEE/ASME 8th IEEE/ASME International Conference on Mechatronic and Embedded Systems and Applications*, Suzhou, China: IEEE, Jul. 2012, pp. 232–240. DOI: 10.1109/MESA.2012.6275567.
- [53] J. K. Ahn, K. H. Jung, D. H. Kim, H. B. Jin, H. S. Kim and S. H. Hwang, 'Analysis of a regenerative braking system for hybrid electric vehicles using an electro-mechanical brake', *International Journal of Automotive Technology*, vol. 10, no. 2, pp. 229–234, Apr. 2009. DOI: 10.1007/s12239-009-0027-z.
- [54] C. Lv, J. Zhang, Y. Li and Y. Yuan, 'Regenerative braking control algorithm for an electrified vehicle equipped with a by-wire brake system', presented at the SAE 2014 World Congress & Exhibition, 1st Apr. 2014, pp. 2014-01-1791. DOI: 10.4271/2014-01-1791.
- [55] D. Sallee and R. Bannatyne, 'Advanced electronic chassis control systems', presented at the Future Transportation Technology Conference & Exposition, 20th Aug. 2001, pp. 2001-01-2534. DOI: 10.4271/2001-01-2534.
- [56] B. Bilgin and A. Emadi, 'Electric motors in electrified transportation: A step toward achieving a sustainable and highly efficient transportation system', *IEEE Power Electronics Magazine*, vol. 1, no. 2, pp. 10–17, Jun. 2014. DOI: 10.1109/MPPEL.2014.2312275.
- [57] M. Ehsani, Ed., *Modern electric, hybrid electric, and fuel cell vehicles: fundamentals, theory, and design*, Power electronics and applications series, Boca Raton: CRC Press, 2005, 395 pp.
- [58] C. Chan, A. Bouscayrol and K. Chen, 'Electric, hybrid, and fuel-cell vehicles: Architectures and modeling', *IEEE Transactions on Vehicular Technology*, vol. 59, no. 2, pp. 589–598, Feb. 2010. DOI: 10.1109/TVT.2009.2033605.
- [59] J. de Santiago *et al.*, 'Electrical motor drivelines in commercial all-electric vehicles: A review', *IEEE Transactions on Vehicular Technology*, vol. 61, no. 2, pp. 475–484, Feb. 2012. DOI: 10.1109/TVT.2011.2177873.
- [60] M. Boerboom, 'Electric vehicle blended braking maximizing energy recovery while maintaining vehicle stability and maneuverability.', p. 97,

- [61] D. Savitski *et al.*, ‘The new paradigm of an anti-lock braking system for a full electric vehicle: Experimental investigation and benchmarking’, *Proceedings of the Institution of Mechanical Engineers, Part D: Journal of Automobile Engineering*, vol. 230, no. 10, pp. 1364–1377, Sep. 2016. DOI: 10.1177/0954407015608548.
- [62] V. Ricciardi, D. Savitski, K. Augsburg and V. Ivanov, ‘Estimation of brake friction coefficient for blending function of base braking control’, *SAE International Journal of Passenger Cars - Mechanical Systems*, vol. 10, no. 3, pp. 774–785, 17th Sep. 2017. DOI: 10.4271/2017-01-2520.
- [63] L. Ahmadi, S. B. Young, M. Fowler, R. A. Fraser and M. A. Achachlouei, ‘A cascaded life cycle: Reuse of electric vehicle lithium-ion battery packs in energy storage systems’, *The International Journal of Life Cycle Assessment*, vol. 22, no. 1, pp. 111–124, Jan. 2017. DOI: 10.1007/s11367-015-0959-7.
- [64] C. Lv, J. Zhang, Y. Li and Y. Yuan, ‘Directional-stability-aware brake blending control synthesis for over-actuated electric vehicles during straight-line deceleration’, *Mechatronics*, vol. 38, pp. 121–131, Sep. 2016. DOI: 10.1016/j.mechatronics.2015.12.010.
- [65] J. Rauh and D. Ammon, ‘System dynamics of electrified vehicles: Some facts, thoughts, and challenges’, *Vehicle System Dynamics*, vol. 49, no. 7, pp. 1005–1020, Jul. 2011. DOI: 10.1080/00423114.2011.582122.
- [66] Y. Gao, L. Chen and M. Ehsani, ‘Investigation of the effectiveness of regenerative braking for EV and HEV’, presented at the Future Transportation Technology Conference & Exposition, 17th Aug. 1999, pp. 1999–01–2910. DOI: 10.4271/1999-01-2910.
- [67] L. Berzi, M. Delogu and M. Pierini, ‘A comparison of electric vehicles use-case scenarios: Application of a simulation framework to vehicle design optimization and energy consumption assessment’, in *2016 IEEE 16th International Conference on Environment and Electrical Engineering (EEEIC)*, Florence, Italy: IEEE, Jun. 2016, pp. 1–6. DOI: 10.1109/EEEIC.2016.7555775.
- [68] Y. Hori, ‘Future vehicle driven by electricity and control-research on four wheel motored "UOT electric march II"’, in *7th International Workshop on Advanced Motion Control. Proceedings (Cat. No.02TH8623)*, Maribor, Slovenia: IEEE, 2002, pp. 1–14. DOI: 10.1109/AMC.2002.1026883.
- [69] C. Mi and A. Masrur, *Hybrid electric vehicles: principles and applications with practical perspectives principles and applications with practical perspectives* (Automotive series), Second edition. Hoboken, NJ, USA: Wiley, 2018, 1 p.
- [70] A. Walker, M. Galea, C. Gerada, A. Mebarki and D. Gerada, ‘A topology selection consideration of electrical machines for traction applications: Towards the FreedomCar 2020 targets’, in *2015 Tenth International Conference on Ecological Vehicles and Renewable Energies (EVER)*, Monte Carlo: IEEE, Mar. 2015, pp. 1–10. DOI: 10.1109/EVER.2015.7112923.
- [71] B. Frieske, M. Kloetzke and F. Mauser, ‘Trends in vehicle concept and key technology development for hybrid and battery electric vehicles’, vol. 6, p. 12, 2013.

- [72] A. Emadi, Young Joo Lee and K. Rajashekara, 'Power electronics and motor drives in electric, hybrid electric, and plug-in hybrid electric vehicles', *IEEE Transactions on Industrial Electronics*, vol. 55, no. 6, pp. 2237–2245, Jun. 2008. DOI: 10.1109/TIE.2008.922768.
- [73] D. A. Crolla and D. Cao, 'The impact of hybrid and electric powertrains on vehicle dynamics, control systems and energy regeneration', *Vehicle System Dynamics*, vol. 50, pp. 95–109, sup1 Jan. 2012. DOI: 10.1080/00423114.2012.676651.
- [74] M. Vignati, M. Belloni, D. Tarsitano and E. Sabbioni, 'Optimal cooperative brake distribution strategy for IWM vehicle accounting for electric and friction braking torques', *Mathematical Problems in Engineering*, vol. 2021, X. Sun, Ed., pp. 1–19, 9th Jul. 2021. DOI: 10.1155/2021/1088805.
- [75] M. Vignati and E. Sabbioni, 'Force-based braking control algorithm for vehicles with electric motors', *Vehicle System Dynamics*, vol. 58, no. 9, pp. 1348–1366, 1st Sep. 2020. DOI: 10.1080/00423114.2019.1621354.
- [76] D.-w. Pi, P.-y. Xue, Q. Cheng, W.-b. Chu, J.-j. Fan and B.-y. Xie, 'Braking-style-based optimization for regenerative braking system of an electric commercial vehicle', In Review, preprint, 7th Oct. 2020. DOI: 10.21203/rs.3.rs-84020/v1.
- [77] S. Cikanek and K. Bailey, 'Regenerative braking system for a hybrid electric vehicle', in *Proceedings of the 2002 American Control Conference (IEEE Cat. No.CH37301)*, Anchorage, AK, USA: IEEE, 2002, 3129–3134 vol.4. DOI: 10.1109/ACC.2002.1025270.
- [78] L.-H. Björnsson and S. Karlsson, 'The potential for brake energy regeneration under swedish conditions', *Applied Energy*, vol. 168, pp. 75–84, Apr. 2016. DOI: 10.1016/j.apenergy.2016.01.051.
- [79] C. Qiu and G. Wang, 'New evaluation methodology of regenerative braking contribution to energy efficiency improvement of electric vehicles', *Energy Conversion and Management*, vol. 119, pp. 389–398, Jul. 2016. DOI: 10.1016/j.enconman.2016.04.044.
- [80] B. Heissing and M. Ersoy, Eds., *Chassis handbook: fundamentals, driving dynamics, components, mechatronics, perspectives*, 1st edition, ATZ, OCLC: ocn832319879, Wiesbaden: Vieweg + Teubner, 2011, 591 pp.
- [81] K. Muta, M. Yamazaki and J. Tokieda, 'Development of new-generation hybrid system THS II - drastic improvement of power performance and fuel economy', presented at the SAE 2004 World Congress & Exhibition, 8th Mar. 2004, pp. 2004–01–0064. DOI: 10.4271/2004-01-0064.
- [82] Y. Aoki, K. Suzuki, H. Nakano, K. Akamine, T. Shirase and K. Sakai, 'Development of hydraulic servo brake system for cooperative control with regenerative brake', presented at the SAE World Congress & Exhibition, 16th Apr. 2007, pp. 2007–01–0868. DOI: 10.4271/2007-01-0868.
- [83] K. Bayar, 'Performance comparison of electric-vehicle drivetrain architectures from a vehicle dynamics perspective', *Proceedings of the Institution of Mechanical Engineers, Part D: Journal of Automobile Engineering*, vol. 234, no. 4, pp. 915–935, Mar. 2020. DOI: 10.1177/0954407019867491.

- [84] R. de Castro, R. E. Araújo, M. Tanelli, S. M. Savaresi and D. Freitas, ‘Torque blending and wheel slip control in EVs with in-wheel motors’, *Vehicle System Dynamics*, vol. 50, pp. 71–94, sup1 Jan. 2012. DOI: 10.1080/00423114.2012.666357.
- [85] Y. Gao, L. Chu and M. Ehsani, ‘Design and control principles of hybrid braking system for EV, 1ev and FCV’, p. 8,
- [86] W. Xu, H. Chen, H. Zhao and B. Ren, ‘Torque optimization control for electric vehicles with four in-wheel motors equipped with regenerative braking system’, *Mechatronics*, vol. 57, pp. 95–108, Feb. 2019. DOI: 10.1016/j.mechatronics.2018.11.006.
- [87] N. Mutoh, Y. Hayano, H. Yahagi and K. Takita, ‘Electric braking control methods for electric vehicles with independently driven front and rear wheels’, *IEEE Transactions on Industrial Electronics*, vol. 54, no. 2, pp. 1168–1176, Apr. 2007. DOI: 10.1109/TIE.2007.892731.
- [88] C. Jo, J. Ko, H. Yeo, T. Yeo, S. Hwang and H. Kim, ‘Cooperative regenerative braking control algorithm for an automatic-transmission-based hybrid electric vehicle during a downshift’, *Proceedings of the Institution of Mechanical Engineers, Part D: Journal of Automobile Engineering*, vol. 226, no. 4, pp. 457–467, Apr. 2012. DOI: 10.1177/0954407011421083.
- [89] J. Ruan, P. D. Walker, P. A. Watterson and N. Zhang, ‘The dynamic performance and economic benefit of a blended braking system in a multi-speed battery electric vehicle’, *Applied Energy*, vol. 183, pp. 1240–1258, Dec. 2016. DOI: 10.1016/j.apenergy.2016.09.057.
- [90] C. Satzger, R. de Castro, A. Knoblach and J. Brembeck, ‘Design and validation of an MPC-based torque blending and wheel slip control strategy’, in *2016 IEEE Intelligent Vehicles Symposium (IV)*, Gotenburg, Sweden: IEEE, Jun. 2016, pp. 514–520. DOI: 10.1109/IVS.2016.7535435.
- [91] S. A. Oleksowicz *et al.*, ‘Regenerative braking strategies, vehicle safety and stability control systems: Critical use-case proposals’, *Vehicle System Dynamics*, vol. 51, no. 5, pp. 684–699, May 2013. DOI: 10.1080/00423114.2013.767462.
- [92] P. Spichartz, T. Bokker and C. Sourkounis, ‘Comparison of electric vehicles with single drive and four wheel drive system concerning regenerative braking’, p. 7,
- [93] J.-Z. Zhang, X. Chen and P.-J. Zhang, ‘Integrated control of braking energy regeneration and pneumatic anti-lock braking’, *Proceedings of the Institution of Mechanical Engineers, Part D: Journal of Automobile Engineering*, vol. 224, no. 5, pp. 587–610, 1st May 2010. DOI: 10.1243/09544070JAUTO1307.
- [94] Zhang Jingming, Song Baoyu and Niu Xiaojing, ‘Optimization of parallel regenerative braking control strategy’, in *2008 IEEE Vehicle Power and Propulsion Conference*, Harbin, Hei Longjiang, China: IEEE, Sep. 2008, pp. 1–4. DOI: 10.1109/VPPC.2008.4677420.
- [95] A. T. Van Zanten, ‘Bosch ESP systems: 5 years of experience’, presented at the SAE 2000 Automotive Dynamics & Stability Conference, 15th May 2000, pp. 2000–01–1633. DOI: 10.4271/2000-01-1633.

- [96] G. De Filippis, B. Lenzo, A. Sorniotti, P. Gruber and W. De Nijs, ‘Energy-efficient torque-vectoring control of electric vehicles with multiple drivetrains’, *IEEE Transactions on Vehicular Technology*, vol. 67, no. 6, pp. 4702–4715, Jun. 2018. DOI: 10.1109/TVT.2018.2808186.
- [97] Z. Wang, U. Montanaro, S. Fallah, A. Sorniotti and B. Lenzo, ‘A gain scheduled robust linear quadratic regulator for vehicle direct yaw moment control’, *Mechatronics*, vol. 51, pp. 31–45, May 2018. DOI: 10.1016/j.mechatronics.2018.01.013.
- [98] B. Lenzo, M. Zanchetta, A. Sorniotti, P. Gruber and W. De Nijs, ‘Yaw rate and sideslip angle control through single input single output direct yaw moment control’, *IEEE Transactions on Control Systems Technology*, vol. 29, no. 1, pp. 124–139, Jan. 2021. DOI: 10.1109/TCST.2019.2949539.
- [99] R. Tchamna and I. Youn, ‘Yaw rate and side-slip control considering vehicle longitudinal dynamics’, *International Journal of Automotive Technology*, vol. 14, no. 1, pp. 53–60, Feb. 2013. DOI: 10.1007/s12239-013-0007-1.
- [100] M. Vignati and E. Sabbioni, ‘A cooperative control strategy for yaw rate and sideslip angle control combining torque vectoring with rear wheel steering’, *Vehicle System Dynamics*, pp. 1–34, 7th Jan. 2021. DOI: 10.1080/00423114.2020.1869273.
- [101] Y. Shibahata, K. Shimada and T. Tomari, ‘Improvement of vehicle maneuverability by direct yaw moment control’, *Vehicle System Dynamics*, vol. 22, no. 5, pp. 465–481, Jan. 1993. DOI: 10.1080/00423119308969044.
- [102] A. T. van Zanten and R. B. GmbH, ‘Evolution of electronic control systems for improving the vehicle dynamic behavior’, p. 9,
- [103] B. Lenzo, A. Sorniotti, P. Gruber and K. Sannen, ‘On the experimental analysis of single input single output control of yaw rate and sideslip angle’, *International Journal of Automotive Technology*, vol. 18, no. 5, pp. 799–811, Oct. 2017. DOI: 10.1007/s12239-017-0079-4.
- [104] T. Johansen, I. Petersen, J. Kalkkuhl and J. Ludemann, ‘Gain-scheduled wheel slip control in automotive brake systems’, *IEEE Transactions on Control Systems Technology*, vol. 11, no. 6, pp. 799–811, Nov. 2003. DOI: 10.1109/TCST.2003.815607.
- [105] L. Xiong, Z. Yu, Y. Wang, C. Yang and Y. Meng, ‘Vehicle dynamics control of four in-wheel motor drive electric vehicle using gain scheduling based on tyre cornering stiffness estimation’, *Vehicle System Dynamics*, vol. 50, no. 6, pp. 831–846, Jun. 2012. DOI: 10.1080/00423114.2012.663921.
- [106] M. Perrelli, G. Carbone, B. Lenzo and D. Mundo, ‘Design of understeer characteristics through torque vectoring on a lumped-parameter full vehicle model’, in *Advances in Italian Mechanism Science*, V. Niola and A. Gasparotto, Eds., vol. 91, Series Title: Mechanisms and Machine Science, Cham: Springer International Publishing, 2021, pp. 768–776. DOI: 10.1007/978-3-030-55807-9\_85.
- [107] F. Assadian and M. Hancock, ‘A comparison of yaw stability control strategies for the active differential’, in *Proceedings of the IEEE International Symposium on Industrial Electronics, 2005. ISIE 2005.*, Dubrovnik, Croatia: IEEE, 2005, pp. 373–378. DOI: 10.1109/ISIE.2005.1528939.

- [108] R. Marino and S. Scalzi, 'Asymptotic sideslip angle and yaw rate decoupling control in four-wheel steering vehicles', *Vehicle System Dynamics*, vol. 48, no. 9, pp. 999–1019, Sep. 2010. DOI: 10.1080/00423110903248686.
- [109] L. De Novellis, A. Sorniotti and P. Gruber, 'Wheel torque distribution criteria for electric vehicles with torque-vectoring differentials', *IEEE Transactions on Vehicular Technology*, vol. 63, no. 4, pp. 1593–1602, May 2014. DOI: 10.1109/TVT.2013.2289371.
- [110] L. De Novellis *et al.*, 'Direct yaw moment control actuated through electric drivetrains and friction brakes: Theoretical design and experimental assessment', *Mechatronics*, vol. 26, pp. 1–15, Mar. 2015. DOI: 10.1016/j.mechatronics.2014.12.003.
- [111] Hongtian Zhang and Jinzhu Zhang, 'Yaw torque control of electric vehicle stability', in *2012 IEEE 6th International Conference on Information and Automation for Sustainability*, Beijing, China: IEEE, Sep. 2012, pp. 318–322. DOI: 10.1109/ICIAFS.2012.6419924.
- [112] B. Li and F. Yu, 'Design of a vehicle lateral stability control system via a fuzzy logic control approach', *Proceedings of the Institution of Mechanical Engineers, Part D: Journal of Automobile Engineering*, vol. 224, no. 3, pp. 313–326, 1st Mar. 2010. DOI: 10.1243/09544070JAUTO1279.
- [113] C. Zhao, W. Xiang and P. Richardson, 'Vehicle lateral control and yaw stability control through differential braking', in *2006 IEEE International Symposium on Industrial Electronics*, Montreal, Que.: IEEE, Jul. 2006, pp. 384–389. DOI: 10.1109/ISIE.2006.295624.
- [114] Cong Geng, L. Mostefai, M. Denai and Y. Hori, 'Direct yaw-moment control of an in-wheel-motored electric vehicle based on body slip angle fuzzy observer', *IEEE Transactions on Industrial Electronics*, vol. 56, no. 5, pp. 1411–1419, May 2009. DOI: 10.1109/TIE.2009.2013737.
- [115] M. Jalali, E. Hashemi, A. Khajepour, S.-k. Chen and B. Litkouhi, 'Integrated model predictive control and velocity estimation of electric vehicles', *Mechatronics*, vol. 46, pp. 84–100, Oct. 2017. DOI: 10.1016/j.mechatronics.2017.07.002.
- [116] G. Palmieri, M. Barić, L. Glielmo and F. Borrelli, 'Robust vehicle lateral stabilisation via set-based methods for uncertain piecewise affine systems', *Vehicle System Dynamics*, vol. 50, no. 6, pp. 861–882, Jun. 2012. DOI: 10.1080/00423114.2012.666353.
- [117] P. Falcone, F. Borrelli, J. Asgari, H. E. Tseng and D. Hrovat, 'Predictive active steering control for autonomous vehicle systems', *IEEE Transactions on Control Systems Technology*, vol. 15, no. 3, pp. 566–580, May 2007. DOI: 10.1109/TCST.2007.894653.
- [118] P. Falcone, H. Eric Tseng, F. Borrelli, J. Asgari and D. Hrovat, 'MPC-based yaw and lateral stabilisation via active front steering and braking', *Vehicle System Dynamics*, vol. 46, pp. 611–628, sup1 Sep. 2008. DOI: 10.1080/00423110802018297.
- [119] B. Ren, H. Chen, H. Zhao and L. Yuan, 'MPC-based yaw stability control in in-wheel-motored EV via active front steering and motor torque distribution', *Mechatronics*, vol. 38, pp. 103–114, Sep. 2016. DOI: 10.1016/j.mechatronics.2015.10.002.

- [120] S. Anwar, 'Generalized predictive control of yaw dynamics of a hybrid brake-by-wire equipped vehicle', *Mechatronics*, vol. 15, no. 9, pp. 1089–1108, Nov. 2005. DOI: 10.1016/j.mechatronics.2005.06.006.
- [121] L. Del Re, Ed., *Automotive model predictive control: models, methods and applications*, Lecture notes in control and information sciences 402, OCLC: ocn471801791, Berlin: Springer, 2010, 284 pp.
- [122] N. Guo, B. Lenzo, X. Zhang, Y. Zou, R. Zhai and T. Zhang, 'A real-time nonlinear model predictive controller for yaw motion optimization of distributed drive electric vehicles', *IEEE Transactions on Vehicular Technology*, vol. 69, no. 5, pp. 4935–4946, May 2020. DOI: 10.1109/TVT.2020.2980169.
- [123] B. Wang, X. Huang, J. Wang, X. Guo and X. Zhu, 'A robust wheel slip ratio control design combining hydraulic and regenerative braking systems for in-wheel-motors-driven electric vehicles', *Journal of the Franklin Institute*, vol. 352, no. 2, pp. 577–602, Feb. 2015. DOI: 10.1016/j.jfranklin.2014.06.004.
- [124] H. Yu, M. Huang and Z. Zhang, 'Direct yaw-moment hinfinity control of motor-wheel driving electric vehicle', in *2013 IEEE Vehicle Power and Propulsion Conference (VPPC)*, Beijing: IEEE, Oct. 2013, pp. 1–5. DOI: 10.1109/VPPC.2013.6671676.
- [125] V. Cerone, M. Milanese and D. Regruto, 'Yaw stability control design through a mixed sensitivity approach', in *2007 IEEE Intelligent Vehicles Symposium*, ISSN: 1931-0587, Istanbul, Turkey: IEEE, Jun. 2007, pp. 805–810. DOI: 10.1109/IVS.2007.4290215.
- [126] Q. Lu, A. Sornioti, P. Gruber, J. Theunissen and J. De Smet, 'H loop shaping for the torque-vectoring control of electric vehicles: Theoretical design and experimental assessment', *Mechatronics*, vol. 35, pp. 32–43, May 2016. DOI: 10.1016/j.mechatronics.2015.12.005.
- [127] A. Gimondi, M. Corno and S. M. Savaresi, 'Linear parameter varying path tracking control for over-actuated electric vehicles', *Frontiers in Control Engineering*, vol. 2, p. 750 190, 27th Oct. 2021. DOI: 10.3389/fcteg.2021.750190.
- [128] S. Zheng, H. Tang, Z. Han and Y. Zhang, 'Controller design for vehicle stability enhancement', *Control Engineering Practice*, vol. 14, no. 12, pp. 1413–1421, Dec. 2006. DOI: 10.1016/j.conengprac.2005.10.005.
- [129] M. Shino, 'Yaw-moment control of electric vehicle for improving handling and stability', *JSAE Review*, vol. 22, no. 4, pp. 473–480, Oct. 2001. DOI: 10.1016/S0389-4304(01)00130-8.
- [130] X. Liu, Y. Wu, Y. Zhang and S. Xiao, 'A control method to make LQR robust: A planes cluster approaching mode', *International Journal of Control, Automation and Systems*, vol. 12, no. 2, pp. 302–308, Apr. 2014. DOI: 10.1007/s12555-012-0435-0.
- [131] L. Li, G. Jia, J. Chen, H. Zhu, D. Cao and J. Song, 'A novel vehicle dynamics stability control algorithm based on the hierarchical strategy with constrain of nonlinear tyre forces', *Vehicle System Dynamics*, vol. 53, no. 8, pp. 1093–1116, 3rd Aug. 2015. DOI: 10.1080/00423114.2015.1025082.

- [132] E. Esmailzadeh, A. Goodarzi and G. Vossoughi, 'Optimal yaw moment control law for improved vehicle handling', *Mechatronics*, vol. 13, no. 7, pp. 659–675, Sep. 2003. DOI: 10.1016/S0957-4158(02)00036-3.
- [133] C. Hu, R. Wang, F. Yan and N. Chen, 'Output constraint control on path following of four-wheel independently actuated autonomous ground vehicles', *IEEE Transactions on Vehicular Technology*, vol. 65, no. 6, pp. 4033–4043, Jun. 2016. DOI: 10.1109/TVT.2015.2472975.
- [134] M. Vignati, E. Sabbioni and D. Tarsitano, 'Torque vectoring control for IWM vehicles', *International Journal of Vehicle Performance*, vol. 2, no. 3, p. 302, 2016. DOI: 10.1504/IJVP.2016.078561.
- [135] K. Nam, H. Fujimoto and Y. Hori, 'Advanced motion control of electric vehicles based on robust lateral tire force control via active front steering', *IEEE/ASME Transactions on Mechatronics*, vol. 19, no. 1, pp. 289–299, Feb. 2014. DOI: 10.1109/TMECH.2012.2233210.
- [136] Q. Lu *et al.*, 'Enhancing vehicle cornering limit through sideslip and yaw rate control', *Mechanical Systems and Signal Processing*, vol. 75, pp. 455–472, Jun. 2016. DOI: 10.1016/j.ymssp.2015.11.028.
- [137] Haiping Du, Nong Zhang and Guangming Dong, 'Stabilizing vehicle lateral dynamics with considerations of parameter uncertainties and control saturation through robust yaw control', *IEEE Transactions on Vehicular Technology*, vol. 59, no. 5, pp. 2593–2597, 2010. DOI: 10.1109/TVT.2010.2045520.
- [138] V. Utkin, 'Sliding mode control design principles and applications to electric drives', *IEEE Transactions on Industrial Electronics*, vol. 40, no. 1, pp. 23–36, Feb. 1993. DOI: 10.1109/41.184818.
- [139] M. Abe, 'Side-slip control to stabilize vehicle lateral motion by direct yaw moment', *JSAE Review*, vol. 22, no. 4, pp. 413–419, Oct. 2001. DOI: 10.1016/S0389-4304(01)00124-2.
- [140] D. Thang Truong, M. Meywerk and W. Tomaske, 'Torque vectoring for rear axle using adaptive sliding mode control', in *2013 International Conference on Control, Automation and Information Sciences (ICCAIS)*, Nha Trang, Vietnam: IEEE, Nov. 2013, pp. 328–333. DOI: 10.1109/ICCAIS.2013.6720577.
- [141] S. Ding, L. Liu and W. X. Zheng, 'Sliding mode direct yaw-moment control design for in-wheel electric vehicles', *IEEE Transactions on Industrial Electronics*, vol. 64, no. 8, pp. 6752–6762, Aug. 2017. DOI: 10.1109/TIE.2017.2682024.
- [142] C. Fu, R. Hoseinnezhad, A. B. Hadiashar and R. N. Jazar, 'Electric vehicle side-slip control via electronic differential', *International Journal of Vehicle Autonomous Systems*, vol. 13, no. 1, p. 1, 2015. DOI: 10.1504/IJVAS.2015.070724.
- [143] M. Hancock, R. Williams, E. Fina and M. Best, 'Yaw motion control via active differentials', *Transactions of the Institute of Measurement and Control*, vol. 29, no. 2, pp. 137–157, Jun. 2007. DOI: 10.1177/0142331207069489.

- [144] M. Vignati, E. Sabbioni, D. Tarsitano and F. Cheli, ‘Electric powertrain layouts analysis for controlling vehicle lateral dynamics with torque vectoring’, in *2017 International Conference of Electrical and Electronic Technologies for Automotive*, Torino, Italy: IEEE, Jun. 2017, pp. 1–5. DOI: 10.23919/EETA.2017.7993204.
- [145] T. Grigoratos and G. Martini, ‘Brake wear particle emissions: A review’, *Environmental Science and Pollution Research*, vol. 22, no. 4, pp. 2491–2504, Feb. 2015. DOI: 10.1007/s11356-014-3696-8.
- [146] M. Nowak and J. Pielecha, ‘Comparison of exhaust emission on the basis of real driving emissions measurements and simulations’, *MATEC Web of Conferences*, vol. 118, J. Pielecha, Ed., p. 00026, 2017. DOI: 10.1051/mateconf/201711800026.
- [147] S. Murata, ‘Innovation by in-wheel-motor drive unit’, *Vehicle System Dynamics*, vol. 50, no. 6, pp. 807–830, Jun. 2012. DOI: 10.1080/00423114.2012.666354.
- [148] K. Bayar, J. Wang and G. Rizzoni, ‘Development of a vehicle stability control strategy for a hybrid electric vehicle equipped with axle motors’, *Proceedings of the Institution of Mechanical Engineers, Part D: Journal of Automobile Engineering*, vol. 226, no. 6, pp. 795–814, Jun. 2012. DOI: 10.1177/0954407011433396.
- [149] Z. Shuai, H. Zhang, J. Wang, J. Li and M. Ouyang, ‘Lateral motion control for four-wheel-independent-drive electric vehicles using optimal torque allocation and dynamic message priority scheduling’, *Control Engineering Practice*, vol. 24, pp. 55–66, Mar. 2014. DOI: 10.1016/j.conengprac.2013.11.012.
- [150] H. Tseng, D. Madau, B. Ashrafi, T. Brown and D. Recker, ‘Technical challenges in the development of vehicle stability control system’, in *Proceedings of the 1999 IEEE International Conference on Control Applications (Cat. No.99CH36328)*, vol. 2, Kohala Coast, HI, USA: IEEE, 1999, pp. 1660–1666. DOI: 10.1109/CCA.1999.801221.
- [151] F. Li, J. Wang and Z. Liu, ‘Motor torque based vehicle stability control for four-wheel-drive electric vehicle’, in *2009 IEEE Vehicle Power and Propulsion Conference*, Dearborn, MI, USA: IEEE, Sep. 2009, pp. 1596–1601. DOI: 10.1109/VPPC.2009.5289613.
- [152] H. Fuse and H. Fujimoto, ‘Fundamental study on driving force control method for independent-four-wheel-drive electric vehicle considering tire slip angle’, in *IECON 2018 - 44th Annual Conference of the IEEE Industrial Electronics Society*, D.C., DC, USA: IEEE, Oct. 2018, pp. 2062–2067. DOI: 10.1109/IECON.2018.8591289.
- [153] B. Guo and Y. Chen, ‘Robust adaptive fault-tolerant control of four-wheel independently actuated electric vehicles’, *IEEE Transactions on Industrial Informatics*, vol. 16, no. 5, pp. 2882–2894, May 2020. DOI: 10.1109/TII.2018.2889292.
- [154] L. Guo, P. Ge and D. Sun, ‘Torque distribution algorithm for stability control of electric vehicle driven by four in-wheel motors under emergency conditions’, *IEEE Access*, vol. 7, pp. 104737–104748, 2019. DOI: 10.1109/ACCESS.2019.2931505.

- [155] P. He, Y. Hori, M. Kamachi, K. Walters and H. Yoshida, 'Future motion control to be realized by in-wheel motored electric vehicle', in *31st Annual Conference of IEEE Industrial Electronics Society, 2005. IECON 2005.*, Raleigh, NC, USA: IEEE, 2005, 6 pp. DOI: 10.1109/IECON.2005.1569322.
- [156] Kanghyun Nam, H. Fujimoto and Y. Hori, 'Lateral stability control of in-wheel-motor-driven electric vehicles based on sideslip angle estimation using lateral tire force sensors', *IEEE Transactions on Vehicular Technology*, vol. 61, no. 5, pp. 1972–1985, 2012. DOI: 10.1109/TVT.2012.2191627.
- [157] J. Kang, J. Yoo and K. Yi, 'Driving control algorithm for maneuverability, lateral stability, and rollover prevention of 4wd electric vehicles with independently driven front and rear wheels', *IEEE Transactions on Vehicular Technology*, vol. 60, no. 7, pp. 2987–3001, Sep. 2011. DOI: 10.1109/TVT.2011.2155105.
- [158] D. Kim and H. Kim, 'Vehicle stability control with regenerative braking and electronic brake force distribution for a four-wheel drive hybrid electric vehicle', *Proceedings of the Institution of Mechanical Engineers, Part D: Journal of Automobile Engineering*, vol. 220, no. 6, pp. 683–693, 1st Jun. 2006. DOI: 10.1243/09544070D00605.
- [159] J. Kim and H. Kim, 'Electric vehicle yaw rate control using independent in-wheel motor', in *2007 Power Conversion Conference - Nagoya*, Nagoya, Japan: IEEE, Apr. 2007, pp. 705–710. DOI: 10.1109/PCCON.2007.373043.
- [160] M. Liu, J. Huang and M. Cao, 'Handling stability improvement for a four-axle hybrid electric ground vehicle driven by in-wheel motors', *IEEE Access*, vol. 6, pp. 2668–2682, 2018. DOI: 10.1109/ACCESS.2017.2784836.
- [161] C. Lv, J. Zhang and Y. Li, 'Extended-kalman-filter-based regenerative and friction blended braking control for electric vehicle equipped with axle motor considering damping and elastic properties of electric powertrain', *Vehicle System Dynamics*, vol. 52, no. 11, pp. 1372–1388, 2nd Nov. 2014. DOI: 10.1080/00423114.2014.938663.
- [162] N. Mutoh, 'Driving and braking torque distribution methods for front- and rear-wheel-independent drive-type electric vehicles on roads with low friction coefficient', *IEEE Transactions on Industrial Electronics*, vol. 59, no. 10, pp. 3919–3933, Oct. 2012. DOI: 10.1109/TIE.2012.2186772.
- [163] B. Najjari, M. Mirzaei and A. Tahouni, 'Constrained stability control with optimal power management strategy for in-wheel electric vehicles', *Proceedings of the Institution of Mechanical Engineers, Part K: Journal of Multi-body Dynamics*, vol. 233, no. 4, pp. 1014–1032, Dec. 2019. DOI: 10.1177/1464419319856953.
- [164] S. Sakai, H. Sado and Y. Hori, 'Motion control in an electric vehicle with four independently driven in-wheel motors', *IEEE/ASME Transactions on Mechatronics*, vol. 4, no. 1, pp. 9–16, Mar. 1999. DOI: 10.1109/3516.752079.
- [165] F. Tahami, S. Farhangi and R. Kazemi, 'A fuzzy logic direct yaw-moment control system for all-wheel-drive electric vehicles', *Vehicle System Dynamics*, vol. 41, no. 3, pp. 203–221, 1st Jan. 2004. DOI: 10.1076/vesd.41.3.203.26510.

- [166] Q. Wang, B. Ayalew and A. Singh, 'Control allocation for multi-axle hub motor driven land vehicles', *SAE International Journal of Alternative Powertrains*, vol. 5, no. 2, pp. 338–347, 5th Apr. 2016. DOI: 10.4271/2016-01-1670.
- [167] G. Yin, R. Wang and J. Wang, 'Robust control for four wheel independently-actuated electric ground vehicles by external yaw-moment generation', *International Journal of Automotive Technology*, vol. 16, no. 5, pp. 839–847, Oct. 2015. DOI: 10.1007/s12239-015-0086-2.
- [168] L. Zhai, T. Sun and J. Wang, 'Electronic stability control based on motor driving and braking torque distribution for a four in-wheel motor drive electric vehicle', *IEEE Transactions on Vehicular Technology*, vol. 65, no. 6, pp. 4726–4739, Jun. 2016. DOI: 10.1109/TVT.2016.2526663.
- [169] J. Chen, J. Yu, K. Zhang and Y. Ma, 'Control of regenerative braking systems for four-wheel-independently-actuated electric vehicles', *Mechatronics*, vol. 50, pp. 394–401, Apr. 2018. DOI: 10.1016/j.mechatronics.2017.06.005.
- [170] Y. Chen, J. K. Hedrick and K. Guo, 'A novel direct yaw moment controller for in-wheel motor electric vehicles', *Vehicle System Dynamics*, vol. 51, no. 6, pp. 925–942, Jun. 2013. DOI: 10.1080/00423114.2013.773453.
- [171] S. Müller, M. Uchanski and K. Hedrick, 'Estimation of the maximum tire-road friction coefficient', *Journal of Dynamic Systems, Measurement, and Control*, vol. 125, no. 4, pp. 607–617, 1st Dec. 2003. DOI: 10.1115/1.1636773.
- [172] 'Monitoring tire-road friction using the wheel slip', *IEEE Control Systems*, vol. 18, no. 4, pp. 42–49, Aug. 1998. DOI: 10.1109/37.710877.
- [173] L. Alvarez, J. Yi, R. Horowitz and L. Olmos, 'Dynamic friction model-based tire-road friction estimation and emergency braking control', *Journal of Dynamic Systems, Measurement, and Control*, vol. 127, no. 1, pp. 22–32, 1st Mar. 2005. DOI: 10.1115/1.1870036.
- [174] K. Yi, K. Hedrick and S.-C. Lee, 'Estimation of tire-road friction using observer based identifiers', *Vehicle System Dynamics*, vol. 31, no. 4, pp. 233–261, 1st Apr. 1999. DOI: 10.1076/vesd.31.4.233.4231.
- [175] C. Lee, K. Hedrick and K. Yi, 'Real-time slip-based estimation of maximum tire-road friction coefficient', *IEEE/ASME Transactions on Mechatronics*, vol. 9, no. 2, pp. 454–458, Jun. 2004. DOI: 10.1109/TMECH.2004.828622.
- [176] D. Piyabongkarn, R. Rajamani, J. Grogg and J. Lew, 'Development and experimental evaluation of a slip angle estimator for vehicle stability control', *IEEE Transactions on Control Systems Technology*, vol. 17, no. 1, pp. 78–88, Jan. 2009. DOI: 10.1109/TCST.2008.922503.
- [177] L. R. Ray, 'Nonlinear tire force estimation and road friction identification: Simulation and experiments', *Automatica*, vol. 33, no. 10, pp. 1819–1833, Oct. 1997. DOI: 10.1016/S0005-1098(97)00093-9.
- [178] L. Ray, 'Nonlinear state and tire force estimation for advanced vehicle control', *IEEE Transactions on Control Systems Technology*, vol. 3, no. 1, pp. 117–124, Mar. 1995. DOI: 10.1109/87.370717.
- [179] 'Tire-road friction-coefficient estimation', *IEEE Control Systems*, vol. 30, no. 4, pp. 54–69, Aug. 2010. DOI: 10.1109/MCS.2010.937006.

- [180] F. Gustafsson, 'Slip-based tire-road friction estimation', *Automatica*, vol. 33, no. 6, pp. 1087–1099, Jun. 1997. DOI: 10.1016/S0005-1098(97)00003-4.
- [181] A. Lutz *et al.*, 'Simulation methods supporting homologation of electronic stability control in vehicle variants', *Vehicle System Dynamics*, vol. 55, no. 10, pp. 1432–1497, 3rd Oct. 2017. DOI: 10.1080/00423114.2017.1322705.
- [182] *ISO26262 road vehicle – functional safety*, in collab. with I. E. C. I. 2018, 2018.
- [183] *IEC-61508, functional safety of electric/ electronic/ programmable safety-related systems*, in collab. with I. E. C. IEC, 2010.
- [184] W. Dieterle, 'Mechatronic systems: Automotive applications and modern design methodologies', *Annual Reviews in Control*, vol. 29, no. 2, pp. 273–277, Jan. 2005. DOI: 10.1016/j.arcontrol.2005.05.002.
- [185] M. Krammer, 'The distributed co-simulation protocol for the integration of real-time systems and simulation environments', in *Proceedings of the 50th Computer Simulation Conference*, University of Bordeaux, Bordeaux, France: Society for Modeling and Simulation International (SCS), 2018. DOI: 10.22360/SummerSim.2018.SCSC.001.
- [186] D. Auslander, 'What is mechatronics?', *IEEE/ASME Transactions on Mechatronics*, vol. 1, no. 1, pp. 5–9, Mar. 1996. DOI: 10.1109/3516.491404.
- [187] L. Berzi, M. Delogu and M. Pierini, 'Development of driving cycles for electric vehicles in the context of the city of florence', *Transportation Research Part D: Transport and Environment*, vol. 47, pp. 299–322, Aug. 2016. DOI: 10.1016/j.trd.2016.05.010.
- [188] J. Demuyneck, D. Bosteels, M. De Paepe, C. Favre, J. May and S. Verhelst, 'Recommendations for the new WLTP cycle based on an analysis of vehicle emission measurements on NEDC and CADC', *Energy Policy*, vol. 49, pp. 234–242, Oct. 2012. DOI: 10.1016/j.enpol.2012.05.081.
- [189] A. Sidhu, D. A. Guenther and G. J. Heydinger, 'Development of a method to assess vehicle stability and controllability in open and closed-loop maneuvers', presented at the SAE 2010 World Congress & Exhibition, 12th Apr. 2010, pp. 2010-01-0111. DOI: 10.4271/2010-01-0111.
- [190] M. Hal, 'Is vehicle characterization in accordance with standard test procedures a necessary prerequisite for validating computer models of a test vehicle?', 2014, Publisher: Dublin Institute of Technology. DOI: 10.21427/D76604.
- [191] J. Pauwelussen, 'The driver experience under extreme lane change conditions', *International Journal of Driving Science*, vol. 1, no. 1, p. 1, 26th Nov. 2018. DOI: 10.5334/ijds.7.
- [192] K. Rahman, N. Patel, T. Ward, J. Nagashima, F. Caricchi and F. Crescimbin, 'Application of direct-drive wheel motor for fuel cell electric and hybrid electric vehicle propulsion system', *IEEE Transactions on Industry Applications*, vol. 42, no. 5, pp. 1185–1192, Sep. 2006. DOI: 10.1109/TIA.2006.880886.
- [193] R. N. Tuncay, O. Ustun, M. Yilmaz, C. Gokce and U. Karakaya, 'Design and implementation of an electric drive system for in-wheel motor electric vehicle applications', in *2011 IEEE Vehicle Power and Propulsion Conference*, Chicago, IL, USA: IEEE, Sep. 2011, pp. 1–6. DOI: 10.1109/VPPC.2011.6043070.

- [194] M. Montani *et al.*, ‘ESC on in-wheel motors driven electric vehicle: Handling and stability performances assessment’, in *2020 IEEE International Conference on Environment and Electrical Engineering and 2020 IEEE Industrial and Commercial Power Systems Europe (EEEIC / I&CPS Europe)*, Madrid, Spain: IEEE, Jun. 2020, pp. 1–6. DOI: 10.1109/EEEIC/ICPSEurope49358.2020.9160768.
- [195] A. M. Dizqah, B. Lenzo, A. Sorniotti, P. Gruber, S. Fallah and J. De Smet, ‘A fast and parametric torque distribution strategy for four-wheel-drive energy-efficient electric vehicles’, *IEEE Transactions on Industrial Electronics*, vol. 63, no. 7, pp. 4367–4376, Jul. 2016. DOI: 10.1109/TIE.2016.2540584.
- [196] ‘Optimal yaw-rate target for electric vehicle torque vectoring system’, in *The Dynamics of Vehicles on Roads and Tracks*, M. Rosenberger, M. Plochl, K. Six and J. Edelmann, Eds., 0th ed., CRC Press, 30th Mar. 2016, pp. 122–129. DOI: 10.1201/b21185-12.
- [197] N. Guo, X. Zhang, Y. Zou, B. Lenzo and T. Zhang, ‘A computationally efficient path-following control strategy of autonomous electric vehicles with yaw motion stabilization’, *IEEE Transactions on Transportation Electrification*, vol. 6, no. 2, pp. 728–739, Jun. 2020. DOI: 10.1109/TTE.2020.2993862.
- [198] L. Pugi, T. Favilli, L. Berzi, E. Locorotondo and M. Pierini, ‘Application of regenerative braking on electric vehicles’, in *2019 IEEE International Conference on Environment and Electrical Engineering and 2019 IEEE Industrial and Commercial Power Systems Europe (EEEIC / I&CPS Europe)*, Genova, Italy: IEEE, Jun. 2019, pp. 1–6. DOI: 10.1109/EEEIC.2019.8783318.
- [199] T. Favilli, L. Pugi, L. Berzi, M. Pierini and N. Tobia, ‘Regenerative fuzzy brake blending strategy on benchmark electric vehicle: The FIAT 500e’, in *2020 IEEE International Conference on Environment and Electrical Engineering and 2020 IEEE Industrial and Commercial Power Systems Europe (EEEIC / I&CPS Europe)*, Madrid, Spain: IEEE, Jun. 2020, pp. 1–6. DOI: 10.1109/EEEIC/ICPSEurope49358.2020.9160584.
- [200] J. Wang, W. Li, J. Li, Y. Liu, B. Song and H. Gao, ‘Modeling a driver’s directional and longitudinal speed control based on racing track features’, *Shock and Vibration*, vol. 2018, pp. 1–12, 2018. DOI: 10.1155/2018/7487295.
- [201] C. C. MacAdam, ‘An optimal preview control for linear systems’, *Journal of Dynamic Systems, Measurement, and Control*, vol. 102, no. 3, pp. 188–190, 1st Sep. 1980. DOI: 10.1115/1.3139632.
- [202] C. C. MacAdam, ‘Application of an optimal preview control for simulation of closed-loop automobile driving’, *IEEE Transactions on Systems, Man, and Cybernetics*, vol. 11, no. 6, pp. 393–399, 1981. DOI: 10.1109/TSMC.1981.4308705.
- [203] J. C. Gerdes and J. K. Hedrick, ‘Brake system modeling for simulation and control’, *Journal of Dynamic Systems, Measurement, and Control*, vol. 121, no. 3, pp. 496–503, 1st Sep. 1999. DOI: 10.1115/1.2802501.

- [204] P. Delaigue and A. Eskandarian, 'A comprehensive vehicle braking model for predictions of stopping distances', *Proceedings of the Institution of Mechanical Engineers, Part D: Journal of Automobile Engineering*, vol. 218, no. 12, pp. 1409–1417, 1st Dec. 2004. DOI: 10.1243/0954407042707641.
- [205] L. K. Ming, 'Hydraulic brake system modeling and control for active control of vehicle dynamics', in *Proceedings of the 1999 American Control Conference (Cat. No. 99CH36251)*, San Diego, CA, USA: IEEE, 1999, 4538–4542 vol.6. DOI: 10.1109/ACC.1999.786447.
- [206] P. G. Anselma, S. P. Patil and G. Belingardi, 'Rapid optimal design of a light vehicle hydraulic brake system', presented at the WCX SAE World Congress Experience, 2nd Apr. 2019, pp. 2019–01–0831. DOI: 10.4271/2019-01-0831.
- [207] J. G. Hayes and G. A. Goodarzi, *Electric powertrain: energy systems, power electronics & drives for hybrid, electric & fuel cell vehicles*. 2018, OCLC: 1156656784.
- [208] W. Enang and C. Bannister, 'Modelling and control of hybrid electric vehicles (a comprehensive review)', *Renewable and Sustainable Energy Reviews*, vol. 74, pp. 1210–1239, Jul. 2017. DOI: 10.1016/j.rser.2017.01.075.
- [209] N. H. Amer, H. Zamzuri, K. Hudha and Z. A. Kadir, 'Modelling and control strategies in path tracking control for autonomous ground vehicles: A review of state of the art and challenges', *Journal of Intelligent & Robotic Systems*, vol. 86, no. 2, pp. 225–254, May 2017. DOI: 10.1007/s10846-016-0442-0.
- [210] L. Pugi, T. Favilli, L. Berzi, E. Locorotondo and M. Pierini, 'Brake blending and torque vectoring of road electric vehicles: A flexible approach based on smart torque allocation.', p. 39,
- [211] X. Zhao, L. Li, X. Wang, M. Mei, C. Liu and J. Song, 'Braking force decoupling control without pressure sensor for a novel series regenerative brake system', *Proceedings of the Institution of Mechanical Engineers, Part D: Journal of Automobile Engineering*, vol. 233, no. 7, pp. 1750–1766, Jun. 2019. DOI: 10.1177/0954407018785740.
- [212] W. Han, L. Xiong and Z. Yu, 'A novel pressure control strategy of an electro-hydraulic brake system via fusion of control signals', *Proceedings of the Institution of Mechanical Engineers, Part D: Journal of Automobile Engineering*, vol. 233, no. 13, pp. 3342–3357, Nov. 2019. DOI: 10.1177/0954407018821016.
- [213] L. Pugi *et al.*, 'Fast modelling and identification of hydraulic brake plants for automotive applications', *International Journal of Fluid Power*, 29th Nov. 2020. DOI: 10.13052/ijfp1439-9776.2122.
- [214] T. D'hondt *et al.*, 'Modeling and identification of an electric vehicle braking system: Thermal and tribology phenomena assessment', presented at the WCX SAE World Congress Experience, 14th Apr. 2020, pp. 2020–01–1094. DOI: 10.4271/2020-01-1094.
- [215] A. Robertson and D. Gross, 'An electrical-analog method for transient heat-flow analysis', *Journal of Research of the National Bureau of Standards*, vol. 61, no. 2, p. 105, Aug. 1958. DOI: 10.6028/jres.061.016.

- [216] J. Wahlström, ‘A comparison of measured and simulated friction, wear, and particle emission of disc brakes’, *Tribology International*, vol. 92, pp. 503–511, Dec. 2015. DOI: 10.1016/j.triboint.2015.07.036.
- [217] S. Andersson, ‘Wear simulation’, in *Advanced Knowledge Application in Practice*, I. Fuerstner, Ed., Sciyo, 2nd Nov. 2010. DOI: 10.5772/10349.
- [218] G. Perricone *et al.*, ‘A concept for reducing PM 10 emissions for car brakes by 50%’, *Wear*, vol. 396–397, pp. 135–145, Feb. 2018. DOI: 10.1016/j.wear.2017.06.018.
- [219] W. Li, X. Zhu and J. Ju, ‘Hierarchical braking torque control of in-wheel-motor-driven electric vehicles over CAN’, *IEEE Access*, vol. 6, pp. 65 189–65 198, 2018. DOI: 10.1109/ACCESS.2018.2877960.
- [220] R. de Castro, R. E. Araújo and D. Freitas, ‘HYBRID ABS WITH ELECTRIC MOTOR AND FRICTION BRAKES’, p. 7,
- [221] L. Berzi *et al.*, ‘Brake blending strategy on electric vehicle co-simulation between MATLAB simulink<sup>®</sup> and simcenter amesim<sup>™</sup>’, in *2019 IEEE 5th International forum on Research and Technology for Society and Industry (RTSI)*, Florence, Italy: IEEE, Sep. 2019, pp. 308–313. DOI: 10.1109/RTSI.2019.8895548.
- [222] A. Adriano *et al.*, ‘Design of a new on-board energy storage and conversion system for a fast charging urban transport electric bus’, in *2021 IEEE International Conference on Environment and Electrical Engineering and 2021 IEEE Industrial and Commercial Power Systems Europe (EEEIC / I&CPS Europe)*, Bari, Italy: IEEE, 7th Sep. 2021, pp. 1–6. DOI: 10.1109/EEEIC/ICPSEurope51590.2021.9584573.
- [223] L. Berzi *et al.*, ‘Smart energy management of auxiliary load for electric vehicles’, in *2020 IEEE International Conference on Environment and Electrical Engineering and 2020 IEEE Industrial and Commercial Power Systems Europe (EEEIC / I&CPS Europe)*, Madrid, Spain: IEEE, Jun. 2020, pp. 1–6. DOI: 10.1109/EEEIC/ICPSEurope49358.2020.9160762.
- [224] K. Yamamoto, M. Ponchant, F. Sellier, T. Favilli, L. Pugi and L. Berzi, ‘48v electric vehicle powertrain optimal model-based design methodology’, in *2020 AEIT International Conference of Electrical and Electronic Technologies for Automotive (AEIT AUTOMOTIVE)*, Turin, Italy: IEEE, 18th Nov. 2020, pp. 1–6. DOI: 10.23919/AEITAUTOMOTIVE50086.2020.9307407.
- [225] Zijian Zhang, Guoqing Xu, Weimin Li and Liang Zheng, ‘Regenerative braking for electric vehicle based on fuzzy logic control strategy’, in *2010 2nd International Conference on Mechanical and Electronics Engineering*, Kyoto, Japan: IEEE, Aug. 2010, pp. V1–319–V1–323. DOI: 10.1109/ICMEE.2010.5558540.
- [226] T. J. Ross, *Fuzzy logic with engineering applications*, 3rd ed. Chichester, U.K: John Wiley, 2010, 585 pp., OCLC: ocn430736639.
- [227] M. Cirstea, A. Dinu and M. McCormick, *Neural and Fuzzy Logic Control of Drives and Power Systems*. Burlington: Elsevier, 2002, OCLC: 437182155.

- [228] S. Onori, P. Spagnol, V. Marano, Y. Guezennec and G. Rizzoni, 'A new life estimation method for lithium-ion batteries in plug-in hybrid electric vehicles applications', *International Journal of Power Electronics*, vol. 4, no. 3, p. 302, 2012. DOI: 10.1504/IJPELEC.2012.046609.
- [229] N. Omar *et al.*, 'Lithium iron phosphate based battery – assessment of the aging parameters and development of cycle life model', *Applied Energy*, vol. 113, pp. 1575–1585, Jan. 2014. DOI: 10.1016/j.apenergy.2013.09.003.
- [230] C. Huang, F. Naghdy, H. Du and H. Huang, 'Fault tolerant steer-by-wire systems: An overview', *Annual Reviews in Control*, vol. 47, pp. 98–111, 2019. DOI: 10.1016/j.arcontrol.2019.04.001.
- [231] S. A. Zulkifli, V. S. Asirvadam, N. Saad, A. R. A. Aziz and A. A. M. Mohideen, 'Implementation of electronic throttle-by-wire for a hybrid electric vehicle using national instruments' CompactRIO and LabVIEW real-time', in *2014 5th International Conference on Intelligent and Advanced Systems (ICIAS)*, Kuala Lumpur, Malaysia: IEEE, Jun. 2014, pp. 1–6. DOI: 10.1109/ICIAS.2014.6869555.
- [232] P. Kafka, 'The automotive standard ISO 26262, the innovative driver for enhanced safety assessment & technology for motor cars', *Procedia Engineering*, vol. 45, pp. 2–10, 2012. DOI: 10.1016/j.proeng.2012.08.112.
- [233] C. Lidstrom, C. Bondesson, M. Nyberg and J. Westman, 'Improved pattern for ISO 26262 ASIL decomposition with dependent requirements', in *2019 IEEE 19th International Conference on Software Quality, Reliability and Security Companion (QRS-C)*, Sofia, Bulgaria: IEEE, Jul. 2019, pp. 28–35. DOI: 10.1109/QRS-C.2019.00019.
- [234] K.-L. Leu, H. Huang, Y.-Y. Chen, L.-R. Huang and K.-M. Ji, 'An intelligent brake-by-wire system design and analysis in accordance with ISO-26262 functional safety standard', in *2015 International Conference on Connected Vehicles and Expo (ICCVEx)*, Shenzhen, China: IEEE, Oct. 2015, pp. 150–156. DOI: 10.1109/ICCVEx.2015.20.
- [235] V. Bernon-Enjalbert, M. Blazy-Winning, R. Gubian, D. Lopez, J.-P. Meunier and M. O'Donnell, 'Safety-integrated hardware solutions to support ASIL-d applications', p. 9,
- [236] M. Hasegawa and T. Kaneko, 'Examination of hazard analysis and risk assessment and exposure research in the real traffic situation of ISO 26262 for motorcycles', *SAE International Journal of Passenger Cars - Electronic and Electrical Systems*, vol. 10, no. 1, pp. 95–101, 8th Nov. 2016. DOI: 10.4271/2016-32-0058.
- [237] R. Rana, M. Staron, C. Berger, J. Hansson, M. Nilsson and F. Törner, 'Improving fault injection in automotive model based development using fault bypass modeling', p. 15,
- [238] H. Ziade, R. Ayoubi and R. Velazco, 'A survey on fault injection techniques', vol. 1, no. 2, p. 16, 2004.
- [239] M. Kooli and G. Di Natale, 'A survey on simulation-based fault injection tools for complex systems', in *2014 9th IEEE International Conference on Design & Technology of Integrated Systems in Nanoscale Era (DTIS)*, Santorini, Greece: IEEE, May 2014, pp. 1–6. DOI: 10.1109/DTIS.2014.6850649.

- [240] Mei-Chen Hsueh, T. Tsai and R. Iyer, ‘Fault injection techniques and tools’, *Computer*, vol. 30, no. 4, pp. 75–82, Apr. 1997. DOI: 10.1109/2.585157.
- [241] L. Pintard, J.-C. Fabre, K. Kanoun, M. Leeman and M. Roy, ‘Fault injection in the automotive standard ISO 26262: An initial approach’, in *Dependable Computing*, M. Vieira and J. C. Cunha, Eds., red. by D. Hutchison *et al.*, vol. 7869, Series Title: Lecture Notes in Computer Science, Berlin, Heidelberg: Springer Berlin Heidelberg, 2013, pp. 126–133. DOI: 10.1007/978-3-642-38789-0\_11.
- [242] M. Malvezzi, P. Presciani, B. Allotta and P. Toni, ‘Probabilistic analysis of braking performance in railways’, *Proceedings of the Institution of Mechanical Engineers, Part F: Journal of Rail and Rapid Transit*, vol. 217, no. 3, pp. 149–165, 1st May 2003. DOI: 10.1243/095440903769012867.
- [243] J. Zhang, Y. Zhang and G. Li, ‘Functional safety design of four-wheel independent brake system on electric vehicle’, *IOP Conference Series: Earth and Environmental Science*, vol. 170, p. 042071, Jul. 2018. DOI: 10.1088/1755-1315/170/4/042071.
- [244] L. Pugi, T. Favilli, L. Berzi, E. Locorotondo and M. Pierini, ‘Brake blending and optimal torque allocation strategies for innovative electric powertrains’, in *Applications in Electronics Pervading Industry, Environment and Society*, S. Saponara and A. De Gloria, Eds., vol. 573, Series Title: Lecture Notes in Electrical Engineering, Cham: Springer International Publishing, 2019, pp. 477–483. DOI: 10.1007/978-3-030-11973-7\_57.
- [245] L. Pugi, T. Favilli, L. Berzi, M. Cappa and M. Pierini, ‘An optimal torque and steering allocation strategy for stability control of road vehicles’, in *2021 IEEE International Conference on Environment and Electrical Engineering and 2021 IEEE Industrial and Commercial Power Systems Europe (EEEIC / I&CPS Europe)*, Bari, Italy: IEEE, 7th Sep. 2021, pp. 1–6. DOI: 10.1109/EEEIC/ICPSEurope51590.2021.9584554.
- [246] T. Favilli, L. Pugi, L. Berzi and M. Pierini, ‘Coordinated steering and torque vectoring lateral stability sliding mode control applied to an electric in-wheel motors vehicle’, in *2021 IEEE International Conference on Environment and Electrical Engineering and 2021 IEEE Industrial and Commercial Power Systems Europe (EEEIC / I&CPS Europe)*, Bari, Italy: IEEE, 7th Sep. 2021, pp. 1–6. DOI: 10.1109/EEEIC/ICPSEurope51590.2021.9584717.
- [247] H. Martin, K. Tschabuschnig, O. Bridal and D. Watzenig, ‘Functional safety of automated driving systems: Does ISO 26262 meet the challenges?’, in *Automated Driving*, D. Watzenig and M. Horn, Eds., Cham: Springer International Publishing, 2017, pp. 387–416. DOI: 10.1007/978-3-319-31895-0\_16.
- [248] T. Novi, R. Capitani and C. Annicchiarico, ‘An integrated artificial neural network–unscented kalman filter vehicle sideslip angle estimation based on inertial measurement unit measurements’, *Proceedings of the Institution of Mechanical Engineers, Part D: Journal of Automobile Engineering*, vol. 233, no. 7, pp. 1864–1878, Jun. 2019. DOI: 10.1177/0954407018790646.

- [249] M. Montani, R. Capitani, M. Fainello and C. Annicchiarico, 'Use of a driving simulator to develop a brake-by-wire system designed for electric vehicles and car stability controls', in *10th International Munich Chassis Symposium 2019*, P. E. Pfeffer, Ed., Series Title: Proceedings, Wiesbaden: Springer Fachmedien Wiesbaden, 2020, pp. 663–684. DOI: 10.1007/978-3-658-26435-2\_46.
- [250] *ISO 21994:2007*, 27th Jan. 2020.
- [251] P. Nag, U. Ghanekar and J. Harmalkar, 'A novel multi-core approach for functional safety compliance of automotive electronic control unit according to ISO 26262', in *2019 IEEE 5th International Conference for Convergence in Technology (I2CT)*, Bombay, India: IEEE, Mar. 2019, pp. 1–5. DOI: 10.1109/I2CT45611.2019.9033841.
- [252] K. Enisz, D. Fodor, I. Szalay and L. Kovacs, 'Reconfigurable real-time hardware-in-the-loop environment for automotive electronic control unit testing and verification', *IEEE Instrumentation & Measurement Magazine*, vol. 17, no. 4, pp. 31–36, Aug. 2014. DOI: 10.1109/MIM.2014.6873729.
- [253] Z. Zhou, H. Liao, X. Wang, S. Mumtaz and J. Rodriguez, 'When vehicular fog computing meets autonomous driving: Computational resource management and task offloading', *IEEE Network*, vol. 34, no. 6, pp. 70–76, Nov. 2020. DOI: 10.1109/MNET.001.1900527.
- [254] E. Sabbioni, F. Cheli, M. Vignati and S. Melzi, 'Comparison of torque vectoring control strategies for a IWM vehicle', *SAE International Journal of Passenger Cars - Electronic and Electrical Systems*, vol. 7, no. 2, pp. 565–572, 1st Apr. 2014. DOI: 10.4271/2014-01-0860.
- [255] L. Pugi, F. Grasso, M. Pratesi, M. Cipriani and A. Bartolomei, 'Design and preliminary performance evaluation of a four wheeled vehicle with degraded adhesion conditions', *International Journal of Electric and Hybrid Vehicles*, vol. 9, no. 1, p. 1, 2017. DOI: 10.1504/IJEHV.2017.082812.
- [256] F. Cheli, M. Pedrinelli, F. Resta, A. Zorzutti, M. Zanchetta and G. Travaglio, 'Development of a control strategy for a semi-active differential for a high performance vehicle', presented at the SAE World Congress & Exhibition, 16th Apr. 2007, pp. 2007-01-0927. DOI: 10.4271/2007-01-0927.
- [257] A. Pulcinelli, L. Pugi, F. Vinattieri, R. Capitani and C. Annicchiarico, 'Design and testing of an innovative electro-hydraulic actuator for a semi-active differential', *Proceedings of the Institution of Mechanical Engineers, Part D: Journal of Automobile Engineering*, vol. 232, no. 11, pp. 1438–1453, Sep. 2018. DOI: 10.1177/0954407017729619.
- [258] X. Gong, W. Ge, J. Yan, Y. Zhang and X. Gongye, 'Review on the development, control method and application prospect of brake-by-wire actuator', *Actuators*, vol. 9, no. 1, p. 15, 5th Mar. 2020. DOI: 10.3390/act9010015.
- [259] G. Burgio and P. Zegelaar, 'Integrated vehicle control using steering and brakes', *International Journal of Control*, vol. 79, no. 5, pp. 534–541, May 2006. DOI: 10.1080/00207170500488970.
- [260] M. Choi and S. B. Choi, 'MPC for vehicle lateral stability via differential braking and active front steering considering practical aspects', *Proceedings of the Institution of Mechanical Engineers, Part D: Journal of Automobile Engineering*, vol. 230, no. 4, pp. 459–469, Mar. 2016. DOI: 10.1177/0954407015586895.

- [261] M. Doumiati, O. Sename, L. Dugard, J.-J. Martinez-Molina, P. Gaspar and Z. Szabo, 'Integrated vehicle dynamics control via coordination of active front steering and rear braking', *European Journal of Control*, vol. 19, no. 2, pp. 121–143, Mar. 2013. DOI: 10.1016/j.ejcon.2013.03.004.
- [262] P. Hang, X. Chen, S. Fang and F. Luo, 'Robust control for four-wheel-independent-steering electric vehicle with steer-by-wire system', *International Journal of Automotive Technology*, vol. 18, no. 5, pp. 785–797, Oct. 2017. DOI: 10.1007/s12239-017-0078-5.
- [263] B. Lee, A. Khajepour and K. Behdinan, 'Vehicle stability through integrated active steering and differential braking', presented at the SAE 2006 World Congress & Exhibition, 3rd Apr. 2006, pp. 2006-01-1022. DOI: 10.4271/2006-01-1022.
- [264] B. Li, H. Du, W. Li and Y. Zhang, 'Side-slip angle estimation based lateral dynamics control for omni-directional vehicles with optimal steering angle and traction/brake torque distribution', *Mechatronics*, vol. 30, pp. 348–362, Sep. 2015. DOI: 10.1016/j.mechatronics.2014.12.001.
- [265] M. Nagai, 'Study on integrated control of active front steer angle and direct yaw moment', *JSAE Review*, vol. 23, no. 3, pp. 309–315, Jul. 2002. DOI: 10.1016/S0389-4304(02)00189-3.
- [266] J. Wang, Z. Luo, Y. Wang, B. Yang and F. Assadian, 'Coordination control of differential drive assist steering and vehicle stability control for four-wheel-independent-drive EV', *IEEE Transactions on Vehicular Technology*, vol. 67, no. 12, pp. 11 453–11 467, Dec. 2018. DOI: 10.1109/TVT.2018.2872857.
- [267] H. Fujimoto, 'Regenerative brake and slip angle control of electric vehicle with in-wheel motor and active front steering', p. 7, 2010.
- [268] A. Hildebrandt, O. Sawodny, R. Trutschel and K. Augsburg, 'Nonlinear control design for implementation of specific pedal feeling in brake-by-wire car design concepts', in *Proceedings of the 2004 American Control Conference*, Boston, MA, USA: IEEE, 2004, 1463–1468 vol.2. DOI: 10.23919/ACC.2004.1386782.
- [269] Wang, 'Linear parameter-varying controller design for four-wheel independently actuated electric ground vehicles with active steering systems', *IEEE Transactions on Control Systems Technology*, vol. 22, no. 4, pp. 1281–1296, Jul. 2014. DOI: 10.1109/TCST.2013.2278237.
- [270] W. Zhao, X. Qin and C. Wang, 'Yaw and lateral stability control for four-wheel steer-by-wire system', *IEEE/ASME Transactions on Mechatronics*, vol. 23, no. 6, pp. 2628–2637, Dec. 2018. DOI: 10.1109/TMECH.2018.2812220.
- [271] T. van der Sande, P. Zegelaar, I. Besselink and H. Nijmeijer, 'A robust control analysis for a steer-by-wire vehicle with uncertainty on the tyre forces', *Vehicle System Dynamics*, vol. 54, no. 9, pp. 1247–1268, Sep. 2016. DOI: 10.1080/00423114.2016.1197407.
- [272] M. W. Oppenheimer, D. B. Doman and M. A. Bolender, 'Control allocation for over-actuated systems', in *2006 14th Mediterranean Conference on Control and Automation*, Ancona, Italy: IEEE, Jun. 2006, pp. 1–6. DOI: 10.1109/MED.2006.328750.

- [273] R. Conti, E. Galardi, E. Meli, D. Nocciolini, L. Pugi and A. Rindi, 'Energy and wear optimisation of train longitudinal dynamics and of traction and braking systems', *Vehicle System Dynamics*, vol. 53, no. 5, pp. 651–671, 4th May 2015. DOI: 10.1080/00423114.2014.990466.
- [274] V. V. Vantsevich, 'Road and off-road vehicle system dynamics. understanding the future from the past', *Vehicle System Dynamics*, vol. 53, no. 2, pp. 137–153, Feb. 2015. DOI: 10.1080/00423114.2014.984726.
- [275] G. Reina and A. Messina, 'Vehicle dynamics estimation via augmented extended kalman filtering', *Measurement*, vol. 133, pp. 383–395, Feb. 2019. DOI: 10.1016/j.measurement.2018.10.030.
- [276] G. Jia, L. Li and D. Cao, 'Model-based estimation for vehicle dynamics states at the limit handling', *Journal of Dynamic Systems, Measurement, and Control*, vol. 137, no. 10, p. 104501, 1st Oct. 2015. DOI: 10.1115/1.4030784.
- [277] S. Nokleby, R. Fisher, R. Podhorodeski and F. Firmani, 'Force capabilities of redundantly-actuated parallel manipulators', *Mechanism and Machine Theory*, vol. 40, no. 5, pp. 578–599, May 2005. DOI: 10.1016/j.mechmachtheory.2004.10.005.
- [278] B. Allotta, L. Pugi, V. Colla, F. Bartolini and F. Cangioli, 'Design and optimization of a semi-active suspension system for railway applications', *Journal of Modern Transportation*, vol. 19, no. 4, pp. 223–232, Dec. 2011. DOI: 10.1007/BF03325762.
- [279] K. Uematsu and J. C. Gerdes, 'A comparison of several sliding surfaces for stability control', *A comparison of several sliding surfaces for stability control*, vol. Proc.of the Intl. Symp. on Advanced Vehicle Control, Japan, 2002.
- [280] C. G. Bobier and J. C. Gerdes, 'Envelope control: Stabilizing within the limits of handling using a sliding surface', *IFAC Proceedings Volumes*, vol. 43, no. 7, pp. 162–167, Jul. 2010. DOI: 10.3182/20100712-3-DE-2013.00012.
- [281] T. Chung, K. Yi, J. Kim and J. Lee, 'Closed-loop evaluation of vehicle stability control (VSC) systems using a combined vehicle and human driving model', presented at the SAE 2004 World Congress & Exhibition, 8th Mar. 2004, pp. 2004–01–0763. DOI: 10.4271/2004-01-0763.
- [282] C. Hu, R. Wang, F. Yan, Y. Huang, H. Wang and C. Wei, 'Differential steering based yaw stabilization using ISMC for independently actuated electric vehicles', *IEEE Transactions on Intelligent Transportation Systems*, vol. 19, no. 2, pp. 627–638, Feb. 2018. DOI: 10.1109/TITS.2017.2750063.
- [283] J. Breuer, 'Analysis of driver-vehicle-interactions in an evasive manoeuvre-results of 'moose test' studies', Proc. 16th ESV Conf 1998.
- [284] J. Pančík and V. Beneš, 'Emulation of wheel speed sensors for automotive electronic control unit', in *Industry 4.0: Trends in Management of Intelligent Manufacturing Systems*, L. Knapčíková and M. Balog, Eds., Series Title: EAI/Springer Innovations in Communication and Computing, Cham: Springer International Publishing, 2019, pp. 111–120. DOI: 10.1007/978-3-030-14011-3\_10.

# Appendix A

## Publications

### A.1 Brake Blending and Optimal Torque Allocation Strategies for Innovative Electric Powertrains [198]

**Published in** 2019 IEEE International Conference on Environment and Electrical Engineering and 2019 IEEE Industrial and Commercial Power Systems Europe (EEEIC / I&CPS Europe)

**Authors** Luca Pugi, Tommaso Favilli, Lorenzo Berzi, Edoardo Locorotondo, Marco Pierini

**Abstract** Development of electric vehicles is not only an opportunity in terms of environmental sustainability but it also offers interesting possibilities in terms of control performances that can be achieved by on board systems devoted to increase vehicle safety and stability by modulating longitudinal efforts applied to tires. It's not only a matter of performances but also of standardization in a single integrated subsystem able to safely control vehicle dynamics of various functions that are currently implemented by different subsystems. This simplification and rationalization of the whole mechatronic system should be of fundamental importance also for the integration of autonomous or assisted driving functionalities making easier and safer system integration.

#### 1 Introduction: Brake Blending for Automotive Applications

[...] With the growing diffusion of electric traction system in the automotive sector is growing the opportunity of exploiting their four quadrant capabilities in order to perform an extensive use of regenerative braking mainly to optimize energy consumptions and consequently the autonomy of the vehicle both for traction<sup>4</sup> or to fed on board subsystems<sup>5</sup>. The amount of recovered energy is related to the characteristics of the typical driving cycle and it can reach values above 20% of the energy spent for traction, especially in urban-suburban context<sup>6</sup>. Since performances of blended braking plants are associated to different reliability and availability levels, blending system have also to assure the requested braking performances compensating limitations arising from current state of motors, drive and storage

systems. In addition, the braking command strategy has to be implemented in order to let the user fully exploit regenerative braking potential while maintaining comfort and intuitiveness<sup>11</sup> for the user.

In this work authors propose and describe innovative criteria in order to easily integrate optimal allocation and blending policies able to fully exploit in a relatively simple way torque vectoring capabilities of distributed electric traction system.

## 2 Reference Benchmark Configuration

[...] For the proposed benchmark configuration, authors supposed a nested layout of standards mechatronics systems that have to access to brake actuation reproducing a common scheme which is also adopted by the most widely diffused and simulation software like Siemens Amesim<sup>TM12</sup> as visible in Figure A.1/a/b: brake demand (Figure A.1/a) is pre-processed by an EBD system able to optimally distribute braking performances between wheels respect to an estimated distribution of normal contact forces. Then this brake demand is modified by an ESP system that should be able to activate and modulate brake demand also during the traction phase in order to correct vehicle behaviour respect to stability criteria mostly based on a comparison between measured kinematic (yaw speed, lateral acceleration) and an expected one (a tolerated trajectory respect to ideal steering conditions). Finally, generated brake demand is processed by an inner loop corresponding to the ABS system able to modulate brake performances on each wheel in order to optimally exploit available wheel-road adhesion avoiding wheel locking and saturation of the available tangential forces which are potentially dangerous also for lateral stability.

Respect to this quite conventional scheme reproduced in Figure A.1/a, authors considered the following generalized approach in which the plant is generalized respect to a more general and innovative approach which is summarized in Figure A.1/b: Since electric motors are able to operate in four quadrants the concept of brake demand is generalized in terms of a generic torque, longitudinal traction braking performances which is split among wheels according powertrain configuration and estimated normal contact forces (modified EBD block in Figure A.1/b). Torque reference on wheels is then modified by the ESP (extended ESP-Torque Vectoring block in Figure A.1/b) that should modify both traction and braking efforts on wheels according chosen powertrain configuration and different limitations of the involved actuation systems. These reference efforts are processed by a hybrid ABS-ASR subsystem since the sign of processed signals should be both positive or negative being the same system devoted both to control traction and braking manoeuvres. Especially in case of braking efforts the system has to manage the application of braking efforts between conventional and electric plant [...]. By comparing the two schemes of Figure A.1/a/b, most noticeable differences among the two plants concern the allocation of longitudinal efforts performed by the extended ESP torque vectoring block and the brake blending one [...].

### 2.1 Optimal allocation of efforts for the enhanced ESP system

In order to correct vehicle trajectory, ESP has to allocate a known correction torque  $M_z$  which is a function of the error between desired  $r_{ref}$  and estimated  $r_{feed}$  yaw rotational speed (A.1).

$$M_z = f(r_{ref}, r_{feed}) \quad (\text{A.1})$$

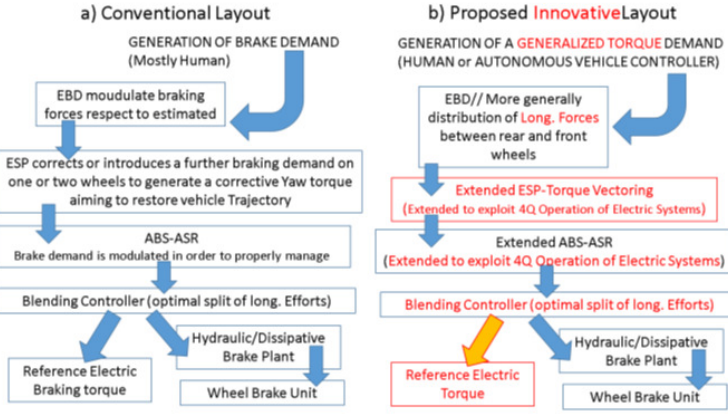


Figure A.1: comparison between conventional a) and innovative b) layouts of the mechatronics on board systems aiming to modulate vehicle braking efforts

In order to allocate the torque  $M_z$  the effort applied on each wheel should be corrected applying a force  $T_{Cij}$  [...]. Applied correction forces has to satisfy at the same time relation (A.2) and constraints  $T_{minij}$ ,  $T_{maxij}$  (A.3) which depend from availability of both actuation systems (electric motors and mech. brakes).

$$M_z = \frac{1}{2}t(T_{fr} - T_{fl} + T_{rr} - T_{rl}) = \overbrace{\begin{bmatrix} \frac{1}{2}t & -\frac{1}{2}t & \frac{1}{2}t & -\frac{1}{2}t \end{bmatrix}}^{\text{Feed-forward}} \left. \begin{bmatrix} T_{fr} \\ T_{fl} \\ T_{rr} \\ T_{rl} \end{bmatrix} \right\} T_C(\text{vector of corrections}) \quad (\text{A.2})$$

$$T_{minij} \leq (T_{*ij} + T_{Cij}) \leq T_{maxij} \quad (\text{A.3})$$

In (A.3)  $T_{*ij}$  and  $T_{ij}$  represent respectively the reference torque and the corrected one (after the application of  $T_{Cij}$ ). Since (A.2) has potentially multiple solutions it should be solved using the Moore-Penrose pseudo-inverse of the torque allocation matrix  $B$  [...]. Solution obtained with the pseudo-inverse approach is optimal since it minimize the norm of the correction vector  $T_C$ : in this way the applied correction is minimal assuring, if possible, the respect of constraints (A.3). Also a well distributed allocation of efforts between wheels is obtained, this should be very useful especially in degraded adhesion conditions avoiding, as possible the saturation of available adhesion on wheel-road contact patches. Calculation is performed iteratively since at each computational step  $T_{ij}$  values that violate constraints (A.3) are saturated on corresponding limits; then pseudo-inverse calculation is repeated. The use of an iterative procedure its not a problem since it's possible to demonstrate that even in worst numerical conditions no more than four iterations are necessary while numerical resources needed to calculate the pseudo-inverse matrix of four or less elements is almost negligible.

### 3 Preliminary Results

Proposed Model was implemented in a preliminary “toy” version using Matlab Simulink 2018a and in particular the new “Vehicle Dynamics Blockset™” which makes available in MATLAB both advanced vehicle multibody models and relatively detailed models of tyre-road interaction based on widely accepted approach proposed by Pacejka. Potential advantages of the proposed approach should be easily understood looking at some preliminary results visible in Figure A.2/a/b/c: the behaviour of a vehicle with four independent in wheel motors, which performs a narrow curve (radius  $18m$ ) with degraded adhesion conditions. In this way it can be easily understood the capability of the proposed model of implementing and representing some typical behaviour of ESP and ABS systems.

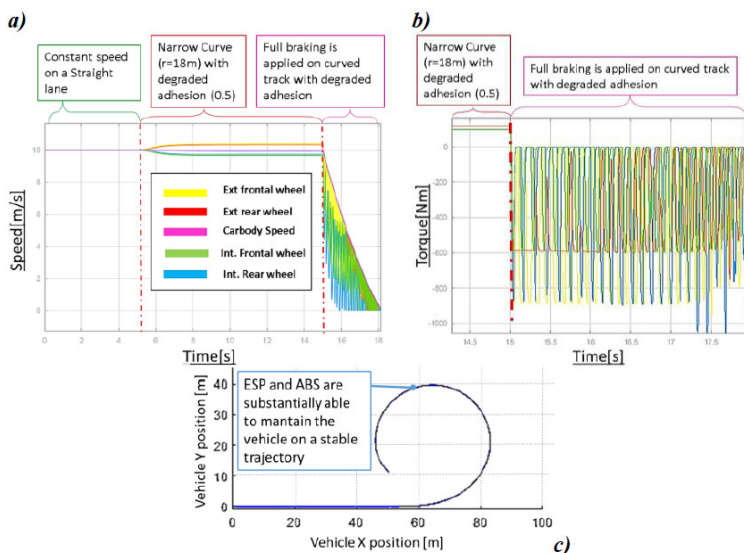


Figure A.2: example of speed a) and torque profiles b) respect to performed trajectory c)

Since the vehicle is equipped with four motors performed manoeuvres involve a negligible usage of the conventional brake, with positive consequences both in terms of friction brake and pads (that are not used) and in terms of recovered energy (since all the braking actuation is almost entirely regenerative).

### Conclusions and Future Developments

Results of current activities applied to a generic vehicle with distributed traction systems are quite encouraging. As previous step authors are working to a further improvement of the proposed approach hoping to be able to generalize and apply this solution to the largest number of possible “Use Cases” that should be made available by the industrial partners of the OBELICS Project (current results are referred to a preliminary toy model). An extended version of this paper describing in detail both modelling methodologies and obtained results should be the natural prosecution of this preliminary work.

## References

1. Gerdes, J.C., Hedrick, J.K. Brake system modelling for simulation and control (1999) *Journal of Dynamic Systems, Measurement and Control, Transactions of the ASME*, 121 (3), pp. 296-503. DOI: 10.1115/1.2802501.
2. Subramanian, S.C., Darbha, S., Rajagopal, K.R. Modeling the pneumatic subsystem of an s-cam air brake system (2004) *Journal of Dynamic Systems, Measurement and Control, Transactions of the ASME*, 126 (1), pp. 36-46. DOI: 10.1115/1.1666893
3. Pugi, L., Malvezzi, M., Papini, S., Vettori, G. Design and preliminary validation of a tool for the simulation of train braking performance, (2013) *Journal of Modern Transportation*, 21 (4), pp. 247-257. DOI: 10.1007/s40534-013-0027-6
4. Lv, C., Zhang, J., Li, Y., Yuan, Y. Mechanism analysis and evaluation methodology of regenerative braking contribution to energy efficiency improvement of electrified vehicles (2015) *Energy Conversion and Management*, 92, pp. 469-482. DOI: 10.1016/j.enconman.2014.12.092
5. Pugi, L., Pagliai, M., Nocentini, A., Lutzemberger, G., Pretto, A. Design of a hydraulic servo-actuation fed by a regenerative braking system (2017) *Applied Energy*, 187, pp. 96-115. DOI: 10.1016/j.apenergy.2016.11.047
6. Berzi, L., Delogu, M., Pierini, M.,. Development of driving cycles for electric vehicles in the context of the city of Florence (2016), *Transportation Research Part D: Transport and Environment* 47, 299–322. <https://doi.org/10.1016/j.trd.2016.05.010>
7. Kukutschová, J., Roubíček, V., Malachová, K., Pavlíčková, Z., Holuša, R., Kubačková, J., Mička, V., MacCrimmon, D., Filip, P Wear mechanism in automotive brake materials, wear debris and its potential environmental impact (2009) *Wear*, 267 (5-8), pp. 807-817 DOI: 10.1016/j.wear.2009.01.034
8. William Pasillas-Lépine (2007) Hybrid modeling and limit cycle analysis for a class of five-phase anti-lock brake algorithms, *Vehicle System Dynamics*, 44:2,173-188, DOI: 10.1080/00423110500385873
9. Fennel, H., & Ding, E. L. (2000). A model-based failsafe system for the continental TEVES electronic-stability-program (ESP) (No. 2000-01-1635). SAE Technical Paper.
10. Pugi, L., Grasso, F., Pratesi, M., Cipriani, M., Bartolomei, A. Design and preliminary performance evaluation of a four wheeled vehicle with degraded adhesion conditions (2017) *International Journal of Electric and Hybrid Vehicles*, 9 (1), pp. 1-32. DOI: 10.1504/IJEHV.2017.082812
11. Zhang, J., Lv, C., Gou, J., Kong, D., Cooperative control of regenerative braking and hydraulic braking of an electrified passenger car (2018).. *Proceedings of the Institution of Mechanical Engineers, Part D: Journal of Automobile Engineering* 226, 1289–1302. <https://doi.org/10.1177/0954407012441884> 12. Siemens Amesim™, Technical documentation release 14.00
12. Pugi, L., Pagliai, M., Allotta, B. A robust propulsion layout for underwater vehicles with enhanced manoeuvrability and reliability features (2017) *Proceedings of the Institution of Mechanical Engineers Part M: Journal of Engineering for the Maritime Environment*,. DOI: 10.1177/1475090217696569

## A.2 Real Time Models of Automotive Mechatronics Systems: Verifications on “Toy Models” [21]

**Published in** Springer International Publishing Mechanisms and Machine Science

**Authors** Lorenzo Berzi, Tommaso Favilli, Edoardo Locorotondo, Marco Pierini, and Luca Pugi

**Abstract** Modern electric vehicles are complex mechatronics systems whose behaviour is highly influenced by the concurrent action of mechanical and electrical systems interfaced with complex control logics aiming to improve several aspect concerning energy management, vehicle stability, comfort and guidance. [...] authors have focused their attention in system integration and model optimization of electric powertrains with a particular attention to the problem of brake blending respect to different applications (smart energy management, vehicle stability, hardware in the loop testing of connected mechatronics systems). In this work authors introduce main features and possible usages of brake models that they have to develop within the OBELICS Project. Proposed models have to be implemented and verified also for real-time implementation with a particular attention to RT-Implementation and Co-Simulation with models provided by other partners of the project. For this reason, authors introduce specifications concerning RTI not only in terms of scheduling of different tasks but also proposing a reference architecture of Real Time controller [...] Finally, a preliminary “toy”, simplified model is proposed in order to verify the feasibility of the proposed architecture respect to a future complete implementation and integration with the product of the research of the other partners of the project.

**Keywords** Mechatronics, Real-time simulation, Multi-scale models, Multi-physics models, Brake blending

### 1 Introduction: Brake Blending, State of the Art and Involved Research Activities

[...] authors are focusing their attention on the problem of brake blending for road electric vehicles.

[...] Finally, it should be noticed that the dynamical response of electric motors/actuation systems are much faster and more controllable respect to conventional internal combustion engines. As a consequence, electric traction should be used to perform a fast and precise multi-quadrant control of exerted torques contributing to modulate longitudinal efforts on wheels contributing to an enhanced behaviour of on board subsystem such as ABS-ASR<sup>8</sup>, ESP etc. In literature<sup>10-12</sup> there is a wide variety of studies concerning this topic. Another interesting topic for research and design optimization is represented by powertrains with multiple traction motors or direct drive in-wheel solutions. These unconventional solutions are very promising both for off-road or urban mobility applications [...].

Investigation and Simulation of Brake blending should be very interesting also for the development of high frequency inverters and energy storage management systems. In particular, high levels of reliability of energy storage systems involve a constant monitoring of high frequency interactions with traction motors and drive systems<sup>16</sup>. For this reason, it should be interesting to verify the behaviour of the system when complex control tasks are performed by traction motors (as example high frequency modulation of exerted torques for torque vectoring). Frequency

content associated fast control transients should be exploited to perform diagnostic identification procedures aiming to verify the current state of health of energy storage systems through on line spectroscopic identification procedures<sup>17</sup>.

## 2 Proposed Task Partitioning and Hardware Implementation for a Modular Real-Time Simulation

As explained in the introduction, advanced simulation of brake blending involves the evaluation of multi-scale and multi-physics phenomena that are described in Table A.1 [...].

Many commercial products (as example from Matworks<sup>TM</sup> or from National Instruments<sup>TM</sup>) allow some automatic or smart distribution of concurrent tasks between different cores. However, a good organization of tasks is fundamental to optimize computational efficiency. Authors adopted a physical based distinction between “Continuous” and “Discrete” subsystems. Continuous models represent physical systems whose mutual interaction has to be modelled minimizing delays introduced by the execution on a real time target which is necessary discrete. Computational delays (due to task execution and data exchange between different tasks) are tolerable only if they are relatively negligible respect to the typical time scale of the phenomena that they have to reproduce as shown in Table A.1.

Table A.1: Simulated Dynamical Behaviour and corresponding integration features

System description	Physical domain	Continuous/ Discrete (Num.Stiffness)	Mean integration freq. (ODE1 solver)
Multibody Vehicle Model	Mechanical	Continuous <sup>a</sup> (Stiff)	$10^3-10^4$ [Hz]
Tire/Road Contact Models	Mechanical	Continuous <sup>a</sup> (Stiff)	$10^3-10^4$ [Hz]
Hydraulic Plant/Brake Models	Mainly Fluid	Continuous <sup>a</sup> (Stiff)	$10^3-10^4$ [Hz]
On board Digital Control Systems	Math/Digital	Discrete (Not stiff)	$10^1-10^3$ [Hz]
Electric Motor and Drives	Electric	Continuous (Stiff)	$10^5-10^9$ [Hz]
Low Lev. Control of Power	Math/Digital	Discrete (Not stiff)	$10^4$ [Hz]
Battery Models	Electro-Chem.	Continuous <sup>a</sup> (Stiff)	$10^3-10^6$ [Hz] <sup>b</sup>
Efficiency, Thermal and Wear Models (friction and power components)	Thermal/Other	Continuous <sup>a</sup> (Stiff)	$10^1-10^2$ [Hz] <sup>b</sup>

Clearly, it should be easier the implementation on different threads of slow processes such as thermal and wear models since delays introduced by data exchange with faster simulated physical phenomena should produce relatively small consequences on accuracy of results. On the other hand, models have to reproduce control algorithms and other processes that are discrete also in the real world. In this case the correct implementation of delays associated to data acquisition, communication and production of outputs are mandatory to correctly reproduce the dynamical behaviour of simulated digital system. A correct implementation of discrete system is also useful to perform task partitioning since delays that have to be reproduced to fit a real physical behaviour should be used to manage communication and data exchange between different threads on the real time platform [...].

### 3 Preliminary Implementation of a Simplified “Toy” Model: Some Results and Observations

According over-introduced specifications, authors have assembled a simplified “toy” model of a vehicle with its main sub-systems. Aim of this activity is to verify feasibility and functionality of the proposed approach while more complex simulation modules (developed by other partners of the project) are still not available, since the activities are still in a preliminary phase [...].

In order to properly simulate brake plant models also other interacting dynamical systems has to be simulated using Matlab Simulink™. For these activities, authors have preliminary considered the usage of simplified vehicle models (quarter vehicle and/or planar 7-DOF one) [...].

Electric Power train is currently simulated in terms of simplified transfer functions. Also a simplified model of the energy storage system is introduced<sup>21</sup>. All the implemented models are integrated separately simulating different sampling frequencies and communication delays. In order to properly verify the portability of the code within different partners of the project each subsystem is compiled as a discrete Matlab-Simulink S-function™. This verification of code portability<sup>22</sup> is useful also for the conversion models also the FMI (Functional Mock-up Interface) format [...].

In A.3/a and b there are some results referred to the simulation of a braking manoeuvre(simplified quarter vehicle model). Considered data approximately correspond to the loads applied to the motorized frontal wheels of city-car like with a total mass of about 1400 kg. In particular, it’s interesting the capability of the model of implementing some typical features of the brake blending: as visible in Figure A.3/b applied electric torque is limited considering torque and power limitations of the drive system, including the unavailability of regenerative braking for very low speed.

In A.3/c same simulation is repeated considering degraded road adhesion conditions. These results are quite interesting to verify model stability and reliability respect to delays and errors introduced by fixed step integrators and relatively large integrations steps. In particular, it’s clearly noticeable the absence of “chatter” phenomena that are typically caused by delays introduced by discrete task partitioning in real time systems.

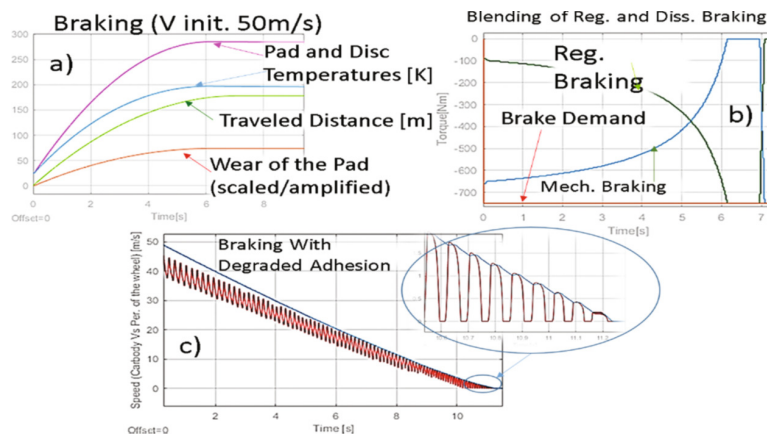


Figure A.3: example of preliminary simulation results, (a) results of braking simulations, (b) blending between mechanical and Electrical Blending, (c) braking with degraded adhesion

## 4 Conclusions and Future Developments

In this work authors have introduced preliminary design activities concerning real time simulation and optimization of brake blending models produced by University of Florence. Most innovative and significant results of these activities mainly concerns implementation procedures aiming to assure portability of produced code within different partners and simulation environments. As further development author wish to be able to further customize and develop the model respect to Use Cases proposed by Industrial Partners of the Project (Example of advanced prototypes of Electric Vehicles that should be simulated using the proposed tools). Also in order to assure the prescribed portability of proposed models authors will verify also FMI implementation and compatibility with advanced models proposed by the other partner of the project.

## References

1. Official site of the Obelics EU Project. <https://obelics.eu/>
2. Pugi, L., Malvezzi, M., Papini, S., Tesi, S.: Simulation of braking performance: the AnsaldoBreda EMU V250 application. *Proc. Inst. Mech. Eng. Part F J. Rail Rapid Transit* 229(2), 160–172 (2015). <https://doi.org/10.1177/0954409713504394>
3. Pugi, L., Malvezzi, M., Conti, R.: Optimization of traction and braking subsystems with respect to mission profile. In: *Civil-Comp Proceedings*, p. 104 (2014)
4. Conti, R., Galardi, E., Meli, E., Nocciolini, D., Pugi, L., Rindi, A.: Energy and wear optimisation of train longitudinal dynamics and of traction and braking systems. *Veh. Syst. Dyn.* 53(5), 651–671 (2015). <https://doi.org/10.1080/00423114.2014.990466>
5. Leigh, M.J.: Brake blending. *Proc. Inst. Mech. Eng. Part F J. Rail Rapid Transit* 208(1), 43–49 (1994)
6. Van Zanten, A.T.: Bosch ESP systems: 5 years of experience (No. 2000-01-1633). SAE Technical Paper (2000)
7. Ren, G., Ma, G., Cong, N.: Review of electrical energy storage system for vehicular applications. *Renew. Sustain. Energy Rev.* 41, 225–236 (2015)

8. Lv, C., Zhang, J., Li, Y., Yuan, Y.: Mechanism analysis and evaluation methodology of regenerative braking contribution to energy efficiency improvement of electrified vehicles. *Energy Convers. Manag.* 92, 469–482 (2015) *Real Time Models of Automotive Mechatronics Systems* 147
9. Huber, W., Jonner, W.D., Demel, H.: Simulation, performance and quality evaluation of ABS and ASR (No. 880323). SAE Technical Paper (1988)
10. Sawase, K., Ushiroda, Y., Miura, T.: Left-right torque vectoring technology as the core of super all wheel control (S-AWC). *Mitsubishi Mot. Tech. Rev.* 18, 16–23 (2006)
11. De Novellis, L., Sorniotti, A., Gruber, P., Pennycott, A.: Comparison of feedback control techniques for torque-vectoring control of fully electric vehicles. *IEEE Trans. Veh. Technol.* 63(8), 3612–3623 (2014)
12. Description of MRT™ freely available the the official site of the IET company.  
<http://www.ietspa.com>
13. Ceraolo, M., Lutzemberger, G., Sani, L., Valenti, G., Pretto, A., Pugi, L.: Full electric and hybrid series vans: cost, performance and efficiency evaluation for different powertrain layout. In: 2017 International Conference of Electrical and Electronic Technologies for Automotive, Article no. 7993205 (2017).  
<https://doi.org/10.23919/eeta.2017.7993205>
14. Technical Documentation on hybrid solutions with torque vectoring performed with multiple electric motor available at the site of Honda Company.  
<http://world.honda.com/Hybrid/>
15. Pugi, L., Grasso, F., Pratesi, M., Cipriani, M., Bartolomei, A.: Design and preliminary performance evaluation of a four wheeled vehicle with degraded adhesion conditions. *Int. J. Electr. Hybrid Veh.* 9(1): 1–32 (2017).  
<https://doi.org/10.1504/ijehv.2017.08281>
16. Doersam, T., Schoerle, S., Hoene, E., Lang, K.D., Spieker, C., Waldmann, T.: High frequency impedance of Li-ion batteries. In: 2015 IEEE International Symposium on Electromagnetic Compatibility (EMC), pp. 714–719. IEEE, August 2015
17. Al Nazer, R., Cattin, V., Granjon, P., Montaru, M., Ranieri, M.: Broadband identification of battery electrical impedance for HEVs. *IEEE Trans. Veh. Technol.* 62(7), 2896–2905 (2013)
18. Gazzarri, J., Shrivastava, N., Jackey, R., Borghesani, C.: Battery pack modeling, simulation, and deployment on a multicore real time target. *SAE Int. J. Aerosp.* 7(2), 207–213 (2014).  
<https://doi.org/10.4271/2014-01-2217>
19. OBELICS Project deliverable D3.1: Standardized model integration, 2017-12-31.
20. Pacejka, H.: *Tire and Vehicle Dynamics*. Elsevier, New York (2005)
21. Locorotondo, E., Pugi, L., Berzi, L., Pierini, M., Lutzemberger, G.: Online identification of Thevenin equivalent circuit model parameters and estimation State of Charge of Lithium-Ion batteries. In: Proceedings of the 18th IEEE EEIC International Conference on Environment and Electrical Engineering, Palermo, 12–15 June 2018 (2018)
22. Stettinger, G., Benedikt, M., Thek, N., Zehetner, J.: On the difficulties of real-time cosimulation. In: V International Conference on Computational Methods for Coupled Problems in Science and Engineering, COUPLED PROBLEMS 2013, Ibiza, Spain (2013)
23. The Functional Mock-up Interface Standard (n.d.).  
<http://fmi-standard.org/downloads/>

## A.3 Application of Regenerative Braking on Electric Vehicles [198]

**Published in** 2019 IEEE International Conference on Environment and Electrical Engineering and 2019 IEEE Industrial and Commercial Power Systems Europe (EEEIC / I&CPS Europe)

**Authors** Luca Pugi, Tommaso Favilli, Lorenzo Berzi, Marco Pierini, Edoardo Locorotondo

**Abstract** Regenerative braking influences several aspects of design and performances of electric vehicles. Improved performances of modern electric drives can be exploited to optimize vehicle efficiency, stability and environmental impact. Braking plant is devoted not only to stop the vehicle but also to the actuate many on board safety related systems. As a consequence of the application of regenerative braking, the system is redundant and over-actuated, so the application of electrical and mechanical efforts has to be carefully optimized. In this study a general approach is proposed and discussed, in terms of used engineering tools and obtained results.

**Keywords** Braking, Brake Blending, Torque Vectoring, Electric Vehicles EV, Energy Efficiency.

### I. Introduction

The greatest opportunities for innovation in the automotive sector offered to designer concern the possibility of using electric traction system. Electric motors can be both speed or torque controlled quite precisely in wider operational ranges, respect to conventional Internal Combustion Engines (ICEs)<sup>1</sup>: modern electric drives allow a precise torque control even in near to standstill conditions<sup>2</sup> and enable, also, a simple four quadrant control, which offers the possibility of performing regenerative braking, allowing to recover a significant part of vehicle kinetic energy during the braking phase<sup>3</sup>.

Therefore, the application of regenerative braking is very important, since can reduce overall energy consumption (improving autonomy and efficiency), maintenance costs and environmental impact related to the worn brake debris, credited as first source of pollution not related to combustion<sup>5</sup>, with not negligible consequences in terms of environmental impact, which is still difficult to be completely quantified. Also, the good bandwidth response of electric drives should be exploited by on board mechatronic systems, in order to maintain vehicle stability and safety, not only during braking and traction phase<sup>6,7</sup>, but also through cornering manoeuvres<sup>8-10</sup> [...]. High power density rate of electric units allows the usage of multiple traction motors to regulate torque efforts among wheels, in order to perform torque vectoring. For these reasons the system has to be designed in order to optimize the synergy between electric and friction braking<sup>13,14</sup>, not only in terms of vehicle longitudinal dynamics but also for lateral stability issues [...].

[...] Aim of this study is to optimize the blending strategy and torque allocation algorithm of electric and conventional friction brake efforts on vehicle's wheels, whit the objective to completely exploit the regenerative brake, while ensuring the provision of a minimum level of braking performance in every operational condition, according to specific driving safety specifications.

A general flexible modelling methodology is developed in order to be easily adapted to different vehicle powertrain and brake plant layouts. Proposed models are designed to be modular, in order to be reassembled and customized for different applications. Finally, implementation is optimized for fixed step integration and easier Real Time Implementation (RTI). These are fundamental features in order to perform Hardware/Software in the Loop (HiL/SiL) testing procedure [...].

## II. Model Description

In Figure A.4 it's introduced a simplified scheme of the proposed approach: the brake plant is supposed to be controlled by a "brake demand", an abstraction of a signal, representing a braking torque reference desired by a human or an autonomous driver. This brake reference should be further modified by on-board subsystems, such as ABS or ESP, devoted to improving vehicle stability and safety.

As a consequence, brake demand is a vector whose scalar components are  $T_{ref-ij}$ , each one representing the requested torque in Nm of the  $ij$ -th vehicle wheel.

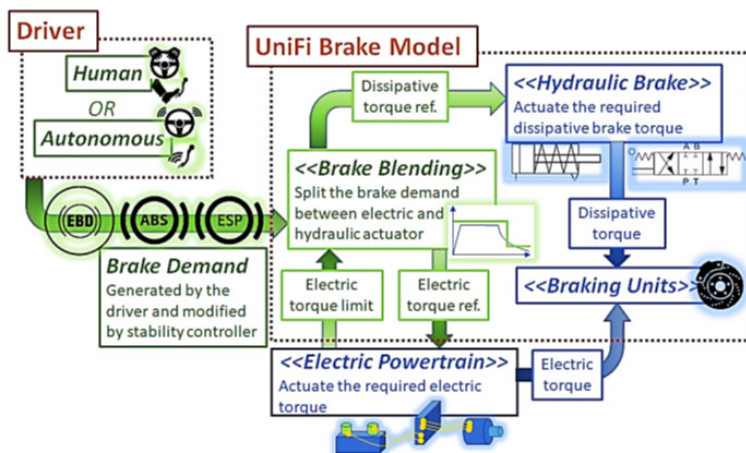


Figure A.4: UniFi Brake Model: layout and main subsystem.

According the scheme of Figure A.4, **UniFi Brake Model (UBM)** is composed by three sub-modules:

- *Brake Blending Controller (BBC)*: an algorithm devoted to executing the brake blending strategy.
- *Hydraulic Brake Plant*: it simulates the hydraulic actuation of the dissipative braking torque.
- *Braking Units*: which reproduce the application of braking torques on vehicle's wheels, including the wear and thermal calculations of disc and pad.

### Brake Blending and Vehicle Stability Controllers

Stability controllers, like ESP, perform vehicle torque vectoring by modulating braking torques applied on left and right wheels: in this way it's possible to apply an equivalent yaw torque  $M_{yaw}$  to the car-body, in order to correct its trajectory.

For this reason, brake blending has to be integrated in a more general optimal torque allocation policy of controllers devoted to keep the lateral/directional stability of the vehicle performing torque vectoring.

Assuming that applied longitudinal efforts can be modulated separately on each wheel, corresponding efforts should be calculated as the ratio between torques  $T_{qref-ij}$  and wheel rolling radius  $r_w$ . Also, half-track  $t_i$  between tire contact patches and vehicle symmetry plane are supposed to be constant and known.

According over-cited simplifications, the correction torque  $M_{yaw}$  produced by the in-wheel motors is described by the following equation (A.4):

$$M_{yaw} = \sum T_{ref-ij} \cdot t_i / r_w \tag{A.4}$$

In order to find a near to optimal solution some constraints have to be respected. First, total braking or traction demand should not be affected by the action of the stability controller: the exerted torques  $T_{ref-ij}^*$  has to be maintained as unaltered as possible respect to  $T_{ref-ij}$ , the torques that should be applied to wheels without any intervention of the stability controller:

$$T_{ref-ij} \simeq T_{ref-ij}^* \tag{A.5}$$

Values of applied  $T_{ref-i}$  have to be constrained in order to respect known limitations of braking and traction units (A.6).

$$T_{min-ij} \leq T_{ref-ij} \leq T_{max-ij} \tag{A.6}$$

Finally “norm 2” of the applied correction has to be minimized (A.7).

$$\|T_{ref-ij} - T_{ref-ij}^*\|_2 = \left( \sum (T_{ref-ij} - T_{ref-ij}^*)^2 \right)^{\frac{1}{2}} \tag{A.7}$$

Minimization of (A.7) contributes to find a solution that respect constraints and limitations described by (A.6). Also, a smoother dynamical behaviour of applied actuation is expected. Proposed implementation is described by following steps: first conditions, corresponding to relations (A.4) and (A.5), are implemented obtaining the linear system (A.8).

$$\overbrace{\begin{bmatrix} -\frac{t_f/2}{r_w} & \frac{t_f/2}{r_w} & -\frac{t_r/2}{r_w} & \frac{t_2/2}{r_w} \\ 1 & 1 & 1 & 1 \end{bmatrix}}^A \begin{bmatrix} T_{ref-fl} - T_{ref-fl}^* \\ T_{ref-fr} - T_{ref-fr}^* \\ T_{ref-rl} - T_{ref-rl}^* \\ T_{ref-rr} - T_{ref-rr}^* \end{bmatrix} = \begin{bmatrix} M_{yaw} \\ 0 \end{bmatrix} \tag{A.8}$$

By solving (A.8), using the Moore-Penrose Pseudo-Inverse matrix of  $A$ , it's possible to calculate the desired correction applied on every wheel. The use of Pseudo-Inverse assures the minimization of the norm 2 of the solution as stated by (A.7). Then it is possible to impose to each torque profile  $T_{ref-ij}$  the saturation constrains(A.6), according (A.9).

$$\begin{cases} \text{if } T_{ref-ij} > T_{max-ij} \Rightarrow T_{ref-ij} = T_{max-ij} \\ \text{if } T_{ref-ij} < T_{min-ij} \Rightarrow T_{ref-ij} = T_{min-ij} \end{cases} \quad (\text{A.9})$$

Calculation of (A.8) is repeated until a valid solution is found or alternatively when every torque profile  $T_{ref-ij}$  is saturated. The resulting calculation is quite efficient, since in the worst case four iterations are needed [...].

## Braking Unit

Braking Unit sub-model is able to calculate the power flows and corresponding energy integrals due to the application of braking efforts on wheels: knowing the amount of dissipated energy on each wheel, the model calculates corresponding thermal and wear behaviour of brake friction components. “Braking model” performs the following sub-functionalities that are described in the scheme of Figure A.5:

- Thermal behaviour of components: which calculate the temperature of the dissipative components.
- Wear of components: volume of pollutant debris produced in the braking phase is evaluated.
- Stability of friction/braking performances: torques applied to wheels are corrected taking count of the thermal behaviour of friction components.

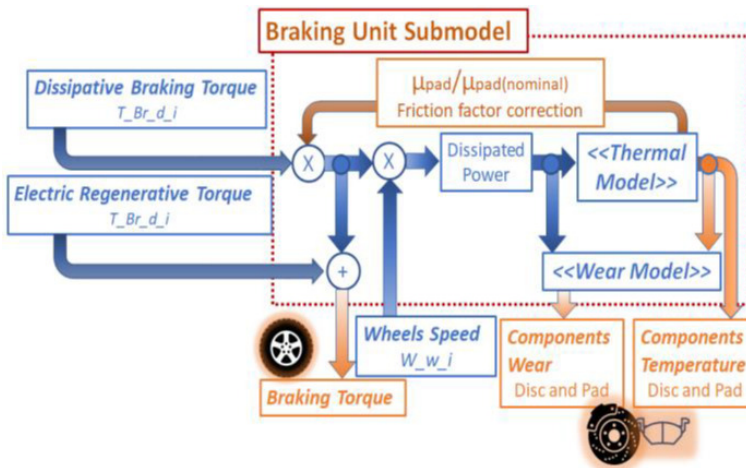


Figure A.5: Braking unit model and corresponding sub-models.

## Thermal Model

$T_{Br-d-i}$  and  $w_{w-i}$  are respectively the dissipative torque applied on the  $i$ -th wheel and the relative rotational speed. Dissipated power on brake-components  $W_{Br-d-i}$  is calculated according (A.10):

$$W_{Br-d-i} = T_{Br-d-i} \cdot w_{w-i} \quad (\text{A.10})$$

Energy is dissipated in the contact interface between pads and discs, so generated heat is transferred to both ones, being  $Q_{pad-i}$  and  $Q_{disc-i}$  respectively the heat flows transferred to pads and disc of the  $i$ -th wheel.

It's possible to define a heat flux distribution coefficient  $\gamma$  (A.11) in order to evaluate how transferred heat flow is divided between pads and discs. By adopting the coefficient  $\gamma$ , a decoupling of the thermal systems (pads and the discs) is introduced<sup>16</sup>.

$$\gamma = \frac{Q_{disc-i}}{Q_{pad-i}} \Rightarrow \begin{cases} Q_{disc-i} = \frac{\gamma}{(\gamma+1)} W_{Br-d-i} \\ Q_{pad-i} = \frac{1}{(\gamma+1)} W_{Br-d-i} \end{cases} \quad (\text{A.11})$$

Once inlet heat flows for each brake component are calculated, it's possible to evaluate the mean temperatures  $T_{disc-i}$  (disc) and  $T_{pad-i}$  (pads), solving the lumped systems described by equations (A.12) and (A.13).

$$Q_{disc-i} = C_{disc-i} \dot{T}_{disc-i} + \left( \overbrace{h_{conv-d-i}}^{convection} + \overbrace{h_{cond-d-i}}^{conduction} + \overbrace{h_{rad-d-i}}^{radiation} \right) (T_{disc-i} - T_{amb}) \quad (\text{A.12})$$

$$Q_{pad-i} = C_{pad-i} \dot{T}_{pad-i} + \left( \overbrace{h_{conv-p-i}}^{convection} + \overbrace{h_{cond-p-i}}^{conduction} + \overbrace{h_{rad-p-i}}^{radiation} \right) (T_{pad-i} - T_{amb}) \quad (\text{A.13})$$

Cooling coefficients adopted in (A.12)-(A.13) and also in the calculation of the heatdistribution factor (A.11), should be tabulated respect to relevant physical parameters (component temperature, disc angular speed, vehicle speed, etc.). In this work these values are assumed constant, except for the convective term, whose value is scheduled in function of vehicle longitudinal speed.

## Wear Model

Wear of friction components it's calculated according an Archard approach corresponding to (A.14) in which it's supposed a proportionality of worn volumes of pads and discs ( $V_{pad}$ ,  $V_{disc}$ ) respect to dissipated energy on brake friction elements ( $E_d$ ).

$$\left. \begin{aligned} V_{pad} &= k_{pad} E_d \\ V_{disc} &= k_{disc} E_d \end{aligned} \right\} \Rightarrow V_{debris} = (k_{pad} + k_{disc}) E_d \quad (\text{A.14})$$

Wear coefficients  $k_{pad}$  and  $k_{disc}$  are supposed to be known. However the main objective of the (A.14) is to evaluate the volume of pollutant debris ( $V_{debris}$ ) produced by conventional braking. In this way it's possible to investigate how electric regeneration can produce a reduction of harmful micro-particles.

### III. Proposed Benchmark Vehicle Model

[...] Proposed approach was tested on a virtual model of a benchmark vehicle whose main parameters have been inspired by a known existing one. This data are freely available on line<sup>17</sup>. However, the latter were not exhaustive, so the model was completed with parameters derived from reasonable heuristic consideration. For the prescribed benchmark authors considered two different powertrain configurations:

- *Single traction Motor*: a conventional powertrain layout in which single electrical motor is used to distribute power to frontal wheels.
- *Four In-wheel Motors*: the same power of the previous case is divided between four identical motors, each one directly connected to a wheel. This second powertrain configuration is not related to any existing application and it's introduced only to evaluate possible advantages arising from different powertrain configurations.

Over described models have been developed in Matlab- Simulink™, where each subsystem is implemented as an independent model instance, allowing a separate execution of threads with different solvers and sampling frequencies. Execution in separated threads allows an efficient execution and the verification of stability troubles due to communication delays between subsystem that also affect the real system.

For the vehicle is adopted a planar 3 DoF model (longitudinal and lateral motion with yaw rotation), also rotation of each wheel is considered. For modelling the tires a Pacejka<sup>18</sup> approach is adopted.

Also high level control sub-systems, are introduced mutating existing simplified sub-models that are used by other simulation tools, such as Amesim™, and inspired by<sup>19</sup> [...].

### VI. Results

[...], proposed brake blending strategy proved to be flexible since it was possible to use the same model for both powertrain configurations proposed for the benchmark vehicle model. In Figure A.6 an example is shown: driver demands a constant braking torque of -700 Nm at the motorized wheels and the algorithm allocates the maximum available braking torque. Only the remaining one is applied through conventional brake system.

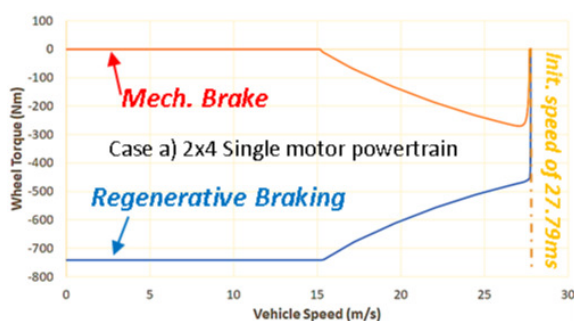


Figure A.6: Brake blending with a constant brake demand of 700 Nm.

In Figure A.7 some results concerning control of brake caliper are shown: it's simulated the application of a full braking followed by a modulation pattern due to ABS intervention with a duty cycle of 50%. Proposed model is clearly able to reproduce some typical features of the plant. It's interesting to notice how, limited bandwidth of brake systems assures a relatively smooth behaviour of applied clamping and braking forces.

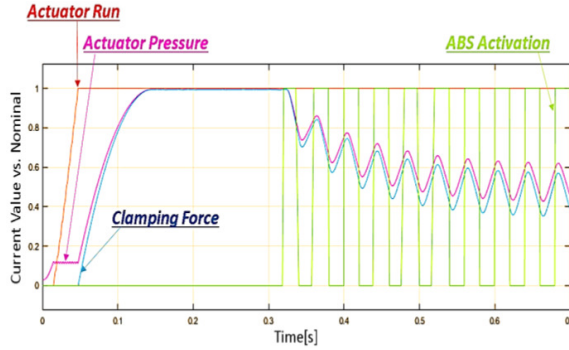


Figure A.7: Example of simulated hydraulic response of a brake caliper

Another interesting feature of the proposed model, its the possibility of reproducing different mission profiles, in order to verify how proposed regeneration strategies, applied to different powertrains, should affect vehicle performances in terms of saved energy and wear of brake pads. Simulations have been repeated for different test cycles (NEDC, WLTP, FTP-75) in order to verify the robustness of obtained results.

Some results are visible in TABLE A.2: as expected, a four inwheel powertrain is absolutely desirable in terms of regenerated energy and stability. Another interesting result is represented by the comparative evaluation of brake pad wear which is far lower for the four in-wheel powertrain.

Table A.2: Consumed vs recovered energy and pad wear

Drive Cycle Simulation Test			
<i>Drive Cycle</i>	<i>Traction Layout</i>	<i>Recovered vs. Consumed energy</i>	<i>Pad Wear Reduction</i>
<b>NEDC</b>	2x4 (A)	0.258	About 60%
	4x4 (B)	0.427	About 99%
<b>WLTP</b>	2x4 (A)	0.287	About 68%
	4x4 (B)	0.454	About 99%
<b>FTP-75</b>	2x4 (A)	0.393	About 66%
	4x4 (B)	0.601	About 99%

These results can be easily explained considering the limited deceleration associated to simulated test cycles: for the four in-wheel powertrain desired deceleration are almost completely assured by regenerative braking.

## V. Conclusions and Future Developments

In this work, some preliminary results concerning the development of modular brake models have been presented. Proposed models offer interesting features for preliminary sizing and optimization of brake blending policies for electric vehicles. The tool is also designed and optimized for real time implementation and hardware in the loop testing.

## References

1. A. Emadi, K. Rajashekara, and Joo L.Y, "Power Electronics and Motor Drives in Electric, Hybrid Electric, and Plug-In Hybrid Electric Vehicles," *IEEE Trans. Ind. Electron.*, vol. 55, pp. 2237–2245, Jun. 2008.
2. J. de Santiago et al., "Electrical Motor Drivelines in Commercial All-Electric Vehicles: A Review," *IEEE Trans. Veh. Technol.*, vol. 61, pp. 475–484, Feb. 2012.
3. Y. Gao, L. Chen, M. E.-S. transactions, and 1999, "Investigation of the Effectiveness of Regenerative Braking for EV and HEV," 1999.
4. T. Grigoratos and G. Martini, "Brake wear particle emissions: a review," *Environ. Sci. Pollut. Res.*, vol. 22, pp. 2491–2504, Oct. 2014.
5. K. Malachova et al., "Toxicity and mutagenicity of low-metallic automotive brake pad materials," *Ecotoxicol. Environ. Saf.*, vol. 131, pp. 37–44, Sep. 2016.
6. R. de Castro, R. E. Araojo, M. Tanelli, S. M. Savaresi, and D. Freitas, "Torque blending and wheel slip control in EVs with in-wheel motors," *Veh. Syst. Dyn.*, vol. 50, pp. 71–94, Jan. 2012.
7. S. D. Cairano, H. E. Tseng, D. Bernardini, and A. Bemporad, "Vehicle Yaw Stability Control by Coordinated Active Front Steering and Differential Braking in the Tire Sideslip Angles Domain," *IEEE Trans. Control. Syst. Technol.*, vol. 21, pp. 1236–1248, Jul. 2013.
8. L. D. Novellis et al., "Direct yaw moment control actuated through electric drivetrains and friction brakes: Theoretical design and experimental assessment," *Mechatronics*, vol. 26, pp. 1–15, Mar. 2015.
9. Y. Hori, "Future vehicle driven by electricity and control-research on four wheel motored 'UOT Electric March II,'" in *7th International Workshop on Advanced Motion Control. Proceedings (Cat. No.02TH8623)*.
10. C. Geng, L. Mostefai, M. Denai, and Y. Hori, "Direct Yaw-Moment Control of an In-Wheel-Motored Electric Vehicle Based on Body Slip Angle Fuzzy Observer," *IEEE Trans. Ind. Electron.*, vol. 56, pp. 1411–1419, May 2009.
11. S. R. Cikanek and K. E. Bailey, "Regenerative braking system for a hybrid electric vehicle," in *Proceedings of the 2002 American Control Conference (IEEE Cat. No.CH37301)*, 2002.
12. "Brake apparatus for an electric vehicle to maximize regenerative energy," US5895100A, 1999.
13. R. Limpert, "Brake design and safety," 1999.
14. L. Berzi, T. Favilli, E. Locorotondo, M. Pierini, and L. Pugi, "Real Time Models of Automotive Mechatronics Systems: Verifications on a Toy Models", *Mechanisms and Machine Science. Springer International Publishing*, pp. 141–148, 01-Oct-2018.
15. L. Pugi, R. Conti, D. Nocciolini, E. G. J. of Fluid , and 2014, "A tool for the simulation of turbo-machine auxiliary lubrication plants," 2014.
16. G. Genta and L. Morello, "L'autotelaio," 2007.
17. "Web-site of an American car seller, <http://www.fiat500usa.com/2013/04/fiat-500e-full-vehicle-specifications.html>." .
18. H. Pacejka, "Tire and vehicle dynamics," 2005.
19. R. Bosch, "Bosch automotive handbook," 1986.
20. "Obelics Project (Optimization of scalaBle rEaltime modeLs and functIonal testing for e-drive ConceptS) , European Unions Horizon 2020 research and innovation programme under grant agreement No. 769506 official site <https://obelics.eu/>."

## A.4 Brake Blending Strategy on Electric Vehicle: Co-simulation Between MATLAB Simulink and Simcenter Amesim [221]

**Published in** 2019 IEEE 5th International forum on Research and Technology for Society and Industry (RTSI)

**Authors** Lorenzo Berzi, Tommaso Favilli, Marco Pierini, Luca Pugi, Gerhard Benedikt Weiß, Nicola Tobia, Matthieu Ponchant

**Abstract** Application of regenerative braking on electric vehicles has to be carefully optimized in order to maximize the system efficiency, maintaining high performance and reliability levels that are required by the automotive sector. Considering complex interactions arising from the interaction of electric brake plant with vehicle dynamics and other on-board sub-systems, there is the necessity of modular scalable models able to merge multiple competences and different engineering tools, aimed at performing accurate simulation activities. In this work authors present some preliminary results concerning the implementation of a model in which the potentialities of co-simulation between different environment are exploited.

**Keywords** Electric Vehicle; Fiat 500e; Brake System; Brake Blending; Mechatronics; Electric Powertrain Optimizazion

### I. Introduction

[...] Four-quadrant capabilities of modern electric drives employed in the automotive field<sup>3,4</sup> allow regenerative braking, increasing autonomy and efficiency of the EVs<sup>5</sup>. Regenerative brake can provide a reduction of 15-20% of the overall consumed energy, as demonstrated in literature<sup>6,7</sup>, on the basis of real-world driving cycles simulation<sup>8</sup> and road testing<sup>9</sup>. Also, an extended application of regenerative braking system involves a drastic reduction in the wear of the brake friction components<sup>10</sup>. This is a very interesting feature, not only in term of maintenance costs: debris produced by worn brakes are one of the most important sources of pollution<sup>11</sup>.

In this work, authors have investigated the opportunities offered by the co-simulation between different tools: MATLAB Simulink and Siemens Simcenter Amesim [...].

The attention is more focused on the simulation of regenerative braking and on the benefits arising from the possibility of exploiting co-simulation features between different simulation tools. In particular, it's proposed a simplified co-simulation layout between a model of the brake plant and a corresponding simplified vehicle model. Data concerning the proposed benchmark vehicle are made available from CRF. The models have been designed in order to allow, in a short-term scenario, the adoption of general purpose interfaces, such as FMI (Functional Mock-up Interface)<sup>21</sup>, in order to demonstrate the possibility of a full interoperability between different simulation environments. Considering multiple possible application of the proposed tools, ranging from preliminary design to HiL testing, authors also optimize model implementation for a possible RT execution, even on distributed networks. In this latter case, to compensate reduced communication bandwidth between distributed computational resources and to allow a more efficient simulation

of weakly coupled system, authors have suggested the application of numerical methods that have been successfully established in previous research activities<sup>22</sup>.

## II. Aim of the Proposed Work

[...], the proposed models are developed in the perspective of preserving the scalability, modularity, flexibility, abstraction and RT capability.

These mentioned features are necessary for achieving the main aims of this work: verify the interoperability between the UniFi Brake Model (UBM), and the so-called Vehicle Model (VM), while ensuring the standardization and the applicability of the models respect to numerous different EVs UCs, proposed by the project's partners. Also, the potentiality of a co-simulation approach is exposed.

## III. Modelling Approach

[...] In Figure A.8 is reported a representation of the simulation layout [...].

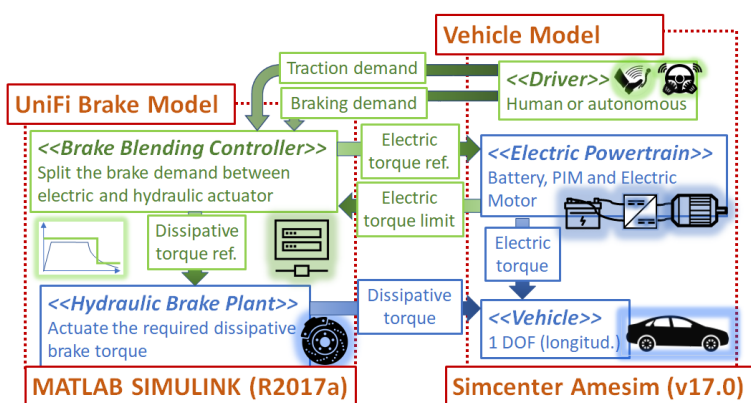


Figure A.8: Co-simulation environmental layout

### A. Unifi Brake Model

The UBM consists of two different subsystems: *Brake Blending Controller* [...]; *Hydraulic Brake Plant* [...].

The Brake Blending Controller (BBC) should consider some limitations, relative to the actuation devices. The availability of several brake sources makes appear the vehicle an over-actuated system, whose effort must be constrained by some steady and variable physical limit conditions [...].

Therefore, according to the aforementioned specifications, the action of the BBC should be able to compensate the unavailability of the actuation systems in several working situations, working adaptively, ensuring at the same time a certain minimum level of performance, able to guarantee a desired vehicle behaviour and safety level.

The Brake Blending Controller is also capable to perform some specific functions, for which is necessary to estimate vehicle longitudinal speed. In particular, for the reference UC, it is advisable to disable the regenerative brake under a specific

vehicle speed value, since the corresponding advantage in terms of recovered energy at very low speed is often negligible respect to additional complexity levels that are introduced in the system management. Finally, the control unit is designed to deliver a “coasting braking torque” (which value is fixed) when none of the accelerator and brake pedals are pressed. This functionality is implemented to reproduce the feeling of the engine brake effect on the pilot, similarly to what happens in conventional ICE vehicles. In this way controllability and drive comfort of the vehicle are highly improved<sup>24</sup> [...].

The Hydraulic Brake Plant is the model of the dissipative brake actuator which delivers the desired braking torques, reproducing the physical phenomena that occur in a real hydraulic braking system. This plant is supposed to be controlled in terms of desired torque performance [...].

### B. Vehicle Model

The modelled vehicle equipment consists of a series of different mechanical, electrical and electronic components, useful for the correct simulation of the vehicle behaviour (during traction and braking phase); i.e.: driver, 1-DoF vehicle chassis, EM, HV battery, Power Inverter Module (PIM), transmission, auxiliary load and LV battery (for accurate calculation of the absorbed energy) [...].

In Figure A.9 are displayed side and top schematic view of the vehicle [...].

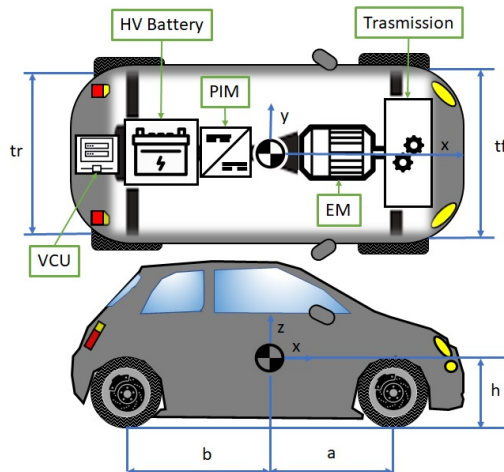


Figure A.9: Representation of the reference UC vehicle

### C. Co-simulation Layout

There are two ways in which the co-simulation between the mentioned software can be performed.

The first one, used in this work, involves the use of a dedicated tools for the concurrent processing among the involved software. It enables a simple and fast data exchange, allowing the independent resolution of the corresponding model. Otherwise, the cooperative simulation could also be performed by exporting both model in the FMI standard (Functional Mock-up Interface) and solving them

through a support interface software (MODELICA language). FMI represents an independent standard tool which supports data exchange between different simulation environments [...].

Figure A.10 shows the implemented configuration in Simcenter Amesim™ and integrates the VCU. Essentially, the VCU is an electronic device which comprises the BBC, that is the corresponding control algorithm implemented in MATLAB. The proposed model appears to be extremely simplified, for which is not considered, for example, the four-quadrant converter for the motor regulation. However, for the battery charging and discharging we impose directly on the BMS model the appropriate Voltage-Current profile<sup>25</sup> [...].

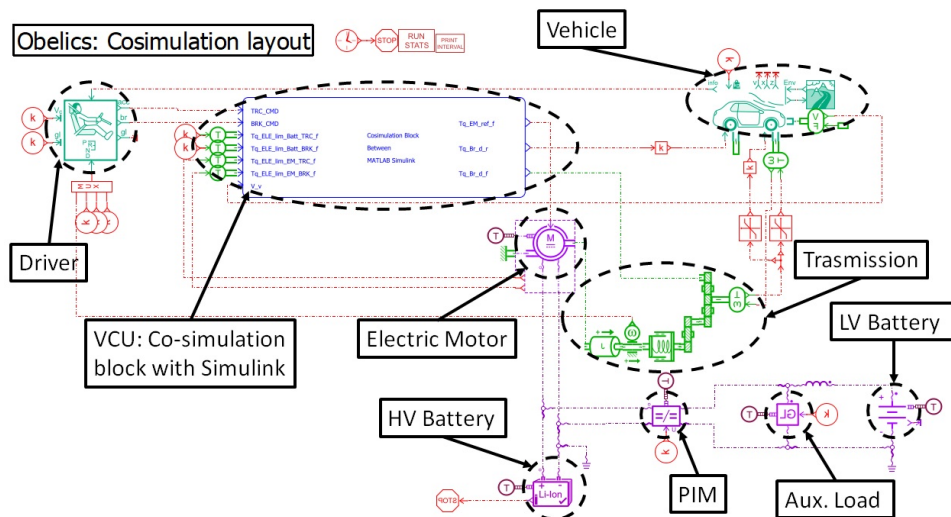


Figure A.10: Co-simulation layout implemented in the Simcenter Amesim™ v17.0 environmental for the reference UC vehicle

It is important to note that the system allows the possibility to adopt different sampling rate between models or sub-models, so the time step of the solvers included in the co-simulation environments may be different. Considering that occurring phenomena characterized by very different time-constants are often simulated together in mechatronics systems, this feature is highly desirable, since allows the use of an optimized resolution configuration according to the need of each subsystem, without compromising the data exchange between them [...].

#### IV. Vehicle Use Cases Description

For this activity we decide to apply the current study to a specific UC, which is an EV developed by one of the project partners: the FIAT 500e [...].

## V. Simulation Results

We can finally present some result arising from the performed simulations.

Firstly, we impose to the vehicle the execution of a certain reference manoeuvre, in order to determine the effectiveness of the blending algorithm. The manoeuvre consists of three different phases:

1. *Traction Phase*: from 0 speed to 144 km/h (40 m/s).
2. *Coasting Phase*: in which no pedals are pressed (both throttle or brake) and the EM provide a coasting braking torque on the driven wheels.
3. *Braking Phase*: where the vehicle slows down until is completely stopped (supposing a constant brake demand).

As visible in Figure A.11, the BBC correctly assign the effort applied by EM (traction and regenerative braking) and the disc brakes (mechanical braking) in order to maximize the recovered energy.

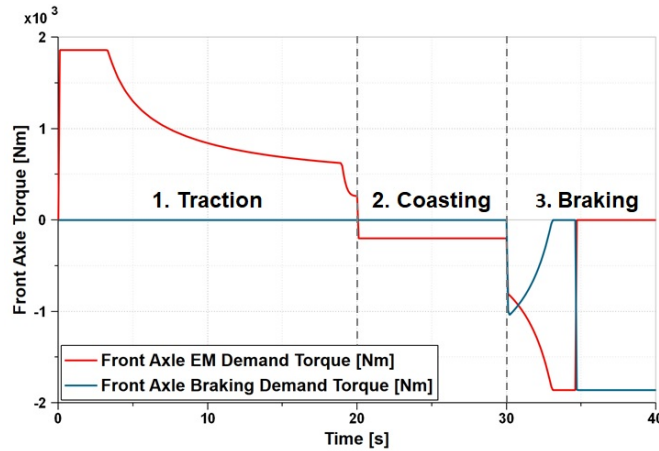


Figure A.11: Demanded torque on front axle during the reference manoeuvre

After this, we impose a well-known (in literature) speed profile to the vehicle, in order to evaluate its energy performances, shown in Figure A.12 [...]: the WLTP.

For comparatively evaluate the results of this simulated scenario we consider multiple vehicle traction layout configuration: without regenerative braking, with regenerative braking on front axle and with regenerative braking in both front and rear axle. In Figure A.13a are expose the consumed and the regenerate energy profile during WLTP class 3 driving cycle for the previously mentioned powertrain configuration, while in Figure A.13b is visible the trend of the battery SOC, also in all mentioned cases. Table A.3, instead, show the overall consumed and regenerated energy, the final  $SOC_f$  of the battery (supposing an initial 60% of charge), along with the percent of the regenerated energy improvement obtained in the reference driving cycle.

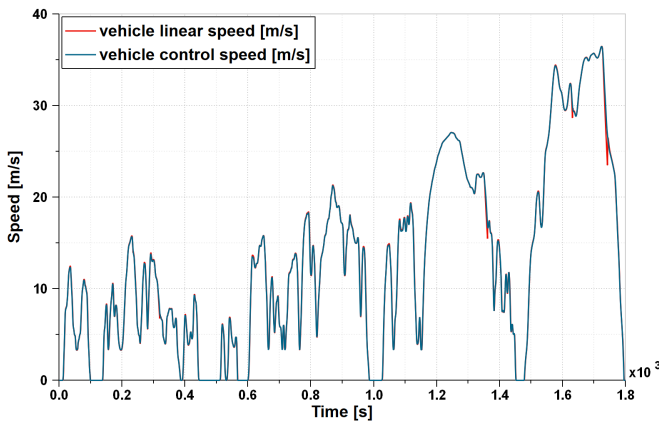
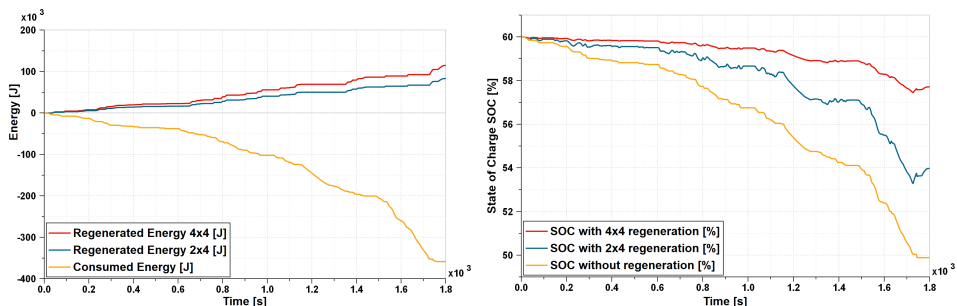


Figure A.12: Vehicle speed during a WLTC Class 3



(a) Consumed and Regenerated Energy during a WLTC class 3 (b) Battery SOC trend during a WLTC class 3

Figure A.13: Energy and SOC during WLTP class 3

Table A.3: Vehicle energy performance during WLTP class 3 cycle

Vehicle Energy Performances				
Cases	Consumed Energy [kJ]	Regenerated Energy [kJ]	Regenerated Energy [%]	SOC <sub>f</sub> [%]
No Regenerative Brake	1582.1 kJ	0 kJ	0%	41.2%
2x4 Regenerative Brake	1353.6 kJ	225.5 kJ	14.25%	43.9%
4x4 Regenerative Brake	1306.3 kJ	275.8 kJ	17.4%	44.5%

## VI. Conclusion and Future Developments

The availability of the regenerative brake system consents to recovery part of the total consumed energy, about 15-18% as visible in Table A.3, depending of the adopted powertrain configuration [...].

The Brake Blending strategy applied in this study appear to be extremely efficient and reliable, since address the maximum of the requested braking effort to the electric motor, in the respect of the corresponding constrains, leaving to the disc brake the burden to compensate a possible gap between the required torque and the one delivered by the EM. For what concern the simulation potentiality, it seems that use a cooperative simulation environment can lead to the possibility to use different solvers and sample times for the integration of the implemented subsystem, while ensuring a fast data exchange between the used software.

The actual implementations allow the coupling between UBM and VM, whose integration is performed with the help of different solvers and sampling steps, reported in Table A.4. The proposed co-simulation layout replicates the behaviour of a realistic EV well, both for what concern the brake system as its energy performance, automatically executing data extrapolation of the input signal, to ensuring the continuity of the exchanges data between the software. This feature is fundamental in order to compensate the delay effect arising by the use of different solver's sample time and communication interval.

Table A.4: Cosimulation Solver and Sample Rate Settings

<b>Cosimulation settings</b>			
<i>System</i>		<i>Sample Time</i>	<i>Solver</i>
UBM	BBC	0.01 [s]	ODE1 (Euler)
	Hydraulic Brake	0.001 [s]	ODE14x (Extrap.)
VM		0.01 [s]	Standard
Communication		0.01 [s]	

## References

1. A. Emadi, Young Joo Lee, and K. Rajashekara, 'Power Electronics and Motor Drives in Electric, Hybrid Electric, and Plug-In Hybrid Electric Vehicles', IEEE Trans. Ind. Electron., vol. 55, no. 6, pp. 2237–2245, Jun. 2008.
2. B. Bilgin and A. Emadi, 'Electric Motors in Electrified Transportation: A step toward achieving a sustainable and highly efficient transportation system', IEEE Power Electron. Mag., vol. 1, no. 2, pp. 10–17, Jun. 2014.
3. A. Walker, M. Galea, C. Gerada, A. Mebarki, and D. Gerada, 'A topology selection consideration of electrical machines for traction applications: towards the FreedomCar 2020 targets', p. 10.
4. L. Pugi, F. Grasso, M. Pratesi, M. Cipriani, and A. Bartolomei, 'Design and preliminary performance evaluation of a four wheeled vehicle with degraded adhesion conditions', Int. J. Electr. Hybrid Veh., vol. 9, no. 1, p. 1, 2017.
5. J. de Santiago et al., 'Electrical Motor Drivelines in Commercial All- Electric Vehicles: A Review', IEEE Trans. Veh. Technol., vol. 61, no. 2, pp. 475–484, Feb. 2012.
6. M. T. Von Srbik and R. F. Martinez-Botas, 'Vehicle optimisation for regenerative brake energy maximisation', in Sustainable Vehicle Technologies, Elsevier, 2012, pp. 165–174.

7. J. A. A. Hartley, R. G. McLellan, J. Richmond, A. J. Day, and I. F. Campean, 'Regenerative braking system evaluation on a full electric vehicle', in *Innovations in Fuel Economy and Sustainable Road Transport*, Elsevier, 2011, pp. 73–86.
8. L. Berzi, M. Delogu, and M. Pierini, 'Development of driving cycles for electric vehicles in the context of the city of Florence', *Transp. Res. Part Transp. Environ.*, vol. 47, pp. 299–322, Aug. 2016.
9. C. Qiu and G. Wang, 'New evaluation methodology of regenerative braking contribution to energy efficiency improvement of electric vehicles', *Energy Convers. Manag.*, vol. 119, pp. 389–398, Jul. 2016.
10. R. Conti, E. Galardi, E. Meli, D. Nocciolini, L. Pugi, and A. Rindi, 'Energy and wear optimisation of train longitudinal dynamics and of traction and braking systems', *Veh. Syst. Dyn.*, vol. 53, no. 5, pp. 651–671, May 2015.
11. T. Grigoratos and G. Martini, 'Brake wear particle emissions: a review', *Environ. Sci. Pollut. Res.*, vol. 22, no. 4, pp. 2491–2504, Feb. 2015.
12. P. Tawadros, N. Zhang, and A. Boretti, 'Integration and performance of regenerative braking and energy recovery technologies in vehicles', in *Alternative Fuels and Advanced Vehicle Technologies for Improved Environmental Performance*, Elsevier, 2014, pp. 541–563.
13. 'Homepage - Obelics | Obelics'. [Online]. Available: <https://obelics.eu/>. [Accessed: 17-Apr-2019].
14. L. Pugi, M. Malvezzi, S. Papini, and S. Tesi, 'Simulation of braking performance: The AnsaldoBreda EMU V250 application', p. 13.
15. K. T. Chau, 'Pure electric vehicles', in *Alternative Fuels and Advanced Vehicle Technologies for Improved Environmental Performance*, Elsevier, 2014, pp. 655–684.
16. C. Satzger, R. de Castro, A. Knoblach, and J. Brembeck, 'Design and validation of an MPC-based torque blending and wheel slip control strategy', in *2016 IEEE Intelligent Vehicles Symposium (IV)*, Gotenburg, Sweden, 2016, pp. 514–520.
17. C. Satzger and R. de Castro, 'Combined wheel-slip control and torque blending using MPC', in *2014 International Conference on Connected Vehicles and Expo (ICCVE)*, Vienna, Austria, 2014, pp. 618–624.
18. C. Lv, H. Wang, and D. Cao, 'Brake-Blending Control of EVs', in *Modeling, Dynamics and Control of Electrified Vehicles*, Elsevier, 2018, pp. 275–308.
19. L. Berzi, T. Favilli, E. Locorotondo, M. Pierini, and L. Pugi, 'Real Time Models of Automotive Mechatronics Systems: Verifications on "Toy Models"', in *Advances in Italian Mechanism Science*, vol. 68, G. Carbone and A. Gasparetto, Eds. Cham: Springer International Publishing, 2019, pp. 141–148.
20. L. Pugi, T. Favilli, L. Berzi, M. Pierini, and E. Locorotondo, 'Application of Regenerative Braking on Electric Vehicles', p. 6.
21. 'The Distributed Co-Simulation Protocol for the Integration of Real- Time Systems and Simulation Environments', in *Proceedings of the 50th Computer Simulation Conference*, University of Bordeaux, Bordeaux, France, 2018.
22. M. Benedikt, D. Watzenig, J. Zehetner, and A. Hofer, 'MACRO-STEP SIZE SELECTION AND MONITORING OF THE COUPLING ERROR FOR WEAK COUPLED SUBSYSTEMS IN THE FREQUENCY-DOMAIN', p. 12.
23. B. Allotta and L. Pugi, *Meccatronica: azionamenti elettrici ed oleodinamici*. Bologna: Esculapio, 2016.
24. S. Murata, 'Innovation by in-wheel-motor drive unit', *Veh. Syst. Dyn.*, vol. 50, no. 6, pp. 807–830, Jun. 2012.
25. Junjun Deng, Siqi Li, Sideng Hu, C. C. Mi, and Ruiqing Ma, 'Design Methodology of LLC Resonant Converters for Electric Vehicle Battery Chargers', *IEEE Trans. Veh. Technol.*, vol. 63, no. 4, pp. 1581–1592, May 2014.
26. 'Model.CONNECTTM - Model.CONNECTTM - IODP Portfolio', AVL. [Online]. Available: <https://www.avl.com>. [Accessed: 24-Apr-2019].
27. S. Georg Stettinger, M. Martin Benedikt, B. Norbert Thek, and Josef Zehetner, *Computational methods for coupled problems in science and engineering V*. Barcelona: International Center for Numerical Methods in Engineering, 2013.

## A.5 Fast modelling and identification of hydraulic brake plants for automotive applications [213]

**Published in** International Journal of Fluid Power

**Authors** Luca Pugi, Federico Alfatti, Lorenzo Berzi, Tommaso Favilli, Marco Pierini, Bart Forrier, Thomas D'Hondt, Mathieu Sarrazin

**Abstract** Diffusion of electric and hybrid vehicles is accelerating the development of innovative braking technologies. Calibration of accurate models of a hydraulic brake plant involves availability of large amount of data whose acquisition is expensive and time consuming. Also, for some applications, such as vehicle simulators and hardware in the loop test rig, a real-time implementation is required. To avoid excessive computational loads, usage of simplified parametric models is almost mandatory. In this work, authors propose a simplified functional approach to identify and simulate the response of a generic hydraulic plant with a limited number of experimental tests. To reproduce complex non-linear behaviours that are difficult to be reproduced with simplified models, piecewise transfer functions with scheduled poles are proposed. This innovative solution has been successfully applied for the identification of the brake plant of an existing vehicle, a Siemens prototype of instrumented vehicle called SimRod, demonstrating the feasibility of proposed method.

**Keywords** Identification, modelling, brake plants, piecewise transfer function, linear systems with scheduled poles.

### 1 Introduction

There is a wide literature<sup>1-5</sup> concerning simulation of conventional automotive brake plants, which is usually performed using customized commercial tools [...].

Different innovation trends of automotive sector are boosting the proliferation of different brake plant configurations.

[...] there is an increasing interest for studies concerning innovative brake plant configurations<sup>15-18</sup> to improve both performances and implemented functionalities.

[...] Literature works<sup>17,19,20</sup> emphasize different aspects of a common topic: the need of an increasing integration between a conventional brake system, electric powertrain and various vehicle systems through VCU (Vehicle Control Unit).

[...], authors have to develop general purpose models that should be used to reproduce and fit the functionalities of different braking plants that are installed on a wide variety of vehicles [...].

In this sense, the work is not only a relevant result of the over-cited research project but also an original research contribution respect to exigences of major automotive industrial players that have sustained not only this specific project but also the whole European research call H2020 in which these topics are widely addressed. Looking at the list of different kind of vehicles, it is difficult to obtain a pure physical model that fit the behaviour of different brake plants by accurately modelling each sub-component. Also a certain level of abstraction of the model should be very important in order to assure the portability of proposed models between different simulation environments [...].As example, in literature there are

specific works dedicated to the modelling of ABS controllers and hydraulic brake plants<sup>21</sup>. Also, it is easy to find brake models which are optimized for a specific vehicle or plant layout. However, there is a gap for what concern simplified general models that can be used to fit plant functionality abstracting from specific physical features of components and subsystems. Also, very accurate models involve the availability of a large amount of data and the calibration of many parameters, which are often not available. For these reasons, a general-purpose procedure is proposed and investigated in this work.

Proposed approach should be usable for different tasks and activities: Preliminary Design, Simulations and Numerical Optimizations; RTI for HiL, SiL and MiL systems; Re-use of proposed models as part of model-based filters, controllers and estimators.

In this work it is proposed a hybrid functional model: simple physical elements are introduced to perform an easy calibration; more complex functionalities are implemented with interpolated piece-wise linear transfer functions, able to fit a wide variability of different behaviours acting on a reduced set of parameters [...].

Piece-wise linear transfer functions are a powerful instrument that is commonly used to approximate systems with a strong non-linear behaviour, minimizing the number of integrated states and maintaining a high level of continuity on calculated states and corresponding derivatives. [...] are widely proposed and adopted in literature<sup>24</sup> to perform robust model reduction of systems with non-linear or badly scaled dynamics<sup>25,26</sup>. Authors have considered an existing electric sport vehicle the Kyburz SimRod as benchmark test vehicle.

Original contributions of this research respect to current literature are mainly two:

- **Functional Decomposition of the Plant:** proposed model it is not simplified physical representation of the plant, but of its functionalities. Simplified physical sub-models are introduced only to make possible an easy tuning of proposed model respect to experimental data.
- **Piece-wise Transfer Functions:** poles of linear transfer functions are scheduled respect to state values and their derivatives. In this way it is possible to reproduce complex non-linear phenomena affecting both amplitude and frequency response of the plant. Resulting model maintains a low number of integrated states and assures a numerically smooth behaviour.

## 2 Brake System Model

Authors started their work from a general scheme of a brake plant taken from literature<sup>27</sup>. Brake Plant is analysed in terms of implemented features and functionalities to better understand how to generalize and simplify proposed simulation model [...].

To fit the functional behaviour of a generic brake plant, authors propose a simplified pseudo-physical model, whose main features are briefly described in Figure A.14. Brake Demand is pre-processed using a piece-wise second order transfer functions. Static gain of the transfer function is scheduled to fit plant response in terms of amplitude.

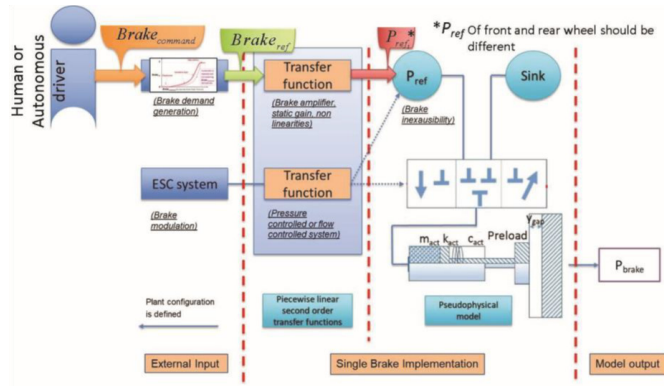


Figure A.14: Simplified pseudo-physical model proposed by university of Florence.

Poles of the transfer function are scheduled respect to system states, to reproduce dynamic response of brake plant including non-linear features. Output of this transfer function is an equivalent pressure reference, corresponding to the desired torque that must be transmitted to braking units. This reference pressure is modulated considering an independent actuation unit for each wheel. In this way it is possible to control the brake force applied on each wheel by controlling the clamping force applied by each calliper. To model the simplified hydraulic plant of callipers, a multi-physics approach<sup>28</sup> is followed. Fluid compressibility is modelled as a single RC that simulate equivalent capacity and losses of the plant. This hydraulic model is coupled with a lumped mechanical able to simulate mechanical response of the calliper. Many on board subsystems have to modulate brake forces on wheels, such as example, ABS and ESP. In order to control the brake force of each wheel, actuation of each calliper is controlled by another valve which is also modelled using piece-wise second order transfer function. Inexhaustible Braking behaviour is current implemented supposing a proper design of the system, so pressure reference is modelled as an ideal pressure source.

However, limitations of a real pumping unit can be easily simulated by considering a real pressure source, whose response is limited by a fixed or a scheduled hydraulic loss coefficient [...].

## 2.1 Brake Demand Generation

[...]  $Brake_{ref}$  represents the required braking performance generated by an input signal called  $Brake_{command}$ . An example is the run of brake pedal which is used by the human driver to activate vehicle brake.  $Brake_{ref}$  is a tabulated function of the input  $Brake_{command}$  and its derivative, as visible in Figure 3. In this way it is possible to reproduce some non-linear behaviour of system response, such as dead-zones, variable gains, saturation effects.

[...] Once desired longitudinal forces  $T_f$  and  $T_r$  are known, corresponding values of steady state pressure, called  $P_{max-i}$ , can be calculated according to (A.15).

$$T_i = (P_{max-i}A - F_{preload} - k_{act}y_{gap}) \frac{r_{brake}f}{r_{wheel}} \quad (A.15)$$

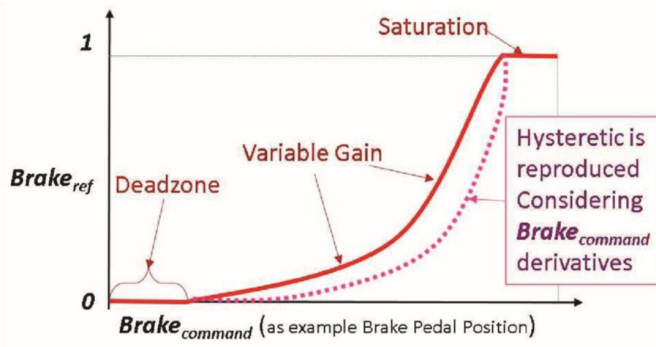


Figure A.15: Example of feed-forward tabulation for brake torque reference respect to the brake command

The following symbology is adopted:  $A$  is the equivalent area of the calliper (including friction surfaces and actuators);  $F_{preload}$ ,  $k_{act}$  and  $y_{gap}$  are respectively the pre-load, stiffness and run of the calliper;  $r_{brake}$  and  $r_{wheel}$  are the mean disc radius and the mean rolling radius of the wheel;  $f$  is the friction factor between brake pads and discs;  $P_{max-i}$  is the steady state value of brake pressure that should be applied to the brake calliper in order to obtain the desired value of longitudinal brake force  $T_i$ , in steady state conditions.

Assuming to model the system as an equivalent pressure-controlled loop, transfer function described in (A.16) is used to represent evolution of Pref respect to the desired steady state value  $P_{max-i}$ :

$$P_{ref}(s) = Brake_{ref}(s)P_{max-i} \overbrace{\frac{\omega_n^2}{s^2 + 2\epsilon\omega_n s + \omega_n^2}}^{G(s) \text{ transfer function}} \tag{A.16}$$

Where in (A.16), following symbology is adopted:  $\omega_n$  is the equivalent eigenfrequency/pole of the pressure loop,  $\epsilon$  is the damping factor. Second Order transfer functions are often used to approximate the dynamical behaviour of both flow-controlled and pressure-controlled valves [...].

Transfer function (A.16) is often a rough approximation of plant response, so authors adopted a piece-wise linear transfer function in which parameters [...] are scheduled as functions of system states. [...] authors implemented the transfer function  $G(s)$  according the scheme of Figure A.16. In this way, it's possible to change the coefficients with continuous smooth behaviour: even a step variation of transfer function coefficients produces an output signal which is at least C1 (continuity of function and of its first derivative). [...] it is possible to properly shape a smooth and continuous behaviour of simulated pressure reference.

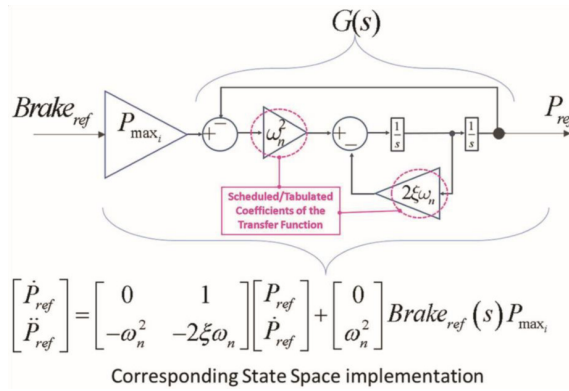


Figure A.16: Implementation of equation (A.16)

## 2.2 Brake Actuator Model

Pressure reference [...] represents from a physical point of view the output pressure provided by the brake amplifier of the plant which is used to feed brake actuators as described by the scheme of Figure A.17:  $P_{ref}$  is modelled as an ideal pressure source which is used to feed the actuator, a single chamber cylinder with pre-load springs through a three way valve. This three-way valve that is normally open when ABS is not working, introduces pressure drops and consequently flow limitations that are useful to properly fit the response of a real plant.

[...] is reproduced the step application of braking forces followed after one second by a step release of the brake: for front and rear brake cylinders is supposed a different braking pressure (65 and 40 bar respectively): this benchmark model is still not calibrated or tuned for a precise case study since the aim of this example is only to demonstrate some potential feature of the proposed approach; [...] application and release of brake effort is delayed by a transient which is mainly influenced by the choice of parameters of (A.16) that describes plant dynamics.

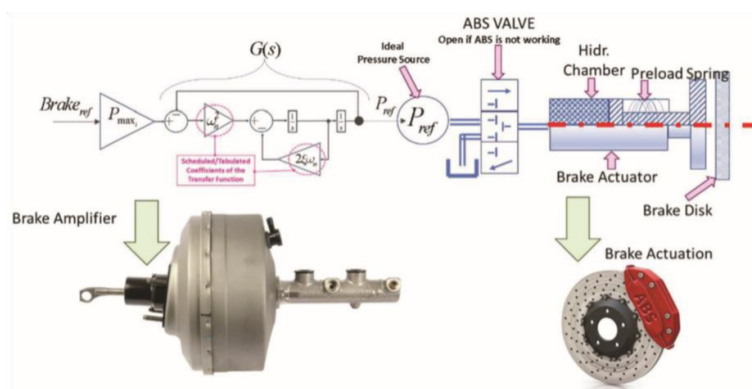


Figure A.17: Implementation of a control loop to used impose the pressure of the actuator

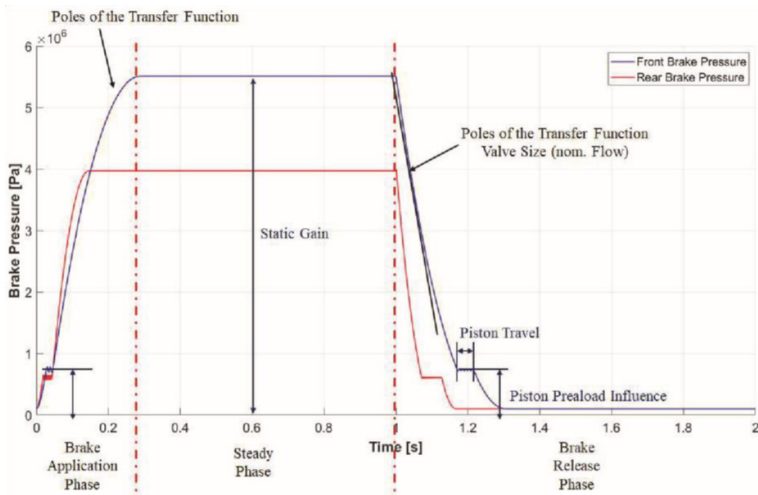


Figure A.18: Example fitting capability of the proposed model

### 2.3 Brake Actuator Model Plant Configuration

On modern vehicles, brake plant is interconnected with several on board control and safety systems, e.g. ABS<sup>33</sup> or ESP<sup>34</sup>. These systems may overrule or modulate demanded braking efforts. This functionality is typically assured by a system of fast response valves which intercepts the fluid flow that is provided for brake clamping [...].

Since ABS operates with high switching frequencies, modelling must take count of the dynamic response of these fast reacting valves. [...] behaviour of these fast reacting valves can be modelled using a 2nd order transfer function  $G_v(s)$  adopting an approach which is substantially like the one adopted in (A.17) to model the dynamic response of brake amplifier. [...]  $G_v(s)$  is the ratio between  $x_{vi}$  and coil current command  $i_{vi}$  [...]; dynamic behaviour of the valve is modelled by tuning only two parameters, natural frequency  $\omega_{nv}$  and damping coefficient  $\epsilon_v$ .

$$G_v(s) = \frac{x_{vi}}{i_{vi}} = \frac{\omega_{nv}^2}{s^2 + 2\epsilon_v\omega_{nv}s + \omega_n^2} \quad (\text{A.17})$$

### 2.4 Inexhaustible Brake Behaviour

In this work we assume the presence of an ideal pressure source  $P_{ref}$ . The amount of fluid and the volume flow rate are considered unlimited, i.e. the brake system is assumed to be “inexhaustible”. A possible extension would be to introduce a flow limitation on  $P_{ref}$ , e.g. for a virtual Hazard and Operability (HazOp) analysis of degraded plant response<sup>27</sup>.

## 3 SimRod Brake Plant

As previously introduced proposed brake plant has been calibrated and validated on experimental data collected from an existing electric vehicle called SimRod that has been assembled by Siemens.

Current version of SimRod prototype is not equipped with any stability mechatronics system aiming to improve vehicle stability; vehicle brake plant is described in Figure A.19: plant is composed by two master cylinders working in parallel; master cylinders amplifies the command provided through a conventional brake pedal. Each master cylinder controls separately the clamping pressure of callipers on front and rear wheels.

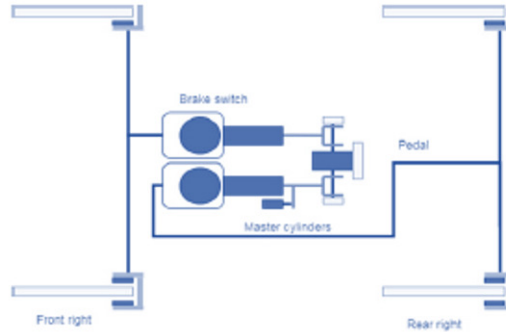


Figure A.19: SimRod Kyburz simplified brake plant scheme

[...] Currently no blending strategy is implemented so electric regenerative braking is applied through a separated command that must be intentionally activated by the driver. For the aim of this work electric regenerative braking was disabled so only the conventional hydraulic brake plant is used to decelerate the vehicle. SimRod was equipped with the measurement system described in Figure A.20:

- Vehicle dynamics and localization: vehicle kinematics and position are identified using a fully integrated OXTSTM RT3003 Inertial Measurement Unit (IMU) (6 D.O.F inertial measurement, GPS and magnetometer);
- Wheel-road interaction: forces exchanged between road and tyres are measured through a 6-axis Wheel Force Transducer (WFT) of the RoaDyn™ series, from Kistler; these sensors are installed on wheels;
- Electric drive system: battery and electric drive are continuously monitored, respectively by BMS and by Motor Control unit MCU;
- Additional sensors: vehicle is customized to be easily adapted to different testing activities (a maximum of about 150 signals not fully listed here can be acquired). Also braking plant is monitored by measuring pressures on callipers and brake pedal position.

All data are collected using a Siemens Simcenter SCADAS. For the particular purpose of this work, hydraulic plant was equipped with additional sensors described in Table A.5. All brake related measurements (displacement measures, forces, pressures, etc.) are acquired with a sampling frequency of 1024 Hz.

This general approach is applicable to several different kind of brake plants, including brake by-wire ones, in which this kind of signals are often generated by different components and subsystems.

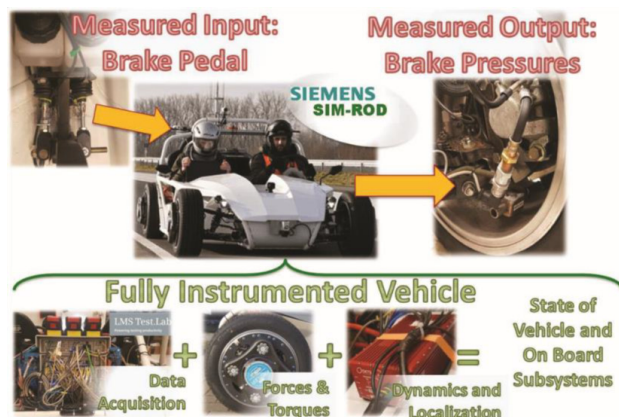


Figure A.20: Main elements of the acquisition system installed on SimRod prototype for the identification of main brake plant features

Table A.5: Vehicle and brake plant data-sheet

Phys. Quantity	Symbol	Sensor	Measured
Force(f)	$F_f$	Strain gauge	Strain [ $\mu\epsilon$ ]
Force(r)	$F_r$	Strain gauge	Strain [ $\mu\epsilon$ ]
Displ(f)	$x_f$	Potentiometer	Displ [mm]
Displ(r)	$x_r$	Potentiometer	Displ [mm]
Pressure(f)	$p_{brake-f}$	Pres. sens.	Pressure [bar]
Pressure(r)	$p_{brake-r}$	Pres. sens.	Pressure [bar]

## 4 Performed Identification Campaign: Methods and Obtained Results

### 4.1 Aim and Organization of Testing Campaign

Aim of performed campaign is to verify how proposed model can fit the response of a real plant with a reduced set of known data and experimental results.

Test campaign have been organized in the as follow:

- Standstill Tests:[...] known inputs are applied to brake pedals, to identify hydraulic plant behaviour, in terms of clamping pressure inside callipers. Model proposed by UNIFI implements a decoupled scheduling of both amplitude and frequency response of brake plant. Thanks to this approach, it was possible to calibrate separately the model first in terms of amplitude response with steady state tests, refining aspects related to frequency response with few dynamic tests [...].
- Dynamic Test on Circuit: [...]authors execute some additional tests to perform a preliminary validation of the model with the vehicle running on a circuit. Purpose of this activity is to verify how various braking patterns performed on a circuit by a driver should be fitted by a model calibrated with a limit number of step test in standstill conditions. These additional tests have been performed on the circuit of Aldenhoven (Germany). Tests were performed on a dedicated "Braking manoeuvre zone", visible in Figure A.21 [...].

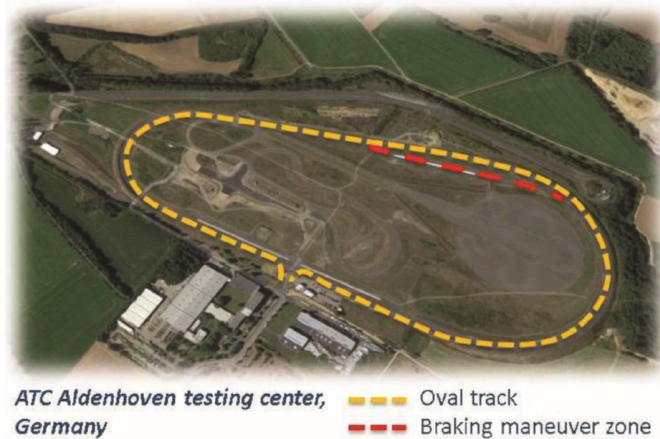


Figure A.21: Testing center of Aldenhoven (Germany).

## 4.2 Amplitude Response Identification

[...] In order to identify the amplitude response of plant, authors execute some simple tests: first, brake pedal is lowered slowly (imposing a linear displacement growth), in order to identify the dead-band or some compliance that has to be recovered in terms of pedal displacements. In this way is possible to produce a non-zero response of the plant, in terms of brake pressure.[...] Then test with multiple braking tests are executed: brake pedal position (input) is imposed and corresponding pressures on callipers (outputs) are measured. In Figure A.22 imposed pistons run profile is shown: in each test brake pedal position is increased from the lower end run to the upper one, with three consecutive steps. Amplitude of each intermediate step is randomly perturbed and their duration is high enough to assure the achievement of steady state conditions before the application of the following step (the duration of twait is much bigger than the observed time constant of the system). [...] After maximum run is reached pedal returns to the lowest position through three falling steps that are generated with the same random procedure used for the rising ones. [...] This cycle is repeated for at least ten times to have data corresponding to a population of at least 60 random steps (30 rising and 30 falling steps).

To calibrate the scheduled relation between pedal displacement and corresponding steady state pressure of brake plant, it is recommended to observe the system output after transient becomes negligible. In Figure A.23 is visible an example of this procedure: when derivatives of observed signals are sufficiently low, we perform a running mean of the observed pressure. In this way, it is possible to evaluate two interpolated curves for the rising and falling values of the reference, that approximately describe the amplitude response of the system, including its hysteresis. In particular, according to the sign of  $Brake_{ref-i}$ , it's possible to define an upper rising gain profile and a falling one. Results of Figure A.23 are scaled respect to maximum input displacements and maximum brake pressure of front and rear callipers, respectively.

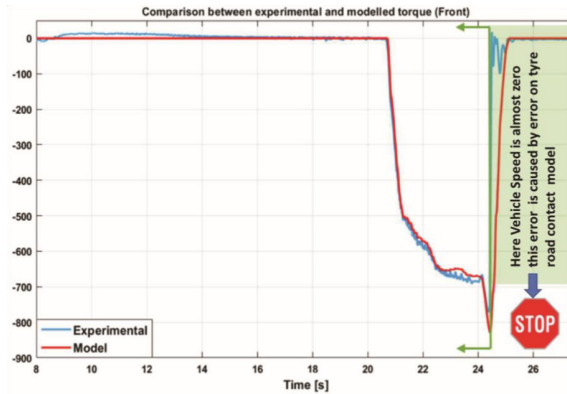


Figure A.22: Experimental three-steps input measurement results: imposed brake piston displacements.

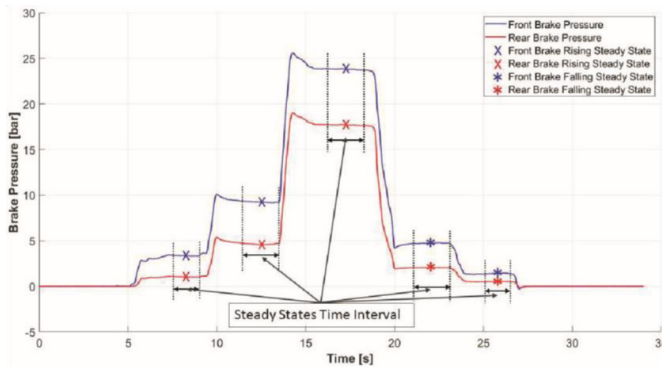


Figure A.23: Evaluation of steady-state values for a three-steps test: brake pressures.

To calibrate the scheduled relation between pedal displacement and corresponding steady state pressure of brake plant, it is recommended to observe the system output after transient becomes negligible. [...] In this way, it is possible to evaluate two interpolated curves for the rising and falling values of the reference, that approximately describe the amplitude response of the system, including its hysteresis. In particular, according to the sign of  $Brake_{ref-i}$ , it's possible to define an upper rising gain profile and a falling one. Results of Figure A.24 are scaled respect to maximum input displacements and maximum brake pressure of front and rear callipers, respectively.

### 4.3 Frequency Response Identification

[...] parameters that have to be tuned, to fit plant response, are  $\omega_n$  and  $\epsilon$  of the second order transfer function (A.16). [...] To fit experimental response of the plant, parameters should be scheduled respect to measured inputs or states and their corresponding derivatives: coefficients are scheduled respect to the sign of the derivatives of  $Brake_{ref-i}$  and  $P_{ref-i}$ , as described in Table (A.6).

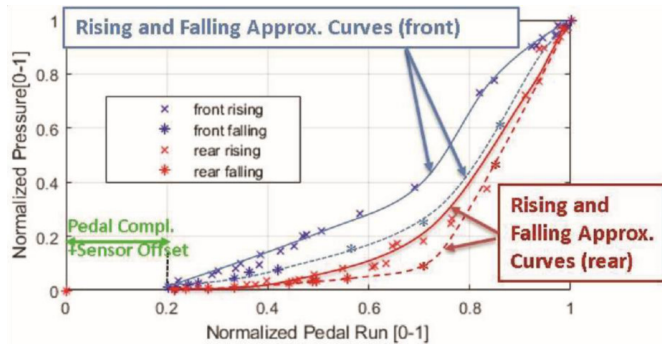


Figure A.24: Normalized pressure plant response vs normalized pedal run.

Table A.6: Frequency response calibration

	$Brake_{ref-i} \geq 0$	$Brake_{ref-i} < 0$
$\dot{P}_{ref-i} \geq 0$	$\begin{cases} \omega_n = 13.5[rad/s] \\ \epsilon = 0.15 \end{cases}$	$\begin{cases} \omega_n = 10[rad/s] \\ \epsilon = 4000 \end{cases}$
$\dot{P}_{ref-i} < 0$	$\begin{cases} \omega_n = 67.5[rad/s] \\ \epsilon = 2.25 \end{cases}$	$\begin{cases} \omega_n = 40[rad/s] \\ \epsilon = 2 \end{cases}$

[...] Since experimental data were naturally noisy pressure and brake command derivatives must be calculated with a relatively aggressive filtering (Butterworth 3rd order with a cutting frequency of about 100 rad/s). This treatment of measured signals proved to be one of the major sources of errors in performed activities.

#### 4.4 Calibration Tests, Some Examples

By applying both over explained amplitude and frequency scheduling described in Figure A.25, authors were able to fit in quite satisfying way experimental behaviour of calibration tests.

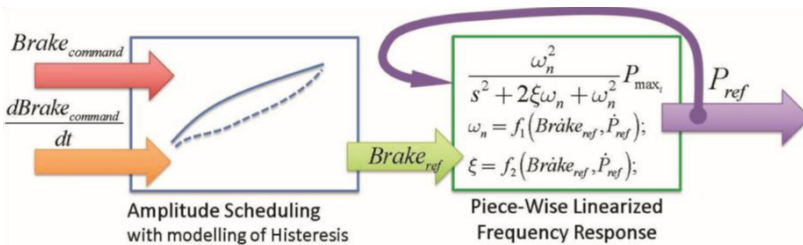


Figure A.25: Application of ampl. and freq. scheduling to the brake command signal

In Figure A.26 proposed model, even with the simple manual calibration, can reproduce some typical non-linearity of performed step tests.

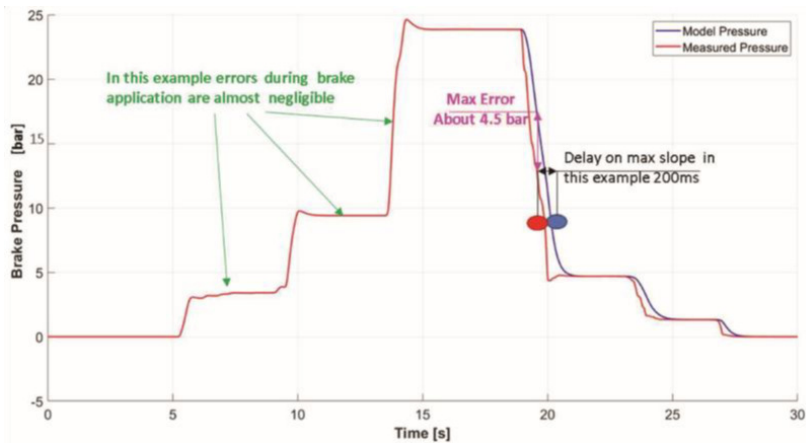


Figure A.26: Example of fitting performance of the brake model with respect to experimental results on three steps (3 rising steps and 3 decreasing steps, measurement referred to front wheels) tests used during calibration tests.

As visible in Table A.7 tests are performed considering a single sequence of brake and release manoeuvre or a sequence of three incremental braking steps followed by three release steps as described in Figure A.26. Results in Table A.7 are mainly evaluated according the following performance criteria: maximum errors between simulated results and experimental measurements in terms of absolute and relative errors; Delay of the maximum gradient on release manoeuvres,[...] aim of this performance index is to evaluate how response of the proposed model should be delayed respect to experimental data when transients do to step excitations occurs. Higher errors are due to the difficult detection of hysteretic phenomena during the transition between braking and release manoeuvres since this evaluation must be performed observing local derivatives which have to be filtered to avoid noisy performances. This trouble causes a delay visible in Figure A.26 (this example was chosen as “worst case” among others to make more evident this effect) between measured and simulated pressure profiles [...].

Table A.7: Evaluation of additional step tests performed during the calibration phase

Test N.	Type	Max Pressure Front//Rear	Max Abs	Max Rel.	Max Slope
			ErrorFront// Rear	ErrorFront// Rear	Delay*Front// Rear
1	Single Step	47.7[bar]//35[bar]	3.1[bar]//4.2[bar]	6.5%/12%	63[ms]//142[ms]
2	Single Step	51.2[bar]//36.9[bar]	4.2[bar]//3.1[bar]	8.2%/8.4%	51[ms]//123[ms]
3	Single Step	61.1[bar]//46.7[bar]	2.2[bar]//3.6[bar]	3.6%/7.7%	89[ms]//87[ms]
4	Single Step	61.1[bar]//46.7[bar]	3.5[bar]//5.1[bar]	5.7%/11.1%	41[ms]//52[ms]
5	Single Step	61.4[bar]//46[bar]	3.9[bar]//3.4[bar]	6.7%/7.4%	63[ms]//63[ms]
6	Single Step	62.5[bar]//48[bar]	3.5[bar]//5.3[bar]	5.6%/11%	52[ms]//42[ms]
7	Single Step	60.8[bar]//48.8[bar]	3.1[bar]//4.1[bar]	5.1%/8.4%	78[ms]//86[ms]
8	Single Step	64.4[bar]//47[bar]	2.9[bar]//3.7[bar]	4.5%/7.9%	143[ms]//78[ms]
9	Single Step	59.2[bar]//40.9[bar]	4.5[bar]//2.9[bar]	7.6%/7.1%	32[ms]//96[ms]
10	Single Step	68.5[bar]//49[bar]	3.7[bar]//2.5[bar]	5.4%/5.1%	69[ms]//113[ms]
11	Single Step	61.2[bar]//47.3[bar]	4.1[bar]//3.5[bar]	6.7%/7.4%	87[ms]//105[ms]
12	3-Step	26.8[bar]//16[bar]	1.5[bar]//1.5[bar]	5.6%/9.4%	35[ms]//132[ms]
13	3-Step	14.3[bar]//9[bar]	2.8[bar]//1.8[bar]	19.6%/20%	42[ms]//69[ms]
14	3-Step	14.4[bar]//8[bar]	1.5[bar]//2.2[bar]	10.4%/27.6%	41[ms]//78[ms]
15	3-Step	13.4[bar]//8[bar]	1.7[bar]//2.3[bar]	12.7%/28.8%	63[ms]//84[ms]

From results of Table A.7 it should be deduced that maximum errors in terms of simulated pressures are limited to few bars (typically around  $2 \sim 2.5 \text{ bar}$ ). However, it should be considered that repeatability of brake tests involves fluctuations on measured exp. Pressures of about 1 bar. Also it should be considered that these high errors are recorded during the brake release phase; also in this case delays measured on the real plant are affected by repeatability errors of about 100 [ms] so it should be concluded that modelling errors are only a bit higher respect to random variations that can be observed on the real plant.

## 5 Validation: Preliminary Results

For the validation process, SimRodTM vehicle was transported to the test circuit of Aldenhoven, where it was possible to perform various manoeuvres at different speed. In this occasion it was possible to measure both brake pedal runs and corresponding brake pressures. By imposing the same recorded input to the calibrated model of the brake plant, it was possible to compare the simulation results respect to corresponding brake pressures measured during the experimental activities. In Figures A.27, some of these comparisons, which are referred to relatively complex brake manoeuvres, are shown: considering the simplicity of the proposed model and the difference between the experimental profiles and the calibration ones, obtained results are very good in terms of fitting capability. [...] higher errors are mainly due to the modelling of hysteretic effects [...] : currently these derivatives are directly evaluated after the application of low pass filters [...].

These relatively aggressive filtering must be introduced to avoid high frequency noise which disturbs a proper estimation of derivatives, but it is also the reason of errors and delays in detecting hysteretic effects.

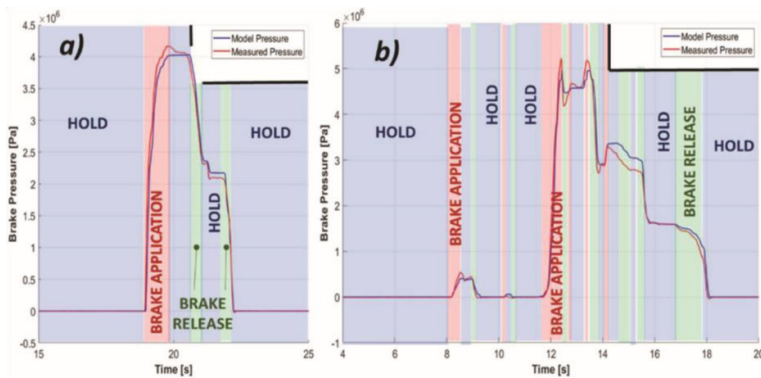


Figure A.27: (a/b) Example of fitting performances of brake model respect to real experimental results measured during real braking manoeuvre performed on the test circuit of Aldenhoven (tests are referred to various braking manoeuvre performed at 50 and 60 km/h).

[...] In FigA.28 simulated brake pressure (on front wheel) are compared with experimental ones (the same brake pedal command is imposed in both cases); knowing the friction factor of the pad simulated brake pad torques are compared with corresponding experimental torque measurements (wheels of Simrod are also equipped with force and torque sensors) as shown in Figure A.29.

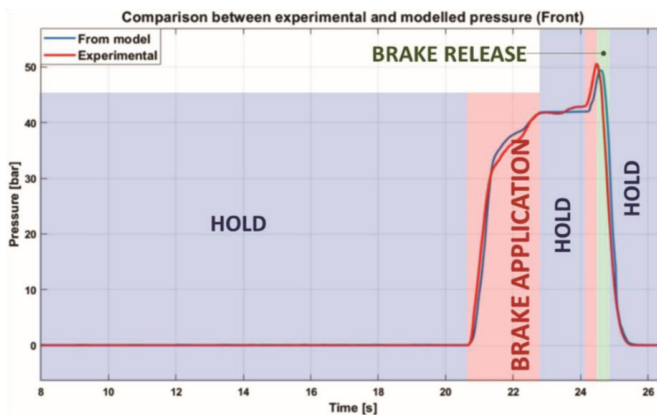


Figure A.28: Comparison of measured and simulated brake pressure during a braking test (simulated results are obtained imposing the same brake pedal displacement).

[...] Finally, by applying the simulated torques to a mechanical model of the vehicle, it's possible to calculate the corresponding speed profile of the carbody, which is compared in Figure A.30 with corresponding experimental value.

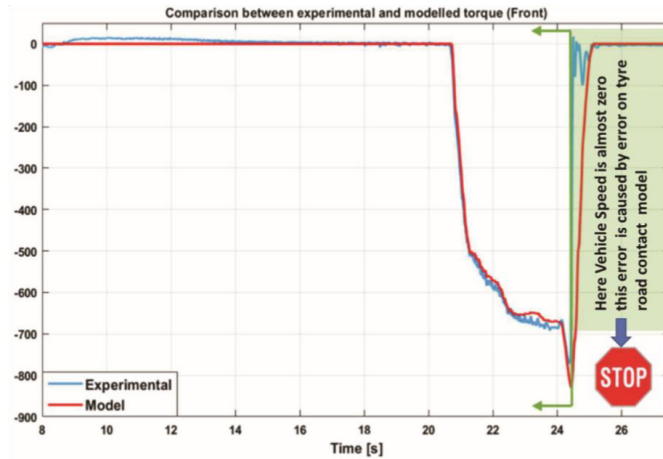


Figure A.29: Comparison of measured and simulated torque profiles during a braking test (simulated results are obtained imposing the same brake pedal displacement).

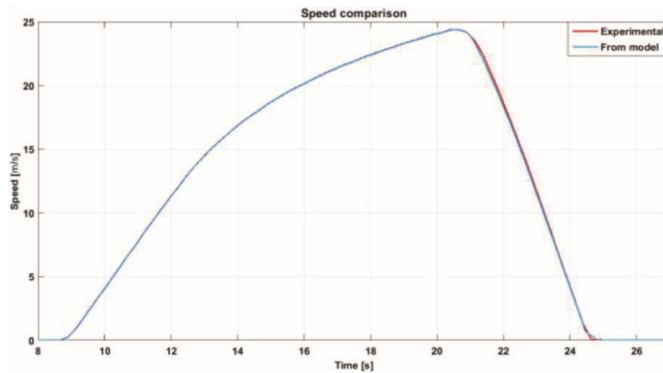


Figure A.30: Comparison of measured and simulated vehicle speed profiles during a braking test (simulated results are obtained imposing the same brake pedal displacement).

Looking at results it's clearly noticeable that brake pressure profiles are well reproduced: in particular errors in terms of brake pressure didn't produce appreciable variations not only in terms of torques but also in term of vehicle speed profile which mainly depends from integral of braking actions. So, it should be further concluded that recorded errors in terms of braking torques are quite acceptable to properly reproduce vehicle dynamical behaviour.

## 6 Conclusions and Future Developments

In this work, authors have proposed a simplified brake model designed to fit the functional behaviour of different brake plants. The model has been applied on a benchmark test vehicle (Siemens SimRod) for which it was not originally designed, proving to be able to fit the real behaviour of a brake plant through a limited set of experimental tests. Also, preliminary validation results obtained on a test circuit are quite encouraging. Results clearly indicate that brake pressures are reproduced quite precisely, and recorded errors produce negligible errors in terms of simulated vehicle dynamics. Residual errors recorded in the comparison of experimental data with simulation results are compatible with signal conditioning of acquired signals and consequent troubles in calculation of state derivatives, so there are also margins for future improvements of proposed methods by introducing a more sophisticated handling of pressure and brake command derivatives.

## References

1. Gerdes JC, Hedrick JK. Brake System Modelling for Simulation and Control. *Journal of Dynamic Systems, Measurement, and Control* 1999; 121: 496–503.
2. Delaigue P, Eskandarian A. A comprehensive vehicle braking model for predictions of stopping distances. *Proceedings of the Institution of Mechanical Engineers, Part D: Journal of Automobile Engineering* 2004; 218: 1409–1417.
3. Savitski D, Ivanov V, Augsburg K, et al. The new paradigm of an anti-lock braking system for a full electric vehicle: experimental investigation and benchmarking. *Proceedings of the Institution of Mechanical Engineers, Part D: Journal of Automobile Engineering* 2016; 230: 1364–1377.
4. Ming L, Kuang. Hydraulic brake system modeling and control for active control of vehicle dynamics. In: *Proceedings of the 1999 American Control Conference (Cat. No. 99CH36251)*. San Diego, CA, USA: IEEE, pp. 4538–4542 vol. 6.
5. Anselma PG, Patil SP, Belingardi G. Rapid Optimal Design of a Light Vehicle Hydraulic Brake System. pp. 2019-01-0831.
6. Bauer F, Fleischhacker J. Hardware-in-the-Loop Simulation of ElectroPneumatic Brake Systems. pp. 2015-01-2745.
7. Li L, Li X, Wang X, et al. Transient switching control strategy from regenerative braking to anti-lock braking with a semibrake-by-wire system. *Vehicle System Dynamics* 2016; 54: 231–257.
8. Zhang J-Z, Chen X, Zhang P-J. Integrated control of braking energy regeneration and pneumatic anti-lock braking. 224: 24.
9. Miller JM. *Electric Powertrain: Energy Systems, Power Electronics and Drives for Hybrid, Electric and Fuel Cell Vehicles* [Book Review
10. . *IEEE Power Electron Mag* 2018; 5: 86–87.
11. Enang W, Bannister C. Modelling and control of hybrid electric vehicles (A comprehensive review). *Renewable and Sustainable Energy Reviews* 2017; 74: 1210–1239.
12. Fagnant DJ. Preparing a nation for autonomous vehicles: opportunities, barriers and policy recommendations. 2015; 15.
13. Gonzalez D, Perez J, Milan´es V, et al. A Review of Motion Planning´ Techniques for Automated Vehicles. *IEEE Transactions on Intelligent Transportation Systems* 2016; 17: 11.
14. Amer NH. Modelling and Control Strategies in Path Tracking Control for Autonomous Ground Vehicles: A Review of State of the Art and Challenges. *J Intell Robot Syst* 2017; 30.
15. Berzi L, Favilli T, Locorotondo E, et al. Real Time Models of Automotive Mechatronics Systems: Verifications on “Toy Models”. In: Carbone G, Gasparetto A (eds) *Advances in Italian Mechanism Science*. Cham: Springer International Publishing, pp. 141–148.

16. Pugi L, Favilli T, Berzi L, et al. Brake Blending and Optimal Torque Allocation Strategies for Innovative Electric Powertrains. In: Saponara S, De Gloria A (eds) Applications in Electronics Pervading Industry, Environment and Society. Cham: Springer International Publishing, pp. 477–483.
17. Pugi L, Favilli T, Berzi L, et al. Application of Regenerative Braking on Electric Vehicles. In: 2019 IEEE International Conference on Environment and Electrical Engineering and 2019 IEEE Industrial and Commercial Power Systems Europe (EEEIC/ICPS Europe). Genova, Italy: IEEE, pp. 1–6.
18. Zhao X, Li L, Wang X, et al. Braking force decoupling control without pressure sensor for a novel series regenerative brake system. Proceedings of the Institution of Mechanical Engineers, Part D: Journal of Automobile Engineering 2019; 233: 1750–1766.
19. Han W, Xiong L, Yu Z. A novel pressure control strategy of an electrohydraulic brake system via fusion of control signals. 16.
20. Ma, L.-X., Yu, L.-Y., Wang, Z.-Z., Song, J. A new type of automotive braking actuator for decentralized electro-hydraulic braking system(2014) Journal of Harbin Institute of Technology (New Series), 21 (1), pp. 1–6.
21. Zhang J, Lv C, Gou J, et al. Cooperative control of regenerative braking and hydraulic braking of an electrified passenger car. Proceedings of the Institution of Mechanical Engineers, Part D: Journal of Automobile Engineering 2012; 226: 1289–1302.
22. Aly, A. A., Zeidan, E. S., Hamed, A., Salem, F. (2011). An antilockbraking systems (ABS) control: A technical review. Intelligent Control and Automation, 2(03), 186.
23. Pugi L, Rindi A, Ercole AG, et al. Preliminary studies concerning the application of different braking arrangements on Italian freight trains. 28.
24. Pugi L, Malvezzi M, Papini S, et al. Simulation of braking performance: The AnsaldoBreda EMU V250 application. Proceedings of the Institution of Mechanical Engineers, Part F: Journal of Rail and Rapid Transit 2015; 229: 160–172.
25. Wang X, Zheng G. Two-step transfer function calculation method and asymmetrical piecewise-linear vibration isolator under gravity. Journal of Vibration and Control 2016; 22: 2973–2991.
26. Rewienski M, White J. A trajectory piecewise-linear approach to model order reduction and fast simulation of nonlinear circuits and micromachined devices. IEEE Trans Comput-Aided Des Integr Circuits Syst 2003; 22: 155–170.
27. Pugi L, Galardi E, Carcasci C, et al. Preliminary design and validation of a Real Time model for hardware in the loop testing of bypass valve actuation system. Energy Conversion and Management 2015; 92: 366–384.
28. Yu L, Liu X, Xie Z, et al. Review of Brake-by-Wire System Used in Modern Passenger Car. In: Volume 3: 18th International Conference on Advanced Vehicle Technologies; 13th International Conference on Design Education; 9th Frontiers in Biomedical Devices. Charlotte, North Carolina, USA: American Society of Mechanical Engineers, p. V003T01A020.
29. Karnopp D, Margolis DL, Rosenberg RC. System dynamics: modelling and simulation of mechatronic systems. 5th ed. Hoboken, NJ: Wiley, 2012.
30. Genta G and Morello L (2007) L' autotelaio 1 and 2. Torino: Libreria universitaria levrotto and bella.
31. W. J. Thayer Transfer Introduction Functions for Moog Servovalves. Moog technical bulletin 103 of Moog Inc. available on line at <http://www.moogvalves.com/>
32. Merrit, H. E. "Hydraulic Control Systems, Jonh Wiley & Sons Inc." New York ISBN 471596175 (1967).
33. Yoshida, F., & Miyakawa, S. (2011). Effect of parameters on frequency characteristics of proportional control valve using tap water. In Proceedings of the 8th JFPS International Symposium on Fluid Power, Okinawa, Japan.
34. Day TD, Roberts SG. A Simulation Model for Vehicle Braking Systems Fitted with ABS. pp. 2002-01–0559.
35. van Zanten AT. Bosch ESP Systems: 5 Years of Experience. SAE International. Epub ahead of print 2000. DOI: 10.4271/2000-01-1633.

36. Kant B. Sensotronic brake control (SBC). In: Reif K (ed) *Automotive Mechatronics*. Wiesbaden: Springer Fachmedien Wiesbaden, pp. 412– 415.
37. Klode H, Omekanda AM, Lequesne B, et al. The Potential of Switched Reluctance Motor Technology for Electro-Mechanical Brake Applications. pp. 2006-01-0296.
38. Pulcinelli A, Pugi L, Vinattieri F, et al. Design and testing of an innovative electro-hydraulic actuator for a semi-active differential. *Proceedings of the Institution of Mechanical Engineers, Part D: Journal of Automobile Engineering* 2017; 232: 1438–1453.
39. D'Hondt, T., Forrier, B., Sarrazin, M., Favilli, T., Pugi, L., Berzi, L., Viviani, R., Pierini, M. Modeling and Identification of an Electric Vehicle Braking System: Thermal and Tribology Phenomena Assessment (2020) SAE Technical Papers, 2020-April (April), DOI: 10.4271/202001-109
40. L. Pugi, A. Reatti, F. Corti and F. Grasso, "A Simplified Virtual Driver for Energy Optimization of Railway Vehicles," 2020 IEEE International Conference on Environment and Electrical Engineering and 2020 IEEE Industrial and Commercial Power Systems Europe (EEEIC/I&CPS Europe), Madrid, Spain, 2020, pp. 1–6, doi:10.1109/EEEIC/ICPSEurope49358.2020.9160715

## A.6 Brake Blending and Torque Vectoring of Road Electric Vehicles: a flexible approach based on Smart Torque Allocation [210]

**Published in** International Journal of Electric and Hybrid Vehicles

**Authors** Luca Pugi, Tommaso Favilli, Lorenzo Berzi, Edoardo Locorotondo, Marco Pierini

**Abstract** Application of regenerative braking on electric vehicles have a large impact on several aspects of design, implemented functionalities and overall performances of road vehicles. In particular, multi-quadrant capabilities and improved control performances of modern electric drives can be fully exploited to improve vehicle efficiency, stability and overall environmental impact. Conventional, Mechanical friction brakes are currently devoted not only to stop the vehicle but also to the actuation of safety related mechatronics systems such as EBD, ABS and ESP. The result is an over-actuated system of electrical (electric motors) and mechanical actuators (friction brakes), whose mixed, blended application has to be carefully optimized. In this work authors propose a simplified approach in which concept transferred from previous studies on high speed trains and autonomous vehicles are re-proposed and adapted in an innovative way to electric road vehicles.

**Keywords** Vehicle Dynamics, Regenerative Braking, Mechatronics, Optimal Thrust, Torque Allocation

### Introduction: Electric Braking on Road Vehicles

[...] Wear and heating of friction brake pads is substantially proportional to dissipated energy<sup>7,8</sup>, so the availability of electric braking offers an important contribution also in improving maintenance costs and environmental impact (in terms of debris and other pollutants that are produced and diffused by worn brake materials). In particular, worn brake debris are credited as the most important source of pollution not related to combustion<sup>9</sup> and its toxicity effects are difficult to be completely quantified considering variety of involved chemical substances and complexity of the involved bio-physical interaction<sup>10,11</sup>. [...] Power to size ratio of electric units is relatively good so it's also feasible the usage of multiple traction motors to precisely distribute torque efforts to different wheels, assuring the possibility of implementing torque vectoring with all the corresponding advantages in terms of overall control of vehicle stability and performances. On these last topics there is wide literature, which is mostly referred to the particular case of a vehicle with four in-wheel motors, that allow a complete control of longitudinal efforts exerted on each wheel<sup>15-22</sup>.

As a consequence, current developments of EV's powertrain are imposing a strong synergy between electric traction-braking system and the conventional friction brake<sup>22-24</sup>, not only to control vehicle longitudinal dynamics, but also in terms of lateral stability<sup>12-14</sup>. The presence of multiple electric and braking units makes the vehicle an over-actuated system, in which the action of each actuator is constrained by fixed or variable physical limits: **Friction Brake Units** are

substantially constrained to work as passive components, able only to dissipate vehicle kinetic energy [...]; **Electric Units** are constrained by thermal, current and power limitations of motors, PIM and electric storage systems<sup>28</sup> [...].

## Objectives and Innovation Content of the Proposed Work

In particular, [...] authors intend to present a general flexible simulation methodology that can be easily adapted to different vehicle powertrains and brake plants using simple modular models that can be reassembled and customized according the considered use-cases. The proposed models are optimized for fixed step integration, in order to make easier Real Time Simulation RTS (both for fast prototyping and Hardware In the Loop HIL and Software In the Loop SIL testing) and co-simulation (integration of proposed brake and control models with other more complex ones provided by external industrial partners). Non-secondary advantages of the proposed approach are Model Partitioning for Multi-Thread Execution, improved model interoperability and computational efficiency of the model.

## General Structure of the Brake Model with Integrated Brake Blending Controller

In Figure 1 it's introduced a simplified scheme of the proposed approach: all the brake plant is supposed to be controlled by a "brake demand" which is an abstraction of a digital or physical signal (as example the brake booster output pressure), which corresponds to a braking torque reference produced by a human or an autonomous driver of the car. These brake demand should be further modified by on-board mechatronics subsystems such as EBD, ABS and ESP in order to improve vehicle stability and safety. Resulting brake demand is a vector of brake reference torques [...].

As visible in Figure A.31, Unifi Brake Model (UBM) is composed by three sub-modules: Brake Blending, Brake Plant and Braking units.

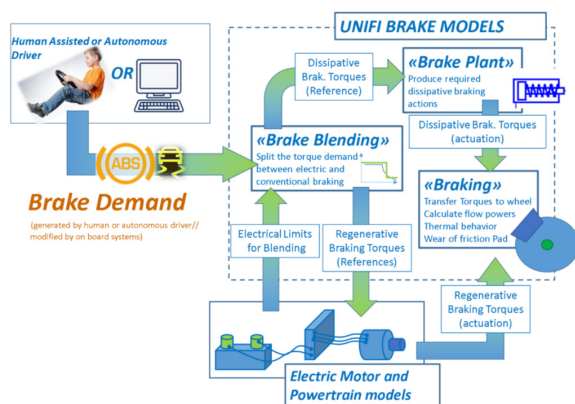


Figure A.31: General layouts and interactions of the UBM with other vehicle subsystems

## Integration of Brake Blending within Vehicle Stability Controllers

BB logic previously described by the scheme of Figure 2 assures an optimal allocation of electric regenerative efforts respect to conventional braking, with the intent to maximize the recovered energy, by taking the full advantage of the electric actuator. However, in modern applications, braking system is not only devoted to control vehicle longitudinal dynamics: a fast differential application of braking torques among wheels is typically used to correct the directional behaviour of the vehicle. Stability controllers like ESP<sup>33</sup> perform vehicle torque vectoring by modulating the braking efforts applied on left and right wheels, in order to produce a desired correction torque  $M_{yaw}$  (A.18) [...].

$$M_{yaw} = \sum_{i=1}^{n=4} \frac{Tq_{ref-ij} - Tq^*_{ref-ij}}{r_w} \cdot y_i \tag{A.18}$$

An optimal BB strategy also corresponds to an optimal torque allocation, so authors also investigate this aspect as a part of the integration of the brake blending controller within the lateral stability one<sup>28-31</sup>. The main focus of this work it's not to further investigate the best way in which a EV cornering or lateral stability control can be implemented, but only find a very simple and efficient way to produce a good allocation of torques on wheels aimed at maintaining vehicle stability while maximizing the recovery of kinetic energy during braking phase, which is significantly a lower layer of the over-cited control stability algorithm<sup>34,35</sup>.

In this work authors consider a simple general torque vectoring approach, supposing that applied longitudinal efforts can be modulated separately on each wheel, being the force calculated as ratio between torques and corresponding wheel rolling radius. Also, transversal distances between tyre contact patches and vehicle symmetry plane are supposed to be constant and completely known as visible in Figure A.32. Finally, in the calculation it's completely neglected the contribution of steering angles whose typical values in normal operating conditions are lower than 0.1-0.12 rad (about 6°-7°).

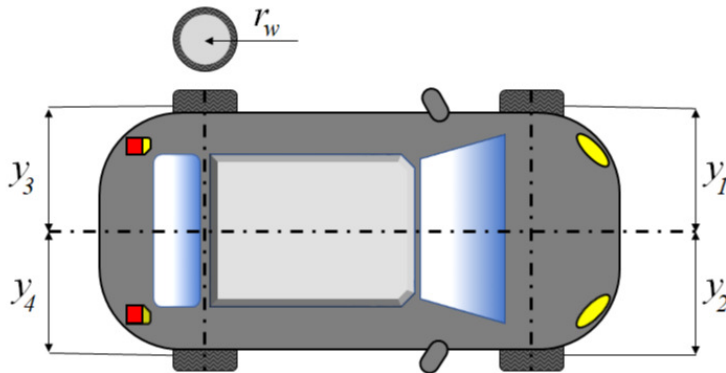


Figure A.32: Simplified vehicle layout adopted to describe brake blending integration in vehicle stability controllers

Considering over-cited simplifications, the system is clearly over-actuated, since four different efforts can be regulated. In order to find a near to optimal solution authors considered some constraints that have to be respected. First, total braking or traction demand should not be affected by the action of the stability controller, so the exerted torques  $Tq_{ref-i}$  has to be maintained as unaltered as possible respect to  $Tq^*_{ref-i}$ , being the latter the torques that should be applied to wheels without any intervention of the stability controller.

$$Tq_{ref-ij} - Tq^*_{ref-ij} \approx 0 \forall ij = fl, fr, rl, rr \tag{A.19}$$

Values of applied torque have to be limited according on available braking and traction performance  $Tq_{min-i}$  and  $Tq_{max-i}$ , which can be scheduled respect to motor shaft speed (which must be controlled in order to perform the motor ideal traction characteristic<sup>34</sup>, and availability of the energy storage system.

$$Tq_{min-i} \leq Tq_{ref-i} \leq Tq_{max-i} \tag{A.20}$$

It should be noticed that for vehicles with independent in-wheel motors also traction efforts on each wheel can be modulated independently; so, sign of  $Tq_{min-ij}$  and  $Tq_{max-ij}$  can be different.

Finally “norm 2” of the applied correction torque has to be minimized (A.21).

$$\|Tq_{ref-ij} - Tq^*_{ref-ij}\|_2 = \left( \sum_{i=1}^{n=4} (Tq_{ref-ij} - Tq^*_{ref-ij})^2 \right)^{\frac{1}{2}} \tag{A.21}$$

In this way the corrections torques are distributed between actuators, improving reliability and energy consumptions. Also, minimization contributes to find a solution that is reasonably far from constraints and limitations. A solution which is far from constraint should finally produce a smoother dynamical behaviour of applied actuation, since a saturation of one or more efforts should produce a discontinuous behaviour across constraints. Authors also propose a numerical implementation of the method, which involves the usage of limited numerical resources that are more than affordable for an industrial RT application.

Proposed implementation is described by following steps. First conditions corresponding to relations (A.18) and (A.19) are implemented obtaining the linear system (A.22).

$$\overbrace{\begin{bmatrix} -\frac{y_1}{r_w} & \frac{y_2}{r_w} & -\frac{y_3}{r_w} & \frac{y_4}{r_w} \\ 1 & 1 & 1 & 1 \end{bmatrix}}^A \begin{bmatrix} Tq_{ref-1} - Tq^*_{ref-1} \\ Tq_{ref-2} - Tq^*_{ref-2} \\ Tq_{ref-3} - Tq^*_{ref-3} \\ Tq_{ref-4} - Tq^*_{ref-4} \end{bmatrix} = \begin{bmatrix} M_{yaw} \\ 0 \end{bmatrix} \tag{A.22}$$

By solving (A.22) using the Moore-Penrose Pseudo-Inverse matrix of  $A$  it's possible to calculate the desired torque correction applied on every wheel. The usage of Pseudo-Inverse assures the minimization of the norm 2 of the solution, automatically involving the respect of conditions. It should be also easily demonstrated that considering the typical symmetry properties of vehicle layouts ( $|y1| = |y2|$ ;  $|y3| = |y4|$ ) the minimization of the norm 2 of the performed correction automatically assure the respect of condition (A.21). Also system (A.22) can be rewritten removing the second row from matrix  $A$ .

Once solution is calculated, it's possible to impose to each torque profile the saturation constrain (A.20). Solution is then recalculated imposing for each saturated torque the corresponding values calculated according (A.23).

$$\begin{cases} \text{if } T_{ref-i} > T_{max-i} \Rightarrow T_{ref-i} = T_{max-i} \\ \text{if } T_{ref-i} < T_{min-i} \Rightarrow T_{ref-i} = T_{min-i} \end{cases} \quad (\text{A.23})$$

As example, if torque of wheel 3 is limited to its maximum, calculation of (A.22) is repeated solving a system in which the value of the third element is locked to the corresponding saturated value.

Calculation is then repeated until a valid solution is found or alternatively when every torque profile is saturated. The resulting method is quite efficient, since in the worst case four iterations are needed. From a computational point of view, the most demanding task is represented by the inversion of the A matrix; however, as number of computational steps increase from one to four, also the size of the problem decreases, further reducing the corresponding computational load [...].

## Brake Plant

### Brake Unit Model

[...] Aim of the “Braking Unit Model” subsystem is to simulate the application of both regenerative/electric and dissipative/mechanical torques to wheels. In this way, we are able to calculate power flows and corresponding energy integrals. Knowing the amount of dissipated energy on each wheel, we can roughly calculate corresponding thermal and wear behaviour of brake friction components (pads and discs). Since brake friction factor depends from thermal and loading conditions, values of applied torques and dissipated energies should be corrected considering fading or more generally load-sensitivity of pads behaviour. So, the Braking Units subsystem satisfies the objective of calculating the performances of brake blending strategies, in terms of: (1) efficiency, (2) safety and (3) improved environmental impact, considering even the volume of pollutant debris produced by wear of brake pads.

The system in question performs the following sub-functionalities, that are described in the scheme of Figure A.33: estimation of the thermal behaviour of components; estimation of the wear of components; stability of friction-braking performance (torques applied to wheels are corrected taking count of the thermal behaviour of friction components and the friction load sensitivity of the contact surface between discs and pads).

### Proposed Benchmark Vehicle

[...] Proposed approach was tested on a virtual model of a benchmark vehicle, whose main parameters have been inspired by a known existing one. Main data are freely available on line<sup>42</sup>. However, latter were not enough to correctly compile and validate the proposed model. So, to completely exploit the system, the model was completed considered a parameter set that was considered reasonable respect to aims of the proposed study, derived by heuristic considerations. It's important to note that this is not a validated model of specific vehicle, but a feasible benchmark with roughly near to realistic features.

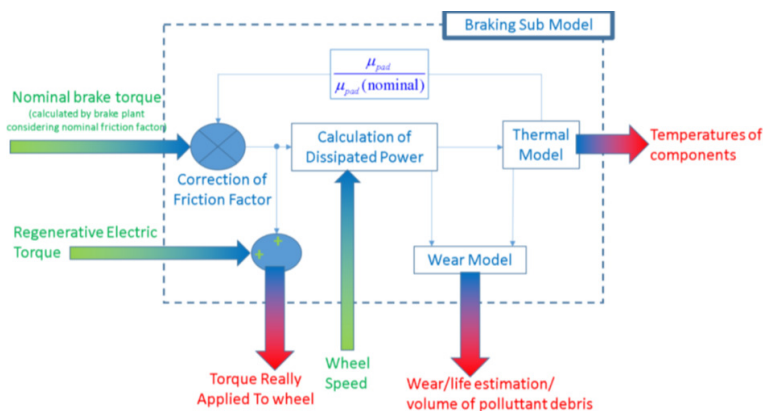


Figure A.33: Braking unit model and corresponding sub-models

Main geometric parameters of the vehicle are described in Figure A.34. Additional data concerning brakes are summarized in Table A.8.

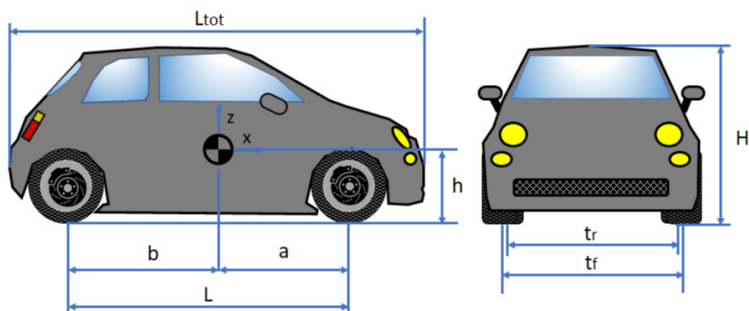


Figure A.34: Main geometrical parameters adopted for the benchmark test vehicle

For the prescribed benchmark authors considered two different powertrain configurations visible in Figure A.35. The first one represented in A.35-a (left side) corresponds to a conventional powertrain layout in which a single electrical motor is used to distribute power to frontal wheels through a differential mechanism [...]. An alternative powertrain solution with four IWM is described in A.35-b (right side): in this second case nominal total installed power is the same of the single motor solution. Therefore, the nominal torque exerted by each WIM is a quarter respect to conventional single motor layout. This powertrain configuration it's introduced to comparatively evaluate the possible advantages arising from different powertrain configurations respect to the conventional one [...].

Table A.8: Main Geometric and Thermal Parameters of the Vehicle's Brake System

<i>Definition</i>	<i>Symbol</i>	<i>Value [unit]</i>
Front Disc ext. Radius	$R_{disc-f-e}$	0.142 [m]
Rear Disc ext. Radius	$R_{disc-r-e}$	0.125 [m]
Disc int. Radius	$R_{disc-i}$	0.0305 [m]
Front Disc Thickness	$S_{disc-f}$	0.022 [m]
Rear Disc Thickness	$S_{disc-r}$	0.022 [m]
Disc Mass Density	$\rho_{disc}$	7230 [ $kgm^{-3}$ ]
Disc Thermal Conductance	$k_{disc}$	4170 [ $Wm^{-1}K^{-1}$ ]
Disc Specific Heat	$C_{disc}$	460 [ $Jkg^{-1}K^{-1}$ ]
Pad Length-Height-Width	$L_{pad} - H_{pad} - S_{pad}$	0.11-0.55-0.014 [mm]
Pad Mass Density	$\rho_{pad}$	2030 [ $kgm^{-3}$ ]
Pad Thermal Conductance	$k_{pad}$	174 [ $Wm^{-1}K^{-1}$ ]
Pad Specific Heat	$C_{pad}$	460 [ $Jkg^{-1}K^{-1}$ ]

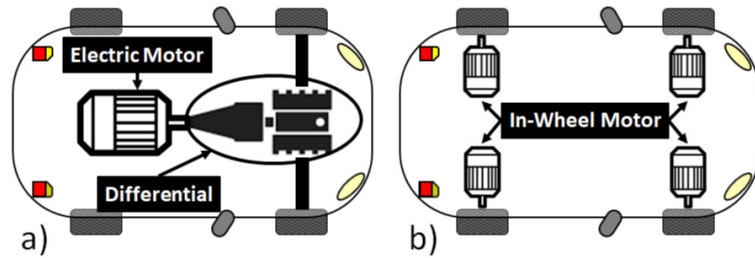


Figure A.35: Simulated vehicle powertrain: a) single motor connected to front wheel by a differential mechanism (conventional); b) four in-wheel motor (considering a different motor for each wheel).

Over described model was implemented in MATLAB Simulink: each subsystem of the vehicle (i.e. driver, chassis, wheels, electric motor, battery, stability controller, brake unit, etc.) are implemented as an independent model instance, allowing a separate execution of each sub-models with different sampling frequencies and solver features. In this way it's possible to perform a fixed step concurrent execution of each plant in separated tasks, allowing a fast RT execution. Execution in separated threads allow to verify potentially negative drawbacks, in terms of stability, due to delay that necessarily affect the communication between time continuous and discrete systems. A maximum integration frequency of 1 kHz has been chosen in order to make reasonably easy a real time implementation of the proposed model.

For high level control sub-systems authors adopted the same simplified logics which are also used by corresponding models available on other commercial software, which apply different torque vectoring techniques [...].

## Preliminary Simulation Results

### Brake Blending Controller

[...] Proposed brake blending strategy proved to be very flexible since it was possible to use the same model for both powertrain configurations proposed for the benchmark test model. Different customization substantially regards model parameters, not functionality aspect [...].

### Brake Plant

[...] When ABS modulation pattern is activated, limited bandwidth of ABS valves and compressibility effects assure a relatively smooth behaviour of applied clamping and braking forces. Therefore, it should be argued that the proposed model, despite to its relative simplicity, is able to reproduce the typical behaviour of a real plant.

Response of the simulated brake plant can be calibrated respect to real experimental data as they become available. In fact, the shape of the system response can be easily changed by managing some parameters, whose physical comprehension is relatively simple. As visible Figure A.36, simulated response of the system can be customized, working on a limited number of parameters:

- Calliper run: represents the run of calliper hydraulic actuation, which simulates the requirement of minimum volume of fluid to produce the desired clamping force. It's very useful to replicate a fixed delay in the plant, without to introducing too much complicated or hard-to-tune dynamics. Increasing the calliper run introduce also a moderate degradation of system bandwidth. This feature is useful to reproduce the fact that the final volume of the simulated plant is slightly increased.
- Bulk modulus and compressibility effects: by reducing fluid bulk modulus a higher volume of oil has to be transferred to the calliper to obtain the same response. As consequence, visible in Figure A.36, by doubling the consistency of the compressibility effects, the response of the system is slower. An equivalent reduction of bulk modulus should be used also to take count of elastic compliance of pipes or additional plant dead volumes, that are difficult to exactly evaluated.
- Hydraulic losses: an increase of friction losses in pipes and valves introduce a slower response of the plant, also increasing fixed delays as visible in the example of Figure A.36, where these losses are doubled.
- Additional parameters: by slight modifying variables, such as applied preloads and equivalent inertia of the calliper, or frequency response of valves, is possible to further reshape the response of the valve making really simple the customization of the plant respect to available experimental data.

Using the simplified vehicle model described in the previous section, it's also possible to simulate the multiple interactions between braking plant and installed on board subsystems, dedicated to the preservation of the vehicle stability (ABS, ESP, etc.). As example, some simulations of a DLC<sup>47</sup> test have been performed. As visible in Table A.9, tests were performed by different powertrain layouts of the vehicle and different adherence conditions, considering also the availability of the stability control, performed by the on-board ESP systems.

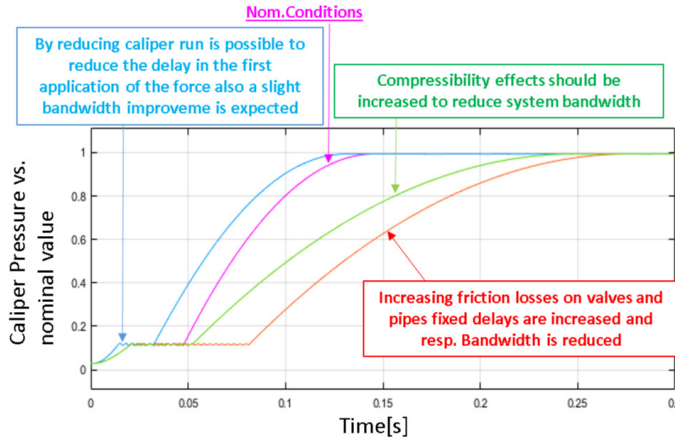


Figure A.36: Response sensitivity of the caliper respect to variation of known input parameters

Some results in terms of maximum speed for which vehicle stability is verified during the DLC manoeuvre are shown: the model highlight the benefit obtained by the application of the ESP control to different powertrain layouts. Model is also able to reproduce the system performances respect to available wheel-road adhesion conditions.

Table A.9: Double lane change test max speed performed by different vehicles powertrain configurations and adherence coefficient.

Double Lane Change Simulation Test			
<i>Adherence</i>	<i>Vehicle Layout</i>	<i>ESP</i>	<i>Maximum Speed</i>
0.5	2x4	No	30 [km/h]
		Yes	35 [km/h]
	4x4	No	35 [km/h]
		Yes	45 [km/h]
0.75	2x4	No	70 [km/h]
		Yes	75 [km/h]
	4x4	No	70 [km/h]
		Yes	80 [km/h]
1	2x4	No	85 [km/h]
		Yes	90 [km/h]
	4x4	No	85 [km/h]
		Yes	90 [km/h]

Results in terms of compared vehicle trajectories are shown in Figure A.37: simulations are performed considering a traveling speed of 80 km/h and the availability of full adhesion conditions ( $\mu = 1$ ). Best performances are obtained by the vehicle equipped with four in-wheel motors and the ESP system able to perform a full torque vectoring of the applied traction efforts. In Figure A.38 instead, results in terms of torque vectoring performed by the ESP controller with four in-wheel motors are shown.

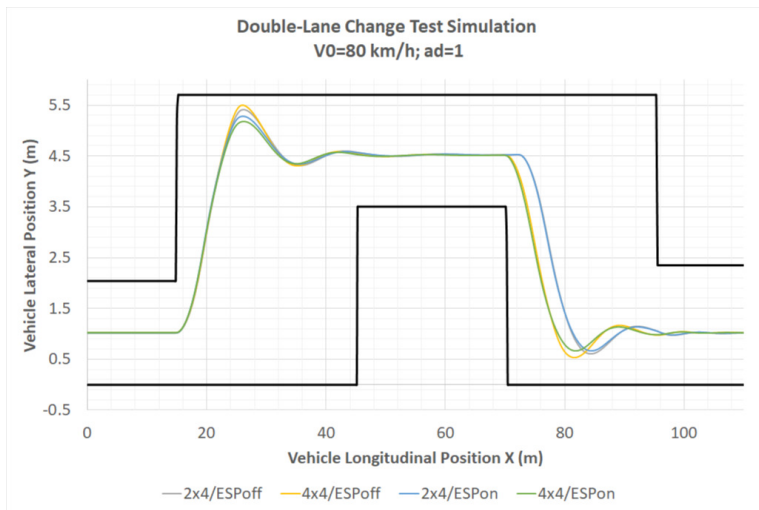


Figure A.37: Trajectories of the benchmark vehicle with different powertrain configuration and the availability of the ESP.

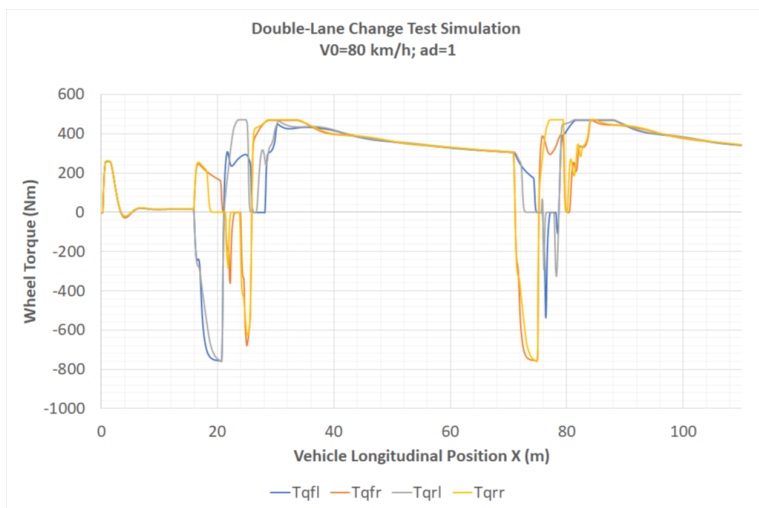


Figure A.38: Torque vectoring during a DLC test at a constant speed of 80 km/h.

## Conclusion and Future Developments

In this work authors have presented some preliminary results concerning the development of modular brake models, that offer interesting features for preliminary the sizing and optimization of brake blending policies for electric vehicles, including RTI for fast prototyping of codes, devoted to HiL simulation. Results presented in this work are mainly referred to a preliminary benchmark test case whose aim is to demonstrate more modelling functionalities than results.

## References

1. A. Emadi, Young Joo Lee, and K. Rajashekara, 'Power Electronics and Motor Drives in Electric, Hybrid Electric, and Plug-In Hybrid Electric Vehicles', *IEEE Transactions on Industrial Electronics*, vol. 55, no. 6, pp. 2237–2245, Jun. 2008.
2. B. Bilgin and A. Emadi, 'Electric Motors in Electrified Transportation: A step toward achieving a sustainable and highly efficient transportation system', *IEEE Power Electronics Magazine*, vol. 1, no. 2, pp. 10–17, Jun. 2014.
3. J. de Santiago et al., 'Electrical Motor Drivelines in Commercial All-Electric Vehicles: A Review', *IEEE Transactions on Vehicular Technology*, vol. 61, no. 2, pp. 475–484, Feb. 2012.
4. A. Walker, M. Galea, C. Gerada, A. Mebarki, and D. Gerada, 'A topology selection consideration of electrical machines for traction applications: towards the FreedomCar 2020 targets', p. 10.
5. T. J. Nicholson, 'DC & AC traction motors', in *IET Professional Development Course on Electric Traction Systems*, Manchester, UK, 2010, pp. 39–51.
6. Y. Gao, L. Chen, and M. Ehsani, 'Investigation of the Effectiveness of Regenerative Braking for EV and HEV', *SAE International*, Warrendale, PA, SAE Technical Paper 1999-01–2910, Aug. 1999.
7. A. Hatam and A. Khalkhali, 'Simulation and sensitivity analysis of wear on the automotive brake pad', *Simulation Modelling Practice and Theory*, vol. 84, pp. 106–123, May 2018.
8. K. Stevens and M. Tirovic, 'Heat dissipation from a stationary brake disc, Part 1: Analytical modelling and experimental investigations', *Proceedings of the Institution of Mechanical Engineers, Part C: Journal of Mechanical Engineering Science*, vol. 232, no. 9, pp. 1707–1733, May 2018. item T. Grigoratos and G. Martini, 'Brake wear particle emissions: a review', *Environ Sci Pollut Res*, vol. 22, no. 4, pp. 2491–2504, Feb. 2015.
9. H. Barosova et al., 'Biological response of an in vitro human 3D lung cell model exposed to brake wear debris varies based on brake pad formulation', *Arch Toxicol*, vol. 92, no. 7, pp. 2339–2351, Jul. 2018.
10. K. Malachova et al., 'Toxicity and mutagenicity of low-metallic automotive brake pad materials', *Ecotoxicology and Environmental Safety*, vol. 131, pp. 37–44, Sep. 2016.
11. R. de Castro, R. E. Araújo, M. Tanelli, S. M. Savaresi, and D. Freitas, 'Torque blending and wheel slip control in EVs with in-wheel motors', *Vehicle System Dynamics*, vol. 50, no. sup1, pp. 71–94, Jan. 2012.
12. S. Di Cairano, H. E. Tseng, D. Bernardini, and A. Bemporad, 'Vehicle Yaw Stability Control by Coordinated Active Front Steering and Differential Braking in the Tire Sideslip Angles Domain', *IEEE Trans. Contr. Syst. Technol.*, vol. 21, no. 4, pp. 1236–1248, Jul. 2013.
13. L. De Novellis et al., 'Direct yaw moment control actuated through electric drivetrains and friction brakes: Theoretical design and experimental assessment', *Mechatronics*, vol. 26, pp. 1–15, Mar. 2015.
14. Y. Hori, 'Future vehicle driven by electricity and control-research on four wheel motored "UOT Electric March II"', in *7th International Workshop on Advanced Motion Control. Proceedings (Cat. No.02TH8623)*, Maribor, Slovenia, 2002, pp. 1–14.
15. Y. Chen, J. K. Hedrick, and K. Guo, 'A novel direct yaw moment controller for in-wheel motor electric vehicles', *Vehicle System Dynamics*, vol. 51, no. 6, pp. 925–942, Jun. 2013.
16. F. Tahami, S. Farhangi, and R. Kazemi, 'A Fuzzy Logic Direct Yaw-Moment Control System for All-Wheel-Drive Electric Vehicles', *Vehicle System Dynamics*, vol. 41, no. 3, pp. 203–221, Jan. 2004.
17. Cong Geng, L. Mostefai, M. Denai, and Y. Hori, 'Direct Yaw-Moment Control of an In-Wheel-Motored Electric Vehicle Based on Body Slip Angle Fuzzy Observer', *IEEE Trans. Ind. Electron.*, vol. 56, no. 5, pp. 1411–1419, May 2009.
18. K. Bayar, J. Wang, and G. Rizzoni, 'Development of a vehicle stability control strategy for a hybrid electric vehicle equipped with axle motors', *Proceedings of the Institution of Mechanical Engineers, Part D: Journal of Automobile Engineering*, vol. 226, no. 6, pp. 795–814, Jun. 2012.

19. L. Pugi, F. Grasso, M. Pratesi, M. Cipriani, and A. Bartolomei, 'Design and preliminary performance evaluation of a four wheeled vehicle with degraded adhesion conditions', *International Journal of Electric and Hybrid Vehicles*, vol. 9, no. 1, p. 1, 2017.
20. J. Wang, Q. Wang, L. Jin, and C. Song, 'Independent wheel torque control of 4WD electric vehicle for differential drive assisted steering', *Mechatronics*, vol. 21, no. 1, pp. 63–76, Feb. 2011.
21. S. Eppler, T. Klenk, and J. Wiedemann, 'Thermal Simulation within the Brake System Design Process', presented at the 20th Annual Brake Colloquium And Exhibition, 2002, pp. 2002-01–2587.
22. S. R. Cikanek and K. E. Bailey, 'Regenerative braking system for a hybrid electric vehicle', in *Proceedings of the 2002 American Control Conference (IEEE Cat. No.CH37301)*, Anchorage, AK, USA, 2002, pp. 3129–3134 vol.4.
23. M. Ito, F. Kawahata, M. Ohkubo, K. Nakamura, A. Sakai, and A. Otomo, 'Brake apparatus for an electric vehicle to maximize regenerative energy', US5895100A, 20-Apr-1999.
24. F. Talati and S. Jalalifar, 'Analysis of heat conduction in a disk brake system', *Heat Mass Transfer*, vol. 45, no. 8, pp. 1047–1059, Jun. 2009.
25. A. Belhocine and M. Bouchetara, 'Thermal analysis of a solid brake disc', *Applied Thermal Engineering*, vol. 32, pp. 59–67, Jan. 2012.
26. D. Savitski et al., 'The new paradigm of an anti-lock braking system for a full electric vehicle: experimental investigation and benchmarking', *Proceedings of the Institution of Mechanical Engineers, Part D: Journal of Automobile Engineering*, vol. 230, no. 10, pp. 1364–1377, Sep. 2016.
27. J. Zhang, C. Lv, J. Gou, and D. Kong, 'Cooperative control of regenerative braking and hydraulic braking of an electrified passenger car', *Proceedings of the Institution of Mechanical Engineers, Part D: Journal of Automobile Engineering*, vol. 226, no. 10, pp. 1289–1302, Oct. 2012.
28. C. Lv, J. Zhang, Y. Li, and Y. Yuan, 'Regenerative Braking Control Algorithm for an Electrified Vehicle Equipped with a By-Wire Brake System', presented at the SAE 2014 World Congress & Exhibition, 2014, pp. 2014-01–1791.
29. C. Lv, J. Zhang, Y. Li, and Y. Yuan, 'Directional-stability-aware brake blending control synthesis for over-actuated electric vehicles during straight-line deceleration', *Mechatronics*, vol. 38, pp. 121–131, Sep. 2016.
30. L. Berzi, T. Favilli, E. Locorotondo, M. Pierini, and L. Pugi, 'Real Time Models of Automotive Mechatronics Systems: Verifications on "Toy Models"', in *Advances in Italian Mechanism Science*, vol. 68, G. Carbone and A. Gasparetto, Eds. Cham: Springer International Publishing, 2019, pp. 141–148.
31. L. Pugi, M. Malvezzi, S. Papini, and S. Tesi, 'Simulation of braking performance: The AnsaldoBreda EMU V250 application', p. 13.
32. C. Satzger and R. de Castro, 'Combined wheel-slip control and torque blending using MPC', in *2014 International Conference on Connected Vehicles and Expo (ICCVE)*, Vienna, Austria, 2014, pp. 618–624.
33. C. Satzger, R. de Castro, A. Knoblach, and J. Brembeck, 'Design and validation of an MPC-based torque blending and wheel slip control strategy', in *2016 IEEE Intelligent Vehicles Symposium (IV)*, Gotenburg, Sweden, 2016, pp. 514–520.
34. L. Pugi, M. Malvezzi, A. Tarasconi, A. Palazzolo, G. Cocci, and M. Violani, 'HIL simulation of WSP systems on MI-6 test rig', *Vehicle System Dynamics*, vol. 44, no. sup1, pp. 843–852, Jan. 2006.
35. G. Genta and L. Morello, Eds., 'Braking System', in *The Automotive Chassis: Vol. 1: Components Design*, Dordrecht: Springer Netherlands, 2009, pp. 269–316.
36. L. Pugi, R. Conti, D. Nocciolini, E. Galardi, A. Rindi, and S. Rossin, 'A Tool for the Simulation of Turbo-Machine Auxiliary Lubrication Plants', *International Journal of Fluid Power*, vol. 15, no. 2, pp. 87–100, May 2014.
37. J. Kukutschová et al., 'Wear mechanism in automotive brake materials, wear debris and its potential environmental impact', *Wear*, vol. 267, no. 5–8, pp. 807–817, Jun. 2009.
38. H.-G. Namgung et al., 'Size distribution analysis of airborne wear particles released by subway brake system', *Wear*, vol. 372–373, pp. 169–176, Feb. 2017.

39. G. Perricone et al., 'A concept for reducing PM 10 emissions for car brakes by 50%', *Wear*, vol. 396–397, pp. 135–145, Feb. 2018.
40. Fiat500USA.com, 'Fiat 500e Full Vehicle Specifications' .
41. H. Pacejka, *Tire and Vehicle Dynamics*. Elsevier, 2005.
42. 'Bosch Automotive Handbook, 10th Edition'. [Online]. Available: <https://www.sae.org/publications/books/content/bosch10/>. [Accessed: 29-Apr-2019].
43. 'Homepage - Obelics | Obelics'. [Online]. Available: <https://obelics.eu/>. [Accessed: 17-Apr-2019].
44. T. Blockwitz et al., 'Functional Mockup Interface 2.0: The Standard for Tool independent Exchange of Simulation Models', presented at the 9th International MODELICA Conference, Munich, Germany, 2012, pp. 173–184.
45. International Organization for Standardization, *Passenger Cars—Test Track for a Severe Lane-change Manoeuvre: Part 1: Double Lane-change*. 1999.
46. Q. Ren, D. A. Crolla, and A. Morris, 'Effect of transmission design on Electric Vehicle (EV) performance', in 2009 IEEE Vehicle Power and Propulsion Conference, Dearborn, MI, 2009, pp. 1260–1265.
47. J. Demuyne, D. Bosteels, M. De Paepe, C. Favre, J. May, and S. Verhelst, 'Recommendations for the new WLTP cycle based on an analysis of vehicle emission measurements on NEDC and CADC', *Energy Policy*, vol. 49, pp. 234–242, Oct. 2012.
48. M. Montazeri-Gh and M. Naghizadeh, 'DEVELOPMENT OF CAR DRIVE CYCLE FOR SIMULATION OF EMISSIONS AND FUEL ECONOMY', p. 6.
49. L. Berzi, M. Delogu, and M. Pierini, 'Development of driving cycles for electric vehicles in the context of the city of Florence', *Transportation Research Part D: Transport and Environment*, vol. 47, pp. 299–322, Aug. 2016.
50. 'Asterics - Homepage'. [Online]. Available: <http://www.asterics-project.eu/>. [Accessed: 02-May-2019].

## A.7 Modeling and Identification of an Electric Vehicle Braking System: Thermal and Tribology Phenomena Assessment [214]

**Published in** International Journal of Fluid Power

**Authors** Thomas D'hondt, Bart Forrier and Mathieu Sarrazin, Tommaso Favilli, Luca Pugi, Lorenzo Berzi, Riccardo Viviani and Marco Pierini

**Abstract** A rapidly shifting market and increasingly stringent environmental regulations require the automotive industry to produce more efficient low-emission Electric Vehicles (EVs). Regenerative braking has proven to be a major contributor to both objectives, enabling the charging of the batteries during braking and a reduction of the load and wear of the brake pads. The optimal sizing of such systems requires the availability of good simulation models to improve their performance and reliability at all stages of the vehicle design. This enables the designer to study both the integration of the braking system with the full vehicle equipment and the interactions between electrical and mechanical braking strategies. This paper presents a generic simulation framework for the identification of thermal and wear behaviour of a mechanical braking system, based on a lumped parameter approach. Additionally, the effect of wear and temperature on the generation of airborne particles is investigated. Subsequently, experimental data collected on a real EV is used to validate and tune the previously described simulation model, following a proposed validation procedure. The instrumentation method and challenges, as well as the experimental procedure used to collect the data on a chassis dynamometer and in real-world driving conditions, are described. Finally, simulation results for different driving scenarios are used to compare virtual and experimental results.

### Introduction

[...] The usage of simulation models throughout the development process can help engineers with the sizing, integration and safety validation issues associated with such complex braking strategies. In order to simulate the behaviour of a vehicle with sufficient fidelity, both accurate models and appropriate parameter calibration methods are required. Therefore, the present paper proposes an enhanced simulation model for the braking system of the SimRod, an EV prototyping platform (Figure A.39). The authors focus on the assessment of the thermal and tribological aspects of its mechanical braking system. This includes the interaction between the pad interface temperature and the available friction coefficient, to define its influence on the vehicle braking performances. Additionally, the wear of the brake pad is simulated, which is one of the major sources of fine particle emissions in EVs<sup>10</sup>. Finally, an approach for the identification of accurate model parameters is proposed and evaluated using data collected on a chassis dynamometer and in real driving conditions [...].

### Simulation of braking systems

The SimRod braking system is represented in Figure A.40. It consists of a TT layout, where one master cylinder controls both front brakes and the other cylinder controls the rear ones.



Figure A.39: SimRod electric test vehicle

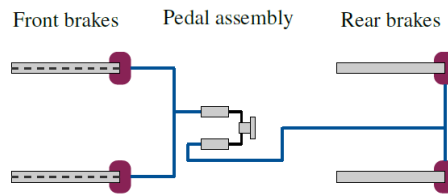


Figure A.40: Overview of the SimRod braking plant

The corresponding brake plant simulation model is divided in multiple sub-models, each representing a specific component of the system or a physical phenomena (Figure A.41). The hydraulics model reproduce the effect of a driver input  $u_b$ , such as the pedal displacement, on the pressure reference  $p_c^i$  in each calliper pistons, where  $i \in \{fl, fr, rl, rr\}$ . This includes the effects of the pedal, master cylinder, brake booster, hydraulic modulator, hydraulic lines and piston displacement. The demanded piston pressure is then transformed into a torque  $\tau^i$  due to the friction between the pad and the braking disk. Together, the braking torques on each wheel affect the dynamic behaviour of the vehicle, which is here summarised by the vehicle longitudinal speed  $\dot{x}$  and acceleration  $\ddot{x}$ . The friction torque, speed and ambient temperature are inputs to the thermal model of the plant. It computes the temperature of different components of the brake system, including the disk-pad interface temperature  $T_{if}^i$ . The latter is fed back to the torque sub-model, since the friction coefficient between the pad and the disk is a function of this temperature. Finally, both the friction torque and the interface temperature affect the wear of the braking pad.

### Torque computation

The friction torque  $\tau^i$  generated at a single wheel is given by (A.24).

$$\tau^i = 2\mu T_{if}^i p_c^i A_{pist}^i \tau^i \quad (\text{A.24})$$

The pad-disk friction coefficient  $\mu$  is assumed to be a function of pad interface temperature  $T_{if}^i$ . A corresponding friction force is generated by the normal force applied by a single pad on the disk. This force is computed using the calliper pressure and the area of the piston  $A_{pist}^i$ .

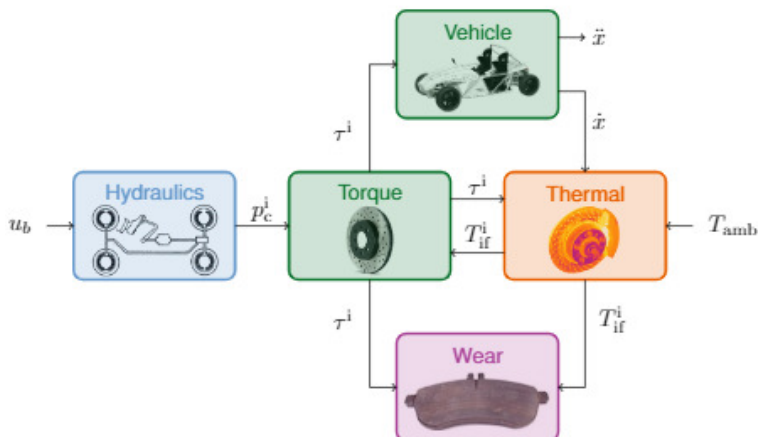


Figure A.41: Decomposition of the braking plat simulation model in sub-models

Finally, this force is transformed into an equivalent torque, assuming an average radius  $r^i$  of application. Due to the floating calliper, this force is applied by both pads on the two sides of the disk, hence the factor two.

### Thermal behaviour

The thermal behaviour of the braking system is modelled using an equivalent electrical circuit<sup>11</sup>. This circuit is composed of multiple basic elements (Figure A.42):

- The temperature source (Figure A.42/a) imposes a constant temperature gradient  $\Delta T = T_s$  across its terminals. It can be used for instance to define the ambient temperature  $T_{amb}$  with respect to the thermal reference.
- The heat transfer rate source (Figure A.42/b) imposes a constant heat rate  $\dot{Q} = \dot{Q}_s$  through its circuit branch. A common application is the modelling of the generated heat at the interface between the braking pad and the disk.
- The thermal resistance (Figure A.42/c) models the heat transfer between two bodies at different temperatures  $\Delta T = R_{th}\dot{Q}$ . This element can be used to model both conduction and convection phenomena.
- The thermal mass (Figure A.42/d) represents the thermal inertia of a body: its ability to store thermal energy. In the present model, it is always referred to the thermal reference on one of its terminals. Therefore, it imposes the temperature of the considered body on its other terminal as a function of the rate of heat  $\dot{Q}$  entering the body  $C_{th} \frac{d\Delta T}{dt} = C_{th} \frac{dT}{dt} = \dot{Q}$ .

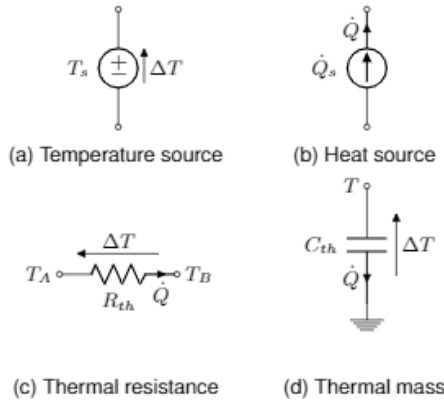


Figure A.42: Equivalent thermal modelling of the brake system using basic elements

The model presented in this paper focuses on the thermal behaviour of the caliper assembly and the non-vented braking disk of one of the rear brakes (Figure A.43). The interface region between the disk and one of the braking pads, indicated in red, is represented by a heat source  $\dot{Q}^i$  and a small equivalent thermal mass  $C_{if}$ . The latter represents the local mass around the pad-disk interface which heats up very quickly during braking manoeuvres and whose temperature is given by  $T_{if}^i$ . The resulting heat is then further propagated, either towards the disk and towards the pad. The disk thermal capacity and resistance are given by  $C_{disk}$  and  $R_{disk}$ , respectively. The hub temperature  $T_{hub}^i$  is then defined by the hub thermal resistance  $R_{hub}$  and capacitance  $C_{hub}$ . On the other side of the model, the heat generated during braking is propagated to the pad, the piston, the caliper and the braking fluid. Their respective thermal resistance and capacitance are indicated in Figure A.43.

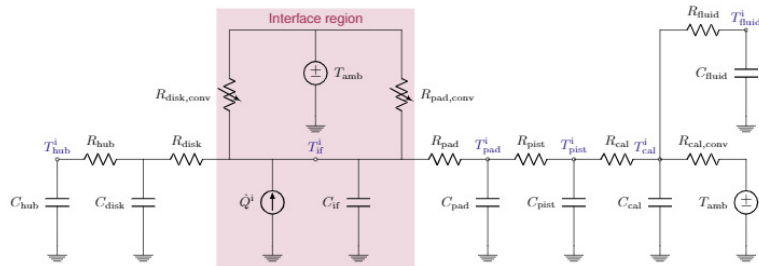


Figure A.43: Equivalent thermal RC network for a single rear brake of the vehicle. Temperature measurement points are indicated with dots.

When the pressure  $p_c^i$  is greater than zero, the pad-to-air convection resistance  $R_{pad,conv}$  is very high, as most of the pad surface is in contact with the disk and no longer with air.

It is assumed that all the energy dissipated by the friction between the pad and the disk is converted into heat. Supposing that this heat is divided equally amongst both brake pads, symmetrically along the half plane of the disk, the injected heat into the thermal model of the braking system is given by (A.25).

$$\dot{Q}^i = \frac{|\tau^i \omega^i|}{2} \quad (\text{A.25})$$

A similar exercise can be done for the simulation of the front brakes of the car. The major difference with the proposed model for the rear brakes, besides the difference in geometry, is that the front disks are vented on the SimRod. This should improve the convection cooling of the system and can be considered using an adapted speed-varying thermal resistance.

### Wear Behaviour

The friction between a braking pad and the disk results in the wear of both components. In this paper, the wear of pad material is modelled according to Archard's law, which can be expressed in polar coordinates as<sup>12,13</sup>:

$$\frac{dh}{d\theta} = kpr \quad (\text{A.26})$$

where  $h$  is the worn height of a pad,  $k$  is the associated specific wear coefficient,  $p$  is the contact pressure between the disk and the pad and  $r$  is the radius at which the wear occurs. After multiplying both sides by  $\frac{d\theta}{dt}$ , this equation can be rewritten as:

$$\frac{dh}{dt} = kpr\omega \quad (\text{A.27})$$

Finally, this equation is applied to a single pad inside one of the brake calipers of the car. It is furthermore assumed that the wear occurs at a constant average radius  $r = r^i$ . Therefore, integrating from the start of the experiment time  $t_0$  until the end  $t_f$ :

$$h^i = \int_{t_0}^{t_f} k p^i r^i \omega^i dt \quad (\text{A.28})$$

In (A.28),  $h^i$  is the worn height of a single pad,  $p^i = p_c^i \frac{A_{pist}^i}{A_{pad}^i}$  the contact pressure between the disk and the pad,  $r^i$  the mean braking radius and  $\omega_i$  the angular speed of the disk.

The wear coefficient  $k$  is a function of the interface temperature  $T_{if}^i$ , which is predicted by the previously described thermal model (Figure A.44). This curve is a bi-linear approximation of the fading phenomenon and represents a wear increase at high temperature due to the degradation of the mechanical properties of the material.

The worn mass  $m_f^i = \rho_{pad} h^i A_{pad}^i$  per pad is obtained assuming that the pads wear uniformly across their surface. The resulting mass of emitted airborne particles in the environment  $m_{PM}^i$  corresponds on average to 35% of the total worn mass  $m_f^i$ <sup>14</sup>. Those particles can then be divided into two main groups, according to their size:

$$\begin{aligned} PM_{10}^i &= 0.8m_{PM}^i \\ PM_{2.5}^i &= 0.63m_{PM}^i \end{aligned} \quad (\text{A.29})$$

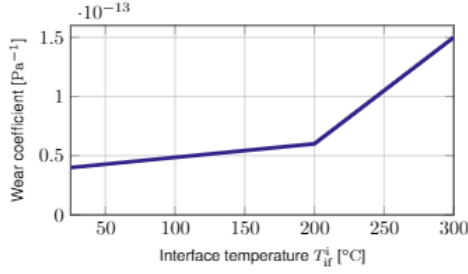


Figure A.44: Pad wear coefficient  $k$  as a function of the pad temperature<sup>13</sup>

One should note that the fraction of particles  $PM_{10}^i$  also includes  $PM_{2.5}^i$ . In order to obtain the total worn mass for the entire car, the wear on the four calipers should be summed, considering two pads per caliper.

$$\begin{aligned}
 PM_{10}^{tot} &= 2 \sum_i PM_{10}^i \\
 PM_{2.5}^{tot} &= 2 \sum_i PM_{2.5}^i
 \end{aligned}
 \tag{A.30}$$

### System instrumentation

The braking system of the SimRod has been instrumented with several thermal sensors for the identification of the simulation model parameters (Figure A.45). They were laid out on the rear-left brake, following the different measurement points indicated in the equivalent thermal RC network. Where appropriate, regular K-type thermocouples were used due to their lower cost and wide availability,. Both a rubbing thermocouple and a 16 points 1D infra-red sensor were used to measure the disk interface temperature. Additionally, a pad thermocouple was used to measure the internal temperature in the pad at a known distance from the surface. This sensors is mounted with a specific epoxy as to not affect the mechanical integrity and the thermal properties of the braking pad during the test campaign. Finally, the ambient temperature is measured using an external sensor.

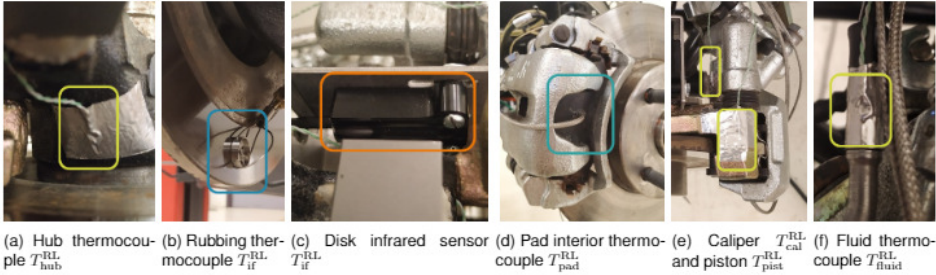


Figure A.45: Thermal sensors instrumented on the left-rear brake of the SimRod

The two types of sensors used to measure the interface temperature were chosen due to their complementary characteristics. Indeed, the rubbing thermocouple will wear over time, measures only at a single radius of the disk and has greater thermal inertia and, hence, a lower bandwidth. On the other hand, the infra-red sensor measures 16 radii simultaneously without direct contact with the disk, giving us a better idea on the distribution of the temperature over the disk surface. However, the low emissivity of the brake disk makes the calibration of the sensor hard, without the reference provided by the rubbing thermocouple<sup>15</sup>.

Other physical quantities were measured on the car during the tests, such as the pressure inside the braking system. The SimRod has a fully-split front and rear braking circuit with two independent master cylinders and no hydraulic modulator. Therefore, the pressure was measured at two points: next to the rear-left and to the front-right callipers. The rotational speed of the rear wheels was acquired using an optical sensor and zebra tape mounted on the rear axle. GPS data was acquired during outdoor measurements. Finally, all of the data was collected using a multi-physical data acquisition system: the Simcenter SCADAS and Testlab.

### Measurement Scenarios

The identification measurements took place in the controlled environment of a chassis dynamometer (Figure A.46). The braking pedal was fixed at a constant displacement using a mechanical assembly installed on the mounting points of the seat for rigidity. Meanwhile, the rear wheels of the car were spinning at a constant speed imposed by the test bed. Different measurement runs were recorded considering several speeds and pedal displacements (Table A.10).

Run	$p_{c,0}^{RL}$ [bar]	$\dot{x}$ [km/h]
1	8	10
2	7	5
3	2	30
4	4	50

Table A.10: Experimental runs evaluated on the chassis dynamometer

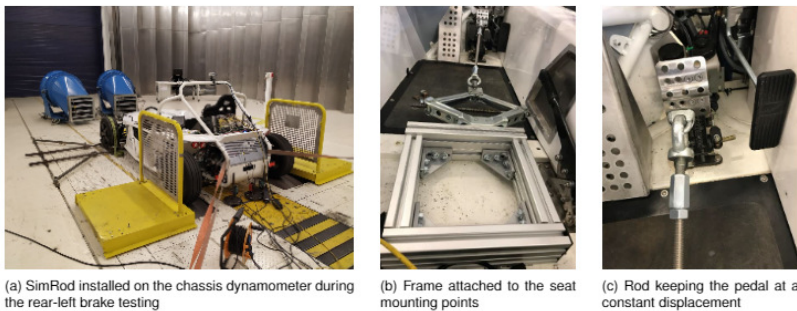


Figure A.46: Chassis dynamometer experimental setup

One should note that the constant displacement imposed to the pedal means that the pressure inside the hydraulic circuit was varying during the experiments. Indeed, the heat generated by the braking action partly propagates to the braking fluid, whose subsequent expansions results in a gradual increase of the pressure in the system. This in turns increases the braking torque and, therefore, the generation of heat. It was consequently decided to stop the measurements when reaching a safe threshold of interface temperature, since no thermal equilibrium was observed. This was also required considering the electrical nature of the car and the fire hazards related to its batteries.

Then, real-world validation tests were performed on a parking using the same instrumentation. Successive run-ups and brake manoeuvres were executed repeatedly to heat up the system. Wheel lock-up was avoided during those experimental runs.

Finally, new braking pads were installed on the car before the first test on the chassis dynamometer. Their weight was measured before and after the runs listed in Table A.10 and the real-world tests for the evaluation of the wear model.

## Identification Methodology

### Friction Coefficient Identification

One of the important parameters in the simulation model is the friction coefficient  $\mu$  between the pad and the disk, as it directly links the braking pressure and the resulting torque. On the dynamometer, the dissipated power  $P_{br}$  is measured, obtained from the product between the rotational speed  $\omega_i$  and the torque  $\tau^i$  of the rear wheels:

$$\begin{aligned} P_{br} &= \omega^{RL} \tau^{RL} + \omega^{RR} \tau^{RR} \\ &= 2\omega^{RL} \tau^{RL} \end{aligned} \tag{A.31}$$

In the last equation, it is assumed that the left and rear side of the car behave equally on the dynamometer. Then, substituting with (A.24):

$$\mu(T_{if}^i) = \frac{P_{br}}{2\omega^{RL} p_c^{RL} A_{pist}^{RL} r^i} \tag{A.32}$$

All values are known or directly measured on the test bed in (A.32). Hence, the friction coefficient  $\mu$  can be computed for all experimental runs as a function of  $T_{if}^i$ . Subsequently, this data was filtered to obtain smoother curves using a zero-phase filter to avoid adding a phase-shift in the system. Finally, those smoothed curves were arithmetically averaged for each interface temperature  $T_{if}^i$  in order to obtain a unique friction curve  $\mu(T_{if}^i)$  which can be used inside the simulation model.

### Thermal Coefficient Identification

Initial approximate values for the thermal capacitances were computed based on the weight of the individual components when accessible. Alternatively, the detailed 3D geometry of the car was used in a CAD software to obtain their volume, which was then used to compute the corresponding mass using their density. Combined with the specific heat of the material, an approximated thermal capacitance can be computed. For the thermal resistances representing conduction and convection,

initial values were used from<sup>17</sup> when available. The final tuning of the different thermal parameters was done manually. Therefore, the dissipated heat at the disc-pad interface was computed based on the acquired data for all measurement runs. It was then imposed as an input to the simulation model and the resulting predicted and measured temperatures were compared. Subsequently, the closest parameters to the interface were tuned to find a good correspondence between experimental and simulated temperatures. Gradually, parameters further away from the interface were tuned to obtain an overall good match. An optimization-based approach could be studied in future work to automate this process.

## Result Discussion

### Friction coefficient results

The friction coefficient  $\mu$  was evaluated for the different runs using (A.32). The results were plotted as a function of the interface temperature  $T_{if}^{RL}$  in Figure A.47.

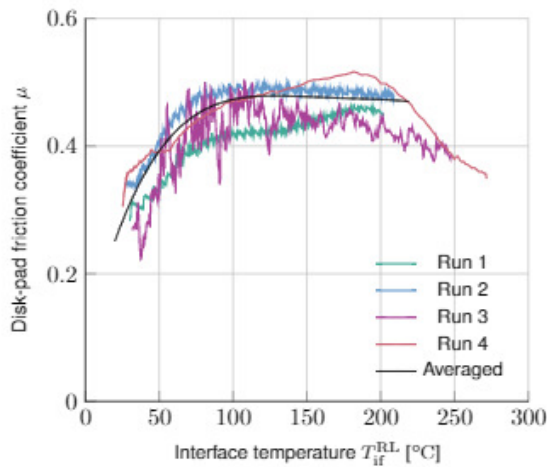


Figure A.47: Estimated friction coefficient for the different measurement runs as a function of interface temperature  $T_{if}^{RL}$

It is observed that for  $T_{if}^{RL} \leq 100^\circ\text{C}$ , the friction coefficient  $\mu$  tends to increase. For  $100^\circ\text{C} < T_{if}^{RL} \leq 200^\circ\text{C}$ ,  $\mu$  stays approximately constant and, finally,  $\mu$  decreases again for higher temperatures.

The run 3 has higher noise with respect to the other runs, which can be explained by a resonance of the mechanical assembly (between dynamometer & car). Indeed, some additional vibrations were directly visible on the car at that speed. Also, lower speed tests tend to have higher noise than other tests conducted at higher speed, as seen in Run 1 and 2. This can be justified by a slight misalignment on the disk or by its imperfect flatness. The rotational-dependency of this noise means that it tends to get filtered out by the system dynamics at higher speeds. All those sources of noise were first filtered out as described in the previous section.

The curve obtained by averaging all the smoothed data is plotted in black in Figure A.47. This curve was used as  $\mu T_{if}^{RL}$  in the following simulations. The authors intend to further investigate the differences in measured  $\mu$  across the

different runs. One possible possible path forward is to also consider the dependency between  $\mu$  and the contact pressure between the pad and the disk. This could affect the physical properties of the micro-contact patches causing a variation in the resulting macroscopic friction coefficient.

### Friction coefficient results

After identifying the different thermal resistances and capacities of the system, the simulation model was executed on the different recorded runs for its validation. For this purpose, measured pressure and speed were imposed directly to the model and the thermal responses of the different braking system components were compared. In the following paragraphs, the results for run 3 are presented.

Firstly, a good match is observed between the measured and the predicted temperatures of the interface region and the piston (Figure A.48). During the first 1500 s of the run, the temperature increases up-to 200 °C. It was not possible to obtain a thermal steady-state due to the increase in pressure in the hydraulic lines linked to the expansion of the braking fluid. Therefore, the test was stopped manually at that time by turning-off shortly the chassis dynamometer. Subsequently, the operators retracted the brake pedal locking mechanism, before restarting the test bed with its initial speed. The short period of time during which the wheels are not rotating corresponds to the slow decrease in interface temperature . Once the dynamometer is restarted, the decrease in temperature accelerates again thanks to the increased convection. It should be noted that a lag exists between the maximum interface and piston temperatures: while the former is already cooling-down, the latter still heats-up due to the thermal inertia of the interposed component. Similarly, a comparison between pad and calliper temperatures is provided (Figure A.48/b).

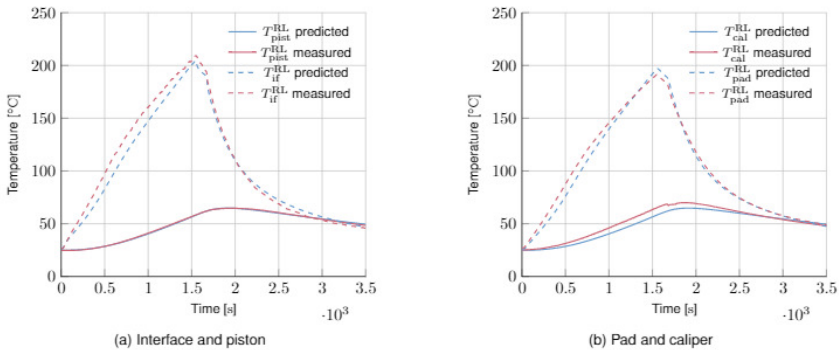


Figure A.48: Comparison between predicted and simulated temperatures for run 3

Finally, the simulation model was used to predict the thermal behaviour of the braking system in a real-world driving scenario (Figure A.49). During the first part of the experiment ( $t \approx 100$  s), the driver was quickly alternating between accelerating and braking manoeuvres, resulting in an increase in temperature. Afterwards, the car was stopped and the system was cooled, thanks to the convection with air, while the brake was still applied to keep the pad-disk contact. The measured pressure and GPS speed were used as inputs to the simulation model. A good match is observed between the predicted and the measured results.

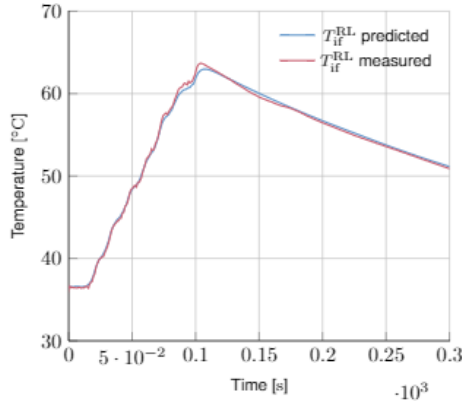


Figure A.49: Comparison between predicted interface temperature and measured interface temperature for consecutive braking manoeuvre during on-road driving

### Pad Wear Evaluation

A first limited validation for the wear model was attempted by comparing the mass of the newly installed braking pad before and after all previously presented runs. The predicted wear mass was also computed by summing the loss of mass over all the corresponding simulations (Table A.11). Although a good match is observed between measured and predicted wear, further tests are required to more accurately validate this part of the simulation model.

Parameter	$m_{pm}^{RL}$ [g]	$h^{RL}$ [mm]
Measured	1.7	$6.5e-2$
Predicted	1.5	$5.9e-2$
Error	11.7%	8.8%

Table A.11: Predicted and measured wear on a single rear-left braking pad

### Conclusion

In this work, a scalable model of the braking system was presented with a focus on the thermal, friction and wear behaviour. An experimental setup and identification methodology were also proposed and evaluated. The resulting parametrized models showed a promising correlation with the experimental results. Finally, simulations on the emissions associated with brake pad wear highlighted that it is important to look not only at the emissions related to ICE, but also at those associated with braking. The resulting simulation model can be used for the sizing, design and validation of electrical and mechanical braking strategies.

## References

1. European Environment Agency, Electric vehicles from life cycle and circular economy perspectives. Technical report, European Environment Agency, 2018.
2. Jiageng Ruan, Paul D. Walker, Peter A. Watterson, and Nong Zhang. The dynamic performance and economic benefit of a blended braking system in a multi-speed battery electric vehicle. *Applied Energy*, 183:1240 – 1258, 2016.
3. Junzhi Zhang, Chen Lv, Jinfang Gou, and De-cong Kong. Cooperative control of regenerative braking and hydraulic braking of an electrified passenger car. *Proceedings of the Institution of Mechanical Engineers, Part D: Journal of Auto-mobile Engineering*, 226(10):1289–1302, 2012.
4. J. de Santiago, H. Bernhoff, B. Ekegard, S. Eriksson, S. Ferhatovic, R. Waters, and M. Leijon. Electrical motor drivelines in commercial all-electric vehicles: A review. *IEEE Transactions on Vehicular Technology*, 61(2):475–484, Feb 2012.
5. Guido Wager, Jonathan Whale, and Thoma sBraunl. Performance evaluation of regenerative braking systems. *Proceedings of the Institution of Mechanical Engineers, Part D: Journal of Automobile Engineering*, 232(10):1414–1427, 2018.
6. Lorenzo Berzi, Tommaso Favilli, Edoardo Locorotondo, Marco Pierini, and Luca Pugi. Realtime models of automotive mechatronics systems: Verifications on “toy models. *IFToM-MITALY 2018: Advances in Italian Mechanism Science*, 68:141–148, 10 2018.
7. Luca Pugi, Tommaso Favilli, Lorenzo Berzi, Edoardo Locorotondo, and Marco Pierini. Brake blending and optimal torque allocation strategies for innovative electric powertrains. *ApplePies2018: Applications in Electronics Pervading Industry, Environment and Society*, 573:477–483, 5 2019.
8. Luca Pugi, Tommaso Favilli, Lorenzo Berzi, Edoardo Locorotondo, and Marco Pierini. Application of regenerative braking on electric vehicles. *IEEE International Conference on Environment and Electrical Engineering and 2019 IEEE Industrial and Commercial Power Systems Eu-rope (EEEIC / I&CPS Europe)*, pages 1–6, 2019.
9. David A. Crolla and Dongpu Cao. The impact of hybrid and electric powertrains on vehicle dynamics, control systems and energy regeneration. *Vehicle System Dynamics*, 50(sup1):95–109, 2012.
10. Theodoros Grigoratos and Giorgio Martini. Brake wear particle emissions: a review. *Environmental science and pollution research inter-national*, 22, 10 2014.
11. A.F. Robertson and Daniel Gross. An electrical-analog method for transient heat-flow analysis. *Journal of Research of the National Bureau of Standards*, 61:105, 08 1958.
12. Jens Wahlstrom. A comparison of measured and simulated friction, wear, and particle emission of disc brakes. *Tribology International*, 92:503–511, 2015.
13. Andersson, S., “Wear simulation,” in *Advanced Knowledge Application in Practice*, Fuerstner, I., Ed. Rijeka: Intech Open, 2010, ch. 2, doi:10.5772/10349
14. Guido Perricone, Vlastimil Matejka, Mattia Alemani, Giorgio Valota, Andrea Bonfanti, Alessandro Ciotti, Ulf Olofsson, Anders Soderberg, Jens Wahlstrom, Oleksii Nosko, Giovanni Straffellini, Stefano Gialanella, and Metinoz Ibrahim. A concept for reducing pm10 emissions for car brakes by 50%. *Wear*, 396-397:135 – 145, 2018.
15. Bhagwan D. Garg, Steven H. Cadle, Patricia A. Mulawa, Peter J. Groblicki, Chris Laroo, and Gra-ham A. Parr. Brake wear particulate matter emissions. *Environmental Science & Technology*, 34(21):4463–4469, 2000.
16. Abdil Kus, Yahya Isik, M. Cemal Cakir, Salih Coskun, and Kadir Ozdemir. Thermocouple and infrared sensor-based measurement of temperature distribution in metal cutting. *Sensors*, 15:1274–91, 01 2014.
17. Genta, G. and Morello, L., *The Automotive Chassis: Vol. 1: Components Design*. Springer Netherlands, 2009, doi:10.1007/978-1-4020-8676-2

## A.8 Smart Energy Management of Auxiliary Load for Electric Vehicles [223]

**Published in** 2020 IEEE International Conference on Environment and Electrical Engineering and 2020 IEEE Industrial and Commercial Power Systems Europe (EEEIC / I&CPS Europe)

**Authors** Lorenzo Berzi, David Delichristov, Tommaso Favilli, Marco Pierini, Luca Pugi, Albi Qehajaj

**Abstract** Energy Consumption of Auxiliary Systems on electric vehicles has an important role in reducing the overall autonomy since their contribution, especially for what concern HVAC Systems, is often not negligible and not correlated to vehicle kinematics. In this work authors propose a quite simple architecture to adopt an intelligent management of on board loads in order to increase the level of correlation between vehicle dynamics and applied auxiliary loads whith the aim to smooth the overall power demand for vehicle storage system, which should be stressed by transients in which both traction and auxiliary loads are applied at the same time.

**Keywords** Smart Energy Management, HVAC, Electric Vehicles

### I. Introduction

Auxiliary loads represent an important source of energy consumption<sup>1</sup> which is weakly correlated to vehicle kinematics. As a consequence, an optimization of mission profile in term of vehicle kinematics, the so-called EcoDriving<sup>2</sup> can take count of these loads but has limited possibilities of intervention. In a mid-term scenario this problem is going more and more important since electric vehicles cannot harvest as conventional ones the thermal power of the internal combustion engine for energy consuming systems such as HVAC one so the whole power demand has to be satisfied by on board energy storage<sup>3</sup>.

[...] In this work authors propose a simple decentralized power management strategy that can be easily implemented to almost every vehicle starting with few interventions on involved system. Aim of the proposed system is force an increased statistical correlation between the applied auxiliary loads and vehicle dynamics: in this way it's possible to safe energy when traction system is requiring more power, shifting as much as possible the application of auxiliary loads to regenerative braking phase when a reverse flow of power can be exploited. So proposed strategy offers important advantages also in terms of protection and duration of batteries employed on in the storage system, smoothing peak currents and reducing the overall quantity of exchanged charge.

### II. Proposed Solution

Proposed system is based on following assumptions:

- There is a wide variety of possible vehicle subsystems with different load profiles and different levels of priority; also considering the wide variety of optional and possible configuration of a commercial vehicle it's almost unrealistic to manage a centralized control for every subsystem.

- BMS plays a key role in protecting the battery from misuse and overloads and thanks to a high level of installed intelligence (sensors and computational power) can identify the state of the storage.
- All power limitations can be approximately treated as equivalent constraints of corresponding delivered currents on a common voltage bus shared by electric power train, storage system and more generally all the power converters that provide energy to connected vehicle auxiliary systems

As visible in the scheme of Figure A.50 proposed system performs the following operation: [...] According the sign of the current required by the powertrain  $I_{trac}$  is possible to determine the quadrant in which is operating the traction system. Current SOC of the battery is estimated through BMS, which also estimates CCL and DCL according battery state.

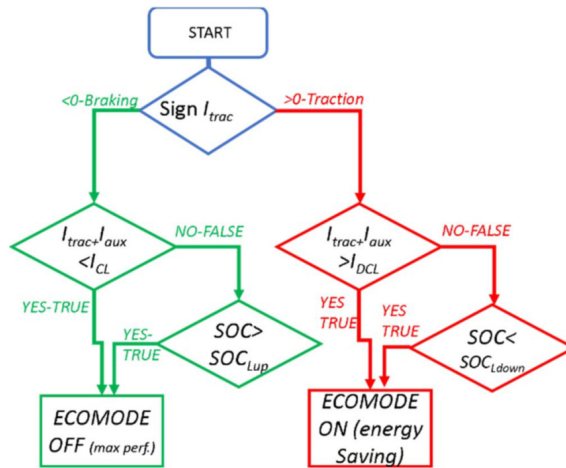


Figure A.50: Proposed Energy Management For Auxiliary Loads

According the value of  $I_{trac}$  respect to CCL and DCL and SOC, it is decided the way in which auxiliary loads are managed in order to preserve battery against power overloads especially for extreme value of the state of charge where the battery is tendentially more sensitive to this kind of troubles. It is defined a binary state briefly called ECOMODE which is sent and shared with the electronic control units of various auxiliary system. According the state of ECOMODE each connected subsystem will define its own energy management policy privileging performance (ECOMODE 'OFF') or energy saving (ECOMODE 'ON'). In this way proposed system simply indicates to connected system the opportunity of privileging a more aggressive or conservative power policy, but the way in which this choice is implemented is strictly implemented and customized in each connected sub-system.

The only exception respect to this policy is represented by the electric powertrain.

For what concern connected subsystems, highest consumptions are statistically related to the HVAC<sup>5</sup> system also considering additional loads related to battery thermal management which can be relatively important also for safety and reliability of the overall vehicle system.

### III. Reference System/Vehicle Model

The model, as visible in Figure A.51 composed by the following elements:

- A planar vehicle model developed using Siemens Simcenter;
- A lumped model of HVAC that was provided by the Siemens after a calibration performed with FCA;
- A simplified model of the NMC battery developed using standard Simcenter sub-models;
- A co-simulation interface between Matlab-Simulink which allows the implementation of controllers developed by the authors;
- Additional blocks modelling many other on board secondary systems;

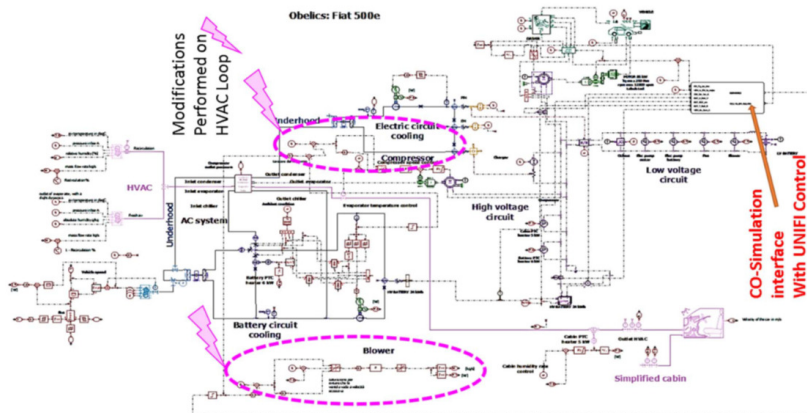


Figure A.51: Vehicle and sub-systems model in Amesim

For what concern the implementation of co-simulation, the Simcenter Amesim model is implemented with its proprietary variable step solver, data are exchanged with the Simulink controller with a communication interval of 100Hz which is the same adopted by the fixed step solver adopted in Simulink.

### IV. Customization of HVAC System

As visible in the general scheme of Figure A.51 HVAC plant is composed by a single refrigeration loop with a single compressor that provide the coolant or more generally the fluid used for thermal exchange to two different temperature loops:

- Evaporator Loop: a first external loop is devoted to control the temperature of the cooled air (in case of air conditioning). Compressor speed is regulated to maintain a reference temperature in this plant section. Power provided by the evaporator should be roughly proportional to heat flux transmitted to the refrigerated fluids, according the efficiency of the performed refrigeration cycle. Compressor also provides the refrigeration power for the other cooling circuits including the battery one.

- Blower Loop: by regulating blower speed is possible to regulate the amount of refrigerated air delivered to the cabin.

In order to implement the proposed control strategy authors, introduce in HVAC system the modifications described: speed of the compressor of the chiller/heat pump is regulated to maintain the temperature of the processed air to a known reference temperature (see Figure A.52). So by adjusting this processed air temperature  $T_{evap}$  is fundamentally regulated the specific heat/enthalpy flow that is transferred to incoming air which have a different inlet temperature  $T_{inlet}$ . Therefore, the heat flow that is exchanged with inlet air to refresh the cabin is roughly proportional to the mass flow multiplied for the specific coefficient  $c_p$ .

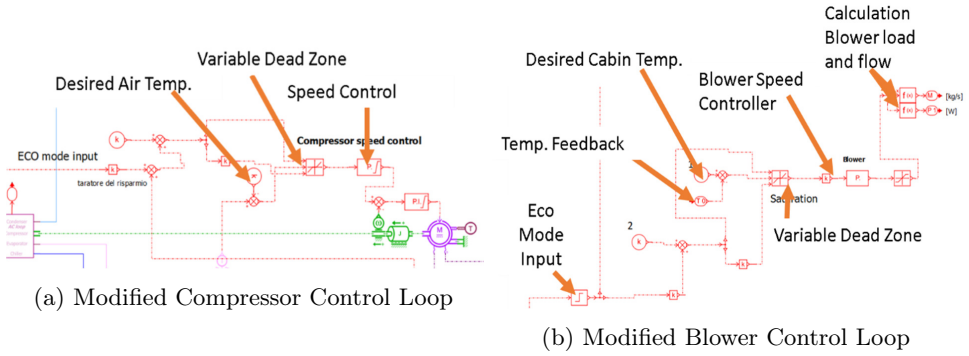


Figure A.52: Control loops

$$Q \approx \dot{m}c_p(T_{evap} - T_{inlet}) \quad (\text{A.33})$$

Value of  $T_{inlet}$  depends from cabin and external temperatures  $T_{ext}$  according the fraction  $k_{rec}$  of recirculating air from the cabin (A.34).

$$T_{inlet} \approx k_{rec}T_{cabin} + (1 - k_{rec})T_{ext} \quad (\text{A.34})$$

Air mass flow is regulated through a speed-controlled blower; blower speed reference is generated by a temperature loop aiming to regulate the internal temperature of the cabin. So, a higher temperature error in the cabin correspond to a greater performance in terms of exchanged heat flows. Respect to the original controller authors introduce the following modifications: both regulators are supposed to be proportional and not controlled by a discrete state logic; also it's introduced a variable dead-band on the evaluation of both Temperature Loop Errors. This dead-band is a function of the ECOMODE state: if ECOMODE state is "ON" (system need to save energy) dead band is increased, otherwise is near to null and performances of both loops are higher.

In order to further protect battery safety, if the temperature of the battery is over a cautious threshold  $T_{warn}$  the application of the ECOMODE On state to the compressor loop is avoided assuring that maximum performances are still available.

On the other hand, in normal operating conditions (battery at acceptable temperature) is fundamental also to manage compressor speed in order to be sure of a proper synchronization of auxiliary power reduction respect to peak of required power from the traction system, since much of the power of the plant is delivered by the compressor and not by the blower.

## V. Simulation Results

Over described model can be used to investigate the behaviour of several different scenario, however in this preliminary work authors focused their attention on a specific situation which is quite useful to understand main features and advantages of proposed solution. Vehicle starts his mission with a relatively low residual charge, outside temperature is high ( $35^{\circ}\text{C}$ ) and the HVAC is switched on setting a setpoint of about  $25^{\circ}\text{C}$ .

For what concern mission profile authors consider a WLTP mission profile. Then mission is continued until battery charge is exhausted [...].

As visible from result of Figure A.53 and Table A.12, proposed system assures a significative increase of residual vehicle autonomy, thanks to energy saved by HVAC: most of the energy saving is assured by a more efficient use of HVAC compressor while the consumption of the blower is almost the same.

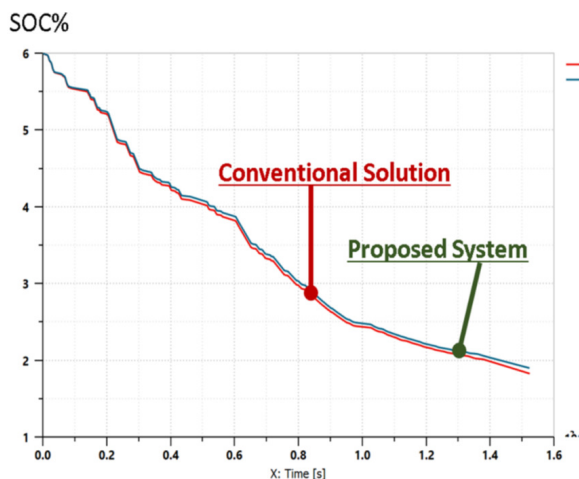


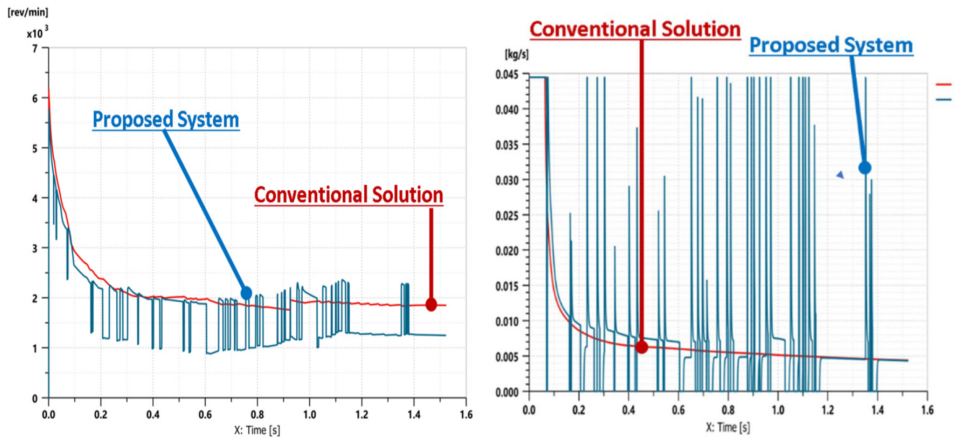
Figure A.53: Behaviour of SOC during performed mission

Table A.12: Comparison in term of energy consumption

	<i>ECOMODE</i>	<i>Conventional</i>	<i>Difference %</i>
Blower Energy	25.8 [Wh]	25.6 [Wh]	-0.8%
Compressor Energy	134 [Wh]	193 [Wh]	-30%
Distance	7234 [m]	6682 [m]	+9%

In Figure A.54a a and b power profiles of compressor and blower are shown: it is quite clear how blower and compressor switching are well synchronized respect to occurring traction and braking maneuvers.

Looking to cabin temperature profiles visible in Figure A.55, it is clearly visible that these relevant improvements are obtained with limited consequences on controlled temperature since the increased dead band produced limited temperature fluctuations of a degree.



(a) Comparison of compressor behaviour (rotational speed) (b) Comparison of blower behaviour in terms of delivered flow

Figure A.54: Comparison of thermal element behaviour before and after the controller implementation

It should be also noticed that this temperature fluctuations should even smaller and smother in a real situation since current model probably underestimates some additional thermal capacity of the plant which should probably contribute to further smooth temperature fluctuations in the cabin. However current fluctuations are less than  $1^\circ\text{C}$  respect to a difference between external and internal temperature of about  $10^\circ\text{C}$  so the recorded increase of efficiency (30%) is largely justified by a more efficient use of available energy.

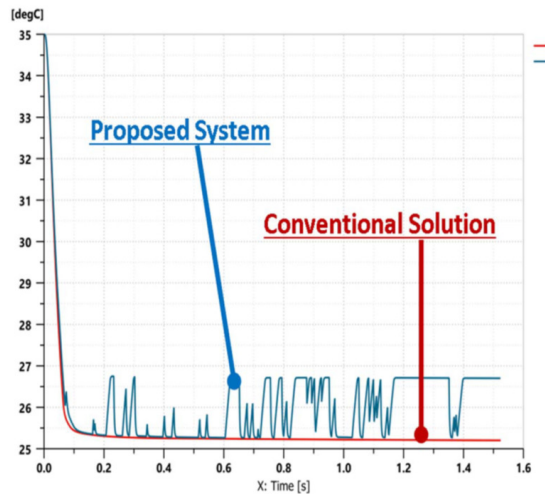


Figure A.55: Thermal Behaviour inside the cabin

All the above tests have been also repeated in the same conditions modifying only the initial temperature of the vehicle to be much higher respect to external vehicle temperature ( $60^\circ\text{C}$ ) and quite near to potentially dangerous limits. As visible in

Figure A.56. Battery temperature behaviour is not affected by the application of the proposed energy management: first, battery is properly cooled when temperature is over the warning limit of  $45^{\circ}$  since as visible in Figure A.57 compressor speed is smoothly modulated by evaporator temperature loop. On the other hand, once battery is cooled under the warning limit of  $45deg$  the compressor speed is regulated by the energy management system, but battery temperature continues to smoothly decrease without being influenced by the modulation of the compressor speed. Therefore, demonstrating the redundancy of the protection that has been implanted in order to protect as much as possible the battery. Therefore, as visible in Table A.13, in the case in which an initial battery overheating is simulated the overall energy consumption is increased in order to assure a fast cooling of the storage system.

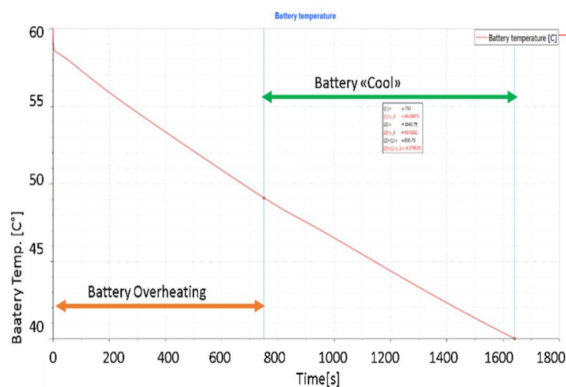


Figure A.56: Temperature Profile

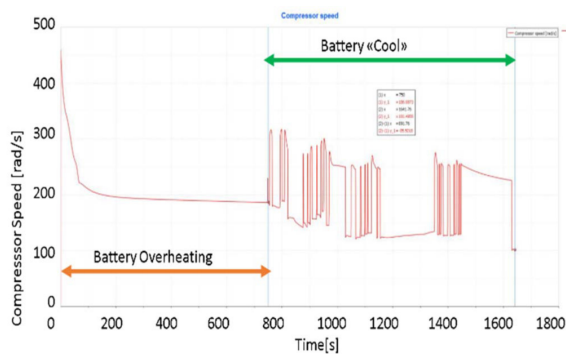


Figure A.57: Temperature Profile

Table A.13: Energy consumption

	<i>ECO batt overheating</i>	<i>ECO batt nominal</i>
Blower Energy	32 [Wh] (+6.2)	25.8 [Wh]
Compressor Energy	186 [Wh] (+62)	124 [Wh]

## VI. Conclusion and Future Developments

In this work authors have proposed a strategy to manage on board auxiliary loads starting from a very simple implementation. Even with this preliminary implementation, advantages of the proposed approach in terms of energy saving and higher reliability of the proposed system are quite important. Current authors are working on the following improvements:

- A more sophisticated control strategy for or even a more advanced configuration of HVAC according more recent improvement proposed in literature<sup>9-11</sup>;
- Modelling and implementation of the proposed approach also on other auxiliary loads also extending the simulation to different operational conditions such.
- The possibility of inserting more complex features on the proposed smart management strategy including load prediction functionality based on the knowledge of the planned route<sup>12,13</sup>.
- A testing campaign on a real vehicle since proposed control logic is very simple to be implemented.

## References

1. Min-Joong KimHueiPengl, Power management and design optimization of fuel cell/battery hybrid vehicles, *Journal of Power Sources* Volume 165, Issue 2, 20 March 2007, Pages 819-832 <https://doi.org/10.1016/j.jpowsour.2006.12.038>
2. Dib, W., Chasse, A., Moulin, P., Sciarretta, A., & Corde, G. (2014). Optimal energy management for an electric vehicle in eco-driving applications. *Control Engineering Practice*, 29, 299-307.
3. Valentina, R., Viehl, A., Bringmann, O., & Rosenstiel, W. (2014, June). HVAC system modeling for range prediction of electric vehicles. In *2014 IEEE Intelligent Vehicles Symposium Proceedings* (pp. 1145-1150). IEEE.
4. Lorenzo Berzi, Tommaso Favilli, Marco Pierini, Luca Pugi, Gerhard Benedikt Weiß, Nicola Tobia, Matthieu Ponchant "Brake Blending Strategy on Electric Vehicle Co-simulation Between MATLAB Simulink® and Simcenter Amesim™," 2019 IEEE 5th International forum on Research and Technology for Society and Industry (RTSI), Florence, Italy, 2019, pp. 308-313.
5. Kambly, K. R., & Bradley, T. H. (2014). Estimating the HVAC energy consumption of plug-in electric vehicles. *Journal of Power Sources*, 259, 117-124.
6. Pugi, L., Favilli, T., Berzi, L., Locorotondo, E., Pierini, M. Application of Regenerative Braking on Electric Vehicles (2019) *Proceedings - 2019 IEEE International Conference on Environment and Electrical Engineering and 2019 IEEE Industrial and Commercial Power Systems Europe, IEEEIC/I and CPS Europe 2019*, art. no. 8783318, .DOI: 10.1109/IEEEIC.2019.8783318
7. Berzi, L., Favilli, T., Locorotondo, E., Pierini, M., Pugi, L. Real time models of automotive mechatronics systems: Verifications on "toy models" (2019) *Mechanisms and Machine Science*, 68, pp. 141-148. DOI: 10.1007/978-3-030-03320-0\_15

8. Pugi, L., Grasso, F., Pratesi, M., Cipriani, M., Bartolomei, A. Design and preliminary performance evaluation of a four wheeled vehicle with degraded adhesion conditions (2017) *International Journal of Electric and Hybrid Vehicles*, 9 (1), pp. 1-32. DOI: 10.1504/IJEHV.2017.082812
9. Maranville, C. W., Schneider, J., Chaney, L., Barnh, T., & Heremans, J. P. (2012). Improving efficiency of a vehicle HVAC system with comfort modeling, zonal design, and thermoelectric devices. *United States Department of Energy*, 18(10).
10. Roscher, M. A., Leidholdt, W., & Trepte, J. (2012). High efficiency energy management in BEV applications. *International Journal of Electrical Power & Energy Systems*, 37(1), 126-130.
11. Huang, P., Huang, G., & Wang, Y. (2015). HVAC system design under peak load prediction uncertainty using multiple-criterion decision making technique. *Energy and Buildings*, 91, 26-36.
12. JOHANNESSON, Lars; NILSSON, Magnus; MURGOVSKI, Nikolce. Look-ahead vehicle energy management with traffic predictions. *IFAC-PapersOnLine*, 2015, 48.15: 244-251.
13. Guo, J., He, H., & Sun, C. (2019). Arima-based road gradient and vehicle velocity prediction for hybrid electric vehicle energy management. *IEEE Transactions on Vehicular Technology*, 68(6),

## A.9 Regenerative Fuzzy Brake Blending Strategy on Benchmark Electric Vehicle: the FIAT 500e [199]

**Published in** 2020 IEEE International Conference on Environment and Electrical Engineering and 2020 IEEE Industrial and Commercial Power Systems Europe (EEEIC / I&CPS Europe)

**Authors** Tommaso Favilli, Luca Pugi, Lorenzo Berzi and Marco Pierini, Nicola Tobia

**Abstract** Enhanced regenerative brake performances and increased battery reliability in modern Electric Vehicles could be allowed by a proper reduction of electric braking applications at severe operative conditions. In this paper, authors intend to develop an algorithm for the optimized coordination between Regenerative Brake System and Hydraulic Brake Plant, also known as Brake Blending strategy. Proposed solution aim at maximizing the recovered energy during braking manoeuvres while ensuring an increased battery durability, by avoiding accelerated ageing phenomena occurring at high temperatures and limit State Of Charge values of the energy storage system. The controller, based on fuzzy logic, is validated through simulation activities on a benchmark electric vehicle showing improved reliability performances and extended lifespan of the storage system.

**Keywords** :electric vehicle, brake blending, electric braking, fuzzy logic, battery reliability

### I. Introduction

The synergetic coordination between electric and hydraulic brakes in modern EV, aimed at ensuring a maximum energy recovery, is a very challenging task due to the complexity of the involved phenomena, which concerns several and heterogeneous physical domains<sup>1,2</sup>. Also, reliability constrains, which inevitably affects electric powertrain systems, should be accounted in the design of the *BB Controller*, making it capable to automatically select the most cautionary conditions<sup>3</sup>. Using a fuzzy logic approach could be a feasible solution for the design of this algorithm, being able to account both modelled and poorly conditioned limitations<sup>4,5</sup>.

Extensive work has been done in literature in order to properly model electric powertrain torques availability and to apply related constrains in the adopted control policies<sup>12</sup>. However, since a deterministic approach can be detrimental and, in some cases, lead to an underestimation of the involved limitations, a probabilistic based approach is proposed. To determine how the brake demand should be split between hydraulic and regenerative braking plant, the so-called *Brake Blending* strategy, we decide to follow a fuzzy logic methodology, which could be a useful tool in the optics of integrating the above mentioned aspects<sup>13,14</sup>.

Despite common fuzzy applications<sup>15</sup>, in which the involved aspects are abstracted to define a probabilistic strategy, in this paper authors successfully build and implement a fuzzy controller which can completely take account of power and energy limitations of battery and EM, based on its own models and their ideal power characteristics. Another non secondary advantages arising by the utilization of *mamdani* inference method concern the reduced perception of the driver during

variations of the efforts exerted by the involved systems. This allows smoother transitions in torques allocation between available braking actuators, ensuring better reliability of the electric driveline and improved dynamics behaviour of the vehicle, avoiding abrupt acceleration variations. This know-how is used to build an effective and efficient FBB controller, which can take account also of bad conditioned and hardly modelled constrain terms, such as the battery temperature and ageing<sup>16</sup>.

In this work, authors intend to evaluate the improvement permitted by the FBB controller in terms of regenerated energy and battery ageing. The proposed solution is validated through simulation activities based on a benchmark vehicle: the **FIAT 500e**. Nevertheless, a wide range of different EVs architectures are investigated in the current State-of-Arts, so the controller is designed to ensure scalability and portability properties, in order to be implementable for several e-powertrain configurations and multiple vehicles UCs.

## II. Simulation Framework

### A. Benchmark Vehicle: FIAT 500e

he investigated vehicle is the *FIAT 500e* [...].

he evaluation of the results is done supposing, for the reference UC, two different powertrain architectures: a) the conventional FWD configuration and b) a 4WD layout, actuated by independents IWMs. The parameters remain the same for both the investigated configurations [...].

The 7 DoF EV model consist of several mechanical, electrical and electronic sub-systems, useful for an accurate simulation of the vehicle behaviour during real driving scenarios, i.e.: **Driver model**, **Torque regulation controller** (constituted by a simple EBD controller (which apply different distribution ratio between front and rear axles torques in function of the longitudinal load transfer), and the proposed FBB controller), **Electric motor model**, **Energy storage model**, **Hydraulic brake model**, **Chassis model**, **Wheel model**.

[...] It is important to note that the gathered experimental data has allowed to estimate the the number of cycle which the battery has already experienced, based on our model. It has been found that the battery has performed about 25 equivalent cycle before tests starts. These results are in agreement with the ones arise from the real vehicle.

### B. Fuzzy Brake Blending Controller

Fuzzy logic can be considered as a simplified neural network whose primary benefit is to approximate systems behaviour when analytic functions or numerical models don't exist, are poorly structured<sup>14</sup> or object of high level of measurement uncertainty<sup>15</sup>.

Proposed FIS logic controller, whose block diagram is represented in Figure A.58, aims at the controlling of the blending strategy of the available braking actuators: RBS and disc brake. For doing that, accounts multiple variables in the process, listed above.

1) **Driver Demand** establish the requested torques on each wheel. As already pointed out, when battery SOC, defined by (A.35), is lower than a certain value, it is recommended to prioritize electric braking, in order to ensure the maximum regeneration. Otherwise, when battery is almost completely charged a de-rating of the EM brake performances should be applied. For medium SOC value instead,

regenerative brake is still desired, but it achieves its maximum value of 1 only if the entity of the requested brake exceeds a threshold, corresponding to an acceptable level of regeneration. Indeed, if the brake command is smaller than this established value, the reduced amounts of recovered energy doesn't justify the increased complexity in the system management. The *Driver demand* is then fuzzified through three different MtFs, respectively *full*, *derate* and *no* for low, medium and high SOC values.

**2) EM shaft speed** essential for the evaluation of the available torque by the electric powertrain and the avoidance of shaft overrunning. Fully exploiting of the EM characteristics is achieved making sure the delivered torque closely trace the ideal traction/braking curve. To realize this assumption in the FIS, we build a 2 MtFs variable dependency: the *start* function, used to avoid vehicle going in reverse direction, and the *stop* function, which turns off the regenerative braking above the maximum admitted shaft speed. Indeed, when the vehicle is approaching 0 speed, regenerative braking is not suggested, since applying negative torque to wheels when the car is in stationary conditions can cause the vehicle going backward. The Iso-Torque and Iso-Power curve are implemented by the signals arising by the MCU.

**3) Battery SOC** fundamental for averting dangerous condition of the storage system. The power constrains are implemented by 3 MtFs named *low*, *medium* and *high*, reflecting the corresponding SOC states defined by (A.35), where  $C_{nominal}$  is the battery capacity.

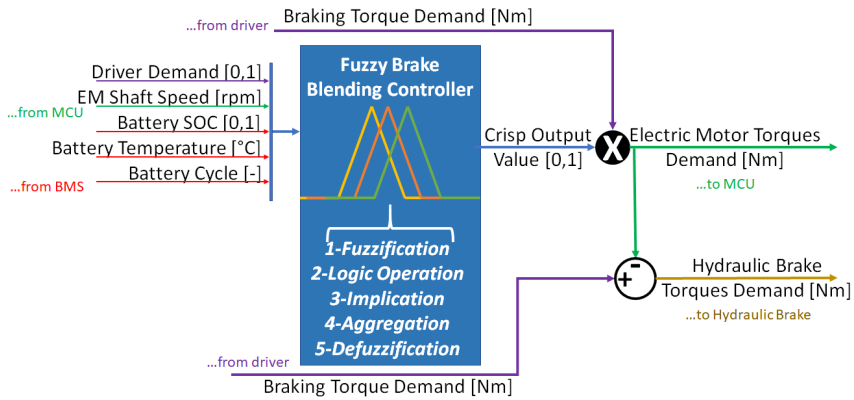


Figure A.58: Fuzzy Brake Blending controller

$$SOC = 100 \left( 1 - \frac{1}{C_{nominal}} \int_0^t i(t) dt \right) \tag{A.35}$$

This variable is essential to avoid fast performances degradation due to high level of requested DOD, as pointed out in<sup>19</sup>, where DOD is defined by (A.36).

$$DOD = 1 - SOC \tag{A.36}$$

**4) Battery Temperature** it is recommended to reduce the power flowing in the battery when low or high temperatures condition occurs. Similarly at the previous case, temperature effects increase the ageing rate of the battery<sup>16,19</sup>. So it is advisable to limit the battery C-rate when operating at temperature that differs

from the nominal. We adopt a Gaussian MtF in function of the battery temperature to reduce the current.

**5) Battery ageing** used to implement energy limitations of storage according to capacity fade effects. As the battery ages its capacity decreases, so it is recommended to limit the amount of power recovered during regenerative braking scenario. Otherwise we could accelerate the decay performances law.

According to<sup>16</sup>, automotive battery are considered at EoL when their capacity drops below 80% of the Beginning of Life (BoL) capacity value  $C_{BoL}$ . For the reference UC we assume an equivalent number of full charge-discharge cycle of  $N_{EoL}=2000$ . However, in EVs applications, only in a restricted number of case batteries are object of full cycles. So, to account the effect of partial cycles we define the battery ageing using the *Ampere-hour throughput* model<sup>19</sup>, a framework for the battery lifetime prediction. The battery nominal Ampere-hour throughput is calculated by (A.37), supposing a DOD of 100% and an ambient temperature of 20°C.

$$Ah - throughput_{\text{nominal}} = \int_0^{t_{EoL}} |i_{\text{nom}}(t)| dt \quad (\text{A.37})$$

Where  $i_{\text{nom}}(t)$  is the nominal current of the battery and  $t_{EoL}$  the instant in which battery capacity reaches the EoL value.

To quantify the ageing effects we consider the severity factor  $\sigma$ , an indicator of the battery degradation respect to the nominal number of admitted cycle  $N_{EoL}$ . In particular, the severity factor, at a given *DOD* and temperature  $T_{\text{batt}}$ , is defined by (A.38), with  $i(t)$  the current actually flowing in the battery.

$$\sigma = \frac{Ah - throughput_{\text{nominal}}}{\int_0^{t_{EoL}} |i(t)| dt} \quad (\text{A.38})$$

Value of  $\sigma$  higher than 1 corresponds to more severe operating conditions respect to the baseline. In<sup>19</sup> the severity factor is mapped respect to *DOD* and  $T_{\text{batt}}$ , highlighting that at higher temperature and depth of discharge the severity factor is increased, as the ageing rate. So, is recommended to reduce the flowing current when the effective battery Ampere-hour throughput is approaching his EoL value. To implement this functionalities we use a single MtF respect to the performed equivalent cycles. The severity factor  $\sigma$  is used as adjusting coefficient for the calculation of the effective battery *Ah-throughput<sub>eff</sub>*, according to (A.39).

$$Ah - throughput_{\text{eff}} = \int_0^t \sigma(t) |i_{\text{batt}}(t)| dt \quad (\text{A.39})$$

At this point the *Ah-throughput<sub>eff</sub>* is used to establish the equivalent number of performed cycles  $N_{\text{eff}}$ , subdividing it by the nominal *Ah* consumed during a cycle in nominal condition, which is double the nominal capacity of the battery supposing a cycle composed by a full charge and discharge process.

**6) Output** the fuzzy logic requires the definition of proper output MtFs to fulfil the implication phases. Those are *max* and *min*.

Once established the inputs fuzzy values using the corresponding MtFs during the fuzzification process, the fuzzified input variables, whose degrees of membership are comprised between 0 and 1, have to be processed according specified rules. Adopted implication rules, summarized in Table A.14, have the objective to join model-based constrains with poor structured reliability aspects of the electric powertrain,

while maximizing the regenerated energy. The resolving of those statement is done according to AND operator logic (min).

Table A.14: Fuzzy controller implication rules

Implication Rules: Statements						
$n^\circ$	$Brake_{CMD}$	$EM_{rpm}$	$SOC_{batt}$	$T_{batt}$	$Cycle_{batt}$	output
1	full	start	low	cycle	T	max
2	derate	start	medium	cycle	T	max
3	no	start	high	cycle	T	min
4	stop	/	/	/	/	min

For each rule a single degree of membership is obtained using an OR operator between fuzzified input and corresponding output MtFs, during the implication phase. The aggregation stages conjugated the previously described rules, while the defuzzification process returns a single crisp final value using a SOM logic. The FIS controller uses a *mamdani-type* inference method and the output signals are continuous (instead of discrete for the *sugeno-type*). This final value corresponds to the desired EM brake ratio that can be exerted by the electric powertrain, respect the maximum requested braking torque. The remaining effort should be burden by the hydraulic brake system [...].

Summarizing, all this recommended specification are integrated by a proper design of the fuzzy controller rules, along with the BB controller developed in<sup>6-9</sup>. It is sufficient to know that the crisp value arise by the fuzzy controller constitute a correctional gain, variable between 0 and 1, which is multiplied to the EM torques command [...]. This solution concretized the attempt to reproduce a model-based concept in a fuzzy controller. Electric powertrain protections should be considered also during traction, so the fuzzy controller functionalities have been extended in order to implement EM and battery constrains, both during deceleration and acceleration phases. However, to ensure the execution of maneuvers according to the pilot's request, the traction fuzzy controller output is used to reduce the torque constrains, not the command.

The above mentioned input and output MtFs are visible in Figure A.59.

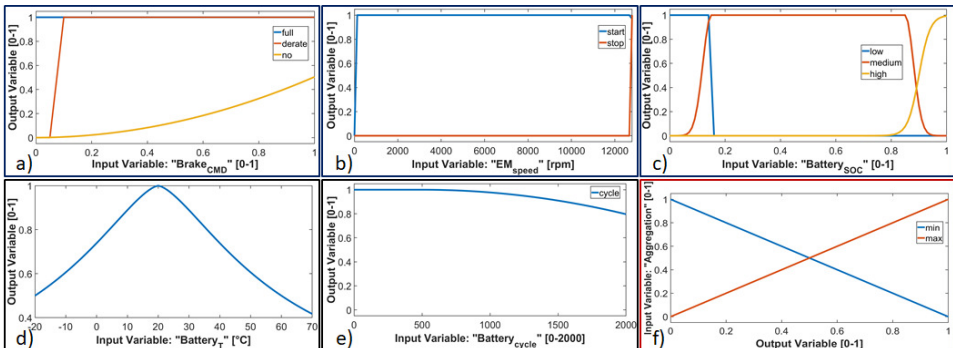


Figure A.59: Membership Function for: a) Brake Comand; b) EM shaft speed; c) Battery SOC; d) Battery Temperature; e) Battery Cycle; f) Aggregation

### III. Simulation Results

For evaluating the performances of the proposed FBB controller, the models of the investigated EV (the *FIAT 500e*) has been implemented in *MATLAB Simulink* environment, according to the scheme of Figure A.60, in order to execute some simulation campaigns [...].

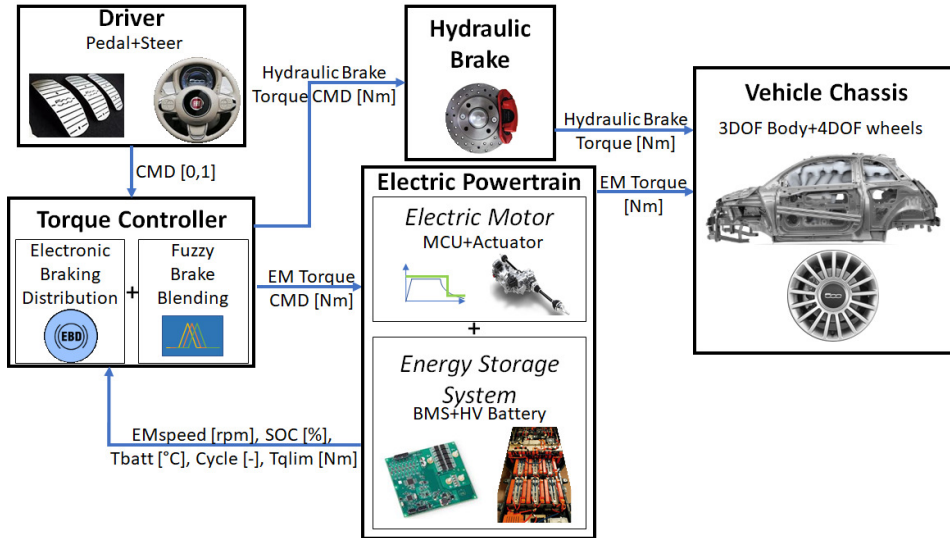


Figure A.60: Simulation layout implemented in MATLAB Simulink

Performed tests can be grouped in two branches:

**Reference Manoeuvres** consist in the execution of straight line deceleration at fixed boundary condition, i.e. battery temperature and initial vehicle speed, varying the corresponding initial charge. In this way it is possible to show the influence of  $Brake_{CMD}$  and  $EM_{speed}$  Membership Functions on the blending strategy.

During these full braking manoeuvres the blending controller prioritizes the RBS when available. Initial vehicle speed  $V_i=27.78\text{ m/s}$  and battery temperature  $T_{batt}=20\text{ }^\circ\text{C}$  are supposed constant, while consecutive simulation have been performed at different battery initial charges  $SOC_i$ . Outcomes of the tests, for the FWD vehicle UC, are the torque references summarized in Figure A.61.

**Driving Cycles** making the vehicle perform specific driving cycles at different initial battery temperature  $T_{batti}$ , in order to account the effect of the FBB controller on storage reliability aspects. Though more significant driving cycles are available and frequently used, e.g. WLTP, which better replicates real driving conditions by involving a wide spectrum of acceleration and speed ranges, we still opted for the NEDC. This is due to the fact that experimental data have been made available by CRF concerning this cycle, useful for the model and controller design.

Tests are repeated, for both the electric powertrain configurations, supposing the unavailability and availability of the FBB controller in order to metrical asses its performances. Interesting output are regenerated energy respect to the consumed one, final  $SOC_f$  and effective Ah-throughput impact on one equivalent performed

cycle (A.40), visible in Table A.14, which show the effect of the FBB on above mentioned variables, assuming the data arise from simulation performed with conventional BB as a reference baseline for the improvement evaluations.

$$Ah - throughput_{\text{impact}} = \frac{Ah - throughput_{\text{eff}}}{2C_{\text{nom}}} \quad (\text{A.40})$$

Concerning the first simulations, results of Figure A.61 show how the proposed controller correctly assign the EM torque references, according to the battery SOC and motor shaft speed: when high level of charge occurs the blending strategies reduces the RBS effort to avoid over-charging. Viceversa, for low and medium level of charge the algorithm prioritize electric braking to ensure a maximum energy recover.

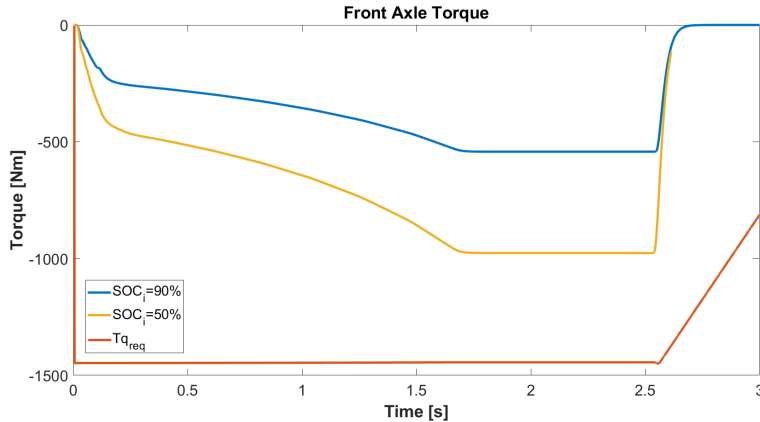


Figure A.61: Straight line deceleration: regenerative torques at different  $SOC_i$

Regarding the driving cycle simulations, we expect a faster performances degradation when the BB strategy do not account thermal and ageing phenomena. Data of Table A.15 are in agreement with these assumptions, since more severe operative conditions accelerates the performances decay: the equivalent performed cycle are higher. Indeed, according equation (A.38)-(A.38) and [228], the impact in the battery ageing of cycles performed at temperatures which differs from the nominal, is greater. Nevertheless, energy performances are reduced in potentially dangerous scenario.

Important consideration about the proposed controller could be done observing that the amount of energy regenerated is minor for higher battery temperatures. A first look at this output could suggest some error in the simulations activities, since we expect a less significant decrease of the energy recovered ratio by the RBS, when the tests are performed at severe temperature conditions. However, these results are justified considering the limited vehicle's accelerations involved by the NEDC. The constrains limitation imposed by the fuzzy controller during acceleration phases are not overcomes by the driver request, which require negligible torques, so the consumed energy remain the same. During braking instead, the performances are reduced, since are applied directly to the driver command, unlike during traction, in which are applied to the e-powertrain limits.

Table A.15: NEDC simulation results at  $SOC_i=85\%$  and  $DOD=5\%$ 

Initial Condition: $T_{batt0}=20^\circ C$ ; $\sigma = 1$				
Layout	Fuzzy BB	$SOC_{battf}[\%]$	$E_{reg}/E_{cons}[\%]$	$Cycle_{impact}[\%]$
FWD	ON	80.1	16.24	3.24
	OFF	80.2	16.28	3.45
4WD	ON	80.5	21.72	3.40
	OFF	80.5	21.76	3.61
Initial Condition: $T_{batt0}=45^\circ C$ ; $\sigma = 1.5$				
Layout	Fuzzy BB	$SOC_{battf}[\%]$	$E_{reg}/E_{cons}[\%]$	$Cycle_{eff}$
FWD	ON	79.9	10.87	4.93
	OFF	80.2	16.28	5.17
4WD	ON	80.0	14.47	5.09
	OFF	80.5	21.76	5.41
Initial Condition: $T_{batt0}=60^\circ C$ ; $\sigma = 2$				
Layout	Fuzzy BB	$SOC_{battf}[\%]$	$E_{reg}/E_{cons}[\%]$	$Cycle_{eff}$
FWD	ON	79.7	8.14	6.42
	OFF	80.1	16.23	6.90
4WD	ON	79.9	10.85	6.57
	OFF	80.5	21.71	7.22

## IV. Conclusion and Future Developments

Most significant results of the simulations are the energy performances and reliability improvements obtained. Supposing different powertrain layouts allows to comparatively evaluate the outcomes, as well as the assessment of scalability and portability properties of the developed control strategy.

In conclusion, to ensure the maximum flexibility of the controller, we have developed an algorithm which owns important scalability and portability properties. This conclusion is due to the fact that the FBB strategies applies effectively to different electric powertrain architectures. In addition, improvements in the driver dynamic feedback are achieved: conventional blending policies could generate abrupt accelerations when passing from the usage of a braking actuators to another. A smoother dynamic instead, as the one proposed in this paper, can reduce the passengers perception.

Results highlight how the proposed fuzzy controller could increase battery reliability and lifespan, selecting more conservative power constrains when limit conditions occurs. However, adopt FBB reduce the overall energy which could be recovered for the RBS in those scenarios. This strategy, attempt to find an optimal comprise between energy regeneration and energy storage system preservation [...].

## References

1. J. Ruan, P. D. Walker, P. A. Watterson, and N. Zhang, ‘The dynamic performance and economic benefit of a blended braking system in a multi-speed battery electric vehicle’, *Applied Energy*, vol. 183, pp. 1240–1258, Dec. 2016, doi:10.1016/j.apenergy.2016.09.057.
2. M. T. Von Srbik and R. F. Martinez-Botas, ‘Vehicle optimisation for regenerative brake energy maximisation’, in *Sustainable Vehicle Technologies*, Elsevier, 2012, pp. 165–174.

3. J. de Santiago et al., ‘Electrical Motor Drivelines in Commercial All-Electric Vehicles: A Review’, *IEEE Transactions on Vehicular Technology*, vol. 61, no. 2, pp. 475–484, Feb. 2012, doi: 10.1109/TVT.2011.2177873.
4. G. J. Klir and B. Yuan, *Fuzzy sets and fuzzy logic: theory and applications*. Upper Saddle River, N.J: Prentice Hall PTR, 1995.
5. M. N. Cirstea, Ed., *Neural and fuzzy logic control of drives and power systems*. Oxford; Burlington, MA: Newnes, 2002.
6. L. Berzi, T. Favilli, E. Locorotondo, M. Pierini, and L. Pugi, ‘Real Time Models of Automotive Mechatronics Systems: Verifications on “Toy Models”’, in *Advances in Italian Mechanism Science*, vol. 68, G. Carbone and A. Gasparetto, Eds. Cham: Springer International Publishing, 2019, pp. 141–148.
7. L. Pugi, T. Favilli, L. Berzi, E. Locorotondo, and M. Pierini, ‘Brake Blending and Optimal Torque Allocation Strategies for Innovative Electric Powertrains’, in *Applications in Electronics Pervading Industry, Environment and Society*, vol. 573, S. Saponara and A. De Gloria, Eds. Cham: Springer International Publishing, 2019, pp. 477–483.
8. L. Pugi, T. Favilli, L. Berzi, E. Locorotondo, and M. Pierini, ‘Application of Regenerative Braking on Electric Vehicles’, in *2019 IEEE International Conference on Environment and Electrical Engineering and 2019 IEEE Industrial and Commercial Power Systems Europe (EEEIC / I and CPS Europe)*, Genova, Italy, 2019, pp. 1–6, doi: 10.1109/EEEIC.2019.8783318.
9. L. Berzi, T. Favilli, E. Locorotondo, M. Pierini, and L. Pugi, ‘Real Time Models of Automotive Mechatronics Systems: Verifications on “Toy Models”’, in *Advances in Italian Mechanism Science*, vol. 68, G. Carbone and A. Gasparetto, Eds. Cham: Springer International Publishing, 2019, pp. 141–148.
10. C. Satzger, R. de Castro, and T. Bunte, ‘A model predictive control allocation approach to hybrid braking of electric vehicles’, in *2014 IEEE Intelligent Vehicles Symposium Proceedings*, MI, USA, 2014, pp. 286–292, doi: 10.1109/IVS.2014.6856529.
11. C. Feng, N. Ding, Y. He, G. Xu, and F. Gao, ‘Control allocation algorithm for over-actuated electric vehicles’, *J. Cent. South Univ.*, vol. 21, no. 10, pp. 3705–3712, Oct. 2014, doi: 10.1007/s11771-014-2354-0.
12. J. A. A. Hartley, R. G. McLellan, J. Richmond, A. J. Day, and I. F. Campean, ‘Regenerative braking system evaluation on a full electric vehicle’, in *Innovations in Fuel Economy and Sustainable Road Transport*, Elsevier, 2011, pp. 73–86.
13. J. Zhang, B. Song, S. Cui, and D. Ren, ‘Fuzzy Logic Approach to Regenerative Braking System’, in *2009 International Conference on Intelligent Human-Machine Systems and Cybernetics*, Hangzhou, Zhejiang, China, 2009, pp. 451–454, doi: 10.1109/IHMSC.2009.120.
14. Zijian Zhang, Guoqing Xu, Weimin Li, and Liang Zheng, ‘Regenerative braking for electric vehicle based on fuzzy logic control strategy’, in *2010 2nd International Conference on Mechanical and Electronics Engineering*, Kyoto, Japan, 2010, pp. V1-319-V1-323, doi: 10.1109/ICMEE.2010.5558540.
15. T. J. Ross, *Fuzzy logic with engineering applications*, 3rd ed. Chichester, U.K: John Wiley, 2010.
16. N. Omar et al., ‘Lithium iron phosphate based battery – Assessment of the ageing parameters and development of cycle life model’, *Applied Energy*, vol. 113, pp. 1575–1585, Jan. 2014, doi: 10.1016/j.apenergy.2013.09.003.
17. Junjun Deng, Siqi Li, Sideng Hu, C. C. Mi, and Ruiqing Ma, ‘Design Methodology of LLC Resonant Converters for Electric Vehicle Battery Chargers’, *IEEE Trans. Veh. Technol.*, vol. 63, no. 4, pp. 1581–1592, May 2014, doi: 10.1109/TVT.2013.2287379.
18. H. Pacejka, *Tire and Vehicle Dynamics*. Elsevier, 2005.]
19. S. Onori, P. Spagnol, V. Marano, Y. Guezennec, and G. Rizzoni, ‘A new life estimation method for lithium-ion batteries in plug-in hybrid electric vehicles applications’, *IJPELEC*, vol. 4, no. 3, p. 302, 2012, doi: 10.1504/IJPELEC.2012.046609.

## A.10 ESC on In-Wheel Motors Driven Electric Vehicle: Handling and Stability Performances Assessment [194]

**Published in** 2020 IEEE International Conference on Environment and Electrical Engineering and 2020 IEEE Industrial and Commercial Power Systems Europe (EEEIC / I&CPS Europe)

**Authors** Margerita Montani, Tommaso Favilli, Lorenzo Berzi, Renzo Capitani, Marco Pierini, Luca Pugi and Claudio Annicchiarico

**Abstract** Improved lateral stability performances of modern Electric Vehicles equipped with In-Wheel Motors could be achieved by a proper design of the adopted control strategy. The possibility to independently regulates braking and traction efforts delivered at each wheel can lead to increased handling properties during cornering manoeuvres, especially if performed in degraded adherence operative conditions. In this activity, authors propose a newly ESC lateral stability algorithm, integrated with longitudinal stability controller (EBD and ABS) and implemented on a benchmark vehicle use case model. The assessment of the performances is done through co-simulation activities, imposing to the vehicle specified reference trajectories according to related standards, in order to evaluate the achieved stability improvements.

**Keywords** electric vehicle, in-wheel motor, lateral stability

### I. Introduction

[...] Challenging well-known and widely diffused control algorithms is intent of the paper, aiming at the development of effective longitudinal and lateral control strategies which can fully exploit the electric powertrain features and, also, to investigate unconventional driveline architectures that can lead to more performances improvements. [...] Thus, the consequent increased complexity in the system architectures and the recent growing interest for IWM driven vehicle, requires the development of control strategies which combines the contribution of all the involved stability controllers: ESC, EBD and ABS<sup>11-13</sup>.

Objectives of the work is to correctly integrate proposed longitudinal and lateral stability controllers, in order to validate the results on a benchmark vehicle through simulation activities. In particular, the results are evaluated supposing an alternative drive-line architecture respect to the conventional layout of the vehicle UC, establishing corresponding improvement through the execution of several reference manoeuvres, according to related standards.

Respect to previously proposed work in literature, in this paper authors develop a newly ESC strategy using an UKF vehicle state estimator<sup>2</sup> and More-Penrose pseudoinverse based torque vectoring technique<sup>3,4</sup>, which aim at minimizing the difference between the driving performances requested by the driver and the controllers, ensuring enhanced stable behaviour by fully exploiting IWM traction and braking characteristic. All the models are developed in co-simulation environments that accurately reproduce the boundary conditions.

## II. Aim Of The Paper

As already pointed out, intent of these activities is to assess the possible improvement arising by an optimized coordination between proposed stability controllers (ESC, EBD and ABS), in terms of vehicle’s dynamical behaviour.

To fulfil these tasks, we decide to build a vehicle model following a co-simulation approach between widely diffused simulation environments: *MATLAB Simulink* and *VI grade Simulator*. In particular, the models developed in the different solutions are coupled using one platform as master and the other one as slave. In order to ensure no losses in the data exchange process during RT simulation tests, proper sample rates and solvers are imposed.

## III. Electric Vehicle Model

The vehicle model, inspired by a real existing car, is a RWD vehicle configuration. However, we suppose a different powertrain layout, in order to investigate the performance improvements allowed by the proposed stability controllers: a 4WD architectures with IWMs, which independently actuate the EV wheels. The main sub-models adopted for this work are: Driver model, Stability Controllers (ESC, EBD and ABS interposed between the driver model and the MCU or the BCU), Electric Motor Model, Hydraulic Brake Plant Model and Vehicle Model [...].

The Hydraulic Brake Plant Model, developed by Meccanica42 company, is composed by four electro-hydraulic units interposed between the main pump and the calliper of the brake system. Each unit is made by a controller and an electric motor which command the hydraulic plant in order to deliver the target braking pressure to the wheel’s calliper. They can be considered as a CAN controlled device and so, can track a target pressure imposed by higher level control systems, thus simplifying the integration of the whole loop.

The interfacing between the *Vehicle Model* and the *Stability Controllers* is done according the block diagram scheme of Figure A.62.

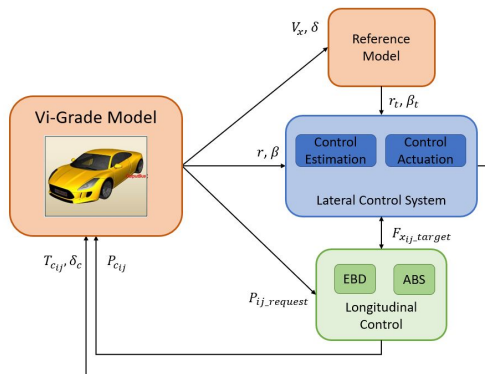


Figure A.62: Lateral Control Strategy Block Diagram

## A. Electronic Stability Program

[...] the controller firstly calculate the expected yaw rate and side slip angles, in function of the imposed trajectory. Then, compare these values with the ones that the vehicle is effectively experiencing, typically estimated through IMU sensors platform and ANN-UKF algorithm, as reported in<sup>15</sup>. If there is a not negligible error, evaluated with a proper dead-zone, the ESC apply torque vectoring and steering control techniques to ensure the vehicle follows as close as possible the desired states (yaw rate and side slip angle), delivering an equivalent yaw moment and a corrective steering angle, according to the driver's command.

In conventional automotive solution, e.g. ICE vehicles, lateral stability strategies differentiates braking efforts between rights and lefts wheels, generating a correction yaw moment [...] However, for the reference UC, lateral stability enhancement could be achieved thanks to IWM specifications. Indeed, each actuator can both accelerate and decelerate, increasing the  $M_{yaw}$  that could be applied to the vehicle body.

The proposed lateral control algorithm, shown in Figure A.62, is composed by three sub-systems: the *Reference Dynamic Model*, the *Control Estimation System* and the *Control Command Actuation*.

**1) Reference Dynamic Model** according to driver commands the vehicle body reference system vary with time. However, to underline inner vehicle characteristics (manoeuvrability) and control the under-steering/over-steering behaviour of the chassis, estimating the steady state values of the yaw rate (A.41) and side slip angle (A.42) it's essential. These variables are expressed as a function of the *under-steering gradient*  $K$ , a coefficient depending from the vehicle wheelbase  $L = a + b$ , mass  $m$  and rear tires cornering stiffness  $C_{yr}$ .

$$r_t = \frac{u}{(a + b) + u^2 K} \delta \quad (\text{A.41})$$

$$\beta_t = \frac{b - \frac{m a u^2}{(a+b)C_{yf}}}{(a + b) + u^2 K} \delta \quad (\text{A.42})$$

To ensure a stable behaviour of the vehicle during cornering manoeuvres, the ESC should control the available actuators in order to make the yaw rate  $r$  and the side slip angle  $\delta$  strictly follow their optimal values, established from the *Reference Dynamic Model*. Nevertheless, expressions (A.41) and (A.42) doesn't accounts degraded adhesion conditions of the wheels, thus their values must be saturated to an upper threshold [...].

**2) Control Estimation System** the implemented ESC strategy is based on a LQR, an optimal control that is able to find, during driving scenario, the desired yaw torque and steering wheel angle which ensure stable behaviour of the chassis and passengers safety, as well as improved dynamic performances. Conventional LQR estimator works for a single linear dynamic model and are tuned specifically to reset the input variable<sup>16</sup>. The proposed LQR solution, as reported in<sup>2</sup>, integrates a gain-scheduling control methodology, able to accurately follows the target value imposed by the *Reference Dynamic Model*, by adaptively tune itself in RT.

The states of the system are the actual yaw rate  $r$  and side slip angle  $\beta$ , estimated by a single track vehicle model, and yaw rate  $r_t$  and nominal side slip angle  $\beta_t$  arises

from the reference model by solving (A.45), where  $A$  (A.43) and  $B$  (A.44) are the coefficients matrices.

$$A = - \begin{bmatrix} \frac{C_{yf}+C_{yr}}{m*vel_x} & \frac{1+C_{yf}*a-C_{yr}*b}{m*vel_x^2} & 0 & 0 \\ \frac{C_{yf}*a-C_{yr}*b}{J} & \frac{C_{yf}*a^2+C_{yr}*b^2}{J*vel_x} & 0 & 0 \\ 0 & 0 & \frac{1}{\tau_\beta} & 0 \\ 0 & 0 & 0 & \frac{1}{\tau_r} \end{bmatrix} \quad (A.43)$$

$$B = \begin{bmatrix} \frac{C_{yf}}{m*vel_x} & 0 \\ \frac{C_{yf}*a}{J} & \frac{1}{J} \\ 0 & 0 \\ 0 & 0 \end{bmatrix} \quad (A.44)$$

$$\begin{Bmatrix} \dot{r} \\ \dot{\beta} \\ \dot{r}_t \\ \dot{\beta}_t \end{Bmatrix} = A * \begin{Bmatrix} r \\ \beta \\ r_t \\ \beta_t \end{Bmatrix} + B * \begin{Bmatrix} \delta_c \\ M_y \end{Bmatrix} \quad (A.45)$$

In (A.45) the dynamic states evolution is expressed by vehicle geometric parameters, i.e., the front and rear wheelbase  $a$  and  $b$ , the vehicle mass  $m$  and yaw moment of inertia  $J$ , the front and rear cornering stiffness,  $C_{yf}$  and  $C_{yr}$  respectively, and the longitudinal vehicle speed, which is scheduled at intervals of 10 m/s.

Defining the output of the controller as the difference between reference and actual states, it's possible to establish the optimal controller gains. This allow to correctly determine the control signals: a steering wheel angle  $\delta_c$ , that has to be added to the driver's steer command, and an equivalent yaw moment  $M_{yaw}$ , which is delivered to the vehicle body by the EM and by the hydraulic brake plant (A.46).

$$\begin{Bmatrix} \delta_c \\ M_{yaw} \end{Bmatrix} = \begin{bmatrix} K_{\delta r} & K_{\delta \beta} & K_{\delta r_t} & K_{\delta \beta_t} \\ K_{M r} & K_{M \beta} & K_{M r_t} & K_{M \beta_t} \end{bmatrix} * \begin{Bmatrix} r \\ \beta \\ r_t \\ \beta_t \end{Bmatrix} \quad (A.46)$$

To be implemented in Real-Time, all the control logic is discretized with a sample time of 0,001 s.

**3) Control Command Actuation** the optimal allocation strategy proposed here is based on the Moore-Penrose pseudoinverse<sup>4</sup>. We would like to accomplish two different tasks: (1) ensure a desired stable lateral behaviour of the vehicle and (2) produce a minimum correction moment, which must be also in accordance with the driver intent. The followed approach appear efficient, since minimize the norm 2 of the functional cost (A.47), which attempt to stabilize the vehicle lateral behaviour, while minimizing the correction efforts.

$$\|T_{cmd-k} - T_{cmd-k} * \|_2 = \left( \sum_{k=1}^{n=4} (T_{cmd-k} - T_{cmd-k}^*)^2 \right)^{1/2} \quad (A.47)$$

where  $k \in \{fl, fr, rl, rr\}$  indicate the wheel (front left, front right, rear left, rear right),  $y_k$  is the half-track of the corresponding wheel,  $R_w$  the tire radius,  $T_{cmd-k}$

and  $T_{\text{cmd-k}}^*$  are the torques requested by the driver and by the ESC controller, respectively.

The reference wheel torques is given by (A.48).

$$\begin{bmatrix} \frac{-y_{fl}}{R_w} & \frac{y_{fr}}{R_w} & \frac{-y_{rl}}{R_w} & \frac{y_{rr}}{R_w} \\ 1 & 1 & 1 & 1 \end{bmatrix} \begin{bmatrix} T_{\text{cmd-fl}} - T_{\text{cmd-fl}}^* \\ T_{\text{cmd-fr}} - T_{\text{cmd-fr}}^* \\ T_{\text{cmd-rl}} - T_{\text{cmd-rl}}^* \\ T_{\text{cmd-rr}} - T_{\text{cmd-rr}}^* \end{bmatrix} = \begin{bmatrix} M_{\text{yaw}} \\ 0 \end{bmatrix} \quad (\text{A.48})$$

As can be seen, the first row correspond to the task (1), while the second row reflect the task (2). The resolution of (A.48) occur in four sequential steps. In each  $k$ -th step the value of  $T_{\text{cmd-k}}^*$  is checked respect to its upper and lower constrain limits. If it exceeds them, is subsequently saturated at this value. At the  $(k+1)$ -th steps (A.48) is recalculated, excluding from the system the row related to the  $k$ -th torque reference, assumed equal to its own limitations.

The algorithm is parameterized respect to the wheels torque constrains, in order to ensure maximum flexibility and portability of the code respect to different vehicle architectures. This ensure that the requested torques are in accordance with the actuators limitations, allowing, in addition, the implementability of advanced torque vectoring techniques. Is the case of the benchmark vehicle investigated in this paper, in which positive and negative efforts could be delivered independently on each wheel, even of the same axis.

## B. Electronic Braking Distribution

The EBD is a control unit widely adopted in the automotive field, used to privilege braking performances of the vehicle's axes, in function of front/rear longitudinal load transfer. According to<sup>17</sup>, the set of optimal points, as the adhesion coefficient in the tire-road interface changes, is a parabola, visible in Figure A.63(a). This curve is calculated by solving (A.49) [...].

$$F_{zf} = \frac{F_{xf}}{\mu} = F_{zf}^0 + \frac{h}{l}(F_{xf} + F_{xr}) \quad (\text{A.49})$$

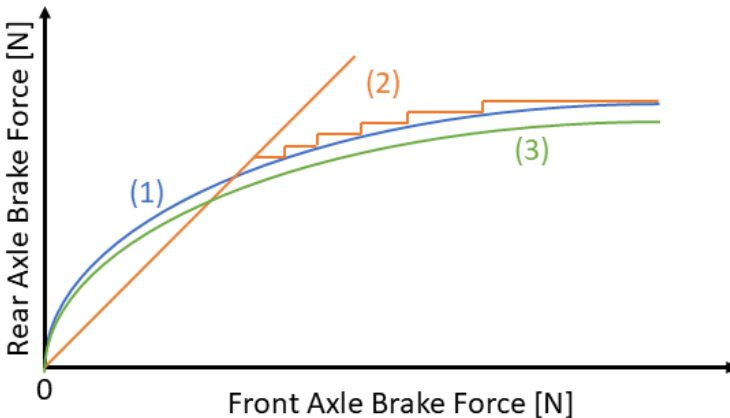


Figure A.63: Front/Rear Axle Braking Force EBD distribution: (1) Ideal; (2) Conventional; (3) Proposed.

The curve define the load distribution coefficients between the axes which, for the specified friction coefficient, maximize the available deceleration while avoiding wheels sliding. Typically, conventional EBD controller approximate this function with a simple ramp which apply a 50/50 ratio axle braking, leaving to the ABS controller the burden to avoid rear wheels sliding (Figure A.63(2)).

Use more conservative strategy could reduce the onset of wheel slippage, but underestimate the available deceleration performances, not allowing to completely exploit the braking actuators and reduce the stopping distance for degraded friction conditions. However, the new architecture of by-wire system used allows to reduce the delay respect to the one in modern EV, thanks to the positioning of the hydraulic component close to the wheel. The use of four independent actuators ensures to obtain the optimal brake distribution and increases system safety with redundancy. In order to compensate the uncertainty of the adhesion coefficient we adopt a parabola which slightly deviate from the ideal curve (Figure A.63(3)). In this way the front/rear braking allocation strategy appear more robust respect to error in the friction value estimation.

### C. Anti-Lock Braking System

To ensure the stability during braking actuation and improve the handling of vehicle, both in longitudinal and cornering manoeuvres, an ABS is recommended (Figure A.62). It is implemented a PID controller that allows to follow the target longitudinal wheel slip<sup>18</sup>, given by the ESC and by the driver's request, at each wheel. [...] The target wheel slip is calculated from the desired longitudinal force, arising from the EBD in case of brake pedal actuation, or from the ESC system. Knowing the longitudinal front and rear stiffness of the tires and assuming a linear behaviour of the latter, target longitudinal slip is calculated through (A.50).

$$\sigma_t = \frac{F_x}{C_x} \quad (\text{A.50})$$

This value is saturated from zero, so that the control only works when braking, to near 0.05, ensuring that the wheel maintain itself in the linear dynamic range.

Instead the actual value of the longitudinal slip is estimated by (A.51).

$$\sigma = \frac{V_x - \omega * R_w}{V_x} \quad (\text{A.51})$$

The PID output is the single pressure which, if applied on every wheel, reduce the error between target and actual value of the slip.

## IV. Simulation Campaign Results

To evaluate the stability performances improvement allowed by the controllers, we make the vehicle perform specific reference manoeuvres. Simulation tests on the proposed EV model, implemented in the co-simulation environment of *MATLAB Simulink* and *VI Grade*, could be grouped in two branch: *Longitudinal Stability tests*, useful for the assessment of EBD and ABS effects on the braking distance; *Lateral Stability tests*, executed to understand the impact of the ESC system on the vehicle lateral behaviour.

## A. Longitudinal Stability Test

Consist in the execution of straight-line deceleration for several friction coefficient values. Indeed, for degraded tire-road adhesion conditions, EBD and ABS controller are essential to ensure the minimum braking performances required by the standards<sup>19</sup>, reducing the corresponding vehicle braking distance. In specific, current regulations recommend a stopping distance under 40 meters for nominal friction values. Results are showed in Figure A.64 and summarized in Table A.16 for the vehicle UC, supposing the availability and unavailability of the ABS controller, to highlight its contribution on the stopping distance reduction, showing also the corresponding improvement in terms of distance percentage. In addition, in Figure A.65 the wheels' and vehicle speed are shown, to underline the avoidance of wheel locking and the driver comfort improvement with the ABS implemented, compared with the conventional bang-bang wheels acceleration controller

Table A.16: Stopping Distance of the Longitudinal Stability Tests for Different Adherence Conditions

Initial Speed: $V_{x-i}=27.78$ [m/s]			
Adherence $\mu$ [0-1]	ABS	Stopping Dist. [m]	Improvement [%]
1	ON	32.56	18.13%
	OFF	39.77	
0.7	ON	44.14	29.02%
	OFF	62.19	
0.5	ON	62.12	22.17%
	OFF	79.82	

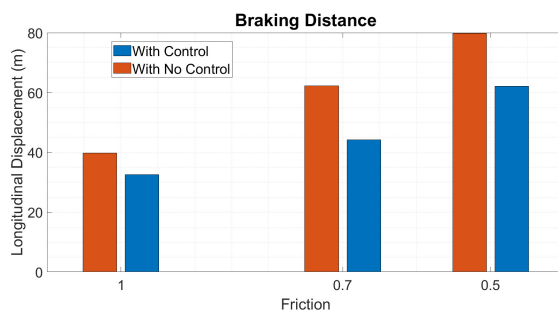


Figure A.64: Vehicle braking distance in longitudinal braking maneuver with a speed of 100 km/h and a friction coefficient of: 1, 0.7 and 0.5, supposing availability and unavailability of the ABS control system.

## B. Lateral Stability Test

These simulations campaign are executed in order to asses the effect of the proposed ESC algorithm on lateral stability performances. Two different tests are executed: the *DLC*<sup>20</sup> and the *Sine With Dwell* tests<sup>21</sup>.

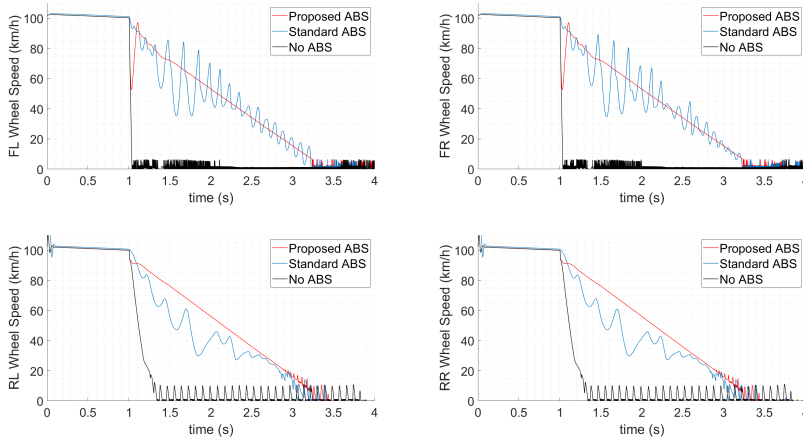


Figure A.65: Vehicle wheels speed in longitudinal braking manoeuvre in accordance to ISO21994 standard specification, supposing availability and unavailability of the proposed ABS control system and a standard on-off controller on the wheels acceleration.

[...] The improvement are evaluated observing the maximum speed at which the vehicle executes the imposed steering manoeuvres without leaving the admitted zone and hitting the corners (Figure A.66). This figure shows how the vehicle equipped by the proposed control is able to perform the manoeuvre at 60 km/h. Instead, vehicle with only standard ESC, i.e. excluding the Moore-Penrose pseudoinverse from the control algorithm, is unable to fulfil test requirements at the same speed. In addition, in Figure A.67 the comparison of the speed during DLC manoeuvre for the investigated UCs, shows a lesser vehicle speed reduction in the second phase of the trajectory and a faster return to target speed, due to a better distribution of the vehicle torque values.

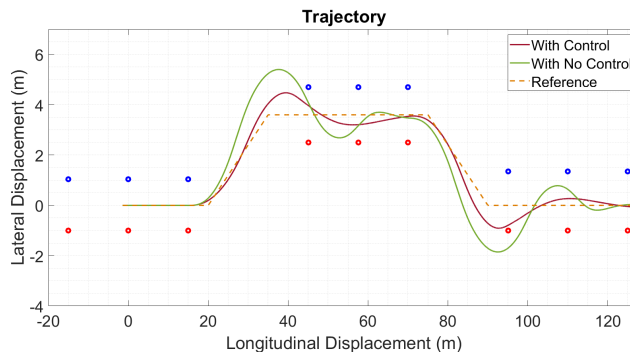


Figure A.66: Vehicle trajectory in a Double Lane Change manoeuvre, with a longitudinal speed of 50 km/h and a friction of 1, supposing availability and unavailability of the ESC control system.

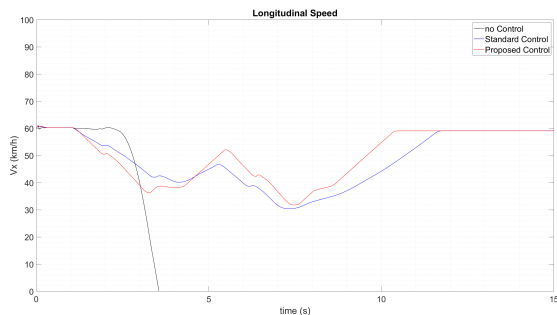


Figure A.67: Vehicle Longitudinal speed during Double Lane Change manoeuvre, with a longitudinal speed of 60 km/h and a friction of 1, supposing availability and unavailability of the ESC control systems.

The performances evaluation of the ESC during the Sine with Dwell manoeuvre (open-loop test) is done evaluating two key parameters: the side slip angle  $\beta$  and the yaw rate  $r$ . [...] Figure A.68 shows the target and actual values of the yaw rate and the side slip angle. Plots displays both the signals the vehicle is experiencing, supposing availability and unavailability of the controller.

[...] The assumption to alternatively suppose availability and unavailability of the stability controller is done in order to comparatively assess the simulation outputs of the performed tests. In particular, the results of the tests in which the controller systems are disabled are assumed as a reference baseline for the metrical evaluation of the obtained improvements.

In Figure A.69 is visible that the stability is reached at higher vehicle speed, ensuring an improved integration between control and driver inputs.

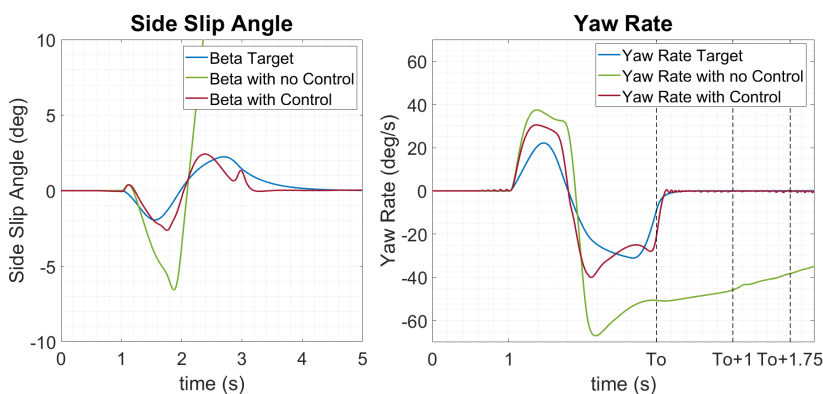


Figure A.68: Target and effective vehicle side slip angle  $\beta$  and yaw rate  $r$  during Sine With Dwell maneuver, with a longitudinal speed of 80 km/h and a steering wheel angle of 270 deg, supposing availability and unavailability of the ESC control system.

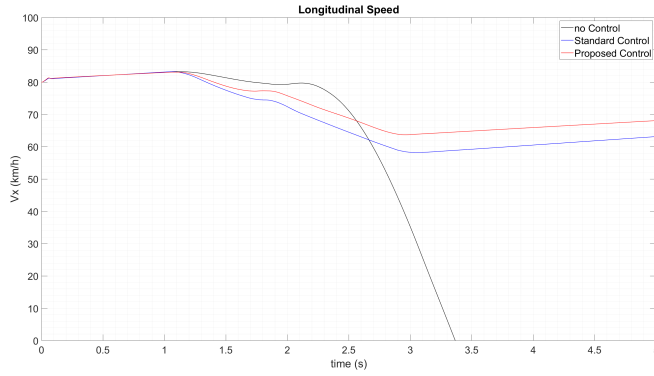


Figure A.69: Vehicle Longitudinal speed during Sine With Dwell maneuver, with a longitudinal speed of 80 km/h and a steering wheel angle of 270 deg, supposing availability and unavailability of the ESC control systems.

## V. Conclusions and Future Developments

Most interesting output of the performed tests campaign concern the dynamical vehicle behaviour improvements allowed by the proposed controllers, both respect to longitudinal and lateral stability.

Assessment of the longitudinal stability enhancement is done in accordance to ISO21994:2007<sup>19</sup>, evaluating the stopping distance of the vehicle, assuming fixed boundary condition. Result of Figure A.64 and Table A.16 suggest that the ABS controller is fundamental to ensure a safe behaviour during straight line deceleration. Instead, Figure A.65 indicates that the proposed ABS strategy, based on PID control logic of the longitudinal slip, makes effective and smoothness the braking effort respect a on-off control on the wheel acceleration. Indeed, for different adherence conditions, the Anti-slip strategy appear effective, since reduce the corresponding longitudinal distance between the starting of the brake manoeuvres and the completely stopping of the vehicle, if compared with the case in which ABS controller is disabled.

It's interesting to note also that, for normal adherence conditions, the adopted policy successfully fulfils the limitations imposed by the mandatory standards.

For the lateral stability, we investigate the performance improvements by observing the result of DLC and Sine with D-well tests. Concerning the Double-Lane Change, it can be stated that, looking at the outputs of Figure A.66 and Table A.17, the proposed ESC strategy can ensure a stable lateral behaviour of the vehicle, by increasing the speed at which the reference trajectory could be executed and by reducing the RSME respect to the ideal curve of the manoeuvre (centered respect to the admitted zone). Results of the Sine with Dwell tests are visible in Figure A.68. The plots clearly show that the ESC controller increase the stability performances, reducing the error between target and real value of  $\beta$  and  $r$  during the execution of the imposed manoeuvre.

Table A.17: Maximum Vehicle Speed During Double Lane Change Tests for Different Adherence Conditions

Double-Lane Change			
<i>Adherence</i> $\mu$ [0-1]	<i>ESP</i>	<i>Max. Speed</i> [km/h]	<i>RSME</i>
1	ON	50	0.52
	OFF	40	0.78
0.7	ON	40	0.40
	OFF	30	0.53
0.5	ON	30	0.11
	OFF	30	0.28

Summarizing, we can conclude by saying that, in this work, the proposed controller are correctly integrated with each other in order to accomplish enhanced stability behaviours of the IWM driven vehicle, both in longitudinal and lateral directions. Possible future developments concerns the further refining of the vehicle models and sub-models, in order to faithfully replicate real driving scenario conditions, along with a better tuning of the controller parameters, aiming at increasing the stability performances.

## References

1. L. Yu, X. Liu, Z. Xie, and Y. Chen, ‘Review of Brake-by-Wire System Used in Modern Passenger Car’, in Volume 3: 18th International Conference on Advanced Vehicle Technologies; Charlotte, North Carolina, USA, 2016, p. V003T01A020, doi: 10.1115/DETC2016-59279.
2. M. Montani, R. Capitani, M. Fainello, and C. Annicchiarico, ‘Use of a driving simulator to develop a brake-by-wire system designed for electric vehicles and car stability controls’, in 10th International Munich Chassis Symposium 2019, P. E. Pfeffer, Ed. Wiesbaden: Springer Fachmedien Wiesbaden, 2020, pp. 663–684, doi: 10.1007/978-3-658-26435-2\_46.
3. L. Berzi, T. Favilli, E. Locorotondo, M. Pierini, and L. Pugi, ‘Real Time Models of Automotive Mechatronics Systems: Verifications on “Toy Models”’, in Advances in Italian Mechanism Science, vol. 68, G. Carbone and A. Gasparetto, Eds. Cham: Springer International Publishing, 2019, pp. 141–148.
4. J. Jin, ‘Modified Pseudoinverse Redistribution Methods for Redundant Controls Allocation’, Journal of Guidance, Control, and Dynamics, vol. 28, no. 5, pp. 1076–1079, Sep. 2005, doi: 10.2514/1.14992.
5. J. de Santiago et al., ‘Electrical Motor Drivelines in Commercial All-Electric Vehicles: A Review’, IEEE Transactions on Vehicular Technology, vol. 61, no. 2, pp. 475–484, Feb. 2012, doi: 10.1109/TVT.2011.2177873.
6. R. de Castro, M. Tanelli, R. E. Araújo, and S. M. Savaresi, ‘Minimum-time manoeuvring in electric vehicles with four wheel-individual-motors’, Vehicle System Dynamics, vol. 52, no. 6, pp. 824–846, Jun. 2014, doi: 10.1080/00423114.2014.902973.
7. C. Feng, N. Ding, Y. He, G. Xu, and F. Gao, ‘Control allocation algorithm for over-actuated electric vehicles’, J. Cent. South Univ., vol. 21, no. 10, pp. 3705–3712, Oct. 2014, doi: 10.1007/s11771-014-2354-0.
8. L. Pugi, T. Favilli, L. Berzi, E. Locorotondo, and M. Pierini, ‘Brake Blending and Optimal Torque Allocation Strategies for Innovative Electric Powertrains’, in Applications in Electronics Pervading Industry, Environment and Society, vol. 573, S. Saponara and A. De Gloria, Eds. Cham: Springer International Publishing, 2019, pp. 477–483.
9. C. Lv, J. Zhang, Y. Li, and Y. Yuan, ‘Regenerative Braking Control Algorithm for an Electrified Vehicle Equipped with a By-Wire Brake System’, presented at the SAE 2014 World Congress & Exhibition, 2014, pp. 2014-01-1791, doi: 10.4271/2014-01-1791.

10. L. Berzi et al., 'Brake Blending Strategy on Electric Vehicle Co-simulation Between MATLAB Simulink (®) and Simcenter Amesim™', in 2019 IEEE 5th International forum on Research and Technology for Society and Industry (RTSI), Florence, Italy, 2019, pp. 308–313, doi: 10.1109/RTSI.2019.8895548.
11. K. Sung-Yeon, K. Ji-Weon, L. Sang-Moon, C. Jae-Seung, and K. Hyunsoo, 'A Study on In-wheel Motor Control to Improve Vehicle Stability Using Human-in-the-Loop Simulation', *Journal of Power Electronics*, vol. 13, no. 4, pp. 536–545, Jul. 2013, doi: 10.6113/JPE.2013.13.4.536.
12. Kanghyun Nam, H. Fujimoto, and Y. Hori, 'Lateral Stability Control of In-Wheel-Motor-Driven Electric Vehicles Based on Sideslip Angle Estimation Using Lateral Tire Force Sensors', *IEEE Trans. Veh. Technol.*, vol. 61, no. 5, pp. 1972–1985, 2012, doi: 10.1109/TVT.2012.2191627.
13. B. Jin, C. Sun, and X. Zhang, 'Research on Lateral Stability of Four Hubmotor- In-Wheels Drive Electric Vehicle', *International Journal on Smart Sensing and Intelligent Systems*, vol. 8, no. 3, pp. 1855–1875, 2015, doi: 10.21307/ijssis-2017-833.
14. H. Pacejka, *Tire and Vehicle Dynamics*. Elsevier, 2005.
15. T. Novi, R. Capitani, C. Annicchiarico, 'An integrated ANN-UKF vehicle sideslip angle estimation based on IMU measurements', in *Proceedings of the Institution of Mechanical Engineers, Part D: Journal of Automobile Engineering*, 233(7), pp. 1864–1878, 2016.
16. P. Falcone, H. Eric Tseng, F. Borrelli, J. Asgari, D. Hrovat, 'MPC-based yaw and lateral stabilisation via active front steering and braking', in *Vehicle System Dynamics* 46, pp. 611–628, 2008.
17. M. Guiggiani, *The science of vehicle dynamics: handling, braking, and ride of road and race cars*. Dodrecht: Springer, 2014.
18. E. Mosca, 'Optimal Predictive and Adaptive Control', in *Prentice Hall information and system sciences series*, Englewood Cliffs, 1995.
19. International Organization for Standardization, 'ISO 21994:2007-Passenger cars—Stopping distance at straight-line braking with ABS — Open-loop test method'.
20. International Organization for Standardization, 'ISO3888-1:1999-Passenger Cars-Test Track for a Severe Lane-change Manoeuvre: Part 1: Double Lane-change'.
21. International Organization for Standardization, 'ISO 19365:2016-Passenger cars — Validation of vehicle dynamic simulation — Sine with dwell stability control testing'.

## A.11 Functional safety and reliability for innovative vehicle braking system and integration with electric traction units [15]

**Published in** IOP Conference Series: Materials Science and Engineering

**Authors** Tommaso Favilli, Massimo Delogu, Luca Pugi, Lorenzo Berzi

**Abstract** Newly electric vehicle architectures require intensive virtual and physical testing for safety assessment, due to the increasing relevance of By-Wire systems and the presence of innovative control algorithms for ordinary driving scenario, potential emergency situations or Advanced Driver-Assistance Systems implementation purpose. To reduce the development time while increasing system reliability and the a priori knowledge about its safety requirements, the evaluation of such aspects should be performed. In accordance to ISO26262 standard, authors propose a systematic approach based on Virtual FMEA, in order to assess the functional safety level of hybrid brake plant. Plant modification and securing strategy as been presented and implemented in target vehicle model, evaluating their performances in simulation environments, in order to met required Automotive Safety Integrity Level. This work is developed in the ambit of OBELICS European Project.

### 1. Introduction

Nowadays, the usage of embedded controller devices in the electric automotive field is further increasing, thanks to the introduction of BW systems<sup>1-3</sup>. Also, interaction between users and E/E systems on board are more frequent, since are becoming more and more active, including drive prediction and ADAS. The growing complexity of such plants, due to the integration of more functionalities and the attribution of safety-related tasks (relieved from the pilot) can lead both to increased fault probability and severity. It's also interesting to notice that in a scenario in which autonomous and assisted driving functionalities are implemented, reliability of underlying automation and actuation systems hast to be further increased, considering the limited awareness of human driver when dealing with complex nested automation layers. Those faults are quite difficult to be correctly interpreted, especially when low-mid level control layers are affected.

Reliability and Safety are crucial factors for the correct operation of a product, especially for E/E devices adopted in the automotive sector, whose developments process must follow rigorous procedures. Indeed, essential drive functionalities are implemented trough CU, so safety-critical active system should be developed in accordance to severe functional reliability concept. Standard *ISO 26262*<sup>4</sup> provide usefull guidelines, assisting designer through all main phases of the V-shape procedure, in order to develop a product which respects required safety performances. Occurrences of faults during operative phases of an E/E systems of EVs, can lead to a deviation from the expected behaviour, with potential risk for the users, especially for those systems dealing with active safety functionalities. So, it is recommended to analyse the fault-modes of the involved devices, to avoid undesired effect in the overall system reliability, using a vFMEA approach. More in detail, relevant examples of BW commands on latest generation vehicles are: throttle, braking and steer. All of them are fundamental for vehicle safety and controllability. Literature experience describe main design criteria for such applications, including appropriate

system topology, and the testing procedures needed to quantify their functional reliability, fault tolerance and applicability on road vehicles<sup>5,6</sup>. In this context, ISO2626 provides a solid framework for system development which is applicable to x-by-wire analysis, possibly integrated with modelling activities<sup>7-12</sup>.

These aspects highlight the importance of ensuring enhanced reliability and safety performances for these systems. To avoid these situations, a systematic procedure for the design, development and validation of automotive systems could be a feasible solution to avoid a dangerous and harmful scenario. The supposed failure mechanisms, determined through FMEA, are related to the vehicle ECU. Faults are supposed permanent (irreversible) and concern hardware and interaction failure. However, proposed solution are effective also for transient and intermittent failures. Such failures are always possible due to the aggressive and dangerous environment of automotive applications and the growing complexity of hardware components and system architecture. The investigation focuses on the proposal of a virtual simulation environment, implemented with a model-based approach, to assess the consequences of a fault on the vehicle behaviour, through FI simulations activities on a vehicle model and related sub-systems.

Proposed methodology, similarly to other performance assessment procedures described in literature<sup>13,14</sup>, concern EV functional safety concept and aims at the safety assessment of investigated brake plant. However, respect to the actual SoA, this solution is developed in accordance with ISO 26262 standard specifications, which strongly suggest to support the validation protocol with FI techniques. In particular, a multi-level FI approach is adopted, which consists in the simulation of investigated failure modes, useful to establish their effects on the vehicle behaviour. The proposed approach allows the validation, tolerance and recovery from a fault condition of the product's functionalities.

Depending on the development phase of the vehicle, two different approaches are selected: In an early phase, starting from the failure rate of single components, the potential combined failure are calculated using Montecarlo approach with simplified models, in order to find out main interactions within component layout; In a second phase, vehicle system topology is reproduced in a Multiphysics simulation environment and the certain faults events (e.g. those highlighted as critical by previous steps) are injected in the system. Such approach is aimed to verify the consequences of the failure itself and develop and verify the functionality of mitigation strategies. Looking at model concept, the approach suggests the modification of typical "model identity cards" adding ports suitable to represent component state-of-function, which can be expressed either as Boolean or progressive variability of performances (e.g. 0 to 100 functionality); in practice, this means that parameters usually adopted to represent component static characteristics are modified as tunable parameters or even as variables. This allows to dynamically change component functionality during simulation itself. The case study presented – a 4WD concept EV – has been used to estimate stopping distance with regular and degraded components; in particular, a parameter strongly influencing the results is the time delay needed for failure recognition, which depends partly on physical construction partly on software decisions (e.g. number of failure confirmation events needed to avoid false positives): in this way, the model can be adopted not only to verify the effectiveness of mitigation strategies, but also for pre-calculate the time-delay that vehicle designer should adopt as target, to prevent the occurrence of dangerous events, thus being also a tool to better set up vehicle specifications

and, thus, reducing development time.

The current activities propose the definition of a systematic methodology based on vFMEA approach and ISO 26262 standard specifications to evaluate and assess the actual and target ASIL for the investigated brake functionalities related to complex vehicle architecture, due to the growing relevance of active stability ECUs and BW systems. This study aim at identify the major weakness of the brake plant and establish proper architecture modification or control strategy to fit the previously determined safety requirement. Results will reduce man-hour and cost of the BBW reliability analysis.

## 2. Proposed Methodology

The purpose of this activity concerns different aspects: ensuring braking performances of the EV and the BBW system reliability, as well as the availability of safety-related functionalities in which brake is involved, despite the operation of the various subsystems dealing with brake effort management (EBD, ABS, ESP or TCS) and application (BB). At this purpose, while reducing time and cost effort, authors define a systematic model-based methodology, to implement vFMEA and FI analysis.

Developed reliability analysis solution consists of different phases:

1. **SoA investigation:** an in-depth literature review is conducted, to identify the failure rate and distribution of the brake component.
2. **FMEA:** Failure Modes and Effects Analysis is executed on the target BBW components. This step aims to identify failure mode, causes and consequences of involved components. FMEA constitutes an essential methodology in the development process of a product, allowing reliable forecast and letting designer focus on most critical plant parts, assisting them in the application of the securing mechanism that should be implemented to fulfil minimum safety requirements.
3. **ISO 26262 guidelines application:** guidelines of the standards have been applied to the reference brake system, in order to evaluate target and actual ASIL, respect to the investigated plant functionalities.
4. **Simulation-based FI:** performed in a virtual simulation environment. This consist in the execution of controlled tests, where the behaviour of the EV is observed when one or more faults are triggered<sup>15,1</sup>. In particular, FI is used to evaluate if the response of the system fulfils the specification when faults occur. ISO 26262 strongly recommends this procedure as a supporting tool to develop fault removal and prevention tasks. Also, the standard encourages the application of multi-level FI, redefining specific solution to increase system reliability and functional safety, to be applied during the whole development process. In this work, a double-level FI approach is used. Firstly, it is applied in the early stages of design, on a high-level abstracted model, to establish the most significant faults. Then, simulations are repeated on a more sophisticated model (developed in *MATLAB Simulink*), to evaluate the appropriateness of the supposed boundary condition, coherence with previous results and effectiveness of proposed securing solutions.

5. **Securing Solutions:** finally, plant modification and securing strategy are proposed and implemented in the *Simulink* environment, to better understand the impact of them in brake system reliability and performance.

For a better understanding of the approach adopted in this activity, a flowchart of the proposed methodology is visible in Figure A.70. Once the benchmark vehicle is chosen, physical and functional scheme of the corresponding BBW system is identified. Failure rates and probability distributions of the brake plant components are identified during the SoA review. Then, proceed with the analysis of the causes, modes and effects of the investigated faults.

This phase is fundamental in order to select most critical malfunctionalities and propose securing solutions. At this point, guidelines of ISO 26262 standard are applied to establish target ASIL and the FI simulation activities performed, to assess the plant reliability aspect, respect to specific functionalities. If the target ASIL is reached, the process ends: it can be state that the system fulfils standard specifications; otherwise, appropriate securing mechanisms are implemented in the vehicle models and simulations repeated, to confirm their effectiveness.

FMEA and FI techniques show strong similarities and share several common goals. Most relevant concerns the identification of the critical system faults. This purpose can be achieved by analysing causes and effects trough FMEA process and observing their impact using FI. Also, both aim at the definition of those subsystems which require a securing mechanism, specifically addressed for diagnostic and mitigation of failures.

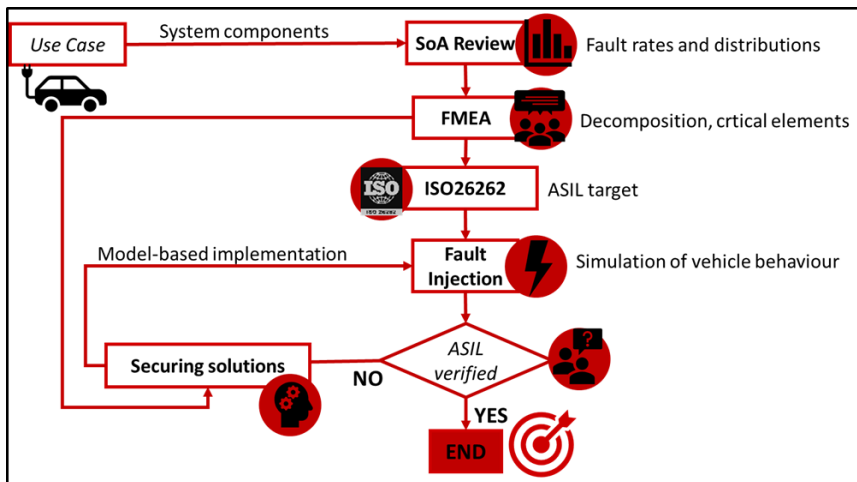


Figure A.70: Flowchart of the proposed methodology

### 3. Benchmark Electric Vehicle

The procedure described in the previous section is applied to a reference UC [...]. Investigated EV is a fully electric concept car developed by *Valeo*, equipped with 4 independent IWMs.

[...] is possible to identify the following elements:

- Brake Pedal Interface: pedal position command is translated in a brake demand that is transferred to an Electronic Brake Control;
- Electronic Brake Control: It's an underlying automation layer which produces an actuation reference according to brake demand, vehicle dynamics and other connected autonomous systems, implementing also active safety functionalities (EBD, ABS, ESP);
- Wheel Brake Control Unit: brake reference is actuated on the wheel, regardless of whatever the torque is applied by disc or electric motor. It includes MCU and BB controller.
- Electric Vehicle equipment: consisting of all the sub-systems of the vehicle, e.g. battery, BMS, inverter, EM, hydraulic brake plant.

This consideration allows a concept abstraction respect to the considered vehicle layout, to propose a flexible methodology which can effectively be applied to different powertrain architectures and UCs, allowing man-hour and cost reduction, thanks to the possibility to automatically adapt the proposed approach to several EV's e-powertrain and brake system configurations.

The layout of Figure A.71 is applicable. However, it should be considered the integration of a multiple braking actuation, in which the mechanical brake system is integrated with the electric one. This makes of the BEV an over-actuated system from the braking functionalities aspects, offering opportunities to achieve increased ASIL, due to the redundancy of the brake plant. Indeed, enhanced brake plant reliability could be reached by the application of innovative BB strategies and the proposal of specific procedures for the vehicle securing, implemented thought control algorithms.

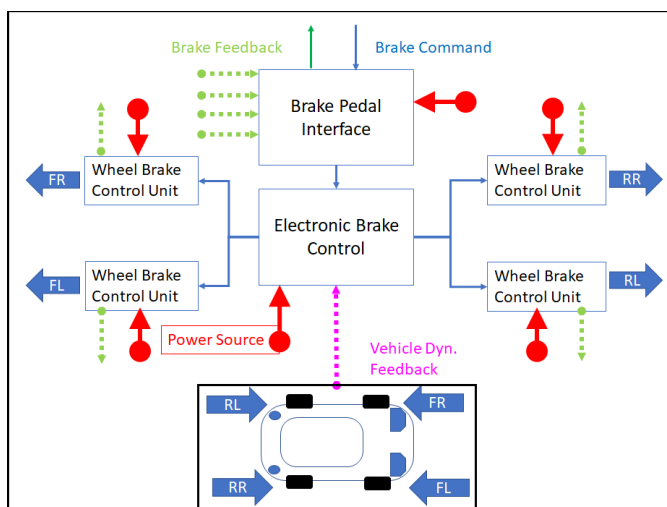


Figure A.71: Reference BBW system layout

It is considered the integration in the system of a BB strategy, using the EV architecture represented in Figure A.72: since each wheel has its independent braking and traction control unit, the brake blending system is integrated at the level of a single wheel. This is an example of lower-level integration which assures a

higher level of redundancy, since the BB ECU failure affects only one wheel. On the other hand, specific securing procedures have to be implemented, to avoid undesired vehicle dynamics behaviour, such possible yaw moment generated by the differential braking between right and left tires.

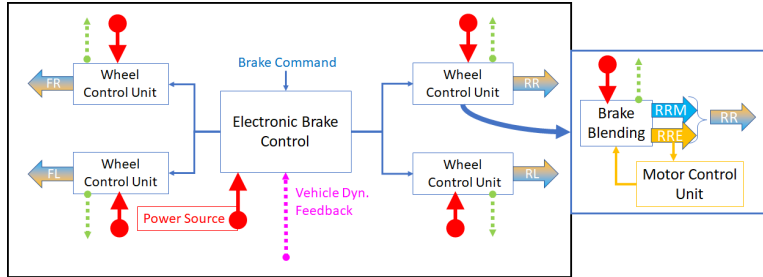


Figure A.72: Reference BBW system layout with BB

Our investigation focuses on this architecture, which is used only with the aim of the higher possible generality to 4WD architectures, allowing to implement the most innovative solution to increase vehicle reliability [...].

### 3.1. State-of-Art review

For this kind of generic BBW system, there are some sources in literature to be considered: works of Sinha et al.<sup>22</sup> simply introduce an analysis of the level of redundancy and reliability of ECUs and communication bus, to ensure the overall reliability requirements of the braking system. Respect to the investigated BBW plant layout of Figure A.72, a preliminary SoA review is performed to find the appropriate fault distribution and MTBF for each of the brake system component.

Despite some tech data-sheet from OEMs suggest a bathtub rate distribution (e.g. Texas Instrument), authors suppose to consider only components in the fit region. So, the adoption a uniform distribution for the CUs is assumed, using the maximum value of failure rate of the fit region, which are summarized in Table A.18.

Table A.18: Failure rate of different components used in our analysis

Component	Failure Rate $\lambda[1/h]$
Pedal sensor	$1 \cdot 10^{-7}$
Wheel speed sensor	$1 \cdot 10^{-7}$
Pressure sensor	$5.69 \cdot 10^{-7}$
ECU	$5.88 \cdot 10^{-7}$
Wires	$1 \cdot 10^{-9}$
CAN bus	$2.58 \cdot 10^{-9}$
Battery	$2 \cdot 10^{-6}$
Inverter	$3.77 \cdot 10^{-7}$

### 3.2. Failure Mode and Effect Analysis

FMEA is a bottom-up failure identification systematic process, applied to the EV layout of Figure A.72. It consist of several stages: plant decomposition in independent unit, identification of functionalities and interconnections between sub-systems and definition of modes and effects of the faults for each unit. This risk analysis is essential in order to identify major weakness of the BBW plant, letting designer to focus mainly on most critical elements and define appropriate securing strategy. FMEA methodology appear versatile and flexible, concerning single element or whole system faults. Output of this phase is the EV layout block diagram of Figure A.73. It is assumed the presence of an additional CU, the *Supervisor Controller*, which superintends at the the securing strategy functionalities.

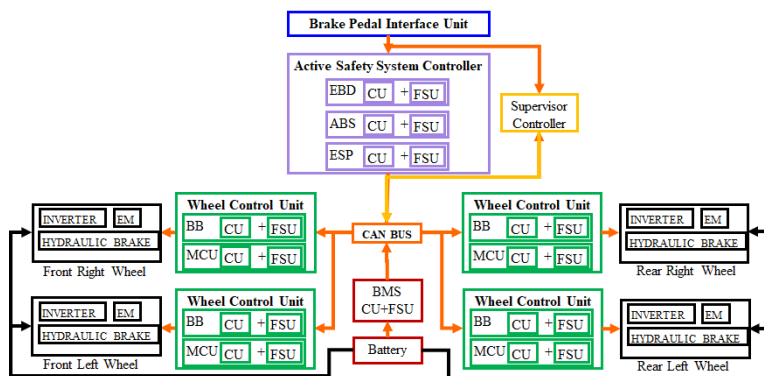


Figure A.73: EV block diagram for the FMEA process

FMEA of the whole EV BBW model components is summarized in Table A.19, where a column is dedicated to the proposal of safety solutions that can be implemented. Also, specific fault mode and effect analysis have been applied to ABS functionalities. Reliability of this device depends not only by the proper operation of the single component but also by their integration: FMEA indeed considers all the existing interaction between the single plant's elements (Table A.20). For this analysis are considered only malfunctionalities related to E/E systems.

Table A.19: FMEA of the reference BBW control units

Component	Failure	Effects	Causes	Securing
Pedal unit	Pedal fail	No pedal stroke No signal to EBD	Power supply fail Sensor fail	Redundancy
EBD	ECU fail	No f/r allocation No signal to ESP	Power supply fail Sensor fail	Redundancy Bypass EBD
ESP	ECU fail	No lateral stability No signal to ABS	Power supply fail Sensor fail	Redundancy Bypass ESP
ABS	ECU fail	Wheels locking No signal to BB	Power supply fail Sensor fail	Redundancy Bypass ABS
BB	ECU fail	No regeneration	Power supply fail Sensor fail	Redundancy Bypass BB
BMS	ECU fail	Overcharging Underdischarging	Power supply fail Sensor fail	Redundancy Hydr. braking
MCU	ECU fail	No electric torque	Power supply fail Sensor fail	Redundancy Hydr. braking
HCU	ECU fail	No hydraulic torque	Power supply fail Sensor fail	Redundancy

Table A.20: FMEA of the ABS control unit

Component	Failure mode	Effects	Causes	RPN	Securing
Sensors	No signal	ABS off	Operative fault	18	Redundancy
	Wrong signal		Operative fault	96	Warning light
Wires	No signal	ABS off	Short circuit	18	Redundancy
	Wrong signal		Disconnection		Warning light
ECU	No signal	ABS off	Operative fault	108	Redundancy
	Wrong diagnostic		Software fault		Warning light
	Wrong signal		Software fault		

RPN: Risk Priority Number

In particular, proposed solutions concern:

- Fault prevention: failure forecasting is done evaluating systems behaviour, respect to injection.
  - Qualitative evaluation: identification and classification of fault mode and/or combinations.
  - Quantitative/probabilistic evaluation: reliability measurements, such as Mean Time Between Failure (MTBF) or failure rate.
- Fault tolerance: integrating technique of management, detection, correction of fault and redundancy, in order to define fault-tolerant system architecture.
- Fault removal: aiming at reducing fault occurrences during the development stage. Consisting of a verification process which leads to the system's weakness diagnosis, useful to investigate possible securing intervention.

### 3.3. ISO 26262

The management of safety-critical decision by the E/E system in automotive sector inevitably increase the complexity of the vehicle architectures. Indeed, risk of systematic and random hardware failure is grater. To assist designers at ensuring the highest safety standards and lead the development of safe automotive systems, specific regulations should be considered. The *ISO 26262 Road Vehicle - Functional Safety* series of standards<sup>4</sup> is the adaptation of IEC 61508<sup>21</sup> to address the sector-specific needs of E/E systems within road vehicles.

This adaptation applies to all activities during the safety life-cycle of safety-related systems, comprised of electrical, electronic and software components. It provides methods and techniques which should be integrated into the development process to ensure the required functional safety level of E/E devices in road vehicles. In particular, it states the necessity to assist traditional reliability assessment solutions, e.g. FMEA, FMECA, FTA or BRD with FI strategy. ASIL of a specific fault modality can be determined through 3 parameters and its values ranging from QM (minimum) to D (maximum). ISO 26262 assist developers in the definition of Severity, Exposure and Controllability.

Estimated ASIL target values for the E/E devices of the benchmark EV of Figure A.73, in accordance with specifications provided by ISO 26262, are visible in Table A.21 and Table A.22, regarding respectively vehicle with human driver or ADAS. In the second case, values of Severity could be increased, since in those failure scenarios, where it is coherent to assume distracted passengers, the consequences could be more dangerous. Only for some failure modes is assumed a major Controllability, related to more sophisticated diagnostic procedures. Generally speaking, ADAS require higher ASIL, since the level of demanded automation is greater. For each scenario which result in  $ASIL > QM$ , one or more *safety goal* are formulated, which represent a safety requirement that should be achieved to avert the risk in dangerous situations. If quite similar safety goals are formulated for several events related to the same sub-component, they must be combined into a single security goal with the highest ASIL among those considered. In this activity, the evaluation of the coherence of the BBW system with the ISO 26262 specifications is performed, respect to the metric of the *Random Hardware Failure Rate*, whose requirements are those of Table A.23.

Table A.21: ASIL target estimation for the EV (autonomous driving level between 0 and 1)

Component	Severity	Exposure	Controllability	ASIL
Pedal CU	S3	E4	C3	D (max)
EBD CU	S2	E4	C2	B
ESP CU	S3	E3	C3	C
ABS CU	S3	E3	C3	C
BB CU	S2	E4	C2	B
BMS CU	S2	E4	C2	B
MCU	S2	E4	C2	B
Hydraulic CU	S3	E4	C3	D (max)

Table A.22: ASIL target estimation for the EV (autonomous driving level greater than 2)

Component	Severity	Exposure	Controllability	ASIL
Pedal CU	S3	E3	C2	B
EBD CU	S3	E4	C2	C
ESP CU	S3	E3	C2	B
ABS CU	S3	E3	C3	C
BB CU	S2	E4	C2	B
BMS CU	S2	E4	C2	B
MCU	S2	E4	C2	B
Hydraulic CU	S3	E4	C3	D (max)

Table A.23: ASIL target respect to Random Hardware Failure Rate

ASIL	Failure Rate $\lambda$ [1/h]
B	$< 10^{-7}$
C	$< 10^{-7}$
D	$< 10^{-8}$

### 3.4. Simulation Based Fault Injection

The Fault Injection (FI)<sup>23-25</sup>, is defined as the reliability validation technique of fault-tolerant systems and consists in the execution of controlled experiments where the behaviour is observed upon the introduction of one or more failures. The injection of faults aims to determine if the response of the system, in the presence of a defined set of faults, corresponds to the specifications. Lot of approaches for the analysis of the safety aspects of systems use this strategy for the validation of results obtained with static analysis of criticality, or for the study of the fault propagation. In particular, is useful to establish proper securing strategy, aiming at fault prevention and removal. Fault prevention solutions are typically based on statistical tests, which simulate distribution and rate of specific failure. Fault removal, instead, is based on functional modelling of the system. The introduction of FI in ISO 26262<sup>26</sup> has renewed the interest in this methodology in the automotive sector. However, this well-established method of verification is now used in different sectors. The standard motivated the adoption of newly solutions for the safety assessment of a product, redefining specific reliability concepts which should be applied during development phases, supporting conventional failure analysis methods. In particular, strongly recommend the usage of simulation-based FI techniques on model with a high level of physical abstraction, in order to identify errors in safety requirements management and propose appropriate securing strategy.

Developed simulation test campaigns consist of two different steps. In the first phase a recursive **Montecarlo simulation campaign** of a simplified vehicle model (high level of physical abstraction) is performed at high computational speed, considering the real value of component's fault occurrences and probability distributions. The impact of several brake system failure modes in the vehicle stopping distance is evaluated, resulting in a quite similar reliable output. High integrity and safety levels of the brake system are involved to embed the current mechatronic system within a higher-level system, related to autonomous or assisted

braking. In this stage, which components of the plant are more inclined to failure and/or had the major impact of vehicle braking performances can be established. A better understanding of those aspects allows the proposal of efficient and robust securing policies for fault prevention, which could be a useful tool for the achievement of target ASIL.

Then, once establish from the latter phase a specific number of dangerous scenarios respect to functional safety, **Model-based simulation campaign** of specific failure events are repeated using a more precise accurate vehicle model, from physical and functional point of view. This allows evaluating the appropriateness of the proposed approach and securing solutions, comparing result obtained at this stage and in the previous one and proposing fault removal solutions. Also, it consent to better identify causes and effects of failure, improving the knowledge of the mechanism of their occurrence and related impact on functional safety, used even to further increase the accuracy of the Montecarlo FI model. In both cases, the simulation environment involves 2 sub-models: *Target system*, which is the vehicle model; *FI controller*, consisting of a *Fault Injector*, which contains the vectors of possible fault and schedule their onset; the *Fault Monitor*, which detects malfunctions and communicates with the *Supervisor controller*.

It is important to note that a delay is considered between the fault occurrences and its detection (Figure A.74). This delay replicates the physiological lag of the communication channels (e.g. flooding of the CAN bus system) and time step interval (of 50 ms). Additional 300 ms time-out is supposed, in order to avoid false positive fault detection by the *Supervisor controller*, whose monitor the failure occurrences, turns on the warning light in the driver dashboard and triggers specific securing algorithms to start failure mitigation procedures.



Figure A.74: Supposed delay between fault occurrences and confirmation

The reason behind the choice of this process is mainly referred to the necessity of reducing the simulation computational effort and time. vFMEA activities require the execution of billion recursive simulations to observe failure event, which are in the magnitude of  $10^{-7} - 10^{-8}$  occurrences per hour. So, it is necessary to identify the system weakness in a shorter time and lower energy/cost consuming, in the optics of implementing fault mitigation solutions in the early phases of system and components design, evaluating also their effectiveness respect to functional safety requirements.

Concerning the specification given by the OBELICS project, developed model has the following characteristics:

- *Numerical efficient*: able to perform a large number of simulations, considering several combinations of faults and performances degradation in different operational conditions and scenarios. RT implementation is required;
- *Simple and standardized*: models flexibility is ensured by proper scalability and portability properties, in order to be easily portable for different vehicle

architecture and layout, as well as for different simulation environments and boundary conditions [...];

- *Robust and reliable*: respect to the physical abstraction, which in some cases can lead to complex dynamic behaviour that introduces further integration problems, especially when a fault occur.

**3.4.1. Montecarlo Simulation.** In this phase, each component of the investigated BBW system is abstracted by its primary functionality and considered as a simplified element<sup>27</sup>, identified only by its own MTBF and fault distribution. Probability of fault occurrences is estimated from SoA, literature investigation, component and system data-sheet and proper technical considerations<sup>16,22,28</sup>.

This abstraction concept, based on system BRD, is useful to implement an efficient and effective Montecarlo recursive study, aimed to establish the stopping distance of the vehicle when one or more component of the brake system experience fault situations. This probabilistic-based implementation, from the computational effort perspective, is designed to perform  $10^3 - 10^{12}$  consecutive iteration, using a simple functional approach devoted to parallel computing (parallel pool and coded functions supported by MATLAB). This type of simulation is also suitable for numerically intensive implementation of GPU hardware, an ideal application for HiL test method.

The Montecarlo simulation campaign is based on the vehicle dynamic equation, according to the simplified formula of the stopping distance calculation related to a braking manoeuvre (A.52):

$$s = \frac{v_0^2}{2a} + v_0d \quad (\text{A.52})$$

Where  $s$  is the stopping distance expressed in meter,  $v_0$  the initial vehicle speed in meter per second,  $a$  the acceleration in meter per square second and  $d$  the time delay in seconds.

The output of this test campaigns constitutes a preliminary supporting tool for the following model-based FI: the information arising from the Montecarlo simulations allows understanding the system weakness and to identify the specific plant components which mainly experience fails. At this point, it is possible to deeply study the select scenario, by their implementation in a more sophisticated simulation environment.

Considered fault event could be of 2 different types:

- **Boolean Fault**: the component can appear as completely healthy (ON) or dead (OFF). When a fault condition occur its functionalities are considered lost;
- **Derating Fault**: the component can be partially available, and its functionalities reduced in the magnitude order of a percentage.

**3.4.2. Model-based Simulations.** A more complete vehicle equipment model is implemented in the *Simulink* environment<sup>17-20</sup> to assess the effect of the BBW E/E devices failure on the car vehicle behaviour. For this work, however, models have been modified to account fault effect by the introduction of FI controller, which allows supposing specific component failure.

The detailed FI model, developed in *MATLAB Simulink* environment (Figure A.75), is designed for  $10^0 - 10^3$  iterative simulations and it is useful to evaluate the consequence of a fault or to validate expected results on a worst-case scenario, established in the previous step. This full vehicle equipment functional model consists in: Driver, Vehicle Chassis (7-DoF), Torque Regulation Controller (EBD, ABS, ASR, ESP, BB controller), Torque Actuation (EM and hydraulic brake system) and Monitor (to check the controllers status and to observe the vehicle dynamic behaviour when one or more faults occur) [...].

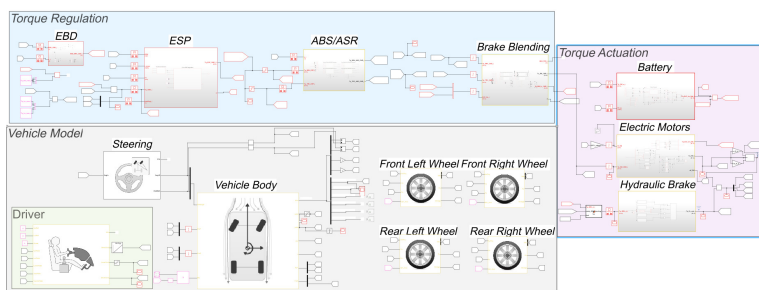


Figure A.75: EV simulation layout of the *Simulink* model

The usage of these more accurate models is devoted mainly to confirm the coherence with the dynamic vehicle behaviour established during the Montecarlo methodology. Moreover, model-based simulations are useful also to endorse the achievement of target ASIL and evaluate the improvement permitted by plant modifications.

### 3.5. Securing Solutions

The proposal of securing solutions to be implemented in the vehicle model concerns the necessity to fulfil the minimum safety performances established from ISO 26262 perspective. Indeed, to reach target ASIL of Table A.21, plant modifications and advanced control algorithm are required to fit functional safety level in accordance to the standard specifications. In relation to Figure A.73, for the vehicle CU is assumed the presence of a redundant electronic controller, called FSU. Also an addition ECU, named *Supervisor Controller* is considered, whose task concerns the application of the securing strategy. Fault detection for ABS/ASR system is done in accordance of the logical scheme of Figure A.76.

When slip is above admitted value and the comparison between torque command, arising from upstream controllers, and output demanded signals is negligible, the fault is detected and confirmed after the time out interval, by turning on the warning light and bypassing ABS functionalities<sup>15</sup>. Other securing strategy, summarized in Table A.20, are realized in analogy with this one.

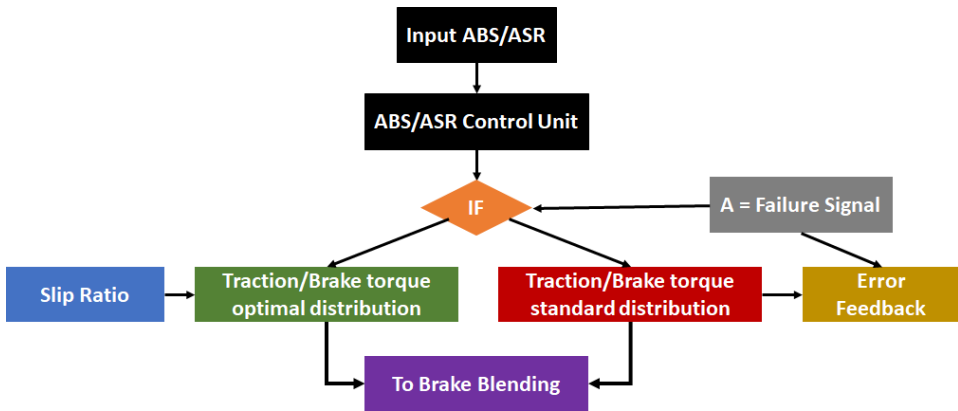


Figure A.76: Proposed ABS fault detection and mitigation logic scheme

#### 4. Results and Discussions

In this section are summarized the result concerning the FI simulation campaign, obtained from the application of the proposed methodology to the benchmark EV, supposing different faults. Also, is assumes a specific fault of the CU related to anti-lock braking functionalities, whose simplified scheme is represented in Figure A.77, in which are evident the interconnection within other BBW components. It is important to know that the proposed *Supervisor Controller* is able to perform diagnostic functions, turning off ABS system when errors are detected. This implemented securing strategy allows the application of braking torque to wheels, which, however, are not modulated to keep the slip in the admitted bandwidth.

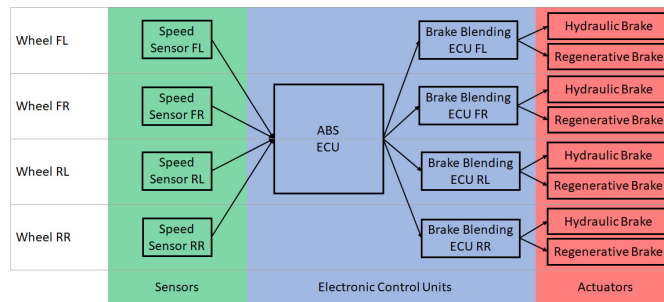


Figure A.77: ABS functional decomposition scheme

For the purpose of this simulation campaigns, the boundary condition of the simulated tests is the one provided by ISO 21994:2007<sup>31</sup>. This standard is related to the determination of the stopping distance in Straight line deceleration with ABS in open-loop test methodology, which should remain under 40 m for braking manoeuvres on good surface, starting from an initial speed of 100 km/h.



Figure A.78: Investigated reference manoeuvres

#### 4.1. Montecarlo Simulation Campaign Results

In this kind of tests, different failures are supposed, whose specifications, respect to the BBW system layout of Figure A.73, are summarized in Table A.24, along with some parametric variable, useful to simulate different braking conditions (e.g. vehicle mass variation). For the E/E control units a redundant solution with FSU is suggested. This consideration is due to the high ASIL required. Results of the tests are in agreement with these assumptions, since the detection of the failure will result in acceptable stopping distance.

Consider the simulation results of Figure A.79, which refers to the fault of ABS CU for a population of 100 millions of straight line deceleration event. These outcomes correspond to about 72 billion of operative hours of the brake system. This fact is due to that executed tests consider the failure rates of Table A.24, which are expressed in terms of occurrences per hour, but the reference manoeuvre only lasts about 5 seconds, so between the rates there is a factor of 720, according to (A.53).

$$\lambda[1/h] = \lambda[1/3600s] = \lambda[1/5s] \cdot \frac{1}{720} \quad (\text{A.53})$$

Table A.24: Investigated failure in the Montecarlo simulation campaign

Sub-sytem	Failure	Rate [1/h]	Distr.	Parameters
Brake Pedal Inter.	ECU (D)	$5.88 \cdot 10^{-7}$	Uniform	$a_{nom}; d_{nom}$
	ECU (ND)	$3.46 \cdot 10^{-13}$	Uniform	$a_{min}; d_{max}$
	CAN bus	$5.69 \cdot 10^{-9}$	Uniform	$a_{min}; d_{max}$
Safety CU	ECU (D)	$5.88 \cdot 10^{-7}$	Uniform	$a_{nom}; d_{nom}$
	ECU (ND)	$3.46 \cdot 10^{-13}$	Uniform	$a_{ABS}; d_{max}$
	CAN bus	$5.69 \cdot 10^{-9}$	Uniform	$a_{min}; d_{max}$
Wheel Brake CU	ECU (ND)	$1 \cdot 10^{-7}$	Uniform	$3/4a_{nom}; d_{nom}$
	CAN bus	$5.69 \cdot 10^{-9}$	Uniform	$a_{min}; d_{max}$
Power Supply	Unavailable	$3.77 \cdot 10^{-7}$	Uniform	$a_{min}; d_{max}$
Load	Variation	/	Normal	$[0.8; 1.2]a_{nom}$
Pad-Disc Friction	Variation	/	Normal	$[0.8; 1.2]a_{nom}$
Slope	Variation	/	Normal	$[0.95; 1.05]a_{nom}$

$$a_{nom} = 9.81m/s^2; d_{nom} = 0.005s; a_{min} = 0.1m/s^2; d_{max} = 0.035s; a_{ABS} = 8m/s^2$$

D: detected; ND: not detected

In particular, Figure A.79 shows how an additional control unit, the FSU, markedly improves braking performance, thanks to the presence of the redundant backup controller, which replaces the primary electronic regulator after the time-out (once fault is confirmed). In the case of a single CU instead, the intervention of the *Supervisor Controller* is needed, applying corresponding securing strategy.

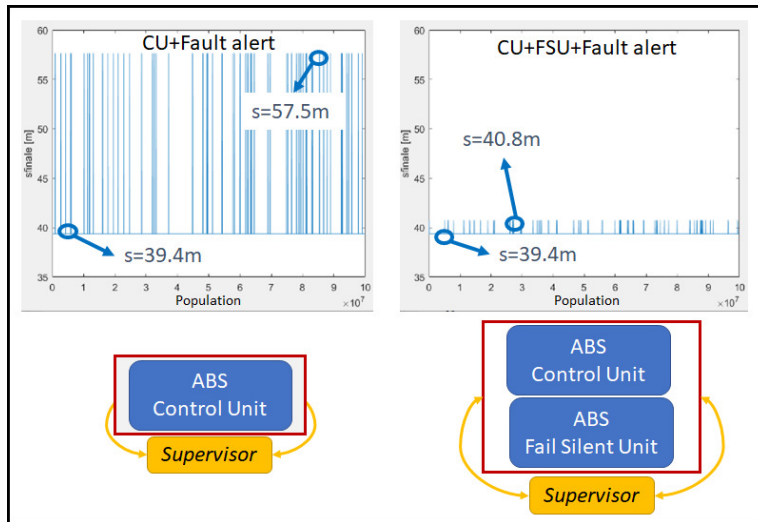


Figure A.79: Final stopping distance supposing and detected ABS CU failure without (left) and with FSU (right) during Montecarlo FI simulations

## 4.2. Model-based FI Campaign Results

The braking manoeuvre<sup>31</sup> is repeated for the full vehicle model, supposing the fault occurrences of all the subsystems dealing with braking performances and BBW functionalities. In the model-based simulation are investigated the effect on vehicle behaviour of the securing strategy.

Output of Figure A.80 shows wheel torques and slips in normal operative condition (left) and ABS control unit fault (right). In the second case the *Supervisor Controller* applies the securing solution of Figure A.76. So, even in the extremely rare case of simultaneous failure of CU and FSU, is still possible to apply braking torques to the wheels. However, these ones are not properly modulated, so wheel locking occurs, resulting in an increased stopping distance (Table A.25).

Making the vehicle replicate, for each investigated faults dealing with braking performances, the same manoeuvre allows to comparatively evaluate the effect on stopping distance related to the different fault mode and sub-systems. Stopping distances are visible in Table A.25. Please note that the first two rows of the table refer to the full working vehicle stopping condition; the first one presents a stopping distance of  $46.6m$ , which corresponds to an efficient vehicle braking on a medium-condition surface; while the second one presents a stopping distance of  $39.3m$ , which corresponds to an efficient vehicle braking on a good-condition surface. All other rows are calculated assuming the same conditions expressed on the first row. For certain cases (e.g. failure of regenerative braking system), the distance increase is assumed to be almost negligible due to the simple mitigation strategy implemented (i.e. increment of mechanical braking torque request to compensate lost regenerative braking torque by the BB controller).

## 5. Conclusions and Future Developments

Results of these tests, as already pointed out, concern several aspects:

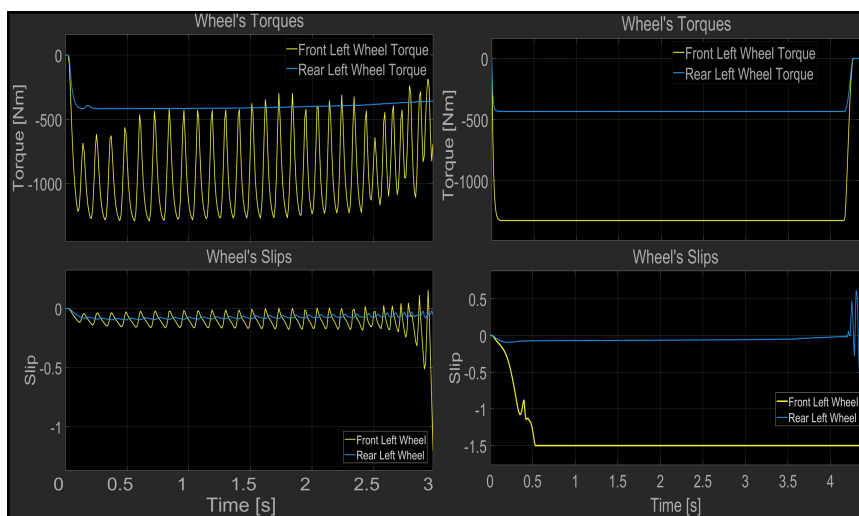


Figure A.80: Wheel torque (top) and slip (bottom) in normal operative condition (left) and fault condition (right) during Model-based FI simulations

Table A.25: Stopping distance of EV in different fault scenario for the BBW subsystems

Case	Stopping Distance [m]	Max Deceleration [ $m/s^2$ ]
Normal	46.6	9.81
Normal (Best Case)	39.3	10.65
EBD Fault	50.6	9.31
ABS Fault	57.1	9.69
BB Fault	47.3	9.88
BMS Fault	47.7	9.84
EM Fault	49.6	9.36
Hydraulic CU Fault	72.6	8.01

1. Definition of the actual Automotive Safety Integrity Level, respect to the investigated brake plant functionalities, summarized in Table A.21 and Table A.22;
2. Proposal of securing intervention, to let the system fulfil the ISO 26262 standard requirements, respect to brake functionalities;
3. Assessment of the procedure coherence and robustness with results arising from functional safety identification methodology, based on vFMEA and FI techniques.

The proposed vFMEA procedure has been applied to several components dealing with EV braking performances. Modified block able to support FI has been proposed and implemented on an existing *MATLAB Simulink* model, representing an electric vehicle equipped with four IWM and a conventional hydraulic braking system, integrated with BB policies. The model is useful to verify the consequences of the events considered more critical and to verify the implications in terms of stopping

distance, considering implemented securing strategy. Simulation campaign involves two environment: Montecarlo and Model-based solution.

In particular, respect to ABS functionality of benchmark vehicle, the simplified Montecarlo model provides quite reliable output (Figure A.79), in accordance with the stopping distance of Table A.25, identified during model-based simulation campaign.

The developed models include the possibility to vary parameters that are sensitive for final performance achievement, such as:

- Failure recognition delay (in this case, set to a total of 350 ms);
  - In real system, part of the delay is unavoidable since it depends on low level communications and physical signals measurements.
  - In both real and simulated system, an additional delay (time-out) has been implemented to represent the need to detect more than 1 single failure alarm to avoid “false positive”.
- Mitigation strategy: actions taken by the system to preserve minimum vehicle performances;
  - Very simple strategies, when possible, have been defined (e.g. brake blending modification in case of total or partial loss of regenerative braking torque).

The model is defined on the basis of “high level” representation, so real system topology is not reproduced. Typical examples are: redundant can-bus communication, here represented through the aggregated failure probability, based on BRD, but not through two data lines modelling; double microprocessor for operator + *Supervisor Controller*. Also, the inclusion of delay and “false positive” mitigation strategy are built in order to simplify implementation on embedded system taking into account the risk of communication limitations (e.g. CAN bus flooding) thus avoiding excessive data transmission rates on the communication lines.

In *conclusion* it can be stated that:

- A tool for the reliability assessment of a target Brake-By-Wire system has been developed, through systematic Virtual Fault Mode and Effect Analysis methodology;
- Proposed solution, in accordance with ISO 26262 standard, adopts Fault Injection technique, applied on vehicle models with different level of detail, in order to let users scale the methodology, according to number and accuracy of desired results;
- Applied to the reference vehicle UC ABS system, allowed verifying the effectiveness of proposed securing solution (redundancy of E/E, application of fault mitigation strategy), making investigated system fulfil standard specifications respect to the random hardware failure metric (Table A.23), which is in the order of  $10^{-12}$  [1/h].

## References

1. Martin H, Krammer M, Winkler B and Schwarzl C 2015 Model-based Engineering Workflow for Automotive Safety Concepts doi: 10.4271/2015-01-0273 pp 0273

2. Yu L, Liu X, Xie Z and Chen Y 2016 Review of Brake-by-Wire System Used in Modern Passenger Car *18th International Conference on Advanced Vehicle Technologies; 13th International Conference on Design Education* **3** (American Society of Mechanical Engineers, Charlotte North Carolina, USA)
3. Martin H, Tschabuschnig K, Bridal O and Watzenig D 2017 Functional Safety of Automated Driving Systems: Does ISO 26262 Meet the Challenges? *Automated Driving: Safer and More Efficient Future Driving* D. Watzenig, E. M. Horn and A. c. d. Cham, Eds., Springer
4. International Electrotechnical Commission IEC 2018 ISO-26262 Road Vehicle – Functional Safety part 1-12
5. Huang C, Naghdy F, Du H and Huang H 2019 Fault tolerant steer-by-wire systems: An overview *Annual Reviews in Control* *47* <https://doi.org/10.1016/j.arcontrol.2019.04.001>, pp 98–111
6. Zulkifli SA, Asirvadam V S, Saad N, Aziz A R A and Mohideen A A M 2014 Implementation of electronic throttle-by-wire for a hybrid electric vehicle using National Instruments' CompactRIO and LabVIEW Real-Time, *2014 5th International Conference on Intelligent and Advanced Systems (ICIAS)*, <https://doi.org/10.1109/ICIAS.2014.6869555>, pp 1–6
7. Kafka P, 2012 The Automotive Standard ISO 26262, the Innovative Driver for Enhanced Safety Assessment and Technology for Motor Cars. *Procedia Engineering, 2012 International Symposium on Safety Science and Technology* **45** <https://doi.org/10.1016/j.proeng.2012.08.112>, pp 2–10
8. Kwon H, Itabashi-Campbell R and McLaughlin K, 2013 ISO 26262 application to electric steering development with a focus on Hazard Analysis, *2013 IEEE International Systems Conference (SysCon)* <https://doi.org/10.1109/SysCon.2013.6549952>, pp 655–61
9. Lidström C, Bondesson C, Nyberg M and Westman J, 2019. Improved Pattern for ISO 26262 ASIL Decomposition with Dependent Requirements *2019 IEEE 19th International Conference on Software Quality, Reliability and Security Companion (QRS-C)* <https://doi.org/10.1109/QRS-C.2019.00019>, pp 28–35
10. Leu K-L, Huang H, Chen Y-Y, Huang L-R and Ji K-M 2015 An intelligent brake-by-wire system design and analysis in accordance with ISO-26262 functional safety standard. *2015 International Conference on Connected Vehicles and Expo (ICCVE) [Internet]*. (Shenzhen, China) Available from: <http://ieeexplore.ieee.org/document/7447585/>, pp 150–6.
11. Bernon-Enjalbert V, Blazy-Winning M, Gubian R, Lopez D, Meunier J-P and O'Donnell M 2015 Safety-Integrated Hardware Solutions to Support ASIL-D Applications.
12. Hasegawa M and Kaneko T 2016 Examination of Hazard Analysis and Risk Assessment and Exposure Research in the Real Traffic Situation of ISO 26262 for Motorcycles *SAE Int J Passeng Cars – Electron Electr Syst* 2016 Nov 8;10(1), pp95–101
13. Nakao S, Shimozawa M and Sugure Y 2014 Virtual FMEA: Simulation-Based ECU Electrical Failure Mode and Effects Analysis Available from: <https://www.sae.org/content/2014-01-0205/> pp 2014-01–0205
14. Nakao S, Hyodo A, Itabashi M, Sakashita T, Obara S and Uno T et al. 2017 Virtual FMEA and Its Application to Software Verification of Electric Power Steering System. Available from: <https://www.sae.org/content/2017-01-0066/>, pp 2017-01–0066.
15. Rana R, Staron M, Berger C, Hansson J, Nilsson M and Törner F 2013 Improving Fault Injection in Automotive Model Based Development using Fault Bypass Modeling *Informatik angepasst an Mensch, Organisation und Umwelt*
16. Zhang J, Zhang Y and Li G 2018 Functional Safety Design of Four-Wheel Independent Brake System on Electric Vehicle *IOP Conf Ser: Earth Environ Sci. Jul;170:042071*
17. Pugi L, Favilli T, Berzi L, Locorotondo E and Pierini M 2019 Brake Blending and Optimal Torque Allocation Strategies for Innovative Electric Powertrains *Saponara S, De Gloria A, editors. Applications in Electronics Pervading Industry, Environment and Society [Internet]*. Cham: Springer International Publishing Available from: [http://link.springer.com/10.1007/978-3-030-11973-7\\_57](http://link.springer.com/10.1007/978-3-030-11973-7_57), pp 477–83
18. Pugi L, Favilli T, Berzi L, Locorotondo E and Pierini M 2019 Application of Regenerative Braking on Electric Vehicles *2019 IEEE International Conference on Environment and Electrical Engineering and 2019 IEEE Industrial and Commercial Power Systems Europe (EEEIC / I&CPS Europe)* (Genova, Italy) Available from: <https://ieeexplore.ieee.org/document/8783318/>, pp 1–6

19. Berzi L, Favilli T, Pierini M, Pugi L, Weib G B and Tobia N et al 2019 Brake Blending Strategy on Electric Vehicle Co-simulation Between MATLAB Simulink ® and Amesim™ 2019 IEEE 5th International forum on Research and Technology for Society and Industry (RTSI) (Florence, Italy) Available from: <https://ieeexplore.ieee.org/document/8895548/>, pp 308–13
20. Pugi L, Favilli T, Berzi L, Locorotondo E and Pierini M 2020 Brake blending and torque vectoring of road electric vehicles: a flexible approach based on smart torque allocation. *IJEHV*
21. International Electrotechnical Commission IEC 2010 IEC-61508, Functional safety of electric/ electronic/ programmable safety-related systems (Geneva)
22. Sinha P 2011 Architectural design and reliability analysis of a fail-operational brake-by-wire system from ISO 26262 perspectives *Reliability Engineering & System Safety* Oct96(10) pp 1349–59
23. Ziade H, Ayoubi R and Velazco R 2004 A Survey on Fault Injection Techniques. *2004;1(2):16*
24. Kooli M and Di Natale G 2014 A survey on simulation-based fault injection tools for complex systems. *2014 9th IEEE International Conference on Design & Technology of Integrated Systems in Nanoscale Era (DTIS) [Internet]* Santorini, Greece: IEEE; 2014 [cited 2020 Sep 9]. Available from: <http://ieeexplore.ieee.org/document/6850649/>, pp 1–6
25. Mei-Chen H, Tsai TK and Iyer RK 1997 Fault injection techniques and tools. *Computer. pr*;30(4) pp 75–82
26. Pintard L, Fabre J-C, Kanoun K, Leeman M and Roy M 2013 Fault Injection in the Automotive Standard ISO 26262: An Initial Approach *Vieira M, Cunha JC, editors. Dependable Computing [Internet] Berlin, Heidelberg: Springer Berlin Heidelberg; 2013 [cited 2020 Sep 9]. (Hutchison D, Kanade T, Kittler J, Kleinberg JM, Mattern F, Mitchell JC, et al., editors. Lecture Notes in Computer Science; vol. 7869) Available from: [http://link.springer.com/10.1007/978-3-642-38789-0\\_11](http://link.springer.com/10.1007/978-3-642-38789-0_11), pp 126–33*
27. Malvezzi M, Presciani P, Allotta B and Toni P 2003 Probabilistic analysis of braking performance in railways *Proceedings of the Institution of Mechanical Engineers, Part F: Journal of Rail and Rapid Transit* 217(3) pp 149–65
28. Linzey G 1996 Development of the Electrical Wiring Interconnection System Risk Assessment Tool *U.S. Department of Transportation Federal Aviation Administration*
29. Pacejka H 2005 Tire and Vehicle Dynamics *Elsevier* pp 657
30. D'hondt T, Forrier B, Sarrazin M, Favilli T, Pugi L, Berzi L et al. 2020 Modeling and Identification of an Electric Vehicle Braking System: Thermal and Tribology Phenomena Assessment Available from: <https://www.sae.org/content/2020-01-1094/> pp 2020-01–1094
31. Technical Committee ISO/TC 22/SC 33 Vehicle dynamics and chassis components ISO 21994:2007 Passenger cars — Stopping distance at straight-line braking with ABS — Open-loop test method

## A.12 48V Electric Vehicle Powertrain Optimal Model-based Design [224]

**Published in** 2020 AEIT International Conference of Electrical and Electronic Technologies for Automotive (AEIT AUTOMOTIVE)

**Authors** Kazusa Yamamoto, Matthieu Ponchant, Franck Sellier, Tommaso Favilli, Luca Pugi, Lorenzo Berzi

**Abstract** Battery autonomy and drive range of Electric Vehicles could be improved by smart control of the power flows requested by equipped systems. In this paper, the authors propose two energy-saving strategies, acting respectively in the electric driveline consumption minimization and in the auxiliary power allocation policy. Developed solutions aim at the reduction of the power demand, both concerning e-powertrain and sub-components, not directly related to traction purpose, enhancing corresponding driveability distance. Evaluation of the result is done through a model-based approach, using a concept e-car proposed by *Valeo* and implemented in a co-simulation environment, between *Amesim* and *Simulink*. The investigated methodology appears as a useful tool for the optimal design of the vehicle sub-system and component.

**Keywords** low voltage electric vehicle, energy efficiency, auxiliary management, thermal management, real driving emission, e-powertrain optimization

### I. Introduction

Another challenging aspect is thermal comfort. Indeed hot sources, in conventional vehicles, are available, which are not the case for EV. So the thermal management has to be considered in the earlier design phase, especially for battery sizing, by adding these new electric consumers (compressor and/or electric heater). Furthermore, thermal comfort could be coupled with electric components cooling systems<sup>13</sup> to balance thermal efficiency and energy balance.

[...] authors intend to propose specific control algorithms and policies, devoted to increasing EVs driving range and autonomy, by a smart allocation and coordination of the power flows. Developed controller address specific needs of scalability and portability properties, as well as real-time capability, in order to be easily tested on several vehicles, use cases. The main challenge of the activity is to reach a 20% efficiency improvement goal, in order to meet the target of the OBELICS project. Hence, this activity is focused on 48V EV powertrain optimal design methodology. To fulfil the aim of this activity, an Equivalent Consumption Minimization Strategy (ECMS) for the electric hub-motors is performed, implemented using *Simcenter Amesim*<sup>TM</sup> tools. Also, an APMC is proposed in *MATLAB Simulink*<sup>®</sup> environment.

[...] Model refinement is also achieved considering cabin thermal regulation system. Then, independent control strategies have been introduced, in order to improve vehicle energy efficiency: on one hand an optimized control for the e-machines, on the other an auxiliary management strategy, both devoted to reduce the power requirement of EM and sub-systems not directly related on traction performances, respectively. Virtual test results, performed using *Amesim*<sup>TM</sup>/*Simulink*<sup>®</sup> co-simulation interface<sup>12</sup>, are shown, highlighting the improvement obtained from the efficiency perspective. Specific driving scenarios are simulated to accurately

reproduce real EV behaviours: so standard urban, ARTEMIS<sup>14</sup> and RDE cycles are performed<sup>15</sup>.

## II. Benchmark Electric Vehicle: 48V architecture

Regarding innovation on small BEV, some low voltage concepts could be highlighted, as the prototype of *Mahle MEET* or *Valeo*, supposed as the reference use case for these activities. Both manufacturers targeted applications for urban mobility, where vehicle maximum speed reaches about 100 km/h and urban traffic autonomy achieves up to 170 km.

Hence, it appears interesting to evaluate the achievable performance over several drive cycles of the investigated BEV, which is inspired by a concept car based on *Valeo* 48 V e-machines characteristics, to meet also rural and motorway requests. However, this control strategy has been successfully applied even to High Voltage (HV) EV [223], so proposed methods are not limited only to Low-Voltage (LV) vehicle solution. [...] a 4WD with independent IWM architecture with a single battery pack has been supposed. The intent is the evaluation of the achievable power and driving range, to meet A/B1 segment car requirement.

### A. Simulation Layout

The 48V electric model has been developed with *Simcenter Amesim*<sup>18</sup>. The hypothetical e-powertrain layout consists of 4 IWM connected to each wheels, where supposed EM are based on real *Valeo* e-machine data (Figure A.81). Their performances (maximum and minimum torque, losses respect to shaft speed) are mapped and implemented through a model-based concept in the simulation environment.

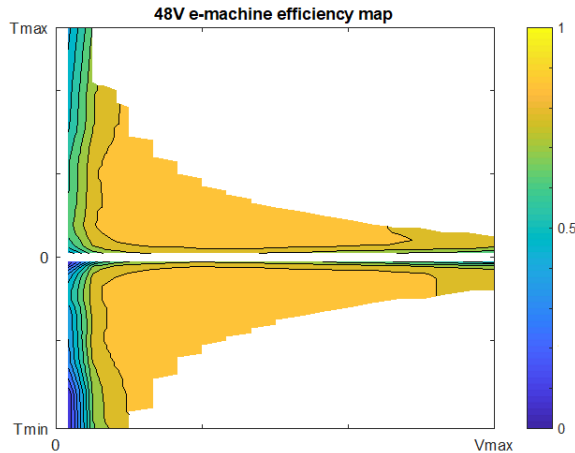


Figure A.81: 48V Valeo concept car

According to pre-sizing results of 4WD EV requirements, HEEDS software<sup>18</sup> has been used to optimize some vehicle parameters, improving the overall performance over WLTC cycle. Then, some variables (*e.g.* gear ratio, the weight of the car and of the battery) is updated through the automated process, subject to optimization objectives and constraints (*e.g.* vehicle maximum range, minimizing acceleration time). The design criteria are summarized in Table A.26 and the resulting 48V

4WD EV concept shows similar performance compared to the recently release high voltage VW e-up which has a close application target (city, rural road, highway). HEEDS has improved over 500 iterations the 4WD EV characteristics. Indeed, a 280 km range is achieved by considering a reduction of the battery SOC from 90% to 10%, which is better than equivalent EVs available on the market and increased the vehicle range by 11% compared to pre-sizing specifications. The selected battery cell chemistry is Nickel Cobalt Aluminium Oxide since it is widely spread in EV industry<sup>17</sup>.

Table A.26: BEV Characteristics

Desing Criteria	48V 4WD BEV	VW e-Up
<i>Range WLTC Class 3</i>	280.8 [km]	258 [km]
<i>Max Acceleration 0 – 100 [km/h]</i>	11.96 [s]	11.9 [s]
<i>Max Speed</i>	140 [km/h]	130 [km/h]
<i>Mass of Vehicle with conductor</i>	1094.4 [kg]	1310 [kg]
<i>Battery Capacity</i>	42.5 [kWh]	36.8 [kWh]
<i>Gear Ratio</i>	8	unk.

## B. Model Refinement

The Air Conditioning (AC) system is also considered to refine the autonomy estimation of the vehicle in a more realistic case. This subsystem could be critical in some specific condition, especially at cold or hot temperature, when its power consumption is not negligible if compared to the driveline power.

## III. Control Strategy

This section is dedicated to the description of the proposed optimal control strategy, implemented on the use case vehicle simulation model. In particular, developed algorithms, ECMS and APMC, have the task of reducing the BEV total power consumption, acting respectively in the e-powertrain and auxiliary system regulation.

### A. Equivalent Consumption Minimization Strategy (ECMS)

Optimal control of the electric machine has been implemented using the *Simcenter Amesim* Hybrid Optimization Tool. It is an interactive interface dedicated to estimating the energetic potential of a vehicle architecture on a given drive cycle. In this case, the 4WD is selected. This tool is based on an optimal control allocation strategy and, specifically, on the method known as Pontryagin's Minimum Principle<sup>19</sup>, which states that at each time step, the optimal values of the degrees of freedom are found by minimizing a function called Hamiltonian (H), that is (A.54)-(A.55) where  $u$  represents the degrees of freedom to optimized and  $P_{exch}$  is the electrochemical consumption of the battery.

$$u^{opt}(t) = argmin H(u, t, SOC) \quad (A.54)$$

$$H = P_{exch} \quad (A.55)$$

## B. Auxiliary Power Management Control (APMC)

Aim of this control strategy is to optimize the usage of HVAC system, in order to reduce its consumption when critical conditions occur, e.g. in low SOC situation, or when high levels of power are demanded by the EMs to fulfil the traction demand. In particular, the APMC will trigger the activation of a so-called *ECO-mode*, useful to increase the remaining vehicle driving range by minimizing the power demanded by the auxiliary system, while ensuring cabin temperature comfort. The activation of this control method is based on the following parameters:

- Battery SOC: when the storage system is approaching the full discharge condition, this control policy is enabled;
- Battery DCL: once evaluated the maximum value of the discharge current the storage system can experience, is evaluated respect to the actual request from the DC bus. When demanded current is higher then DCL, which is estimated from SOC and temperature of the battery<sup>20</sup>, ECO-mode will trigger.

Based on this information, it is evident that the APMC require a integration with the vehicle CU, especially BMS and Motor CU, which estimate specific parameters, fundamental for the strategy application.

ECO-mode regards the controlling policies of the AC system. Intervention concern the regulation of the admitted temperature bandwidth for the cabin and related control gains, acting on the thermal regulation loops. The involved sub-systems are:

- Blower: the device which establishes the mass of mixed air flowing in the cabin. It's a composition of fresh and recirculated air. ECO-mode activation enlarge the dead-zone of the temperature control loop;
- Evaporator: similarly at the blower intervention, in ECO-mode higher output temperature are tolerated;
- Compressor: its regulation method involves two nested feedback control loops, temperature and speed. Intervention concern only the first one, reducing the PID controller gains and increasing temperature dead-zone.

A simplified flow chart of the APMC is visible in Fig. A.82. At the vehicle starts, an initialization procedure begins, consisting in the data acquisition from the main vehicle CU. This task, recursively iterated ad each time steps of the APMC, allows the verification of two different *if* statements: (1) the value of current SOC is below a specified desired value? (2) The total requested current is above admitted DCL? Results of the rules are evaluated through an OR logical operator. If verified, ECO-mode will trigger, otherwise, no action on auxiliary systems regulation is performed.

## IV. Simulation Results

Proposed campaign tests, performed in the model of Figure A.83 and implemented in a co-simulation environment, can be grouped into two branches:

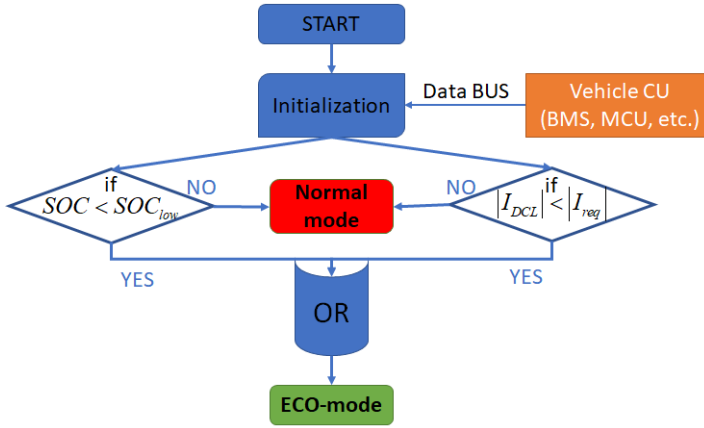


Figure A.82: APMC flow chart

- *Standard Driving Cycles*: mainly used for the model verification and the controllers' calibrations; results concern these tests are also useful to assess the performances of proposed ECMS control policy and different thermal system solutions, if compared to the output of simulations performed on a baseline 4WD EV;
- *RDE Cycles*: adopted for the purpose of accurately estimated BEV performances and Efficiency Improvement (Eff Imp) allowed by proposed control strategies, accounting road slope and external temperature variations.

## A. Standard Driving Cycles

**1) Model Verification** Vehicle model has been verified on *JC08* driving cycle under different initial SOC conditions. This test is repeated several times to assess the effect of the ECMS controller functionalities. The Eff Imp is calculated according to (A.56), considering the average energy consumption (kWh/100km) of the 4WD model without a thermal regulation system, as a reference baseline for the metrical evaluation.

$$\eta = \frac{E_{baseline} - E_{ECMS}}{E_{baseline}} [\%] \quad (\text{A.56})$$

Looking at Table A.27, could be noticed that a strong efficiency improvement is achieved, allowed by the usage of optimal e-motor controlling method, especially in urban conditions. On investigated standard driving cycles (*JC08* and *WLTP*), an increase of more than 10% is reached. Nevertheless, such cycles consider neither the thermal effect nor the landscape, e.g. the slope of the road. So these enhancements should be considered overestimated if compared with a more realistic operating scenario.

**2) Thermal model verification** *ARTEMIS* drive cycles<sup>14</sup> has been used, dedicated to accurately simulate thermal effects on BEV performances in different external weather conditions, as well as cabin target temperatures. With such cycles, different HVAC technologies (Heat pump & electric heater) have been investigated

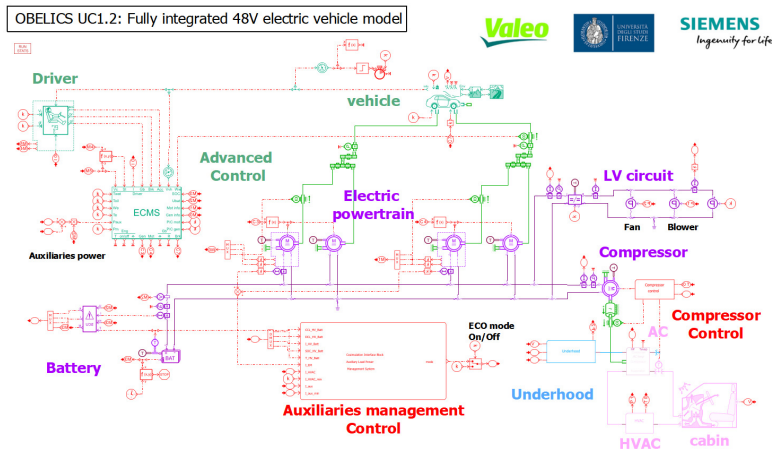


Figure A.83: Fully integrated 48 V electric vehicle model

Table A.27: Standard driving cycles simulation results

Initial battery conditions: SOC 90% and 20°C		
Control	Driving Cycle	Eff. Imp. [%]
ECMS	WLTC	16.5
	JC08	10.3

for the reference benchmark case. As shown in the plots of Figure A.84, heat pumps allow improving energy consumption, if compared to electric heaters (SOC increases of 7% and thermal energy consumption reduced by 53.6%) while ensuring same heating performances: both steady states are at 20°C target temperature, with almost the same transient phase, though the electric heater is 100 s faster at reaching desired value. Indeed, the heat pump coefficient of performance is about 3.

## B. Real Driving Emission Cycles

RDE cycles are frequently used and widely adopted in recent literature<sup>15</sup>, since they can give to designer a more accurate performance overview of the vehicle, by accounting more variables for their definition. In particular, different operative conditions respect to time, besides speed reference, can be considered, e.g. temperature, altitude and so on. Performed cycles reply to the real driving condition of *Barcelona* and *Gratz* cities (Figure A.85), specifying different temperature and altitude values during the tests. The model Accuracy Improvement (Acc Imp) is calculated considering the refined 4WD Amesim model at 20°C as a baseline. The average energy consumption increases due to activation of the thermal systems (AC, heat pump) and the growth are visible in Table A.28. Thus, final SOC is reduced in a hot case by 4% and cold case by 9% compared to baseline, as shown in Figure A.86. Indeed, the required thermal system power is rather high to reach expected cabin temperature. At cold and hot ambient condition, the influence of the AC system on the battery range is not negligible and must be taken into account in the early design phase of the EV, especially for the battery sizing.

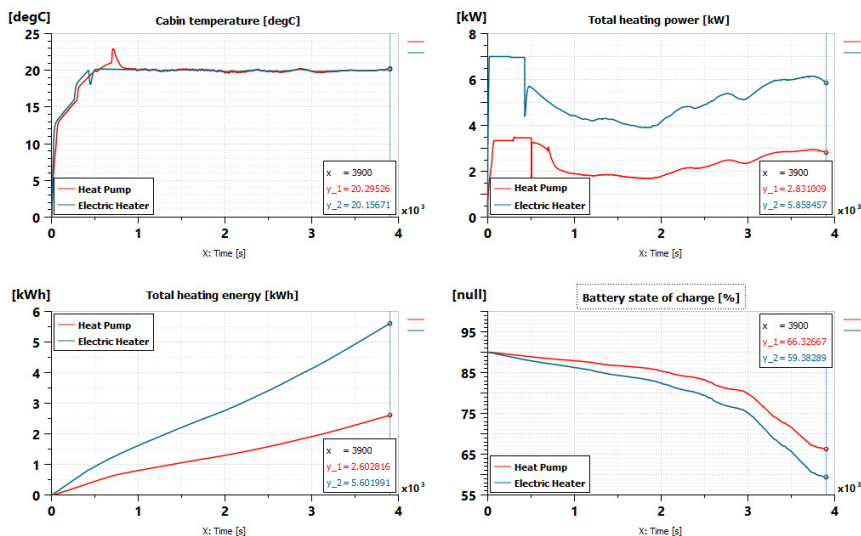


Figure A.84: Thermal system solutions comparison on ARTEMIS cycle: Cabin temperature (top-left); Heating power (top-right); Heating energy (bottom-left) and SOC (bottom-right)

Table A.28: Performance comparison under realistic conditions

RDE cycle simulation results		
<i>RDE Cycle</i>	<i>Temperature</i>	<i>Acc. Imp. [%]</i>
Gratz	35°C	13.9
	0°C	29.6
Barcelona	35°C	14.2
	0°C	28.6

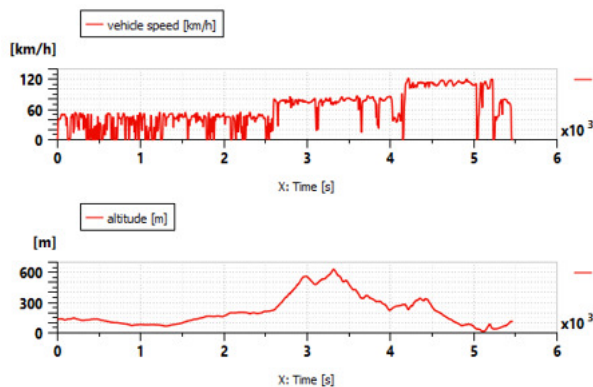


Figure A.85: RDE cycles province of Barcelona

### C. Subsystem integration

After studying subsystems in standalone, the next step in the development process is their integration in the EV model, in order to verify the consistency of the fully

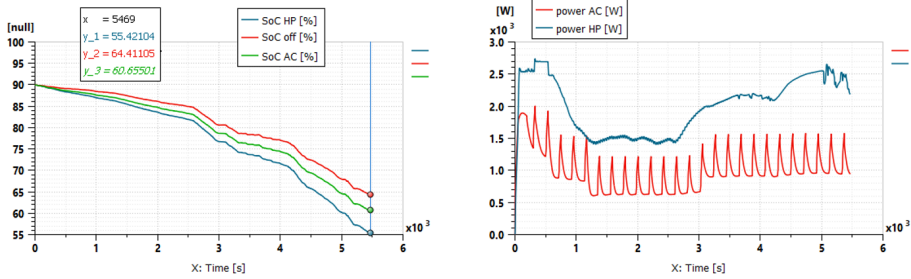


Figure A.86: Comparison on RDE province of Barcelona at different ambient temperature: SOC (left) and thermal system power (right)

integrated solution. Comparison study has been performed with RDE cycles at 35°C, to ensure realistic behaviour in the vehicle energy consumption estimation. To go further, it appears interesting to study the effect of APMC on the average consumption, based on the previous model integrating ECMS and AC thermal system. The whole co-simulation environment, already introduced in Figure A.83, allows estimation of the Eff Imp in realistic condition, assessed on RDE Gratz and Barcelona cycles. The results of Table A.29 show that energy improvement is achieved thanks to APMC. Indeed, as illustrated in Fig. A.87 the ECO mode reduces the HVAC system current consumption, increasing battery autonomy.

Table A.29: Influence of the auxiliaries management control on the vehicle model with optimal e-motor control

Initial conditions: SOC 90% and 35°C			
<i>Layout</i>	<i>RDE Cycle</i>	<i>APMC</i>	<i>Eff. Imp. [%]</i>
ECMS	Gratz	OFF	4.46
		ON	7.4
ECMS	Barcelona	OFF	5.44
		ON	8.79

A non-secondary advantage of this implementation is computational time efficiency, even considering the increasing complexity of the phenomena involved by vehicle sub-systems models. Indeed, virtual tests are running 11.5 times faster than real-time. So, models can be easily integrated into Hardware in the Loop target to validate the control algorithms.

## V. Conclusions and Future Developments

In conclusion, e-powertrain architecture, vehicle characteristics and components sizing have been investigated through vehicle model simulation in *Amesim*. EV performance improvement is reached through optimization of vehicle parameters (HEEDS tool), development of advanced control strategies (ECMS, APMC) and innovative components (heat pump): Fig. A.87 summarizes the achievement permitted by the investigated thermal system solutions. Moreover, realistic conditions

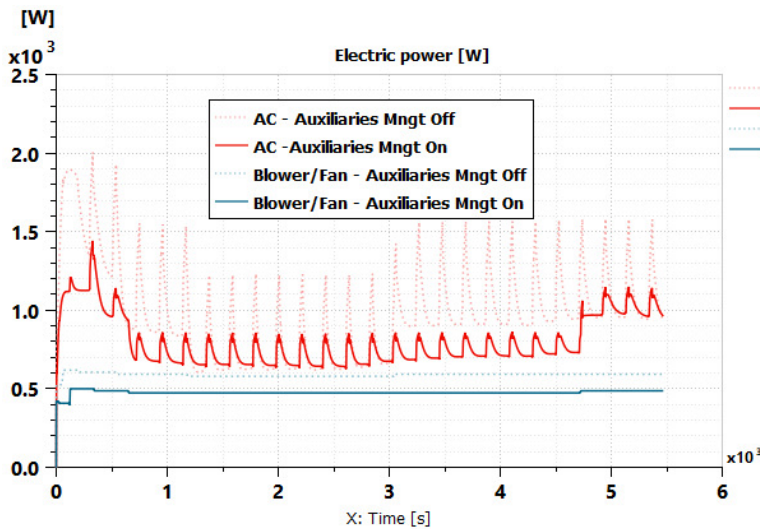


Figure A.87: influence of the APMC on the EV model with advanced e-motor control during RDE Barcelona cycle, (battery SOC on top, HVAC solutions power on bottom)

are considered employing specific driving cycles (ARTEMIS, RDE), to refine average consumption. In particular, multiple 48V EV simulation models have been developed to investigate efficiency improvement within a short development time.

## References

1. European Parliament, Council of the European Union, Regulation (EC) No 715/2007 of the European Parliament and of the Council of 20 June 2007 on type approval of motor vehicles with respect to emissions from light passenger and commercial vehicles (Euro 5 and Euro 6).
2. <https://www.c40.org/other/green-and-healthy-streets>
3. M. Ehsani, Ed., Modern electric, hybrid electric, and fuel cell vehicles: fundamentals, theory, and design. Boca Raton: CRC Press, 2005.
4. J. de Santiago et al., 'Electrical Motor Drivelines in Commercial All-Electric Vehicles: A Review', IEEE Transactions on Vehicular Technology, vol. 61, no. 2, pp. 475–484, Feb. 2012, doi: 10.1109/TVT.2011.2177873.
5. R. Mounce and J. D. Nelson, 'On the potential for one-way electric vehicle car-sharing in future mobility systems', Transportation Research Part A: Policy and Practice, vol. 120, pp. 17–30, Feb. 2019, doi: 10.1016/j.tra.2018.12.003.
6. B. Frieske, M. Kloetzke, and F. Mauser, 'Trends in Vehicle Concept and Key Technology Development for Hybrid and Battery Electric Vehicles', vol. 6, p. 12, 2013.
7. L. Pugi, T. Favilli, L. Berzi, E. Locorotondo, and M. Pierini, 'Brake Blending and Optimal Torque Allocation Strategies for Innovative Electric Powertrains', in Applications in Electronics Pervading Industry, Environment and Society, vol. 573, S. Saponara and A. De Gloria, Eds. Cham: Springer International Publishing, 2019, pp. 477–483.
8. L. Pugi, T. Favilli, L. Berzi, E. Locorotondo, and M. Pierini, 'Brake blending and torque vectoring of road electric vehicles: a flexible approach based on smart torque allocation', IJEHV, vol. 12, no. 2, p. 87, 2020, doi: 10.1504/IJEHV.2020.106339.
9. L. Yu, X. Liu, Z. Xie, and Y. Chen, 'Review of Brake-by-Wire System Used in Modern Passenger Car', in Volume 3: 18th International Conference on Advanced Vehicle Technologies; Charlotte, North Carolina, USA, 2016, p. V003T01A020, doi: 10.1115/DETC2016-59279.

10. L. Berzi, T. Favilli, E. Locorotondo, M. Pierini, and L. Pugi, 'Real Time Models of Automotive Mechatronics Systems: Verifications on "Toy Models"', in *Advances in Italian Mechanism Science*, vol. 68, G. Carbone and A. Gasparetto, Eds. Cham: Springer International Publishing, 2019, pp. 141–148.
11. Y. Hori, 'Future vehicle driven by electricity and control-research on four wheel motored "UOT Electric March IP"', in *7th International Workshop on Advanced Motion Control. Proceedings (Cat. No.02TH8623)*, Maribor, Slovenia, 2002, pp. 1–14, doi: 10.1109/AMC.2002.1026883.
12. L. Berzi et al., 'Brake Blending Strategy on Electric Vehicle Co-simulation Between MATLAB Simulink® and Simcenter Amesim™', in *2019 IEEE 5th International forum on Research and Technology for Society and Industry (RTSI)*, Florence, Italy, Sep. 2019, pp. 308–313, doi: 10.1109/RTSI.2019.8895548.
13. N. Tobia, M., Ponchant, 'Methodology applied to couple 1D & 3D models on HPC in context of electric vehicle Fiat 500e thermal management design', in *32nd Electric vehicle Symposium*, Lyon, France, May 2019, pp. 308–313.
14. M. André, 'The ARTEMIS European driving cycles for measuring car pollutant emissions', *Science of The Total Environment*, vol. 334–335, pp. 73–84, Dec. 2004, doi: 10.1016/j.scitotenv.2004.04.070.
15. M. Nowak and J. Pielecha, 'Comparison of exhaust emission on the basis of Real Driving Emissions measurements and simulations', *MATEC Web Conf.*, vol. 118, p. 00026, 2017, doi: 10.1051/mateconf/201711800026.
16. L. Berzi et al., 'Smart Energy Management of Auxiliary Load for Electric Vehicles', in *2020 IEEE International Conference on Environment and Electrical Engineering and 2020 IEEE Industrial and Commercial Power Systems Europe (EEEIC / I&CPS Europe)*, Madrid, Spain, Jun. 2020, pp. 1–6, doi: 10.1109/EEEIC/ICPSEurope49358.2020.9160762.
17. Y. Miao, P. Hynan, A. von Jouanne and A. Yokochi, 'Current Li-Ion Battery Technologies in Electric Vehicles and Opportunities for Advancements', *Energies* 2019, 12, 1074, doi:10.3390/en12061074
18. <https://www.plm.automation.siemens.com/global/fr/products/simcenter/simcenter-amesim.html>
19. Dabadie, J., Sciarretta, A., Font, G., and Le Berr, F., 'Automatic Generation of Online Optimal Energy Management Strategies for Hybrid Powertrain Simulation', *SAE Technical Paper 2017-24-0173*, 2017, DOI:10.4271/2017-24-0173.
20. S. Onori, P. Spagnol, V. Marano, Y. Guezennec, and G. Rizzoni, 'A new life estimation method for lithium-ion batteries in plug-in hybrid electric vehicles applications', *IJPELEC*, vol. 4, no. 3, p. 302, 2012, doi: 10.1504/IJPELEC.2012.046609.

## A.13 Design of a new On-board Energy Storage and Conversion System for a Fast Charging Urban Transport Electric Bus [222]

**Published in** 2021 IEEE International Conference on Environment and Electrical Engineering and 2021 IEEE Industrial and Commercial Power Systems Europe (EEEIC / I&CPS Europe)

**Authors** Adriano Alessandrini, Lorenzo Berzi, Fabio Cignini, Tommaso Favilli, Antonino Genovese, Alessandro Lidozzi, Fernando Ortenzi, Luca Pugi, Domenico Staffa

**Abstract** Battery autonomy and drive range of Electric Vehicles could be improved by smart control of the power flows requested by equipped systems. In this paper, the authors propose two energy-saving strategies, acting respectively in the electric driveline consumption minimization and in the auxiliary power allocation policy. Developed solutions aim at the reduction of the power demand, both concerning e-powertrain and sub-components, not directly related to traction purpose, enhancing corresponding driveability distance. Evaluation of the result is done through a model-based approach, using a concept e-car proposed by *Valeo* and implemented in a co-simulation environment, between *Amesim* and *Simulink*. The investigated methodology appears as a useful tool for the optimal design of the vehicle sub-system and component.

### I. Introduction

The necessity of reducing the polluting emission of modern transport system in accordance to the recent European council specifications<sup>1,2</sup> and the rapid transition of the current automotive sector towards electrified vehicle's traction system<sup>3</sup> are boosting both academic and industrial interest respect to more sustainable public transport solutions<sup>4</sup>. Main challenge is represented by the limited drive range autonomy. Public transportation systems require a prolonged autonomy and fast recharge times to meet severe mission profiles and high reliability issues. To overcome these open problems, authors intend to design and develop a urban transport solution which involves the use of an e-bus able to perform a fast recharge of an on board high power battery using an infrastructure that is able to release a large amount of power in an affordable and profitable way<sup>5</sup>, exploiting a flywheel storage.

The recharge infrastructure will comprise an inertial energy storage system (flywheel) and HV contact dome (350V) to host the vehicle pantograph equipment<sup>10-13</sup>. The traction system of the vehicle instead, work with LV DC motor drivers (72V). The reference UC vehicle was previously investigated for different applications, to evaluate the feasibility of the proposed solution, both under economical and technical aspects<sup>14,15</sup>. A general scheme of the investigated system is visible in Figure A.88.

In this paper a vehicle model of the reference e-bus is developed to size battery and the recharge station system in accordance with the required specifications. In particular, the vehicle should be able to perform several designated driving path of the line before requiring a charge. This cautious specification is imposed to assure a high level of reliability respect to perturbations of mission parameters including availability of recharge stations that are quite mandatory for a public

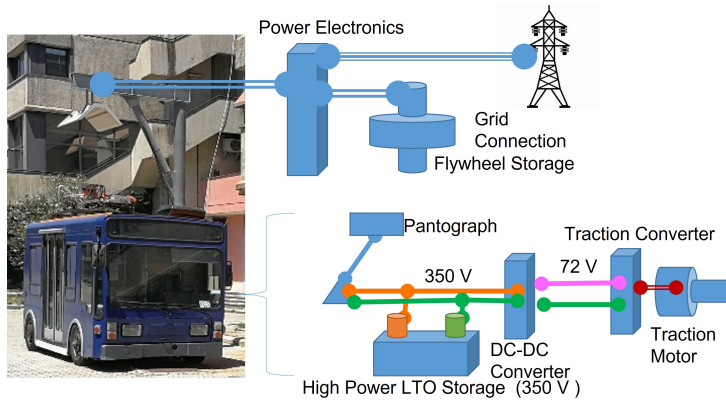


Figure A.88: Simplified Scheme of Proposed System

service. Outcomes are related to the simulation of specific telemetry driving cycles that have been detected during several bus routes, which will be comparatively evaluated respect to the log of electric signals acquired during the experimental testing campaigns.

## II. Benchmark Electric Bus Vehicle

[...] Sizing of the bus storage system have been based on recorded mission profiles on ROMA line 117. One of the investigated drive cycle is visible in Figure A.89. Despite the usage of a high LTO battery, the "bottleneck" of the system which is still limiting the maximum recharge rate of the vehicle is represented by the battery<sup>17</sup>. However, authors are almost confident in further improvement of battery storage technologies so pantograph and more generally the overall system is sized for far larger currents.

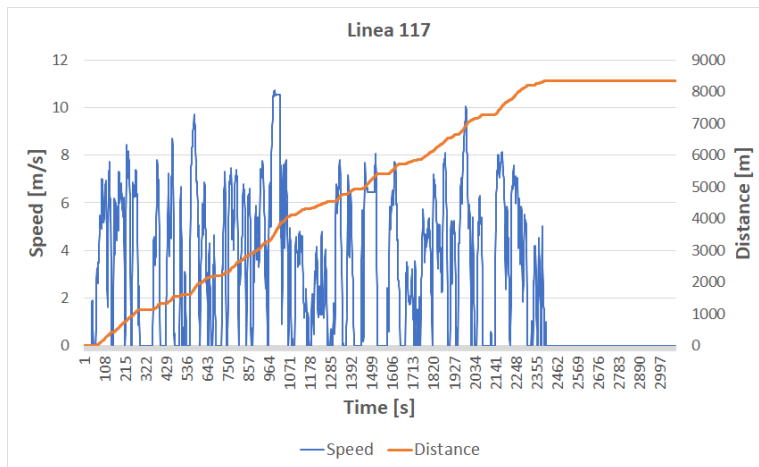


Figure A.89: Graphic plot of speed and distance recorded of ATAC line 117

This choice is also justified by the fact that the current size of the prototype is quite limited, most common size of public buses are at least two three times larger, so the general sizing of the infrastructure and current collection system is far more generous.

#### IV. Modeling Approach

[...] A model of Tecnobus vehicle visible in Figure A.90 has been developed and implemented in *MATLAB Simulink* environment to assess the achievable energy performances respect to the simulated driving cycles.

Indeed, making the e-bus model replicate the reference mission profiles let us to establish the system consumption, useful to verify the effectiveness and the compatibility of the proposed storage/recharge system respect to required drive range specifications. The 5 DoF vehicle model consist of several component which reproduce the behaviour of different vehicle sub-systems: Driver; Brake Blending Controller; Energy Storage System; Electric Motor; Hydraulic Brake; Vehicle Body: a 1-DoF; Wheel/Road Contact; Auxiliary System (a simplified modelling approach used to simulate the power consumption of the vehicle auxiliary load, e.g. compressor for the doors and suspensions, cabin lights, on-board ECU, cooling. It's value is tuned using the consumption of the bus acquired during performed real word test campaigns, when vehicle is in stand-still conditions) [...].

For future activities, involving the testing of ADAS on the same UC vehicle, is available a full model of the e-bus with 9-DoF. Indeed, to properly simulate the lateral behaviour, lateral and yaw motion of the body are needed in addition to longitudinal chassis dynamics, as well as the adoption of 2-DoF independent wheel models, which include longitudinal slip and lateral side-slip effects.

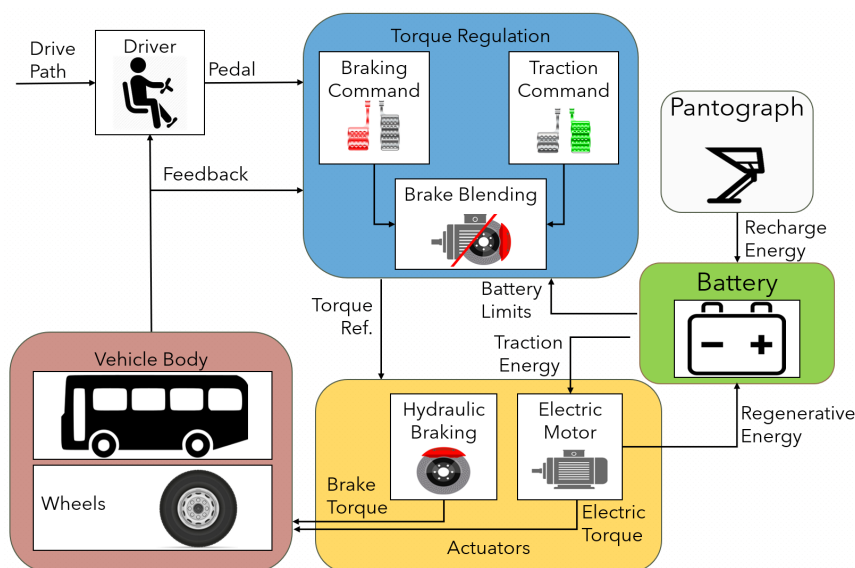


Figure A.90: Simplified block diagram of the proposed simulation model

## V. Preliminary Model Validation with Experimental Results

Results of the performed drive cycles are compared with the simulated ones in order to evaluate the accuracy of the developed models. These calibration data are taken from previous experimental campaigns in which the same bus was equipped with a different storage system (an hybrid battery and super-capacitor system). Aim of these calibration activities is to verify how the developed model is able to emulate a real mission profile in terms of consumed energy. In this way it is possible to assess the proposed model as a tool to further design and optimize the fast recharge system. Assessment metrics are the consumed energy per kilometre  $E_{cons}$  by the vehicle, which are calculated from the logged data of real word testing according (A.57), where  $V$  and  $I$  are respectively battery voltage and current,  $d$  the travel distance and  $\eta$  the efficiency of the traction system. The latter is defined using the efficiency motor map of Figure A.91.

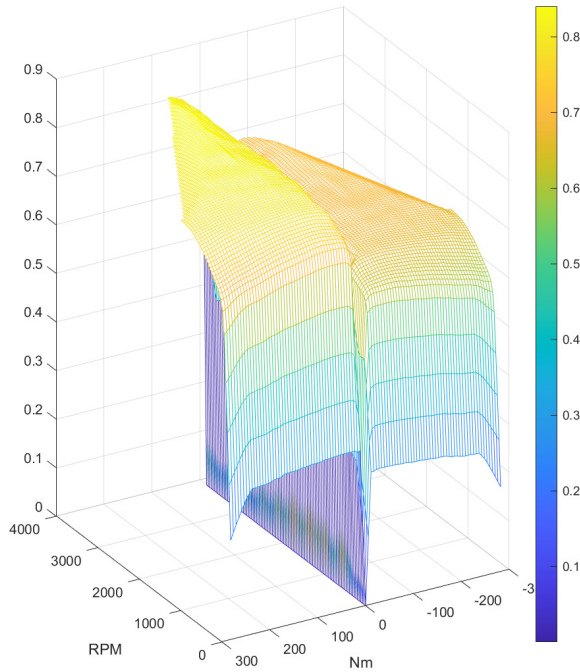


Figure A.91: Electric Motor efficiency map

$$E_{cons} = \frac{V \cdot I}{d \cdot 3600} \eta \tag{A.57}$$

Performed simulations campaign can be divided in two phases:

1. *Calibration tests*: some short-term drive cycles are used to calibrate the models. The reference e-bus was equipped with current and voltage sensors for the calculation of instantaneous power demand and overall energy consumption;
2. *Real bus route tests*: once the calibration is performed, the same model is adopted for reproducing the acquired path of the 117 bus line.

References calibration mission profiles are visible in Figure A.92, which show the GPS track of the e-bus route performed during real word scenario.



Figure A.92: Test route used during real world bus tests and replicated in the simulation environment

Outcomes are summarized in Table A.30, while specific mission profile related to route 3,5 and 8 are visible in Figure A.93, Figure A.94 and Figure A.95, showing the drive cycle along with total energy demand. Its easy to understand, looking at the last column, that the model estimated the real vehicle consumption with acceptable accuracy. However, precision of the simulation results appear variable between 1% to 24%. This effect can be attributable both to the auxiliary system and road slope. Indeed, additional vehicle power consumption is hardly to estimate during traction and braking operative conditions, since its values are negligible respect to e-motor driver power: during these phases the energy required for the compressor can increase significantly.

Table A.30: Consumption of the bus during calibration tests

Test N.	Exp. Cons.	Simul. Cons.	Distance	Error
1	496.5 [Wh/km]	480.9 [Wh/km]	0.86[km]	3.1[%]
2	480 [Wh/km]	455.2 [Wh/km]	0.85[km]	5.2[%]
3	509.7 [Wh/km]	467.1 [Wh/km]	0.86[km]	8.4[%]
4	476.6 [Wh/km]	485.8 [Wh/km]	0.86[km]	-1.9[%]
5	579.2 [Wh/km]	521.9 [Wh/km]	0.58[km]	9.9[%]
6	473.6 [Wh/km]	490.3 [Wh/km]	0.86[km]	-3.5[%]
7	500.8 [Wh/km]	486.5 [Wh/km]	0.86[km]	2.9[%]
8	504.8 [Wh/km]	486.6 [Wh/km]	0.94[km]	3.6[%]
9	747.2 [Wh/km]	555.5 [Wh/km]	0.96[km]	25.7[%]
10	639.7 [Wh/km]	517.1 [Wh/km]	0.95[km]	19.2[%]

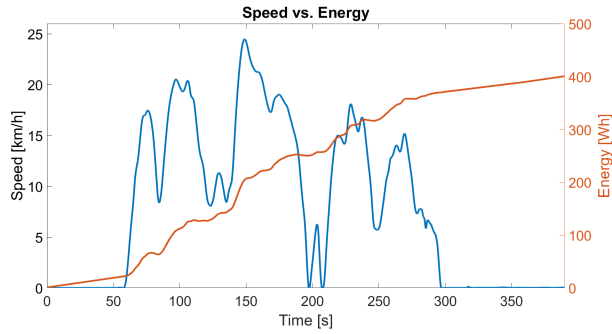


Figure A.93: Speed and Power vs. Time for test n.3

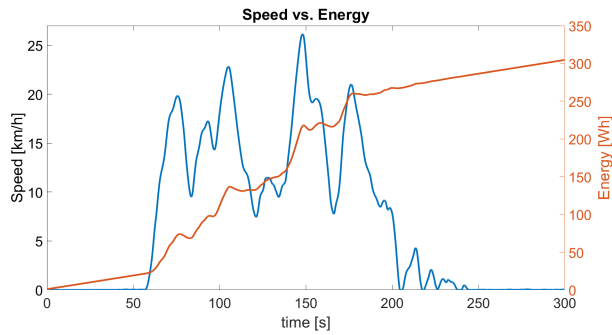


Figure A.94: Speed and Power vs. Time for test n.5

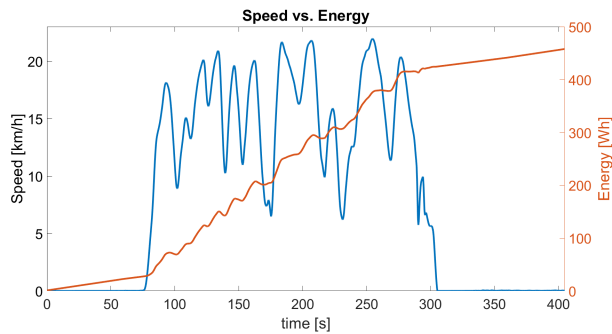


Figure A.95: Speed and Power vs. Time for test n.8

Also, test of route 9 and 10 were performed in tracks with different slope variations (Figure A.96), so, according to Orchi et al.<sup>25</sup>, higher energy demand are justified.

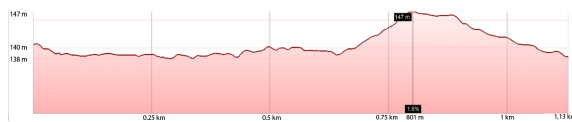


Figure A.96: Altimetry of the calibration test route

Real bus route test results are reported in Figure A.97, Figure A.98 and Figure A.99. Energy consumption and final battery SOC are calculated and summarized in Table A.31 for a comparative evaluation and to assess the appropriateness of the the e-bus battery respect to required performances. What we find out is that the model calibration is quite good, since the output of the line 117 drive cycles simulations agree with results of Table A.30. Consumption per kilometres are slightly under-estimated with respect to real word testing. This is ascribable to the speed achieved during real bus route. Indeed, higher engine speed require much larger wheel torques, benefiting of enhanced traction system efficiency, as visible in Fig. A.91.

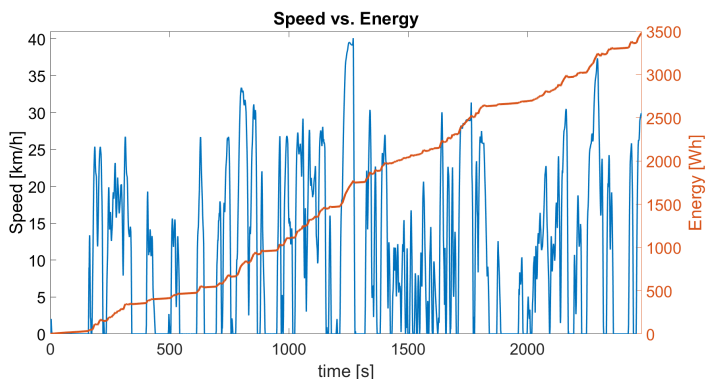


Figure A.97: Speed and Power vs. Time for line 117, run 1

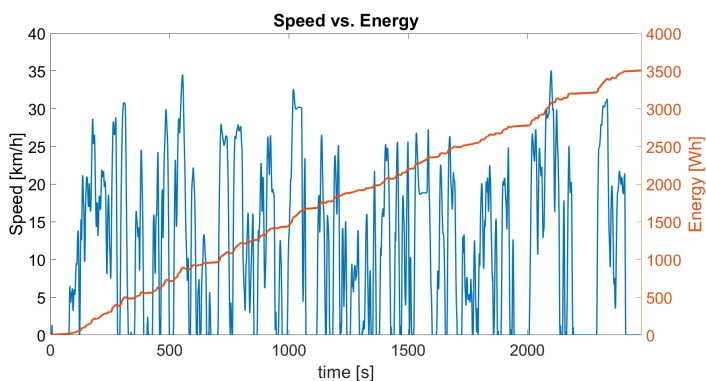


Figure A.98: Speed and Power vs. Time for line 117, run 2

Final values of the storage system SOC are satisfying, since ensure that the bus can cover more routes of the line before requiring a full recharge.

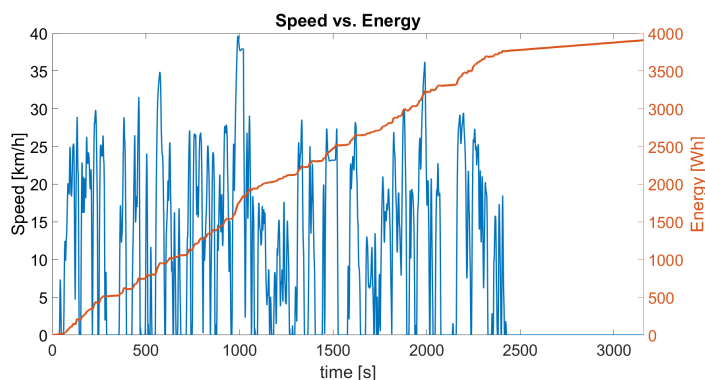


Figure A.99: Speed and Power vs. Time for line 117, run 3

Table A.31: Consumption of the Vehicle during line 117 simulation tests

Test N.	Distance	Simul. Cons.	Final SOC
1	7,73 [km]	481,4 [Wh/km]	79,4 [%]
2	7,73 [km]	452,9 [Wh/km]	80,6 [%]
3	8,34 [km]	470,5 [Wh/km]	78,3 [%]

## VI. Conclusion and Future Developments

In this work authors have presented an innovative fast recharge system and a Matlab-Simulink model that is able to reproduce its behaviour. The latter is currently used to proper design the system that will be assembled and tested at ENEA research laboratories of Casaccia (Rome,Italy). Proposed solution has been preliminary tuned with respect to energy data taken on the same bus from a previous experimental campaign. Then the calibrated model is validated using different drive cycles of ATAC 117 line, acquired trough GPS sensors.

Results appear accurate and reliable, since high level of correspondence between energy consumption per km between experimental and simulated data are achieved [...].

## References

1. R. Smith, ‘Regulation (EC) No 764/2008 of the European Parliament and of the Council’, in *Core EU Legislation*, London: Macmillan Education UK, 2015, pp. 183–186. doi: 10.1007/978-1-137-54482-7\_19.
2. S. R. Adheesh, M. S. Vasisht, and S. K. Ramasesha, ‘Air-pollution and economics: diesel bus versus electric bus’, *CURRENT SCIENCE*, vol. 110, no. 5, p. 5, 2016.
3. B. Bilgin and A. Emadi, ‘Electric Motors in Electrified Transportation: A step toward achieving a sustainable and highly efficient transportation system’, *IEEE Power Electronics Magazine*, vol. 1, no. 2, pp. 10–17, Jun. 2014, doi: 10.1109/MPPEL.2014.2312275.
4. D. Göhlich, T.-A. Fay, D. Jefferies, E. Lauth, A. Kunith, and X. Zhang, ‘Design of urban electric bus systems’, *Des. Sci.*, vol. 4, p. e15, 2018, doi: 10.1017/dsj.2018.10.
5. X. Wang, C. Yuen, N. U. Hassan, N. An, and W. Wu, ‘Electric Vehicle Charging Station Placement for Urban Public Bus Systems’, *IEEE Trans. Intell. Transport. Syst.*, vol. 18, no. 1, pp. 128–139, Jan. 2017, doi: 10.1109/TITS.2016.2563166.

6. F. Ortenzi, G. Pede, and P. Antonini, 'Design of the Storage System of a High Performance Hybrid Vehicle', Sep. 2015, pp. 2015-24–2544. doi: 10.4271/2015-24-2544.
7. G. Sethuraman, P. R. Tran, A. Ongel, M. Lienkamp, and P. Raksincharoensak, 'Development of a parametric packaging and sizing tool for autonomous electric bus system', Proceedings of the Institution of Mechanical Engineers, Part D: Journal of Automobile Engineering, vol. 235, no. 6, pp. 1713–1733, May 2021, doi: 10.1177/0954407020972268.
8. A. Alessandrini, F. Cignini, F. Ortenzi, G. Pede, and D. Stam, 'Advantages of retrofitting old electric buses and minibuses', Energy Procedia, vol. 126, pp. 995–1002, Sep. 2017, doi: 10.1016/j.egypro.2017.08.260.
9. L. Berzi et al., 'Structural and energy storage retrofit of an electric bus for high-power flash recharge', Procedia Structural Integrity, vol. 24, pp. 408–422, 2019, doi: 10.1016/j.prostr.2020.02.038.
10. A. Alessandrini et al., 'A Flash Charge System for Urban Transport', in 2019 IEEE International Conference on Environment and Electrical Engineering and 2019 IEEE Industrial and Commercial Power Systems Europe (EEEIC / I&CPS Europe), Genova, Italy, Jun. 2019, pp. 1–6. doi: 10.1109/EEEIC.2019.8783867.
11. A. Alessandrini et al., 'Design and Testing of a Flash Recharge System for a Bus including foreseen effects in terms of Storage Life Extension', in 2020 IEEE 20th Mediterranean Electrotechnical Conference (MELECON), Palermo, Italy, Jun. 2020, pp. 63–68. doi: 10.1109/MELECON48756.2020.9140606.
12. A. Alessandrini et al., 'Design and Development of a Prototype of Flash Charge Systems for Public Transportation', in Applications in Electronics Pervading Industry, Environment and Society, vol. 627, S. Saponara and A. De Gloria, Eds. Cham: Springer International Publishing, 2020, pp. 293–299. doi: 10.1007/978-3-030-37277-4\_34.
13. F. Ortenzi, M. Pasquali, P. P. Prosini, A. Lidozzi, and M. Di Benedetto, 'Design and Validation of Ultra-Fast Charging Infrastructures Based on Supercapacitors for Urban Public Transportation Applications', Energies, vol. 12, no. 12, p. 2348, Jun. 2019, doi: 10.3390/en12122348.
14. F. Ortenzi, S. Orchi, and G. Pede, 'Technical and economical evaluation of hybrid flash-charging stations for electric public transport', in 2017 IEEE International Conference on Industrial Technology (ICIT), Toronto, ON, Mar. 2017, pp. 549–554. doi: 10.1109/ICIT.2017.7915417.
15. F. Cignini et al., 'Experimental Data Comparison of an Electric Minibus Equipped with Different Energy Storage Systems', Batteries, vol. 6, no. 2, p. 26, Apr. 2020, doi: 10.3390/batteries6020026.
16. M. Evzelman, M. M. Ur Rehman, K. Hathaway, R. Zane, D. Costinett, and D. Maksimovic, 'Active Balancing System for Electric Vehicles With Incorporated Low-Voltage Bus', IEEE Trans. Power Electron., vol. 31, no. 11, pp. 7887–7895, Nov. 2016, doi: 10.1109/TPEL.2015.2513432.
17. J.-Q. Li, 'Battery-electric transit bus developments and operations: A review', International Journal of Sustainable Transportation, vol. 10, no. 3, pp. 157–169, Mar. 2016, doi: 10.1080/15568318.2013.872737.
18. M. di Benedetto, F. Ortenzi, A. Lidozzi, and L. Solero, 'Design and Implementation of Reduced Grid Impact Charging Station for Public Transportation Applications', WEVJ, vol. 12, no. 1, p. 28, Feb. 2021, doi: 10.3390/wevj12010028.
19. A. Alessandrini et al., 'Design of a Hybrid Storage for Road Public Transportation Systems', in Advances in Italian Mechanism Science, vol. 68, G. Carbone and A. Gasparetto, Eds. Cham: Springer International Publishing, 2019, pp. 149–157. doi: 10.1007/978-3-030-03320-0\_16.
20. R. Krishnan, Electric motor drives: modeling, analysis, and control. Upper Saddle River, N.J: Prentice Hall, 2001.
21. L. Pugi, T. Favilli, L. Berzi, E. Locorotondo, and M. Pierini, 'Brake Blending and Optimal Torque Allocation Strategies for Innovative Electric Powertrains', in Applications in Electronics Pervading Industry, Environment and Society, vol. 573, S. Saponara and A. De Gloria, Eds. Cham: Springer International Publishing, 2019, pp. 477–483. doi: 10.1007/978-3-030-11973-7\_57.

21. L. Berzi et al., 'Brake Blending Strategy on Electric Vehicle Co-simulation Between MATLAB Simulink <sup>®</sup> and Simcenter Amesim<sup>™</sup>', in 2019 IEEE 5th International forum on Research and Technology for Society and Industry (RTSI), Florence, Italy, Sep. 2019, pp. 308–313. doi: 10.1109/RTSI.2019.8895548.
22. X. Zhang, H. Peng, H. Wang, and M. Ouyang, 'Hybrid Lithium Iron Phosphate Battery and Lithium Titanate Battery Systems for Electric Buses', IEEE Trans. Veh. Technol., vol. 67, no. 2, pp. 956–965, Feb. 2018, doi: 10.1109/TVT.2017.2749882.
23. H. Pacejka, Tire and Vehicle Dynamics. Elsevier, 2005.
24. S. Orchi, F. Ortenzi, G. Valenti, M. P. Valentini, and V. Fabrizi, 'Analisi di elettrificazione del TPL in contesti ITC: lo smart ring dell'Aquila', p. 62.

